CERN-2003-002-corr
10 October 2003
Experimental
Physics Division

ORGANISATION EUROPÉENNE POUR LA RECHERCHE NUCLÉAIRE
CERN EUROPEAN ORGANIZATION FOR NUCLEAR RESEARCH

THE CKM MATRIX AND THE UNITARITY TRIANGLE

Based on the workshop held at CERN, 13–16 February 2002

PROCEEDINGS

Editors: M. Battaglia, A.J. Buras,
P. Gambino and A. Stocchi

GENEVA
2003

Abstract

This report contains the results of the Workshop on the CKM Unitarity Triangle, held at CERN on 13–16 February 2002, to study the determination of the Cabibbo–Kobayashi–Maskawa (CKM) matrix from the available data of K, D, and B physics. This is a coherent document with chapters covering the determination of CKM elements from tree-level decays and K- and B-meson mixing and the global fits of the unitarity triangle parameters. The impact of future measurements is also discussed.

Contributors

D. Abbaneo[1], *A. Ali*[2], *P. Amaral*[3], *V. Andreev*[4], *M. Artuso*[5], *E. Barberio*[6], *M. Battaglia*[1], *C. Bauer*[6], *D. Becirevic*[8], *M. Beneke*[9], *I. Bigi*[10], *C. Bozzi*[11], *T. Brandt*[12], *G. Buchalla*[13], *A.J. Buras*[14,a], *M. Calvi*[15], *D. Cassel*[16], *V. Cirigliano*[17,b], *M. Ciuchini*[18], *G. Colangelo*[19,b,c], *A. Dighe*[20], *G. Dubois-Felsmann*[21,d], *G. Eigen*[22,d], *K. Ecklund*[16], *P. Faccioli*[23], *R. Fleischer*[1], *J. Flynn*[24], *R. Forty*[1], *E. Franco*[8], *P. Gagnon*[25], *P. Gambino*[1,e], *R. Gupta*[26,f], *S. Hashimoto*[27], *R. Hawkings*[1], *D. Hitlin*[21,d], *A. Hoang*[20], *A. Hocker*[28], *T. Hurth*[1], *G. Isidori*[1,29,b], *T. Iijima*[30], *D. Jaffe*[31], *M. Jamin*[32], *Y.Y. Keum*[30,g], *A. Khodjamirian*[33], *C.S. Kim*[34,h], *P. Kluit*[35], *A. Kronfeld*[36,i], *H. Lacker*[28], *S. Laplace*[28], *F. Le Diberder*[28], *L. Lellouch*[37,l], *A. Lenz*[38], *C. Leonidopoulos*[36,i], *A. Le Yaouanc*[39,b], *Z. Ligeti*[40], *D. Lin*[24], *G. Lopez-Castro*[41,k], *V. Lubicz*[18], *D. Lucchesi*[42], *T. Mannel*[33], *M. Margoni*[42], *G. Martinelli*[8], *D. Melikhov*[32], *M. Misiak*[43,l], *V. Morénas*[44], *H.G. Moser*[20], *U. Nierste*[36,i], *J. Ocariz*[51], *L. Oliver*[39,b], *F. Parodi*[45], *M. Paulini*[46,m], *C. Paus*[47], *O. Pène*[39,b], *M. Pierini*[8], *F. Porter*[21,d], *D. Počanić*[48], *J.-C. Raynal*[39,b], *J.L. Rosner*[3,n], *P. Roudeau*[28], *Y. Sakai*[27], *K.R. Schubert*[12], *C. Schwanda*[27,o], *B. Sciascia*[29], *O. Schneider*[49], *B. Serfass*[12], *L. Silvestrini*[8], *M. Smizanska*[50], *J. Stark*[51], *B. Stech*[32], *A. Stocchi*[28], *N. Uraltsev*[15], *M. Villa*[23], *A. Warburton*[16,52], *C. Weiser*[33], *L.H. Wilden*[12], *G. Wilkinson*[53], *S. Willocq*[54], *N. Yamada*[27]

[1]*CERN, CH-1211 Geneva, Switzerland* [2]*DESY, D-22603 Hamburg, Germany* [3]*Chicago Univ., Chicago, IL 60637, USA* [4]*INP, 188350 St. Petersburg, Russia* [5]*Syracuse Univ., Syracuse, NY 13244, USA* [6]*Southern Methodist Univ., Dallas, TX 75275, USA* [7]*Univ. of California, San Diego, La Jolla, CA 92093 USA* [8]*Univ. Roma La Sapienza, Roma, Italy* [9]*RWTH, D-52056 Aachen, Germany* [10]*Univ. of Notre Dame, Notre Dame, IN 46556, USA* [11]*INFN, I-44100 Ferrara, Italy* [12]*Technische Univ. Dresden, D-01069 Dresden, Germany* [13]*Ludwig-Maximilians-Univ. München, D-80799 Munich, Germany* [14]*Technische Univ. München, D-85748 Garching, Germany* [15]*Univ. Milano Bicocca and INFN Milano, Milano, Italy* [16]*Cornell Univ., Ithaca, NY 14853, USA* [17]*IFIC, Univ. de Valencia, E-46071 Valencia, Spain* [18]*Univ. Roma Tre, Roma, I-00146 Rome, Italy* [19]*University of Bern, CH-3012 Bern, Switzerland* [20]*MPI, D-80805 Munich, Germany* [21]*California Inst. of Technology, Pasadena, CA 91125, USA* [22]*Univ. of Bergen, 5020 Bergen, Norway* [23]*INFN, I-40126 Bologna, Italy* [24]*Univ. of Southampton, Southampton S017 1BJ, England, UK* [25]*Indiana Univ., Bloomington, IN 47405 USA* [26]*LANL, Los Alamos, NM 87545, USA* [27]*KEK, Tsukuba, 305-0801, Japan* [28]*LAL, F-91898 Orsay, France* [29]*LNF, I-00044 Frascati, Italy* [30]*Nagoya Univ., Nagoya, 464-6801, Japan* [31]*BNL, Upton, NY 11973, USA* [32]*Univ. Heidelberg, D-69120 Heidelberg, Germany* [33]*Univ. Karlsruhe, D-76128 Karlsruhe, Germany* [34]*Yonsei Univ., Seoul 120-749, South Korea* [35]*NIKHEF, 1009 DB Amsterdam. Netherlands* [36]*Fermi National Accelerator Laboratory, P.O. Box 500, Batavia, IL 60510, USA* [37]*CPT, F-13288 Marseille, France* [38]*Univ. Regensburg, D-93053 Regensburg, Germany* [39]*LPTHE, F-91405 Orsay, France* [40]*LBL, Berkeley, CA 94720, USA* [41]*CINVESTAV, 07000 Mexico, Mexico* [42]*INFN, I-35100 Padova, Italy* [43]*Univ. of Warsaw, PL-00 681 Warsaw, Poland* [44]*LPC, F-63177 Clermont Ferrand, France* [45]*INFN, I-16146 Genova, Italy* [46]*Carnegie Mellon Univ., Pittsburgh, PA 15213, USA* [47]*MIT, Cambridge, MA 02139, USA* [48]*Univ. of Virgina, Charlottesville, VA 22901, USA* [49]*Univ. of Lausanne, CH-1015 Lausanne, Switzerland* [50]*Univ. of Lancaster, Lancaster LA1 4YB, England, UK* [51]*LPNHE, 75252 Paris, France* [52]*McGill Univ., Montréal, Québec H3A 2T8, Canada* [53]*Univ. of Oxford, Oxford OX13RH, England, UK* [54]*Univ. of Massachusetts, Amherst, MA 01003, USA*

Grant Acknowledgements [a] Contract 05HT1WOA3 of German Bundesministerium für Bildung und Forschung and DFG Project Bu. 706/1-1. [b] EU contract HPRN-CT-2002-00311 (EURIDICE). [c] Partially supported by Schweizerische Nationalfonds. [d] Grant DE-FG03-92-ER40701 of the U.S. Department of Energy. [e] Marie Curie Fellowship No. HPMF-CT-2000-01048. [f] Grant KA-04-01010-E161 of the U.S. Department of Energy. [g] Grant No. NSC-90-2811-M-002 of Science Council of R.O.C. and Grant in Aid for Scientific Research from Ministry of Education, Science and Culture of Japan. [h] Grant No. 2001-042-D00022 of the KRF. [i] Fermilab is operated by Universities Research Association, Inc., under contract with the U.S. Department of Energy. [j] Contract HPRN-CT-2000-00145, Hadrons/Lattice QCD, of the EU Human Potential Program. [k] Conacyt, Mexico. [l] Grant 2 $P03B$ 121 20 of the Polish Committee for Scientific Research. [m] DOE grant DE-FG02-91ER40682. [n] Grant No. DE FG02 90ER40560 of the U.S. Department of Energy. [o] Japan Society for the Promotion of Science.

Participants

Z. Ajaltouni, P. Aliani, T. Allmendingen, G. Altarelli, P. Amaral, V. Andreev, V. Antonelli, S. Aoki, M. Artuso, P. Ball, E. Barberio, M. Battaglia, C. Bauer, D. Becirevic, M. Beneke, I. Bigi, T. Blum, S. Blyth, W. Bonivento, G. Bonneaud, S. Bosch, C. Bosio, E. Bouhova-Thacker, T. Bowcock, C. Bozzi, G. Branco, T. Brandt, G. Buchalla, A.J. Buras, M. Calvi, F. Caravaglios, C. Caso, D. Cassel, G. Cavoto, P. Charpentier, J. Chauveau, N. Christ, V. Cirigliano, M. Ciuchini, G. Colangelo, P. Colangelo, D. Costa, N. Crosetti, G. D'Ambrosio, S. Dasu, A. De Angelis, S. De Cecco, F. De Fazio, N. De Groot, N.J. De Mello, A. Deandrea, F. Di Lodovico, A. Dighe, H. Dijkstra, J. Drees, G.P. Dubois-Felsmann, K. Ecklund, G. Eigen, N. Ellis, M. Elsing, M. Fabbrichesi, R. Faccini, P. Faccioli, F. Ferroni, R. Fleischer, J. Flynn, R. Forty, E. Franco, P. Gagnon, P. Gambino, P. Gavillet, S. Giagu, L. Giusti, B. Golob, C. Greub, M. Gronau, Y. Grossman, M. Gupta, R. Gupta, U. Haisch, T. Hansmann, S. Hashimoto, R. Hawkings, P. Henrard, D. Hitlin, A. Hoang, A. Hoecker, T. Hurth, P. Igo-Kemenes, T. Iijima, G. Isidori, D. Jaffe, M. Jamin, S. Katsanevas, T. Ketel, Y.-Y. Keum, A. Khodin, A. Khodjamirian, C.S. Kim, P. Kluit, P. Koppenburg, E. Kou, A. Kronfeld, H. Lacker, S. Laplace, F. Le Diberder, R. Legac, L. Lellouch, A. Lenz, C. Leonidopoulos, A. Le Yaouanc, O. Leroy, T. Lesiak, J. Libby, Z. Ligeti, A. Likhoded, D. Lin, A. Lipniacka, G. Lopez Castro, M. Lovetere, V. Lubicz, D. Lucchesi, F. Machefert, F. Mandl, T. Mannel, D. Manolis, M. Margoni, G. Martinelli, C. Matteuzzi, S. Mele, B. Melic, D. Melikhov, S. Menzemer, M. Misiak, W. Mitaroff, M. Moch, K. Moenig, V. Morénas H.-G. Moser, F. Muheim, H. Murayama, U. Nierste, J. Ocariz, L. Oliver, T. Onogi, A. Oyanguren, C. Padilla, H. Palka, F. Palla, F. Parodi, E. Paschos, S. Passaggio, A. Passeri, M. Paulini, C. Paus, O. Pène, R. Perez Ramos, P. Perret, A. Petrov, M. Piai, M. Piccolo, M. Pierini, F. Porter, D. Počanić, J.-C. Raynal, M. Rebelo, B. Renk, M. Rescigno, G. Ricciardi, S. Rigolin, K. Rinnert, E. Robutti, J. Rosiek, J. Rosner, P. Rosnet, P. Roudeau, T. Ruf, A. Ruiz-Jimeno, S. Ryan, Y. Sakai, L. Salmi, M. Sannino, R. Santacesaria, A. Sarti, A. Satta, O. Schneider, K. Schubert, M.-H. Schune, C. Schwanda, B. Sciascia, I. Scimemi, B. Serfass, R. Sharafiddinov, L. Silvestrini, F. Simonetto, S. Slabospitsky, M. Smizanska, A. Soni, P. Spagnolo, P. Sphicas, J. Stark, A. Starodumov, B. Stech, H. Stefanicic, A. Stocchi, A. Strumia, O. Tchikilov, C. Troncon, N. Uraltsev, U. Uwer, A. Villa, M. Villa, S. Viret, A. Warburton, C. Weiser, S. Willocq, H. Wittig, S. Xella Hansen, N. Yamada, W. Yao.

Foreword

This report contains the results of the Workshop on the CKM Unitarity Triangle that was held at CERN on 13-16 February 2002. There had been several Workshops on B physics that concentrated on studies at e^+e^- machines, at the Tevatron, or at LHC separately. Here we brought together experts of different fields, both theorists and experimentalists, to study the determination of the CKM matrix from all the available data of K, D, and B physics. The analysis of LEP data for B physics is reaching its end, and one of the goals of the Workshop was to underline the results that have been achieved at LEP, SLC, and CESR. Another goal was to prepare for the transfer of responsibility for averaging B physics properties, that has developed within the LEP community, to the present main actors of these studies, from the B factory and the Tevatron experiments. The optimal way to combine the various experimental and theoretical inputs and to fit for the apex of the Unitarity Triangle has been a contentious issue. A further goal of the Workshop was to bring together the proponents of different fitting strategies, and to compare their approaches when applied to the same inputs.

Since lattice QCD plays a very important role in the determination of the non-perturbative parameters needed to constrain the CKM unitarity triangle, the first Workshop was seen as an excellent opportunity to bring together lattice theorists with the aim of establishing a working group to compile averages for phenomenologically relevant quantities. Representatives from lattice collaborations around the world were invited to attend a meeting during the Workshop. A consensus was reached to set up three test working groups, collectively known as the *CKM Lattice Working Group*, to review a number of well-studied quantities: quark masses, the kaon B-parameter, and the matrix elements relevant for neutral B-meson mixing.

This report is organized as a coherent document with chapters covering the domains of activity of the working groups. It deals mainly with the present determination of the CKM matrix in the Standard Model with a brief outlook on the near future. The impact of future measurements and of physics beyond the Standard Model will be developed further in forthcoming Workshops with the same title. Indeed, the Workshop was conceived as the first of a series. The second one will take place on 5-9 April 2003 in Durham and will focus on the results from the B-factories.

Geneva, March 2003

Contents

Chapter 1

INTRODUCTION

M. Battaglia, A.J. Buras, J. Flynn, R. Forty, P. Gambino, P. Kluit, P. Roudeau, O. Schneider, A. Stocchi

1. Setting the scene

The understanding of flavour dynamics, and of the related origin of quark and lepton masses and mixings, is among the most important goals in elementary particle physics. In this context, weak decays of hadrons, and in particular the CP violating and rare decay processes, play an important role as they are sensitive to short distance phenomena. Therefore the determination of the Cabibbo-Kobayashi-Maskawa (CKM) matrix [1,2] that parametrizes the weak charged current interactions of quarks is currently a central theme in particle physics. Indeed, the four parameters of this matrix govern all flavour changing transitions involving quarks in the Standard Model (SM). These include tree level decays mediated by W bosons, which are essentially unaffected by new physics contributions, as well as a vast number of one-loop induced flavour changing neutral current (FCNC) transitions responsible for rare and CP violating decays in the SM, which involve gluons, photons, $W^{\pm}$, Z^0 and H^0, and are sensitive probes of new physics. This role of the CKM matrix is preserved in most extensions of the SM, even if they contain new sources of flavour and CP violation.

An important goal is then to find out whether the SM is able to describe the flavour and CP violation observed in nature. All the existing data on weak decays of hadrons, including rare and CP violating decays, can at present be described by the SM within the theoretical and experimental uncertainties. On the other hand, the SM is an incomplete theory: some kind of new physics is required in order to understand the patterns of quark and lepton masses and mixings, and generally to understand flavour dynamics. There are also strong theoretical arguments suggesting that new physics cannot be far from the electroweak scale, and new sources of flavour and CP violation appear in most extensions of the SM, such as supersymmetry. Consequently, for several reasons, it is likely that the CKM picture of flavour physics is modified at accessible energy scales. In addition, the studies of dynamical generation of the baryon asymmetry in the universe show that the size of CP violation in the SM is too small to generate a matter-antimatter asymmetry as large as that observed in the universe today. Whether the physics responsible for the baryon asymmetry involves only very short distance scales like the GUT or the Planck scales, or it is related to CP violation observed in experiments performed by humans, is an important question that still has to be answered.

To shed light on these questions the CKM matrix has to be determined with high accuracy and well understood errors. Tests of its structure, conveniently represented by the unitarity triangle, have to be performed; they will allow a precision determination of the SM contributions to various observables and possibly reveal the onset of new physics contributions.

The major theoretical problem in this program is the presence of strong interactions. Although the gluonic contributions at scales $\mathcal{O}(M_{\rm W}, M_{\rm Z}, m_{\rm t})$ can be calculated within the perturbative framework, owing to the smallness of the effective QCD coupling at short distances, the fact that hadrons are bound states of quarks and antiquarks forces us to consider QCD at long distances as well. Here we have to rely on the existing non-perturbative methods, which are not yet fully satisfactory. On the experimental side, the basic problem in extracting CKM parameters from the relevant rare and CP violating transitions is the smallness of the branching ratios, which are often very difficult to measure. As always in the presence of large theoretical and systematic uncertainties, their treatment in the context of global fits is a problematic and divisive issue.

In the last decade considerable progress in the determination of the unitarity triangle and the CKM matrix has been achieved through more accurate experiments, short distance higher order QCD calculations, novel theoretical methods like Heavy Quark Effective Theory (HQET) and Heavy Quark Expansion (HQE), and progress in non-perturbative methods such as lattice gauge simulation and QCD sum rules. It is the purpose of these proceedings to summarize the present status of these efforts, to identify the most important remaining challenges, and to offer an outlook for the future.

While many decays used in the determination of the CKM matrix are subject to significant hadronic uncertainties, there are a handful of quantities that allow the determination of the CKM parameters with reduced or no hadronic uncertainty. The prime examples are the CP asymmetry $a_{\psi K_S}$, certain strategies in B decays relevant for the angle γ in the unitarity triangle, the branching ratios for $\mathrm{K}^+ \to \pi^+\nu\bar{\nu}$ and $\mathrm{K_L} \to \pi^0\nu\bar{\nu}$, and suitable ratios of the branching ratios for rare decays $\mathrm{B}_{d,s} \to \mu^+\mu^-$ and $\mathrm{B} \to X_{d,s}\nu\overline{\nu}$ relevant for the determination of $|V_{td}|/|V_{ts}|$. Also the ratio $\Delta M_d/\Delta M_s$ is important in this respect.

The year 2001 opened a new era of theoretically clean measurements of the CKM matrix through the discovery of CP violation in the B system ($a_{\psi K_S} \neq 0$) and further evidence for the decay $\mathrm{K}^+ \to \pi^+\nu\bar{\nu}$. In 2002 the measurement of the angle β in the unitarity triangle by means of $a_{\psi K_S}$ has been considerably improved. It is an exciting prospect that new data on CP violation and rare decays as well as $\mathrm{B}^0_s - \overline{\mathrm{B}}^0_s$ mixing coming from a number of laboratories in Europe, USA and Japan will further improve the determination of the CKM matrix, possibly modifying the SM description of flavour physics.

Recently, there have been several workshops on B physics [3–5] that concentrated on studies at e^+e^- machines, at the Tevatron or at LHC, separately. Here we focus instead on the discussion of the CKM matrix and its determination from all available data at different machines.

2. CKM matrix and the Unitarity Triangle

2.1. General remarks

The unitary CKM matrix [1,2] connects the *weak eigenstates* (d', s', b') and the corresponding *mass eigenstates* d, s, b:

$$\begin{pmatrix} d' \\ s' \\ b' \end{pmatrix} = \begin{pmatrix} V_{ud} & V_{us} & V_{ub} \\ V_{cd} & V_{cs} & V_{cb} \\ V_{td} & V_{ts} & V_{tb} \end{pmatrix} \begin{pmatrix} d \\ s \\ b \end{pmatrix} \equiv \hat{V}_{\rm CKM} \begin{pmatrix} d \\ s \\ b \end{pmatrix}. \tag{1}$$

Several parametrizations of the CKM matrix have been proposed in the literature; they are classified in [6]. We will use two in these proceedings: the standard parametrization [7] recommended by the Particle Data Group [8] and a generalization of the Wolfenstein parametrization [9] as presented in [10].

2.2. Standard parametrization

With $c_{ij} = \cos\theta_{ij}$ and $s_{ij} = \sin\theta_{ij}$ $(i, j = 1, 2, 3)$, the standard parametrization is given by:

$$\hat{V}_{\rm CKM} = \begin{pmatrix} c_{12}c_{13} & s_{12}c_{13} & s_{13}e^{-i\delta} \\ -s_{12}c_{23} - c_{12}s_{23}s_{13}e^{i\delta} & c_{12}c_{23} - s_{12}s_{23}s_{13}e^{i\delta} & s_{23}c_{13} \\ s_{12}s_{23} - c_{12}c_{23}s_{13}e^{i\delta} & -s_{23}c_{12} - s_{12}c_{23}s_{13}e^{i\delta} & c_{23}c_{13} \end{pmatrix}, \tag{2}$$

where δ is the phase necessary for CP violation. c_{ij} and s_{ij} can all be chosen to be positive and δ may vary in the range $0 \le \delta \le 2\pi$. However, measurements of CP violation in K decays force δ to be in the range $0 < \delta < \pi$.

From phenomenological studies we know that s_{13} and s_{23} are small numbers: $\mathcal{O}(10^{-3})$ and $\mathcal{O}(10^{-2})$, respectively. Consequently to an excellent accuracy the four independent parameters can be chosen as

$$s_{12} = |V_{us}|, \quad s_{13} = |V_{ub}|, \quad s_{23} = |V_{cb}| \quad \text{and} \ \ \delta. \tag{3}$$

As discussed in detail in Chapters 2 and 3, the first three parameters can be extracted from tree level decays mediated by the transitions $s \to u$, $b \to u$ and $b \to c$, respectively. The phase δ can be extracted from CP violating transitions or loop processes sensitive to $|V_{td}|$. We will analyse this in detail in Chapters 4–6.

2.3. Wolfenstein parametrization and its generalization

The absolute values of the elements of the CKM matrix show a hierarchical pattern with the diagonal elements being close to unity, the elements $|V_{us}|$ and $|V_{cd}|$ being of order 0.2, the elements $|V_{cb}|$ and $|V_{ts}|$ of order $4 \cdot 10^{-2}$ whereas $|V_{ub}|$ and $|V_{td}|$ are of order $5 \cdot 10^{-3}$. The Wolfenstein parametrization [9] exhibits this hierarchy in a transparent manner. It is an approximate parametrization of the CKM matrix in which each element is expanded as a power series in the small parameter $\lambda = |V_{us}| \approx 0.22$,

$$\hat{V} = \begin{pmatrix} 1 - \frac{\lambda^2}{2} & \lambda & A\lambda^3(\varrho - i\eta) \\ -\lambda & 1 - \frac{\lambda^2}{2} & A\lambda^2 \\ A\lambda^3(1 - \varrho - i\eta) & -A\lambda^2 & 1 \end{pmatrix} + \mathcal{O}(\lambda^4)\,, \tag{4}$$

and the set (3) is replaced by

$$\lambda, \qquad A, \qquad \varrho, \qquad \text{and} \ \ \eta\,. \tag{5}$$

Because of the smallness of λ and the fact that for each element the expansion parameter is actually λ^2, it is sufficient to keep only the first few terms in this expansion.

The Wolfenstein parametrization is certainly more transparent than the standard parametrization. However, if one requires sufficient level of accuracy, the terms of $\mathcal{O}(\lambda^4)$ and $\mathcal{O}(\lambda^5)$ have to be included in phenomenological applications. This can be done in many ways [10]. The point is that since (4) is only an approximation the *exact* definition of the parameters in (5) is not unique in terms of the neglected order $\mathcal{O}(\lambda^4)$. This situation is familiar from any perturbative expansion, where different definitions of expansion parameters (coupling constants) are possible. This is also the reason why in different papers in the literature different $\mathcal{O}(\lambda^4)$ terms in (4) can be found. They simply correspond to different definitions of the parameters in (5). Since the physics does not depend on a particular definition, it is useful to make a choice for which the transparency of the original Wolfenstein parametrization is not lost.

In this respect a useful definition adopted by most authors in the literature is to go back to the standard parametrization (2) and to *define* the parameters $(\lambda, A, \varrho, \eta)$ through [10,11]

$$s_{12} = \lambda\,, \qquad s_{23} = A\lambda^2\,, \qquad s_{13}e^{-i\delta} = A\lambda^3(\varrho - i\eta) \tag{6}$$

to *all orders* in λ. It follows that

$$\varrho = \frac{s_{13}}{s_{12}s_{23}}\cos\delta, \qquad \eta = \frac{s_{13}}{s_{12}s_{23}}\sin\delta. \tag{7}$$

The expressions (6) and (7) represent simply the change of variables from (3) to (5). Making this change of variables in the standard parametrization (2) we find the CKM matrix as a function of $(\lambda, A, \varrho, \eta)$ which satisfies unitarity exactly. Expanding next each element in powers of λ we recover the matrix in (4) and in addition find explicit corrections of $\mathcal{O}(\lambda^4)$ and higher order terms. Including $\mathcal{O}(\lambda^4)$ and $\mathcal{O}(\lambda^5)$ terms we find

$$\hat{V} = \begin{pmatrix} 1-\frac{1}{2}\lambda^2-\frac{1}{8}\lambda^4 & \lambda+\mathcal{O}(\lambda^7) & A\lambda^3(\varrho-i\eta) \\ -\lambda+\frac{1}{2}A^2\lambda^5[1-2(\varrho+i\eta)] & 1-\frac{1}{2}\lambda^2-\frac{1}{8}\lambda^4(1+4A^2) & A\lambda^2+\mathcal{O}(\lambda^8) \\ A\lambda^3(1-\overline{\varrho}-i\overline{\eta}) & -A\lambda^2+\frac{1}{2}A\lambda^4[1-2(\varrho+i\eta)] & 1-\frac{1}{2}A^2\lambda^4 \end{pmatrix} \tag{8}$$

where [10]

$$\overline{\varrho} = \varrho(1-\frac{\lambda^2}{2}), \qquad \overline{\eta} = \eta(1-\frac{\lambda^2}{2}). \tag{9}$$

We emphasize that by definition the expression for V_{ub} remains unchanged relative to the original Wolfenstein parametrization and the corrections to V_{us} and V_{cb} appear only at $\mathcal{O}(\lambda^7)$ and $\mathcal{O}(\lambda^8)$, respectively. The advantage of this generalization of the Wolfenstein parametrization over other generalizations found in the literature is the absence of relevant corrections to V_{us}, V_{cd}, V_{ub} and V_{cb} and an elegant change in V_{td} which allows a simple generalization of the so-called unitarity triangle to higher orders in λ [10] as discussed below.

2.4. Unitarity Triangle

The unitarity of the CKM-matrix implies various relations between its elements. In particular, we have

$$V_{ud}V_{ub}^* + V_{cd}V_{cb}^* + V_{td}V_{tb}^* = 0. \tag{10}$$

Phenomenologically this relation is very interesting as it involves simultaneously the elements V_{ub}, V_{cb} and V_{td} which are under extensive discussion at present. Other relevant unitarity relations will be presented as we proceed.

The relation (10) can be represented as a *unitarity triangle* in the complex $(\overline{\varrho}, \overline{\eta})$ plane. The invariance of (10) under any phase-transformations implies that the corresponding triangle is rotated in the $(\overline{\varrho}, \overline{\eta})$ plane under such transformations. Since the angles and the sides (given by the moduli of the elements of the mixing matrix) in this triangle remain unchanged, they are phase convention independent and are physical observables. Consequently they can be measured directly in suitable experiments. One can construct five additional unitarity triangles [12] corresponding to other orthogonality relations, like the one in (10). Some of them should be useful when the data on rare and CP violating decays improve. The areas (A_Δ) of all unitarity triangles are equal and related to the measure of CP violation $J_{\rm CP}$ [13]: $\mid J_{\rm CP} \mid = 2 \cdot A_\Delta$.

Noting that to an excellent accuracy $V_{cd}V_{cb}^*$ in the parametrization (2) is real with $|V_{cd}V_{cb}^*| = A\lambda^3 + \mathcal{O}(\lambda^7)$ and rescaling all terms in (10) by $A\lambda^3$ we indeed find that the relation (10) can be represented as the triangle in the complex $(\overline{\varrho}, \overline{\eta})$ plane as shown in Fig. 1.1.

Let us collect useful formulae related to this triangle:

- We can express $\sin(2\alpha_i)$, $\alpha_i = \alpha, \beta, \gamma$, in terms of $(\overline{\varrho}, \overline{\eta})$ as follows:

$$\sin(2\alpha) = \frac{2\overline{\eta}(\overline{\eta}^2+\overline{\varrho}^2-\overline{\varrho})}{(\overline{\varrho}^2+\overline{\eta}^2)((1-\overline{\varrho})^2+\overline{\eta}^2)}, \tag{11}$$

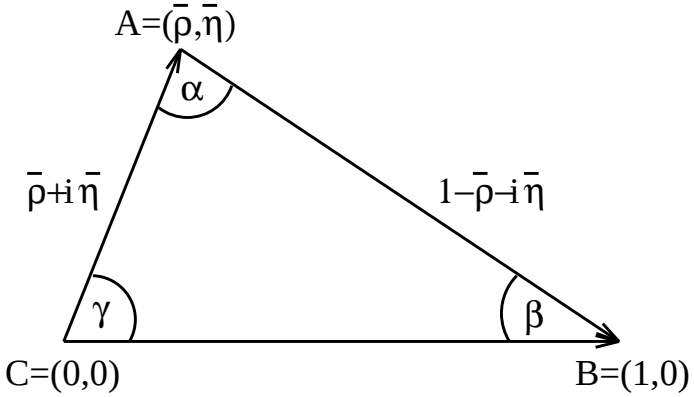

Fig. 1.1: *Unitarity Triangle.*

$$\sin(2\beta) = \frac{2\overline{\eta}(1-\overline{\varrho})}{(1-\overline{\varrho})^2+\overline{\eta}^2}, \tag{12}$$

$$\sin(2\gamma) = \frac{2\overline{\varrho\eta}}{\overline{\varrho}^2+\overline{\eta}^2} = \frac{2\varrho\eta}{\varrho^2+\eta^2}. \tag{13}$$

- The lengths CA and BA to be denoted by R_b and R_t, respectively, are given by

$$R_b \equiv \frac{|V_{ud}V_{ub}^*|}{|V_{cd}V_{cb}^*|} = \sqrt{\overline{\varrho}^2+\overline{\eta}^2} = (1-\frac{\lambda^2}{2})\frac{1}{\lambda}\left|\frac{V_{ub}}{V_{cb}}\right|, \tag{14}$$

$$R_t \equiv \frac{|V_{td}V_{tb}^*|}{|V_{cd}V_{cb}^*|} = \sqrt{(1-\overline{\varrho})^2+\overline{\eta}^2} = \frac{1}{\lambda}\left|\frac{V_{td}}{V_{cb}}\right|. \tag{15}$$

- The angles β and $\gamma = \delta$ of the unitarity triangle are related directly to the complex phases of the CKM-elements V_{td} and V_{ub}, respectively, through

$$V_{td} = |V_{td}|e^{-i\beta}, \quad V_{ub} = |V_{ub}|e^{-i\gamma}. \tag{16}$$

- The unitarity relation (10) can be rewritten as

$$R_b e^{i\gamma} + R_t e^{-i\beta} = 1\ . \tag{17}$$

- The angle α can be obtained through the relation

$$\alpha + \beta + \gamma = 180^\circ \tag{18}$$

  expressing the unitarity of the CKM-matrix.

Formula (17) shows transparently that the knowledge of (R_t, β) allows to determine (R_b, γ) through [14]

$$R_b = \sqrt{1+R_t^2-2R_t\cos\beta}, \qquad \cot\gamma = \frac{1-R_t\cos\beta}{R_t\sin\beta}. \tag{19}$$

Similarly, (R_t, β) can be expressed through (R_b, γ):

$$R_t = \sqrt{1+R_b^2-2R_b\cos\gamma}, \qquad \cot\beta = \frac{1-R_b\cos\gamma}{R_b\sin\gamma}. \tag{20}$$

These formulae relate strategies (R_t, β) and (R_b, γ) for the determination of the unitarity triangle that we will discuss in Chapter 6.

The triangle depicted in Fig. 1.1, together with $|V_{us}|$ and $|V_{cb}|$, gives the full description of the CKM matrix. Looking at the expressions for R_b and R_t, we observe that within the SM the measurements

of four CP *conserving* decays sensitive to $|V_{us}|$, $|V_{ub}|$, $|V_{cb}|$ and $|V_{td}|$ can tell us whether CP violation ($\overline{\eta} \neq 0$) is predicted in the SM. This fact is often used to determine the angles of the unitarity triangle without the study of CP violating quantities.

Indeed, R_b and R_t determined in tree-level B decays and through $\mathrm{B}^0_d - \overline{\mathrm{B}}^0_d$ mixing respectively, satisfy (see Chapters 3 and 4)

$$1 - R_b < R_t < 1 + R_b, \tag{21}$$

and $\overline{\eta}$ is predicted to be non-zero on the basis of CP conserving transitions in the B-system alone without any reference to CP violation discovered in $\mathrm{K_L} \to \pi^+\pi^-$ in 1964 [15]. Moreover one finds

$$\overline{\eta} = \pm\sqrt{R_b^2 - \overline{\varrho}^2}\,, \qquad \overline{\varrho} = \frac{1 + R_b^2 - R_t^2}{2}. \tag{22}$$

Several expressions for $\overline{\varrho}$ and $\overline{\eta}$ in terms of R_b, R_t, α, β and γ are collected in Chapter 6.

2.5. The special role of $|V_{us}|$, $|V_{ub}|$ and $|V_{cb}|$ elements

What do we know about the CKM matrix and the unitarity triangle on the basis of *tree level* decays? Here the semi-leptonic K and B decays play the decisive role. As discussed in detail in Chapters 2 and 3 the present situation can be summarized by

$$|V_{us}| = \lambda = 0.2240 \pm 0.0036 \qquad |V_{cb}| = (41.5 \pm 0.8) \cdot 10^{-3}, \tag{23}$$

$$\frac{|V_{ub}|}{|V_{cb}|} = 0.086 \pm 0.008, \qquad |V_{ub}| = (35.7 \pm 3.1) \cdot 10^{-4} \tag{24}$$

implying

$$A = 0.83 \pm 0.02, \qquad R_b = 0.37 \pm 0.04\,. \tag{25}$$

This tells us only that the apex A of the unitarity triangle lies in the band shown in Fig. 1.2. While this

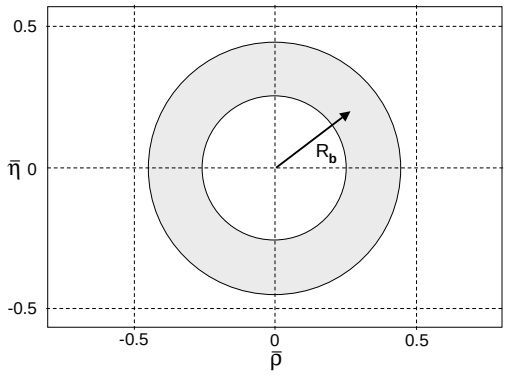

Fig. 1.2: *"Unitarity Clock"*

information appears at first sight to be rather limited, it is very important for the following reason. As $|V_{us}|$, $|V_{cb}|$, $|V_{ub}|$ and R_b are determined here from tree level decays, their values given above are to an excellent accuracy independent of any new physics contributions. That is, they are universal fundamental constants valid in any extension of the SM. Therefore their precise determination is of utmost importance. To find where the apex A lies on the *unitarity clock* in Fig. 1.2 we have to look at other decays. Most promising in this respect are the so-called *loop induced* decays and transitions and CP violating B decays

which will be discussed in Chapters 4–6. They should allow us to answer the important question of whether the Cabibbo-Kobayashi-Maskawa picture of CP violation is correct and more generally whether the Standard Model offers a correct description of weak decays of hadrons. In the language of the unitarity triangle the question is whether the various curves in the $(\overline{\varrho}, \overline{\eta})$ plane extracted from different decays and transitions using the SM formulae cross each other at a single point, as shown in Fig. 1.3, and whether the angles (α, β, γ) in the resulting triangle agree with those extracted from CP asymmetries in B decays and from CP conserving B decays.

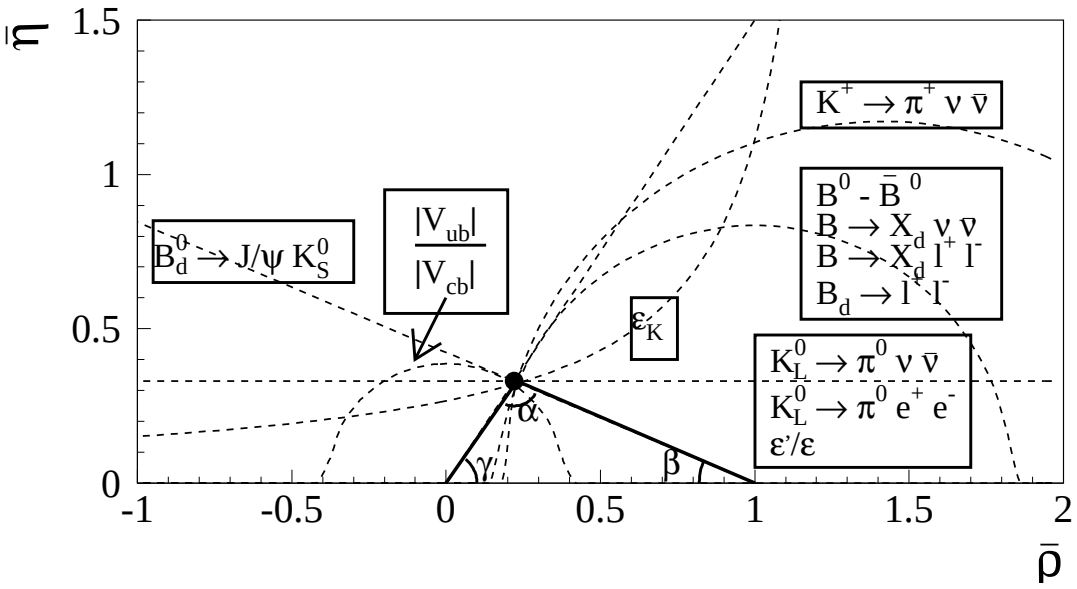

Fig. 1.3: *The ideal Unitarity Triangle*

Any inconsistencies in the $(\overline{\varrho}, \overline{\eta})$ plane will then give us some hints about the physics beyond the SM. One obvious inconsistency would be the violation of the constraint (21). Another signal of new physics would be the inconsistency between the unitarity triangle constructed with the help of rare K decays alone and the corresponding one obtained by means of B decays. Also $(\overline{\varrho}, \overline{\eta})$ extracted from loop induced processes and CP asymmetries lying outside the unitarity clock in Fig. 1.2 would be a clear signal of new physics.

In this context the importance of precise measurements of $|V_{ub}|$ and $|V_{cb}|$ should be again emphasised. Assuming that the SM with three generations and a unitary CKM matrix is a part of a bigger theory, the apex of the unitarity triangle has to lie on the unitarity clock obtained from tree level decays. That is, even if SM expressions for loop induced processes put $(\overline{\varrho}, \overline{\eta})$ outside the unitarity clock, the corresponding expressions of the grander theory must include appropriate new contributions so that $(\overline{\varrho}, \overline{\eta})$ is shifted back to the band in Fig. 1.2. In the case of CP asymmetries, this could be achieved by realizing that in the presence of new physics contributions the measured angles α, β and γ are not the true angles of the unitarity triangle but sums of the true angles and new complex phases present in extensions of the SM. Various possibilities will be discussed in the forthcoming CKM workshops. The better $|V_{ub}|$ and $|V_{cb}|$ are known, the thinner the band in Fig. 1.2 becomes, improving the selection of the correct theory. Because the branching ratios for rare and CP violating decays depend sensitively on the parameter A, precise knowledge of $|V_{cb}|$ is very important.

In order for us to draw such thin curves as in Fig. 1.3, we require both experiments and theory to be under control. Let us then briefly discuss the theoretical framework for weak decays.

3. Theoretical framework

3.1. Operator Product Expansion

The present framework describing weak decays is based on the operator product expansion (OPE) that allows short (μ_{SD}) and long distance (μ_{LD}) contributions to weak amplitudes to be separated, and on renormalization group (RG) methods that allow us to sum large logarithms $\log \mu_{SD}/\mu_{LD}$ to all orders in perturbation theory. A full exposition of these methods can be found in [16,17].

The OPE allows us to write the effective weak Hamiltonian for $\Delta F = 1$ transitions as an expansion in inverse powers of M_W. The leading term is simply

$$\mathcal{H}_{\rm eff} = \frac{G_F}{\sqrt{2}} \sum_i V^i_{\rm CKM} C_i(\mu) Q_i \tag{26}$$

with an analogous expression for $\Delta F = 2$ transitions. Here G_F is the Fermi constant and Q_i are the relevant local operators, built out of quark, gluon, photon and lepton fields, which govern the decays in question. The Cabibbo-Kobayashi-Maskawa factors $V^i_{\rm CKM}$ [1,2] and the Wilson coefficients $C_i(\mu)$ describe the strength with which a given operator enters the Hamiltonian. The latter coefficients can be considered as scale dependent *couplings* related to *vertices* Q_i and as discussed below can be calculated using perturbative methods, as long as μ is not too small. A well known example of Q_i is the $(V-A)\otimes(V-A)$ operator relevant for $\mathrm{K}^0 - \overline{\mathrm{K}}^0$ mixing

$$Q(\Delta S = 2) = \overline{s}\gamma_\mu(1-\gamma_5)d \otimes \overline{s}\gamma^\mu(1-\gamma_5)d. \tag{27}$$

We will encounter other examples later on.

An amplitude for a decay of a given meson $M = \mathrm{K}, \mathrm{B}, ..$ into a final state $F = \pi\nu\overline{\nu},\ \pi\pi,\ \mathrm{D\,K}$ is then simply given by

$$A(M \to F) = \langle F|\mathcal{H}_{\rm eff}|M\rangle = \frac{G_F}{\sqrt{2}} \sum_i V^i_{\rm CKM} C_i(\mu) \langle F|Q_i(\mu)|M\rangle, \tag{28}$$

where $\langle F|Q_i(\mu)|M\rangle$ are the matrix elements of Q_i between M and F, evaluated at the renormalization scale μ. An analogous formula exists for particle-antiparticle mixing.

The essential virtue of the OPE is that it allows the problem of calculating the amplitude $A(M \to F)$ to be separated into two distinct parts: the *short distance* (perturbative) calculation of the coefficients $C_i(\mu)$ and the *long-distance* (generally non-perturbative) calculation of the matrix elements $\langle Q_i(\mu)\rangle$. The scale μ separates, roughly speaking, the physics contributions into short distance contributions contained in $C_i(\mu)$ and the long distance contributions contained in $\langle Q_i(\mu)\rangle$. Thus C_i include the top quark contributions and those from other heavy particles such as W-, Z-bosons and charged Higgs or supersymmetric particles in the supersymmetric extensions of the SM. Consequently $C_i(\mu)$ depend generally on m_t and also on the masses of new particles if extensions of the SM are considered. This dependence can be found by evaluating so-called *box* and *penguin* diagrams with full W-, Z-, top- and new particles exchanges and properly including short distance QCD effects. The latter govern the μ-dependence of $C_i(\mu)$.

The value of μ can be chosen arbitrarily but the final result must be μ-independent. Therefore the μ-dependence of $C_i(\mu)$ has to cancel the μ-dependence of $\langle Q_i(\mu)\rangle$. In other words it is a matter of choice what exactly belongs to $C_i(\mu)$ and what to $\langle Q_i(\mu)\rangle$. This cancellation of the μ-dependence generally involves several terms in the expansion in (28). The coefficients $C_i(\mu)$ depend also on the renormalization scheme. This scheme dependence must also be cancelled by that of $\langle Q_i(\mu)\rangle$, so that physical amplitudes are renormalization scheme independent. Again, as in the case of the μ-dependence, cancellation of the renormalization scheme dependence generally involves several terms in the expansion (28).

Although μ is in principle arbitrary, it is customary to choose μ to be of the order of the mass of the decaying hadron. This is $\mathcal{O}(m_{\rm b})$ and $\mathcal{O}(m_{\rm c})$ for B decays and D decays respectively. For K decays the typical choice is $\mu = \mathcal{O}$(1-2 GeV) rather than $\mathcal{O}(m_K)$ that would be much too low for any perturbative calculation of the couplings C_i. Now since $\mu \ll M_{W,Z},\ m_t$, large logarithms $\ln M_{\rm W}/\mu$ compensate in the evaluation of $C_i(\mu)$ the smallness of the QCD coupling constant α_s, and terms $\alpha_s^n(\ln M_{\rm W}/\mu)^n$, $\alpha_s^n(\ln M_{\rm W}/\mu)^{n-1}$ etc. have to be resummed to all orders in α_s before a reliable result for C_i can be obtained. This can be done very efficiently by renormalization group methods. The resulting *renormalization group improved* perturbative expansion for $C_i(\mu)$ in terms of the effective coupling constant $\alpha_s(\mu)$ does not involve large logarithms. The related technical issues are discussed in detail in [16] and [17].

Clearly, in order to calculate the amplitude $A(M \to F)$ the matrix elements $\langle Q_i(\mu)\rangle$ have to be evaluated. Since they involve long distance contributions one is forced in this case to use non-perturbative methods such as lattice calculations, the 1/N expansion (where N is the number of colours), QCD sum rules, hadronic sum rules, chiral perturbation theory and so on. In the case of certain B-meson decays, the *Heavy Quark Effective Theory* (HQET) and *Heavy Quark Expansion* (HQE) also turn out to be useful tools. These approaches will be described in Chapter 3. Needless to say, all these non-perturbative methods have some limitations. Consequently the dominant theoretical uncertainties in the decay amplitudes reside in the matrix elements $\langle Q_i(\mu)\rangle$ and non-perturbative parameters present in HQET and HQE.

The fact that in many cases the matrix elements $\langle Q_i(\mu)\rangle$ cannot be reliably calculated at present is very unfortunate. The main goal of the experimental studies of weak decays is the determination of the CKM factors ($V_{\rm CKM}$) and the search for the physics beyond the SM. Without a reliable estimate of $\langle Q_i(\mu)\rangle$ these goals cannot be achieved unless these matrix elements can be determined experimentally or removed from the final measurable quantities by taking suitable ratios and combinations of decay amplitudes or branching ratios. Classic examples are the extraction of the angle β from the CP asymmetry in $\mathrm{B} \to \psi \mathrm{K_S}$ and the determination of the unitarity triangle by means of $\mathrm{K} \to \pi\nu\overline{\nu}$ decays. Flavour symmetries like $SU(2)_{\rm F}$ and $SU(3)_{\rm F}$ relating various matrix elements can also be useful in this respect, provided flavour breaking effects can be reliably calculated. However, the elimination of hadronic uncertainties from measured quantities can be achieved rarely and often one has to face directly the calculation of $\langle Q_i(\mu)\rangle$.

One of the outstanding issues in the calculation of $\langle Q_i(\mu)\rangle$ is the compatibility (*matching*) of $\langle Q_i(\mu)\rangle$ with $C_i(\mu)$. $\langle Q_i(\mu)\rangle$ must have the correct μ and renormalization scheme dependence to ensure that physical results are μ- and scheme-independent. Non-perturbative methods often struggle with this problem, but lattice calculations using non-perturbative matching techniques can meet this requirement.

Finally, we would like to emphasize that in addition to the hadronic uncertainties, any analysis of weak decays, and in particular of rare decays, is sensitive to possible contributions from physics beyond the SM. Even if the latter are not discussed in this document and will be the subject of future workshops, it is instructive to describe how new physics would enter into the formula (28). This can be done efficiently by using the master formula for weak decay amplitudes given in [18]. It follows from the OPE and RG, in particular from (28), but is more useful for phenomenological applications than the formal expressions given above. This formula incorporates SM contributions but also applies to any extension of the SM:

$$\mathrm{A(Decay)} = \sum_i B_i \eta^i_{\rm QCD} V^i_{\rm CKM}[F^i_{\rm SM} + F^i_{\rm New}] + \sum_k B^{\rm New}_k [\eta^k_{\rm QCD}]^{\rm New} V^k_{\rm New}[G^k_{\rm New}]\,. \qquad (29)$$

The non-perturbative parameters B_i represent the matrix elements $\langle Q_i(\mu)\rangle$ of local operators present in the SM. For instance in the case of $\mathrm{K^0 - \overline{K}^0}$ mixing, the matrix element of the operator $Q(\Delta S = 2)$ in (27) is represented by the parameter $\hat{B}_K$. An explicit expression is given in Chapter 4. There are other non-perturbative parameters in the SM that represent matrix elements of operators Q_i with different colour and Dirac structures. Explicit expressions for these operators and their matrix elements will be given in later chapters.

The objects $\eta^i_{\rm QCD}$ are the QCD factors resulting from RG-analysis of the corresponding operators. They summarise the contributions from scales $m_b \leq \mu \leq m_t$ and 1-2 GeV$\leq \mu \leq m_t$ in the case of B and K decays, respectively. Finally, $F^i_{\rm SM}$ stand for the so-called Inami-Lim functions [19] that result from the calculations of various box and penguin diagrams. They depend on the top-quark mass. $V^i_{\rm CKM}$ are the CKM-factors we want to determine.

New physics can contribute to our master formula in two ways. First, it can modify the importance of a given operator, already relevant in the SM, through a new short distance function $F^i_{\rm New}$ that depends on new parameters in extensions of the SM, such as the masses of charginos, squarks, and charged Higgs particles, or the value of $\tan\beta = v_2/v_1$, in the Minimal Supersymmetric Standard Model (MSSM). These new particles enter the new box and penguin diagrams. Second, in more complicated extensions of the SM new operators (Dirac structures) that are either absent or very strongly suppressed in the SM, can become important. Their contributions are described by the second sum in (29) with $B^{\rm New}_k, [\eta^k_{\rm QCD}]^{\rm New}, V^k_{\rm New}, G^k_{\rm New}$ the analogues of the corresponding objects in the first sum of the master formula. The $V^k_{\rm New}$ show explicitly that the second sum describes generally new sources of flavour and CP violation beyond the CKM matrix. This sum may, however, also include contributions governed by the CKM matrix that are strongly suppressed in the SM but become important in some extensions of the SM. A typical example is the enhancement of the operators with Dirac structures $(V-A)\otimes(V+A)$, $(S-P)\otimes(S\pm P)$ and $\sigma_{\mu\nu}(S-P)\otimes\sigma^{\mu\nu}(S-P)$ contributing to $\rm K^0$-$\overline{\rm K}^0$ and $\rm B^0_{d,s}$-$\overline{\rm B}^0_{d,s}$ mixings in the MSSM with large $\tan\beta$ and in supersymmetric extensions with new flavour violation. The latter may arise from the misalignment of quark and squark mass matrices. The most recent compilation of references to existing next-to-leading (NLO) calculations of $\eta^i_{\rm QCD}$ and $[\eta^k_{\rm QCD}]^{\rm New}$ can be found in [20].

The new functions $F^i_{\rm New}$ and $G^k_{\rm New}$ as well as the factors $V^k_{\rm New}$ may depend on new CP violating phases, making the phenomenological analysis considerably more complicated. On the other hand, in the simplest class of the extensions of the SM where the flavour mixing is still entirely given by the CKM matrix and only the SM low energy operators are relevant [21] the formula (29) simplifies to

$$\mathrm{A(Decay)} = \sum_i B_i \eta^i_{\rm QCD} V^i_{\rm CKM}[F^i_{\rm SM} + F^i_{\rm New}] \tag{30}$$

with $F^i_{\rm SM}$ and $F^i_{\rm New}$ real. This scenario is often called *Minimal Flavour Violation* (MFV) [21], although one should be mindful that for some authors MFV means a more general framework in which also new operators can give significant contributions [22].

The simplicity of (30) allows to eliminate the new physics contributions by taking suitable ratios of various quantities, so that the CKM matrix can be determined in this class of models without any new physics uncertainties. This implies a universal unitarity triangle [21] and a number of relations between various quantities that are universal in this class of models [23]. Violation of these relations would indicate the relevance of new low energy operators and/or the presence of new sources of flavour violation. In order to see possible violations of these relations and consequently the signals of new sources of flavour violation it is essential to have a very precise determination of the CKM parameters. We hope that the material presented in this document is a relevant step towards this goal.

3.2. Importance of lattice QCD

Lattice calculations of the matrix elements $\langle Q_i(\mu)\rangle$ are based on a first-principles evaluation of the path integral for QCD on a discrete space-time lattice. They have the advantage of being systematically improvable to approach continuum QCD results with no additional parameters beyond those of QCD itself. Indeed, lattice QCD can be applied to determine these QCD parameters — the quark masses and the coupling constant. The most notable application of lattice QCD for CKM-fitting is to the mixing parameters for neutral kaons (B_K) and neutral B-mesons (F_B and B_B). Uncertainties in these quantities are now dominant in CKM fits. Lattice calculations are also important for determining form factors used

to extract $|V_{ub}|$ from exclusive semileptonic B decays to light pseudoscalars or vectors, and for providing the endpoint form factor normalization needed to extract $|V_{cb}|$ from semileptonic B to $\mathrm{D}^{(*)}$ decays. With the advent of CLEO-c, the current round of lattice calculations for charm physics will be tested at the few-percent level. The charm calculations share several features with their analogues in the b sector, so a favourable outcome would bolster confidence in lattice techniques.

In recent years much effort has been devoted to non-perturbative techniques for improvement, to reduce discretization errors, and for renormalization and matching, to relate lattice results either directly to physical quantities or to quantities defined in some continuum renormalization scheme. With non-perturbative matching, the μ- and scheme-dependence of the matrix elements $\langle Q_i(\mu)\rangle$ is correctly matched with that of the $C_i(\mu)$.

The outstanding issue for the lattice is the inclusion of dynamical quark effects or *unquenching*. Many phenomenologically important quantities have been or are being calculated with dynamical quarks. However the dynamical quarks cannot be simulated with light enough masses to describe physical up and down quarks (the state-of-the-art is a mass of about $m_s/5$). Likewise, the *valence* quarks, whose propagators are used to evaluate matrix elements, also cannot be simulated with physical up and down masses. The combined extrapolations (chiral extrapolations) of both kinds of masses to realistic values are a major current focus of activity.

For heavy quarks the issue is to avoid discretization errors proportional to positive powers of $m_Q\,a$ where m_Q is the mass of the heavy quark and a the lattice spacing. Since present-day inverse lattice spacings are in the range $2\,\mathrm{GeV} < a^{-1} < 4\,\mathrm{GeV}$ or so, $m_b\,a$ is intolerably large for the b-quark. One approach is to restrict calculations to masses around that of charm and extrapolate to the b-quark regime guided by HQET, but the extrapolation can be significant and may amplify the $m_Q\,a$ errors, unless a continuum limit is taken first. In the last few years much has been learned about how to disentangle heavy quark mass-dependence and discretization effects using an effective theory approach where QCD is expanded in powers of μ/m_Q, where μ denotes other dimensionful scales in the problem, and discretization errors are proportional to powers of μa (so that μ should be smaller than m_Q and a^{-1}). This has been pioneered by the Fermilab group and implemented by them and others in numerical simulations for B-meson decay constants and semileptonic decay form factors. Lattice discretizations of HQET and NRQCD are also effective theory approaches which are used in simulations. In the effective theories one has to ensure that corrections in powers of $1/m_Q$ are calculated accurately, which involves issues of renormalization and the proliferation of terms as the power of $1/m_Q$ increases. By combining lattice HQET with direct simulations around the charm mass, the b-quark can be reached by interpolation, but this makes sense only if the continuum limit is taken for both calculations first. Currently, results obtained with different approaches to treating heavy quarks agree fairly well for b-physics.

An important theoretical advance in 1998 was the realization that full chiral symmetry could be achieved at finite lattice spacing, allowing the continuum and chiral limits to be separated. Lattice actions incorporating chiral symmetry are being used notably in calculations for kaon physics, including B_K, the $\Delta I = 1/2$ rule and ϵ'/ϵ, where the symmetry can be used to simplify the structure of the calculation. However, these calculations are currently quenched and have not yet had much impact on phenomenology.

4. Experimental aspects of B physics and the CKM matrix elements

In this report we will review B decay properties relevant for the measurement of the $|V_{ub}|$ and $|V_{cb}|$ CKM matrix elements, and $\mathrm{B}^0 - \overline{\mathrm{B}}^0$ oscillations which constrain $|V_{td}|$ and $|V_{ts}|$, allowing to test the Standard Model through the CKM Unitarity Triangle. However, many additional measurements of B mesons properties (masses, branching fractions, lifetimes etc.) are necessary to constrain Heavy Quark theories to enable a precise extraction of the CKM parameters. These measurements are also important because they propagate to the CKM-related measurements as systematic errors.

4.1. B physics at colliders

In the last 15 years — before the start of asymmetric B-factories — the main contributors to B hadron studies have been symmetric e^+e^- colliders operating at the $\Upsilon(4S)$ and at the Z^0 resonance, and also the Tevatron $p\overline{p}$ collider (see Table 1.1).

Experiments	Number of $b\overline{b}$ events ($\times$ 10^6)	Environment	Characteristics
ALEPH, DELPHI	$\sim$ 1 per expt.	Z^0 decays	back-to-back 45 GeV b-jets
OPAL, L3		($\sigma_{bb} \sim$ 6nb)	all B hadrons produced
SLD	~ 0.1	Z^0 decays	back-to-back 45 GeV b-jets
		($\sigma_{bb} \sim$ 6nb)	all B hadrons produced
			beam polarized
ARGUS	~ 0.2	$\Upsilon(4S)$ decays	mesons produced at rest
		($\sigma_{bb} \sim$ 1.2nb)	B^0_d and B^+
CLEO	~ 9	$\Upsilon(4S)$ decays	mesons produced at rest
		($\sigma_{bb} \sim$ 1.2nb)	B^0_d and B^+
CDF	$\sim$ several	$p\overline{p}$ collisions	events triggered with leptons
		$\sqrt{s}$ = 1.8 TeV	all B hadrons produced

Table 1.1: *Summary of the recorded statistics for experiments at different facilities and their main characteristics.*

At the $\Upsilon(4S)$ peak, B^+B^- and $B^0_d\ \overline{B}^0_d$ meson pairs are produced on top of a continuum background, with a cross section of about 1.2 nb. At the energy used, only $B^\pm$ and B^0_d mesons are produced, almost at rest, with no additional hadrons. The constraint that the energy taken by each B meson is equal to the beam energy is useful for several measurements which rely on kinematic reconstruction.

At the Z^0 resonance the production cross section is $\sim$ 6 nb, about five times larger than at the $\Upsilon(4S)$, and the fraction of $b\overline{b}$ in hadronic events, is $\sim 22\%$, very similar to that obtained at the $\Upsilon(4S)$. Further, at the Z^0 peak B^0_s mesons and B baryons are produced in addition to $B^\pm$ and B_d mesons. B hadrons carry, on average, about 70% of the available beam energy, resulting in a significant boost which confines their decay products within well-separated jets. The resulting flight distance of a B hadron, $L = \gamma\beta c\tau$, is on average about 3 mm at these energies. Since the mean charged multiplicity in B decays is about five, it is possible to tag B hadrons using a lifetime tag based on the track topology. Additional hadrons are created in the fragmentation process which can be distinguished from the heavy hadron decay products using similar procedures.

Finally, at $p\overline{p}$ colliders b quarks are produced predominantly through gluon-gluon fusion. At the Tevatron energy of $\sqrt{s}$ = 1.8 TeV the b-production cross section is observed to be around 100 μb, which is huge. As the B decay products are contained in events with a much greater multiplicity than at the Z^0 pole and as backgrounds are important, only specific channels, such as fully reconstructed final states, can be studied with a favourable signal-to-background ratio.

Most of the precision measurements in B physics performed since SLC/LEP startup have been made possible by the development of high resolution Vertex Detectors, based on Silicon sensors. As the average flight distance of the b quark is of the order of 3 mm at Z^0 energies and as the typical displacement of secondary charged particles from the event primary vertex is of the order of 200 μm, secondary particles can be identified and the decay topology of short-lived B hadrons can be measured. The typical resolution of silicon detectors varies between a few and a few tens of microns depending

on particle momentum and on detector geometry. A typical LEP $b\overline{b}$ event is shown in Fig. 1.4. In spite of a smaller Z^0 data set, the SLD experiment has proven to be highly competitive, due to a superior CCD-based vertex detector, located very close to the interaction point.

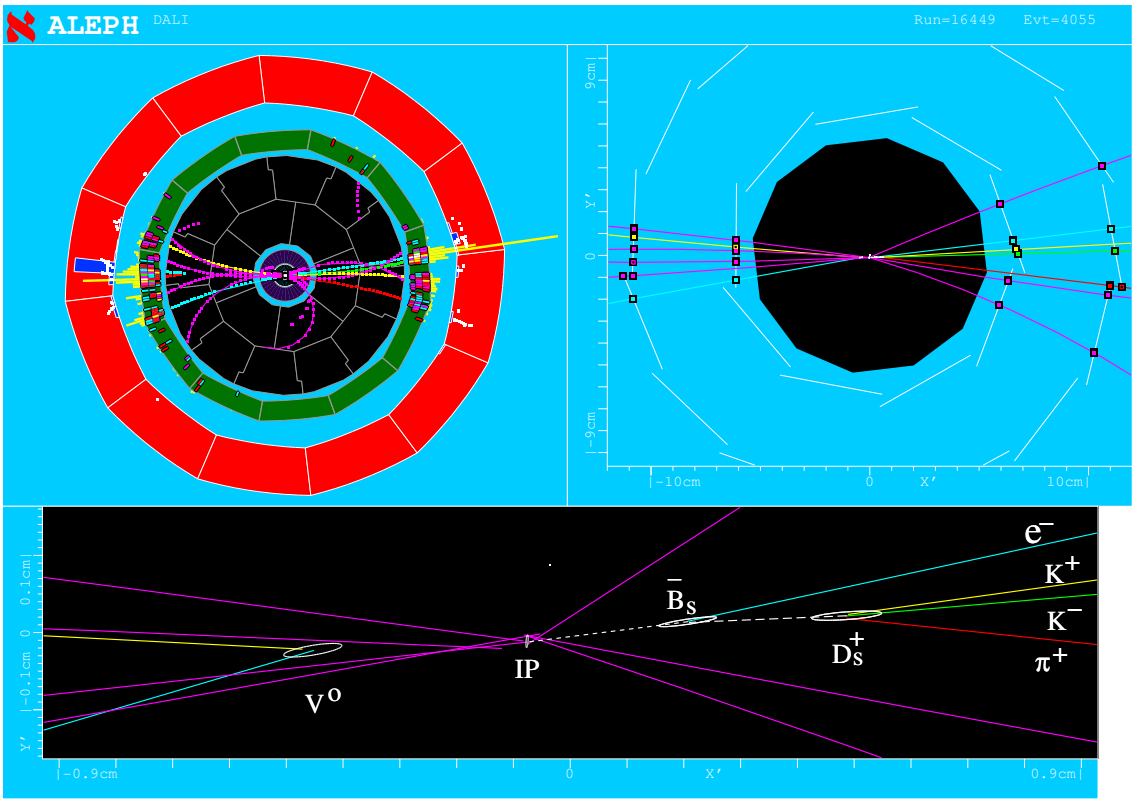

Fig. 1.4: *A $b\overline{b}$ event at LEP recorded by the ALEPH detector. The event consists of two jets containing the decay products of the two B hadrons and other particles. In one hemisphere a $\overline{\mathrm{B}}^0_s$ decays semileptonically : $\overline{\mathrm{B}}^0_s \to D_s^+ e^- \overline{\nu}_e X$, $D_s^+ \to K^+K^-\pi^+$ (tertiary vertex).*

The physics output from the data taken on the Z^0 resonance at LEP and SLC has continued to improve, with a better understanding of the detector response and new analysis techniques. Better-performing statistical treatments of the information have been developed. As a result, the accuracy of several measurements and the reach of other analyses have been considerably enhanced.

In 1984, six years after the discovery of the $b\overline{b}$ bound state Υ, the first experimental evidence for the existence of $\mathrm{B_d}$ and B^+ mesons was obtained by ARGUS at DORIS and CLEO at CESR and the B mesons joined the other known hadrons in the Review of Particle Physics listings. By the time LEP and SLC produced their first collisions in 1989, the inclusive b lifetime was known with about 20% accuracy from measurements at PEP and PETRA. The relatively long b lifetime provided a first indication for the smallness of the $|V_{cb}|$ matrix element. Branching fractions of $\mathrm{B_d}$ and B^+ meson decays with values larger than about few 10^{-3} had been measured.

In the early 90's the B sector landscape was enriched by the observation of new states at LEP. Evidence of the Λ_b baryon was obtained in the $\Lambda_b \to \Lambda \ell \nu X$ decay mode [24]. This was followed by the observations of the B^0_s meson, in the decay $\overline{\mathrm{B}}^0_s \to \mathrm{D}^+_s \ell^- \overline{\nu}_\ell$, in 1992 and of the Ξ_b baryon in 1994. These analyses used semileptonic decays with a relatively large branching ratio of the order of a few % in combination with a clean exclusive final state (D_s , Λ or Ξ). Using right and wrong sign combinations, the background could be controlled and measured using the data. Selection of those signals is shown

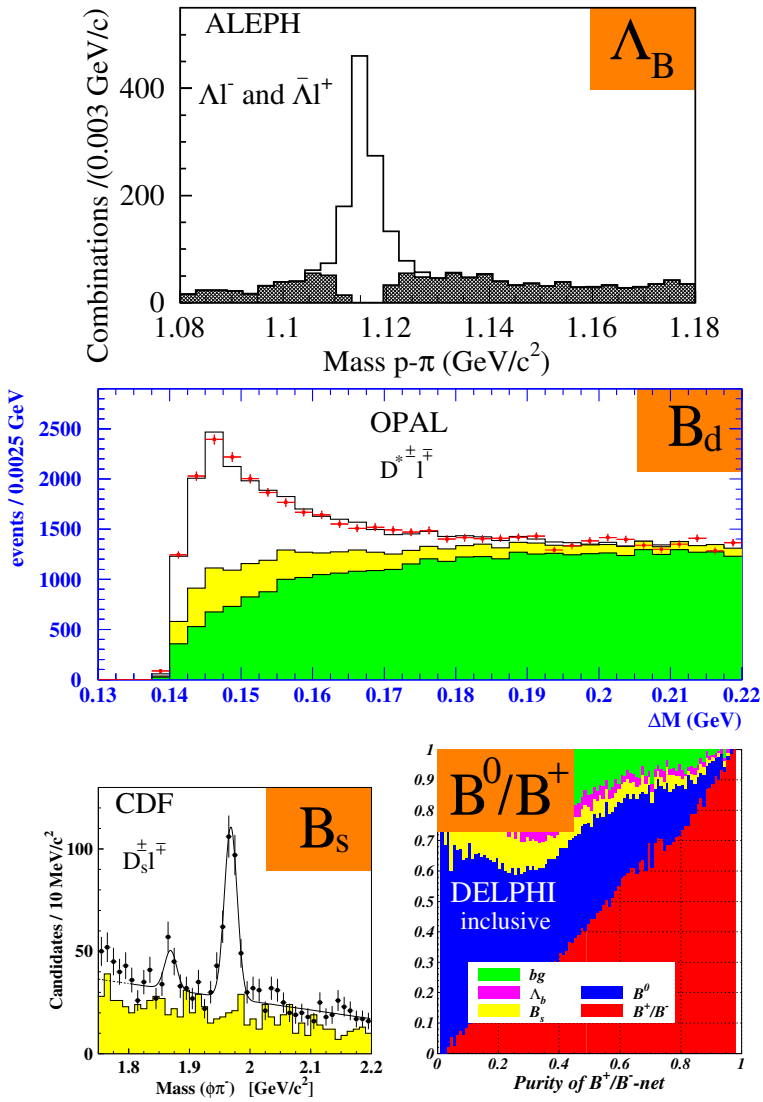

Fig. 1.5: *Signals from B hadrons. From top left to bottom left are the invariant mass spectra of* Λ, $((\mathrm{D}^0\pi) - \mathrm{D}^0)$, $\mathrm{D_s}$ *which are obtained in correlation with an opposite sign lepton. These events are attributed mainly to the semileptonic decays of* Λ_b, $\mathrm{B_d^0}$ *and* $\mathrm{B_s^0}$ *hadrons, respectively. The bottom right figure shows the possibility of distinguishing charged from neutral B mesons based on inclusive techniques.*

in Fig. 1.5. The orbitally excited B hadrons ($L = 1$) (B^{**}) [25] were also found and studied starting in 1994. These analyses were mostly based on partial reconstruction, profiting from the characteristic decay topology, and estimated the backgrounds relying to a large extent on the data themselves.

In parallel with studies on B spectroscopy, inclusive and individual B_d^0, B^+, B_s^0 and b-baryon exclusive lifetimes were measured at LEP, SLD and CDF with increasing accuracies (as shown in Fig. 1.6) down to the present final precision, of a few percent.

Rare decays have been traditionally a hunting ground for the CLEO experiment, which benefited from the large statistics recorded at CESR. With about 9M $\mathrm{B\overline{B}}$ meson pairs registered, B decay modes with branching fractions down to 10^{-5} could be observed. The first signal for the loop-mediated $\mathrm{B} \to K^*\gamma$ decay was obtained in 1993. Evidence for charmless decay of B mesons followed [26] (see Fig. 1.7). At LEP, where the data sets were smaller, topological decay reconstruction methods and the efficient separation of decay products from the two heavy mesons allowed access to some transitions having branching fractions of order 10^{-4}–10^{-5} [27].

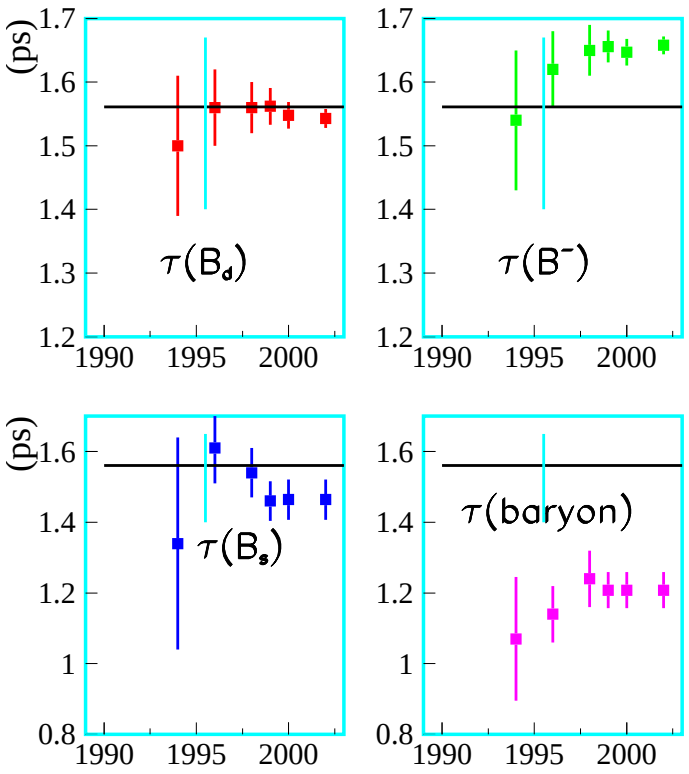

Fig. 1.6: *Evolution of the combined measurement of the different B hadron lifetimes over the years (the last point for* B_d^0 *and* B^- *meson lifetimes includes measurement obtained at b-factories). The horizontal lines indicate the values of the inclusive b lifetime, while the vertical lines indicate the end of LEP data taking at the* Z^0 *resonance.*

A value close to 10% for the semileptonic (s.l.) b branching fraction was not expected by theorists in the early 90's. More recent theoretical work suggests measuring both the s.l. branching fraction and the number of charmed particles in B decays. In fact, a s.l. branching ratio of 10% favours a low value of the charm mass and a value for the B branching ratio into double charm $b \to c\bar{c}s$ of about 20%. Much experimental effort has been made in recent years by the CLEO and LEP collaborations, allowing a coherent picture to emerge. The interplay among data analyses and phenomenology has promoted these studies to the domain of precision physics. The s.l. B branching fraction is presently known with about 2% accuracy and much data has become available for fully inclusive, semi-inclusive and exclusive decays. Inclusive and exclusive s.l. decays allow the extraction of $|V_{cb}|$ and $|V_{ub}|$ with largely independent sources of uncertainties and underlying assumptions. The inclusive method is based on the measured inclusive s.l. widths for $b \to X_{c,u}\ell\overline{\nu}_\ell$ interpreted on the basis of the Operator Product Expansion predictions. The exclusive method uses processes such as $\overline{\mathrm{B}}_d^0 \to \mathrm{D}^{*+}\ell^-\overline{\nu}$ and $\mathrm{B}^- \to \rho\ell\overline{\nu}$ and relies on Heavy Quark Effective Theory and form factor determinations. The requirements of precision tests of the unitarity triangle are now setting objectives for further improving our understanding of these decays and their application in the extraction of the CKM parameters.

The second major source of information on the magnitude of the relevant elements in the CKM matrix comes from oscillations of neutral B mesons. A B^0 meson is expected to oscillate into a $\overline{\mathrm{B}}^0$ with a probability given by: $P_{\mathrm{B}_q^0 \to \mathrm{B}_q^0(\overline{\mathrm{B}}_q^0)} = \frac{1}{2}e^{-t/\tau_q}(1 \pm \cos\Delta M_q t)$ where ΔM_q is proportional to the

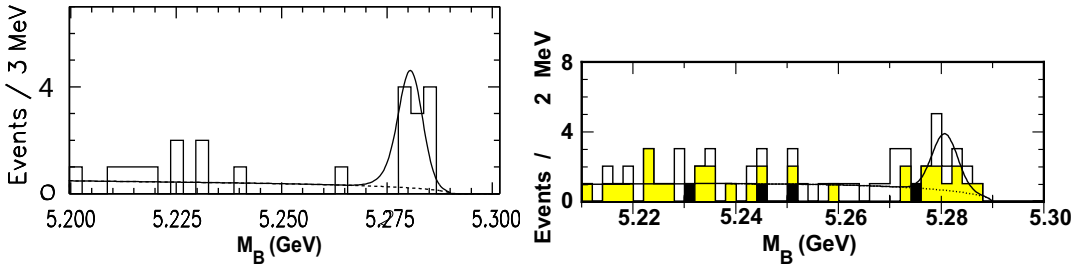

Fig. 1.7: *Left Plot: the* $\mathrm{K}^*\gamma$ *mass spectrum reconstructed by CLEO in the* $\mathrm{B} \to \mathrm{K}^*\gamma$ *decay modes. Right Plot : charmless B decays observed by CLEO :* $\pi\pi$ *and K*π *mass spectrum in the* $\mathrm{B} \to \pi\pi(\mathrm{K}\pi)$ *decay modes. In dark the events with an identified pion. The plots show the updated signals in 1995.*

magnitude of the V_{tq} element squared. The first signals for B_d mixing were obtained in 1987 by the ARGUS [28] and CLEO [29] experiments. The UA1 experiment at the CERN S$p\overline{p}$S collider showed evidence for mixing due to combined contributions from both B^0_d and B^0_s mesons [30].

At energies around the Z^0 peak, where both B^0_d and B^0_s mesons are produced with fractions f_{B_d} and f_{B_s}, the mixing parameter χ is given by $\chi = f_{B_d}\chi_d + f_{B_s}\chi_s$ (where $\chi_{d(s)}$ is the probability to observe a $\overline{\mathrm{B}}^0_{d(s)}$ meson starting from a $\mathrm{B}^0_{d(s)}$ meson and $f_{B_{d(s)}}$ is the $\mathrm{B}^0_{d(s)}$ production fraction). Owing to the fast B^0_s oscillations, the χ_s value is close to 0.5 and becomes very insensitive to ΔM_s. Therefore even a very precise measurement of χ_s does not provide a determination of $|V_{ts}|$.

It became clear that only the observation of time evolution of $\mathrm{B}^0 - \overline{\mathrm{B}}^0$ oscillations, for B_d and B_s mesons separately, would allow measurement of ΔM_d and ΔM_s. Time dependent $\mathrm{B}^0_d - \overline{\mathrm{B}}^0_d$ oscillation was first observed [31] in 1993. The precision of the measurement of the B_d oscillation frequency has significantly improved in recent years. Results have been extracted from the combination of more than thirty-five analyses which use different event samples from the LEP/SLD/CDF experiments. At present, new results from the B-factories are also being included. The evolution of the combined results for the ΔM_d frequency measurement over the years is shown in Fig. 1.8, reaching, before the contribution from the B-factories, an accuracy of $\sim 2.5\%$. New, precise measurements performed at the B-factories further improved this precision by a factor of 2.

As the B^0_s meson is expected to oscillate more than 20 times faster than the B^0_d meson ($\sim 1/\lambda^2$) and as B_s mesons are less abundantly produced, the search for $\mathrm{B}^0_s - \overline{\mathrm{B}}^0_s$ oscillations is much more difficult. To observe these fast oscillations, excellent resolution on the proper decay time is mandatory. Improvements in the ΔM_s sensitivity are depicted in Fig. 1.9. As no signal for $\mathrm{B}^0_s - \overline{\mathrm{B}}^0_s$ oscillations has been observed so far, the present limit implies that B^0_s mesons oscillate at least 30 times faster than B^0_d mesons. The impact of such a limit on the determination of the unitarity triangle parameters is already significant.

5. Heavy flavour averages

5.1. Motivation and history

Averaging activities have played an important role in the LEP community and several different working groups were formed to address the issue of combining LEP results. The first working group to appear was the LEP Electroweak WG with members from ALEPH, DELPHI, L3 and OPAL, soon followed in 1994

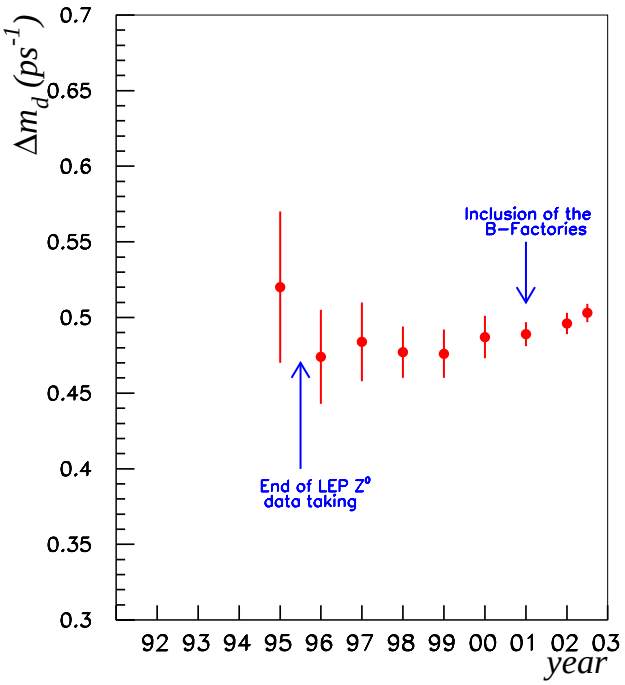

Fig. 1.8: *Evolution of the average of ΔM_d frequency measurements over the years.*

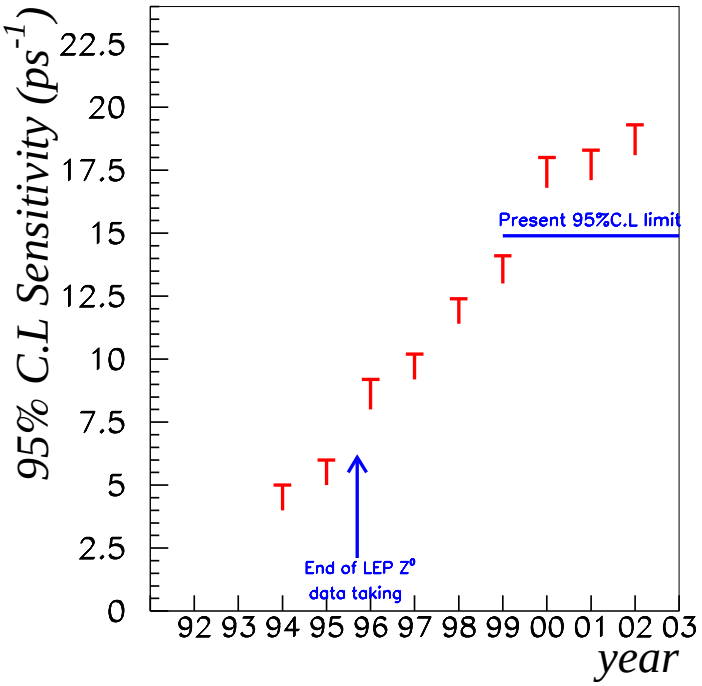

Fig. 1.9: *Evolution of the combined ΔM_s sensitivity over the last decade.*

by the b-hadron lifetime WG. They both rather quickly felt the need to enlarge their scope, and provide *world averages* rather than just LEP averages, so these groups have grown to include also representatives from the SLD collaboration, as well as from the CDF collaboration in the case of the lifetime WG. The B oscillations WG was formed in 1996 (once the need for combining B mixing results arose), and was also joined by SLD and CDF a year later.

In fall 1998, the four LEP collaborations decided to create the Heavy Flavour Steering Group (HFS), with members from the ALEPH, CDF, DELPHI, L3, OPAL and SLD collaborations. Within the scope of heavy flavour physics — in particular beauty physics — its mandate was to identify new areas where combined results are useful, and coordinate the averaging activities.

The HFS quickly spawned three new working groups on $\Delta\Gamma_s$, $|V_{cb}|$ and $|V_{ub}|$, and also supported or initiated activities in other areas like charm-counting in b-hadron decays, determination of the b-fragmentation function, and extraction of the CKM parameters. The coordination of all these activities resulted in better communication between experimenters and theorists and, as a product, a more coherent set of averages in b physics updated on a regular basis [32]. In order to provide world averages, contacts have also been established with representatives of other collaborations (CLEO, and more recently BABAR and BELLE).

The results of the b-lifetime WG were used by the Particle Data Group from 1996 onwards; later also averages from the B oscillation and b-fractions (1998), the $|V_{cb}|$ and the $|V_{ub}|$ Working Groups (2000) were also included. During this Workshop an Open Forum was organised for an orderly hand-over of the responsibility for heavy flavour physics world averages. This forum was chaired by HFS and PDG members. As a result, in the future, after the HFS group disbands, these averaging activities will be continued in the framework of a new Heavy Flavour Averaging Group [33], in which the Particle Data Group is also taking part.

In 2000 and 2001, the HFS group has produced reports [34] containing combined results on b-hadron production rates and decay properties from the ALEPH, CDF-1, DELPHI, L3, OPAL and SLD experiments. A final report is expected soon after all major results from these experiments have been published. In the remainder of this chapter, we will give some information on the combination procedures used for extracting averages for the b-hadron lifetimes, oscillations parameters and b-hadron fractions, $|V_{cb}|$ and $|V_{ub}|$. More details as well as technical aspects can be found in [34].

5.2. Averages of b-hadron lifetimes

Methods for combining b-hadron lifetime results were established in 1994, following a study [35] triggered by a rather puzzling fact: the world averages for the B_s^0 lifetime quoted by independent reviewers at the 1994 Winter Conferences differed significantly, although they were based essentially on the same data. Different combination methods have been developed [36] in the b-hadron lifetime WG to take into account the underlying exponential behaviour of the proper time distribution, as well as handling the resulting asymmetric uncertainties and biases in low statistics measurements.

The b-hadron lifetime WG provides the following averages: the B^+ lifetime, the mean B^0 lifetime, the $\mathrm{B}^+/\mathrm{B}^0$ lifetime ratio, the mean B_s^0 lifetime, the b-baryon lifetime (averaged over all b-baryon species), the Λ_b^0 lifetime, the Ξ_b lifetime (averaged over the two isospin states), and various average b-hadron lifetimes (e.g. for an unbiased mixture of weakly decaying b-hadrons). These averages take into account all known systematic correlations, which are most important for the inclusive and semi-inclusive analyses: physics backgrounds (e.g. $\mathrm{B} \to \mathrm{D}^{**}\ell\nu$ branching ratios), bias in momentum estimates (from b fragmentation, decay models and multiplicities, branching ratios of b- and c-hadrons, b-baryon polarization, etc.), and the detector resolution. For the B^+ and B^0 lifetimes, the fractions of weakly-decaying b-hadrons determined by the B oscillation WG (see Sec. 5.4. below) are used as an input to the averaging procedure. The b-lifetime averages are used as input by the other working groups for the determination of other b-physics averages.

5.3. Averages of B oscillation frequencies

The main motivation for the creation of the B oscillation WG was to combine the different lower limits obtained on ΔM_s. In 1995, the ALEPH collaboration proposed the so-called *amplitude method* [37], as a way to present the ΔM_s results in a form which allowed them to be combined in a straightforward manner. Each analysis provides the measured value of the B_s oscillation amplitude as a function of the oscillation frequency, normalized in such a way that a value of 1 is expected for a frequency equal to ΔM_s, and 0 for a frequency much below ΔM_s. A limit on ΔM_s can be set by excluding a value of 1 in a certain frequency range, and the results can be combined by averaging the measurements of this amplitude at each test frequency, using standard techniques.

The B oscillation working group played a major role in promoting this method, which was eventually adopted by each experiment studying B_s oscillations. As a result, all published papers on ΔM_s since 1997 give the *amplitude spectrum*, i.e. the B_s oscillation amplitude as a function of the oscillation frequency. As the individual ΔM_s results are limited by the available statistics (rather than by systematics), the overall sensitivity to ΔM_s is greatly increased by performing a combination of the results of the ALEPH, CDF, DELPHI, OPAL and SLD experiments.

It should be noted that the sensitivity of the inclusive analyses depends on the assumed value for the fraction of B_s mesons in a sample of weakly decaying b-hadrons. This is taken into account in the combination procedure, which is performed assuming the latest average value for this fraction (see Sec. 5.4. below).

The B oscillation working group also combines the many measurements of ΔM_d: in February 2002, 34 measurements were available from 8 different experiments. Several correlated systematic (and statistical) uncertainties are taken into account. Systematic uncertainties come from two main sources: experimental effects (which may be correlated amongst analyses from the same experiment), and imperfect knowledge of physics parameters like the b-hadron lifetimes and b-hadron production fractions which are common to all analyses. Since different individual results are assuming different values for the physics parameters, all measurements are re-adjusted to a common (and recent) set of average values for these parameters before being combined.

The average ΔM_d value is also combined with the B^0 lifetime to get a value for x_d, and with the time-integrated measurements of χ_d performed at ARGUS and CLEO, to get world averages of ΔM_d and χ_d.

5.4. Averages of *b*-hadron fractions in *b*-jets

Knowledge of the fractions of the different hadron species in an unbiased sample of weakly-decaying b hadrons produced in high-energy b jets is important for many b physics measurements. These fractions are rather poorly known from direct branching ratio measurements: for example the fraction of B_s mesons is only known with a $\sim 25\%$ uncertainty. However, mixing measurements allow this uncertainty to be reduced significantly, roughly by a factor 2.

Because these fractions play an important role in time-dependent mixing analyses, the B oscillation WG was also committed to provide b-hadron fractions (as well as a complete covariance matrix) that incorporate all the available information. A procedure was developed by this group, in which the determinations from direct measurements are combined with the world average of χ_d and the value of $\overline{\chi}$ (the mixing probability averaged over all b-hadron species) provided by the LEP electroweak WG, under the assumption that $\chi_s = 1/2$ (as is known from the limit on ΔM_s).

The b-hadron fractions are used as input for the ΔM_d combination procedure. Because the final fractions can only be known once the average ΔM_d is computed (and vice versa), the calculation of the b-hadron fractions and the ΔM_d averaging are part of the same fitting procedure, in such a way that the final results form a consistent set. The fractions are also used as input for the ΔM_s combination, for the lifetime averages, and for the $|V_{cb}|$ average.

5.5. Averages of $|V_{cb}|$ and $|V_{ub}|$ elements

The $|V_{cb}|$ working group started to combine LEP results and has by now evolved in a worldwide effort including results from the collaborations BABAR, BELLE, CDF, and CLEO. Only the case of exclusive $b \to c$ transitions presents specific problems. To combine the different results, central values and uncertainties on $\mathcal{F}(1)|V_{cb}|$ and ρ^2 have been rescaled to a common set of input parameters and ranges of values. The $\mathcal{F}(1)|V_{cb}|$ central value has then been extracted using the parametrization of Ref. [38], which is based on the experimental determination of the R_1 and R_2 vector and axial form factors. LEP results have been rescaled accordingly. In the averaging, the correlations between the different measurements and that between $\mathcal{F}(1)|V_{cb}|$ and ρ^2 have been taken into account. The working group also provides the combination of inclusive and exclusive determinations.

In order to average the inclusive charmless semileptonic branching fraction results from the LEP experiments, uncorrelated and correlated systematic errors are carefully examined. The correlated systematical errors come from the description of background $b \to c$ and from the theoretical modelling of signal $b \to u$ transitions. They are assumed to be fully correlated between the different measurements. The four measurements of BR($b \to X_u \ell \overline{\nu}$) have been averaged using the Best Linear Unbiased Estimate technique [39].

From this average branching fraction, using as an input the average b lifetime value, the probability density function for $|V_{ub}|$ has been derived. To obtain this function all the errors have been convoluted assuming that they are Gaussian in BR($b \to X_u \ell \overline{\nu}$) with the exception of the HQE theory error which is assumed to be Gaussian in $|V_{ub}|$. The negligible part of this function in the negative unphysical $|V_{ub}|$ region is discarded and the probability density function renormalised accordingly. The median of this function has been chosen as the best estimate of the $|V_{ub}|$ value and the corresponding errors are obtained from the probability density function.

6. Outline

This document is organized as follows:

Chapters 2 and 3 are dedicated to the determination of the elements V_{ud}, V_{us}, V_{cb} and V_{ub} by means of tree level decays. In Chapter 2 we summarize the present status of the elements V_{ud} and V_{us}. In Chapter 3 we discuss in detail the experimental and theoretical issues related to the determination of V_{cb} and V_{ub} from semileptonic inclusive and exclusive B decays and we discuss status and perspectives for B^0-$\overline{\mathrm{B}}^0$ lifetime differences and for the ratios of the lifetime of B hadrons.

In Chapter 4 we consider the determination of the elements $|V_{ts}|$ and $|V_{td}|$, or equivalently of $\overline{\varrho}, \overline{\eta}$ by means of $\mathrm{K}^0 - \overline{\mathrm{K}}^0$ and $\mathrm{B}^0_{d,s} - \overline{\mathrm{B}}^0_{d,s}$ mixings. The first part of this chapter recalls the formalism for ε_K and the mass differences ΔM_d and ΔM_s. Subsequently, the present status of the non-perturbative calculations of $\hat{B}_K$, $\sqrt{\hat{B}_{B_d}} F_{B_d}$, $\sqrt{\hat{B}_{B_s}} F_{B_s}$, and ξ is reviewed. The final part of this chapter deals with the measurements of $\mathrm{B}^0_{d,s} - \overline{\mathrm{B}}^0_{d,s}$ oscillations, parameterized by the mass differences $\Delta M_{d,s}$.

In Chapter 5 we describe two different statistical methods for the analysis of the unitarity triangle: the Bayesian approach and the frequentist method. Subsequently, we compare the results obtained in the two approaches, using in both cases the same inputs from Chapters 2-4. We also investigate the impact of theoretical uncertainties on the CKM fits.

Chapter 6 deals with topics that will be the focus of future CKM workshops. In this respect it differs significantly from the previous chapters and consists of self-contained separate contributions by different authors. After a general discussion of future strategies for the determination of the Unitarity Triangle, a few possibilities for the determination of its angles α, β and γ in B decays are reviewed. The potential of radiative and rare leptonic B decays and of $\mathrm{K} \to \pi \nu \overline{\nu}$ for the CKM determination is also considered.

Finally, Chapter 7 has a summary of the main results of this workshop and the conclusion.

References

[1] N. Cabibbo, Phys. Rev. Lett. **10** (1963) 531.

[2] M. Kobayashi and T. Maskawa, Prog. Theor. Phys. **49** (1973) 652.

[3] The BaBar Physics Book, eds. P. Harrison and H. Quinn, (1998), SLAC report 504.

[4] B Decays at the LHC, eds. P. Ball, R. Fleischer, G.F. Tartarelli, P. Vikas and G. Wilkinson, hep-ph/0003238.

[5] B Physics at the Tevatron, Run II and Beyond, K. Anikeev et al., hep-ph/0201071.

[6] H. Fritzsch and Z.Z. Xing, Prog. Part. Nucl. Phys. **45** (2000) 1.

[7] L.L. Chau and W.-Y. Keung, Phys. Rev. Lett. **53** (1984) 1802.

[8] Particle Data Group, Euro. Phys. J. C **15** (2000) 1.

[9] L. Wolfenstein, Phys. Rev. Lett. **51** (1983) 1945.

[10] A.J. Buras, M.E. Lautenbacher and G. Ostermaier, Phys. Rev. D **50** (1994) 3433.

[11] M. Schmidtler and K.R. Schubert, Z. Phys. C **53** (1992) 347.

[12] R. Aleksan, B. Kayser and D. London, Phys. Rev. Lett. **73** (1994) 18;
J.P. Silva and L. Wolfenstein, Phys. Rev. D **55** (1997) 5331;
I.I. Bigi and A.I. Sanda, hep-ph/9909479.

[13] C. Jarlskog, Phys. Rev. Lett. **55**, (1985) 1039; Z. Phys. C **29** (1985) 491.

[14] A.J. Buras, P.H. Chankowski, J. Rosiek and Ł. Sławianowska, Nucl. Phys. B **619** (2001) 434.

[15] J.H. Christenson, J.W. Cronin, V.L. Fitch and R. Turlay, Phys. Rev. Lett. **13** (1964) 128.

[16] A.J. Buras, hep-ph/9806471, in *Probing the Standard Model of Particle Interactions*, eds. R. Gupta, A. Morel, E. de Rafael and F. David (Elsevier Science B.V., Amsterdam, 1998), p. 281.

[17] G. Buchalla, A.J. Buras and M. Lautenbacher, Rev. Mod. Phys **68** (1996) 1125.

[18] A.J. Buras, in *Kaon 2001*, eds. F. Constantini, G. Isidori and M. Sozzi, Frascati Physics Series, p. 15, hep-ph/0109197.

[19] T. Inami and C.S. Lim, Progr. Theor. Phys. **65** (1981) 297.

[20] A.J. Buras, in *Theory and Experiment Heading for New Physics*, ed. A. Zichichi, World Scientific, 2001, page 200, hep-ph/0101336.

[21] A.J. Buras, P. Gambino, M. Gorbahn, S. Jäger and L. Silvestrini, Phys. Lett. B **500** (2001) 161.

[22] C. Bobeth, T. Ewerth, F. Krüger and J. Urban, Phys. Rev. D: **64** (2001) 074014; **66** (2002) 074021;
G. D'Ambrosio, G.F. Giudice, G. Isidori and A. Strumia, Nucl. Phys. B **645** (2002) 155.

[23] S. Bergmann and G. Perez, Phys. Rev. D **64** (2001) 115009, JHEP **0008** (2000) 034;
A.J. Buras and R. Fleischer, Phys. Rev. D **64** (2001) 115010;

S. Laplace, Z. Ligeti, Y. Nir and G. Perez, Phys. Rev. D **65** (2002) 094040;
A.J. Buras, hep-ph/0303060.

[24] ALEPH Coll., Phys. Lett. B **297** (1992) 449; Phys. Lett. B **294** (1992) 145;
OPAL Coll., Phys. Lett. B **316** (1992) 435; Phys. Lett. B **281** (1992) 394;
DELPHI Coll., Phys. Lett. B **311** (1993) 379.

[25] OPAL Coll., Zeit. Phys. C **66** (1995) 19;
DELPHI Coll., Phys. Lett. B **345** (1995) 598;
ALEPH Coll., Zeit. Phys. C **69** (1996) 393.

[26] CLEO Coll., Phys. Rev. Lett. **71** (1993) 3922.

[27] P. Kluit, Nucl Instr. Meth. A **462** (2001) 108.

[28] ARGUS Coll., Phys. Lett. B **192** (1987) 245.

[29] CLEO Coll., Phys. Rev. Lett. **58** (1987) 18.

[30] UA1 Coll., Phys. Lett. B **186** (1987) 247, erratum ibid B **197** (1987) 565.

[31] ALEPH Coll., Phys. Lett. B **313** (1993) 498; DELPHI Coll., Phys. Lett. B **332** (1994) 488;
OPAL Coll., Phys. Lett. B **336** (1994) 585.

[32] The LEP Heavy Flavour Steering group maintains a web page at
`http://www.cern.ch/LEPHFS/` with links to the web sites of each of the different working groups, where the latest averages can be found.

[33] The HFAG Steering group maintains a web page at
`http://www.slac.stanford.edu/xorg/hfag/` with links to the web sites of each of the different working groups, where the latest averages can be found.

[34] D. Abbaneo *et al*, LEP Heavy Flavour Steering group and the different Heavy Flavour working groups (for the ALEPH, CDF, DELPHI, L3 OPAL, and SLD collaborations), CERN-EP/2000-096 and update in *idem*, CERN-EP/2001-050.

[35] R. Forty, CERN-PPE/94-144.

[36] L. Di Ciaccio *et al.*, OUNP 96-05, ROM2F/96/09.

[37] ALEPH Coll., contributed paper EPS 0410 to Int. Europhysics Conf. on High Energy Physics, Brussels, July 1995; the amplitude method is described in H.-G. Moser and A. Roussarie, Nucl. Instrum. Meth. A **384** (1997) 491.

[38] R. A. Briere *et al.* [CLEO Coll.], Phys. Rev. Lett. **89** (2002) 081803, [hep-ex/0203032].

[39] L. Lyons, D. Gibaut and G. Burdman, Nucl. Instrum. Meth. A **270** (1988) 110. The fit program code blue.f (author: P. Checchia) has been employed by the COMBOS program (authors: O. Schneider and H. Seywerd) developed by the LEP B Oscillation Working Group
(see `http://www.cern.ch/LEPOSC/combos/`).

Chapter 2

DETERMINATION OF THE CABIBBO ANGLE

Convener : G. Isidori
Contributors : V. Cirigliano, G. Colangelo, G. Lopez-Castro, D. Počanić, and B. Sciascia

1. Introduction

The determinations of $|V_{us}|$ and $|V_{ud}|$ provide, at present, the most precise constraints on the size of CKM matrix elements. This high-precision information is extracted from the semileptonic transitions $s \to u$ and $d \to u$ which, although occurring in low-energy hadronic environments, in a few cases can be described with excellent theoretical accuracy. In particular, the best determination of $|V_{us}|$ is obtained from $\mathrm{K} \to \pi\ell\nu$ decays ($K_{\ell 3}$), whereas the two most stringent constraints on $|V_{ud}|$ are obtained from superallowed Fermi transitions (SFT), i.e. beta transitions among members of a $J^P = 0^+$ isotriplet of nuclei, and from the neutron beta decay. From a theoretical point of view, the beta decay of charged pions could offer a third clean alternative to determine $|V_{ud}|$; however, at present this is not competitive with the first two because of the experimental difficulty in measuring the tiny π_{e3} branching fraction ($\sim 10^{-8}$) at the desired level of precision.

In all cases, the key observation which allows a precise extraction of the CKM factors is the non-renormalization of the vector current at zero momentum transfer in the $SU(N)$ limit (or the conservation of the vector current) and the Ademollo Gatto theorem [1]. The latter implies that the relevant hadronic form factors are completely determined up to tiny isospin-breaking corrections (in the $d \to u$ case) or $SU(3)$-breaking corrections (in the $s \to u$ case) of second order. As a result of this fortunate situation, the accuracy on $|V_{us}|$ has reached the 1% level and the one on $|V_{ud}|$ can be pushed below 0.1%.

Interestingly enough, if we make use of the unitarity relation

$$U_{uu} = |V_{ud}|^2 + |V_{us}|^2 + |V_{ub}|^2 = 1 \,, \tag{1}$$

the present level of accuracy on $|V_{ud}|$ and $|V_{us}|$ is such that the contribution of $|V_{ub}|$ to Eq. (1) can safely be neglected, and the uncertainty of the first two terms is comparable. In other words, $|V_{ud}|$ and $|V_{us}|$ lead to two independent determinations of the Cabibbo angle both at the 1% level.

In the following four sections we review the determinations of $|V_{us}|$ and $|V_{ud}|$ from the four main observables mentioned above. These results are then summarized and combined in the last section, where we shall discuss the accuracy to which Eq. (1) is satisfied and we shall provide a final global estimate of the Cabibbo angle.

2. Determination of $|V_{us}|$

The amplitudes of $\mathrm{K}(k) \to \pi(p)\ell\nu$ decays can be expressed in terms of the two form factors ($f_\pm$) that determine the matrix element of the vector current between a pion and a kaon:

$$\mathcal{M}(K_{\ell 3}) \;=\; \frac{G_\mu}{\sqrt{2}} V_{us}^* C_K \left[f_+(t)(k+p)_\mu + f_-(t)(k-p)_\mu \right] L^\mu \,, \qquad t = (k-p)^2 \,, \tag{2}$$

Here C_K is a Clebsh-Gordan coefficient, equal to 1 ($2^{-1/2}$) for neutral (charged) kaon decays, and L^μ is the usual leptonic part of the matrix element. The corresponding decay rate reads

$$\Gamma(K_{\ell 3}) = \frac{G_\mu^2}{192\pi^3} M_K^5 |V_{us}|^2 C_K^2 |f_+(0)|^2 I(f_+, f_-) \;\; , \tag{3}$$

where $I(f_+, f_-)$ is the result of the phase space integration after factoring out $f_+(0)$. We recall that the dependence of $I(f_+, f_-)$ on f_- is proportional to $(m_\ell/M_K)^2$, thus f_- is completely irrelevant for the electron modes (K_{e3}). Moreover, it is customary to trade $f_-(t)$ for the so-called scalar form factor $f_0(t)$, defined as:

$$f_0(t) = f_+(t) \;+\; \frac{t}{M_K^2 - M_\pi^2}\, f_-(t) \,. \tag{4}$$

The momentum dependence of the form factors, which is relevant for the integral over the phase space is often described in terms of a single parameter, the slope at $t = 0$

$$f_{+,0}(t) = f_+(0) \left(1 + \lambda_{+,0} \frac{t}{M_\pi^2} \right) \;\; . \tag{5}$$

In this approximation the phase space integral depends explicitly only on the slope parameters, and we use the notation $I(f_+, f_-) \to I(\lambda_+, \lambda_0)$.

The steps necessary to extract $|V_{us}|$ from the experimental determination of $K_{\ell 3}$ decay rates can be summarized as follows:

1. theoretical evaluation of $f_+(0)$, including strong isospin violations;
2. measurement (or, if not available, theoretical evaluation) of the momentum dependence of $f_\pm(t)$;
3. theoretical treatment of photonic radiative corrections [note that Eq. (3) is not yet general enough to account for these effects, see below].

The first analysis that included all these ingredients was performed by Leutwyler and Roos [2]. In summary, they

1. relied on Chiral Perturbation Theory (CHPT) to $O(p^4)$ for the evaluation of $f_+(0)$, and on a quark model for the estimate of higher-order corrections (see below for more details), obtaining

$$f_+^{K^0\pi^-}(0) = 0.961 \pm 0.008 \quad \text{and} \quad f_+^{K^+\pi^0}(0)/f_+^{K^0\pi^-}(0) = 1.022 \,; \tag{6}$$

2. relied on CHPT at $O(p^4)$ for the evaluation of $\lambda_{+,0}$ (obtaining, in particular, $\lambda_+ = 0.031$);
3. relied on previous work on the photonic radiative corrections, both for the short- (Sirlin [3]) and the long-distance (Ginsberg [4]) part of this contribution; for the latter, they estimated an effect on the rate of the form

$$\Gamma(K_{e3}) \to \Gamma(K_{e3})(1+\delta) \,, \quad \delta \simeq \pm 1\% \,. \tag{7}$$

Using all these ingredients, they finally obtained

$$|V_{us}| = 0.2196 \pm 0.0023 \,. \tag{8}$$

An update of the same analysis, with substantially unchanged final numerical outcome, has recently been performed by Calderon and Lopez-Castro [5]. On the other hand, new analytical ingredients were brought to this kind of analysis by Cirigliano *et al.* [6], who did the first complete $O(p^4, \epsilon p^2)$ analysis of isospin breaking corrections in the framework of CHPT (ϵ stands for both e^2 and $m_u - m_d$).

2.1. Electromagnetic corrections

The first observation to be made in order to account for electromagnetic corrections is the fact that photon loops modify the very structure of the amplitude:

1. The form factors now depend on another kinematical variable

$$f_\pm(t) \to f_\pm(t,v) \simeq \left[1 + \frac{\alpha}{4\pi}\Gamma_c(v,\lambda_{IR})\right] f_\pm(t) \,,$$

   where $v = (p_K - p_l)^2$ in K^+ decays and $v = (p_\pi + p_l)^2$ in K^0 decays. The function $\Gamma_c(v,\lambda_{IR})$ encodes universal long distance corrections, depending only on the charges of the external particles. This contribution is infrared divergent, hence it depends upon the regulator λ_{IR}. Since the dependence on the second kinematical variable can be factored out (to a very good approximation), the notion of effective form factor $f_\pm(t)$ survives and proves useful in the subsequent analysis.
2. New local contributions appear in the effective form factors $f_\pm(0)$. These, together with the chiral logarithms, are truly structure dependent corrections, which can be described in a model independent way within the CHPT approach. Let us note here that the universal short-distance electroweak corrections to semileptonic charged-current amplitudes [3,7,8] belong in principle to this class of corrections. In fact, they can be related to one of the local couplings of CHPT (X_6) [6]. However, for consistency with previous literature, we keep the short distance correction explicit, and denote it by $S_{\rm ew}$. Its numerical value is fixed to 1.0232, corresponding to renormalization group evolution between M_Z and M_ρ.

The second observation is that one has to consider how radiation of real photons affects the various observables (e.g. Dalitz Plot density, spectra, branching ratios). For the purpose of extracting $|V_{us}|$, we need to assess the effect of real photon emission to the partial widths. As is well known, a given experiment measures an inclusive sum of the parent mode and radiative modes:

$$d\Gamma_{\rm obs} = d\Gamma(K_{\ell 3}) \;+\; d\Gamma(K_{\ell 3\gamma}) \;+\; \cdots$$

From the theoretical point of view, only such an inclusive sum is free of infrared singularities. At the precision we aim to work at, a meaningful comparison of theory and experiment can be done only once a clear definition of the inclusive observable is given. In practice this means that the phase space integrals are calculated using the same cuts on real photons employed in the experimental analysis.

In summary, all long distance QED effects, due to both virtual photons [$\Gamma_c(v,\lambda_{IR})$] and real photons [$d\Gamma(K_{\ell 3\gamma})$], can be combined to produce a correction to the phase space factor in the expression for the decay width. This term comes, in principle, with no theoretical uncertainty. The structure dependent electromagnetic corrections, as well as the chiral corrections to the $SU(3)$ results, are in the form factor $f_+(0)$, where all of the theoretical uncertainty concentrates.

Based on the above considerations, we can write the partial widths for the $K_{\ell 3}$ modes as:

$$\Gamma_i = \mathcal{N}_i \, |V_{us}|^2 \, S_{\rm ew} \, |f_+^i(0)|^2 \, I_i(\lambda_+,\lambda_0,\alpha) \,, \tag{9}$$

where the index i runs over the four $K_{\ell 3}$ modes ($K_{e3}^{\pm,0}, K_{\mu 3}^{\pm,0}$) and we defined

$$\mathcal{N}_i \;=\; \frac{G_\mu^2 M_{K_i}^5}{192\pi^3}\, C_i^2 \tag{10}$$

$$I_i(\lambda_+,\lambda_0,\alpha) \;=\; I_i(\lambda_+,\lambda_0,0)\left[1 + \Delta I_i(\lambda_+,\lambda_0)\right] . \tag{11}$$

In the above relation G_μ indicates the Fermi constant as extracted from the muon decay rate after inclusion of radiative corrections at order α.

2.2. Estimates of $f_+^i(0)$

The estimate of the four $f_+^i(0)$ is the key (and most delicate) theoretical ingredient in the extraction of $|V_{us}|$. We choose to "normalize" them to $f_+^{K^0\pi^-}(0)$, evaluated in absence of electromagnetic corrections. Differences between the various form factors are due to isospin breaking effects, both of strong ($\delta^i_{SU(2)}$) and electromagnetic ($\delta^i_{e^2p^2}$) origin, which have been evaluated at $\mathcal{O}(\epsilon p^2)$ in the chiral expansion (see Ref. [6]):

$$f_+^i(0) \;\; = \;\; f_+^{K^0\pi^-}(0)\,(1+\delta^i_{SU(2)})\,(1+\delta^i_{e^2p^2})\;. \tag{12}$$

The expansion of $f_+^{K^0\pi^-}(0)$ in the quark masses has been analysed up to the next-to-next-to-leading order [2]. At this level of accuracy we write

$$f_+^{K^0\pi^-}(0) \;\; = \;\; 1+f_2+f_4+\mathcal{O}(p^6)\;, \tag{13}$$

where the identity $f_0=1$ follows from current conservation in the chiral limit. Because of the Ademollo-Gatto theorem [1], which states that corrections to $f_+(0)=1$ have to be quadratic in the $SU(3)$ breaking, local terms are not allowed to contribute to f_2. An explicit calculation gives

$$f_2 = H_{K^0\pi}+\frac{1}{2}H_{K^+\pi}+\frac{3}{2}H_{K^+\eta}+\varepsilon\sqrt{3}\,(H_{K\pi}-H_{K\eta}) \quad , \tag{14}$$

where H_{PQ} is a loop function

$$H_{PQ} = -\frac{1}{128\pi^2F_\pi^2}\left[M_P^2+M_Q^2+\frac{2M_P^2M_Q^2}{M_P^2-M_Q^2}\ln\frac{M_Q^2}{M_P^2}\right] \quad , \tag{15}$$

and ε is the $\pi^0-\eta$ mixing angle, $\tan 2\varepsilon = \sqrt{3}/2(m_d-m_u)/(m_s-\hat{m})$. The absence of low-energy constants in the expression for f_2 allows a numerical evaluation which is practically free of uncertainties:

$$f_2 = -0.023 \;\; . \tag{16}$$

As for f_4 the situation is much less clear, because low energy constants (LECs) of the p^6 Lagrangian can now contribute. Before entering the discussion of various evaluations of f_4 which can be found in the literature, it is useful to recall a model-independent bound on $f_+(0)$. A sum rule discovered in the sixties [9] implies:

$$\left|f_+^{K^0\pi^-}(0)\right|^2 = 1-\sum_{n\neq\pi^-}\left|\langle K^0|Q^{us}|n\rangle\right|^2 \quad , \tag{17}$$

where Q^{us} is the vector charge, thus $f_+(0)$ has to be smaller than one.

Various estimates of the size of f_4 have been given:

1 Leutwyler and Roos [2] relate this form factor at zero momentum transfer to the matrix element of the vector charge between a kaon and a pion in the infinite-momentum limit. The latter matrix element is then given as a superposition of the wave functions of the constituents of the kaon and of the pion. If one defines the asymmetry between the two wave functions with a function δ:

$$\varphi_K = (1+\delta)\varphi_\pi \quad , \tag{18}$$

the average of the square of the asymmetry (calculated with the pion wave function as a weight) gives the deviation of $f_+(0)$ from one:

$$f_+(0) = 1-\frac{1}{2}\langle\delta^2\rangle_\pi \;\; . \tag{19}$$

Instead of performing an explicit model calculation of the asymmetry δ, they only made a simple parametrization of δ, and estimated the parameters on the basis of the $SU(3)$ rule of thumb: $SU(3)$ breaking effects are expected to be at the 30% level. Despite this large amount of symmetry breaking (which yields a consistent description of the ratio F_K/F_π), the numerical estimate of f_4 turns out to be very suppressed because of the quadratic dependence from δ in Eq. (19). Assigning a conservative 50% error to the effect thus found, Leutwyler and Roos finally quoted

$$f_4 = -0.016 \pm 0.008 \quad . \tag{20}$$

2 Evaluations of $f_+(0)$ in a constituent quark model description of the kaon and the pion have been made by several authors (see Refs. [10,11] and references therein). In particular, the result

$$f_+(0) = 0.96 \pm 0.013 \tag{21}$$

can be found in Ref. [10], which also provides a good summary of earlier literature on the subject (as an estimate of the uncertainty we took the sensitivity of the result to the constituent strange quark mass).* It should be stressed that in this framework no chiral logs are generated – the quark masses which appear as parameters of the model are constituent quark masses and do not vanish in the chiral limit. In this sense, these models can only give an estimate of the local part of f_4, whereas a complete estimate of $f_+(0)$ seems to require also the contribution from f_2. The approach followed in constituent quark models is internally consistent, since the parameters of the model are also fixed ignoring the presence of chiral logs. However, the potential difference of chiral logs in $f_+(0)$ and the physical observables used to constrain the model could induce sizable uncertainties. As far as we could see, nobody has addressed this point. Note that this problem is absent in the estimate of Leutwyler and Roos, which consistently took into account the chiral logs.

3 From the point of view of the pure chiral expansion, the only parameter-free prediction which one can make for f_4 concerns the chiral logs. A first step in this direction was made by Bijnens, Ecker and Colangelo [13], who calculated the double chiral logs contribution to this quantity. The size of this term, however, depends on the renormalization scale μ. By varying the latter within a reasonable range, the numerical estimate $|f_4|_{\text{chiral logs}} \leq 0.5\%$ was obtained.

Post and Schilcher [14] recently completed a full two-loop evaluation of f_4, which besides the double chiral logs contains single ones and polynomial contributions. The latter contain LECs of the p^6 Lagrangian, whose value is basically unknown, and make a numerical estimate difficult. The authors simply set to zero the LECs of order p^6 (at $\mu = M_\rho$) and obtained

$$f_4\Big|_{[O(p^6)\ \text{LECs} = 0]} = 0.018 \quad . \tag{22}$$

Notice the sign difference with respect to Leutwyler and Roos [and most model calculations, which according to the sum rule (17) obtain negative results]. There is, however, no contradiction between the two calculations: the neglected $O(p^6)$ constants may well give a negative contribution roughly twice as large as the part evaluated by Post and Schilcher.

This brief summary clearly indicates the need for more theoretical work on this issue. In particular it appears within reach an analysis that combines model calculations with the contribution of the chiral logs in a consistent way at next-to-next-to-leading order in the chiral expansion. Since the parameters of the constituent quark models are usually fixed with simple observables (like the decay constants), whose chiral expansion is already known at the required level of precision, it appears to us that all the ingredients for such an analysis are already available in the literature.

* A very similar result, with a larger uncertainty, has been reported more recently in Ref. [12].

Mode	BR (%)	λ_+	λ_0
K^+_{e3}	4.87 $\pm$ 0.06	0.0278 $\pm$ 0.0019	
K^0_{e3}	38.79 $\pm$ 0.27	0.0291 $\pm$ 0.0018	
$K^+_{\mu 3}$	3.27 $\pm$ 0.06	0.033 $\pm$ 0.010	0.004 $\pm$ 0.009
$K^0_{\mu 3}$	27.18 $\pm$ 0.25	0.033 $\pm$ 0.005	0.027 $\pm$ 0.006

Table 2.1: *$K_{\ell 3}$ branching ratios (BR) and slopes from Ref. [17]. The lifetimes used as input are: $\tau_{K^\pm} = (1.2384 \pm 0.0024) \times 10^{-8}\ s$ and $\tau_{K_L} = (5.17 \pm 0.04) \times 10^{-8}\ s$.*

	$\delta_{SU(2)}(\%)$	$\delta_{e^2p^2}(\%)$	$\Delta I(\lambda_+, \lambda_0)(\%)$	$\delta_K(\%)$
K^+_{e3}	2.4 $\pm$ 0.2	0.32 $\pm$ 0.16	-1.27	-0.63 $\pm$ 0.32
K^0_{e3}	0	0.46 $\pm$ 0.08	+0.37	+ 1.30 $\pm$ 0.16
$K^+_{\mu 3}$	2.4 $\pm$ 0.2	0.006 $\pm$ 0.16		
$K^0_{\mu 3}$	0	0.15 $\pm$ 0.08		

Table 2.2: *Summary of isospin-breaking factors from Ref. [6].*

In absence of such a complete analysis, for the time being we believe that the best choice is to stick to Leutwyler and Roos' estimate – keeping in mind that, e.g., a value of f_4 two sigmas away from the central value in (20) is not strictly forbidden, but rather unlikely.

Let us close this section with a comment on lattice calculations: we are not aware of any attempts to calculate $f_+(0)$ on the lattice. We believe, however, that in the long run this is the only method that offers any hope to improve the model independent estimate of Leutwyler and Roos, and eagerly wait for the first calculations. It goes without saying that the precision required to have an impact on the determination of V_{us} is extremely challenging.

2.3. Numerical evaluation of $|V_{us}|$

The $K_{\ell 3}$ widths reported in Table 2.1 allow us to obtain four determinations of $|V_{us}| \cdot f_+^{K^0\pi^-}(0)$ which are independent, up to the small correlations of theoretical uncertainties from isospin-breaking corrections $\delta_{e^2p^2}$ and $\delta_{SU(2)}$ (almost negligible at present, see Table 2.2). The master formula for a combined analysis of these modes is:

$$|V_{us}| \cdot f_+^{K^0\pi^-}(0) = \left[\frac{\Gamma_i}{\mathcal{N}_i\, S_{\rm ew}\, I_i(\lambda_+, \lambda_0, 0)}\right]^{1/2} \frac{1}{1 + \delta^i_{SU(2)} + \delta^i_{e^2p^2} + \frac{1}{2}\Delta I_i(\lambda_+, \lambda_0)} \tag{23}$$

The radiative correction factor $\delta_K(i)$, often quoted in the literature, is recovered in our framework by combining the phase space correction and the structure dependent electromagnetic corrections:

$$\delta_K(i) = 2\,\delta^i_{e^2p^2} \;+\; \Delta I_i(\lambda_+, \lambda_0)\;. \tag{24}$$

In the Table 2.2 we report estimates of these isospin-breaking parameters based on Ref. [6], and subsequent work on the K^0_{e3} mode.[†]

The phase space corrections refer to the definition of photon-inclusive width given by Ginsberg (see Refs. [4,6]). The analysis of muonic modes is incomplete, as the phase space corrections have

[†] Very recently a new calculation of electromagnetic corrections to the K^+_{e3} mode has been presented [18]. Although the approach followed in Ref. [18] is not coherent with the model-independent CHPT approach of Ref. [6], the results obtained are numerically consistent with those reported in Table 2.2.

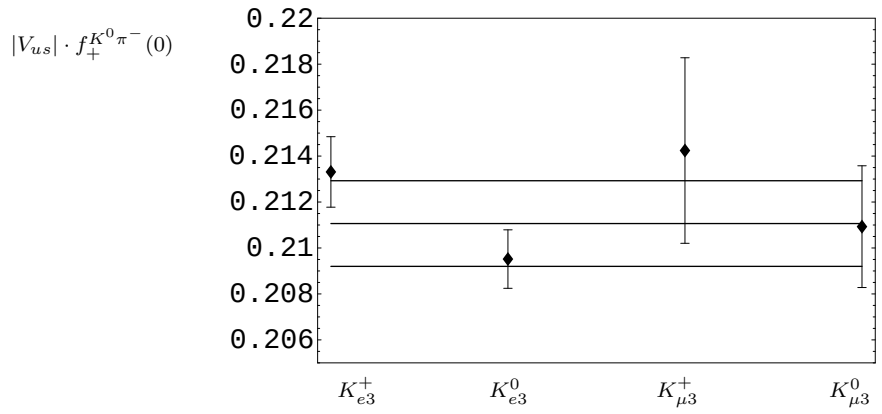

Fig. 2.1: $|V_{us}| \cdot f_+^{K^0\pi^-}(0)$ *from the four* $K_{\ell 3}$ *modes (and average over the electronic modes).*

not yet been evaluated (hence the blank spaces in Table 2.2). In order to include these modes in the phenomenological analysis, we can use the estimates $\delta_K(K^+_{\mu 3}) = -0.06\%$ and $\delta_K(K^0_{\mu 3}) = +2.02\%$ obtained by Ginsberg [4]. However, there are systematic uncertainties in Ginsberg's approach which cannot be easily estimated. They arise because these results depend on the UV cutoff ($\Lambda = m_p$ was used in obtaining the above numbers), and on the ratio $f_-(0)/f_+(0)$ (set to zero to obtain the above numbers). Therefore, in the following analysis, we assign an uncertainty of $\pm 1\%$ to $\delta_K(K^{+,0}_{\mu 3})$. ‡

Using the above input for the isospin-breaking factors and the Particle Data Group (PDG) averages for branching ratios and slopes (see Table 2.1), we obtain the following results for $|V_{us}| \cdot f_+^{K^0\pi^-}(0)$:

$$|V_{us}| \cdot f_+^{K^0\pi^-}(0) = 0.2133 \pm 0.0016 \qquad (K^+_{e3}) \tag{25}$$

$$|V_{us}| \cdot f_+^{K^0\pi^-}(0) = 0.2095 \pm 0.0013 \qquad (K^0_{e3}) \tag{26}$$

$$|V_{us}| \cdot f_+^{K^0\pi^-}(0) = 0.2142 \pm 0.0040 \qquad (K^+_{\mu 3}) \tag{27}$$

$$|V_{us}| \cdot f_+^{K^0\pi^-}(0) = 0.2109 \pm 0.0026 \qquad (K^0_{\mu 3}) \tag{28}$$

In the above determination we have added in quadrature all the uncertainties involved. The final error is completely dominated by experimental uncertainties (rates and slopes). We note that the muonic decays imply larger uncertainties compared to the electronic modes (see also Fig. 2.1), as a consequence of larger uncertainties in branching ratios and slopes. In a weighted average the muonic modes are seen to be irrelevant. Therefore, also in view of the incomplete knowledge of radiative corrections, we conclude that at present the inclusion of muonic decays does not allow us to improve the extraction of $|V_{us}|$. An average over the electronic modes brings to:

$$|V_{us}| \cdot f_+^{K^0\pi^-}(0) = 0.2110 \pm 0.0018 \,, \tag{29}$$

where the error has been multiplied by a scale factor $S = 1.85$, as defined by the PDG [17]. Finally, if we use the Leutwyler-Roos estimate of f_4, or $f_+^{K^0\pi^-}(0) = 0.961 \pm 0.008$, we obtain

$$\begin{aligned} |V_{us}| &= 0.2196 \pm 0.0019_{\rm exp} \pm 0.0018_{{\rm th}(f_4)} \\ &= 0.2196 \pm 0.0026 \,. \end{aligned} \tag{30}$$

‡ As for the electronic modes, let us note that Ginsberg's results $\delta_K(K^+_{e3}) = -0.45\%$ and $\delta_K(K^0_{e3}) = +1.5\%$ are consistent with the ranges reported in Table 2.2.

As can be noted, the above result has an error larger with respect to the estimate made almost 20 years ago by Leutwyler and Roos. The reasons is the decreased consistency of the two $|V_{us}| \cdot f_+^{K^0\pi^-}(0)$ determinations from K_{e3} modes (and the corresponding large scale factor) after a revised average of (old) measurements of K_{e3} branching ratios [17]. This seems to suggest that some experimental errors have been underestimated, or unduly reduced by the PDG averaging procedure, as different experimental input might have common systematic errors (especially the ones related to radiative corrections). We stress, in particular, that the latest rate measurements were performed in the 70's and it is not clear if these correspond to photon-inclusive widths.

This issue should soon be clarified by the high-statistics measurements of $K_{\ell 3}$ widths expected from recently-completed or ongoing experiments, such as BNL-E865 [15] and KLOE (which is presently analysing the four $K_{\ell 3}$ modes in the same experimental setup, with systematic uncertainties rather different from those of the existing measurements) [16]. In our opinion, a reliable extraction of $|V_{us}|$ might come in the near future by using experimental input coming solely from such high-statistics measurements. Indeed, apart from the great improvement in the statistical signal, we can expect a substantial improvement also in the treatment of radiative corrections. As an illustration of this scenario, we use the preliminary result from E865 [15]

$$\begin{aligned} \mathrm{BR}(K^+_{e3}) &= (5.13 \pm 0.02_{\mathrm{stat.}} \pm 0.08_{\mathrm{syst.}} \pm 0.04_{\mathrm{norm.}})\% & (31)\\ &= (5.13 \pm 0.09)\% \,, & (32) \end{aligned}$$

to obtain $|V_{us}| \cdot f_+^{K^0\pi^-}(0) = 0.2189 \pm 0.0021$, and hence:

$$\begin{aligned} |V_{us}| &= 0.2278 \pm 0.0022_{\mathrm{exp}} \pm 0.0019_{\mathrm{th}(f_4)} \\ &= 0.2278 \pm 0.0029 \,. & (33) \end{aligned}$$

We show this number only for illustrative purpose (we do not include it in the average) since it is based on a preliminary result, and it is not clear if it corresponds to the photon-inclusive branching ratio. On the other hand, it should be noted how a single present-day measurement allows us to extract $|V_{us}|$ at the $\sim 1\%$ level [same as in Eq.(30)], and could offer the advantage of a clear understanding of all sources of uncertainty.

2.4. Other determinations of $|V_{us}|$

To conclude the discussion about $|V_{us}|$, we briefly comment about other possibilities to determine this quantity, alternative to $K_{\ell 3}$ decays:

Tau decays. A novel strategy to determine V_{us} has been proposed very recently in Ref. [19]. The method relies on the following facts:

- The possibility to express theoretically, via the OPE,[§] the hadronic width of the τ lepton (R_τ) and the appropriate moments (R^{kl}_τ) [20], for both Cabibbo-allowed ($\bar{u}d$) and Cabibbo-suppressed ($\bar{u}s$) sectors. The relevant moments are denoted respectively by $R^{kl}_{\tau,V+A}$ and $R^{kl}_{\tau,S}$.
- The measurements of hadronic branching fractions (and moments) in τ decays [21].
- The strong sensitivity of the flavour-breaking difference

$$\delta R^{kl}_\tau = \frac{R^{kl}_{\tau,V+A}}{|V_{ud}|^2} - \frac{R^{kl}_{\tau,S}}{|V_{us}|^2} \qquad (34)$$

to the strange-quark mass (m_s) and the CKM matrix elements.

[§] In addition, a phenomenological parameterisation for the longitudinal contribution is adopted.

Originally these features have been exploited to determine m_s, using $|V_{us}|$ as input. The authors of Ref. [19] have inverted this line of reasoning: they have determined $|V_{us}|$ from (34), with $k = l = 0$, using the theoretical input $\delta R_\tau^{00} = 0.229 \pm 0.030$ and the range $m_s(2\,\mathrm{GeV}) = 105 \pm 20$ MeV, derived from other observables. Assuming CKM unitarity to relate $|V_{ud}|$ to $|V_{us}|$ in (34) one finds [19]:

$$|V_{us}| = 0.2179 \pm 0.0044_{\rm exp} \pm 0.0009_{\rm th} = 0.2179 \pm 0.0045\ . \tag{35}$$

The theoretical error reflects the uncertainty in m_s, while the experimental one (by far the dominant error), reflects the inputs $R_{\tau,S} = 0.1625 \pm 0.0066$ and $R_{\tau,V+A} = 3.480 \pm 0.014$ [21]. Relaxing the assumption of CKM unitarity and employing the extremely safe range $|V_{ud}| = 0.9739 \pm 0.0025$, leads to:

$$|V_{us}| = 0.2173 \pm 0.0044_{\rm exp} \pm 0.0009_{\rm th} \pm 0.0006_{V_{ud}} = 0.2173 \pm 0.0045\ . \tag{36}$$

A reduction in the uncertainty of $R_{\tau,S}$ by a factor of two would make this extraction of $|V_{us}|$ competitive with the one based on K_{e3} decays. To this purpose, it would be highly desirable also to estimate the systematic uncertainty of the method (e.g. extracting V_{us} from higher $R_{\tau,S}^{kl}$ moments, and obtaining additional constraints on the m_s range). Future precise measurements of $R_{\tau,S}^{kl}$ and of the $SU(3)$-breaking differences δR_τ^{kl} at B factories could allow to reach this goal. However, at the moment we believe it is safer not to include this (weak) constraint in the average value of $|V_{us}|$.

Hyperon semileptonic decays. As in the case of the neutron beta decay, both vector and axial vector currents contribute to Hyperon semileptonic decays (HSD). However, data on decay rates and asymmetries of three different HSD can not be adequately fitted by existing models of form factors (see e.g. Ref [22)]. On the basis of this conclusion, and given the large discrepancies among different calculations of the leading vector form factors (of up to 13% in the case of Σ^- [22]) at zero momentum transfer, we decided not to include the HSD constraints on $|V_{us}|$ in this review.

3. $|V_{ud}|$ from superallowed Fermi transitions

Currently, SFT provide the most precise determination of $|V_{ud}|$. Several features combine for this purpose. First, the calculation of SFT are simplified by the fact that only the nuclear matrix elements of the vector current contribute to the decay amplitude. Second, since the SFT occur within members of a given isotriplet, the conservation of the vector current helps to fix the normalization of the nuclear form factors. A third important theoretical ingredient is that the calculation of isospin breaking and radiative corrections have achieved a level suited to match the accuracy of experimental data.

From the experimental side, the input information has reached an accuracy that challenges present theory calculations. Accurate measurements of the half-lives t, branching fractions and Q values for nine different $J^P = 0^+ \to 0^+$ beta nuclear transitions have been reported so far [23]. These experimental input allows to compute the ft values, where f is essentially the nuclear-dependent phase space factor, with high accuracy for each transition (see the first column in Table 2.4). At present, the final uncertainty in the determination of $|V_{ud}|$ is further reduced by taking the average over the nine different measurements of SFT. Thus, the high accuracy attained in $|V_{ud}|$ can largely be attributed to a statistical origin despite the fact that a nuclear environment is being used for this purpose.

Due to the spin and parity quantum numbers of the initial and final nuclei, only the vector current is involved in SFT at the tree-level. In the limit where isospin is an exact symmetry, the nuclear matrix elements are fixed by the conservation of the vector current and are given by:

$$\langle p_f; 0^+ | \bar{u}\gamma_\mu d | p_i; 0^+ \rangle = \sqrt{2}(p_i + p_f)_\mu\ . \tag{37}$$

An important check in the determination of $|V_{ud}|$ from SFT is to verify that after removing nuclear-dependent corrections from the observables, the common nuclear matrix elements share the universality predicted by Eq. (37).

Decaying nucleus	δ_C (in %) (Ref. [24])	δ_C (in %) (Ref. [25])	Averages adopted in [26]
^{10}C	0.18	0.15	0.16(3)
^{14}O	0.28	0.15	0.22(3)
^{26m}Al	0.33	0.30	0.31(3)
^{34}Cl	0.64	0.57	0.61(3)
^{38m}K	0.64	0.59	0.62(3)
^{42}Sc	0.40	0.42	0.41(3)
^{46}V	0.45	0.38	0.41(3)
^{50}Mn	0.47	0.35	0.41(3)
^{54}Co	0.61	0.44	0.52(3)

Table 2.3: *Isospin breaking corrections (δ_C, in % units) to the decay rates of SFT.*

Isospin breaking corrections introduce a (nucleus-dependent) correction factor $(1 - \delta_C/2)$ on the right-hand side of Eq. (37). This correction arises from the incomplete overlap of initial and final nuclear wave functions. This mismatch effect has its origin in the Coulomb distortions due to the different number of protons in the decaying and daughter nuclei [24,25]. The two different calculations of δ_C used by the authors of Ref. [26] for the nine measured decaying nuclei are shown in Table 2.3. The error assigned to δ_C is chosen to cover the typical spread between the central values obtained in both calculations. As we shall show in the following, at present this error is not the dominant source of uncertainty on $|V_{ud}|$: doubling it, for a more conservative approach, would induce an increase of the total uncertainty on $|V_{ud}|$ of about 25%.

After including radiative and isospin breaking corrections, it becomes convenient to define the $\mathcal{F}t$ values for each transition, namely:

$$\mathcal{F}t \equiv ft(1+\delta_R)(1-\delta_C) = \frac{\pi^3 \ln 2}{G_\mu^2 m_e^5 (1+\Delta_R)|V_{ud}|^2} \,. \tag{38}$$

By this way all the nucleus-dependent corrections are included in the definition of the $\mathcal{F}$ constants and the right-hand side contains only the nucleus-independent piece of radiative corrections Δ_R (see below) and fundamental constants. Thus, the equality of the $\mathcal{F}t$ values of the nine SFT provides a good consistency check of the conservation of the vector current.

The radiative corrections are split into a nucleus-dependent piece δ_R (also called *outer* corrections) and a nucleus-independent piece Δ_R (also called *inner* corrections). The outer corrections have been computed by two different groups [27] finding good agreement with each other. These corrections include basically model-independent virtual and real QED corrections and the calculations include terms up to $O(Z^2\alpha^3)$ as required by experiments (see Table 2.4). The inner corrections on the other hand, include the short distance electroweak corrections and other pieces of model-dependent (but nucleus-independent) radiative corrections [7,28]. Since a large $\ln(m_Z/m_p)$ term appears at leading order, a resummation of higher order logarithms is required. This improved calculation lead to the following updated numerical value of inner corrections [28,29]:

$$\Delta_R = (2.40 \pm 0.08)\% \,. \tag{39}$$

The uncertainty in the inner corrections has its origin in the lower value for the cutoff used for the axial-induced photonic corrections [28] and it turns out to be the dominant theoretical uncertainty in the current

Decaying nucleus	ft (sec.)	δ_R (%)	δ_C (%)	$\mathcal{F}t$ (sec.)
^{10}C	3038.7(45)	1.30(4)	0.16(3)	3072.9(48)
^{14}O	3038.1(18)	1.26(5)	0.22(3)	3069.7(26)
^{26m}Al	3035.8(17)	1.45(2)	0.31(3)	3070.0(21)
^{34}Cl	3048.4(19)	1.33(3)	0.61(3)	3070.1(24)
^{38m}K	3049.5(21)	1.33(4)	0.62(3)	3071.1(27)
^{42}Sc	3045.1(14)	1.47(5)	0.41(3)	3077.3(23)
^{46}V	3044.6(18)	1.40(6)	0.41(3)	3074.4(27)
^{50}Mn	3043.7(16)	1.40(7)	0.41(3)	3073.8(27)
^{54}Co	3045.8(11)	1.40(7)	0.52(3)	3072.2(27)
Average	3043.9(6)			3072.3(9)
χ^2/dof	6.38			1.10

Table 2.4: *Tree-level (ft) and corrected ($\mathcal{F}t$) values for SFT [26].*

determination of $|V_{ud}|$ from SFT [26]. As a final comment, we should mention that the factorization of inner and outer radiative corrections introduces spurious terms of $O(\alpha^2)$ in the *r.h.s* of Eq. (38). However, these additional terms are not relevant at the present level of accuracy, since they affect the determination of $|V_{ud}|$ at the level of $\delta_R \Delta_R/2 \sim 0.0001$.

Table 2.4 illustrates how quantum corrections are crucial to offer a high-precision test of the conservation of the vector current. As it was mentioned above, this implies that the $\mathcal{F}t$ values should be the same for the nine nuclear transitions under consideration. This test is evident from the χ^2/dof of the fit, which substantially improves in going from the tree-level ft values to the quantum corrected $\mathcal{F}t$ values.

Inserting the weighted average of $\mathcal{F}t$, reported in Table 2.4, into Eq. (38) we obtain:

$$\begin{aligned} |V_{ud}| &= 0.9740 \pm \sqrt{(0.0001)^2_{\rm exp} + (0.0004)^2_{\Delta_R} + (0.0002)^2_{\delta_c}} \\ &= 0.9740 \pm 0.0005 \; . \end{aligned} \tag{40}$$

In the above result we have explicitly separated the different contributions to the total uncertainty in $|V_{ud}|$. As can be noted, at present the dominant error is induced by Δ_R, or by the choice of a low-energy cutoff for the axial-induced photonic corrections [28].

Based on the work of Ref. [30], the Particle Data Group [17] adopt the conservative approach of doubling the error in Eq. (40). According to Ref. [30], isospin breaking at the quark level would increase the size of the corrections δ_C. However, we stress that this proposed manifestation of quarks degrees of freedom at the level of nuclear structure may lead to a double counting of isospin breaking effects [26]. Moreover, we note that δ_C is not the dominant uncertainty at present. For these reasons, we prefer not to modify the uncertainty in Eq. (40) and to quote this result as the best information on $|V_{ud}|$ available at present from SFT.

4. $|V_{ud}|$ from neutron beta decay

The neutron beta decay ($n \to p e^- \overline{\nu}_e$) is another place where measurements and theory are getting accurate enough to provide a determination of $|V_{ud}|$ at the level of 0.1%. This happens despite the fact

that both axial and vector weak currents contribute to the hadronic matrix element. Indeed the axial form factor normalized to the vector one (g_A/g_V) can be determined from data and, once this is known, theory can provide a calculation of the decay rate as a function of $|V_{ud}|$ at the level of a few parts in 10^{-4} [29]. Similarly to SFT, the main theoretical uncertainty arises from the low-energy cut-off of the axial-induced photonic corrections [see Eq. (39)]. However, the present major source of uncertainty in this determination of $|V_{ud}|$ comes from the measurements of g_A/g_V.

In the last twenty years several authors contributed to derive a master formula for the beta decay rate of the neutron precise at the level of a few parts in 10^{-4} [28,29,31,32]. At this level of accuracy, only two momentum-independent form factors, $g_{A,V}$, are required to describe the hadronic amplitude:

$$\langle p|\overline{u}\gamma_\mu(1-\gamma_5)d|n\rangle = \overline{u}_p\gamma_\mu(g_V + g_A\gamma_5)u_n \; . \tag{41}$$

By including the radiative corrections up to order $O(\alpha^2)$ in an additive form [29], and assuming that the beta decay (inclusive of photon corrections) is the only relevant neutron decay mode, we can write

$$|V_{ud}|^2 = \frac{2\pi^3}{G_\mu^2 m_e^5 (1+\Delta_R) g_V^2 [1+3(g_A/g_V)^2] f_R \tau_n} \; , \tag{42}$$

where τ_n denotes the lifetime of the neutron. The factor $f_R = 1.71312 \pm 0.00002$ is essentially the integrated electron spectrum folded with the energy-dependent radiative corrections which are required up to order α^2 [29,31]. Here, an important numerical remark is in order. Our expression for f_R contains the radiative corrections in an additive form, contrary to some other expressions currently used in the literature (see for example Ref. [26,33]). In fact, other analyses use a factorization prescription of the dominant Coulomb term (or Fermi-function) and the remaining $O(\alpha, \alpha^2)$ corrections (see the discussion in Ref. [29]). This factorization introduces spurious terms at the order α^2 which affect the decay rate at the level of 10^{-4}. For instance, using the factorized formula of Ref. [33] and Ref. [26,31] would lead to a decrease of $|V_{ud}|$ of about 5×10^{-4} and 10×10^{-4}, respectively.

Let us now focus on the value of g_V. In the limit where isospin is an exact symmetry, the CVC hypothesis is useful to fix the value of the vector form factor, namely $g_V^{CVC} = 1$. Owing to the Ademollo-Gatto theorem [1], the correction δg_V to this value is expected to be very small. The evaluations of δg_V present in the literature indicate that δg_V is of order 10^{-5} [32]. Thus, at the accuracy level of 10^{-4}, we can safely set $g_V = 1$ in Eq. (42).

As already mentioned, the determination of $|V_{ud}|$ requires two experimental inputs: τ_n and g_A/g_V. At present, the set of data used to extract the average of the neutron lifetime is consistent and very accurate, leading to the world average [17]

$$\tau_n^{\rm exp} = (885.7 \pm 0.8) \; {\rm sec} \; , \tag{43}$$

with an associated scale factor of $S = 1.07$. The situation concerning g_A/g_V does not share the same consistency. In Table 2.5 we show a collection of the most precise measurements of this ratio, together with the corresponding determinations of $|V_{ud}|$. Although other measurements have been reported so far (see Ref. [17]), those shown in Table 2.5 are the most relevant ones for the determination of $|V_{ud}|$ in neutron beta decay [29].

The quoted uncertainty for $|V_{ud}|$ in the third column of Table 2.5 has been computed by adding in quadrature theoretical and experimental uncertainties, following the formula

$$\Delta|V_{ud}| = \pm\sqrt{(0.00044)^2_{\tau_n} + (0.00036)^2_{\rm r.c.} + [0.64\Delta(g_A/g_V)]^2} \; , \tag{44}$$

where the subscript 'r.c.' denote the irreducible theoretical error of axial-induced photonic corrections. Similarly to the SFT case, the latter contribute at the level of 0.04%.

Clearly, the present uncertainty in $|V_{ud}|$ from neutron beta decay is largely dominated by the error in the measurements of g_A/g_V. It should also be noted that there is some inconsistency among

Reference	g_A/g_V	$\lvert V_{ud}\rvert$
[34]	-1.262 ± 0.005	0.9794 ± 0.0032
[35]	-1.2594 ± 0.0038	0.9811 ± 0.0025
[36] [*]	-1.266 ± 0.004	0.9768 ± 0.0026
[37] [*]	-1.2686 ± 0.0046	0.9752 ± 0.0030
[33] [*]	-1.2739 ± 0.0019	0.9718 ± 0.0013
Total average	$-1.2694 \pm 0.0014\ (0.0028)$	$0.9746 \pm 0.0010\ (0.0019)$
Average [*]	$-1.2720 \pm 0.0016\ (0.0022)$	$0.9731 \pm 0.0011\ (0.0015)$

Table 2.5: *Experimental values of g_A/g_V and the determination of $|V_{ud}|$ from neutron beta decay; the [*] denotes recent experiments with a polarization larger than 90%; the errors between brackets in the last two rows are multiplied by the corresponding scale factor.*

the measurements of this ratio (in fact, this is at the origin of the large scale factor quoted in the total average). On the other hand, if only the recent measurements of g_A/g_V performed with a high degree of polarization are considered (entries denoted by [*] in Table 2.5), as recommended by the PDG [17], then a good consistency is recovered. For this reason, we consider the result in the last row (scale factor included),

$$|V_{ud}| = 0.9731 \pm 0.0015\ , \tag{45}$$

as the best information available at present from neutron beta decay.

5. $|V_{ud}|$ from π_{e3} decay

Another interesting possibility to extract $|V_{ud}|$, which shares the advantages of both Fermi transitions (pure vector transition, no axial-vector contribution) and neutron β-decay (no nuclear structure dependent radiative corrections) is provided by the β-decay of the charged pion. The difficulty here lies in the extremely small branching ratio, of order 10^{-8}. Nevertheless, such a measurement is presently being performed at PSI by the PIBETA collaboration, with the aim of measuring the branching ratio with 0.5% accuracy. At this level of precision, radiative corrections have to be taken into account, and Ref. [38] addresses this problem, within the effective theory formalism for processes involving light pseudoscalar mesons, photons and leptons [39].

The decay amplitude for $\pi^+(p_+) \to \pi^0(p_0)\, e^+(p_e)\, \nu_e(p_\nu)$ is determined by the vector pion form factor $f_+^{\pi^\pm\pi^0}(t)$, entering in the current matrix element

$$\langle \pi^0(p_0)|\bar{u}\gamma_\mu d|\pi^+(p_+)\rangle = \sqrt{2}\left[f_+^{\pi^\pm\pi^0}(t)\,(p_+ + p_0)_\mu + f_-^{\pi^\pm\pi^0}(t)\,(p_+ - p_0)_\mu\right], \tag{46}$$

where $t = (p_+ - p_0)^2$. As usual, in the isospin limit $f_+^{\pi^\pm\pi^0}(0) = 1$ and the kinematical dependence from t is parameterised by a linear slope λ. The effect of f_-, suppressed by $(m_e/M_\pi)^2$ and by isospin breaking, can safely be neglected.

Accounting for isospin-breaking and radiative corrections (see analogous discussion for $K_{\ell 3}$ decays), the decay rate can be written as

$$\Gamma_{\pi_{e3[\gamma]}} = \mathcal{N}_\pi\, |V_{ud}|^2\, S_{\rm ew}\, |f_+^{\pi^\pm\pi^0}(0)|^2\, I_\pi(\lambda,\alpha) \tag{47}$$

with $\mathcal{N}_\pi = G_\mu^2 M_{\pi^\pm}^5/(64\pi^3)$ and

$$I_\pi(\lambda,\alpha) = I_\pi(\lambda,0)\left[1 + \Delta I_\pi(\lambda)\right]\ , \quad f_+^{\pi^\pm\pi^0}(0) = (1+\delta^\pi_{SU(2)})\,(1+\delta^\pi_{e^2p^2})\ . \tag{48}$$

Thus we obtain:

$$|V_{ud}| = \left[\frac{\Gamma_{\pi_{e3[\gamma]}}}{\mathcal{N}_\pi\, S_{\rm ew}\, I_\pi(\lambda,0)}\right]^{1/2} \frac{1}{1+\delta^\pi_{SU(2)}+\delta^\pi_{e^2p^2}+\frac{1}{2}\Delta I_\pi(\lambda)}\,.$$

The recent analysis of Ref. [38] shows that

$$\delta^\pi_{SU(2)} \sim 10^{-5}\,, \qquad \delta^\pi_{e^2p^2} = (0.46\pm 0.05)\%\,, \qquad \Delta I_\pi(\lambda) = 0.1\%\,, \tag{49}$$

with a total effect of radiative corrections consistent with previous estimates [7,40].

The present experimental precision for the branching ratio of the pionic beta decay cannot compete yet with the very small theoretical uncertainties of SFT and neutron beta decay: using the latest PDG value $\mathrm{BR} = (1.025 \pm 0.034) \times 10^{-8}$ [17], we find

$$\begin{aligned} |V_{ud}| &= 0.9675 \pm 0.0160_{\rm exp} \pm 0.0005_{\rm th} \\ &= 0.9675 \pm 0.0161. \end{aligned} \tag{50}$$

However, a substantial improvement of the experimental accuracy is to be expected in the near future. Inserting the present preliminary result obtained by the PIBETA Collaboration [41], $\mathrm{BR} = (1.044 \pm 0.007(\mathrm{stat.}) \pm 0.009(\mathrm{syst.})) \times 10^{-8}$, we find

$$\begin{aligned} |V_{ud}| &= 0.9765 \pm 0.0056_{\rm exp} \pm 0.0005_{\rm th} \\ &= 0.9765 \pm 0.0056\,, \end{aligned} \tag{51}$$

where the error should be reduced by about a factor of 3 at the end of the experiment.

6. CKM unitarity and the determination of the Cabibbo angle

The two measurements of $|V_{ud}|$ from SFT and nuclear beta decay, reported in Eqs. (40) and (45) respectively, are perfectly compatible. Combining them in quadrature we obtain

$$|V_{ud}| = 0.9739 \pm 0.0005\,, \tag{52}$$

a result which is not modified by the inclusion in the average of the present π_{e3} data. Due to the small differences in the treatment of radiative corrections and theory errors discussed in the previous sections, this value is slightly different, but perfectly compatible, with the one quoted by the PDG: $|V_{ud}| = 0.9735 \pm 0.0008$ [17].

The compatibility of SFT and nuclear beta decay results is clearly an important consistency check of Eq. (52). However, it should also be stressed that the theoretical uncertainty of inner radiative corrections (which contribute at the level of $\pm 0.04\%$) can be considered to a good extent a common systematic error for both determinations. Thus the uncertainty quoted in Eq. (52) is mainly of theoretical nature and should be taken with some care.

Using the unitarity relation (1) we can translate Eq. (52) into a prediction for $|V_{us}|$:

$$|V_{us}|_{\rm unit.} = 0.2269 \pm 0.0021\,, \tag{53}$$

to be compared with the direct determination in Eq. (30). The 2.2σ discrepancy between these two determinations could be attributed to: i) an underestimate of theoretical and, more in general, systematic errors; ii) an unlikely statistical fluctuation; iii) the existence of new degrees of freedoms which spoil the unitarity of the CKM matrix. Since theoretical errors provide a large fraction of the total uncertainty in both cases, the solution i), or at least a combination of i) and ii), appears to be the most likely scenario. Barring the possibility iii), and in absence of a clear indication of which of the errors is underestimated,

a conservative approach is obtained by treating the two determinations on the same footing and introducing the PDG scale factor. Following this procedure, our final estimate of $|V_{us}|$ imposing the unitarity constraint is

$$\boxed{|V_{us}|_{\mathrm{unit.}+K_{\ell 3}} = 0.2240 \pm 0.0036 \ .} \tag{54}$$

References

[1] M. Ademollo and R. Gatto, Phys. Rev. Lett. **13** (1964) 264.

[2] H. Leutwyler and M. Roos, The Kobayashi-Maskawa Matrix," Z. Phys. C **25** (1984) 91.

[3] A. Sirlin, Nucl. Phys. B **196** (1982) 83, and references therein.

[4] E. S. Ginsberg, Phys. Rev. **162** (1967) 1570 [Erratum, ibid. **187** (1969) 2280];
Phys. Rev. **171** (1968) 1675 [Erratum, ibid. **174** (1968) 2169]; Phys. Rev. D **1** (1970) 229.

[5] G. Calderon and G. Lopez Castro, Phys. Rev. D **65** (2002) 073032 [hep-ph/0111272].

[6] V. Cirigliano, M. Knecht, H. Neufeld, H. Rupertsberger and P. Talavera, Eur. Phys. J. C **23** (2002) 121 [hep-ph/0110153]; V. Cirigliano, M. Knecht, H. Neufeld, H. Pichl, in preparation.

[7] A. Sirlin, Rev. Mod. Phys. **50** (1978) 579.

[8] W.J. Marciano, A. Sirlin, Phys. Rev. Lett. **71** (1993) 3629.

[9] G. Furlan, F.G. Lannoy, C. Rossetti, and G. Segré, Nuovo Cim. **38** (1965) 1747.

[10] H. M. Choi and C. R. Ji, Phys. Rev. D **59** (1999) 034001 [hep-ph/9807500].

[11] W. Jaus, Phys. Rev. D **60** (1999) 054026.

[12] V. Antonelli, R. Ferrari, M. Picariello, E. Torrente-Lujan, A. Vicini, IFUM-726-FT.

[13] J. Bijnens, G. Colangelo and G. Ecker, Phys. Lett. B **441** (1998) 437 [hep-ph/9808421].

[14] P. Post and K. Schilcher, hep-ph/0112352.

[15] A. Sher (E865 Collaboration), talk given at the DPF 2002 Meeting (College of William & Mary, Williamsburg, May 2002), see `http://www.dpf2002.org`

[16] E. De Lucia, talk given at the Workshop On Quark Mixing and CKM Unitarity (Heidelberg, Germany, September 2002), to appear in the proceedings.

[17] K. Hagiwara *et al.*, Particle Data Group Phys. Rev. D **66** (2002) 010001.

[18] V. Bytev, E. Kuraev, A. Baratt and J. Thompson, hep-ph/0210049.

[19] E. Gamiz, M. Jamin, A. Pich, J. Prades and F. Schwab, hep-ph/0212230.

[20] F. Le Diberder and A. Pich, Phys. Lett. B **289** (1992) 165.

[21] M. Davier and C. Yuan, hep-ex/0211057.

[22] R. Flores-Mendieta, A. Garcia and G. Sanchez-Colon, Phys. Rev. D **54** (1996) 6855 [hep-ph/9603256].

[23] J. C. Hardy *et al.*, Nucl. Phys. A **509** (1990) 429;
B. K. Fujikawa *et al.*, life of C-10 with GAMMASPHERE," nucl-ex/9806001;
I. S. Towner *et al.*, nucl-th/9507004.

[24] I. S. Towner and J. C. Hardy, Nucl. Phys. A **284** (1977) 269.

[25] W. E. Ormand and B. A. Brown, nucl-th/9504017.

[26] I. S. Towner and J. C. Hardy, nucl-th/9809087.

[27] A. Sirlin and R. Zucchini, Phys. Rev. Lett. **57** (1986) 1994;
W. Jaus and G. Rasche, Phys. Rev. D **35** (1987) 3420.

[28] W. J. Marciano and A. Sirlin, Phys. Rev. Lett. **56** (1986) 22;
I. S. Towner, Nucl. Phys. A **540** (1992) 478.

[29] A. García, J. L. García-Luna and G. López Castro, Phys. Lett. B **500** (2001) 66.

[30] K. Saito and A. W. Thomas, Phys. Lett. B **363** (1995) 157.

[31] D. H. Wilkinson, Nucl. Phys. A **377** (1982) 474.

[32] N. Paver and Riazuddin, Phys. Lett. B **260** (1991) 421;
J. F. Donoghue and D. Wyler, Phys. Lett. B **241** (1990) 243;
N. Kaiser, Phys. Rev. C **64** (2001) 028201.

[33] H. Abele *et al.*, Phys. Rev. Lett. **88** (2002) 211801.

[34] P. Bopp *et al.*, Phys. Rev. Lett. **56** (1986) 919 [Erratum, ibid. **57** (1986) 1192].

[35] B. Erozolimsky, *et al.*, Phys. Lett. B **412** (1997) 240.

[36] P. Liaud, *et al.*, Nucl. Phys. A **612** (1997) 53.

[37] Yu. A. Mostovoi *et al.*, Phys. Atom. Nucl. **64** (2001) 1955.

[38] V. Cirigliano, M. Knecht, H. Neufeld, H. Pichl, hep-ph/0209226.

[39] M. Knecht, H. Neufeld, H. Rupertsberger, P. Talavera, Eur. Phys. J. C **12** (2000) 469.

[40] W. Jaus, Phys. Rev. D **63** (2001) 053009.

[41] PIBETA Collaboration, M. Bychkov *et al.*, PSI Scientific Report 2001, Vol.1, p. 8, eds. J. Gobrecht *et al.*, Villigen PSI (2002).

Chapter 3

CKM ELEMENTS FROM TREE-LEVEL B DECAYS AND LIFETIMES

Conveners: E. Barberio, L. Lellouch, K.R. Schubert
Contributors: M. Artuso, M. Battaglia, C. Bauer, D. Becirevic, M. Beneke, I. Bigi, T. Brandt, D. Cassel, M. Calvi, M. Ciuchini, A. Dighe ,K. Ecklund, P. Gagnon, P. Gambino, S. Hashimoto, A. Hoang, T. Hurth, A. Khodjamirian, C.S. Kim, A. Kronfeld, A. Lenz, A. Le Yaouanc, Z. Ligeti, V. Lubicz, D. Lucchesi, T. Mannel, M. Margoni, G. Martinelli, D. Melikhov, V. Morénas, H.G. Moser, L. Oliver, O. Pène, J.-C. Raynal, P. Roudeau, C. Schwanda, B. Serfass, M. Smizanska, J. Stark, B. Stech, A. Stocchi, N. Uraltsev, A. Warburton, L.H. Wilden.

Tree level semileptonic (s.l.) decays of B mesons are crucial for determining the $|V_{ub}|$ and $|V_{cb}|$ elements of the CKM matrix. In this Chapter we review our present understanding of inclusive and exclusive s.l. B decays and give an overview of the experimental situation. The second part of the Chapter is devoted to B mesons lifetimes, whose measurement are important for several reasons. Indeed, these lifetimes are necessary to extract the s.l. widths, while the B^0 lifetime differences and the ratios of lifetimes of individual species provide a test of the OPE.

After a brief introduction to the main concepts involved in theoretical analysis of the inclusive decays, we discuss the determination of the relevant parameters — b quark mass and non-perturbative parameters of the Operator Product Expansion (OPE) — and underlying assumption of quark-hadron duality. We then review the inclusive determination of $|V_{ub}|$ and $|V_{cb}|$. The extraction of these two CKM elements from exclusive s.l. B decays is discussed in the two following sections, after which we review the theoretical framework and the measurements of the lifetimes and lifetime differences.

1. Theoretical tools

1.1. The Operator Product Expansion for inclusive decays

Sometimes, instead of identifying all particles in a decay, it is convenient to be ignorant about some details. For example, we might want to specify the energy of a charged lepton or a photon in the final state, without looking at the specific accompanying hadron. These decays are inclusive in the sense that we sum over final states which can be produced as a result of a given short distance interaction. Typically, we are interested in a quark-level transition, such as $b \to c\ell\bar{\nu}$, $b \to s\gamma$, etc., and we would like to extract the corresponding short distance parameters, $|V_{cb}|$, $C_7(m_b)$, etc., from the data. To do this, we

need to be able to model independently relate the quark-level operators to the experimentally accessible observables.

In the large m_b limit, we have $M_W \gg m_b \gg \Lambda_{\rm QCD}$ and we can hope to use this hierarchy to organize an expansion in $\Lambda_{\rm QCD}/m_b$, analogous to the one in $1/M_W$ introduced in Chapter 1, already based on the OPE. Since the energy released in the decay is large, a simple heuristic argument shows that the inclusive rate may be modelled simply by the decay of a free b quark. The b quark decay mediated by weak interactions takes place on a time scale that is much shorter than the time it takes the quarks in the final state to form physical hadronic states. Once the b quark has decayed on a time scale $t \ll \Lambda_{\rm QCD}^{-1}$, the probability that the final states will hadronize somehow is unity, and we need not know the probability of hadronization into specific final states. Moreover, since the energy release in the decay is much larger than the hadronic scale, the decay is largely insensitive to the details of the initial state hadronic structure. This intuitive picture is formalized by the OPE, which expresses the inclusive rate as an expansion in inverse powers of the heavy quark mass, with the leading term corresponding to the free quark decay [1,2] (for a pedagogical introduction to the OPE and its applications, see [3,4]).

Let us consider, as an example, the inclusive s.l. $b \to c$ decay, mediated by the operator $O_{\rm sl} = -4G_F/\sqrt{2}\, V_{cb}\, (J_{bc})^\alpha\, (J_{\ell\nu})_\alpha$, where $J^\alpha_{bc} = (\overline{c}\,\gamma^\alpha P_L\, b)$ and $J^\beta_{\ell\nu} = (\overline{\ell}\,\gamma^\beta P_L\, \nu)$. The decay rate is given by the square of the matrix element, integrated over phase space and summed over final states,

$$\Gamma(\mathrm{B} \to X_c \ell\bar\nu) \sim \sum_{X_c} \int \mathrm{d[PS]}\, |\langle X_c \ell\bar\nu | O_{\rm sl} | \mathrm{B}\rangle|^2 \,. \tag{1}$$

Since the leptons have no strong interaction, it is convenient to factorize the phase space into $\mathrm{B} \to X_c W^*$ and a perturbatively calculable leptonic part, $W^* \to \ell\bar\nu$. The nontrivial part is the hadronic tensor,

$$\begin{aligned} W^{\alpha\beta} &\sim \sum_{X_c} \delta^4(p_B - q - p_{X_c})\, |\langle \mathrm{B}|\mathrm{J}^{\alpha\dagger}_{\rm bc}|\mathrm{X_c}\rangle\, \langle \mathrm{X_c}|\mathrm{J}^{\beta}_{\rm bc}|\mathrm{B}\rangle|^2 \\ &\sim \mathrm{Im} \int \mathrm{d}x\, e^{-iq\cdot x}\, \langle \mathrm{B}|\, \mathrm{T}\{\mathrm{J}^{\alpha\dagger}_{\rm bc}(\mathrm{x})\, \mathrm{J}^{\beta}_{\rm bc}(0)\}\, |\mathrm{B}\rangle \,, \end{aligned} \tag{2}$$

where the second line is obtained using the optical theorem, and T denotes the time ordered product of the two operators. This is convenient because the time ordered product can be expanded in local operators in the $m_b \gg \Lambda_{\rm QCD}$ limit. In this limit the time ordered product is dominated by short distances, $x \ll \Lambda_{\rm QCD}^{-1}$, and one can express the nonlocal hadronic tensor $W^{\alpha\beta}$ as a sum of local operators. Schematically,

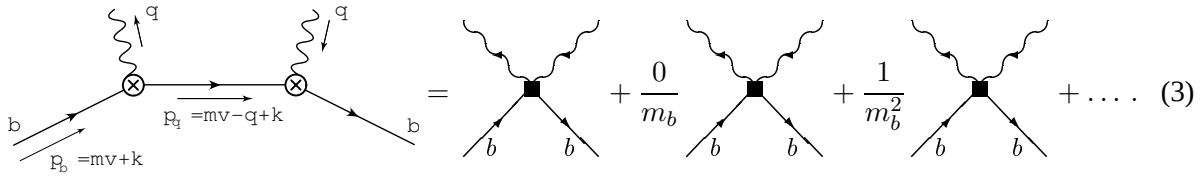

(3)

At leading order the decay rate is determined by the b quark content of the initial state, while subleading effects are parametrized by matrix elements of operators with increasing number of derivatives that are sensitive to the structure of the B meson. There are no $O(\Lambda_{\rm QCD}/m_b)$ corrections, because the B meson matrix element of any dimension-4 operator vanishes. As the coefficients in front of each operator are calculable in perturbation theory, this leads to a simultaneous expansion in powers of the strong coupling constant $\alpha_s(m_b)$ and inverse powers of the heavy b quark mass (more precisely, of $m_b - m_q$). The leading order of this expansion is the parton model s.l. width

$$\Gamma_0 = \frac{G_F^2 |V_{cb}|^2 m_b^5}{192\pi^3} \left(1 - 8\rho + 8\rho^3 - \rho^4 - 12\rho^2 \ln\rho\right) \,, \tag{4}$$

where $\rho = m_q^2/m_b^2$. Non-perturbative corrections are suppressed by at least two powers of m_b [2]. The resulting expression for the total rate of the s.l. $\mathrm{B} \to X_c \ell \bar{\nu}$ has the form

$$\Gamma^{b\to c} = \Gamma_0 \left[1 + A\left[\frac{\alpha_s}{\pi}\right] + B\left[\left(\frac{\alpha_s}{\pi}\right)^2 \beta_0\right] + 0\left[\frac{\Lambda}{m_b}\right] + C\left[\frac{\Lambda^2}{m_b^2}\right] + O\left(\alpha_s^2, \frac{\Lambda^3}{m_b^3}, \frac{\alpha_s}{m_b^2}\right)\right], \qquad (5)$$

where the coefficients A, B, C depend on the quark masses $m_{c,b}$. The perturbative corrections are known up to order $\alpha_s^2\beta_0$. Non-perturbative corrections are parameterized by matrix elements of local operators. The $O(\Lambda^2/m_b^2)$ corrections are given in terms of the two matrix elements

$$\begin{aligned} \lambda_1 &= \frac{1}{2M_B}\left\langle \mathrm{B}|\bar{h}_v (iD)^2 h_v|\mathrm{B}\right\rangle, \\ \lambda_2 &= \frac{1}{6M_B}\left\langle \mathrm{B}\left|\bar{h}_v \frac{g}{2}\sigma_{\mu\nu}G^{\mu\nu}h_v\right|\mathrm{B}\right\rangle. \end{aligned} \qquad (6)$$

The dependence on these matrix elements is contained in the coefficient $C \equiv C(\lambda_1, \lambda_2)$. Up to higher-order corrections, the connection to an alternative notation is $\lambda_1 = -\mu_\pi^2$ and $\lambda_2 = \mu_G^2/3$. At order $1/m_b^3$ there are two additional matrix elements. Thus, the total decay rate depends on a set of non-perturbative parameters, including the quark masses, with the number of such parameters depending on the order in $\Lambda_{\mathrm{QCD}}/m_b$ one is working.

Similar results can be derived for differential distributions, as long as the distributions are sufficiently inclusive. To quantify this last statement, it is crucial to remember that the OPE does not apply to fully differential distributions but requires that such distributions be smeared over enough final state phase space. The size of the smearing region Δ introduces a new scale into the expressions for differential rates and can lead to non-perturbative corrections being suppressed by powers of $\Lambda_{\mathrm{QCD}}^n/\Delta^n$ rather than $\Lambda_{\mathrm{QCD}}^n/m_b^n$. Thus, a necessary requirement for the OPE to converge is $\Delta \gg \Lambda_{\mathrm{QCD}}$, although a quantitative understanding of how experimental cuts affect the size of smearing regions is difficult.

1.2. Heavy Quark Effective Theory

The bound state problem for exclusive decays of hadrons composed of a heavy quark Q and light degrees of freedom simplifies in the limit $m_Q \gg \Lambda_{QCD}$. The size of such heavy-light hadrons is $\sim 1/\Lambda_{QCD}$ and hence, the typical momenta exchanged between the heavy and light degrees of freedom are of order Λ_{QCD}. Such momenta do not permit the light constituents to resolve the quantum numbers of the heavy quark, whose Compton wavelength is $\sim 1/m_Q$. It follows that the light constituents of hadrons which differ only by the flavour or spin of their heavy quark have the same configuration. For N_Q heavy-quark flavours, this invariance results in an $SU(2N_Q)_v$ symmetry which acts on the spin and flavour components of the heavy-quark multiplet and under which the strong interactions are invariant at energies much smaller than m_Q [5,6,7,8,9]. The subscript v on $SU(2N_Q)_v$ labels the velocity of the heavy quark on which the configuration of the light constituents obviously depends.

The spin-flavour symmetry leads to many interesting relations between the properties of hadrons containing a heavy quark. The most immediate consequences concern the spectra of these states [9]. Indeed, since the spin of the heavy quark decouples, states occur in mass-degenerate doublets corresponding to the two possible orientations of the heavy-quark spin.* Examples are the meson doublets $(\mathrm{B}, \mathrm{B}^*)$ and $(\mathrm{D}, \mathrm{D}^*)$ or the baryon doublets (Σ_b, Σ_b^*) and (Σ_c, Σ_c^*). Moreover, the flavour symmetry implies that the energy carried by the light constituents in a heavy-light hadron must be the same whether the heavy quark is a beauty or a charm. Thus, in the symmetry limit, we have relations such as $M_{\Lambda_b} - M_B = M_{\Lambda_c} - M_D$ and $M_{B_s} - M_B = M_{D_s} - M_D$. All of these relations are satisfied experimentally to the expected accuracy, that is up to terms of order Λ_{QCD}/m_b or Λ_{QCD}/m_c, depending on whether the charm quark is present.

*An exception to this rule are the ground state baryons Λ_b and Λ_c: their light constituents carry no angular momentum.

Another set of consequences of heavy quark symmetry concerns current matrix elements and, in particular, $\mathrm{B} \to \mathrm{D}^{(*)}$ transitions [7,8,9]. Consider the matrix element of the b-number current between B meson states of given velocities:

$$\langle \mathrm{B}(v')|\bar{b}\gamma^\mu b|\mathrm{B}(v)\rangle = M_B(v+v')^\mu F_B(t_{BB}) \tag{7}$$

with $t_{BB} = M_B^2(v-v')^2 = 2M_B^2(1-w)$, where $w = v\cdot v'$. $F_B(t_{BB})$ simply measures the overlap of the wave-function of light constituents around a b quark of velocity v with that of light constituents around a b quark of velocity v'. In the heavy-quark limit, flavour symmetry implies that this same form factor describes the matrix element obtained by replacing one or both of the beauty quarks by a charm quark of same velocity. The spin symmetry implies that this form factor parametrizes matrix elements in which the initial and/or final pseudo-scalar meson is replaced by the corresponding vector meson. It further requires the same form factor to parametrize matrix elements in which a vector current such as $\bar{c}\gamma^\mu b$ is replaced by any other $b \to c$ current. This means that in the heavy-quark limit, the s.l. decays $\mathrm{B} \to \mathrm{D}\ell\nu$ and $\mathrm{B} \to \mathrm{D}^*\ell\nu$, which are governed by the hadronic matrix elements, $\langle \mathrm{D}^{(*)}|\bar{c}\gamma^\mu(\gamma^5)b|\mathrm{B}\rangle$, are described by a single form factor, $\xi(w) = F_B(t_{BB}(w)) + O(1/m_b)$, instead of the six form factors allowed by Lorentz invariance. Moreover, this form factor, known as the Isgur-Wise function, is normalized to one at zero-recoil, i.e. $\xi(1) = 1$ for $v = v'$ or $w = 1$, because the b-number current is conserved.

The normalization imposed by heavy quark symmetry is the basis for the measurement of $|V_{cb}|$ from exclusive s.l. B decays described in Sec. 3.. Symmetry is used to the same effect elsewhere in the determination of CKM matrix elements: isospin symmetry normalizes the form factor in β decays, yielding $|V_{ud}|$, and $SU(3)$ flavour symmetry of light quarks approximatively normalizes the form factor in K_{l3} decays, yielding $|V_{us}|$.

In order to explore the consequences of heavy quark symmetry more systematically and compute corrections to the symmetry limit, which are essential for reaching the accuracies required for precise determinations of CKM parameters, it is convenient to construct an effective field theory which displays this symmetry explicitly and gives a simplified description of QCD at low energies [10]. The idea behind effective theories is a separation of scales such that the effective theory correctly reproduces the long-distance physics of the underlying theory. For the case at hand, we are after a theory which duplicates QCD on scales below a cutoff μ such that:

$$\Lambda_{QCD} \ll \mu \ll m_Q \; . \tag{8}$$

The construction of heavy quark effective theory (HQET)[†] begins with the observation that the heavy quark bound inside a heavy-light hadron is nearly on-shell and that its four-velocity is approximately the hadron's velocity, v. Its momentum can thus be written

$$p^\mu = m_Q v^\mu + k^\mu \; , \tag{9}$$

where the components of the residual momentum k^μ are much smaller than m_Q and where $v^2 = 1$. The heavy-quark field is then decomposed into its "particle" and "anti-particle" components, h_v and H_v, as

$$Q(x) = e^{-im_Q v\cdot x}\left[\frac{1+\not{v}}{2}h_v(x) + \frac{1-\not{v}}{2}H_v(x)\right] \; . \tag{10}$$

This decomposition shifts the zero of four-momentum in such a way that the heavy-quark degrees of freedom become massless while the anti-quark degrees of freedom acquire a mass $2m_Q$.[‡] The latter are the heavy degrees of freedom which are integrated out in the construction of the effective theory.

[†]There exist many reviews of heavy quark effective theory. See for instance [11–13].

[‡]A description of heavy anti-quarks is obtained by performing a shift in four-momentum of opposite sign.

Performing this operation in the path integral and expanding the result in powers of terms of order $1/2m_Q$, one finds the following leading order effective Lagrangian:

$$\mathcal{L}_{eff} = \mathcal{L}_0 + O\left(\frac{1}{2m_Q}\right) = \bar{h}_v iv\cdot D h_v + O\left(\frac{1}{2m_Q}\right) \ . \tag{11}$$

At subleading order it becomes:

$$\mathcal{L}_{eff} = \mathcal{L}_0 + \mathcal{L}_1 + O\left(\frac{1}{4m_Q^2}\right) = \mathcal{L}_0 + \frac{1}{2m_Q}\bar{h}_v (iD_\perp)^2 h_v + \frac{g}{2m_Q}\bar{h}_v \sigma_{\mu\nu} G^{\mu\nu} h_v + O\left(\frac{1}{4m_Q^2}\right) \ , \tag{12}$$

with $D_\perp^\mu = D - v^\mu v\cdot D$.

The absence of Dirac structure and of masses in $\mathcal{L}_0$ signals the existence of the heavy quark spin-flavour symmetry. This symmetry is broken at order $1/m_Q$. In Eq. (12), the first correction corresponds to the gauge-invariant extension of the kinetic energy arising from the residual motion of the heavy quark and breaks only the flavour component of the symmetry. The second term describes the colour-magnetic coupling of the heavy-quark spin to the gluons and breaks both the spin and the flavour components of the symmetry.

In order to incorporate the weak interactions of heavy quarks, one must also consider the expansion of weak operators in powers of $1/2m_Q$. Introducing a source in the path integral for the quark field, $Q(x)$, one finds that this source couples to

$$\begin{aligned} Q(x) &= e^{-im_Q v\cdot x}\left[1 + \frac{1}{iv\cdot D + 2m_Q} i\not{D}_\perp\right] h_v(x) \\ &= e^{-im_Q v\cdot x}\left[1 + \frac{i\not{D}_\perp}{2m_Q} + O(1/4m_Q^2)\right] h_v(x) \ , \end{aligned} \tag{13}$$

once the substitution of Eq. (10) and the integral over the "anti-quark" mode H_v are performed. Thus, the expansion of weak currents involving heavy quarks in powers of $1/2m_Q$ is obtained by replacing occurrences of $Q(x)$ by the expansion of Eq. (13).

The construction described up until now correctly reproduces the long-distance physics of QCD, (below μ of Eq. (8)). However, this procedure does not take into account the effects of hard gluons whose virtual momenta can be of the order of the heavy-quark mass, or even larger [6]. Such gluons can resolve the flavour and the spin of the heavy quark and thus induce symmetry breaking corrections. Schematically, the relation between matrix elements of an operator $\mathcal{O}$ in the full and in the effective theory is

$$\langle \mathcal{O}(\mu)\rangle_{QCD} = C_0(\mu,\bar{\mu})\langle \bar{\mathcal{O}}_0(\bar{\mu})\rangle_{HQET} + \frac{C_1(\mu,\bar{\mu})}{2m_Q}\langle \bar{\mathcal{O}}_1(\bar{\mu})\rangle_{HQET} \ , \tag{14}$$

where $\bar{\mu}\sim\mu$ and where we have assumed, for simplicity, that only one HQET operator appears at leading and at sub-leading order in the $1/2m_Q$ expansion. The short-distance coefficients $C_i(\mu,\bar{\mu})$ are defined by this equation, and should be accurately calculable order by order in perturbation theory because α_s is small in the region between μ and m_Q. One typically obtains $C_i = 1 + O(\alpha_s)$. The way in which these virtual processes break the heavy quark symmetry is by inducing a logarithmic dependence of the C_i on m_Q and by causing mixing with operators which have a different spin structure (not shown here).

Since the effective theory is constructed to reproduce the low-energy behaviour of QCD, the matching procedure must be independent of long-distance effects such as infrared singularities or the nature of the external states used. It is therefore possible and convenient to perform the matching using external on-shell quark states. Furthermore, if the logarithms of m_Q/μ which appear in the short-distance coefficients are uncomfortably large, it is possible to resum them using renormalization group techniques.

It is important to note that the matrix elements in the effective theory, such as $\bar{\mathcal{O}}_0(\bar{\mu})\rangle_{HQET}$ and $\langle\bar{\mathcal{O}}_1(\bar{\mu})\rangle_{HQET}$ in Eq. (14), involve long-distance strong-interaction effects and therefore require non-perturbative treatment. It is also important to note that the separation between short-distance perturbative and long-distance non-perturbative contributions is ambiguous, though these ambiguities must cancel in the calculation of physical observables. These ambiguities require one to be careful in combining results for short-distant coefficients and for the non-perturbative HQET matrix elements. In particular, one has to make sure that these coefficients are combined with matrix elements which are defined at the same order and, of course, in the same renormalization scheme.

2. Inclusive semileptonic *b* decays

2.1. Bottom and charm quark mass determinations

In the framework of B physics the bottom quark mass parameter is particularly important because theoretical predictions of many quantities strongly depend on m_b. Thus, uncertainties on m_b can affect the determination of other parameters. However, due to confinement and the non-perturbative aspect of the strong interaction the concept of quark masses cannot be tied to an intuitive picture of the weight or the rest mass of a particle, such as for leptons, which are to very good approximation insensitive to the strong interactions. Rather, quark masses have to be considered as couplings of the Standard Model Lagrangian that have to be determined from processes that depend on them. As such, the bottom quark mass is a scheme-dependent, renormalized quantity. For recent reviews on the determination of the b quark mass, see [14].

2.1.1. Quark mass definitions in perturbation theory

In principle, any renormalization scheme, or definition for quark masses is possible. In the framework of QCD perturbation theory the difference between two mass schemes can be determined as a series in powers of α_s. Therefore, higher-order terms in the perturbative expansion of a quantity that depends on quark masses are affected by which scheme is employed. There are schemes that are more appropriate and more convenient for some purposes than others. In this section we review the prevalent perturbative quark mass definitions, focusing on the case of the bottom quark.

Pole mass

The bottom quark pole mass m_b is defined as the solution to

$$\not{p} - m_b - \Sigma(p, m_b)\Big|_{p^2=m_b^2} = 0\,, \tag{15}$$

where $\Sigma(p, m_b)$ is the bottom quark self energy. The pole mass definition is gauge-invariant and infrared-safe [15] to all orders in perturbation theory and has been used as the standard mass definition of many perturbative computations in the past. By construction, the pole mass is directly related to the concept of the mass of a free quark, which is, however, problematic because of confinement. In practical applications the pole mass has the disadvantage that the perturbative series relating it to physical quantities are in general quite badly behaved, due to a strong sensitivity of the pole mass definition itself to infrared gluons [16].

There is nothing wrong to use the pole mass as an intermediate quantity, as long as it is used in a consistent way. In particular, the presence of a renormalon ambiguity [16] requires considering the numerical value of the pole mass as an order-dependent quantity. Because this makes estimates of uncertainties difficult, the pole mass definition should be avoided for analyses where quark mass uncertainties smaller than $\Lambda_{\rm QCD}$ are necessary. The problems of the pole mass definition can be avoided if one uses quark mass definitions that are less sensitive to small momenta and do not have an ambiguity

of order $\Lambda_{\rm QCD}$. Such quark mass definitions are generically called "short-distance" masses. They have a parametric ambiguity or order $\Lambda_{\rm QCD}^2/m_b$ or smaller.

$\overline{\rm MS}$ mass

The most common short-distance mass parameter is the $\overline{\rm MS}$ mass $\overline{m}_b(\mu)$, which is defined by regulating QCD with dimensional regularization and subtracting the divergences in the $\overline{\rm MS}$ scheme. Since the subtractions do not contain any infrared sensitive terms, the $\overline{\rm MS}$ mass is only sensitive to scales of order or larger than m_b. The relation between the pole mass and the $\overline{\rm MS}$ mass is known to $\mathcal{O}(\alpha_s^3)$ [17,18] and reads ($\bar\alpha_s \equiv \alpha_s^{(n_l=4)}(\overline{m}_b(\overline{m}_b))$)

$$\frac{m_{b,\rm pole}}{\overline{m}_b(\overline{m}_b)} = 1 + \frac{4\bar\alpha_s}{3\pi} + \left(\frac{\bar\alpha_s}{\pi}\right)^2 \left(13.44 - 1.04\,n_f\right) + \left(\frac{\bar\alpha_s}{\pi}\right)^3 \left(190.8 - 26.7\,n_f + 0.65\,n_f^2\right) + \dots \,. \quad (16)$$

The bottom quark $\overline{\rm MS}$ mass arises naturally in processes where the bottom quark is far off-shell. The scale μ in the $\overline{\rm MS}$ mass is typically chosen of the order of the characteristic energy scale of the process under consideration since perturbation theory contains logarithmic terms $\sim \alpha_s(\mu)^n \ln(Q^2/\mu^2)$ that would be large otherwise. Using the renormalization group equation for $\overline{m}_b(\mu)$ the value of the $\overline{\rm MS}$ mass for different μ can be related to each other. The $\overline{\rm MS}$ mass definition is less useful for processes where the bottom quark is close to its mass-shell, i.e. when the bottom quark has non-relativistic energies.

Threshold masses

The shortcomings of the pole and the $\overline{\rm MS}$ masses in describing non-relativistic bottom quarks can be resolved by so-called threshold masses [19]. The threshold masses are free of an ambiguity of order $\Lambda_{\rm QCD}$ and, at the same time, are defined through subtractions that contain contributions that are universal for the dynamics of non-relativistic quarks. Since the subtractions are not unique, an arbitrary number of threshold masses can be constructed. In the following the threshold mass definitions that appear in the literature are briefly reviewed.

Kinetic mass

The kinetic mass is defined as [20,21]

$$m_{b,\rm kin}(\mu_{\rm kin}) \;=\; m_{b,\rm pole} - \left[\bar\Lambda(\mu_{\rm kin})\right]_{\rm pert} - \left[\frac{\mu_\pi^2(\mu_{\rm kin})}{2m_{b,\rm kin}(\mu_{\rm kin})}\right]_{\rm pert} + \dots \,, \quad (17)$$

where $\left[\bar\Lambda(\mu_{\rm kin})\right]_{\rm pert}$ and $\left[\mu_\pi^2(\mu_{\rm kin})\right]_{\rm pert}$ are perturbative evaluations of HQET matrix elements that describe the difference between the pole and the B meson mass.

The relation between the kinetic mass and the $\overline{\rm MS}$ mass is known to $\mathcal{O}(\alpha_s^2)$ and $\mathcal{O}(\alpha_s^3\beta_0)$ [22,33]. The formulae for $[\bar\Lambda(\mu_{\rm kin})]_{\rm pert}$ and $[\mu_\pi^2(\mu_{\rm kin})]_{\rm pert}$ at $\mathcal{O}(\alpha_s^2)$ read [33]

$$\left[\bar\Lambda(\mu)\right]_{\rm pert} \;=\; \frac{4}{3}C_F\mu_{\rm kin}\frac{\alpha_s(\bar m)}{\pi}\left\{1 + \frac{\alpha_s}{\pi}\left[\left(\frac{4}{3} - \frac{1}{2}\ln\frac{2\mu_{\rm kin}}{\bar m}\right)\beta_0 - C_A\left(\frac{\pi^2}{6} - \frac{13}{12}\right)\right]\right\}, \quad (18)$$

$$\left[\mu_\pi^2(\bar m)\right]_{\rm pert} \;=\; C_F\mu^2\frac{\alpha_s(\bar m)}{\pi}\left\{1 + \frac{\alpha_s}{\pi}\left[\left(\frac{13}{12} - \frac{1}{2}\ln\frac{2\mu_{\rm kin}}{\bar m}\right)\beta_0 - C_A\left(\frac{\pi^2}{6} - \frac{13}{12}\right)\right]\right\}. \quad (19)$$

where $\bar m = \overline{m}_b(\overline{m}_b)$, $C_F = 4/3$, and $\beta_0 = 11 - \frac{2}{3}\,n_f$. For $\mu_{\rm kin} \to 0$ the kinetic mass reduces to the pole mass.

Potential-subtracted mass

The potential-subtracted (PS) mass is similar to the kinetic mass, but arises considering the static energy of a bottom-antibottom quark pair in NRQCD [23].The PS mass is known to $\mathcal{O}(\alpha_s^3)$ and its relation to the pole mass reads

$$m_{b,\mathrm{PS}}(\mu_{\mathrm{PS}}) \;=\; m_{b,\mathrm{pole}} - \frac{C_F\alpha_s(\mu)}{\pi}\,\mu_{\mathrm{PS}}\Bigg[1+\frac{\alpha_s(\mu)}{4\pi}\left(a_1-\beta_0\left(\ln\frac{\mu_{\mathrm{PS}}^2}{\mu^2}-2\right)\right) \\ +\left(\frac{\alpha_s(\mu)}{4\pi}\right)^2\left(a_2-(2a_1\beta_0+\beta_1)\left(\ln\frac{\mu_{\mathrm{PS}}^2}{\mu^2}-2\right)+\beta_0^2\left(\ln^2\frac{\mu_{\mathrm{PS}}^2}{\mu^2}-4\ln\frac{\mu_{\mathrm{PS}}^2}{\mu^2}+8\right)\right)\Bigg], \tag{20}$$

where $\beta_0 = 11-\frac{2}{3}\,n_f$ and $\beta_1 = 102-\frac{38}{3}\,n_f$ are the one- and two-loop beta functions, and $a_1 = \frac{31}{3}-\frac{10}{9}\,n_f$, $a_2 = 456.749 - 66.354\,n_f + 1.235\,n_f^2$ (see Refs. [24]). For $\mu_{\mathrm{PS}}\to 0$ the PS mass reduces to the pole mass.

1S mass

The kinetic and the potential-subtracted mass depend on an explicit subtraction scale to remove the universal infrared sensitive contributions associated with the non-relativistic heavy quark dynamics. The 1S mass [25,26] achieves the same task without a factorization scale, since it is directly related to a physical quantity. The bottom 1S mass is defined as one half of the perturbative contribution to the mass of the $n=1$, $^{2s+1}L_j = {}^3S_1$ quarkonium bound state in the limit $m_b \gg m_b v \gg m_b v^2 \gg \Lambda_{\mathrm{QCD}}$. To three loop order the 1S mass is defined as

$$\frac{m_{b,\mathrm{1S}}}{m_{b,\mathrm{pole}}} \;=\; 1-\frac{(C_F\alpha_s(\mu))^2}{8}\left\{1+\left(\frac{\alpha_s(\mu)}{\pi}\right)\left[\beta_0\left(L+1\right)+\frac{a_1}{2}\right] \right. \\ +\left(\frac{\alpha_s(\mu)}{\pi}\right)^2\left[\beta_0^2\left(\frac{3}{4}L^2+L+\frac{\zeta_3}{2}+\frac{\pi^2}{24}+\frac{1}{4}\right)+\beta_0\,\frac{a_1}{2}\left(\frac{3}{2}\,L+1\right)\right. \\ \left.\left.+\frac{\beta_1}{4}\left(L+1\right)+\frac{a_1^2}{16}+\frac{a_2}{8}+\left(C_A-\frac{C_F}{48}\right)C_F\pi^2\right]\right\}, \tag{21}$$

where $L\equiv\ln(\mu/(C_F\alpha_s(\mu)\,m_{b,\mathrm{pole}}))$ and $\zeta_3 = 1.20206$. The expression for the 1S mass is derived in the framework of the non-relativistic expansion, where powers of the bottom quark velocity arise as powers of α_s in the 1S mass definition. Thus, to achieve the renormalon cancellation for B decays in the 1S mass scheme it is mandatory to treat terms of order α_s^{n+1} in Eq. (21) as being of order α_s^n. This prescription is called "upsilon expansion" [25] and arises because of the difference between the non-relativistic power counting and the usual counting in numbers of loops of powers of α_s.

Renormalon-subtracted mass

The renormalon-subtracted mass [27] is defined as the perturbative series that results from subtracting all non-analytic pole terms from the Borel transform of the pole-$\overline{\mathrm{MS}}$ mass relation at $u=1/2$ with a fixed choice for the renormalization scale $\mu=\mu_{\mathrm{RS}}$. The scale μ_{RS} is then kept independent from the renormalization scale used for the computation of the quantities of interest. To order α_s the relation between RS mass and pole mass reads,

$$M_{\mathrm{RS}}(\mu_{\mathrm{RS}}) \;=\; m_{\mathrm{pole}} - c\,\alpha_s\,\mu_{\mathrm{RS}} + \ldots\,, \tag{22}$$

where the constant c depends on the number of light quark species and has an uncertainty because the residue at $u=1/2$ in the Borel transform of the pole-$\overline{\mathrm{MS}}$ mass relation is known only approximately.

In Table 3.1 the various b quark mass parameters are compared numerically taking the $\overline{\mathrm{MS}}$ mass $\overline{m}_b(\overline{m}_b)$ as a reference value for different values for the strong coupling. Each entry corresponds to the mass using the respective 1-loop/2-loop/3-loop relations.

$\overline{m}_b(\overline{m}_b)$	$m_{b,\rm pole}$	$m_{b,\rm kin}(1\,\text{GeV})$	$m_{b,\rm PS}(2\,\text{GeV})$	$m_{b,\rm 1S}$
$\alpha_s^{(5)}(m_Z) = 0.116$				
4.10	4.48/4.66/4.80	4.36/4.42/4.45*	4.29/4.37/4.40	4.44/4.56/4.60
4.15	4.53/4.72/4.85	4.41/4.48/4.50*	4.35/4.42/4.45	4.49/4.61/4.65
4.20	4.59/4.77/4.90	4.46/4.53/4.56*	4.40/4.48/4.51	4.54/4.66/4.71
4.25	4.64/4.83/4.96	4.52/4.59/4.61*	4.46/4.53/4.56	4.60/4.72/4.76
4.30	4.69/4.88/5.01	4.57/4.64/4.67*	4.51/4.59/4.62	4.65/4.77/4.81
$\alpha_s^{(5)}(m_Z) = 0.118$				
4.10	4.49/4.69/4.84	4.37/4.44/4.46*	4.30/4.38/4.41	4.45/4.57/4.62
4.15	4.55/4.74/4.89	4.42/4.49/4.52*	4.36/4.43/4.47	4.50/4.63/4.67
4.20	4.60/4.80/4.94	4.47/4.55/4.57*	4.41/4.49/4.52	4.55/4.68/4.73
4.25	4.65/4.85/5.00	4.52/4.60/4.63*	4.46/4.54/4.58	4.61/4.73/4.78
4.30	4.71/4.91/5.05	4.58/4.66/4.69*	4.52/4.60/4.63	4.66/4.79/4.84
$\alpha_s^{(5)}(m_Z) = 0.120$				
4.10	4.51/4.72/4.88	4.37/4.45/4.48*	4.31/4.39/4.43	4.46/4.59/4.64
4.15	4.56/4.77/4.93	4.43/4.51/4.54*	4.36/4.45/4.48	4.51/4.64/4.70
4.20	4.61/4.83/4.99	4.48/4.56/4.59*	4.42/4.50/4.54	4.56/4.70/4.75
4.25	4.67/4.88/5.04	4.54/4.62/4.65*	4.47/4.56/4.59	4.62/4.75/4.80
4.30	4.72/4.94/5.10	4.59/4.67/4.71*	4.53/4.61/4.65	4.67/4.81/4.86

Table 3.1: *Numerical values of b quark masses in units of GeV for a given* $\overline{\rm MS}$ *mass for* $\overline{m}_b(\overline{m}_b)$ *for* $\mu = m_b(m_b)$, $n_l = 4$ *and three values of* $\alpha_s^{(5)}(m_Z)$. *Flavor matching was carried out at* $\mu = \overline{m}_b(\overline{m}_b)$. *Numbers with a star are given in the large-*β_0 *approximation.*

2.1.2. Bottom quark mass from spectral sum rules

The spectral sum rules for $\sigma(e^+e^- \to b\bar{b})$ start from the correlator of two electromagnetic bottom quark currents

$$(g_{\mu\nu}\, q^2 - q_\mu\, q_\nu)\, \Pi(q^2) \;\; = \;\; -\, i \int dx\, e^{i\, qx}\, \langle\, 0 \,|\, T\, j_\mu^b(x)\, j_\nu^b(0) \,|\, 0 \,\rangle\,, \tag{23}$$

where $j_\mu^b(x) \equiv \bar{b}(x)\gamma_\mu b(x)$. Using analyticity and the optical theorem one can relate theoretically calculable derivatives of Π at $q^2 = 0$ to moments of the total cross section $\sigma(e^+e^- \to b\bar{b})$,

$$\mathcal{M}_n \;=\; \frac{12\,\pi^2\, Q_b^2}{n!} \left(\frac{d}{dq^2}\right)^n \Pi(q^2)\Big|_{q^2=0} \;=\; \int \frac{ds}{s^{n+1}}\, R(s)\,, \tag{24}$$

where $R = \sigma(e^+e^- \to b\bar{b})/\sigma(e^+e^- \to \mu^+\mu^-)$. From Eq. (24) it is possible to determine the bottom quark mass [28]. From the theoretical point of view n cannot be too large because the effective energy range contributing to the moment becomes of order or smaller than $\Lambda_{\rm QCD}$ and non-perturbative effects become uncontrollable. Since the effective range of $\sqrt{s}$ contributing to the spectral integral is of order m_b/n one finds the range

$$n \lesssim 10\,, \tag{25}$$

author		$\overline{m}_b(\overline{m}_b)$	other mass	comments, Ref.
spectral sum rules				
Voloshin	95		$m_{\rm pole} = 4.83 \pm 0.01$	$8 < n < 20$, NLO; no theo.uncert. [29]
Kühn	98		$m_{\rm pole} = 4.78 \pm 0.04$	$10 < n < 20$, NLO [30]
Penin	98		$m_{\rm pole} = 4.78 \pm 0.04$	$10 < n < 20$, NNLO [31]
Hoang	98		$m_{\rm pole} = 4.88 \pm 0.13$	$4 < n < 10$, NLO [32]
Hoang	98		$m_{\rm pole} = 4.88 \pm 0.09$	$4 < n < 10$, NNLO [32]
Melnikov	98	4.20 ± 0.10	$M_{\rm kin}^{\rm 1GeV} = 4.56 \pm 0.06$	$x < n < x$, NNLO [33]
Penin	98		$m_{\rm pole} = 4.80 \pm 0.06$	$8 < n < 12$, NNLO [31]
Jamin	98	4.19 ± 0.06		$7 < n < 15$ [34]
Hoang	99	4.20 ± 0.06	$M_{\rm 1S} = 4.71 \pm 0.03$	$4 < n < 10$, NNLO [35]
Beneke	99	4.26 ± 0.09	$M_{\rm PS}^{\rm 2GeV} = 4.60 \pm 0.11$	$6 < n < 10$, NNLO [36]
Hoang	00	4.17 ± 0.05	$M_{\rm 1S} = 4.69 \pm 0.03$	$4 < n < 10$, NNLO, $m_c \neq 0$ [37]
Kühn	01	4.21 ± 0.05		$1 < n < 4$, $\mathcal{O}(\alpha_s^2)$ [38]
Erler	02	4.21 ± 0.03		$\mathcal{O}(\alpha_s^2)$ [39]
Eidemüller	02	4.24 ± 0.10	$M_{\rm PS}^{\rm 2GeV} = 4.56 \pm 0.11$	$3 < n < 12$ [40]
Bordes	02	4.19 ± 0.05		$\mathcal{O}(\alpha_s^2)$ [41]
Corcella	02	4.20 ± 0.09		$1 < n < 3$, $\mathcal{O}(\alpha_s^2)$ [42]
$\Upsilon(1S)$ mass				
Pineda	97		$m_{\rm pole} = 5.00^{+0.10}_{-0.07}$	NNLO [43]
Beneke	99	4.24 ± 0.09	$M_{\rm PS}^{\rm 2GeV} = 4.58 \pm 0.08$	NNLO [36]
Hoang	99	4.21 ± 0.07	$M_{\rm 1S} = 4.73 \pm 0.05$	NNLO [44]
Pineda	01	4.21 ± 0.09	$M_{\rm RS}^{\rm 2GeV} = 4.39 \pm 0.11$	NNLO [27]
Brambilla	01	4.19 ± 0.03		NNLO, pert. th. only [45]

Table 3.2: *Collection in historical order in units of GeV of recent bottom quark mass determinations from spectral sum rules and the $\Upsilon(1S)$ mass. Only results where α_s was taken as an input are shown. The uncertainties quoted in the respective references have been added quadratically. All numbers have been taken from the respective publications.*

where a reliable extraction of the bottom quark mass is feasible. In this range one can distinguish two regions. In the large-n region, $4 \lesssim n \lesssim 10$, the $b\bar{b}$-dynamics is predominantly non-relativistic and threshold masses are the suitable mass parameters that can be determined. In the small-n region, $1 \leq n \lesssim 4$, the $b\bar{b}$ dynamics is predominantly relativistic and the $\overline{\rm MS}$ mass is the appropriate mass parameter. In the following the advantages and disadvantages of the two types of sum rules are reviewed. Results for bottom quark masses obtained in recent sum rule analyses have been collected in Table 3.2.

Non-relativistic sum rules

The large-n sum rules have the advantage that the experimentally unknown parts of the $b\bar{b}$ continuum cross section above the Υ resonance region are suppressed. A crude model for the continuum cross section is sufficient and causes an uncertainty in the b quark mass below the 10 MeV level. Depending on which moment is used the overall experimental uncertainties in the b quark mass are between 15 and 20 MeV. Over the past years there has been a revived interest in non-relativistic sum rules because new

theoretical developments allowed for the systematic determination of $\mathcal{O}(v^2)$ (NNLO) corrections to the spectral moments [31–33,35–37]. All analyses found that the NNLO corrections were as large or even larger than the NLO corrections and various different methods were devised to extract numerical values for the bottom quark mass. In Refs. [33,35–37] threshold masses were implemented accounting for the renormalon problem. This removed one source of the bad perturbative behaviour, but it was found that a considerable theoretical uncertainty remained, coming from the theoretical description of the production and annihilation probability of the $b\bar{b}$ pair. In Refs. [33] and [36] the kinetic and the PS mass were determined from fits of individual moments. It was found that the NLO and NNLO results for the bottom mass differ by about 200 MeV. In Ref. [33] it was argued that the results form an alternating series and a value of $m_{b,\mathrm{kin}}(1\,\mathrm{GeV}) = 4.56 \pm 0.06(\mathrm{ex,th})$ GeV was determined. In Ref. [36] only the NNLO results were accounted based on consistency arguments with computations of the $\Upsilon(1\mathrm{S})$ mass and the result $m_{b,\mathrm{PS}}(2\,\mathrm{GeV}) = 4.60 \pm 0.02(\mathrm{ex}) \pm 0.10(\mathrm{th})$ GeV was obtained. In Ref. [35] the 1S mass was employed and a χ^2-fit based on four different moments was carried out. It was found that the large normalization uncertainties drop out at NLO and NNLO and that the results for the mass at NLO and NNLO showed good convergence. The result was $m_{b,1\mathrm{S}} = 4.71 \pm 0.02(\mathrm{ex}) \pm 0.02(\mathrm{th})$ GeV. A subsequent analysis [37] which included the effects of the nonzero charm mass yielded $m_{b,1\mathrm{S}} = 4.69 \pm 0.02(\mathrm{ex}) \pm 0.02(\mathrm{th})$ GeV.

Relativistic sum rules

The small-n sum rules have the disadvantage that the unknown parts of the $b\bar{b}$ continuum cross section above the Υ resonance region constitute a substantial contribution to the spectral moments. The advantage is that the computation of the theoretical moments is less involved since usual perturbation theory in powers of α_s can be employed. In Ref. [38] the theoretical moments were determined at order $\mathcal{O}(\alpha_s^2)$ and it was found that the perturbative behaviour of the theoretical moments is quite good. For the bottom quark mass determination it was assumed that the unknown experimental continuum cross section agrees with the perturbation theory prediction and subsequently the result $\overline{m}_b(\overline{m}_b) = 4.21 \pm 0.05$ GeV was determined. A more conservative analysis in Ref. [42] obtained the result $\overline{m}_b(\overline{m}_b) = 4.20 \pm 0.09$ GeV.

2.1.3. Bottom quark mass from the mass of the $\Upsilon(1\mathrm{S})$

Among the earliest values of the b quark mass were determinations that were based on analysis of the observed spectrum of the Υ mesons. However, since these determinations used potential models to describe the $b\bar{b}$ dynamics they have little value for present analyses in B physics. The same conceptual advances that led to the progress in the determination of the $\mathcal{O}(v^2)$ corrections to the spectral moments also allowed to systematically determine $\mathcal{O}(v^2)$ corrections to the spectrum of quark-antiquark bound states, which provides another method to determine a bottom quark threshold mass. The disadvantage of this method is that the theoretical tools only apply to the case in which the binding energy $\sim m_b\, v^2$ is larger than Λ_{QCD}, which is unlikely for higher radial excitations and questionable for the ground state. As such, also the theoretical methods to determine the effects of non-perturbative corrections, which are based on Shifman et al. [46], could be unreliable. In recent analyses (see Tab. 3.2) only the $\Upsilon(1\mathrm{S})$ mass has been used for a bottom mass extraction. The uncertainty is completely dominated by the estimate of the non-perturbative effects.

2.1.4. Summary of m_b determinations from sum rules

Comparing the results from the recent bottom quark mass determinations (see Tab. 3.2) one finds a remarkable consistency among the various analyses. However, the impression could be misleading because all methods have problematic issues. Therefore, it is prudent to adopt a more conservative view in averaging and interpreting the results. For the workshop is was agreed that the $\overline{m}_b(\overline{m}_b)$ shall be used as reference mass and that the respective threshold masses shall be determined from it. This leads to an enhancement of the theoretical error in the threshold masses, due to their dependence on α_s. An averaging

prescription for the results in Tab. 3.2 has not been given, and it was agreed on the value

$$\boxed{\overline{m}_b(\overline{m}_b) \;=\; 4.21 \pm 0.08 \text{ GeV}.} \tag{26}$$

Future work should aim to reduce the uncertainty to a level of 50 MeV.

2.1.5. Charm quark mass from sum rules

The charm mass plays a less important role than m_b in applications related to the CKM determination, although it certainly is a fundamental parameter. Perhaps because of that, the determination of m_c from $e^+e^- \to$ hadrons has so far received less attention than that of m_b and has not reached the same level of maturity; we will not discuss the subject here. The most recent analyses can be found in [40,47,38]. Typical results for the $\overline{\rm MS}$ mass $\overline{m}_c(\overline{m}_c)$ range between 1.19 and 1.37 GeV, with uncertainties varying between 30 and 110 MeV.

2.1.6. Charm and bottom quark masses from Lattice QCD

The determination of both heavy and light quark masses is one of the most important field of activity of lattice QCD simulations. Two major theoretical advances have allowed to increase the accuracy of these determinations. The first one has been the development of non-perturbative renormalization techniques. The renormalized quark mass $m_q(\mu)$, in a given renormalization scheme, is related to the bare quark mass $m_q(a)$, which is a function of the lattice spacing a, through a multiplicative renormalization constant,

$$m_q(\mu) = Z_m(\mu\, a)\, m_q(a)\,. \tag{27}$$

The bare quark mass $m_q(a)$ (with $q = u,\, d,\, s,\, c, \ldots$) is a free parameter of the QCD Lagrangian. It can be computed on the lattice by requiring the mass of some physical hadron ($\pi,\, \mathrm{K},\, \mathrm{D},\, \mathrm{B}, \ldots$), determined from the numerical simulation, to be equal to the corresponding experimental value. Therefore, one experimental input is needed to fix the value of the quark mass for each flavour of quark.

The quark mass renormalization constant, $Z_m(\mu\, a)$, can be computed in principle in perturbation theory. Its perturbative expansion, however, is known only at one loop and the corresponding theoretical uncertainty is therefore rather large. The non-perturbative renormalization techniques allow to compute Z_m in a non-perturbative way directly from a numerical simulation, with an accuracy which is at the level of few per cent. The two most important non-perturbative renormalization methods developed so far are based on the so called RI/MOM [48] and Schrödinger functional [49] schemes.

The other important theoretical progress, in lattice QCD calculations, has been the introduction of improved actions and operators, which allow to reduce discretization errors (finite cut-off effects) from $\mathcal{O}(a)$ to $\mathcal{O}(a^2)$. This improvement has been particularly relevant for the lattice determination of the charm quark mass. Typical values of the lattice cut-off, in current numerical simulations, are in the range $a^{-1} \sim 3 - 4$ GeV. With these values, leading discretization effects proportional to $m_c\, a$ can be of the order of 30% or larger, and they would represent the major source of systematic uncertainty in lattice determinations of the charm quark mass. The use of improved actions, combined with the extrapolation to the continuum limit ($a \to 0$) of the results obtained at fixed lattice spacing, allows to reduce discretization errors well below the 10% level.

Two lattice determinations of the charm quark mass, which use both non-perturbative renormalization and a non-perturbatively improved action, have been performed so far. The results, in the $\overline{\rm MS}$ scheme, read [50,51]

$$\begin{aligned} \overline{m}_c(\overline{m}_c) &= 1.26 \pm 0.04 \pm 0.12\text{GeV} \\ \overline{m}_c(\overline{m}_c) &= 1.301 \pm 0.034\text{GeV}\,. \end{aligned} \tag{28}$$

The first of these results has been obtained at a fixed value of the lattice spacing, corresponding to $a^{-1} \simeq 2.7$ GeV. The second one also involves an extrapolation to the continuum limit, and therefore the prediction is more accurate in this case. At fixed value of the lattice spacing the two calculations are in very good agreement. The only uncertainty which is not quoted in Eq. (28) is due to the use of the quenched approximation. For the b-quark mass the quenching effect has been found to be very small, of the order of 1–2% [52,53], while determinations of this effect for light quarks are more uncertain, lying in the range between 10 and 25%. In order to account for the quenching error in the case of the charm quark mass, a (probably conservative) estimate consists in adding a systematic uncertainty of the order of 10% to the result of Eq. (28). This gives, as best lattice estimate for the charm quark mass, the value

$$\overline{m}_c(\overline{m}_c) = 1.30 \pm 0.03 \pm 0.15\text{GeV}\,. \tag{29}$$

Lattice determinations of the b-quark mass have reached, at present, a very high level of both statistical and systematic accuracy. Since the mass of the b quark is larger than the UV cut-off (the inverse of the lattice spacing) used in current lattice calculations, the b quark cannot be simulated directly on the lattice. Therefore, one is led to use an effective theory, like HQET or NRQCD, in which the heavy degrees of freedom associated with the b quark are integrated out. Within the effective theory, the pole mass of the b quark is related to the B meson mass M_B through the relation

$$M_B = m_b^{\rm pole} + \varepsilon - \delta m\,, \tag{30}$$

which is valid up to $\mathcal{O}(1/m_b^2)$ corrections. In Eq. (30), ε is the so called binding energy and δm is a mass counterterm induced by radiative corrections. Neither ε nor δm are real physical quantities, and indeed they are separately power divergent. The binding energy ε is the quantity which is directly measured in the numerical simulations of the effective theory on the lattice. At the same time, an accurate determination of δm is necessary in order to achieve a precise estimate of the b-quark mass.

The most accurate determination of the b-quark mass on the lattice has been obtained with the HQET [53]. It relies on the NNLO perturbative calculation of the residual mass performed in Ref. [54]. The final unquenched ($N_f = 2$) result for the b-quark mass in the $\overline{\rm MS}$ scheme reads

$$\overline{m}_b(\overline{m}_b) = 4.26 \pm 0.06 \pm 0.07\text{GeV}\,, \tag{31}$$

in which the combined statistical and systematic uncertainty is at the level of 2%. Other lattice determinations of the b-quark mass have been also obtained by using NRQCD [55]. Since the systematic is rather different in the latter case, it is quite reassuring to find that the lattice-NRQCD results are in very good agreement with the prediction of Eq. (31).

The lattice determinations of the b-quark mass can be further improved. In the quenched case, the residual mass δm has been computed at $\mathcal{O}(\alpha_s^3)$ by implementing the so called numerical stochastic perturbation theory [56]. The same NNNLO accuracy could be achieved also for the unquenched theory. More recently, a completely non-perturbative approach to the calculation of δm has been proposed. The corresponding (preliminary) quenched result for the b-quark mass is $\overline{m}_b(\overline{m}_b) = 4.53(5)(7)$GeV [57], which is larger than the lattice determination of Eq. (31) and than the non-lattice estimates reviewed in the previous subsection. Since the approach of Ref. [57] is new, it deserves further investigations. On the other hand, being completely non-perturbative, it is quite promising for future and even more accurate lattice determinations of the b-quark mass.

2.2. Extraction of heavy-quark parameters from semileptonic moments

Important information on the parameters of the OPE can be extracted from the moments of the differential distributions in s.l. and radiative B decays, which encode the shape of these spectra. Recently, the first few moments of the hadronic, leptonic, and photonic spectra in s.l. and radiative B decays have been

measured by several experiments [58,59,60]. We define the moments of the leptonic energy distribution as

$$M_1^\ell = \frac{1}{\Gamma}\int dE_\ell\, E_\ell \frac{d\Gamma}{dE_\ell}; \qquad M_n^\ell = \frac{1}{\Gamma}\int dE_\ell \left(E_\ell - M_1^\ell\right)^n \frac{d\Gamma}{dE_\ell} \quad (n>1), \tag{32}$$

and the moments of the distribution of M_X, the invariant hadronic mass, as

$$M_1^X = \frac{1}{\Gamma}\int dM_X^2\, (M_X^2 - \bar{M}_D^2)\frac{d\Gamma}{dM_X^2}; \qquad M_n^X = \frac{1}{\Gamma}\int dM_X^2\, (M_X^2 - \langle M_X^2\rangle)^n \frac{d\Gamma}{dM_X^2} \quad (n>1), \tag{33}$$

where $\bar{M}_D = 1.973$ GeV is the spin averaged D meson mass and Γ is the total s.l. width. In general, n can also be fractional. Some experiments apply a lower cut on the lepton energy. In that case two truncated leptonic moments, originally suggested by Gremm *et al.* [61] and defined as

$$R_0 = \frac{\int_{1.7}(d\Gamma_{sl}/dE_l)dE_l}{\int_{1.5}(d\Gamma_{sl}/dE_l)dE_l} \quad \text{and} \quad R_1 = \frac{\int_{1.5} E_l(d\Gamma_{sl}/dE_l)dE_l}{\int_{1.5}(d\Gamma_{sl}/dE_l)dE_l}, \tag{34}$$

are often used in the experimental analysis. The theoretical framework to interpret these data has long been known and is based on the OPE. Different formulations exist, depending on the way the quark masses are treated. For instance, the m_b and m_c masses can be taken as independent parameters or subject to a constraint on $m_b - m_c$, imposed from the measured $\mathrm{B}^{(*)}$ and $D^{(*)}$ meson masses. The second choice introduces a $1/m_c$ expansion. Another option concerns the normalization scheme used for quark masses and non-perturbative parameters. As explained in the previous section, one can use short-distance masses, such as the low-scale running masses, or pole masses.

The moments M_n^ℓ, R_i, and M_n^X are highly sensitive to the quark masses and to the non-perturbative parameters of the OPE. For instance, the hadronic moments M_n^X vanish at the parton level and are generated only by real gluon emission at $O(\alpha_s)$ and by non-perturbative effects suppressed by powers of the b quark mass. The OPE expresses lepton moments through quark masses as a double expansion in α_s and $1/m_b$:

$$M_n^\ell = \left(\frac{m_b}{2}\right)^n \left[\varphi_n(r) + \bar{a}_n(r)\frac{\alpha_s}{\pi} + \bar{b}_n(r)\,\frac{\mu_\pi^2}{m_b^2} + \bar{c}_n(r)\,\frac{\mu_G^2}{m_b^2} + \bar{d}_n(r)\,\frac{\rho_D^3}{m_b^3} + \bar{s}_n(r)\,\frac{\rho_{LS}^3}{m_b^3} + ...\right], \tag{35}$$

where $r = (m_c/m_b)^2$. Analogous expressions hold for the truncated moments R_i. The higher coefficient functions $\bar{b}(r)$, $\bar{c}(r)$, ... are also perturbative series in α_s. The functions φ_n in Eq. (35) are well-known parton expressions, given e.g. in [62]. The expectation values of only two operators contribute to $O(1/m_b^3)$: the Darwin term ρ_D^3 and the spin-orbital term ρ_{LS}^3. Due to the kinematic definition of the hadronic invariant mass M_X^2, the general expression for the hadronic moments includes M_B explicitly, but it is otherwise similar to Eq. (35):

$$\begin{aligned} M_n^X \;=\; & m_b^{2n}\sum_{l=0}\left[\frac{M_B - m_b}{m_b}\right]^l \left(E_{nl}(r) + a_{nl}(r)\frac{\alpha_s}{\pi} + b_{nl}(r)\frac{\mu_\pi^2}{m_b^2} + c_{nl}(r)\frac{\mu_G^2}{m_b^2}\right. \\ & \left. + d_{nl}(r)\frac{\rho_D^3}{m_b^3} + s_{nl}(r)\frac{\rho_{LS}^3}{m_b^3} + ...\right). \end{aligned} \tag{36}$$

It is possible to re-express the heavy quark masses, m_Q, in the above equations, in terms of the meson masses, M_{H_Q}, through the relation [21]:

$$M_{H_Q} = m_Q + \bar{\Lambda} + \frac{\mu_\pi^2 - a_{H_Q}\mu_G^2}{2m_Q} + \frac{\rho_D^3 + a_{H_Q}\rho_{LS}^3 - \rho_{nl}^3}{4m_Q^2} + \mathcal{O}\left(\frac{1}{m_Q^3}\right), \tag{37}$$

where $a_{H_Q} = 1$ and $-1/3$ for pseudo-scalar and vector mesons, respectively. The use of these expressions introduces an explicit dependence on the non-local correlators contributing to ρ_{nl}^3. In the notation of [63], ρ_{nl}^3 corresponds to linear combinations of $\mathcal{T}_{1-4}$.

	φ_n	$\bar{a}_n$	$\bar{b}_n$	$\bar{c}_n$	$\bar{d}_n$	$\bar{s}_n$
M_1^ℓ	0.6173	0.015	0.31	-0.73	-3.7	0.2
$M_2^\ell\,(\times 10)$	0.3476	0.026	1.7	-1.0	-10.2	-0.9
$M_3^\ell\,(\times 10^2)$	-0.3410	0.066	3.4	1.3	-23	-4.2

Table 3.3: *Numerical values of the coefficients in Eq.(35) evaluated at r=0.06 and $m_{b,\rm kin}(1\,{\rm GeV}) = 4.6\,{\rm GeV}$ and without a lepton energy cut.*

i	E_{i1}	E_{i2}	E_{i3}	a_{i0}	a_{i1}	b_{i0}	b_{i1}	c_{i0}	c_{i1}	d_{i0}	s_{i0}
1	0.839	1	0	0.029	0.013	-0.58	-0.58	0.31	0.87	3.2	-0.4
2	0	0.021	0	- 0.001	-0.002	0.16	0.34	0	-0.05	-0.8	0.05
3	0	0	-0.0011	0.0018	0.0013	0	0.034	0	0	0.15	0

Table 3.4: *Numerical values of the coefficients in Eq.(36) evaluated at r=0.06 and $m_{b,\rm kin}(1\,{\rm GeV})$ = 4.6 GeV and without a lepton energy cut.*

The moments of the photon spectrum in inclusive radiative B decays, $\mathrm{B} \to X_s\gamma$, are also useful to constrain the non-perturbative parameters. The relevant formulae can be found in [65] and Refs. therein.

Of all the possible formalisms we discuss here only two extreme cases.[§] The first formalism is based on the kinetic running masses, $m_Q(\mu)$, and non-perturbative parameters, introduced in [20,66]. No charm mass expansion is assumed. The second formalism employs quark pole masses and the $\mathrm{B}^{(*)}$ and $D^{(*)}$ meson mass relations. Contributions through $O(\alpha_s^2\beta_0)$ [67,68] and $O(1/m_b^3)$ [1,2,62,63,69,61,70] to the moments are available. Depending on the formulation adopted, the number of parameters involved at this order ranges from six to nine. Some of these parameters, like m_b and $\lambda_2 \simeq \mu_G^2/3$, are relatively well known. Others, notably those which appear at $O(1/m_b^3)$, are virtually unknown.

2.2.1. The $m_{b,\rm kin}(\mu)$, $m_{c,\rm kin}(\mu)$ and $\mu_\pi^2(\mu)$ formalism

The quark masses are here identified by the running kinetic quark masses $m_{b,\rm kin}(\mu)$ and $m_{c,\rm kin}(\mu)$, and since no relation like Eq. (37) is used, they are two independent parameters. Apart from $\mu_\pi^2(\mu)$ and $\mu_G^2(\mu)$, defined here as expectation values in the actual B meson, there are two $1/m_b^3$ parameters, ρ_D^3 and ρ_{LS}^3. The effect of ρ_{LS}^3 turns out to be numerically small. In Eqs. (35) and (36) the mass ratio r is given by $(m_{c,\rm kin}(\mu)/m_{b,\rm kin}(\mu))^2$, and the b quark mass is understood as $m_{b,\rm kin}(\mu)$. The perturbative coefficients additionally depend on μ/m_b and the mass normalization scale μ is set at $\mu = 1$ GeV. To illustrate the size of different contributions to M_n^ℓ, we give the relevant coefficients for the first three moments in the case without a cut on the lepton energy in Table 3.3, using $m_{b,\rm kin}$(1 GeV) = 4.6 GeV and $r = 0.06$ [71] (the $O(\alpha_s^2\beta_0)$ corrections are also available [68]). In the case of hadronic moments, keeping terms up to $1/m_b^3$, we discard in Eq. (36) coefficients b_{nl}, c_{nl} with $l>1$, and d_{nl}, s_{nl} with $l>0$. The only non-vanishing E_{i0} coefficient is $E_{10} = r - \bar{M}_D^2/m_b^2$. The value of the other coefficients, at $r = 0.06$ and again without a cut on the hadron energy, are listed in Table 3.4. The $O(\alpha_s^2\beta_0)$ corrections to hadronic moments are not yet available in this scheme.

[§] A few different possibilities are considered in [65].

2.2.2. The $\bar{\Lambda}$ and λ_1 formalism

This widely used scheme results from the combination of the OPE with the HQET. Following the notation of Ref. [70], the moments are expressed in the following general form:

$$M_n = M_B^k \left[a_0 + a_1 \frac{\alpha_s(\overline{M}_B)}{\pi} + a_2 \beta_0 \frac{\alpha_s^2}{\pi^2} + b_1 \frac{\bar{\Lambda}}{\overline{M}_B} + b_2 \frac{\alpha_s}{\pi} \frac{\bar{\Lambda}}{\overline{M}_B} + \frac{c_1\,\lambda_1 + c_2\,\lambda_2 + c_3\,\bar{\Lambda}^2}{{\overline{M}_B}^2} + \frac{1}{\overline{M}_B^3} \left(d_1\,\lambda_1 \bar{\Lambda} + d_2\,\lambda_2 \bar{\Lambda} + d_3\,\bar{\Lambda}^3 + d_4\,\rho_1 + d_5\,\rho_2 + \sum_{i=1,4} d_{5+i} \mathcal{T}_i \right) + O\left(\frac{\Lambda_{QCD}^4}{m_Q^4} \right) \right] \quad (38)$$

where $k = n$ and $k = 2n$ for leptonic and hadronic moments, respectively, while $a_0 = 0$ for hadronic moments. Analogous expressions hold for the truncated moments. $\overline{M}_B = 5.3135$ GeV is the spin-averaged B meson mass, and $\beta_0 = 11 - 2/3 n_f$, with $n_f = 3$. The terms $O(\alpha_s^2 \beta_0)$ and $O(\alpha_s \bar{\Lambda})$ are not known in the case of the third hadronic moment. The coefficients a_i, b_i, c_i, d_i for the first three leptonic, $M_{1,2,3}^{\ell}$, and hadronic moments, $M_{1,2,3}^{X}$, without a cut on the lepton energy are given in [71]. The coefficients for $i = 1, 2$ with a cut on the lepton energy and for $R_{0,1}$ can be found in [65]. The non-perturbative parameters in Eq.(38) are related to those in Sec. 2.2.1. by the following relations, valid up to $\mathcal{O}(\alpha_s)$:

$$\mu_\pi^2 = -\lambda_1 - \frac{\mathcal{T}_1 + 3\mathcal{T}_2}{m_b}; \quad \mu_G^2 = 3\lambda_2 + \frac{\mathcal{T}_3 + 3\mathcal{T}_4}{m_b}; \quad \rho_D^3 = \rho_1\,; \quad \rho_{LS}^3 = 3\rho_2\,. \quad (39)$$

Perturbative corrections introduce a significant numerical difference between the parameters in the two schemes. At $\mu = 1$ GeV:

$$\bar{\Lambda} \simeq M_B - m_{b,\mathrm{kin}}(1\ \mathrm{GeV}) - \frac{\mu_\pi^2 - \mu_G^2}{2 m_b} - 0.26\ \mathrm{GeV}\,; \qquad -\lambda_1 \simeq \mu_\pi^2(1\ \mathrm{GeV}) - 0.17\ \mathrm{GeV}^2\,. \quad (40)$$

As anticipated in the previous Section, the use of the ill-defined pole quark mass induces in this formalism large perturbative corrections, which are however expected to cancel in the relation between physical observables, as long as all observables involved in the analysis are computed at the same order in α_s. We also note that, as a consequence of the HQET mass relations for the mesons, the intrinsic expansion parameter in Eq.(38) is $1/M_D$, rather than $1/M_B$. The convergence of this expansion has been questioned, in view of indications [72,73] that the matrix elements $\mathcal{T}_i$ of some non-local operators could be larger than that expected from dimensional estimates.

Higher moments are generally more sensitive to the $1/m_b^3$ corrections, but the uncertainty due to unknown perturbative and non-perturbative higher orders prevents a precision determination of the related parameters. Higher moments contain nonetheless useful information: as we will see below, they have been employed in the first analyses based on multi-parameter fits [65,71].

Measurements of the moments and non-perturbative parameters

The study of moments in B meson s.l. decays and $\mathrm{B} \to X_s\gamma$ allows to perform several independent determinations of the non-perturbative parameters and is now pursued by different experiments. Here we summarize the measurements performed by the CLEO collaboration, taking data at the CESR e^+e^- collider, and by the DELPHI Collaboration at LEP. Measurements of the first hadronic moment in $\mathrm{B} \to X_c \ell \bar{\nu}$ with different minimum charged lepton momentum have also been reported by the BaBar Collaboration [78].

CLEO and BaBar measurements have been performed at the $\Upsilon(4S)$ resonance. While there is an obvious advantage in measuring the spectra in events where the decaying B rest frame almost coincides with the laboratory frame, low energy particles cannot be identified there. It is thus necessary to rely on models for extrapolating the lepton energy spectrum to zero energy or to resort to computations for a truncated spectrum. On the other hand, performing the analysis at energies around the Z^0 peak, the

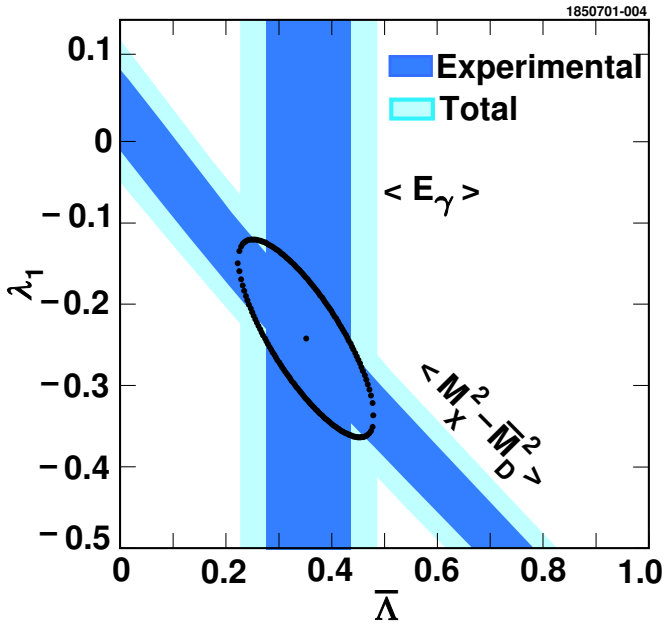

Fig. 3.1: *Constraints on $\bar{\Lambda}$ (GeV), λ_1 (GeV^2) from the first hadronic moment and the first moment of the photon energy spectrum in $b \to s\gamma$ [58,74]. The inner bands show the experimental error bands. The light gray extensions show the theoretical errors.*

large momentum of the b-hadrons ensures sensitivity to almost the full lepton spectrum, thus reducing modelling assumptions. The main challenge put by the higher energy is the accurate determination of the B rest frame.

2.2.3. Moments of hadronic mass and $b \to s\gamma$ photon energy spectra at CLEO

The first experimental determination of the HQE parameters based on the shape variables was performed by the CLEO collaboration [58]. The analysis was based on the measurement of the photon spectrum above 2.0 GeV in $b \to s\gamma$ inclusive decays [74] and on s.l. inclusive decays. CLEO measured the first two moments of the photon spectrum in radiative decays,

$$\langle E_\gamma \rangle = 2.346 \pm 0.032 \pm 0.011 \text{ GeV} \text{ and } \langle E_\gamma^2 \rangle - \langle E_\gamma \rangle^2 = 0.0226 \pm 0.0066 \pm 0.0020 \text{ GeV}^2$$

the first of which is related to half the value of the b quark pole mass, and thus to $\overline{\Lambda}$, of course up to $1/M_B^3$ corrections. The parameter λ_1 was then extracted from a measurement of the first moment, M_1^X, of the mass of the hadronic system recoiling against the ℓ-$\bar{\nu}$ pair in s.l. decays. This measurement takes advantage of the ability of the CLEO experiment to reconstruct the ν 4-momentum with high efficiency and resolution, by virtue of the hermeticity of the detector and the simplicity of the initial state in $\Upsilon(4S) \to B\bar{B}$. CLEO applied a 1.5 GeV/c lower cut on the charged lepton momentum. The explicit relation between M_1^X and the HQE parameters $\overline{\Lambda}$, λ_1, etc. is given in that case in [58]. CLEO found

$$M_1^X = 0.251 \pm 0.023 \pm 0.062 \text{ GeV}^2 \quad \text{and} \quad M_2^X = 0.576 \pm 0.048 \pm 0.163 \text{ GeV}^4,$$

where the first error is statistical and the second is systematic. From M_1^X and $\langle E_\gamma \rangle$, CLEO extracted $\overline{\Lambda}$ and λ_1, obtaining $\overline{\Lambda} = 0.35 \pm 0.07 \pm 0.10$ GeV , and $\lambda_1 = -0.236 \pm 0.071 \pm 0.078$ GeV^2 . Here, the first error is governed by the experimental measurements of the moments, and the second error reflects theoretical uncertainties, and in particular those related to $O(1/m_b^3)$ contributions. Figure 3.1 shows the bands corresponding to these two constraints as well as the $\Delta\chi^2 = 1$ ellipse in the $\overline{\Lambda}, \lambda_1$ plane.

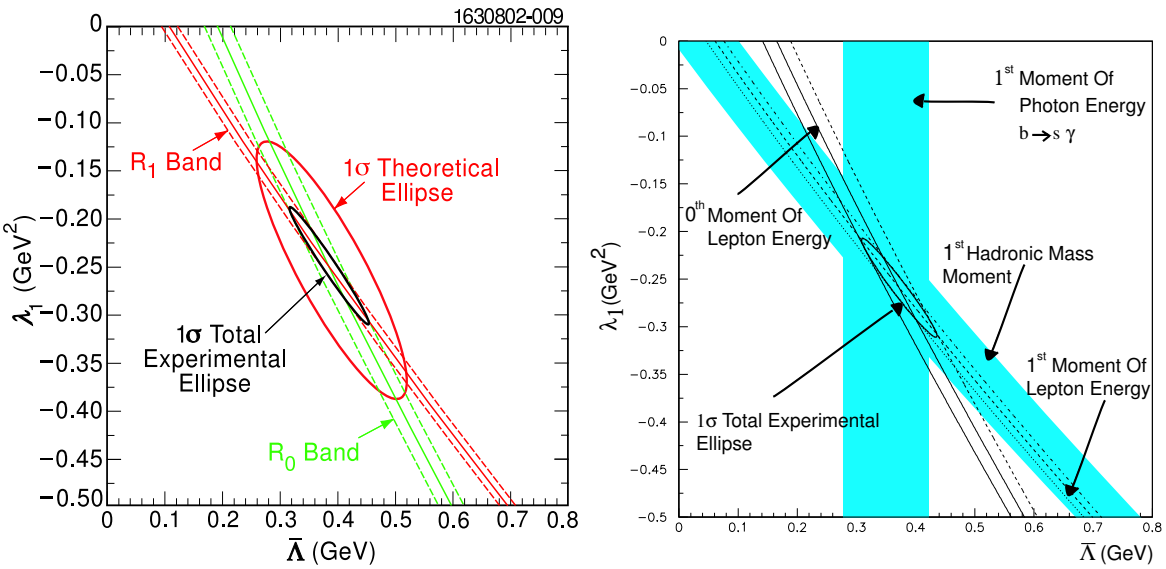

Fig. 3.2: *Left: constraints from combined electron and muon $R_{0,1}$ moments, with $\Delta\chi^2 = 1$ contours for total experimental and theoretical uncertainties [75]. Right: comparison of the same constraints with those in Fig. 3.1. λ_1 and $\bar{\Lambda}$ are computed in the $\overline{MS}$ scheme to order $1/M_B^3$ and $\beta_0\alpha_s^2$.*

2.2.4. Moments of the leptonic spectrum at CLEO

A recent CLEO analysis [75] reports the measurement of the truncated moments of the lepton spectrum, with a momentum cut of $p_\ell \geq 1.5$ GeV/c in the B meson rest frame [75]. This choice for the lepton momentum cut decreases the sensitivity of the measurement to the secondary leptons from the cascade decays ($b \to c \to s/d\ell\bar{\nu}$). The small contribution coming from charmless s.l. decays $b \to u\ell\bar{\nu}$ is included by adding the contribution from $d\Gamma_u/dE_\ell$, scaled by $|V_{ub}/V_{cb}|^2$ [61,64]. CLEO results for $R_{0,1}$ are given in Table 3.5. The values of the HQE parameters and their experimental uncertainties are obtained by calculating the χ^2 from the measured moments R_0^{exp} and R_1^{exp} and the covariance matrix $\mathrm{E}_{R_0R_1}$. The theoretical uncertainties on the HQE parameters are determined by varying, with flat distributions, the input parameters within their respective errors: $|\frac{V_{ub}}{V_{cb}}| = 0.09 \pm 0.02$, $\alpha_s = 0.22 \pm 0.027$, $\lambda_2 = 0.128 \pm 0.010$ GeV^2, $\rho_1 = \frac{1}{2}(0.5)^3 \pm \frac{1}{2}(0.5)^3$ GeV^3, $\rho_2 = 0 \pm (0.5)^3$ GeV^3, and $\mathcal{T}_i = 0.0 \pm (0.5)^3$ GeV^3. The contour that contains 68% of the probability is shown in Fig. 3.2. This procedure for evaluating the theoretical uncertainty from the unknown expansion parameters that enter at order $1/M_B^3$ is similar to that used by Gremm and Kapustin [63] and Bauer and Trott [64], but different from the procedure used in the CLEO analysis discussed above [58]. The dominant theoretical uncertainty is related to the $1/M_B^3$ terms in the non-perturbative expansion discussed before. Ref. [65] has explored the convergence of the perturbative and non-perturbative series appearing in the expressions for the moments described in the previous Section. The most conservative estimate gives a truncation error of at most 20%. The theoretical

	R_0^{exp}	R_1^{exp}
$e^\pm$	$0.6184 \pm 0.0016 \pm 0.0017$	$1.7817 \pm 0.0008 \pm 0.0010$
$\mu^\pm$	$0.6189 \pm 0.0023 \pm 0.0020$	$1.7802 \pm 0.0011 \pm 0.0011$
Combined	$0.6187 \pm 0.0014 \pm 0.0016$	$1.7810 \pm 0.0007 \pm 0.0009$

Table 3.5: *Measured truncated lepton moments for $e^\pm$ and $\mu^\pm$, and for the sum.*

uncertainties presented in this CLEO analysis do not include this truncation error. The extracted λ_1 and $\bar{\Lambda}$ are given in Table 3.6. The rhs in Fig. 3.2 shows a comparison of these CLEO results with the ones in Ref. [58]. The errors shown correspond to the experimental errors only: the agreement is good, although the theoretical uncertainties do not warrant a very precise comparison.

	$\lambda_1(\mathrm{GeV}^2)$	$\bar{\Lambda}(\mathrm{GeV})$
$e^{\pm}$	$-0.28 \pm 0.03\vert_{stat} \pm 0.06\vert_{syst} \pm 0.14\vert_{th}$	$0.41 \pm 0.04\vert_{stat} \pm 0.06\vert_{syst} \pm 0.12\vert_{th}$
$\mu^{\pm}$	$-0.22 \pm 0.04\vert_{stat} \pm 0.07\vert_{syst} \pm 0.14\vert_{th}$	$0.36 \pm 0.06\vert_{stat} \pm 0.08\vert_{syst} \pm 0.12\vert_{th}$
$\ell^{\pm}$	$-0.25 \pm 0.02\vert_{stat} \pm 0.05\vert_{syst} \pm 0.14\vert_{th}$	$0.39 \pm 0.03\vert_{stat} \pm 0.06\vert_{syst} \pm 0.12\vert_{th}$

Table 3.6: *Values λ_1 and $\bar{\Lambda}$ extracted from CLEO measurement of $R_{0,1}$, including statistical, systematic, and theoretical errors. The last row shows the results obtained combining $e^{\pm}$ and $\mu^{\pm}$ samples.*

CLEO also performed an analysis of the truncated leptonic moments in terms of the short distance $m_b^{1\mathrm{S}}$ mass instead of the pole mass scheme implicit in the $\lambda_1, \overline{\Lambda}$ formalism. The results in Ref. [64] are used to extract $m_b^{1\mathrm{S}}$, or rather $\bar{\Lambda}^{1\mathrm{S}} \equiv \bar{M}_B - m_b^{1\mathrm{S}}$. Table 3.7 summarizes the values of $\bar{\Lambda}^{1\mathrm{S}}$ and $m_b^{1\mathrm{S}}$ extracted from $R_{0,1}$ for electrons and muons samples separately, and for their sum. The final result $m_b^{1\mathrm{S}} = (4.82 \pm 0.07\vert_{exp} \pm 0.11\vert_{th})\mathrm{GeV}/c^2$ is in good agreement with the estimates of $m_b^{1\mathrm{S}}$ [35,76] discussed in Sec. 2.1.

	$\bar{\Lambda}^{1S}(\mathrm{GeV})$	$m_b^{1\mathrm{S}}(\mathrm{GeV}/c^2)$
$e^{\pm}$	$0.52 \pm 0.04\vert_{stat} \pm 0.06\vert_{syst} \pm 0.11\vert_{th}$	$4.79 \pm 0.07\vert_{exp} \pm 0.11\vert_{th}$
$\mu^{\pm}$	$0.46 \pm 0.05\vert_{stat} \pm 0.08\vert_{syst} \pm 0.11\vert_{th}$	$4.85 \pm 0.09\vert_{exp} \pm 0.11\vert_{th}$
Combined	$0.49 \pm 0.03\vert_{stat} \pm 0.06\vert_{syst} \pm 0.11\vert_{th}$	$4.82 \pm 0.07\vert_{exp} \pm 0.11\vert_{th}$

Table 3.7: *Values of $\bar{\Lambda}^{1\mathrm{S}}$ and $m_b^{1\mathrm{S}}$ extracted from $R_{0,1}$. The quoted errors reflect statistical, systematic, and theoretical uncertainties, respectively.*

We have mentioned in the previous Section that one can also consider fractional moments. Bauer and Trott [64] have explored different lepton energy moments, by varying the exponent of the energy in the integrands and the lower limits of integration. In particular, they identify several moments that provide constraints for $m_b^{1\mathrm{S}}$ and λ_1 that are less sensitive to higher order terms in the non-perturbative expansion. The shape of the truncated lepton spectrum recently measured by CLEO [77] allows to measure the following ones

$$\mathrm{R}_a^{(3)} = \frac{\int_{1.7} E_l^{0.7} (d\Gamma_{sl}/dE_l) dE_l}{\int_{1.5} E_l^2 (d\Gamma_{sl}/dE_l) dE_l}, \quad \mathrm{R}_b^{(3)} = \frac{\int_{1.6} E_l^{0.9} (d\Gamma_{sl}/dE_l) dE_l}{\int_{1.7} (d\Gamma_{sl}/dE_l) dE_l}, \tag{41}$$

$$\mathrm{R}_a^{(4)} = \frac{\int_{1.6} E_l^{0.8} (d\Gamma_{sl}/dE_l) dE_l}{\int_{1.7} (d\Gamma_{sl}/dE_l) dE_l}, \quad \mathrm{R}_b^{(4)} = \frac{\int_{1.6} E_l^{2.5} (d\Gamma_{sl}/dE_l) dE_l}{\int_{1.5} E_l^{2.9} (d\Gamma_{sl}/dE_l) dE_l}. \tag{42}$$

Tables 3.8 and 3.9 summarize the measured values, as well as the statistical and systematic errors. Fig. 3.3 shows the values of $\bar{\Lambda}^{1\mathrm{S}}$ and λ_1 extracted from these two sets of observables, as well as the constraints derived from the moments R_0 and R_1. Although these results confirm that the $1/M_B^3$ terms induce much smaller uncertainties using $R_{a,b}^{(3,4)}$, the experimental errors are larger in this case because of the similar slopes for the two constraints. However, the different relative importance of experimental and theoretical errors makes these results complementary to the previous ones reported.

	$R_a^{(3)}(\mathrm{GeV}^{-1.3})$	$R_b^{(3)}(\mathrm{GeV}^{0.9})$
$e^{\pm}$	$0.3013 \pm 0.0006\|_{stat} \pm 0.0005\|_{syst}$	$2.2632 \pm 0.0029\|_{stat} \pm 0.0026\|_{syst}$
$\mu^{\pm}$	$0.3019 \pm 0.0009\|_{stat} \pm 0.0007\|_{syst}$	$2.2611 \pm 0.0042\|_{stat} \pm 0.0020\|_{syst}$
$\ell^{\pm}$	$0.3016 \pm 0.0005\|_{stat} \pm 0.0005\|_{syst}$	$2.2621 \pm 0.0025\|_{stat} \pm 0.0019\|_{syst}$

Table 3.8: *Measured truncated lepton moments $R_{a,b}^{(3)}$ for $e^{\pm}$, $\mu^{\pm}$, and their weighted average.*

	$R_a^{(4)}(\mathrm{GeV}^{0.8})$	$R_b^{(4)}(\mathrm{GeV}^{-0.4})$
$e^{\pm}$	$2.1294 \pm 0.0028\|_{stat} \pm 0.0027\|_{syst}$	$0.6831 \pm 0.0005\|_{stat} \pm 0.0007\|_{syst}$
$\mu^{\pm}$	$2.1276 \pm 0.0040\|_{stat} \pm 0.0015\|_{syst}$	$0.6836 \pm 0.0008\|_{stat} \pm 0.0014\|_{syst}$
$\ell^{\pm}$	$2.1285 \pm 0.0024\|_{stat} \pm 0.0018\|_{syst}$	$0.6833 \pm 0.0005\|_{stat} \pm 0.0006\|_{syst}$

Table 3.9: *Measured truncated $R_{4a,b}$ moments for $e^{\pm}$, $\mu^{\pm}$, and their weighted average.*

Bauer and Trott [64] also identify moments that are insensitive to m_b^{1S} and λ_1. They suggest that a comparison between a theoretical evaluations of these "duality moments" and their experimental values may provide useful constraints on possible quark-hadron duality violations in s.l. processes. CLEO measures two such "duality moments", defined as

$$\mathrm{D}_3 = \frac{\int_{1.6} E_l^{0.7}(d\Gamma_{sl}/dE_l)dE_l}{\int_{1.5} E_l^{1.5}(d\Gamma_{sl}/dE_l)dE_l}, \quad \mathrm{D}_4 = \frac{\int_{1.6} E_l^{2.3}(d\Gamma_{sl}/dE_l)dE_l}{\int_{1.5} E_l^{2.9}(d\Gamma_{sl}/dE_l)dE_l}. \tag{43}$$

The theoretical predictions from Ref. [64] are compared with the measured $D_{3,4}$ from the combined lepton sample in Table 3.10. The agreement is excellent and thus no internal inconsistency of the theory is uncovered in this analysis.

	Experimental	Theoretical
D_3	$0.5193 \pm 0.0008\|_{exp}$	$0.5195 \pm 0.0006\|_{\lambda_1,\bar{\Lambda}^{1S}} \pm 0.0003\|_{th}$
D_4	$0.6036 \pm 0.0006\|_{exp}$	$0.6040 \pm 0.0006\|_{\lambda_1,\bar{\Lambda}^{1S}} \pm 0.0005\|_{th}$

Table 3.10: *Measured duality moments and theoretical predictions using the values λ_1 and $\bar{\Lambda}^{1S}$ [77]. The errors reflect the experimental uncertainties in these parameters and the theoretical errors, respectively.*

2.2.5. Moments of leptonic and hadronic mass spectra at DELPHI

Results obtained by the DELPHI collaboration for the first three moments of the lepton energy and the hadronic mass spectra have been presented at ICHEP02 [59]. The analyses were based on b-hadron s.l. decays into electrons and muons, selected from a sample of about 3×10^6 $e^+e^- \to Z^0 \to q\bar{q}$ events recorded with the DELPHI detector at LEP. Electrons and muons were required to have a momentum greater than 2-3 GeV/c in the laboratory frame. For the lepton energy spectrum measurement an inclusive reconstruction of the secondary vertex of the charm hadron decay was performed. The energy of the B hadron was estimated as the energy sum of the identified lepton, the secondary hadronic system and the neutrino energy, evaluated from the event missing energy. The identified lepton was then boosted back to the reconstructed B rest frame and its energy E_ℓ re-computed in this frame. Results for the first three

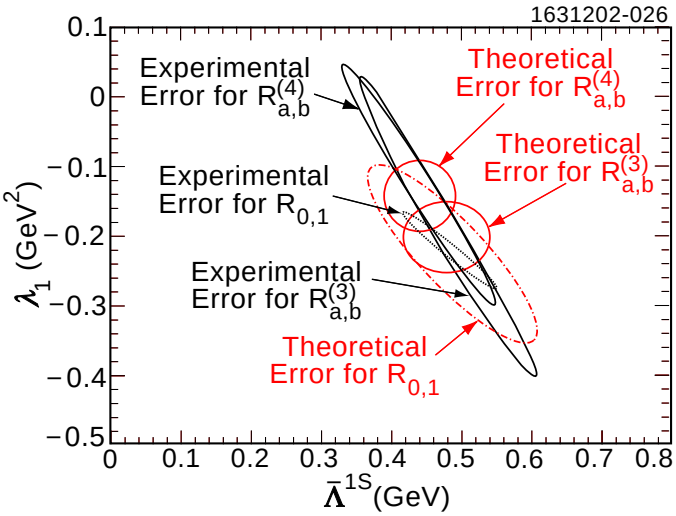

Fig. 3.3: *Constraints on the HQE parameters λ_1 and $\bar{\Lambda}^{1S}$ from different CLEO measured spectral moments.*

moments are summarized in Table 3.11. In order to study the hadronic mass distribution the exclusive reconstruction of $\bar{B}^0_d \to D^{**}\ell\bar{\nu}$ states was performed and the total D^{**} production in b-hadron s.l. decays was determined. Moments of the hadronic mass distribution were measured for D^{**} candidates and moments of the hadronic mass distribution in inclusive b-hadron s.l. decays, M_X, were derived including $b \to D$ and $D^*\ell^-\overline{\nu}_\ell$ channels. Results for the first three moments are summarized in Table 3.11. As we will discuss in the next subsection, the DELPHI results have been used in [71] as inputs of a multi-parameter fit to determine the heavy quark masses and non-perturbative parameters of the HQE. The use of higher moments guarantees a sensitivity to the $1/m_b^3$ parameters and the simultaneous use of the hadronic and leptonic spectra ensures that a larger number of parameters can be kept free in the fit.

Moment	Result	(stat)	(syst)	
$M_1(E_\ell)$	(1.383	$\pm$ 0.012	$\pm$0.009)	GeV
$M_2(E_\ell)$	(0.192	$\pm$ 0.005	$\pm$0.008)	GeV^2
$M_3(E_\ell)$	(-0.029	$\pm$ 0.005	$\pm$0.006)	GeV^3
$M_1(M_X)$	(0.534	$\pm$ 0.041	$\pm$ 0.074)	GeV^2
$M_2(M_X)$	(1.226	$\pm$ 0.158	$\pm$ 0.152)	GeV^4
$M_3(M_X)$	(2.970	$\pm$ 0.673	$\pm$ 0.478)	GeV^6

Table 3.11: *DELPHI results for the first three leptonic and hadronic moments.*

2.2.6. Multi-parameter fits of heavy-quark parameters and outlook

A recent and promising development, in view of the greater precision expected at the B-factories, consists in combining leptonic and hadronic moments in a multi-parameter fit to determine not just m_b and $\lambda_1 \sim -\mu_\pi^2$ but also the dominant $O(1/m_b^3)$ parameters. The first comprehensive analyses that employ this approach [65,71] have shown that present data are consistent with each other (with the possible exception of the preliminary BaBar data [78]) and with our theoretical understanding, most notably with the underlying assumption of quark-hadron duality.

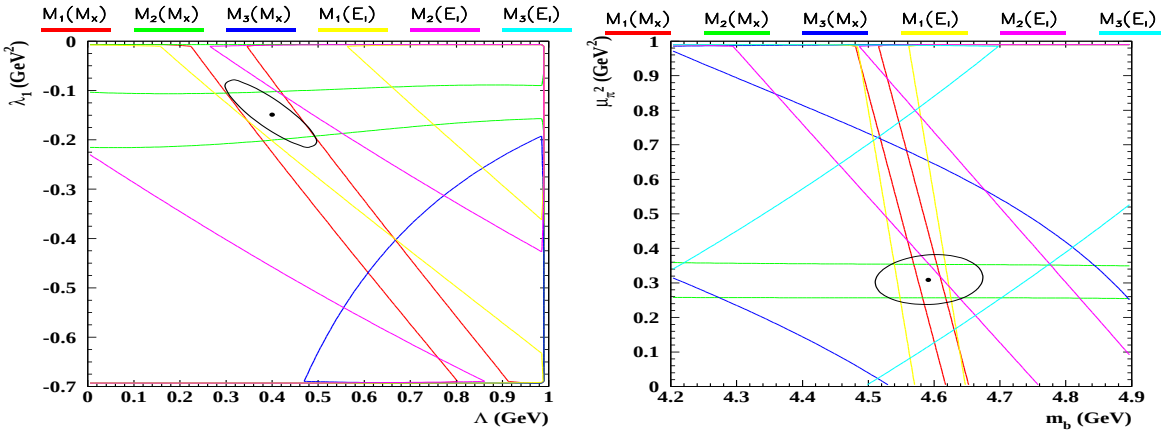

Fig. 3.4: *Projection of the constraints from the six DELPHI moments on the ($m_b(1\ \mathrm{GeV})$, μ_π^2) and ($\overline{\Lambda}$, λ_1) planes [71]. The bands correspond to the total experimental error and given keeping all the other parameters at their central values. The ellipses represent the 1σ contour.*

The analysis of [71] is based solely on the DELPHI data in Table 3.11, and performed in the two theoretical framework described above in Secs. 2.2.1. and 2.2.2. The projection of the various constraints on the ($m_{b,\mathrm{kin}}(1\ \mathrm{GeV})$, μ_π^2) and ($\overline{\Lambda}$, λ_1) planes are given in Fig. 3.4, which shows very good consistency. The results of the fits are shown in Tables 3.12 and 3.13. In the framework of Sec. 2.2.1. the charm mass is a free parameter of the fit, though strongly correlated to the bottom mass. Given a precise determination $\delta m_{b,\mathrm{kin}}(1\ \mathrm{GeV}) \sim 50$ MeV, the charm mass could therefore be extracted with $\delta m_c \sim 90$ MeV, a competitive determination [71] (Cfr. Sec. 2.1.).

Fit Parameter	Fit Values	Fit Uncertainty	Syst. Uncertainty	
$m_{b,\mathrm{kin}}$ (1 GeV)	4.59	$\pm$ 0.08	$\pm$ 0.01	GeV
$m_{c,\mathrm{kin}}$ (1 GeV)	1.13	$\pm$ 0.13	$\pm$ 0.03	GeV
μ_π^2 (1 GeV)	0.31	$\pm$ 0.07	$\pm$ 0.02	GeV^2
ρ_D^3	0.05	$\pm$ 0.04	$\pm$ 0.01	GeV^3

Table 3.12: *Results of fits to the moments of Table 3.11 for the $m_b(\mu)$, $m_c(\mu)$ and $\mu_\pi^2(\mu)$ formalism [71].*

The analysis of Ref. [65] includes the first two hadronic moments measured by CLEO and DELPHI, $R_{0,1}$ measured by CLEO, the first two leptonic DELPHI moments, and the first two moments of the photon spectrum in $\mathrm{B} \to X_s\gamma$. The results in one of the formalisms adopted are shown in Table 3.14. They are in good agreement with both CLEO and DELPHI analyses mentioned above. The preferred ranges for the heavy quark masses and for the non-perturbative parameters in Tables 3.12, 3.13, and 3.14 are in agreement with theoretical expectations and with each other, although the analyses [65,71] differ in several respects (data employed, additional constraints, scheme adopted, treatment of theoretical errors).

In summary, the experimental information appears so far consistent with the theoretical framework, with the possible exception of the preliminary BaBar result. The emerging experimental information from the B factories will eventually lead to a more complete assessment of our present understanding of inclusive s.l. decays.

Fit Parameter	Fit Values	Fit Uncertainty	Syst. Uncertainty	
$\overline{\Lambda}$	0.40	$\pm$ 0.10	$\pm$ 0.02	GeV
λ_1	-0.15	$\pm$ 0.07	$\pm$ 0.03	GeV^2
λ_2	0.12	$\pm$ 0.01	$\pm$ 0.01	GeV^2
ρ_1	-0.01	$\pm$ 0.03	$\pm$ 0.03	GeV^3
ρ_2	0.03	$\pm$ 0.03	$\pm$ 0.01	GeV^3

Table 3.13: *Results of fit to the moments of Table 3.11 for the $\bar{\Lambda} - \lambda_1$ formalism [71].*

Fit Parameter	Fit Values	Fit Uncertainty	
m_b^{1S}	4.74	$\pm$ 0.10	GeV
$\lambda_1 + \frac{\mathcal{T}_1+3\mathcal{T}_3}{m_b}$	-0.31	$\pm$ 0.17	GeV^2
ρ_1	0.15	$\pm$ 0.12	GeV^3
ρ_2	-0.01	$\pm$ 0.11	GeV^3

Table 3.14: *Results of fit for the m_b^{1S}-λ_1 formalism [65].*

2.3. Parton–hadron duality in B decays

Parton-hadron duality [¶] – or duality for short – is invoked to connect quantities evaluated on the quark-gluon level to the (observable) world of hadrons. It is used all the time, often without explicit reference to it. A striking example of the confidence high-energy physicists have in the asymptotic validity of duality was provided by the discussion of the width $\Gamma(Z^0 \to H_b H_b' X)$. There was about a 2% difference between the predicted and measured decay width, which lead to lively debates on its significance vis-a-vis the *experimental* error, before disappearing when the analysis was improved. No concern was expressed about the fact that the Z^0 width was calculated on the quark-gluon level, yet measured for hadrons. Likewise the strong coupling $\alpha_{\rm s}(\rm M_Z)$ is routinely extracted from the perturbatively computed hadronic Z^0 width with a stated theoretical uncertainty of 0.003 which translates into a theoretical error in $\Gamma_{had}(Z^0)$ of about 0.1%.

There are, however, several different versions and implementations of the concept of duality. The problem with invoking duality implicitly is that it is very often unclear which version is used. In B physics – in particular when determining $|V_{cb}|$ and $|V_{ub}|$ – the measurements have become so precise that theory can no longer hide behind experimental errors. To estimate theoretical uncertainties in a meaningful way one has to give clear meaning to the concept of duality; only then can one analyse its limitations. In response to the demands of B physics a considerable literature has been created on duality over the last few years, which we summarize here. Technical details can be found in the references.

Duality for processes involving time-like momenta was first addressed theoretically in the late '70's in references [79] and [80]. Using the optical theorem, the cross section for $e^+e^- \to \rm hadrons$ at

[¶] This name might be more appropriate than the more frequently used *quark*-hadron duality since gluonic effects have to be included as well into the theoretical expressions.

leading order in α_{em} can be expressed as

$$\sigma(s) = \frac{16\pi^2\alpha_{em}}{s}\mathrm{Im}\ \Pi(s) \tag{44}$$

where $\Pi(s)$ is defined through the correlator of electromagnetic currents:

$$T_{\mu\nu}(q^2) = i\int d^4x\, e^{iqx}\,\langle 0|T\left(J_\mu(x)J_\nu(0)\right)|0\rangle = (g_{\mu\nu}q^2 - q_\mu q_\nu)\Pi(q^2)\ . \tag{45}$$

One might be tempted to think that by invoking QCD's asymptotic freedom one can compute $\sigma(\mathrm{e}^+\mathrm{e}^- \to \mathrm{hadrons})$ for large c.m. energies $\sqrt{s} \gg \Lambda_{QCD}$ in terms of quarks (and gluons) since it is shaped by short distance dynamics. However production thresholds like those for charm induce singularities that vitiate such a straightforward computation. Under such circumstances, duality between the QCD-inferred cross section and the observed one looks problematic. It was suggested in [79] that the equality between the two would be restored after averaging or "smearing" over an energy interval:

$$\langle T_{\mu\nu}^{hadronic}\rangle_w \simeq \langle T_{\mu\nu}^{partonic}\rangle_w \tag{46}$$

where $\langle ...\rangle_w$ denotes the smearing which is an average using a smooth weight function $w(s)$:

$$\langle ...\rangle_w = \int ds\, ...\, w(s) \tag{47}$$

The degree to which $\langle T_{\mu\nu}^{partonic}\rangle_w$ can be trusted as a theoretical description of the observable $\langle T_{\mu\nu}^{hadronic}\rangle_w$ depends on the weight function, in particular its width. It can be broad compared to the structures that may appear in the hadronic spectral function, or it could be quite narrow, as an extreme case even $w(s) \sim \delta(s - s_0)$. It has become customary to refer to the first and second scenarios as *global* and *local* duality, respectively. Other authors use different names, and one can argue that this nomenclature is actually misleading. Below these items are described in more detail without attempting to impose a uniform nomenclature.

Irrespective of names, a fundamental distinction concerning duality is often drawn between s.l. and non-leptonic widths. Since the former necessarily involves smearing with a smooth weight function due to the integration over neutrino momenta, it is often argued that predictions for the former are fundamentally more trustworthy than for the latter. However, such a categorical distinction is overstated and artificial. Of much more relevance is the differentiation between distributions and fully integrated rates.

No real progress beyond the more qualitative arguments of Refs. [79] and [80] occurred for many years. For as long as one has very limited control over non-perturbative effects, there is little meaningful that can be said about duality violation. Yet this has changed for heavy flavour physics with the development of heavy quark expansions, since within this OPE framework we can assess non-perturbative effects as well as duality violation.

2.3.1. What is parton–hadron duality?

In order to discuss possible violations of duality one has to give first a more precise definition of this notion, which requires the introduction of some theoretical tools. Here the arguments given in the extensive reviews of Ref. [81] and [82][‖] are followed closely.

The central ingredient in the definition of duality that will be used here is the method of the Wilsonian OPE frequently used in field theory to perform a separation of scales. In practical terms this means that we can write

$$i\int d^4x\, e^{iqx}\,\langle A|T\left(J^\mu(x)J^\nu(0)\right)|A\rangle \simeq \sum_n \left(\frac{1}{Q^2}\right)^n c_n^{\mu\nu}(Q^2;\lambda)\langle A|\mathcal{O}_n|A\rangle_\lambda \tag{48}$$

[‖] It can be noted that even the authors of Ref. [81] and [82] – although very close in the substance as well as the spirit of their discussion – do not use exactly the same terminology concerning different aspects of duality.

for $Q^2 = -q^2 \to \infty$. The following notation has been used: $|A\rangle$ denotes a state that could be the vacuum – as for $e^+e^- \to hadrons$ considered above – or a B meson when describing s.l. beauty decays. J^μ denote electro-magnetic and weak current operators ($b \to c$ or u) for the former and the latter processes, respectively; for other decays like non-leptonic or radiative ones one employs different $\Delta B = 1$ operators; the $\mathcal{O}_n$ are local operators of increasing dimension. The operator of lowest dimension yields the leading contribution. In e^+e^- annihilation it is the unit operator $\mathcal{O}_0 = 1$, for B decays $\mathcal{O}_0 = \bar{b}b$. As we have seen in Sec. 1.1., they lead (among other things) to the naive partonic results. Yet the OPE allows us to systematically improve the naive partonic result. The coefficients $c_n^{\mu\nu}$ contain the contributions from short distance dynamics calculated perturbatively based on QCD's asymptotic freedom. Following Wilson's prescription a mass scale λ has been introduced to separate long and short distance dynamics; both the coefficients and the matrix elements depend on it, but their product does not.

The perturbative expansion takes the form

$$c_n^{\mu\nu} = \sum_i \left(\frac{\alpha_s(Q^2)}{\pi} \right)^i a_{n,i}^{\mu\nu} \tag{49}$$

and is performed in terms of quarks and gluons. The expectation values for the local operators provide the gateways through which non-perturbative dynamics enters.

The crucial point is that the OPE result is obtained in the Euclidean domain, far from any singularities induced by hadronic thresholds, and has to be continued analytically into the Minkowskian regime relating the OPE result to observable hadronic quantities. As long as QCD is the theory of the strong interactions, it does not exhibit unphysical singularities in the complex Q^2 plane, and the analytical continuation will not induce additional contributions. To conclude: *duality between* $\langle T_{\mu\nu}^{hadronic} \rangle_w$ *and* $\langle T_{\mu\nu}^{partonic} \rangle_w$ *arises due to the existence of an OPE that is continued analytically*. It is thus misleading to refer to duality as an additional assumption.

Up to this point the discussion was quite generic. To specify it for s.l. B decays one chooses the current J_μ to be the weak charged current related to $b \to c$ or $b \to u$. As already noted in Sec. 1.1., the expansion parameter for inclusive s.l. decays is given by the energy release $\sim 1/(m_b - m_c)$ $[1/m_b]$ for $b \to c$ $[b \to u]$.

2.3.2. Duality violation and analytic continuation

One of the main applications of the heavy quark expansion is the reliable extraction of $|V_{cb}|$ and $|V_{ub}|$. One wants to be able to arrive at a meaningful estimate of the theoretical uncertainty in the values obtained. There are three obvious sources of theoretical errors:

1. unknown terms of higher order in α_s;
2. unknown terms of higher order in $1/m_Q$;
3. uncertainties in the input parameters α_s, m_Q and the expectation values of local operators which appear in the OPE.

Duality violations constitute additional uncertainties.They arise from the fact that at finite order in $1/m_Q$, the Euclidean OPE is insensitive to contributions of the type $e^{-m_Q/\mu}$, with μ denoting some hadronic scale. While such a term is probably innocuous for beauty, it needs not be for charm quarks. Furthermore, under analytic continuation these terms turn into potentially more dangerous oscillating terms of the form $\sin(m_Q/\mu)$.

Though there is not (yet) a full theory for duality and its violations, progress has come about in the last few years for the following reasons:

- the understanding of the physical origins of duality violations has been refined as due to
  - hadronic thresholds;

  - so-called 'distant cuts';
  - the suspect validity of $1/m_c$ expansions.
- The issues surrounding the exponentially small terms discussed above and their analytic continuation have been understood.
- There is an increasing array of field-theoretical toy models, chief among them the 't Hooft model, which is QCD in 1+1 dimensions in the limit of $N_c \to \infty$. It is solvable and thus allows an unequivocal comparison of the OPE result with the exact solution.
- For the analysis of $b \to c$ transitions the small-velocity (SV) expansion is a powerful tool [7].

Based on general expectations as well as on analysing the models one finds that indeed duality violations are described by highly power suppressed 'oscillating' terms of the form

$$T(m_Q) \sim \left(\frac{1}{m_Q}\right)^k \sin(m_Q/\mu) \tag{50}$$

for some integer power k. More generally one can state:

- Duality will not be exact at finite masses. It represents an approximation the accuracy of which will increase with the energy scales in a way that depends on the process in question.
- Limitations to duality can enter only in the form of an oscillating function of energy or m_Q (or have to be exponentially suppressed), i.e. duality violation cannot modify all decay rates in the same way.
- The OPE equally applies to s.l. as well as to non-leptonic decay rates. Likewise both widths are subject to duality violations. The difference here is quantitative rather than qualitative; at finite heavy quark masses corrections are generally expected to be larger in the non-leptonic widths. In particular, duality violations there can be boosted by the accidental nearby presence of a narrow hadronic resonance. Similar effects could arise in s.l. rates, but are expected to be highly suppressed there.
- It is not necessary to have a proliferation of decay channels to reach the onset of duality, either approximate or asymptotic. Instructive examples are provided by the SV kinematics in s.l. decays and by non-leptonic rates in the 't Hooft model. For example, in the SV limit, the ground-state doublet of D mesons alone saturates the inclusive s.l. decay rate and is dual to the partonic rate [83]. The point here is that the large energy release would allow a large number of states to contribute kinematically, but only two channels are actually allowed by the dynamics.

Putting everything together it has been estimated by the authors of Ref. [82] – that *duality violations in the integrated s.l. width of B mesons cannot exceed the fraction of a percent.* As such we do not envision it to ever become the limiting factor in extracting $|V_{cb}|$ and $|V_{ub}|$ since the uncertainties in the expression for the s.l. width due to fixed higher order contributions will remain larger than this level. The oscillatory nature of duality violating contributions is a main ingredient in this conclusion. It also shows that duality violations could become quite sizeable if an only partially integrated width – let alone a distribution – is considered. Generally, for distributions the expansion parameter is not the heavy mass, rather it is a quantity such as $1/[m_Q(1-x)]$ where x is e.g. the rescaled charged lepton energy of a s.l. decay. From Eq. (50) one would expect that contributions the form $\sin(m_Q[1-x]/\mu)/[m_Q(1-x)]^k$ would appear in differential distributions.

2.3.3. How can we check the validity of parton–hadron duality?

If in the future a discrepancy between the measured and predicted values for, say, a CP asymmetry in B decays is found, one has to check very diligently all ingredients upon which the prediction was based, in particular the values for $|V_{cb}|$ and $|V_{ub}|$, before one could make a credible claim to have uncovered

New Physics. This means one needs a measure for potential duality violations that is not based purely on theoretical arguments.

Most theoretical uncertainties do not have a statistical nature. As in the case of experimental systematics, the most convincing way to control them is to determine the same quantity in independent ways and analyse their consistency. The heavy quark expansions lend themselves naturally to such an approach since they allow the description of numerous decay rates in terms of a handful of basic parameters, namely quark masses and hadronic expectation values. Of course, such independent determinations of the same quantity only probe the overall theoretical control: by themselves they cannot tell whether a failure is due to unusually large higher order contributions or to a breakdown of duality.

The fact that both the inclusive and exclusive methods for extracting $|V_{cb}|$ and $|V_{ub}|$ yield consistent values (see Secs. 2.4.,2.5., 3., and 4.) is such a test. Theoretical corrections are nontrivial and essential for the agreement. As discussed in Sec. 2.2., the study of moments offers another important consistency check. In particular, we emphasize that the b quark mass extracted from the shape variables is consistent, within errors, with the one extracted from sum rules and lattice calculations (see Sec. 2.1.), and that the analyses of CLEO and DELPHI data, and those of the leptonic and hadronic moments point to very similar values for the kinetic energy parameter $\lambda_1 \sim -\mu_\pi^2$. This suggests that no anomalously large higher order corrections or unexpectedly sizeable duality violating contributions are present in the HQE used to described inclusive s.l. $b \to c$ decays. However, once again, we stress that these comparisons do not represent direct tests of duality.

2.3.4. Model based investigations of duality

It is desirable to study in more explicit detail how duality comes about, how it is approached and what its limitations are. This can be done in the context of exactly soluble field theories, in particular the 't Hooft model, which is QCD in 1+1 dimensions with the number of colours going to infinity [84]. There one finds duality to be achieved very quickly, i.e. after a mere handful of channels open up.

For detailed studies in 1+3 dimensions one is at present limited to the use of quark models employing certain types of potential. However, one has to handle these models with care, as they have sometimes led to confusion. In particular, it has been argued in Ref.[86] that within quark models one could have an $\mathcal{O}(1/m_Q)$ contribution to the ratio of inclusive to free quark total decay rate. Such terms are absent in the OPE, and therefore violate duality. The arguments presented in [86] and similar papers have been discussed in [82], where their internal flaws have been pointed out. One of the important lessons is that such models exhibit automatically the proper behaviour in the Shifman-Voloshin (SV) limit [7], where $\Lambda_{QCD} \ll \delta m = m_b - m_c \ll m_b$. In particular, they have to satisfy a set of sum rules. Once one realizes that such models are automatically in compliance with what we know to be true in QCD, it becomes clear that no $1/m_Q$ terms can appear [88,89,90]. Of particular importance in this context are the Bjorken sum rule for $\mathcal{O}(\frac{(\delta m)^2}{m_b^2})$ terms and the Voloshin sum rule for $\mathcal{O}(\frac{\delta m}{m_b})$ terms[**]. Other terms are suppressed by higher powers of $1/m_b$ or powers of $\Delta/\delta m$, Δ being the level spacing of $O(\Lambda_{QCD})$, *i.e.* the difference between the ground state and the first excited level. Once such models have been brought into compliance with what we know to be true in QCD – like the validity of the SV sum rules – then they can play a significant heuristic role in educating our intuition about the onset of duality.

In Ref. [90] a detailed study of the cancellations required for duality to hold have been performed using a harmonic oscillator (HO) potential. The interest of this model is that the truncation of states to the first band of orbital excitations (lowest D^{**}) becomes exact to the relevant order $1/m_b^2$, which allows us to perform a complete and explicit numerical or analytical calculation. Furthermore, this model is

[**] It also has been demonstrated explicitly that, contrary to what suggested in note 3 of Ref. [86], no term of $\mathcal{O}(\frac{\delta m}{m_b^2})$ exist in QCD [87].

close to the ones used in [86], so that one can check precisely the various statements made there. Using a constant for the leptonic interaction one finds in the harmonic oscillator model

$$R_{sl} = \frac{\Gamma_{inclusive}}{\Gamma_{free\ quark}} = 1 + \frac{3}{R^2 m_b^2}(\frac{1}{4} - \frac{\Delta}{\delta m}) + \text{smaller terms} \tag{51}$$

where $\Delta = \frac{1}{m_d R^2}$ is a model parameter containing the square of the harmonic oscillator radius R and the light-quark mass m_d. Note that the first term inside the parentheses originates from the kinetic energy operator. In fact, it can be proven [89] that for *regular* potentials the whole series, directly calculated in the model, is *exactly* the one given by OPE.

What is then the explanation of the apparent disagreement with [86]? First, there is a misunderstanding induced by the expression "$1/m_Q$ duality violation", used sometimes in a misleading way. Ref. [86] does not dispute that the OPE is basically right and that the equality with free quark decay is satisfied within the expected accuracy in the region of phase space where the energy release is large $(t_{max}^{1/2} - t^{1/2})/\Delta \gg 1$, i.e. where many states are kinematically allowed ($t = q^2$). This is certainly true when t is small. What may cause problems, according to [86], is only the region near t_{max} where this condition is not satisfied and large effects can be generated. According to the authors of [89], one can certainly produce effects which violate the equality with free quark over the region of phase space *where only the ground state is opened*, of relative order $1/m_Q$ if this "relative order " means that one compares to the corresponding free quark decay *over the same region* of phase space. But they object that such effects be related to the *total* free quark decay which is much larger. Indeed, such effects are not of order $1/m_Q$ with respect to the total free quark decay rate, but much smaller, suppressed by powers of $2\Delta/\delta m$ [89]. This suppression factor amounts, in the standard $1/m_Q$ expansion at fixed ratio of heavy masses, to further powers of the heavy mass, because then $\delta m \propto m_b$. Also, numerically, they are small since $2\Delta/\delta m$ is small.

The first example given by Isgur is that the decrease of the ground state contribution with decreasing t (or increasing $|\vec{q}|$) due to the form factor must be compensated by the increase of the excited states to maintain duality with free quarks. This is exactly guaranteed by the Bjorken sum rule in the heavy quark limit, but it is no longer exact at finite mass, because there is a region below the D^{**} threshold where only the ground state $\mathrm{D} + \mathrm{D}^*$ contribute. Quantitatively, the term pointed out in [86] with a constant leptonic interaction reads (the choice of this interaction is not crucial):

$$\frac{\delta\Gamma}{\Gamma_{free}} \simeq -\rho^2 \frac{\int_{(\delta m-\Delta)^2}^{(\delta m)^2} dt |\vec{q}| \frac{|\vec{q}|^2}{m_b^2}}{\int_0^{(\delta m)^2} dt |\vec{q}|} \tag{52}$$

where $|\vec{q}|^2 \simeq (\delta m)^2 - t$, $-\rho^2 \frac{|\vec{q}|^2}{m_b^2}$ describes the falloff of the ground state (ρ^2 is the slope of the Isgur-Wise function), and the integration limits are approximated to the desired accuracy. At the lower limit of the numerator integral $t = (\delta m - \Delta)^2$ this falloff attains its maximum, $-\rho^2 \frac{2\Delta\delta m}{m_b^2}$. This term is by itself the expression of a $1/m_Q$ term in the SV limit [86]. However, the real magnitude is much smaller because one must integrate over a limited phase space, while the integral of the free quark decay in the denominator extends over a much larger region [90]:

$$\frac{\delta\Gamma}{\Gamma_{free}} \simeq -\frac{3}{5}\rho^2 \frac{2\Delta\delta m}{m_b^2} \left(\frac{2\Delta}{\delta m}\right)^{3/2} = -\frac{3}{5}\frac{m_d \delta m}{m_b^2} \left(\frac{2\Delta}{\delta m}\right)^{3/2} \tag{53}$$

where $\rho^2\Delta = \frac{m_d}{2}$ in the HO model. Parametrically, this is suppressed with respect to $1/m_Q$ because of the factor $(\frac{2\Delta}{\delta m})^{3/2}$.

In another example relying on a model of two-body decay, Isgur [86] tries to take into account also the larger effect due to the $\frac{m_d \delta m}{m_b^2}$ terms present in *partial rates*. Such terms, which corresponds to

$1/m_Q$, are present *separately* in the various exclusive channels. For instance one has for the ratio of the ground state to the free quark decay rates:

$$R_{sl}^{(ground\ state)} = 1 + \frac{3}{2}\frac{m_d \delta m}{m_b^2} + ..., \tag{54}$$

but they cancel in the total decay rate. Then, if the kinematical situation is such that only the ground state is produced, the total ratio R_{sl} would depart from 1 by $\frac{\frac{3}{2} m_d \delta m}{m_b^2}$. However, this effect is for t above the D** threshold $(M_B - M_{D^{**}})^2$, i.e. in a limited region of phase space. Hence, taking the ratio of this effect to the total rate, one gets:

$$\frac{\delta\Gamma}{\Gamma_{free}} \simeq \frac{3}{2}\frac{m_d \delta m}{m_b^2} \frac{\int_{(\delta m-\Delta)^2}^{(\delta m)^2} dt |\vec{q}\,|}{\int_0^{(\delta m)^2} dt |\vec{q}\,|} \simeq \frac{3}{2}\frac{m_d \delta m}{m_b^2} \left(\frac{2\Delta}{\delta m}\right)^{3/2}, \tag{55}$$

which is once more parametrically smaller by the factor $(\frac{2\Delta}{\delta m})^{3/2}$.

In conclusion, both effects are not $\mathcal{O}(1/m_Q)$ but much smaller. Thus the model dependent investigations of possible duality violations do not hint at any effect beyond the OPE of full QCD. In particular, taking into account the sum rules valid in full QCD allows us to show explicitly the absence of contributions at order $1/m_Q$, which would be a gross violation of OPE or, likewise, of duality.

2.3.5. Conclusion

All we currently know from purely theoretical considerations indicates that duality violations should be safely below one percent in the s.l. branching ratio. This is likely to remain in the noise of theoretical uncertainties due to higher order perturbative and non-perturbative ($O(1/m_b^3)$ and higher) corrections. Hence we will not assign additional uncertainty to the extraction of $|V_{cb}|$ from possible duality violation in inclusive decays. As discussed above, this picture will be tested through an intense program of high precision measurements in the near future, and most notably by the study of different moments of the s.l. distributions – even separately in the decays of B_d, B^- and B_s mesons.

2.4. Review and future prospects for the inclusive determination of $|V_{cb}|$

The value of the CKM matrix element $|V_{cb}|$ can be obtained by comparing the measured value of the b-quark s.l. decay partial width with its prediction in the context of the OPE. Experimentally, this partial width is obtained by measuring the inclusive s.l. decay rate of B-hadrons and their lifetime(s). Present measurements are rather accurate and experimental uncertainties lead to a relative error of about 1% on $|V_{cb}|$. The main limitation for a precise determination of $|V_{cb}|$ comes from theory, as the expression for the s.l. decay width depends on several poorly known parameters that are introduced by perturbative and non-perturbative QCD effects. Only recently, as discussed in Sec. 2.2., some of the non-perturbative parameters describing corrections of order $\mathcal{O}(1/m_b)$, $\mathcal{O}(1/m_b^2)$, and $\mathcal{O}(1/m_b^3)$ have been constrained experimentally. As a result, not only has the accuracy on $|V_{cb}|$ improved, but also a large fraction of the previous systematic uncertainty has changed nature.

In the following, we briefly summarize the main ingredients of the evaluation of $|V_{cb}|$ from inclusive b s.l. decay measurements. As discussed in Sec. 2.3., a possible violation of parton-hadron duality can be legitimately neglected at the present level of accuracy, and we will not include it in our estimate of the error associated with $|V_{cb}|$.

2.4.1. Perturbative QCD corrections

Using the pole mass definition for quark masses, the first order QCD perturbative corrections to the s.l. b-decay width have been given in [67,92] and dominant second order (BLM) corrections have been

obtained in [91]; the subdominant two-loop corrections have been estimated in [94]. The s.l. width can be written as

$$\Gamma(b\to c\ell\overline{\nu}_\ell)=\frac{G_F^2 m_b^5|V_{cb}|^2\mathcal{A}_{ew}}{192\pi^3}F(z)\left\{1-\frac{\alpha_s(m_b)}{\pi}\frac{2}{3}f(z)-\frac{\alpha_s^2}{\pi^2}\left[\beta_0\chi^{\rm BLM}(z)+\chi_0(z)\right]\right\}. \quad (56)$$

In this expression:

- the phase space factor $F(z)=1-8z+8z^3-z^4-12z^2\ln z$, with $z=m_c^2/m_b^2$, accounts for the mass of the final quark, and both m_c and m_b are pole masses;
- $\beta_0=11-\frac{2}{3}n_f$, where n_f is the number of active flavours;
- $\mathcal{A}_{ew}\simeq 1+2\frac{\alpha}{\pi}\ln\frac{m_Z}{m_b}$ and corresponds to the electroweak correction, cfr. Eq. (107) below;
- $f(x)=h(x)/F(x)$ with

$$\begin{aligned} h(x) &= -(1-x^2)\left(\frac{25}{4}-\frac{239}{3}x+\frac{25}{4}x^2\right)+x\ln x\left(20+90x-\frac{4}{3}x^2+\frac{17}{3}x^3\right)\\ &\quad +x^2\ln^2 x(36+x^2)+(1-x^2)\left(\frac{17}{3}-\frac{64}{3}x+\frac{17}{3}x^2\right)\ln(1-x)\\ &\quad -4(1+30x^2+x^4)\ln x\ln(1-x)-(1+16x^2+x^4)\left[6Li_2(x)-\pi^2\right]\\ &\quad -32x^{3/2}(1+x)\left[\pi^2-4Li_2(\sqrt{x})+4Li_2(-\sqrt{x})-2\ln x\ln\frac{1-\sqrt{x}}{1+\sqrt{x}}\right] \end{aligned} \quad (57)$$

  Numerical values for $f(x)$ can be found in [93] and are reported in Table 3.15.

$\frac{m_c}{m_b}$	0.	0.1	0.2	0.3	0.4	0.5	0.6	0.7	0.8	0.9	1
$f(\frac{m_c^2}{m_b^2})$	3.62	3.25	2.84	2.50	2.23	2.01	1.83	1.70	1.59	1.53	1.50

Table 3.15: *Values of $f(x)$ for several values of m_c/m_b.*

- $\chi^{\rm BLM}$, corresponding to the BLM corrections, is equal to 1.68 for $m_c/m_b=0.3$;
- χ_0, corresponding to the non-BLM corrections, is equal to -1.4 ± 0.4 for $m_c/m_b=0.3$.

The convergence of the perturbative series in Eq. (56) appears problematic. It has been demonstrated that this expansion can be much better controlled – within a few % – using a properly normalized short-distance mass [95,20]. This is the case, for instance, of the kinetic running mass* defined in Eq. (17). Replacing in Eq. (56) the pole quark masses by kinetic running masses through Eq. (17) and expanding in α_s, one obtains:

$$\Gamma(b\to c\ell\overline{\nu}_\ell)=\frac{G_F^2 m_b(\mu)^5|V_{cb}|^2\mathcal{A}_{ew}}{192\pi^3}F(z(\mu))\left[1+a_1(\mu)\frac{\alpha_s(m_b)}{\pi}+a_2(\mu)\left(\frac{\alpha_s(m_b)}{\pi}\right)^2\right], \quad (58)$$

where $z(\mu)=m_c^2(\mu)/m_b^2(\mu)$. A typical value for μ is 1 GeV. The explicit expressions for $a_{1,2}(\mu)$ can be found in [98,97].

2.4.2. Non-perturbative QCD corrections

Non-perturbative corrections in the OPE start at second order in $1/m_Q$ [2]. Including those of $O(1/m_b^2)$ [1,2] and $O(1/m_b^3)$ [63], and changing the scale at which α_s is evaluated to an arbitrary value q, Eq. (58)

*Other definitions for quark masses can be adopted, which do not suffer from problems attached to the pole mass definition, see Sec. 2.1.

becomes:

$$\Gamma(b\to c\ell\overline{\nu}_\ell)=\frac{G_F^2 m_b(\mu)^5|V_{cb}|^2\mathcal{A}_{ew}}{192\pi^3}\quad\left[1+b_1(\mu)\frac{\alpha_s(q)}{\pi}+b_2(\mu,q)\left(\frac{\alpha_s(q)}{\pi}\right)^2\right]\left\{F(z(\mu))\left(1-\frac{\mu_\pi^2}{2m_b^2(\mu)}\right)\right.$$
$$\left.-G(z(\mu))\frac{1}{2m_b^2(\mu)}\left(\mu_G^2-\frac{\rho_{LS}^3}{m_b(\mu)}\right)+H(z(\mu))\frac{\rho_D^3}{6m_b^3(\mu)}\right\}\qquad(59)$$

where $b_1(\mu)=a_1(\mu)$ and $b_2(\mu,q)=a_2(\mu)+a_1(\mu)\frac{\beta_0}{2}\ln\frac{q}{m_b}$, and where we have introduced the functions ($z=(m_c/m_b)^2$)

$$G(z)=3-8z+24z^2-24z^3+5z^4+12z^2\ln z,$$
$$H(z)=77-88z+24z^2-8z^3+5z^4+12(4+3z^2)\ln z.$$

A very recent analysis [97] contains a comprehensive discussion of all the aspects of the Γ_{sl} calculation and several improvements. In particular, it includes BLM corrections to all orders in the scheme with running kinetic masses and non-perturbative parameters. The effect of the resummed BLM corrections is small, 0.1% of the s.l. width, if compared to the perturbative corrections calculated in Eq. (59) at $q=m_b$. Ref. [97] also discusses the role played by four-quark operators containing a pair of charm quark fields in the higher orders of the OPE. These operators give in principle $O(1/m_b^3)$ contributions that are not necessarily negligible and require further study.

In the quark pole mass approach, quark masses are usually re-expressed in terms of heavy hadron masses, using the HQET relation of Eq. (37): the corresponding expression for the s.l. width can be found in [58] and is quoted below for completeness:

$$\Gamma(b\to c\ell\overline{\nu}_\ell)=\frac{G_F^2\overline{M}_B^5|V_{cb}|^2}{192\pi^3}0.3689\quad\left[1-1.54\frac{\alpha_s}{\pi}-1.43\beta_0\frac{\alpha_s^2}{\pi^2}-1.648\frac{\overline{\Lambda}}{\overline{M}_B}\left(1-0.87\frac{\alpha_s}{\pi}\right)\right.$$
$$-0.946\frac{\overline{\Lambda}^2}{\overline{M}_B^2}-3.185\frac{\lambda_1}{\overline{M}_B^2}+0.02\frac{\lambda_2}{\overline{M}_B^2}-0.298\frac{\overline{\Lambda}^3}{\overline{M}_B^3}-3.28\frac{\overline{\Lambda}\lambda_1}{\overline{M}_B^3}$$
$$+10.47\frac{\overline{\Lambda}\lambda_2}{\overline{M}_B^3}-6.153\frac{\rho_1}{\overline{M}_B^3}+7.482\frac{\rho_2}{\overline{M}_B^3}-7.4\frac{\mathcal{T}_1}{\overline{M}_B^3}+1.491\frac{\mathcal{T}_2}{\overline{M}_B^3}$$
$$\left.-10.41\frac{\mathcal{T}_3}{\overline{M}_B^3}-7.482\frac{\mathcal{T}_4}{\overline{M}_B^3}+\mathcal{O}\left(\frac{1}{\overline{M}_B^4}\right)\right]\qquad(60)$$

In this equation, $\overline{M}_B=\frac{M_B+3M_{B^*}}{4}=5.313$ GeV and the corresponding value for charmed mesons is taken to be equal to 1.975 GeV. The relations between the parameters used in the two formalisms have been recalled in Eq. (39). The value of μ_G^2 is strongly constrained by the mass splitting between B* and B mesons, for instance one finds $\mu_G^2(1\text{ GeV})=0.35^{+0.03}_{-0.02}$ GeV^2 [72]. For the other non-perturbative parameters one has to rely on theoretical estimates. Alternately, they can be constrained by measuring other observables: as explained in Sec. 2.2., the moments of differential distributions in b-hadron s.l. decays and the moments of the photon energy distribution in $b\to s\gamma$ decays depend on the same parameters that enter the $|V_{cb}|$ determination. Measurements of these quantities can therefore be used to determine the OPE parameters and to verify the overall consistency of the formalism.

2.4.3. $|V_{cb}|$ determination

The value for $|V_{cb}|$ is obtained by comparing the theoretical and experimental determinations of the inclusive s.l. decay partial width:

$$\Gamma_{sl}|_{th}=\text{BR}_{sl}|_{exp}\times\tau_b|_{exp}\qquad(61)$$

In PDG2000 [99], the uncertainty attached to $|V_{cb}|$ was of $O(5\%)$ and was dominated by the theoretical uncertainty related to the heavy quark parameters. Using the analysis of the first hadronic moment and

the first moment of the photon energy distribution in $b \to s\gamma$ decays mentioned in Sec. 2.2., together with Eq. (60), CLEO has obtained [58]:

$$|V_{cb}| = 40.4 \times (1 \pm 0.022|_{exp} \pm 0.012|_{\overline{\Lambda},\lambda_1} \pm 0.020|_{th}) \times 10^{-3} \tag{62}$$

The first uncertainty corresponds to the experimental measurements of the s.l. branching fraction, of the B_d^0 and B^+ fractions as obtained by CLEO, and of the B_d^0 and B^+ lifetimes given in PDG2000. The second uncertainty corresponds to the errors on $\overline{\Lambda}$ and λ_1 in the analysis of the moments. The last uncertainty corresponds to the remaining theoretical error coming from contributions of $\mathcal{O}(1/m_b^3)$ and higher order perturbative corrections, estimated from the uncertainty on the scale at which α_s has to be evaluated [†]. It appears that the corresponding variation of $\alpha_s = 0.22 \pm 0.05$ gives the largest contribution (± 0.017). Remaining contributions to the theory error have been obtained by varying the values of parameters contributing at $\mathcal{O}(1/m_b^3)$ within $\pm(0.5)^3$ GeV^3, a rather arbitrary range, based only on naive dimensional analysis.

CLEO's result on $|V_{cb}|$ was improved, at the Workshop, mainly by using all experimental measurements on b-hadron s.l. branching fraction and lifetime [101]. Recent experimental results, made available at the ICHEP 2002 Conference in Amsterdam, and obtained by the LEP experiments [102], by BaBar [103] and by BELLE [104] have been combined [105], including previous measurements of these quantities given in [106]:

$$\begin{aligned}
\Gamma_{sl}|_{\Upsilon(4S)}(b \to X_c \ell^- \overline{\nu}_\ell) &= 0.431 \times (1 \pm 0.019 \pm 0.016) \times 10^{-10}\ \text{MeV} \\
\Gamma_{sl}|_{LEP}(b \to X_c \ell^- \overline{\nu}_\ell) &= 0.438 \times (1 \pm 0.024 \pm 0.015) \times 10^{-10}\ \text{MeV} \\
\Gamma_{sl}|_{Average}(b \to X_c \ell^- \overline{\nu}_\ell) &= 0.434 \times (1 \pm 0.018) \times 10^{-10}\ \text{MeV}
\end{aligned} \tag{63}$$

In these expressions the second contribution to the errors corresponds to uncertainties in the decay modelling and in the subtraction of the $b \to u\ell^-\overline{\nu}_\ell$ component. Using the above result, the corresponding uncertainty in Eq. (62) can be reduced by about a factor two. Keeping the same values for the two remaining uncertainties and correcting for the slightly different central values of BR_{sl} and τ_b, one finds

$$|V_{cb}| = 40.7 \times (1 \pm 0.010|_{exp} \pm 0.012|_{\overline{\Lambda},\lambda_1} \pm 0.020|_{th}) \times 10^{-3} \tag{64}$$

This approach was adopted to obtain the value of $|V_{cb}|$ quoted in the corresponding mini-review [107] of PDG2002 [106][‡]. However, the result quoted in the main CKM section of the PDG2002, $|V_{cb}| = (41.2 \pm 2.0) \times 10^{-3}$, does not take into account this progress, and still assigns a large uncertainty of 2.0×10^{-3}, which is meant to account for possible parton-hadron duality violation.

As summarized in Sec. 2.2., progress has been achieved soon after the Workshop both on theoretical and experimental aspects of the $|V_{cb}|$ determination. On the theoretical side, the moments of the s.l. distributions have been studied using schemes that avoid the problems related to the pole mass [64,65,71]. The inclusion of higher order moments has been reconsidered in [71,65] and, as we have seen, some of the corresponding measurements have been used in these analyses. On the experimental side, new measurements of moments have been presented by BaBar [78], CLEO [75,77], and DELPHI [59].

The analysis of [65] employs first, second, and truncated moments to fit the values of the $\overline{\Lambda}$, λ_1 parameters and obtain constraints on $\mathcal{O}(1/m_b^3)$ contributions. Four different definitions of the heavy quark masses have also been considered. A consistent picture for inclusive b-hadron s.l. decays is obtained when theoretical uncertainties are taken into account, especially if the BaBar preliminary data [78] are excluded. Using the average given in Eq. (63), the result of [65] for $|V_{cb}|$ in the 1S scheme is

$$|V_{cb}| = (41.2 \pm 0.9) \times 10^{-3}. \tag{65}$$

[†] In that analysis the range is taken to be $[m_b/2,\ 2m_b]$.

[‡] In PDG2002, the value given in the corresponding mini-review for $|V_{cb}| = (40.4 \pm 0.5 \pm 0.5 \pm 0.8) \times 10^{-3}$ is slightly different as it depends on the values of experimental results available at that time.

In the analysis of Ref. [71], which is based on DELPHI data and includes third order moments, the low-scale running mass approach is used to extract μ_π^2 and the two parameters contributing at order $\mathcal{O}(1/m_b^3)$. Neither the moments nor $|V_{cb}|$ are actually sensitive to ρ_{LS}^3. The other parameter appearing at this order, $\rho_D^3 = (0.05 \pm 0.05)\ \mathrm{GeV}^3$, is found to be in good agreement with some theoretical expectation (about 0.1 GeV^3 [72]). In the low-scale running mass scheme the uncertainty related to the scale at which α_s is computed has also been reduced with respect to the pole mass analysis. Employing the average s.l. width given in Eq. (63), the result of Ref. [71] is

$$|V_{cb}| = 41.7 \times (1 \pm 0.010|_{exp} \pm 0.015|_{m_b,m_c,\mu_\pi^2,\mu_G^2,\rho_D^3,\rho_{LS}^3} \pm 0.010|_{pert\ QCD} \pm 0.010|_{th}) \times 10^{-3}. \quad (66)$$

The last two uncertainties in this equation are theoretical and correspond to the scale ambiguity for α_s and to possible contributions from $\mathcal{O}(1/m_b^4)$ terms for which an upper limit corresponding to the contribution of the previous order term has been used. The above estimate of the overall theoretical error agrees well with that of [97].

All the results presented in this Section are preliminary. They indicate a promising future for the approach where all non-perturbative parameters, up to order $\mathcal{O}(1/m_b^3)$, are experimentally constrained. Only the preliminary BaBar analysis [78] does not seem to fit the picture: it seems difficult to reconcile the dependence of BaBar first hadronic moment on the lepton momentum cut with the other measurements in the context of the OPE. Although a high lepton momentum cut could in principle spoil the convergence of the power expansion, this point definitely needs to be fully understood.

2.4.4. Prospects

Impressive improvements have been obtained in the determination of $|V_{cb}|$ from inclusive b-hadron s.l. decay measurements during and just after this Workshop. The moments in inclusive s.l. and radiative decays have been studied in new theoretical frameworks. Preliminary analyses of recent experimental measurements of such moments indicate that all parameters contributing to $\mathcal{O}(1/m_b^3)$ included can be constrained by experiment. The results for $|V_{cb}|$ in Eqs. (65) and (66) are very similar. We can adopt a central value given by their average with a 2.3% accuracy:

$$\boxed{|V_{cb}| = 41.4 \cdot (1 \pm 0.018|_{exp} \pm 0.014|_{th}) \times 10^{-3}\ .} \quad (67)$$

in which the largest fraction of the uncertainty depends on experimental measurements. These analyses have to be confirmed, as most of them correspond to preliminary results, and the possible discrepancy raised by BaBar data has to be investigated, especially with respect to the impact of the lepton energy cut, by lowering the cut as much as possible. If the present picture remains valid, more effort has to be invested in the control of remaining theoretical errors, namely $i)$ the uncertainty related to the truncation of the perturbative QCD expansion and $ii)$ the importance of four-quark operators containing the charm quark and of $\mathcal{O}(1/m_b^n),\ n \geq 4$ corrections.

2.5. Review and future prospects for the inclusive determination of $|V_{ub}|$

The charmless s.l. decay channel $b \to u\ell\bar{\nu}$ can in principle provide a clean determination of $|V_{ub}|$ along the lines of that of $|V_{cb}|$. The main problem is the large background from $b \to c\ell\bar{\nu}$ decay, which has a rate about 60 times higher than that for the charmless s.l. decay. The experimental cuts necessary to distinguish the $b \to u$ from the $b \to c$ transitions enhance the sensitivity to the non-perturbative aspects of the decay, like the Fermi motion of the b quark inside the B meson, and complicate the theoretical interpretation of the measurement.

The inclusive decay rate $\mathrm{B} \to X_u\ell\bar{\nu}$ is calculated using the OPE. At leading order, the decay rate is given by the parton model decay rate. As we have seen, non-perturbative corrections are suppressed by at least two powers of $1/m_b$ and to $O(1/m_b^2)$ they are parameterized by the two universal matrix elements

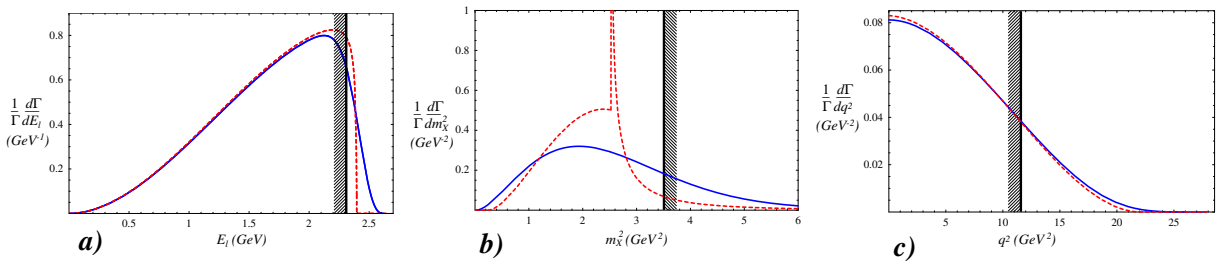

Fig. 3.5: *The distribution of the three main discriminating variables in inclusive* $\mathrm{B} \to X_u \ell \bar{\nu}$ *analyses: lepton energy* E_ℓ *(left), hadronic invariant mass* M_X^2 *(center) and di-lepton invariant mass* q^2 *(right), as given by* $O(\alpha_s)$ *parton level decay (dashed curves), and including the Fermi motion model (solid curves) with typical parameters. The vertical line marks the cut necessary to eliminate the* $b \to c$ *transitions in each case.*

μ_π^2 and μ_G^2 (or λ_1 and λ_2), see Sec. 1.1. At $O(1/m_b^3)$, the Darwin term ρ_D^3 reduces $\Gamma(\mathrm{B} \to l\nu X_u)$ by 1 - 2 %. Perturbative corrections are known through order α_s^2 [108]. All this allows to relate the total inclusive decay rate directly to $|V_{ub}|$ [109]

$$|V_{ub}| = 0.0040 \times (1 \pm 0.03|_{m_b} \pm 0.025|_{QCD}) \left(\frac{\mathrm{BR}(\mathrm{B} \to l\nu X_u)}{0.0016}\right)^{\frac{1}{2}} \left(\frac{1.55 \text{ ps}}{\tau_B}\right)^{\frac{1}{2}} \tag{68}$$

where in the second error both perturbative and non-perturbative uncertainties are included. The uncertainty due to the b mass assumes $\delta m_b \sim 60$ MeV and can easily be rescaled to accommodate the error in Eq. (26). The errors reported in Eq. (68) are very similar to those given in [25]. In fact, despite the use of slightly different inputs, and of different formalisms, the results of Refs. [109] and [25] are remarkably consistent, their central values differing by only 1.7%. Information from the moments of the s.l. distributions is unlikely to decrease significantly the overall uncertainty in Eq. (68).

The large background from $\mathrm{B} \to X_c \ell \bar{\nu}$ makes the direct measurement of the inclusive rate a very challenging task. In principle, there are several methods to suppress this background and all of them restrict the phase space region where the decay rate is measured. Hence, great care must be taken to ensure that the OPE is valid in the relevant phase space region.

There are three main kinematical cuts which separate the $b \to u\ell\bar{\nu}$ signal from the $b \to c\ell\bar{\nu}$ background:

1. A cut on the lepton energy $E_\ell > (M_B^2 - M_D^2)/2M_B$ [110]
2. A cut on the hadronic invariant mass $M_X < M_D$ [111]
3. A cut on the leptonic invariant mass $q^2 > M_B^2 - M_D^2$ [112]

These cuts correspond to about 10%, 80% and 20% respectively of the signal selected. The simplest kinematical discriminator for $b \to u$ versus $b \to c$ is the endpoint in the ℓ inclusive spectrum, where the first evidence for $|V_{ub}| \neq 0$ was seen [110]. However, in this case the remaining phase space is characterized by $\Delta E_\ell = M_D^2/2M_B = 320$ MeV $\sim \Lambda_{QCD}$. Because of this cut on the lepton energy, the selected hadronic system has large energy and small invariant mass, and is placed in a kinematic region where the OPE is not expected to converge. Measurements done using this method have given [110] $|V_{ub}|/|V_{cb}| = (0.08 \pm 0.02)$, where the 25% error is dominated by the theoretical uncertainty.

In the original analyses [110] several models [113,114] were used to estimate the rate at the endpoint. In fact, the exact fraction of signal decays selected depends strongly on a *shape function*, as illustrated in Fig. 3.5, where the spectrum in the parton model is compared to the one including the structure function. Physically, the *shape or structure function* (sometimes also called light-cone distribution function) encodes the Fermi motion of the b quark inside the B meson, which is inherently

non-perturbative. To estimate the effect of the structure function on the rate measured in the endpoint region, several models for the shape function have been constructed. They are constrained by the values of the first few moments of the shape function, which are related to physical quantities like m_b and $\mu_\pi^2 \sim -\lambda_1$ [115–117]. The model dependence of the measurement can be reduced by noting that the shape function, like the Fermi motion inside the meson, is a universal property of the B meson, independent of the decay process. Consequently, the shape function can in principle be extracted from a different $\mathrm{heavy} \to \mathrm{light}$ process and then employed in the inclusive $\mathrm{B} \to X_u \ell \bar{\nu}$ decay [116–118]. The best way is to use the $\mathrm{B} \to X_s \gamma$ decay. At leading order in $1/m_b$ and α_s, the photon spectrum in the radiative decay is proportional to the light cone distribution function. This strategy for determining $|V_{ub}|$ has three main drawbacks:

- The b quark distribution function is the same in $\mathrm{B} \to l\nu X_u$ and $\mathrm{B} \to \gamma X_s$ only at leading order in $1/m_b$ and in α_s; perturbative QCD corrections complicate its extraction [119,120];
- There are process specific corrections of order $1/m_b$ which still need to be evaluated reliably. In Ref. [121] it is argued that these corrections could be quite sizeable. Even after a precise measurement of the photon spectrum there are unknown and not-calculable contributions $\sim \mathcal{O}(1/m_b)$ in $\mathrm{B} \to l\nu X_u$ which could spoil the accurate extraction of $|V_{ub}|$. It has also been pointed out [122] that there are contributions of dimension six operators, suppressed by $1/m_b^3$, but enhanced by a phase space factor of $16\pi^2$. They arise from so called *weak annihilation* (WA) contributions, and their total contribution survives any cut used to reject the $b \to c\ell\nu$ background. The size of WA contributions is hard to estimate, as very little is known about the values of the relevant four-quark operator matrix elements. They could in principle be constrained by a comparison of B^0 and $\mathrm{B}^\pm$ decay rates. While their impact on the integrated width is modest ($\lesssim 2\%$), in the endpoint region WA terms could give effects of up to 20% [123]. This conclusion, however, is challenged in [124], according to which the uncertainty induced by subleading shape functions is safely below 10%, for lepton energy cuts $E_\ell \leq 2.2$ GeV. See also [118].
- Finally, the endpoint region represents such a narrow slice of the phase space that may be vulnerable to violations of *local* parton-hadron duality.

The first analysis combining $\mathrm{B} \to l\nu X_u$ and $\mathrm{B} \to \gamma X_s$ was performed by CLEO [125]. To account for the distortion of the endpoint spectrum due to the motion of the B mesons, the initial state radiation and the experimental resolution, CLEO fit for the observed data using a theoretical momentum spectrum to model these distortions. They find

$$|\mathrm{V_{ub}}| = (4.12 \pm 0.34 \pm 0.44 \pm 0.23 \pm 0.24) \times 10^{-3}$$

in the lepton momentum range 2.2–2.6 GeV/c. Here the first error combines statistical and experimental uncertainty on the measured rate, the second error is the uncertainty on the fraction of leptons within the acceptance, derived from the uncertainty in the $b \to s\gamma$ shape function, the third error is the theoretical uncertainty on the extraction of $|V_{ub}|$ from the total rate, the fourth error is an estimate of the uncertainty that results from the unknown power corrections in applying the $b \to s\gamma$ shape function to $b \to u\ell\nu$. To evaluate this last uncertainty, the parameters of the shape function are varied by the expected order of the corrections: $\Lambda_{QCD}/M_B \approx 10\%$. Clearly, this sets only the *scale* of that uncertainty.

In principle, the hadronic recoil mass provides the single most efficient kinematical discriminator against the $b \to c\ell\nu$ background. The $b \to c\ell\nu$ background is separated from the signal imposing $M_X < M_D$. After this cut, more than 80% of the signal survives. However, due to the experimental resolution, the $b \to c\ell\nu$ transitions contaminate the $M_X < M_D$ region, and therefore either the cut is lowered, or a different strategy has to be employed. When the cut on the hadronic recoil mass is used, the main theoretical issue arises from the knowledge of the fraction of $b \to u\ell\nu$ events with M_X below a given cut-off mass, M_{cut}:

$$\Phi_{SL}(M_{\mathrm{cut}}) \equiv \frac{1}{\Gamma(B \to l\nu X_u)} \int_0^{M_{\mathrm{cut}}} dM_X \frac{d\Gamma}{dM_X}$$

where $\Phi(0) = 0$ and $\Phi(M_B) = 1$. The M_X spectrum is in fact sensitive to the values of the HQE parameters m_b, μ_π^2, etc. It also depends on the heavy quark shape function, although the dependence is weaker than for the lepton energy in the endpoint region. To set the scale of the problem: a very rough estimate for $\Phi_{SL}(1.7\ \mathrm{GeV})$ lies between 0.55 and 0.9; i.e. a measurement of $\Phi_{SL}(1.7\ \mathrm{GeV})$ yields a value for $|V_{ub}|$ with *at most* a $\pm 12\%$ uncertainty, and possibly less. The actual uncertainty in realistic experimental analyses has been estimated by the experimental collaborations. Since a cut on the hadronic invariant mass allows for a much larger portion of the decay rate to survive, the uncertainties from weak annihilation contributions are safely below the 5% level. The subleading shape functions contributions can in this case be analysed using the same method as in [121]. A preliminary discussion can be found in [118].

The above observations motivated an intense effort to measure $|V_{ub}|$ using inclusive analyses at LEP, where B hadrons are produced with a large and variable momentum and in most of the cases the B decay products are contained into narrow jets in $Z^0 \to b\bar{b}$ events. These characteristics make the LEP measurements complementary to the ones at the $\Upsilon(4S)$. All four LEP experiments have provided a measurement of $|V_{ub}|$ using inclusive methods, although the actual procedures differ significantly.

DELPHI [126] perform an inclusive reconstruction of the hadronic mass of the system emitted together with the lepton in the B hadron decay. The B s.l. sample is split into $b \to u\ell\nu$ enriched and depleted samples based on the separation between tertiary and secondary vertices (taking advantage of the finite charm lifetime) and on the presence of tagged kaons in the final state. The mass of the hadronic system M_X is used to subdivide further the sample into a $b \to X_u\ell\nu$–favoured region ($M_X < 1.6$ GeV) and a $b \to X_c\ell\nu$–dominated region. The signal is extracted from a simultaneous fit to the number of decays classified according to the four different categories and the distributions of the lepton energy in the reconstructed B rest frame.

The leptonic invariant mass, $q^2 = (p_\ell + p_\nu)^2$, can also suppress the $b \to c$ background [112]. This cut allows to measure $|V_{ub}|$ without requiring knowledge of the structure function of the B meson (see Fig. 3.5c). The acceptance of this cut on q^2 can be calculated using the usual local OPE. Depending on the value of the cut, the fraction of selected signal events can range between 10 and 20%, but the theoretical uncertainty on $|V_{ub}|$, dominated by higher order power corrections, can range from 15% for $q^2_{\mathrm{cut}} = M_B^2 - M_D^2 = 11.6\,\mathrm{GeV}^2$ to 25% for $q^2_{\mathrm{cut}} = 14\,\mathrm{GeV}^2$ (see also [127]). The q^2 method allows to measure $|V_{ub}|$, albeit with larger uncertainties than when one combines the lepton energy or the hadron invariant mass cut with data from $\mathrm{B} \to X_s\gamma$ decay.

Recently, a strategy relying on the combination of q^2 and M_X cuts has been proposed [128]. The M_X cut is used to reject the charm background, while the q^2 cut is used to eliminate the high energy, low invariant mass region. Rejecting the region at small q^2 reduces the impact of the shape function in the M_X analysis. Strong interaction effects on M_X are maximal there due to the significant recoil [128]. Imposing, for instance, $q^2 \geq 0.35 m_b^2$ eliminates the impact of the primordial Fermi motion encoded in $M_X < 1.7$ GeV events. Up to 50% of all $\mathrm{B} \to X_u\ell\bar{\nu}$ events survive this cut, making possible to measure $|V_{ub}|$ with uncertainties safely below the 10% level.

CLEO has presented the first experimental attempt to implement this method [129]. The analysis is based on a full fit to $q^2/(E_\ell + E_\nu)^2$, M_X and $\cos\theta_{W\ell}$. Models are needed to extract the sample composition and to relate the regions of higher sensitivity and theoretically safer to the inclusive charmless s.l. branching fraction. However, imposing these additional cuts has drawbacks. The overall energy scale governing the intrinsic hardness of the reaction gets smaller since it is driven at large q^2 by $m_b - \sqrt{q^2}$ rather than m_b. This enhances the impact of higher-order contributions which are not calculated, like in the case of the direct cut on q^2. Furthermore, cutting simultaneously on M_X and q^2 decreases the fraction of the full width retained in the sample, and exposes the calculation to violations of duality. Finally, the cut on q^2 removes the possibility to incorporate in full the constraints on the spectrum which follow from the properties of the shape function, because it dissolves the connection between the M_X spectrum and the shape function.

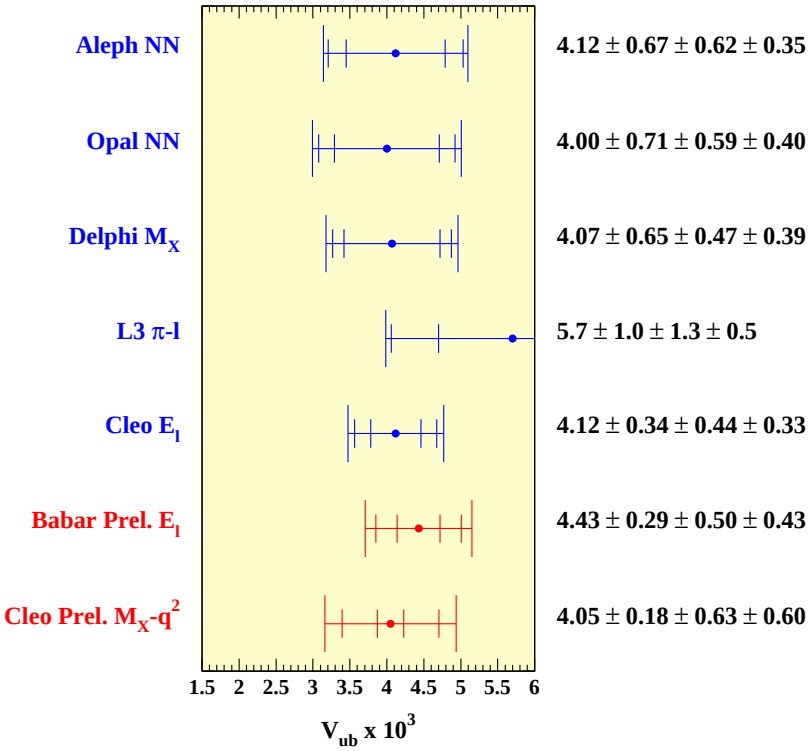

Fig. 3.6: *Summary of the inclusive determinations of* $|V_{ub}|$.

Yet another approach has been followed by the ALEPH and OPAL collaborations in their analyses [130]. They use neural networks, which input a large number of kinematic variables (20 in ALEPH, 7 in OPAL) to discriminate between the $b \to c\ell\nu$ and the $b \to u\ell\nu$ decays. In both experiments, the signal is extracted from a fit to the network output, restricted to a region enriched in signal events. The observation of s.l. $b \to u\ell\nu$ decays at LEP has been very challenging. These analyses pioneered new approaches for extracting $|V_{ub}|$. Their main drawback is the S/B ratio, that requires the control of the background level to better than 5% . Concerns, discussed within the community, include the modelling of the uncertainties on the non-D and D* components of the background from B decays, the modelling of the $\mathrm{B_s}$ and b-baryon s.l. decays and the estimation of the $b \to u\ell\nu$ modelling uncertainties due to the uneven sampling of the decay phase space.

Since tight selections are needed to extract the signal, the effects of these experimental cuts trimming the inclusive distributions must be understood. In particular, it is important to make sure the the inclusive analyses are probing the selected phase space in an even and uniform way. Neural network analyses bias the phase space toward the region of large E_ℓ and low M_X, where the signal-to-background ratio is larger. The uncertainty quoted by ALEPH accounts for the range of models tested. In this case, it would be desirable to test more unbiased methods. DELPHI, on the other hand, has shown that the M_X analysis has a reasonably uniform sensitivity in the M_X-E_ℓ plane and a recent CLEO analysis, repeated for different sets of M_X-q^2 selections, finds results compatible with LEP.

Finally, L3 applies a sequential cut analysis using the kinematics of the lepton and of the leading hadron in the same jet for discrimination of the signal events [131]. The uncertainty (see Fig. 3.6) is larger than in other analyses, mainly because the result depends on a few exclusive final states only.

All the analyses discussed in this Section have an individual accuracy of about 15% and, as can be seen in Fig. 3.6, their central values agree within that uncertainty. One can distinguish two sets of inclusive determinations of $|V_{ub}|$ which rely on roughly the same theoretical assumptions and are extracted within the same OPE framework. The LEP inclusive results have been averaged accounting for correlated systematics. The uncertainty of the CLEO determination from the lepton end-point and the

$b \to s\gamma$ spectrum can be re-expressed in a way corresponding to that used for the LEP averaging. The results read

$$\boxed{\begin{array}{l} |V_{ub}|^{incl}_{LEP} = [4.09^{+0.36\ +0.42\ +0.24}_{-0.39\ -0.47\ -0.26} \pm 0.21] \times 10^{-3}, \\ |V_{ub}|^{incl}_{CLEO} = [4.08 \pm 0.44 \pm 0.27 \pm 0.33 \pm 0.21] \times 10^{-3}, \end{array}} \tag{69}$$

where the first error corresponds to statistical and experimental systematics, the second to the dominant $b \to c$ background, the third to $b \to u$ modelling, and the last one to the relation between $|V_{ub}|$ and the branching fraction, see Eq. (68). A first exercise aimed at understanding the relationship between the different sources of systematics in these determinations and to obtain a global average was started at the workshop. A conservative approach consists in taking the systematic uncertainties as fully correlated. This combined result has a total uncertainty of $\pm 14\%$ and is used in Chapter 5 (see Table 5.1). However, the uncertainties are only partly correlated and more precise measurements are becoming available: once the systematics and their correlation are better understood there is room for considerable improvement.

As the B factories start focusing on the inclusive measurements of $|V_{ub}|$, there is potential for considerable progress. A more precise evaluation of the $b \to s\gamma$ photon spectrum will lead to a more precise effective shape function and we now have several methods to employ it efficiently in the extraction of $|V_{ub}|$. A recent proposal [132], for instance, uses the s.l. differential distribution in M_X/E_X together with the $b \to s\gamma$ photon spectrum to build a short distance ratio from which $|V_{ub}|/|V_{cb}|$ can be extracted, testing at the same time some of the underlying assumptions. The use of event samples with one fully reconstructed B will reduce the contamination from $b \to c\ell\bar{\nu}$ decays in the reconstruction of the hadronic recoil mass and of q^2 and will allow for useful cross-checks [133]. Hence, experimental uncertainties should be reduced. If the various methods will give consistent central values while their precision improves, we will be confident that theoretical uncertainties are not biasing $|V_{ub}|$ beyond the level of precision which has been reached in the individual measurements.

3. Exclusive determination of $|V_{cb}|$

As we have seen in the previous section, inclusive $b \to c$ semileptonic (s.l.) decay rates have a solid description via the OPE. Exclusive s.l. decays have a similarly solid description in terms of heavy-quark effective theory (HQET). The main difference is that the non-perturbative unknowns in the inclusive rates can be determined from experimental measurements, while those arising in exclusive rates must be calculated. Thus, there is a major theoretical challenge here as non-perturbative QCD calculations have to performed. Experimentally, the D and D* mesons have to be reconstructed using several decay channels, to gain in statistics, and the signal has to be isolated from higher excited states. Moreover, the theory is under best control at the kinematic endpoint, where the rate vanishes. Consequently, not only must the differential decay rate be measured, it also must be extrapolated to the endpoint. Despite these experimental difficulties, and given the ongoing progress in lattice QCD, these channels provide a valuable cross-check at present and hold considerable promise for the future.

The exclusive determination of $|V_{cb}|$ is obtained by studying $\mathrm{B} \to \mathrm{D}^*\ell\nu$ and $\mathrm{B} \to \mathrm{D}\ell\nu$ decays, where ℓ stands for either e or μ. The differential rates for these decays are given by

$$\begin{aligned} \frac{d\Gamma(\mathrm{B} \to \mathrm{D}^*\ell\nu)}{dw} &= \frac{G_\mu^2 |V_{cb}|^2}{48\pi^3} \eta_{\mathrm{EW}}^2 \, (M_B - M_{D^*})^2 \, M_{D^*}^3 (w^2-1)^{1/2} (w+1)^2 \\ &\quad \times \left[1 + \frac{4w}{w+1} \, \frac{1 - 2w\, r_* + r_*^2}{(1-r_*)^2} \right] |\mathcal{F}(w)|^2 \,, \end{aligned} \tag{70}$$

$$\frac{d\Gamma(\mathrm{B} \to \mathrm{D}\ell\nu)}{dw} = \frac{G_\mu^2 |V_{cb}|^2}{48\pi^3} \eta_{\mathrm{EW}}^2 \, (M_B + M_D)^2 \, M_D^3 (w^2-1)^{3/2} |\mathcal{G}(w)|^2 \,, \tag{71}$$

where $w = v_B \cdot v_{D^{(*)}}$ is the product of the velocities of the initial and final mesons, and $r_* = M_{D^*}/M_B$. The velocity transfer is related to the momentum q transferred to the leptons by $q^2 = M_B^2 - 2wM_BM_{D^{(*)}} + M_{D^{(*)}}^2$, and it lies in the range $1 \leq w < (M_B^2 + M_{D^{(*)}}^2)/2M_BM_{D^{(*)}}$. Electroweak radiative corrections introduce the muon decay constant $G_\mu = 1.1664 \times 10^{-5}$ GeV^{-2} (instead of G_F) and the factor $\eta_{\rm EW}^2$ (see Sec. 3.4.).

In the heavy-quark limit, the form factors $\mathcal{F}(w)$ and $\mathcal{G}(w)$ coincide with the Isgur-Wise function $\xi(w)$, which describes the long-distance physics associated with the light degrees of freedom in the heavy mesons [8,9]. This function is normalized to unity at zero recoil, corresponding to $w = 1$. There are corrections to heavy-quark limit from short distances, which can be calculated in perturbation theory in $\alpha_s(\sqrt{m_c m_b})$. There are also corrections from long distances, which are suppressed by powers of the heavy quark masses. The separation of the two sets of contributions can be achieved with HQET, which is reviewed, for example, in [12,13]. The calculation of the small corrections to this limit is explained below in Secs. 3.2. and 3.3. With a satisfactory calculation of these corrections, $|V_{cb}|$ can be determined accurately by extrapolating the differential decay rates to $w = 1$, yielding $|V_{cb}|\mathcal{F}(1)$ and $|V_{cb}|\mathcal{G}(1)$. Uncertainties associated with this extrapolation can be reduced using model-independent constraints on the shape of the form factors, derived with dispersive methods. These techniques are briefly reviewed in Sec. 3.1.

At present $\mathrm{B} \to \mathrm{D}^*\ell\nu$ transitions yield a more precise value of $|V_{cb}|$ than $\mathrm{B} \to \mathrm{D}\ell\nu$. The statistics are three times higher. More importantly, phase space suppresses $\mathrm{B} \to \mathrm{D}^*\ell\nu$ by only $(w-1)^{1/2}$, but $\mathrm{B} \to \mathrm{D}\ell\nu$ by $(w-1)^{3/2}$. Finally, the theoretical calculation of $\mathcal{F}(1)$ is under better control than that of $\mathcal{G}(1)$. Nevertheless, $\mathrm{B} \to \mathrm{D}\ell\nu$ provides a useful check. For example, $|V_{cb}|$ drops out of the (experimental) ratio $|V_{cb}|\mathcal{F}(1)/|V_{cb}|\mathcal{G}(1)$, which can be used to test the theoretical calculations.

3.1. Theory-guided extrapolation in w

Dispersive methods allow the derivation of rigorous, model-independent constraints on the form factors in exclusive s.l. or radiative decays. The derivation is based on first principles: the analyticity properties of two-point functions of local current operators and the positivity of the corresponding hadronic spectral functions. Analyticity relates integrals of these spectral functions to the behaviour of the two-point functions in the deep Euclidean region, where they can be calculated using the operator product expansion. Positivity guarantees that the contributions of the states of interest to these spectral functions are bounded from above. Constraints on the relevant form factors are then derived, given the latter's analyticity properties. The beauty of these techniques is that the bounds can be improved with information about the form factors, such as their value or derivatives at different kinematic points, or their phase along various cuts. These techniques also have the advantage that the constraints they yield are optimal for any given input.

Here we focus on the application of these methods to $\mathrm{B} \to \mathrm{D}^{(*)}\ell\nu$ decays. The first such application was carried out in [136], where three-parameter descriptions of the corresponding differential decay rates were presented. In [137], it was shown how a judicious change of variables can be used to reduce the number of parameters. The most recent analyses [138,139] take two-loop and non-perturbative corrections to the relevant two-point correlators into account and make use of heavy-quark spin symmetry in the ground-state doublets $(\mathrm{B}, \mathrm{B}^*)$ and $(\mathrm{D}, \mathrm{D}^*)$. Ref. [139] uses spin symmetry more extensively, and accounts for the dominant $1/m_Q$ and radiative corrections. The results are one-parameter descriptions of the form factors $\mathcal{G}(w)$ and $A_1(w) = \mathcal{F}(w)/\mathcal{K}(w)$, with $\mathcal{K}(w)$ defined below in Eq. (73), that are accurate to better than 2% over the full kinematic range.

In the case of $\mathrm{B} \to \mathrm{D}^*\ell\nu$ transitions, it is convenient to constrain the form factor $A_1(w)$ instead of $\mathcal{F}(w)$ in order to avoid large, kinematically enhanced corrections to the heavy-quark limit. This yields

for $\mathcal{F}(w)$ [139]:

$$\frac{\mathcal{F}(w)}{\mathcal{F}(1)} \approx \mathcal{K}(w) \left\{ 1 - 8\rho^2_{A_1} z + (53.\rho^2_{A_1} - 15.)z^2 - (231.\rho^2_{A_1} - 91.)z^3 \right\} , \tag{72}$$

with z given in Eq. (76) and where the only parameter, the slope parameter $\rho^2_{A_1}$ of $A_1(w)$ at zero recoil, is constrained by the dispersive bounds to lie in the interval $-0.14 < \rho^2_{A_1} < 1.54$. This constraint on $\rho^2_{A_1}$ is somewhat weaker than the one derived from the inclusive heavy-quark sum rules of Bjorken [143] and Voloshin [144] which require $0.4 \leq \rho^2_{A_1} \leq 1.3$ once $O(\alpha_s)$ corrections have been included [145]. A stronger lower bound has been derived by Uraltsev [146]. This is to be compared with the world experimental average $\rho^2_{A_1} = 1.50 \pm 0.13$ given in Sec. 3.6.1.

In Eq. (72), the function $\mathcal{K}(w)$ is

$$\mathcal{K}(w)^2 = \frac{2\,\dfrac{1 - 2wr_* + r_*^2}{(1-r_*)^2} \left[1 + \dfrac{w-1}{w+1}\, R_1(w)^2 \right] + \left[1 + \dfrac{w-1}{1-r_*} \Big(1 - R_2(w) \Big) \right]^2}{1 + \dfrac{4w}{w+1}\, \dfrac{1 - 2wr_* + r_*^2}{(1-r_*)^2}} , \tag{73}$$

where r_* is given after Eq. (71), and $R_1(w)$ and $R_2(w)$ describe corrections to the heavy-quark limit. They are usually expanded in Taylor series around $w = 1$. Using QCD sum rules [140,141,142] one finds [139]

$$\begin{aligned} R_1(w) &\approx 1.27 - 0.12(w-1) + 0.05(w-1)^2 , \\ R_2(w) &\approx 0.80 + 0.11(w-1) - 0.06(w-1)^2 . \end{aligned} \tag{74}$$

The sum-rule calculation is supported by measurements reported by the CLEO Collaboration [188], $R_1(1) = 1.18 \pm 0.30 \pm 0.12$ and $R_2(1) = 0.71 \pm 0.22 \pm 0.07$. These values are obtained assuming that $R_1(w)$ and $R_2(w)$ are constant in w and that $A_1(w)$ is linear in w. CLEO also find that $R_1(1)$ and $R_2(1)$ are not sensitive either to the form of $A_1(w)$ or the w dependence of the form factors, consistent with the mild w dependence in Eq. (74). Note that the extractions of $|V_{cb}|$ by CLEO and BELLE discussed in Sec. 3.6.1. use CLEO's measurements of $R_1(1)$ and $R_2(1)$.

For $\mathrm{B} \to \mathrm{D}\ell\nu$ decays, the parametrization of [139] is

$$\frac{\mathcal{G}(w)}{\mathcal{G}(1)} \approx 1 - 8\rho^2_{\mathcal{G}} z + (51.\rho^2_{\mathcal{G}} - 10.)z^2 - (252.\rho^2_{\mathcal{G}} - 84.)z^3 , \tag{75}$$

with

$$z = \frac{\sqrt{w+1} - \sqrt{2}}{\sqrt{w+1} + \sqrt{2}} , \tag{76}$$

and where the only parameter, the slope parameter $\rho^2_{\mathcal{G}}$ at zero recoil is constrained by the dispersive bounds to lie in the interval $-0.17 < \rho^2_{\mathcal{G}} < 1.51$ which can be compared with the world experimental average $\rho^2_{\mathcal{G}} = 1.19 \pm 0.19$ given in Sec. 3.6.2.

It is interesting to note that heavy quark symmetry breaking in the difference of the slope and curvature parameters of the form factors $\mathcal{F}(w)$ and $\mathcal{G}(w)$, together with measurements of the ratios R_1 and R_2 may strongly constrain the calculations which determine $\mathcal{F}(1)$ and $\mathcal{G}(1)$ [189]. More importantly, a better knowledge of the slope parameters will reduce the error on $|V_{cb}|$, because of the large correlation between the two parameters [189] (see Fig. 3.8).

3.2. Theoretical calculations of the form factor $\mathcal{F}(1)$ for $\mathrm{B} \to \mathrm{D}^* \ell\nu$ decays

The zero-recoil form factor $\mathcal{F}(1)$ must be calculated non-perturbatively in QCD. At zero recoil ($w = 1$), all $\mathrm{B} \to \mathrm{D}^* \ell\nu$ form factors but h_{A_1} are suppressed by phase space, and

$$\mathcal{F}(1) = h_{A_1}(1) = \langle \mathrm{D}^*(v)|A^\mu|\overline{\mathrm{B}}(v)\rangle, \tag{77}$$

where A^μ is the $b \to c$ axial vector current. Thus, the theoretical information needed is contained in one relatively simple hadronic matrix element, which heavy-quark symmetry [7,8,9] requires to be close to unity. Heavy-quark *spin* symmetry would imply $\langle \mathrm{D}^*(v)|A^\mu|\overline{\mathrm{B}}(v)\rangle = \langle \mathrm{D}(v)|V^\mu|\overline{\mathrm{B}}(v)\rangle$, where V^μ is the $b \to c$ vector current. If, in addition, heavy-quark *flavor* symmetry is used, these amplitudes can be equated to $\langle \mathrm{B}(v)|V^\mu|\overline{\mathrm{B}}(v)\rangle$. The last matrix element simply counts the number of b quarks in a $\overline{\mathrm{B}}$ meson and is, hence, exactly 1. Deviations from the symmetry limit arise at short distances, from the exchange of gluons with $m_c < k < m_b$, and also at long distances. Short-distance corrections are suppressed by powers of $\alpha_s(\sqrt{m_c m_b})$, and long-distance corrections are suppressed by powers of the heavy-quark masses. The heavy-quark symmetries also require the corrections of order $1/m_Q$ to vanish, a result known as Luke's theorem [147]. In summary, thanks to heavy-quark symmetry, uncertainties from treating the long-distance, non-perturbative QCD are suppressed by a factor of order $(\bar{\Lambda}/2m_c)^2 \sim 5\%$, where $\bar{\Lambda} \sim 500$MeV is the contribution of the light degrees of freedom to the mass of the mesons. Owing to these constraints from heavy-quark symmetry, the exclusive technique is sometimes called model-independent [134], but in practice model dependence could appear at order $1/m_c^2$, through estimates of the deviation of $h_{A_1}(1)$ from 1.

To date three methods have been used to estimate $h_{A_1}(1) - 1$. One approach starts with a rigorous inequality relating the zero-recoil form factor to a spectral sum over excited states [148,21]. Here some contributions can be measured by moments of the inclusive s.l. decay spectrum (cf. Sec. 2.4.), but others can be estimated only qualitatively. The other two methods both start with HQET to separate long- and short-distance contributions [149]. The short-distance contributions are calculated in perturbative QCD. The long-distance contributions are intrinsically non-perturbative. Several years ago they were estimated in a non-relativistic quark model [149,135]. More recently, the HQET technique has been adapted to lattice gauge theory [150,151], and an explicit calculation, in the so-called quenched approximation, has appeared [152].

The three methods all quote an uncertainty on $\mathcal{F}(1)$, and hence $|V_{cb}|$, of around 4%. The errors arising in the sum rule and the quark model calculations are difficult to quantify and do not appear to be reducible. In the lattice gauge theory calculations, there are several ways to reduce the error, notably by removing the quenched approximation and in improving the matching of lattice gauge theory to HQET and continuum QCD. It is conceivable that one could reduce the uncertainty to the percent level over the next few years.

3.2.1. Sum rule method

Here the main result of a sum rule that puts a rigorous bound on $h_{A_1}(1)$ is quoted. For a lucid and brief derivation, the reader may consult a classic review of the heavy-quark expansion [153]. Based on the optical theorem and the operator-product expansion, one can show that

$$|h_{A_1}(1)|^2 + \frac{1}{2\pi}\int_0 d\epsilon\, w(\epsilon) = 1 - \Delta_{1/m^2} - \Delta_{1/m^3} \tag{78}$$

where $\epsilon = E - M_{D^*}$ is the relative excitation energy of higher resonances and non-resonant $D\pi$ states with $J^{PC} = 1^{-+}$, and $w(\epsilon)$ is a structure function for the vector channel. The contributions Δ_{1/m^n} describe corrections to the axial vector current for finite-mass quarks. The excitation integral is related to finite-mass corrections to the bound-state wave functions—hence the "sum" over excited states. The Δ_{1/m^n} and the excitation integral are positive, so Eq. (78) implies $|h_{A_1}(1)| < 1$.

Let first consider the excitation integral. For $\epsilon \gg \bar{\Lambda}$, the hadronic states are dual to quark-gluon states. Introducing a scale μ to separate this short-distance part from the long-distance part (which must be treated non-perturbatively), one writes

$$\frac{1}{2\pi}\int_0 d\epsilon\, w(\epsilon) = \frac{1}{2\pi}\int_0^\mu d\epsilon\, w(\epsilon) + [1-\eta_A^2(\mu)]. \tag{79}$$

Here the short-distance quantity $\eta_A(\mu)$ lumps together the short-distance ($\epsilon > \mu$) contribution. Then, rearranging Eq. (78),

$$h_{A_1}(1) = \eta_A(\mu) - \frac{1}{2}\Delta_{1/m^2} - \frac{1}{2}\Delta_{1/m^3} - \frac{1}{4\pi}\int_0^\mu d\epsilon\, w(\epsilon) \tag{80}$$

and $\eta_A(\mu)$ is computed perturbatively (to two loops [154]). The other contributions arise from long distances and must be taken from other considerations. There is a good handle on the second term on the right-hand side of Eq. (80), namely,

$$\Delta_{1/m^2} = \frac{\mu_G^2}{3m_c^2} + \frac{\mu_\pi^2(\mu)-\mu_G^2}{4}\left(\frac{1}{m_c^2} + \frac{2/3}{m_c m_b} + \frac{1}{m_b^2}\right), \tag{81}$$

where μ_G^2 and $\mu_\pi^2(\mu)$ are matrix elements of the chromomagnetic energy and kinetic energy (of the b quark) in the $\overline{\rm B}$ meson. Note that the kinetic energy μ_π^2 depends on the scale μ. Apart from subtleties of renormalization conventions, μ_G^2 and $\mu_\pi^2(\mu)$ are related to the quantities λ_2 and λ_1, given in the discussion of inclusive s.l. decays. Ignoring this subtlety for the moment, $\mu_G^2 = 3\lambda_2 = 3(M_{B^*}^2 - M_B^2)/4$ and $\mu_\pi^2 = -\lambda_1$. The last term in Eq. (80), from higher hadronic excitations, is unconstrained by data.

To make a numerical determination, one must choose a conventional value for the separation scale to μ, usually 1 GeV. The choice of μ alters $\eta_A(\mu)$ and $\mu_\pi^2(\mu)$, as well as the excitation integral, in ways that can be computed in perturbative QCD. A recent review [4] of the heavy quark expansion takes

$$\frac{1}{4\pi}\int_0^{1\ {\rm GeV}} d\epsilon\, w(\epsilon) = 0.5 \pm 0.5, \tag{82}$$

but emphasises that this is a heuristic estimate. Ref. [4] found $h_{A_1}(1) = 0.89 \pm 0.04$, using a then-current value of μ_π^2. With CLEO's analysis of moments of the inclusive s.l. decay spectrum in hand, one can convert that determination of λ_1 to a determination of $\mu_\pi^2(1\ {\rm GeV})$. The updated sum-rule becomes [4]

$$\mathcal{F}(1) = h_{A_1}(1) = 0.900 \pm 0.015 \pm 0.025 \pm 0.025, \tag{83}$$

where the uncertainties are, respectively, from the two-loop calculation of $\eta_A(1\ {\rm GeV})$, the excitation integral [*i.e.*, Eq. (82)], and an estimate of Δ_{1/m^3} based on dimensional analysis. The uncertainty from $\eta_A(\mu)$ could be reduced, in principle, with a three-loop calculation, but it is already smaller than the other two, which appear to be irreducible.

3.2.2. HQET-based methods

The main drawback of the sum rule method is that the excitation integral is not well constrained. Using HQET one can characterize it in more detail. Based on heavy-quark symmetry one can write

$$h_{A_1}(1) = \eta_A\left[1 + \delta_{1/m^2} + \delta_{1/m^3}\right] \tag{84}$$

where η_A is a short-distance coefficient, which is discussed in more detail below. Heavy-quark symmetry implies the normalization of the first term in brackets [8,9] and the absence of a correction $\delta_{1/m}$ of

order $1/m_Q$ [147]. The corrections δ_{1/m^n} of order $1/m_Q^n$ contain long-distance matrix elements. Simply from enumerating possible terms at second and third order, they have the structure

$$\delta_{1/m^2} = -\frac{\ell_V}{(2m_c)^2} + \frac{2\ell_A}{(2m_c)(2m_b)} - \frac{\ell_P}{(2m_b)^2}, \tag{85}$$

$$\delta_{1/m^3} = -\frac{\ell_V^{(3)}}{(2m_c)^3} + \frac{\ell_A^{(3)}\Sigma}{(2m_c)(2m_b)} + \frac{\ell_D^{(3)}\Delta}{(2m_c)(2m_b)} - \frac{\ell_P^{(3)}}{(2m_b)^3}, \tag{86}$$

where $\Sigma = 1/(2m_c) + 1/(2m_b)$ and $\Delta = 1/(2m_c) - 1/(2m_b)$.

HQET is a systematic method for separating out the long- and short-distance corrections to the symmetry limit, making efficient use of the constraints of heavy-quark symmetry. It provides a detailed description of the ℓs [149,158], of the form

$$\ell_X = \sum_i c_i(\mu)\mathcal{M}_i(\mu), \tag{87}$$

where the $c_i(\mu)$ are short-distance coefficients and the $\mathcal{M}_i(\mu)$ matrix elements defined in the effective field theory. The scale μ is now the renormalization scale of HQET. Some contributions on the right-hand side come from the $1/m_Q$ expansion of the physical B and D^* mesons and others from the expansion of the axial vector current. The latter coincide with the λ_1 and λ_2 (or μ_π^2 and μ_G^2) terms in Eq. (81). The long-distance corrections of the states are, in Eq. (80), contained in $\int_0^\mu d\epsilon w(\epsilon)$.

It is well-known that intermediate quantities defined in effective field theories depend on the renormalization scheme, but physical quantities do not. We dwell on it briefly here, for reasons that will become clear below. At one-loop level, the short-distance coefficient is

$$\eta_A(c) = 1 + \frac{4}{3}\frac{\alpha_s}{4\pi}\left[3\frac{m_b+m_c}{m_b-m_c}\ln\frac{m_b}{m_c} - 8\right] + \frac{4}{3}\frac{\alpha_s}{4\pi}c\mu^2\left(\Delta^2 + 2\Sigma^2\right) \tag{88}$$

where the constant c is characteristic of the scheme for renormalizing operators in HQET. In minimal subtraction schemes $c = 0$, whereas the energy cutoff in Eq. (79) implies $c = 4/3$ (cf. Eq. (19)). Similarly, the scheme (and μ) dependence of the ℓs is, to order α_s,

$$\ell_V(c) = \ell_V(0) + \frac{4}{3}\frac{\alpha_s}{4\pi}3c\mu^2, \tag{89}$$

$$\ell_A(c) = \ell_A(0) - \frac{4}{3}\frac{\alpha_s}{4\pi}\,c\mu^2, \tag{90}$$

$$\ell_P(c) = \ell_P(0) + \frac{4}{3}\frac{\alpha_s}{4\pi}3c\mu^2. \tag{91}$$

Combining the above formulae, one can check that the scheme dependence drops out of $h_{A_1}(1)$.

As long as one is careful to keep track of the scheme, it does not matter which is used. For many purposes it is simplest to define all operator insertions in minimal subtraction, for which $c = 0$. This is not a problem, as long as one knows how to calculate the ℓs in the same scheme. (For example, the $-\lambda_1$ and μ_π^2 are defined by the same HQET matrix element, renormalized such that $c = 0$ and $4/3$, respectively.)

The HQET formalism does not provide numerical estimates for the ℓs: that requires a non-perturbative approach to QCD. The first estimates [149,135] used the non-relativistic quark model, which, though not QCD, can be a useful guide and tends to yield rather small δ_{1/m^2}. The more recent of these estimates [135] takes δ_{1/m^2} to be -0.055 ± 0.025, and relies on sum rule constraints. Combining it with the two-loop calculation of η_A [155,156], one obtains

$$\mathcal{F}(1) = h_{A_1}(1) = 0.907 \pm 0.007 \pm 0.025 \pm 0.017, \tag{92}$$

where the quoted uncertainties [135,155] are from perturbation theory, errors in the quark model estimate of the $1/m_Q^2$ terms, and the omission of $1/m_Q^3$ terms. Uncertainties from α_s and the quark masses are not included. This result does not pay close attention to the scheme dependence mentioned above, because it uses the standard ($c = 0$) result for η_A, corresponding to a minimal subtraction definition of the matrix elements in Eq. (87). The quark model, on the other hand, presumably yields the ℓs in some other scheme (with unknown $c \neq 0$). In that case, Eq. (92) over- or undercounts the contribution at the interface of long and short distances. Moreover, we note that estimates of the perturbative error based on BLM resummation [157,66] are larger than in Eq. (92).

Now let us turn to the recent lattice calculation of $h_{A_1}(1)$. A direct calculation of the matrix element $\langle \mathrm{D}^*|A^\mu|\mathrm{B}\rangle$ in Eq. (77) would be straightforward, but not interesting: similar matrix elements like $\langle 0|A^\mu|\mathrm{B}\rangle$ and $\langle \pi|V^\mu|\mathrm{B}\rangle$ have 15–20% errors [159]. One must involve heavy-quark symmetry from the outset: if one can focus on $h_{A_1} - 1$, there is a chance of success, because a 20% error on $h_{A_1} - 1$ is interesting. The key here is to observe that lattice gauge theory with Wilson fermions has the same heavy-quark symmetries as continuum QCD, for all $m_Q a$ [160]. Consequently, one can build up a description of lattice gauge theory using HQET, with the same logic and structure as above [150,151,161]. In this description the ℓs in Eqs. (85) and (86) are the same as for continuum QCD, apart from lattice effects on the light quarks and gluons. Discretization effects of the heavy quark appear at short distances, where perturbation theory can be used. Thus, the principal change from the usual application of HQET is in the short-distance coefficients.

To calculate the ℓs in lattice gauge theory, one needs some quantities with small statistical and normalization errors, whose heavy-quark expansion contains the ℓs. Work on $\mathrm{B} \to \mathrm{D}$ form factors [162] showed that certain ratios have the desired low level of uncertainty. For the problem at hand one needs

$$\frac{\langle \mathrm{D}|\bar{c}\gamma^4 b|\mathrm{B}\rangle\langle \mathrm{B}|\bar{b}\gamma^4 c|\mathrm{D}\rangle}{\langle \mathrm{D}|\bar{c}\gamma^4 c|\mathrm{D}\rangle\langle \mathrm{B}|\bar{b}\gamma^4 b|\mathrm{B}\rangle} = \left\{\eta_V^{\mathrm{lat}}\left[1 - \ell_P \Delta^2 - \ell_P^{(3)}\Delta^2\Sigma\right]\right\}^2, \tag{93}$$

$$\frac{\langle \mathrm{D}^*|\bar{c}\gamma^4 b|\mathrm{B}^*\rangle\langle \mathrm{B}^*|\bar{b}\gamma^4 c|\mathrm{D}^*\rangle}{\langle \mathrm{D}^*|\bar{c}\gamma^4 c|\mathrm{D}^*\rangle\langle \mathrm{B}^*|\bar{b}\gamma^4 b|\mathrm{B}^*\rangle} = \left\{\eta_V^{\mathrm{lat}}\left[1 - \ell_V \Delta^2 - \ell_V^{(3)}\Delta^2\Sigma\right]\right\}^2, \tag{94}$$

$$\frac{\langle \mathrm{D}^*|\bar{c}\gamma^j\gamma_5 b|\mathrm{B}\rangle\langle \mathrm{B}^*|\bar{b}\gamma^j\gamma_5 c|\mathrm{D}\rangle}{\langle \mathrm{D}^*|\bar{c}\gamma^j\gamma_5 c|\mathrm{D}\rangle\langle \mathrm{B}^*|\bar{b}\gamma^j\gamma_5 b|\mathrm{B}\rangle} = \left\{\check{\eta}_A^{\mathrm{lat}}\left[1 - \ell_A \Delta^2 - \ell_A^{(3)}\Delta^2\Sigma\right]\right\}^2. \tag{95}$$

For lattice gauge theory, the heavy-quark expansions in Eqs. (93)–(95) have been derived in Ref. [150], leaning heavily on Refs. [149,158]. One-loop perturbation theory for η_V^{lat} and $\check{\eta}_A^{\mathrm{lat}}$ is in Ref. [151]. Thus, these ratios yield all three terms in δ_{1/m^2} and three of four terms in δ_{1/m^3} (including the largest, $\ell_V^{(3)}/(2m_c)^3$).

The method then proceeds as follows. First, one computes the ratios on the left-hand sides of Eqs. (93)–(95) with standard techniques of lattice gauge theory, for many combinations of the heavy quark masses. Meanwhile one calculates the short-distance coefficients η_V^{lat} and $\check{\eta}_A^{\mathrm{lat}}$ in perturbation theory. Then, one fits the numerical data to the HQET description, obtaining the ℓs as fit parameters. One can then combine these results with the perturbative calculation of η_A to obtain $h_{A_1}(1)$. The scheme mismatch that arises with the quark model calculation of the ℓs is absent here, as long as one uses the same scheme to calculate η_V^{lat} and $\check{\eta}_A^{\mathrm{lat}}$ on the one hand, and η_A on the other.

As expected, ℓ_V is the largest of the $1/m_Q^2$ matrix elements. Because of the fit, the value of ℓ_V is highly correlated with that of $\ell_V^{(3)}$, but the physical combination is better determined.

Matching uncertainties arise here, as it is usually the case with HQET. In Ref. [152] they are of order α_s^2, $\alpha_s \cdot (\bar{\Lambda}/m_c)^2$, and $(\bar{\Lambda}/m_Q)^3$. These can be improved in the future through higher-order matching calculations. Another uncertainty comes from the dependence of the ratios on the light spectator quark, whose mass lies in the range $0.4 \leq m_q/m_s \leq 1$. There turns out to be a slight linear dependence on m_q, whose main effect is to increase the statistical error. In addition, there is a pion loop contribution [164] that is mistreated in the quenched approximation [165]. The omission of this effect is treated

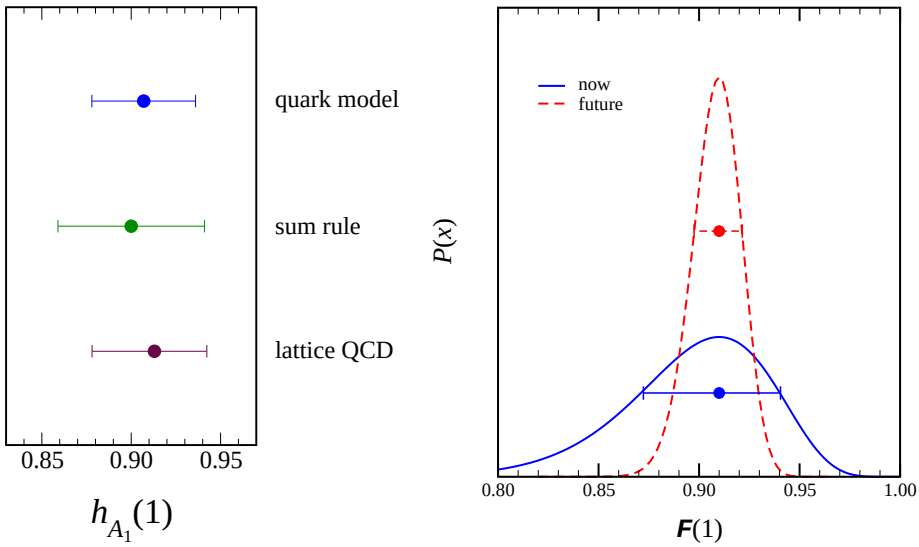

Fig. 3.7: *(a) Comparison of methods for $\mathcal{F}(1)$. Note that the result labelled "quark model" actually uses sum rule constraints. (b) Model likelihood function for $\mathcal{F}(1)$, now and with projected smaller errors in the future.*

as a systematic error. After reconstituting $h_{A_1}(1)$ [152]

$$\mathcal{F}(1) = h_{A_1}(1) = 0.913^{+0.024}_{-0.017} \pm 0.016^{+0.003+0.000+0.006}_{-0.014-0.016-0.014}, \tag{96}$$

where the uncertainties stem, respectively, from statistics and fitting, HQET matching, lattice spacing dependence, the chiral extrapolation, and the effect of the quenched approximation.

3.2.3. Comparison and summary

In Fig. 3.7(a) we compare the three results for $\mathcal{F}(1)$ from Eqs. (83), (92), and (96). All are compatible with

$$\mathcal{F}(1) = 0.91^{+0.03}_{-0.04} \tag{97}$$

The agreement is remarkable, even when one considers that all rely on heavy-quark symmetry (and, so, compute the deviation from 1), and all compute the short-distance part in perturbation theory (roughly half of the deviation). It is worth recalling the defects of the techniques. The quark model omits some dynamics (more than the quenched approximation in lattice QCD), and it is not clear that it gives the ℓs in the same scheme as η_A. The sum rule has an incalculable contribution from excitations with $(M - M_{D^*})^2 < \mu^2$, which can only be estimated. The present lattice result is in the quenched approximation, but errors associated with quenching can, in this case, be estimated and are given in the last two error bars in Eq. (96).

When using Eq. (97) in a global fit to the CKM matrix, one should appreciate the quality of the theoretical information. A flat distribution based on Eq. (97) would be incorrect: the three methods agree well and, more significantly, part of the uncertainty in Eq. (96) is statistical, and other uncertainties are under some control. Also, one cannot rule out a tail for lower values, $\mathcal{F}(1) < 0.87$; they are just unexpected. Finally, we know that $\mathcal{F}(1) \leq 1$ from the sum rule in Eq. (78). A simple function that captures these features is the Poisson distribution (for $x > 0$)

$$P(x) = N x^7 e^{-7x}, \quad x = \frac{1 - \mathcal{F}(1)}{0.090}, \tag{98}$$

where N normalizes the distribution. This distribution differs slightly from a synopsis of the lattice result [163]. The most probable value has been shifted from 0.913 to 0.910, mindful of the central value

from the sum rule. [The average based on Eq. (98) is 0.90.] Future work with lattice gauge theory could reduce the uncertainty by a factor of 3, with unquenched calculations to reduce several of the systematic errors, higher-order HQET matching to reduce the others, and higher statistics to reduce the statistical errors. Fig. 3.7(b) sketches how the resulting distribution would look. Recent developments [168] in the treatment of systematic errors (except quenching) will allow lattice calculations to provide a distribution that directly reflects statistical and systematic uncertainties, instead of a schematic distribution as in Eq. (98).

3.3. Theoretical calculations of the form factor $\mathcal{G}(1)$ for $\mathrm{B} \to \mathrm{D}\ell\nu$ decays

The form factor $\mathcal{G}(W)$ for $\mathrm{B} \to \mathrm{D}\ell\nu$ is given by

$$\mathcal{G}(w) = h_+(w) - \frac{M_B - M_D}{M_B + M_D} h_-(w), \tag{99}$$

where the form factors $h_\pm(w)$ are defined by

$$\langle \mathrm{D}(v')|V^\mu|\mathrm{B}(v)\rangle = \sqrt{M_B M_D}\left[(v'+v)^\mu h_+(w) - (v'-v)^\mu h_-(w)\right]. \tag{100}$$

Even at zero-recoil both form factors remain. With HQET one can derive expressions analogous to Eq. (84). Neglecting contributions of order α_s/m_Q^n, one finds [149,158,150],

$$h_+(1) = \eta_V\left[1 - \left(\frac{1}{2m_c} - \frac{1}{2m_b}\right)^2 \ell_P\right], \tag{101}$$

$$h_-(1) = \beta_V + \left(\frac{1}{2m_c} - \frac{1}{2m_b}\right)\Lambda_- + \left(\frac{1}{(2m_c)^2} - \frac{1}{(2m_b)^2}\right)\ell_-, \tag{102}$$

where β_V is of order α_s. Like the ℓs above, Λ_- and ℓ_- are (combinations of) matrix elements of HQET. They must be obtained by a non-perturbative method. Note that the matrix element ℓ_P appearing in $h_+(1)$ is the same as in $\mathcal{F}(1)$.

Luke's theorem, applied to $\mathrm{B} \to \mathrm{D}\ell\nu$, explains why there is no $1/m_Q$ term in $h_+(1)$. The other form factor $h_-(1)$ is not protected by Luke's theorem, and, unfortunately, it appears in $\mathcal{G}$ even at zero recoil [134]. Moreover, although some constraint might be obtained from sum rules, there is presently no useful bound analogous to that implied by Eq. (78). In conclusion, there is less theoretical control over $\mathcal{G}(1) - 1$ than $\mathcal{F}(1) - 1$.

There are several calculations of $\mathcal{G}(1)$. Using the quark model, Scora and Isgur find [166]

$$\mathcal{G}(1) = 1.03 \pm 0.07. \tag{103}$$

As mentioned above for $\mathcal{F}(1)$, the quark model presumably has a problem with scheme dependence, though it may be a useful guide. There have been a few calculations of ℓ_P, Λ_-, and ℓ_- with QCD sum rules. Including the full α_s^2 correction and using the sum-rule results of [142], one finds [167]:

$$\mathcal{G}(1) = 1.02 \pm 0.08. \tag{104}$$

Although this result is based on QCD, it is unlikely that the error bar can be reduced further. Finally, Hashimoto *et al.* have used lattice QCD and a strategy similar to that for $\mathcal{F}(1)$, which homes in on $\mathcal{G}(1) - 1$. They find [162]

$$\mathcal{G}(1) = 1.058^{+0.021}_{-0.017}, \tag{105}$$

where errors from statistics, tuning of heavy quark masses, and omitted radiative corrections have been added in quadrature. One should also expect some uncertainty from the quenched approximation, perhaps 15–20% of $\mathcal{G}(1) - 1$. Unlike the calculation of by $\mathcal{F}(1)$ by the same group [152], here the dependence on the lattice spacing was not studied. These issues could be cleared up, by completing calculations

of (lattice) radiative corrections needed to improve the calculation of $h_-(1)$, and then carrying out the Monte Carlo calculation of $h_-(1)$ at several lattice spacings.

In conclusion, the status of the theoretical calculations of $\mathcal{G}(1)$ is less satisfactory than for $\mathcal{F}(1)$. We believe that

$$\mathcal{G}(1) = 1.04 \pm 0.06 \tag{106}$$

fairly summarizes the present theoretical knowledge of $\mathcal{G}(1)$.

3.4. Electroweak corrections

For completeness, we close with a brief summary of electroweak corrections to exclusive s.l. decays. Some of these effects are shared by the radiative corrections to muon decay, and that is why the muon decay constant G_μ appears in Eqs. (70) and (71).Another effect is simply radiation of photons from the outgoing charged lepton, which could be important in semi-electronic decays, if the experimental acceptance is non-uniform in the electron's energy. A complete treatment is not available, but an adequate prescription is given in Ref. [169]. If the decaying B meson is electrically neutral, one must multiply the right-hand side of Eq. (71) with a factor [170] $1 + \alpha\pi$ to account for the Coulomb attraction of the outgoing charged lepton and charged D^*. This corresponds to a shift in $|V_{cb}|$ of about 1%.

There are also virtual corrections from diagrams with W and Z bosons. The leading parts of these effects are enhanced by the large logarithm $\ln(M_Z/M_B)$, which arise from distances much shorter than the QCD scale, and their net effect is the factor η_{EW}^2 in Eq. (71). One finds [171]

$$\eta_{\mathrm{EW}} = 1 + \frac{\alpha}{\pi}\ln(m_Z/\mu) \tag{107}$$

where the scale μ separates weak and strong effects. It is natural to set $\mu = M_B$, in which case $\eta_{\mathrm{EW}} = 1.0066$. Should the accuracy of the QCD form factor $\mathcal{F}$ fall below 1%, it might be necessary to go beyond the leading log description of Eq. (107), but that could require the introduction of new form factors besides $\mathcal{F}$, so a general treatment is difficult.

3.5. Semileptonic B decays to a hadronic system heavier than D or D*

Semileptonic B decays into p-wave charm mesons are the most important sources of background polluting the measurement of the $\mathrm{B} \to \mathrm{D}^*\ell\nu$ decay rate. The hadronic system heavier than $\mathrm{D}^{(*)}$ is commonly identified as 'D^{**}'.

In infinite quark mass limit, hadrons containing a single heavy quark can be classified by their total spin J and by the angular momentum j of their light degree of freedom. In this limit, heavy quark mesons come in degenerate doublets with total spin $J = j \pm \frac{1}{2}$. Therefore, the four charm meson states 'D^{**}' corresponding to the angular momentum $l = 1$ are classified in two doublets: $\mathrm{D}_0, \mathrm{D}^*{}_1$ with $j = \frac{1}{2}$ and $J^P = (0^+, 1^+)$, and $\mathrm{D}_1, \mathrm{D}^*{}_2$ with $j = \frac{3}{2}$ and $J^P = (1^+, 2^+)$. Both D_1 and $\mathrm{D}^*{}_2$ are narrow states ($\Gamma \simeq 20$ MeV). This small width is a consequence of their strong decay proceeding through d-wave transitions. The resonances of the other doublet are expected to be rather broad, as they decay through s-wave pion emission.

The existence of the narrow resonant states is well established [106] and a signal for a broad resonance has been seen by CLEO [177], but the decay characteristics of these states in b-hadron s.l. decays have large uncertainties. The average of ALEPH [178], CLEO [179] and DELPHI [181] narrow state branching fractions show that the ratio

$$R_{**} = \frac{\mathcal{B}(\overline{\mathrm{B}} \to \mathrm{D}_2^*\ell\bar{\nu})}{\mathcal{B}(\overline{\mathrm{B}} \to \mathrm{D}_1\ell\bar{\nu})} \tag{108}$$

is smaller than one (< 0.6 at 95% C.L.[182]), in disagreement with HQET calculations where an infinite quark mass is assumed [183], but in agreement with calculations which take into account finite quark mass corrections [184].

To estimate the 'D^{**}', the LEP experiments use the treatment of narrow D^{**} proposed in [184] which accounts for $\mathcal{O}(1/m_c)$ corrections. Ref. [184] provides several possible approximations of the 'D^{**}' form factors, that depend on five different expansion schemes (A, A_{inf}, B_{inf}, B_1, B_2) and on three input parameters ($\eta_{ke}, t_{h1}, z_{h1}$).

Each proposed scheme is tested with the relevant input parameters varied over a range consistent with the experimental limit on R_{**}. The $\mathcal{F}(1)V_{cb}$ analysis is repeated for each allowed point of the scan and the systematic error is the maximal difference from the central value obtained in this way. Non-resonant terms may not be modelled correctly in this approach.

3.6. Review and future prospects for the exclusive determination of $|V_{cb}|$

3.6.1. $|V_{cb}|$ from $\mathrm{B} \to \mathrm{D}^*\ell\nu$ decays

The decay $\mathrm{B} \to \mathrm{D}^*\ell\nu$ has been studied in experiments performed at the $\Upsilon(4S)$ center of mass energy and at the Z^0 center of mass energy at LEP. At the $\Upsilon(4S)$, experiments have the advantage that the w resolution is good. However, they have more limited statistics near $w = 1$ in the decay $\overline{\mathrm{B}}^0 \to \mathrm{D}^{*+}\ell^-\bar{\nu}_\ell$, because of the lower reconstruction efficiency of the slow pion, from the $\mathrm{D}^{*+} \to \pi^+\mathrm{D}^0$ decay. The decay $\mathrm{B}^- \to \mathrm{D}^{*0}\ell^-\bar{\nu}_\ell$ is not affected by this problem and CLEO [172] uses both channels. In addition, kinematic constraints enable $\Upsilon(4S)$ experiments to identify the final state without a large contamination from the poorly known s.l. B decays to 'D^{**}'. At LEP, B's are produced with a large momentum (about 30 GeV on average). This makes the determination of w dependent upon the neutrino four-momentum reconstruction, thus giving a relatively poor resolution and limited physics background rejection capabilities. The advantage that LEP experiments have is an efficiency which is only mildly dependent upon w.

Experiments determine the product $(\mathcal{F}(1) \cdot |V_{cb}|)^2$ by fitting the measured $d\Gamma/dw$ distribution. Measurements at the $\Upsilon(4S)$ have been performed by CLEO [172] and BELLE [173]. At LEP data are available from ALEPH [175], DELPHI [174] and OPAL [176]. At LEP, the dominant source of systematic error is the uncertainty on the contribution to $d\Gamma/dw$ from s.l. $\mathrm{B} \to \mathrm{D}^{**}$ decays. The "D^{**}" includes both narrow orbitally excited charmed meson and non-resonant or broad species. The treatment of the "D^{**}" spectra is described in 3.5., while branching ratios of the processes which affect the value of $|V_{cb}|$ are taken from [182].

experiment	$\mathcal{F}(1)\lvert V_{\mathrm{cb}}\rvert$ ($\times 10^3$)	$\rho^2_{A_1}$	$\mathrm{Corr}_{\mathrm{stat}}$	References
ALEPH published	31.9$\pm$ 1.8$\pm$ 1.9	0.31$\pm$ 0.17$\pm$ 0.08	92%	[175]
ALEPH update	31.5$\pm$ 2.1$\pm$ 1.3	0.58$\pm$ 0.25$\pm$ 0.11	94%	[182]
DELPHI	35.5$\pm$ 1.4$\pm$ 2.4	1.34$\pm$ 0.14$\pm$ 0.23	94%	[174]
OPAL	37.1$\pm$ 1.0$\pm$ 2.0	1.21$\pm$ 0.12$\pm$ 0.20	90%	[176]
BELLE	35.8$\pm$ 1.9$\pm$ 1.8	1.45$\pm$ 0.16$\pm$ 0.20	90%	[173]
CLEO	43.1$\pm$ 1.3$\pm$ 1.8	1.61$\pm$ 0.09$\pm$ 0.21	86%	[172]

Table 3.16: *Experimental results as published by the collaborations. LEP numbers use theoretical predictions for R_1 and R_2. The published ALEPH result is obtained using a linear fit and the old ISGW model [114] for D^{**}. The updated ALEPH numbers (used in our average) are obtained using the same fit parameterization and D^{**} models as the other LEP experiments [185]. The BELLE result listed in the Table uses R_1 and R_2 from CLEO data.*

Parameter	Value	Reference
$\mathrm{R_b} = \Gamma(Z \to b\bar{b})/\Gamma(Z \to had)$	(21.64 $\pm$ 0.07)%	[180]
$\mathrm{f_d} = \mathcal{B}(b \to \mathrm{B}_d)$	(40.0 $\pm$1.1)%	[186]
$\tau(\mathrm{B}^0)$	(1.54 $\pm$ 0.015) ps	[187]
$x_E{}^{LEP} = E(\mathrm{B\ meson})/\sqrt{\mathrm{s}}$	0.702 $\pm$ 0.008	[180]
$\mathcal{B}(\mathrm{D}^{*+} \to \mathrm{D}^0\pi^+)$	(67.7 $\pm$ 0.5) %	[106]
$\mathrm{R_1}$	1.18 ± 0.32	[188]
$\mathrm{R_2}$	0.71 ± 0.23	[188]
$\mathcal{B}(\bar{\mathrm{B}} \to \tau\bar{\nu_\tau}\mathrm{D}_s^+)$	(1.27 $\pm$ 0.21)%	[182]
$\mathcal{B}(\mathrm{B}^- \to \mathrm{D}^{*+}\pi^-\ell\bar{\nu})$	(1.29$\pm$0.16) %	[182]
$\mathcal{B}(\bar{\mathrm{B}}^0_\mathrm{d} \to \mathrm{D}^{*+}\pi^0\ell\bar{\nu})$	(0.61 ± 0.08)%	[182]
$\mathcal{B}(\mathrm{B}_s \to \mathrm{D}^{\star+}\mathrm{K}\ell\bar{\nu})$	(0.65 ± 0.23)%	[182]

Table 3.17: *Values of the most relevant parameters affecting the measurement of $|V_{cb}|$. The three D^{**} production rates are fully correlated.*

Table 3.16 summarizes all published data as quoted in the original papers. To combine the published data, the central values and the errors of $\mathcal{F}(1)|V_{cb}|$ and $\rho^2_{A_1}$ are re-scaled to the same set of input parameters. These common inputs are listed in Table 3.17. The $\mathcal{F}(1)|V_{cb}|$ values used for obtaining an average are extracted with the parametrization of Eq. (72), taking on the experimental determinations of the vector and axial form factor ratios R_1 and R_2 [188]. The LEP data, which originally used theoretical values for these ratios, are re-scaled accordingly [185]. Table 3.18 summarizes the corrected data. The averaging procedure [185] takes into account statistical and systematic correlations between $\mathcal{F}(1)|V_{cb}|$ and $\rho^2_{A_1}$. Averaging the measurements in Table 1, we get:

$$\mathcal{F}(1)|V_{cb}| = (38.3 \pm 1.0) \times 10^{-3}$$

and

$$\rho^2_{A_1} = 1.5 \pm 0.13$$

with a confidence level [§] of 5.1%. The error ellipses for the corrected measurements and for the world average are shown in Fig. 3.8.

The main contributions to the systematic error in $\mathcal{F}(1)|V_{cb}|$ are from the uncertainty on the $\mathrm{B} \to \mathrm{D}^{**}\ell\nu$ shape and on $\mathcal{B}(b \to \mathrm{B}_d)$ (0.57×10^{-3}), fully correlated among the LEP experiments, the branching fraction of D and D^* decays (0.4×10^{-3}), fully correlated among all the experiments, and the slow pion reconstruction from BELLE and CLEO (0.28×10^{-3}), which are uncorrelated. The main contribution to the systematic error on $\rho^2_{A_1}$ is from the uncertainties in the CLEO's measurement of $\mathrm{R_1}$ and $\mathrm{R_2}$ (0.12), fully correlated among experiments. Because of the large contribution of this uncertainty to the non-diagonal terms of the covariance matrix, the averaged $\rho^2_{A_1}$ is higher than one would naively expect. This situation will improve substantially in the next few years through a better determination of R_1 and R_2, using the higher statistics samples being accumulated at the B-factories, as well as through the full exploration of the s.l. B decays to D^{**}.

Using $\mathcal{F}(1) = 0.91 \pm 0.04$, as given in Sec. 3.2. but with a symmetrized error, one gets

$$\boxed{|V_{cb}| = (42.1 \pm 1.1_{exp} \pm 1.9_{th}) \times 10^{-3}.} \qquad (109)$$

[§]The χ^2 per degree of freedom is less than 2, and we do not scale the error.

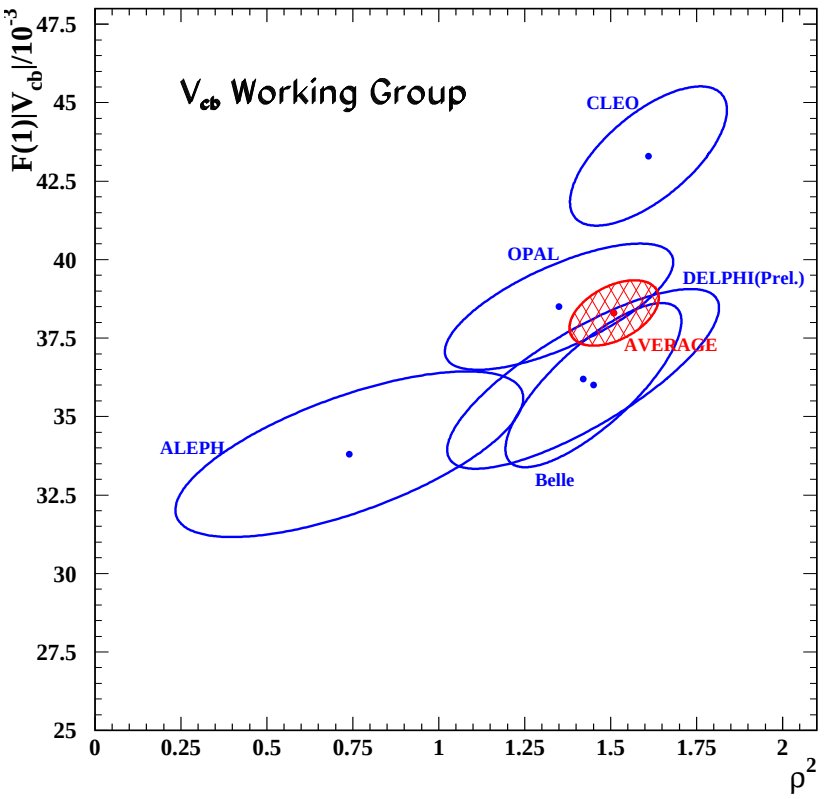

Fig. 3.8: *The error ellipses for the corrected measurements and world average for $\mathcal{F}(1)|V_{cb}|$ vs $\rho^2_{A_1}$. The ellipses correspond to a 39% C.L.*

experiment	$\mathcal{F}(1)\lvert V_{\rm cb}\rvert$ $(\times 10^{-3})$	$\rho^2_{A_1}$	$\rm Corr_{stat}$
ALEPH	33.8± 2.1± 1.6	0.74± 0.25± 0.41	94%
DELPHI	36.1± 1.4± 2.5	1.42± 0.14± 0.37	94%
OPAL	38.5± 0.9± 1.8	1.35± 0.12± 0.31	89%
BELLE	36.0± 1.9± 1.8	1.45± 0.16± 0.20	90%
CLEO	43.3± 1.3± 1.8	1.61± 0.09± 0.21	86%
World average	38.3 ± 0.5± 0.9	1.51± 0.05± 0.12	86%

Table 3.18: *Experimental results after the correction to common inputs and world average. The LEP numbers are corrected to use R_1 and R_2 from CLEO data. $\rho^2_{A_1}$ is the slope parameter as defined in Eq. (72) at zero recoil.*

experiment	$\mathcal{G}(1)\|V_{cb}\|(\times 10^{-3})$	$\rho^2_{\mathcal{G}}$	References
Published values			
ALEPH	31.1± 9.9± 8.6	0.20± 0.98± 0.50	[175]
BELLE	41.1± 4.4± 5.2	1.12± 0.22± 0.14	[190]
CLEO	44.4± 5.8± 3.7	1.27± 1.25± 0.14	[191]
Scaled values			
ALEPH	37.7± 9.9± 6.5	0.90 ± 0.98± 0.38	
BELLE	41.2± 4.4± 5.1	1.12± 0.22± 0.14	
CLEO	44.6± 5.8± 3.5	1.27± 0.25± 0.14	
World average	41.3 ± 2.9± 2.7	1.19± 0.15± 0.12	

Table 3.19: *Experimental results before and after the correction to common inputs and world average. $\rho^2_{\mathcal{G}}$ is the slope parameter as defined in Eq. (75).*

The dominant error is theoretical, but there are good prospects to reduce it through improvements in lattice QCD calculations, particularly removing the quenched approximation.

3.6.2. $|V_{cb}|$ from $\mathrm{B} \to \mathrm{D}\ell\nu$ decays

The strategy to extract $|V_{cb}|\mathcal{G}(1)$ is identical to that used for $|V_{cb}|\mathcal{F}(1)$ in $\mathrm{B} \to \mathrm{D}\ell\nu$ decays. As discussed above, theoretical estimates of $\mathcal{G}(1)$ are not, at this time, as accurate. This channel is much more challenging also from the experimental point of view because $d\Gamma_D/dw$ is more heavily suppressed near $w = 1$ than $d\Gamma_{D^*}/dw$, due to the helicity mismatch between initial and final states, and because it is hard to isolate from the dominant background, $\mathrm{B} \to \mathrm{D}^*\ell\nu$, as well as from fake D-ℓ combinations. Thus, the extraction of $|V_{cb}|$ from this channel is less precise than the one from the $\mathrm{B} \to \mathrm{D}^*\ell\nu$ decay. Nevertheless, the $\mathrm{B} \to \mathrm{D}\ell\nu$ channel provides a consistency check.

BELLE [190] and ALEPH [175] have studied the $\overline{\mathrm{B}}^0 \to \mathrm{D}^+\ell^-\bar{\nu}$ channel, while CLEO [191] has studied both $\mathrm{B}^+ \to \mathrm{D}^0\ell^+\bar{\nu}$ and $\overline{\mathrm{B}}^0 \to \mathrm{D}^+\ell^-\bar{\nu}$ decays. The parametrization used in these studies for the extrapolation to zero recoil is that of Eq. (75). The published results are shown in Table 3.19, together with the results scaled to common inputs. Averaging the latter according to the procedure of [185], we get $\mathcal{G}(1)|V_{cb}| = (41.3 \pm 4.0) \times 10^{-3}$ and $\rho^2_{\mathcal{G}} = 1.19 \pm 0.19$, where $\rho^2_{\mathcal{G}}$ is the slope parameter of $\mathcal{G}(w)$ at zero recoil.

Using $\mathcal{G}(1) = 1.00 \pm 0.07$, as given in Sec. 3.3., we get

$$|V_{cb}| = (41.3 \pm 4.0_{exp} \pm 2.9_{theo}) \times 10^{-3}, \tag{110}$$

consistent with Eq. (109) from $\mathrm{B} \to \mathrm{D}^*\ell\nu$ decay, but with an uncertainty about twice as large.

Since $|V_{cb}|$ drops out of the measured ratio $\mathcal{G}(w)/\mathcal{F}(w)$, this can be compared to theoretical calculations independently of their basis. In the heavy-quark limit, both form factors are given by the same function of w. A precise measurement of their ratio would provide information about the size of symmetry-breaking corrections away from zero recoil. Some experiments have also looked at the differential decay rate distribution to extract the ratio $\mathcal{G}(w)/\mathcal{F}(w)$. However, data are not precise enough to measure the symmetry-breaking corrections away from zero recoil. From the measured values of $\mathcal{G}(1)|V_{cb}|$ and $\mathcal{F}(1)|V_{cb}|$, we get $\mathcal{G}(1)/\mathcal{F}(1) = 1.08 \pm 0.09$, consistent with the form factor values that we used.

4. Exclusive determination of $|V_{ub}|$

As seen in Sec. 2.5., $|V_{ub}|$ can be measured from the inclusive $b \to u l \nu$ rate — blind to the particular decay mode. Such measurements require, however, that kinematic selections be made to discriminate against the dominant $b \to c l \nu$ background. This introduces additional theoretical uncertainties that can be significant.

An alternative route to measure $|V_{ub}|$ is the exclusive reconstruction of particular $b \to u l \nu$ final states. Experimentally this provides some extra kinematical constraints for background suppression, and theoretically the uncertainties are of a different nature. The extraction of $|V_{ub}|$ is complicated by the fact that the quarks are not free, but bound inside mesons. The probability that the final state quarks will form a given meson is described by form factors. And unlike exclusive $b \to c l \nu$ decays, heavy quark symmetry does not help to normalize these form factors at particular kinematic points. A variety of calculations of these form factors exists, based on lattice QCD, QCD sum rules, perturbative QCD, or quark models. At present, none of these methods allows for a fully model-independent determination of $|V_{ub}|$, though lattice calculations should, in time, provide a means to reach this goal. It is thus very important to obtain a consistent measurement of $|V_{ub}|$ with both the inclusive and exclusive approach and also to find consistent results for the various exclusive modes. The simplest mode theoretically is $\mathrm{B} \to \pi l \nu$, since a description of its rate involves only one form factor in the limit of vanishing lepton mass, instead of the three required for vector final states.

The differential rate for $\mathrm{B}^0 \to \pi^- l^+ \nu$ decays ($l = e$ or μ) is given by

$$\frac{1}{|V_{ub}|^2}\frac{d\Gamma}{dq^2} = \frac{G_F^2}{24\pi^3}\left[(v\cdot k)^2 - m_\pi^2\right]^{3/2} |f_{B\pi}^+(q^2)|^2, \tag{111}$$

where the form factor $f_{B\pi}^+(q^2)$ is defined through

$$\langle \pi^-(k)|\bar{b}\gamma^\mu u|\mathrm{B}^0(p)\rangle = f_{B\pi}^+(q^2)\left[(p+k)^\mu - \frac{M_B^2 - m_\pi^2}{q^2}q^\mu\right] + f_{B\pi}^0(q^2)\frac{M_B^2 - m_\pi^2}{q^2}q^\mu, \tag{112}$$

with q^2 the momentum transfer squared, $q^2 = (p-k)^2 = M_B^2 + m_\pi^2 - 2M_B v\cdot k$, and $p = M_B v$. In the s.l. domain, q^2 takes values in the range from 0 to $q^2_{\max} \equiv (M_B - m_\pi)^2$ which corresponds to $v\cdot k$ varying from $M_B/2 + m_\pi^2/(2M_B)$ to m_π. The form factor $f_{B\pi}^0(q^2)$ does not contribute to the rate in the limit of vanishing lepton mass.

4.1. Lattice QCD determinations of semileptonic heavy-to-light form factors

Lattice QCD simulations potentially provide a means of calculating heavy-to-light decay form factors from first principles[¶]. These calculations are model independent in the sense that they are based on approximations of QCD that can be systematically improved to arbitrarily high accuracy. In practice, however, all calculations to date have been performed in the quenched approximation, where the effect of sea quarks is treated as a mean field. This introduces a systematic error that is difficult to estimate *a priori*, though experience shows that for many hadronic quantities, the deviations induced by the quenched approximation are in the 10 to 15% range.

Besides the quenched approximation, which will be lifted (at least partially) in the near future, there are two major practical limitations in the lattice calculation of heavy-to-light form factors. One is that the spatial momenta of the initial and final state hadrons are restricted to be less than about 2 GeV, to avoid large discretization errors. The other is that light-quark masses are much larger than their physical value and the corresponding "pion" mass is $m_\pi \gtrsim$ 400 MeV, so that an extrapolation to the physical light quarks is needed (the so-called chiral extrapolation). As a result, the available region for q^2 is limited to values above about $q^2_{\max}/2$.

[¶] An introductory, though slightly dated, review of some of the subjects covered in this section can be found in [192]

4.1.1. Results for $\mathrm{B}^0 \to \pi^- l^+ \nu$ *form factors*

In addition to the extrapolations in light-quark mass, an understanding of the dependence of the form factors on heavy-quark mass is necessary. For both these purposes, the HQET motivated form factors [202] $f_1(v\cdot k)$ and $f_2(v\cdot k)$ are useful. They are related to the form factors $f^+_{B\pi}$ and $f^0_{B\pi}$ of Eq. (112) through

$$f^+_{B\pi}(q^2) = \sqrt{M_B}\left\{\frac{f_2(v\cdot k)}{v\cdot k}+\frac{f_1(v\cdot k)}{M_B}\right\}, \tag{113}$$

$$f^0_{B\pi}(q^2) = \frac{2}{\sqrt{M_B}}\frac{M_B^2}{M_B^2-m_\pi^2}\left\{[f_1(v\cdot k)+f_2(v\cdot k)] - \frac{v\cdot k}{M_B}\left[f_1(v\cdot k)+\frac{m_\pi^2}{(v\cdot k)^2}f_2(v\cdot k)\right]\right\}. \tag{114}$$

The HQET form factors are defined such that the heavy quark scaling with $M_B \to \infty$ is manifest, namely, $f_{1,2}(v\cdot k)$ become independent of M_B up to logarithms coming from the renormalization of the heavy-light current. The corrections due to finite M_B are then described as a power series in $1/M_B$. At leading order in the $1/M_B$ expansion, $f^+_{B\pi}(q^2)$ is proportional to $f_2(v\cdot k)$, while $f^0_{B\pi}(q^2)$ is proportional to a linear combination $f_1(v\cdot k)+f_2(v\cdot k)$. Thus, the heavy quark scaling of $f^+_{B\pi}(q^2)$ and $f^0_{B\pi}(q^2)$ is given by,

$$f^+_{B\pi}(q^2) \sim \sqrt{M_B}, \tag{115}$$

$$f^0_{B\pi}(q^2) \sim \frac{1}{\sqrt{M_B}}, \tag{116}$$

for fixed $v\cdot k$, up to logarithms and $1/M_B$ corrections.

Recently four major lattice groups, UKQCD [193], APE [194], Fermilab [195], and JLQCD [196], have performed quenched calculations of $\mathrm{B}\to\pi l\nu$ form factors. The UKQCD [193] and APE [194] collaborations use non-perturbatively $O(a)$-improved Wilson fermions [197,198,199]) and treat heavy quarks relativistically. In this formalism, the leading discretization errors induced by the heavy-quark mass, m_Q, are reduced from am_Q to $(am_Q)^2$, with a the lattice spacing. To keep these errors under control with the lattice spacing $a \sim 1/2.7\,\mathrm{GeV}$ available to them, they have to perform the calculations for heavy-quark masses in the neighborhood of the charm-quark mass and extrapolate to the bottom. The drawback of this approach is that the extrapolation can be significant and that discretization errors may be amplified if this extrapolation is performed before a continuum limit is taken. The Fermilab group [195], on the other hand, uses a formalism for heavy quarks in which correlation functions computed with Wilson-type fermions are reinterpreted using HQET [160,161]. In this way, they can reach both the charm and bottom quarks without extrapolation, and they investigate the discretization errors using three lattice spacings (β = 6.1, 5.9 and 5.7) covering $1/a \sim$ 1.2–2.6 GeV. The JLQCD collaboration [196] employs a lattice NRQCD action [200,201] for heavy quarks so that the bottom quark mass is covered by interpolation, and the calculation is done on a coarse lattice, $1/a \sim$ 1.6 GeV (β = 5.9). Both the Fermilab and NRQCD approach are based on expansions of QCD in powers of $1/m_Q$ and precision calculations at the physical b-quark mass require the inclusion of corrections proportional to powers of $1/m_b$ which can be difficult to compute accurately. In the case of NRQCD, one is also confronted with the fact that the continuum limit cannot be taken. All groups use an $O(a)$-improved Wilson action [197] for light quarks. Fig. 3.9 shows a comparison of recent results for the $\mathrm{B}^0 \to \pi^- l^+ \nu$ form factors $f^+_{B\pi}(q^2)$ and $f^0_{B\pi}(q^2)$ from the four groups [193,194,195,196]. For convenience, the values of these form factors are also reported in Table 3.20. The lattice results are available only for the large q^2 region ($13\ \mathrm{GeV}^2 \gtrsim q^2 \gtrsim\ 23\ \mathrm{GeV}^2$) corresponding to small spatial momenta of the initial B and final pion.

Good agreement is found amongst the different groups for $f^+_{B\pi}(q^2)$, while the results for $f^0_{B\pi}(q^2)$ show a slight disagreement. To assess where these differences may come from and, more generally, to estimate systematic errors, the heavy and light quark extrapolations, which form a core part of the underlying analysis, are now briefly reviewed.

Ref.	q^2 [GeV^2]	$f^0_{B\pi}(q^2)$	$f^+_{B\pi}(q^2)$	$1/\|V_{ub}\|^2 d\Gamma/dq^2$ [ps^{-1}GeV^{-2}]
APE	13.6	$0.46(7)^{+5}_{-8}$	$0.70(9)^{+10}_{-3}$	$0.33(9)^{+\ 9}_{-\ 3}$
APE	15.0	$0.49(7)^{+6}_{-8}$	$0.79(10)^{+10}_{-4}$	$0.31(8)^{+\ 8}_{-\ 3}$
APE	16.4	$0.54(6)^{+5}_{-9}$	$0.90(10)^{+10}_{-4}$	$0.28(6)^{+\ 6}_{-\ 3}$
UKQCD	16.7	$0.57^{+6\ +5}_{-6\ -20}$	$0.9^{+1\ +2}_{-2\ -1}$	$0.29^{+10\ +11}_{-\ 9\ -\ 6}$
FNAL	17.23	$0.64^{+\ 9+10}_{-\ 3-10}$	$1.13^{+24+17}_{-\ 9-17}$	$0.35^{+15}_{-\ 6}(11)$
JLQCD	17.79	0.407(92)	1.03(22)	0.25(11)
APE	17.9	$0.59(6)^{+4}_{-10}$	$1.05(11)^{+10}_{-6}$	$0.25(5)^{+\ 5}_{-\ 3}$
UKQCD	18.1	$0.61^{+6\ +6}_{-6\ -19}$	$1.1^{+2\ +2}_{-2\ -1}$	$0.27^{+8\ +11}_{-7\ -1}$
FNAL	18.27	$0.70^{+\ 9+11}_{-\ 4-11}$	$1.36^{+23+20}_{-\ 9-20}$	$0.37^{+13}_{-\ 5}(11)$
JLQCD	18.29	0.421(92)	1.09(21)	0.240(94)
JLQCD	18.80	0.435(98)	1.16(21)	0.231(84)
APE	19.3	$0.64(6)^{+4}_{-10}$	$1.25(13)^{+9}_{-8}$	$0.22(5)^{+\ 3}_{-\ 3}$
JLQCD	19.30	0.45(11)	1.24(21)	0.221(76)
FNAL	19.31	$0.76^{+10+11}_{-\ 4-11}$	$1.59^{+21+24}_{-\ 7-24}$	$0.36^{+10}_{-\ 3}(11)$
UKQCD	19.5	$0.66^{+5\ +6}_{-5\ -17}$	$1.4^{+2\ +3}_{-2\ -1}$	$0.25^{+7\ +11}_{-6\ -1}$
JLQCD	19.81	0.47(12)	1.33(22)	0.210(71)
JLQCD	20.31	0.49(13)	1.43(24)	0.199(68)
FNAL	20.35	$0.83^{+10+12}_{-\ 4-12}$	$1.72^{+18+26}_{-\ 8-26}$	$0.28^{+\ 6}_{-\ 3}(9)$
APE	20.7	$0.71(6)^{+3}_{-10}$	$1.53(17)^{+8}_{-11}$	$0.19(4)^{+\ 2}_{-\ 3}$
JLQCD	20.82	0.51(14)	1.54(27)	0.187(66)
UKQCD	20.9	$0.72^{+5\ +6}_{-4\ -14}$	$1.8^{+2\ +4}_{-2\ -1}$	$0.23^{+6\ +11}_{-5\ -1}$
FNAL	21.38	$0.89^{+10+13}_{-\ 4-13}$	1.84^{+20+27}_{-14-27}	$0.20^{+\ 4}_{-\ 3}(6)$
APE	22.1	$0.80(6)^{+1}_{-12}$	$1.96(23)^{+6}_{-18}$	$0.16(4)^{+\ 1}_{-\ 3}$
FNAL	22.41	$0.95^{+12+14}_{-\ 3-14}$	1.96^{+24+29}_{-20-29}	$0.13^{+\ 3}_{-\ 3}(4)$
FNAL	23.41	$1.00^{+13+15}_{-\ 3-15}$	2.10^{+29+32}_{-25-32}	$0.09^{+\ 2}_{-\ 2}(2)$

Table 3.20: Form factors and differential rate for $B^0 \to \pi^- l\nu$ decays from UKQCD [193], APE [194], FNAL [195] and JLQCD [196]. The first set of errors is statistical and the second, systematic. In the case of JLQCD, these two sets of errors were combined quadratically.

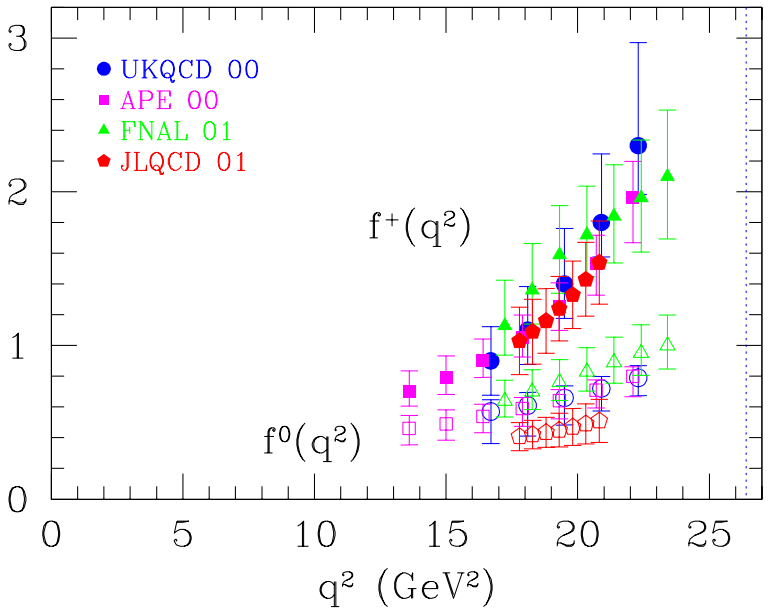

Fig. 3.9: *Recent lattice results for* $\mathrm{B}^0 \to \pi^- l^+ \nu$ *form factors* $f^+_{B\pi}(q^2)$ *and* $f^0_{B\pi}(q^2)$. *Statistical and systematic errors are added in quadrature.*

Heavy quark scaling

At a fixed value of $v \cdot k$, the $1/M_B$ dependences of the form factors $f^+_{B\pi}(q^2)/\sqrt{M_B}$ and $f^0_{B\pi}(q^2)\sqrt{M_B}$ from JLQCD are compared to those of APE [194] in Fig. 3.10. Both collaborations agree that there is no significant $1/M_B$ dependence in $f^+_{B\pi}(q^2)/\sqrt{M_B}$. For $f^0_{B\pi}(q^2)\sqrt{M_B}$, on the other hand, the APE [194] result has a significant slope, which is also supported by the Fermilab result [195] (not shown in the plot), while JLQCD do not see such dependence. The reason for this disagreement is not clear, but it partly explains the smaller value of $f^0_{B\pi}(q^2)$ of JLQCD data in Fig. 3.9.

Chiral extrapolation

The chiral extrapolation of the HQET form factors $f_1(v \cdot k) + f_2(v \cdot k)$ and $f_2(v \cdot k)$ is demonstrated in Fig. 3.11. This extrapolation is performed at fixed $v \cdot k$ by fitting the form factors to a power series in the light quark mass, as suggested in [193]. No attempt is made to account for chiral logarithms because they are not correctly reproduced in the quenched theory [206,207]. The figure shows that the extrapolation is insignificant for $f_2(v \cdot k)$ (or $f^+_{B\pi}(q^2)$), while a large extrapolation is involved in $f_1(v \cdot k) + f_2(v \cdot k)$ (or $f^0_{B\pi}(q^2)$).

Summary of current status

The current status of quenched lattice calculations of the $\mathrm{B} \to \pi l \nu$ form factors may be summarized as follows:

- The physical form factor $f^+_{B\pi}(q^2)$ has small $1/M_B$ corrections in the range of recoils explored. As a result, neither the extrapolation from the charm-quark-mass region (in the UKQCD and APE results) nor the truncation of the $1/M_B$ expansion (in the Fermilab and JLQCD results) is a dominant source of systematic error. $f^0_{B\pi}(q^2)$ is more sensitive to $1/M_B$ corrections, and the agreement among different groups is poorer.
- The form factor $f^+_{B\pi}(q^2)$ is relatively insensitive to light-quark mass, and simple polynomial chiral extrapolations are stable. This is not the case for $f^0_{B\pi}(q^2)$, which displays significant light-quark-mass dependence.
- The agreement amongst the four groups for $f^+_{B\pi}(q^2)$ as shown in Fig. 3.9 is remarkable, because

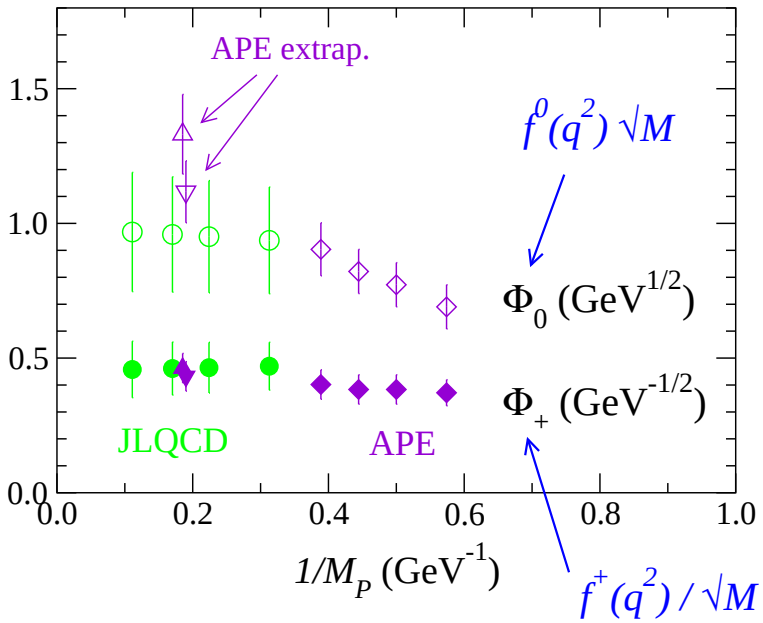

Fig. 3.10: $1/M_B$ *scaling of the form factors* $f^+_{B\pi}(q^2)/\sqrt{M_B}$ *(filled symbols) and* $f^0_{B\pi}(q^2)\sqrt{M_B}$ *(open symbols) at fixed* $v\cdot k \sim 0.95$ GeV. *Data from APE [194] (diamonds) and JLQCD [196] (circles).*

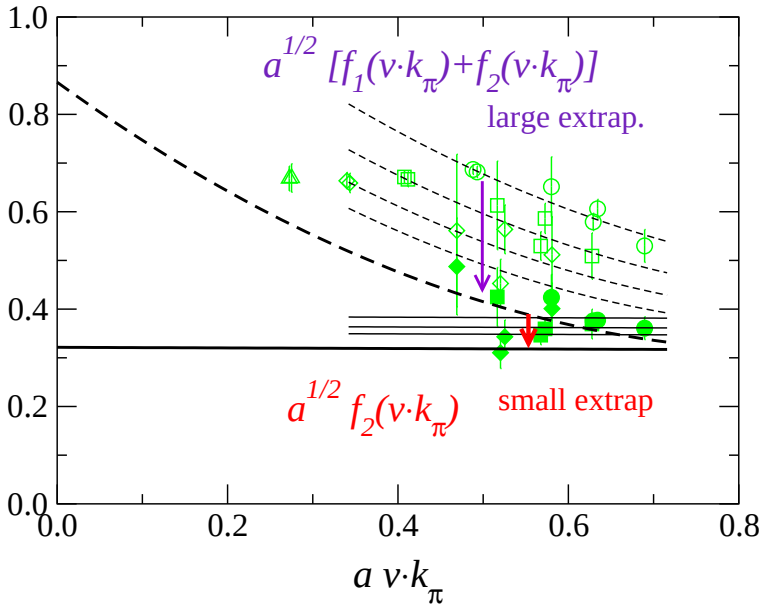

Fig. 3.11: *The chiral extrapolation of the HQET form factors* $f_1(v\cdot k)+f_2(v\cdot k)$ *(open symbols) and* $f_2(v\cdot k)$ *(filled symbols) is indicated by the vertical, downward-pointing arrows. Data from JLQCD [196].*

the groups use different methods for modelling the b quark, for matching the lattice current to the continuum one, for performing chiral extrapolations, *etc.* This agreement is probably due to the fact that this form factor is relatively insensitive to heavy- and light-quark masses, as long as $q^2_{\rm max}$ is not approached too closely.

These observations allow us to conclude that the systematic error is under control at the level of accuracy shown in Fig. 3.9.

On the other hand, the lattice calculations reviewed have important drawbacks:

- They are performed in the quenched approximation.
- The available lattice results are restricted to the large q^2 region. They may be used to predict the partially integrated decay rate, but predictions for the total decay rate usually introduce some model dependence.
- For the physical form factor $f^+_{B\pi}(q^2)$, the current error is of order 20% for all groups and a significant reduction in error will be challenging.

Strategies for determining $|V_{ub}|$

With the quenched lattice results for $\mathrm{B}^0 \to \pi^- l^+ \nu$ decays presented above, the only unknown in the expression of Eq. (111) for the differential decay rate is $|V_{ub}|$. To illustrate this point, the results of the four collaborations for this rate are reproduced in Table 3.20. It is clear, then, that $|V_{ub}|$ can be determined without assumptions about the q^2 dependence of form factors, once experiments measure the differential or partially integrated rate in the range of q^2 values reached in these calculations. Future lattice calculations in full, unquenched QCD will permit completely model-independent determinations of $|V_{ub}|$.

The total rate or the differential rate closer to $q^2 = 0$ can also be used to extract $|V_{ub}|$, but then an extrapolation becomes necessary. This extrapolation usually introduces model dependence and the resulting $|V_{ub}|$ thus inherits a systematic error that is difficult to quantify.

Pole dominance models suggest the following momentum dependence for the form factors,

$$f^i_{B\pi}(q^2) = \frac{f_{B\pi}(0)}{(1 - q^2/M_i^2)^{n_i}}, \tag{117}$$

where $i = +,\ 0$, n_i is an integer exponent and the kinematical constraint $f^+_{B\pi}(0) = f^0_{B\pi}(0)$ has already been imposed. Combining this with the HQS scaling relations of Eq. (115) implies $n_+ = n_0 + 1$. Light-cone sum rule scaling further suggests $n_0 = 1$ [211] [‖]. Another pole/dipole parametrization for $f^0_{B\pi}$ and $f^+_{B\pi}$, which accounts for the B^* pole in $f^+_{B\pi}$ correctly, has been suggested by Becirevic and Kaidalov (BK) [241]:

$$\begin{aligned} f^+_{B\pi}(q^2) &= \frac{f_{B\pi}(0)}{(1 - q^2/m^2_{B^\star})(1 - \alpha q^2/m^2_{B^\star})} \\ f^0_{B\pi}(q^2) &= \frac{f_{B\pi}(0)}{(1 - q^2/\beta m^2_{B^\star})}. \end{aligned} \tag{118}$$

Fitting this parametrization to the results of each of the four collaborations yields the results summarized in Table 3.21. Though uncertainties are still quite large, consistency amongst the various lattice predictions, as well as with the LCSR result, is good.

Using the results of these fits, UKQCD [193] and APE [194], obtain the following total rate:

$$\Gamma(\mathrm{B}^0 \to \pi^- l^+ \nu)/|V_{\rm ub}|^2 = \left\{ \begin{array}{ll} 9^{+3+3}_{-2-4}\ \mathrm{ps}^{-1} & \text{UKQCD [193]} \\ 7.0 \pm 2.9\ \mathrm{ps}^{-1} & \text{APE [194]} \end{array} \right. , \tag{119}$$

[‖] Pole/dipole behaviour for $f^0_{B\pi}$ and $f^+_{B\pi}$ was also suggested in [212].

Ref.	$f_{B\pi}(0)$	α	β
UKQCD M-I[193]	0.30^{+6+4}_{-5-9}	0.46^{+9+37}_{-10-5}	1.27^{+14+4}_{-11-12}
APE M-II [194]	$0.28(6)^{+5}_{-5}$	$0.45(17)^{+6}_{-13}$	$1.20(13)^{+15}$
APE M-I [194]	$0.26(5)^{+4}_{-4}$	$0.40(15)^{+9}_{-9}$	$1.22(14)^{+15}$
FNAL M-I[195]	0.33^{+2}_{-3}	0.34^{+9}_{-3}	1.31^{+3}_{-9}
JLQCD M-II[196]	0.23^{+4}_{-3}	0.58^{+12}_{-9}	1.28^{+12}_{-20}
LCSR [213]	0.28(5)	0.32^{+21}_{-7}	

Table 3.21: Results of fits of the lattice results from the four groups to the BK parametrization of Eq. (118). In the results of UKQCD and APE, the second set of uncertainties corresponds to systematic errors. Method I (M-I) consists in first extrapolating the form factors obtained from the simulation in light-quark mass, heavy-quark mass etc. and then fitting to the BK parametrization. Method II (M-II) corresponds to first fitting the BK parametrization to the form factors obtained from the simulation, before any chiral, heavy-quark, ... extrapolations, and then peforming the extrapolations on the fit parameters. The row entitled LCSR corresponds to a fit to light-cone sum rule results.

where the first error in the UKQCD result is statistical and the second is the systematic error, which includes the difference between the parametrizations of Eqs. (117) and (118). In the APE result, where a fit to the pole/dipole parametrization is not considered, the error includes statistical and systematic errors summed in quadrature. Nevertheless, because of the model dependence of these results, a larger systematic error cannot be excluded.

4.1.2. Future directions

In the following we discuss the directions that should be explored in the near future to improve the accuracy in the determination of $|V_{ub}|$.

Extension toward lower q^2

As already discussed, it is not straightforward to extend lattice calculations of heavy-to-light form factors to the low q^2 region, though finer lattices will eventually get us there. Extrapolations to lower q^2 values can be performed using models which incorporate many of the known constraints on the form factors, but this introduces a model dependence which is difficult to quantify. It has been proposed, however, to use dispersion relations together with lattice data to obtain model-independent bounds for the form factors over the entire q^2 range [208,209,137]. These techniques are based on the same ingredients as those used to constrain the shape of the form factors for $\mathrm{B} \to \mathrm{D}^{(*)} l\nu$ decays, briefly presented in Sec. 3.1., though details of the implementation are quite different. An example is shown in Fig. 3.12. The bounds in that figure were obtained using the lattice results for $\mathrm{B} \to \pi l\nu$ form factors from [210], the most complete set available at the time.

Since then lattice calculations have improved significantly and it would be interesting to derive new bounds by combining modern lattice results for the form factors with the techniques developed in [209]. It may also be advantageous to take into account additional constraints on the form factors. Furthermore, other ways of extending the range of lattice calculations to lower values of q^2 should be investigated.

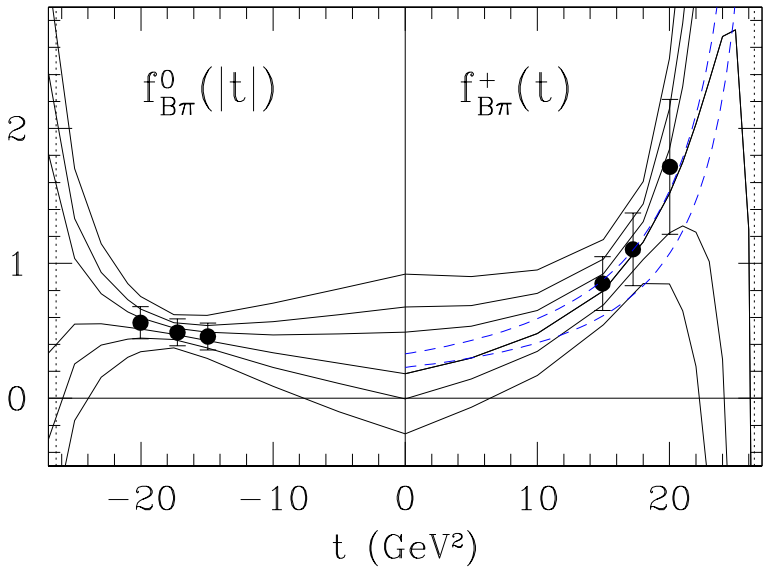

Fig. 3.12: *Dispersive bounds for $f_0(|t|)$ and $f_+(t)$ in $\mathrm{B}^0 \to \pi^- \ell^+ \nu$ decays [209]. The points are the lattice results of [210] with added systematic errors. The pairs of fine curves are, from the outermost to the innermost, the 95%, 70% and 30% bounds, where percentages represent the likelihood that the form factor take a value between the corresponding pair of curves at the given t. The dashed curves are the LCSR results of Eq. (129) [213]. Comparable results are given in Eq. (130) [235].*

Unquenching

Lattice calculations have to be performed with dynamical sea quarks to yield truly model independent results. Some groups already have gauge configurations for two flavours of sea quarks with degenerate masses $\gtrsim m_s/2$ (instead of the two very light u and d quarks and the lightish s quark found in nature). The study of B meson decays on these backgrounds presents no conceptual difficulty.

In practice, however, the chiral extrapolations required to reach the u and d quark masses may be rather delicate as it is not clear that the light-quark masses used in the simulations are light enough to be sensitive to the so-called chiral logarithms which are expected to dominate the small mass behaviour of many physical quantities (see e.g. [214–217] for recent discussions). It will be very important to control this light-quark-mass behaviour to obtain accuracies better than 10%.

Using $\mathrm{D} \to \pi \mathrm{l} \nu$ decays to improve predictions for $\mathrm{B} \to \pi \mathrm{l} \nu$ form factors

In the heavy charm and bottom limit, heavy quark symmetry relates the $\mathrm{B} \to \pi \mathrm{l} \nu$ form factors to $\mathrm{D} \to \pi \mathrm{l} \nu$. Burdman *et al.* [202] proposed to consider the ratio

$$\left.\frac{d\Gamma(\mathrm{B}^0 \to \pi^- l^+ \nu)/d(v\cdot k)}{d\Gamma(\mathrm{D}^0 \to \pi^- l^+ \nu)/d(v\cdot k)}\right|_{\text{same } v\cdot k} = \left|\frac{V_{ub}}{V_{cd}}\right|^2 \left(\frac{M_B}{M_D}\right)^2 \left|\frac{f^+_{B\pi}/\sqrt{M_B}}{f^+_{D\pi}/\sqrt{M_D}}\right|^2 , \tag{120}$$

from which one may extract the ratio of CKM matrix elements $|V_{ub}/V_{cd}|$. In view of the high-precision measurements of D decays promised by CLEO-c, such an approach to determining $|V_{ub}|$ is becoming increasingly relevant.

It is convenient to factorize the nearest pole contribution to $f^+_{B\pi}(q^2)$, which is expected to dominate the q^2 behaviour of this form factor in the heavy-quark limit, at least close to zero recoil. Thus, the breaking of heavy quark symmetry may be parametrized as

$$\frac{f^+_{B\pi}/\sqrt{M_B}}{f^+_{D\pi}/\sqrt{M_D}} = \frac{v\cdot k + \Delta_D}{v\cdot k + \Delta_B} R_{BD}(v\cdot k), \tag{121}$$

where $\Delta_{B,D} \equiv m_{B^*,D^*} - m_{B,D}$ and $(R_{BD}(v\cdot k)-1)$ describes the $1/M_{D,B}$ corrections to be calculated on the lattice. The question then becomes whether $R_{BD}(v\cdot k)$ can be calculated more accurately on the lattice than $f^+_{B\pi}(q^2)$. The answer is "yes" as a number of uncertainties are expected to cancel in the ratio. It is also encouraging that the heavy-quark-mass dependence of $f_2(v\cdot k)$ appears to be mild, as discussed previously.

To reach a level of 5% accuracy or better, the systematic errors associated with the heavy quark have to be under good control for both charm and bottom quarks. These errors should also be as similar as possible in the two regimes in order for them to cancel effectively. For these reasons, the relativistic and Fermilab approaches seem to be preferable to the use of NRQCD. Indeed, NRQCD involves an expansion of QCD in powers of $1/(am_Q)$ which requires either the inclusion of high-orders or coarse lattices ($a^{-1} \ll m_Q$) when m_Q approaches the charm mass. High orders are difficult to implement in practice and coarse lattices imply large discretization errors.

To reach such levels of accuracy, it is also important to study carefully the extent to which uncertainties associated with the chiral extrapolation of the form factors and with the presence of chiral logarithms cancel in the ratio of bottom to charm amplitudes.

B to vector meson semileptonic decays

The rate for $\mathrm{B} \to \rho \mathrm{l} \nu$ is less strongly suppressed kinematically near $q^2_{\rm max}$ than is the rate for $\mathrm{B} \to \pi l \nu$ and it is larger overall. Thus, the number of events will be larger in the region where the lattice can compute the relevant matrix elements reliably. In [218], the UKQCD collaboration suggested that $|V_{ub}|$ be obtained directly from a fit to the differential decay rate around $q^2_{\rm max}$, with the overall normalization of this rate, up to a factor of $|V_{ub}|^2$, determined using lattice results. With their lattice results, such a measurement would allow an extraction of $|V_{ub}|$ with a 10% statistical and a 12% systematic error coming from theory. [**] A first measurement of this differential rate has actually already been performed by CLEO [219].

Very recently, two lattice collaborations (UKQCD [222] and SPQcdR [223]) have begun revisiting $\mathrm{B} \to \rho l \nu$ decays. Their calculations are performed in the quenched approximation and results are still preliminary. Shown in Fig. 3.13 are the four independent form factors required to describe the $\mathrm{B} \to \rho$ s.l. matrix elements, as obtained by SPQcdR [223] at two values of the lattice spacing. Also shown are results from light-cone sum rule calculations [228] which are expected to be reliable for lower values of q^2. These sum rule results look like very natural extensions of the form factors obtained on the finer lattice. Combining the LCSR results for $q^2 \le 10\,\mathrm{GeV}^2$ with the results on the finer lattice for $q^2 > 10\,\mathrm{GeV}^2$ yields $\Gamma(\mathrm{B}^0 \to \rho^- l\nu) = (19 \pm 4)|V_{ub}|^2\,\mathrm{ps}^{-1}$ [223]. It will be interesting to see what the calculations of [222,223] give for the differential rate above $10\,\mathrm{GeV}^2$ once they are finalized.

As was the case for $\mathrm{B} \to \pi l \nu$ decays, derivation of the full q^2 dependence of the form factors from lattice data involves a large extrapolation from $q^2 > 10\,\mathrm{GeV}^2$ all the way down to $q^2 = 0$. Here, the use of dispersion relations is complicated by the singularity structure of the relevant correlation functions and form factors. There exist, however, lattice-constrained parametrizations of $\mathrm{B} \to \rho l \nu$ form factors, which are consistent with lattice results and heavy-quark scaling relations at large q^2, and with kinematic constraints and light-cone sum rule scaling at $q^2 = 0$ [211]. These parametrizations provide simple, few-parameter descriptions of s.l. form factors. [††] However, at values of the recoil for which there are not lattice results (i.e. low q^2), they are not predictions of (quenched) QCD.

[**] Other early lattice work on $\mathrm{B} \to \rho l \nu$ can be found in [220,221].

[††] Away from $q^2 = 0$, these parametrizations are actually not fully consistent with the large-recoil symmetry relations derived in [212] amongst the soft contributions to the relevant form factors. For completeness, let us mention that the α_s corrections to these symmetry relations were calculated in [224] and corrections in powers of $1/m_b$ were investigated in [225,226,227]

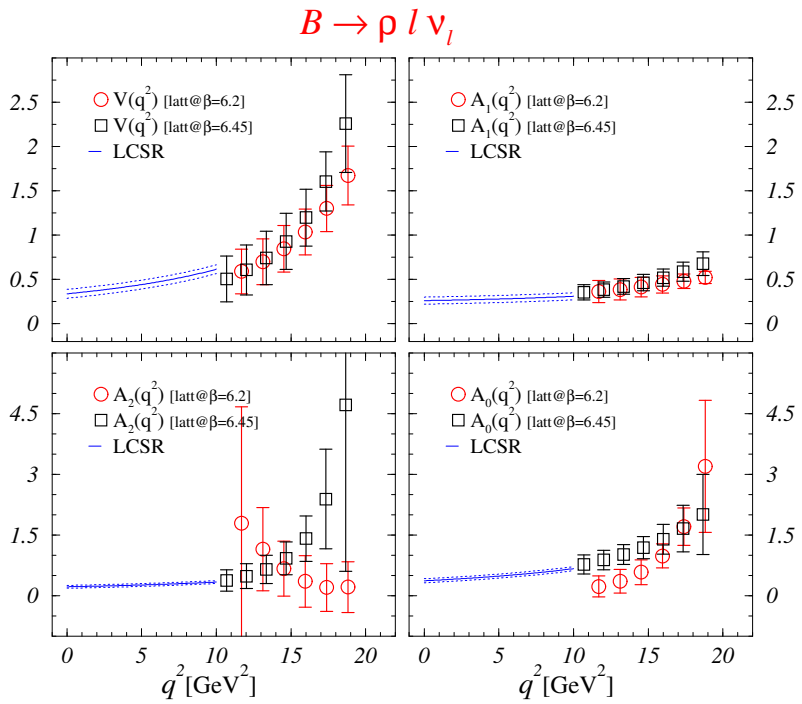

Fig. 3.13: *Example of quenched lattice results for* $\mathrm{B} \to \rho l \nu$ *form factors plotted as a function of* q^2 *[223]. These results were obtained at two values of the inverse lattice spacing* $1/a = 3.7\,\mathrm{GeV}$ *and* $2.7\,\mathrm{GeV}$*, corresponding to bare couplings values* $\beta = 6.45$ *and* 6.2 *respectively. Also shown at low* q^2 *are the light-cone sum rule results of [228].*

4.1.3. Summary

Four groups have recently performed quenched lattice calculations of $\mathrm{B} \to \pi l \nu$ form factors for $q^2 \gtrsim 12\,\mathrm{GeV}^2$ and their results agree. Agreement is best for $f_{B\pi}^+$ which determines the rate for these decays in the limit of vanishing lepton mass. The error on this form factor is of order 20%. The main sources of remaining systematic errors are quenching and light-quark-mass extrapolations for all the groups, and heavy-quark-mass extrapolations, discretization, and perturbative matching, depending on the group.

A substantial reduction in the error (i.e. below 10%) will be difficult to achieve solely in lattice QCD. This is where the use of ratios of s.l. B and D rates, such as the one given in Eq. (120), could be very helpful.

There is still a substantial number of improvements to be made to present calculations. The list includes unquenching, the use of dispersive bounds or other means of extending the kinematic reach of lattice calculations, the determination of ratios of s.l. B and D rates, and more investigations of $\mathrm{B} \to \rho l \nu$ decays.

4.2. Heavy-to-light form factors from light-cone sum rules

The QCD light-cone sum rules (LCSR) [230,231] provide estimates of various heavy-to-light transition form factors. In particular, $\mathrm{B} \to P, V$ form factors ($P = \pi, \mathrm{K}$ and $V = \rho, \mathrm{K}^*, \phi$) have been calculated at small and intermediate momentum transfers, typically at $0 < q^2 \leq m_b^2 - 2 m_b \Lambda_{QCD}$. The upper part of this interval overlaps with the region accessible to the lattice calculations of the same form factors, allowing one to compare the results of two methods. In what follows we will concentrate on the LCSR prediction for the $\mathrm{B} \to \pi$ form factor $f_{B\pi}^+$ [232–234]. Its accuracy has been recently improved in Ref. [235]. For the LCSR $\mathrm{B} \to V$ form factors we refer to the NLO calculation in Ref. [228] and to the resulting parametrization in Ref. [236].

The LCSR approach to calculate $f^+_{B\pi}$ employs a specially designed theoretical object, the vacuum-to-pion correlation function

$$F_\mu(p,q) = i\int d^4x e^{iqx}\langle\pi^+(p)|\, T\{\bar{u}\gamma_\mu b(x), m_b\bar{b}i\gamma_5 d(0)\}\,|0\rangle = F((p+q)^2,q^2)p_\mu + O(q_\mu)\,, \quad (122)$$

where the $b \to u$ weak current is correlated with the quark current which has the B meson quantum numbers, and $p^2 = m_\pi^2$. Writing down the dispersion relation for the invariant amplitude F:

$$F((p+q)^2,q^2) = \frac{2f_B f^+_{B\pi}(q^2)M_B^2}{M_B^2-(p+q)^2} + \sum_{B_h}\frac{2f_{B_h}f^+_{B_h\pi}(q^2)m^2_{B_h}}{m^2_{B_h}-(p+q)^2}\,, \quad (123)$$

one represents the correlation function (122) in terms of hadronic degrees of freedom in the B channel. The ground-state contribution in Eq. (123) contains a product of the B meson decay constant f_B and the form factor $f^+_{B\pi}(q^2)$ we are interested in, whereas the sum over B_h accounts for the contributions of excited and continuum B states.

The dispersion relation is then matched to the result of QCD calculation of $F((p+q)^2,q^2)$ at large virtualities, that is, at $|\ (p+q)^2 - m_b^2\ | \gg \Lambda^2_{QCD}$ and $q^2 \ll m_b^2$. In this region the operator-product expansion (OPE) near the light-cone $x^2 = 0$ is employed:

$$F((p+q)^2,q^2) = \sum_{t=2,3,4}\int Du_i \sum_{k=0,1}\left(\frac{\alpha_s}{\pi}\right)^k T_k^{(t)}((p+q)^2,q^2,u_i,m_b,\mu)\varphi_\pi^{(t)}(u_i,\mu)\,. \quad (124)$$

This generic expression is a convolution of calculable short-distance coefficient functions $T_k^{(t)}$ and universal pion light-cone distribution amplitudes (DA) $\varphi_\pi^{(t)}(u_i,\mu)$ of twist t. Here, m_b is the one-loop b-quark pole mass, μ is the factorization scale and the integration goes over the pion momentum fractions $u_i = u_1, u_2, ...$ distributed among quarks and gluons, so that $Du_i \equiv du_1 du_2 ... \delta(1-\sum_i u_i)$. In particular, $\varphi_\pi^{(2)}(u_1,u_2,\mu) = f_\pi\varphi_\pi(u,\mu)$, ($u_1 = u, u_2 = 1-u$) where φ_π is the lowest twist 2, quark-antiquark pion DA normalized to unity:

$$\varphi_\pi(u,\mu) = 6u(1-u)\left(1+\sum_n a_{2n}(\mu)C_{2n}^{3/2}(2u-1)\right)\,. \quad (125)$$

In the above, C_{2n} are Gegenbauer polynomials and the oefficients $a_n(\mu)$, that are suppressed logarithmically at large μ, determine the deviation of $\varphi_\pi(u)$ from its asymptotic form. Importantly, the contributions to Eq. (124) corresponding to higher twist and/or higher multiplicity pion DA are suppressed by inverse powers of the b-quark virtuality $(m_b^2-(p+q)^2)$, allowing one to retain a few low twist contributions in this expansion. Furthermore, one uses quark-hadron duality to approximate the sum over B_h in Eq. (123) by a dispersion integral over the quark-gluon spectral density, introducing a threshold parameter s_0^B. The final step involves a Borel transformation $(p+q)^2 \to M^2$, where the scale of the Borel parameter M^2 reflects the characteristic virtuality at which the correlation function is calculated.

The resulting sum rule relation obtained by matching Eqs. (123) and (124) can be cast in the following form:

$$f_B f^+_{B\pi}(q^2) = \frac{1}{M_B^2}\exp\left(\frac{M_B^2}{M^2}\right)\sum_{t=2,3,4}\ \sum_{k=0,1}\left(\frac{\alpha_s}{\pi}\right)^k \mathcal{F}_k^{(t)}(q^2,M^2;m_b,s_0^B,\mu;\{\mathrm{DA}\}^{(t)})\,, \quad (126)$$

where the double expansion (in twists and in α_s) and the dependence on the relevant parameters are made explicit. In particular, $\{DA\}^{(t)}$ denotes the non-perturbative normalization constant and non-asymptotic coefficients for each given twist component, e.g., for φ_π: $\{DA\}^{(2)} = \{f_\pi, a_i\}$. The sum rule (126) includes all zeroth order in α_s, twist 2,3,4 contributions containing quark-antiquark and quark-antiquark-gluon DA of the pion. The perturbative expansion has NLO accuracy, including the $O(\alpha_s)$ corrections

to the twist 2 [233] and twist 3 coefficient functions, the latter recently calculated in Ref. [235]. More details on the derivation of LCSR (126) and the explicit expressions can be found in the review papers [237–239].

For the B meson decay constant entering LCSR (126) one usually employs the conventional SVZ sum rule [46] for the two-point correlator of $\bar{b}i\gamma_5 q$ currents with $O(\alpha_s)$ accuracy (a recent update of this sum rule [240] is discussed in Chapter 4 of the present document):

$$f_B = \sum_{d=0,3\div 6} \sum_{k=0,1} \left(\frac{\alpha_s}{\pi}\right)^k C_k^{(d)}(\overline{M}^2, m_b, s_0^B, \mu)\langle 0|\Omega_d(\mu)|0\rangle\,, \tag{127}$$

where the expansion contains the perturbative term with dimension $d = 0$ ($\Omega_0 = 1$), and, at $d \geq 3$, goes over condensates, the vacuum averages of operators $\Omega_d = \bar{q}q, G^a_{\mu\nu}G^{a\mu\nu}, ...$, multiplied by calculable short-distance coefficients $C_k^{(d)}$. The Borel parameter $\overline{M}$ is correlated with M. The LCSR prediction for the $\mathrm{B} \to \pi$ form factor is finally obtained dividing Eq. (126) by Eq. (127):

$$f^+_{B\pi}(q^2) = (f_B f^+_{B\pi}(q^2))_{LCSR}/(f_B)_{2ptSR}\,. \tag{128}$$

In order to demonstrate that the expansion in both twist and α_s in this relation works well, we present the approximate percentage of various contributions to the resulting form factor (128):

twist	DA	LO	$O(\alpha_s)$ NLO
2	$\bar{q}q$	~ 50 %	~ 5%
3	$\bar{q}q$	~ 40 %	~ 1%
4	$\bar{q}q$	~ 5 %	-
3+4	$\bar{q}qG$		

The input parameters used in the numerical analysis of the sum rules (126) and (127) have a limited accuracy. The theoretical uncertainty is estimated by varying these inputs within the allowed regions and adding up linearly the separate uncertainties induced by these variations in the numerical prediction for $f^+_{B\pi}$. The resulting total uncertainties are given below, together with the parametrizations of the form factor. A detailed theoretical error analysis can be found in Ref. [213]. To summarize it briefly, one source of uncertainty is the value of the b-quark one-loop pole mass. The two most recent LCSR analyses use $m_b = 4.7 \pm 0.1$ GeV [213] and $m_b = 4.6 \pm 0.1$ GeV [235]. In both studies, the threshold s_0^B is not an independent parameter, being determined by stabilizing f_B calculated from Eq. (127) at a given b-quark mass. The uncertainty induced by varying the factorization scale μ (adopted simultaneously as the normalization scale for α_s) is very small, firstly, because the NLO approximation is implemented for both dominant twist 2 and 3 terms, and, secondly, because the relatively large $O(\alpha_s)$ corrections to the twist 2 contribution and to the f_B sum rule cancel in the ratio (128). Another source of uncertainty is our limited knowledge of the non-asymptotic part in the pion DA (determined by the coefficients a_{2n} and the analogous coefficients in twist 3,4 DA). In Ref. [213] these coefficients were varied from a certain non-asymptotic ansatz of DA (motivated by QCD sum rules) to purely asymptotic DA. Such a substantial variation covers the existing constraints on non-asymptotic coefficients obtained from LCSR for pion form factors. The latter constraints have been used in Ref. [235]. In fact, LCSR involve integration over normalized DA, therefore it is natural that the results only moderately depend on the non-asymptotic coefficients. Finally, to assess the reliability of the LCSR procedure one has to comment on the use of quark-hadron duality, which is the most sensitive point in the sum rule approach. We expect that the sensitivity to the duality approximation is substantially reduced: 1) by restricting the Borel parameter at not too large values and 2) by dividing out the f_B sum rule which depends on the same threshold. The fact that the QCD sum rule prediction for f_B (see Chapter 4 and [240]) is in a good agreement with the lattice results indicates that quark-hadron duality is indeed valid in the B channel.

For a convenient use in the experimental analysis, the LCSR results for $\mathrm{B} \to \pi$ form factor are usually fitted to simple parametrizations. One of them, suggested in Ref. [213] employs the ansatz [241] based on the dispersion relation for $f^+_{B\pi}(q^2)$. The latter is fitted to the LCSR predictions for $f^+_{B\pi}$ in its validity region $0 < q^2 \leq 14 - 16$ GeV^2. For the B^*-pole term the $\mathrm{B}^* B\pi$ coupling [242] is determined from the same correlation function (124). The result is:

$$f^+_{B\pi}(q^2) = \frac{0.23 \div 0.33}{(1 - q^2/M^2_{B^*})(1 - \alpha_{B\pi} q^2/M^2_{B^*})}\,. \tag{129}$$

where the values of the slope parameter correlated with the lower and upper limits of the interval for $f^+_{B\pi}(0)$ are almost equal: $\alpha_{B\pi} = 0.39 \div 0.38$. A different parametrization was suggested recently in Ref. [235]:

$$\begin{aligned} f^+_{B\pi}(q^2) \quad &= \frac{0.26 \pm 0.06 \pm 0.05}{1 - a(q^2/M^2_B) + b(q^2/M^2_B)^2}, \quad q^2 < q^2_0, \\ &= \frac{c}{1 - q^2/M^2_{B^*}}, \quad q^2 > q^2_0\,, \end{aligned} \tag{130}$$

where the LCSR result is extrapolated to large q^2 using the B^*-pole form. In Eq. (130) the ranges of fitted parameters, $a = 2.34 \div 1.76$, $b = 1.77 \div 0.87$, $c = 0.384 \div 0.523$, and $q^2_0 = 14.3 \div 18.5$ GeV^2, are correlated with the first error in $f^+_{B\pi}(0)$, whereas the second error is attributed to the uncertainty of the quark-hadron duality approximation. Note that all values within the uncertainty intervals in Eqs. (129) and (130) have to be considered as equally acceptable theoretical predictions, without any "preferred central value". The numerical differences between the form factors (129) and (130) are smaller than the estimated uncertainties and are caused by slightly different inputs and by the small $O(\alpha_s)$ correction to the twist 3 term taken into account in Eq. (130) but not in Eq. (129) (where an additional uncertainty was attributed to this missing correction).

Having at hand the form factor, one can predict the $\mathrm{B} \to \pi l \nu$ decay distribution using Eq. (111), as is shown in Fig. 3.14 in the case of the form factor (129). The corresponding integrated s.l. width is

$$\Gamma(\mathrm{B}^0 \to \pi^- \mathrm{l}^+ \nu) = (7.3 \pm 2.5)|\mathrm{V_{ub}}|^2 \mathrm{ps}^{-1}\,, \tag{131}$$

where the indicated error is mainly caused by the uncertainty of $f^+_{B\pi}(0)$, whereas the uncertainty of the form factor shape is insignificant. This prediction [213] was recently used by BELLE in their preliminary analysis of $\mathrm{B} \to \pi l \nu$ decay (see Sec. 4.3.1.). A similar estimate of $|V_{ub}|$ was obtained in Ref. [213] using the older CLEO measurement [245] of the $\mathrm{B} \to \pi l \nu$ width.

The advantage of LCSR is that one can easily switch from the $\mathrm{B} \to \pi$ to $\mathrm{D} \to \pi$ form factor replacing b quark by c quark in the underlying correlation function (124). The LCSR prediction for $f^+_{D\pi}$ obtained in Ref. [213] and parametrized in the form analogous to Eq. (129) yields a D^*-pole dominance:

$$f^+_{D\pi} = \frac{0.65 \pm 0.11}{1 - q^2/m^2_{D^*}}\,, \tag{132}$$

at $0 < q^2 < (M_D - m_\pi)^2$. The corresponding s.l. width $\Gamma(\mathrm{D}^0 \to \pi^- e^+ \nu_e)/|V_{cd}|^2 = 0.13 \pm 0.05$ ps^{-1} calculated with the known value of $|V_{cd}|$ is, within errors, in agreement with the experimental number 0.174 ± 0.032 ps^{-1} [106]. To make this comparison more decisive it would be very important to have new, more accurate measurements of the decay distribution and integrated width of $\mathrm{D}^0 \to \pi^- e^+ \nu_e$.

Are further improvements of the LCSR result for $f^+_{B\pi}$ and $f^+_{D\pi}$ possible? As we have seen, the accuracy of OPE for the correlation function is quite sufficient. The $O(\alpha_s^2)$ level recently achieved in the sum rule for f_B [240] is certainly not an immediate task for LCSR, being also technically very difficult. More important is to improve the accuracy of the input parameters by 1) narrowing the interval of the b quark mass and 2) gaining a better control over the parameters of pion DA. For the latter, in particular,

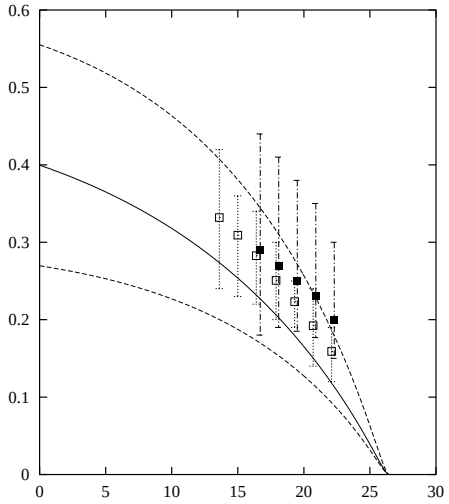

Fig. 3.14: *LCSR prediction for the* $\mathrm{B} \to \pi l\nu$ *decay distribution [213] at the nominal values of inputs (solid), with the interval of theoretical uncertainties (dashed), compared with some of the recent lattice calculations taken from Refs. [243] (solid points) and [194] (open points).*

one needs more precise data on pion form factors, especially on $\gamma^*\gamma \to \pi^0$ (the latter form factor can in principle be measured at the same e^+e^- B-factories) and, eventually, lattice QCD simulations of $\varphi_\pi(u)$ and other DA. A better control over duality approximation in the B and D channels can be achieved if radially excited B and D states are accurately identified with their masses and widths. Optimistically, one may hope to reduce the overall uncertainty of the LCSR prediction for $f^+_{B\pi}$ and other heavy-to-light form factors to the level of $\pm 10\%$, which is a natural limit for any QCD sum rule prediction.

In conclusion, we emphasize that, in addition to providing estimates of the form factors, LCSR help in understanding important physical aspects of the heavy-to-light transitions. First of all, LCSR allow to *quantitatively* assess the role of the soft (end-point) vs hard (perturbative gluon exchange) contributions to the form factors, because both contributions are taken into account in this approach. Secondly, using LCSR one is able to predict [231] the $m_b \to \infty$ limit, $f^+_{B\pi}(0) \sim 1/m_b^{3/2}$, which is used in some lattice extrapolations. Last but not least, LCSR can be expanded in powers of $1/m_b$ and $1/E_\pi$ assessing the size of $1/m_b$ and $1/E$ corrections to various relations predicted in effective theories for heavy-to-light decays.

4.3. Review and future prospects for the exclusive determination of $|V_{ub}|$

4.3.1. Measurements of $BR(\mathrm{B} \to \pi\ell\nu)$

The first exclusive measurement of the mode $\mathrm{B} \to \pi\ell\nu$ was presented by the CLEO collaboration in 1996 [245]. The neutrino momentum is inferred from the missing momentum in the event, using the hermeticity of the detector. Events with multiple charged leptons or a non-zero total charge are rejected, resulting in a reduced efficiency in favour of an improved neutrino momentum resolution. Isospin relations for the relative partial width are used to combine the B^+ and B^0 modes. A fit is performed using the variables $M_{cand} = \sqrt{E^2_{\mathrm{beam}} - |\vec{p}_\nu + \vec{p}_\ell + \vec{p}_{\rho,\omega,\pi}|^2}$ and $\Delta E = (E_{\rho,\omega,\pi} + E_\ell + |\vec{p}_{\mathrm{miss}}|c) - E_{\mathrm{beam}}$, where E_{beam} is the well known beam energy. The modes $\mathrm{B} \to \rho\ell\nu$ (with ρ^0 and ρ^-) and $\mathrm{B} \to \omega\ell\nu$ are also included in the fit because of cross-feed between these modes and $\mathrm{B} \to \pi\ell\nu$. The ρ (ω) mode uses the invariant two (three) π mass in the fit to distinguish better between resonant and non-resonant final states. Backgrounds from continuum processes are subtracted using off-resonance data. The shape of

the five signal contributions, the $b \to c$, and $b \to u$ backgrounds are provided by Monte Carlo simulation. The final results for the branching ratio and $|V_{ub}|$ are obtained by averaging over four separate form factor calculations: two quark models (ISGW2 [246] and Melikhov [247]), a model by Wirbel Stech and Bauer [248], and a hybrid model that uses a dispersion-relation-based calculation of the $\pi\ell\nu$ form factor [249] and combines lattice calculation of the $\rho\ell\nu$ form factors [250] with predicted $\rho\ell\nu$ form factor relations [251]. The dominant systematic uncertainties arise from uncertainties in the detector simulation and modelling of the $b \to u\ell\nu$ backgrounds. The result using 2.66 fb^{-1} on resonance data is

$$\mathcal{B}(\mathrm{B}^0 \to \pi^- e^+ \nu) = (1.8 \pm 0.4 \pm 0.3 \pm 0.2) \times 10^{-4}\,, \text{ and} \quad (133)$$

$$|V_{ub}| = (3.3 \pm 0.2\,^{+0.3}_{-0.4} \pm 0.78) \times 10^{-3}\,. \quad (134)$$

The errors given are statistical, systematic, and theoretical, in the order shown. Note that the above value of $|V_{ub}|$ is extracted using both the π and ρ modes. At ICHEP 2002 BELLE presented a preliminary result using 60 fb^{-1} on-peak and 9 fb^{-1} off-peak data [253]. Results are quoted for the UKQCD model [211]

$$\mathcal{B}(\mathrm{B}^0 \to \pi^- e^+ \nu) = (1.35 \pm 0.11 \pm 0.21) \times 10^{-4}\,, \text{ and} \quad (135)$$

$$|V_{ub}| = (3.11 \pm 0.13 \pm 0.24 \pm 0.56) \times 10^{-3} \quad (136)$$

and for the LCSR model [213]

$$\mathcal{B}(\mathrm{B}^0 \to \pi^- e^+ \nu) = (1.31 \pm 0.11 \pm 0.20) \times 10^{-4}\,, \text{ and} \quad (137)$$

$$|V_{ub}| = (3.58 \pm 0.15 \pm 0.28 \pm 0.63) \times 10^{-3}\,. \quad (138)$$

The CLEO collaboration submitted a preliminary updated analysis [257] to ICHEP 2002 based on 9.7×10^6 B$\overline{\mathrm{B}}$ pairs. In addition to more data compared to Ref. [245], the analysis has been improved in several ways: the signal rate is measured differentially in three q^2 regions so as to minimize modelling uncertainties arising from the q^2 dependence of the form factors (this is the first time this has been done in the $\mathrm{B} \to \pi\ell\nu$ mode); minimum requirements on the signal charged lepton momentum were lowered for both the pseudoscalar and vector modes, thereby increasing the acceptance and also reducing the model dependence; and the $X_u\ell\nu$ feed-down modelling included a simulation of the inclusive process using a parton-level calculation by De Fazio and Neubert [258], its non-perturbative parameters measured in the CLEO analysis of the $\mathrm{B} \to X_s\gamma$ photon energy spectrum [117,74], with the ISGW2 [246] model used to describe a set of expected resonant states[‡‡]. The preliminary CLEO result [257] for the branching fraction was

$$\mathcal{B}(\mathrm{B}^0 \to \pi^- e^+ \nu) = (1.376 \pm 0.180\,^{+0.116}_{-0.135} \pm 0.008 \pm 0.102 \pm 0.021) \times 10^{-4}, \quad (139)$$

where the uncertainties are statistical, experimental systematic, and the estimated uncertainties from the $\pi\ell\nu$ form factor, the $\rho\ell\nu$ form factors, and from modelling the other $\mathrm{B} \to X_u\ell\nu$ feed-down decays, respectively. By extracting rates independently in three separate q^2 ranges, the CLEO analysis demonstrated a significant reduction in the model dependence due to efficiency variations as a function of q^2.

In a preliminary effort to reduce the impact of theoretical uncertainties on the form factor normalization, the CLEO collaboration [257] used q^2-dependent partial branching fractions to extract $|V_{ub}|$ using a $\pi\ell\nu$ form factor from light cone sum rules in the range $q^2 < 16$ GeV^2 and from lattice QCD calculations above this range to obtain the averaged preliminary result

$$|V_{ub}| = (3.32 \pm 0.21 \pm {}^{+0.17}_{-0.19} \pm {}^{+0.55}_{-0.39} \pm 0.12 \pm 0.07) \times 10^{-3}, \quad (140)$$

where the uncertainties represent the same quantities defined in the branching-fraction expression above. In addition, by performing simple χ^2 fits of $|V_{ub}|$ across the three q^2 ranges with a given form factor model, the CLEO method can discriminate between competing form factor model shapes on the basis of χ^2 probabilities in the fits to the data. The CLEO technique has been used, for example, to demonstrate that the ISGW2 [246] model is likely to be unreliable for the extraction of $|V_{ub}|$ from the $\pi\ell\nu$ mode.

[‡‡]Note that the inclusive rate is reduced to allow for that portion of the total rate that is treated exclusively by the ISGW2 model.

4.3.2. Measurements of $BR(\mathrm{B} \to \rho\ell\nu)$

Analyses that are optimized for the modes $\mathrm{B} \to \rho\ell\nu$ were performed by CLEO [219] and BaBar [254]. BELLE also presented a preliminary result at ICHEP 2002 [255]. Again the modes $\mathrm{B}^+ \to \rho^0\ell^+\nu$, $\mathrm{B}^0 \to \rho^-\ell^+\nu$, $\mathrm{B}^+ \to \omega\ell^+\nu$, $\mathrm{B}^+ \to \pi^0\ell^+\nu$, and $\mathrm{B}^0 \to \pi^-\ell^+\nu$ (with $\rho^0 \to \pi^+\pi^-$, $\rho^- \to \pi^0\pi^-$, and $\omega \to \pi^0\pi^+\pi^-$) are fully reconstructed, the inclusion of charge conjugate decays is implied throughout. The neutrino momentum is inferred from the missing momentum in the event. The selection is somewhat looser than for the other analysis (see above), resulting in a higher efficiency but decreased ΔE resolution. Off-resonance data, taken below the $\Upsilon(4S)$ resonance, are used for continuum subtraction. The shape of the five signal contributions, the $b \to c$, and $b \to u$ background are provided by Monte Carlo simulation. A fit with the two variables $M_{\pi\pi(\pi)}$ and ΔE is performed, simultaneously for the five decay modes and for two (for CLEO three) lepton-energy regions. $M_{\pi\pi(\pi)}$ is the invariant hadronic mass of the ρ (ω) meson and ΔE is the difference between the reconstructed and the expected B meson energy, $\Delta E \equiv E_{\rho,\omega,\pi} + E_\ell + |\vec{p}_{\mathrm{miss}}|c - E_{\mathrm{beam}}$. These analyses are most sensitive for lepton energies above 2.3 GeV, below that backgrounds from $b \to c\ell\nu$ decays dominate. Isospin and quark model relations are again used to couple the B^+ and B^0 and ρ and ω modes. The dominant systematic uncertainties arise from uncertainties in the detector simulation and modelling of the $b \to u\ell\nu$ backgrounds.

The CLEO and BaBar analyses obtain their results for the branching ratio and $|V_{ub}|$ by averaging over five separate form factor calculations: two quark models (ISGW2 [246] and Beyer/Melikhov [256]), a lattice calculation (UKQCD [211]), a model based on light cone sum rules (LCSR [228]), and a calculation based on heavy quark and $SU(3)$ symmetries by Ligeti and Wise [259]. CLEO published the result [219]

$$\mathcal{B}(\mathrm{B}^0 \to \rho^-\, e^+\, \nu) = (2.69 \pm 0.41\, ^{+0.35}_{-0.40} \pm 0.50) \times 10^{-4}\,, \text{and} \quad (141)$$

$$|V_{ub}| = (3.23 \pm 0.24\, ^{+0.23}_{-0.26} \pm 0.58) \times 10^{-3}\,. \quad (142)$$

BaBar uses 50.5 fb^{-1} on resonance and 8.7 fb^{-1} off-resonance data and obtains the preliminary result [254]

$$\mathcal{B}(\mathrm{B}^0 \to \rho^-\, e^+\, \nu) = (3.39 \pm 0.44 \pm 0.52 \pm 0.60) \times 10^{-4}\,, \text{and} \quad (143)$$

$$|V_{ub}| = (3.69 \pm 0.23 \pm 0.27\, ^{+0.40}_{-0.59}) \times 10^{-3}\,. \quad (144)$$

BELLE quotes preliminary results only for the ISGW2 model (without theoretical error) using 29 fb^{-1} on resonance and 3 fb^{-1} off-resonance data

$$\mathcal{B}(\mathrm{B}^+ \to \rho^0\ell^+\nu) = (1.44 \pm 0.18 \pm 0.23) \times 10^{-4}\,, \text{and} \quad (145)$$

$$|V_{ub}| = (3.50 \pm 0.20 \pm 0.28) \times 10^{-3}\,. \quad (146)$$

Another result was obtained by CLEO earlier (this analysis was described in the previous Section [245])

$$\mathcal{B}(\mathrm{B}^0 \to \rho^-\, e^+\, \nu) = (2.5 \pm 0.4\, ^{+0.5}_{-0.7} \pm 0.5) \times 10^{-4}\,, \text{and} \quad (147)$$

$$|V_{ub}| = (3.3 \pm 0.2\, ^{+0.3}_{-0.4} \pm 0.78) \times 10^{-3} \text{ (as in Eq. 134).}$$

Note that the above value of $|V_{ub}|$ is extracted using both the π and ρ modes. CLEO quotes the following average result for the two analyses that were presented in Refs. [245,219]:

$$|V_{ub}| = (3.25 \pm 0.14\, ^{+0.21}_{-0.29} \pm 0.55) \times 10^{-3}\,. \quad (148)$$

More recently, the CLEO collaboration has presented a preliminary analysis [257] that uses the neutrino-reconstruction technique to reconstruct the modes $\mathrm{B} \to \rho\ \ell\ \nu$ in a self-consistent way along with the other experimentally accessible $b \to u\ \ell\ \nu$ exclusive modes. Whereas the analyses described in Refs. [219,254,255] are principally sensitive to the lepton endpoint region above 2.3 GeV, the improved CLEO measurement [257] imposes a charged-lepton momentum criterion of 1.5 GeV/c with a view to reducing the dominating theoretical uncertainties. Due to the large uncertainties in $\rho\ell\nu$ from modelling the simulated feed-down $\mathrm{B} \to X_u\ell\nu$ backgrounds, at the time of ICHEP 2002 the $\rho\ell\nu$ mode was not used by CLEO to determine a preliminary $|V_{ub}|$ value.

4.3.3. *Measurements of $BR(\mathrm{B} \to \omega\ell\nu)$*

A first preliminary result was presented at ICHEP 2002 by the BELLE collaboration [260]. The analysis uses electrons with $E > 2.2$ GeV and is based on 60 fb^{-1} on resonance and 6 fb^{-1} off-resonance data. Events are selected by requiring that the missing mass is consistent with zero ($M^2_{\rm miss} < 3.0$ GeV$/c^2$), and that the Dalitz amplitude is 75% of its maximum amplitude ($A = |p_{\pi^+} \times p_{\pi^-}| > 0.75 \times A_{\rm max}$). After subtraction of all backgrounds, 59 ± 15 signal events remain. The dominant systematic error is the background estimation (18%). The preliminary result using the ISGW2 form factors is

$$\mathcal{B}(\mathrm{B}^+ \to \omega e^+ \nu) = (1.4 \pm 0.4 \pm 0.3) \times 10^{-4} \,. \tag{149}$$

No value for $|V_{ub}|$ is given for this analysis.

4.3.4. *Measurements of $BR(\mathrm{B} \to \eta\ell\nu)$*

As in the case of the $\mathrm{B} \to \pi\ell\nu$ mode, the decay $\eta\ell\nu$ is described by only one form factor; however, the extraction of $|V_{ub}|$ is complicated by the $\eta - \eta'$ mixing. Experimentally, the η has a clear signal and, due to its large mass, one can study the region of low η momenta, where lattice calculations are most reliable. $\mathrm{B} \to \eta\ell\nu$ decays can be related via Heavy Quark Symmetry to $\mathrm{D} \to \eta\ell\nu$. It is envisioned that future measurements of the latter mode by CLEO-c can be used to calibrate the lattice calculations, and the B-factories can then use the calibrated lattice to measure $\mathrm{B} \to \eta\ell\nu$. A first preliminary result using approximately 9.7×10^6 $\mathrm{B\overline{B}}$ events was presented at DPF 2002 by the CLEO collaboration [261]:

$$\mathcal{B}(\mathrm{B}^+ \to \eta\ell^+\nu) = (0.39^{+0.18+0.09}_{-0.16-0.08}) \times 10^{-4} \,. \tag{150}$$

The separate CLEO global exclusive study [257], submitted to ICHEP 2002, also found evidence for the mode $\mathrm{B}^+ \to \eta\ell^+\nu$ with a significance of 2.5σ. No value for $|V_{ub}|$ was determined from these analyses.

4.3.5. *Summary*

Several mature measurements of the channels $\mathrm{B} \to \pi\ell\nu$ and $\mathrm{B} \to \rho\ell\nu$ exist and can be used to extract the value of $|V_{ub}|$. That these results are limited by the large theoretical uncertainties on the heavy-to-light form factor shapes and normalizations renders the exclusive approaches important to help clarify the non-perturbative QCD aspect of these decays, besides providing an alternative avenue to $|V_{ub}|$. With larger data samples, increased experimental acceptances, and improvements in our understanding of the background processes, the competing form factor models and calculations can now begin to be tested through shape-sensitive comparisons with data. A summary of some of the results is shown in Fig. 3.15. For the BELLE $\mathrm{B} \to \pi\ell\nu$ result the average of the two form factor model results is shown.

A combined value (the last row in Fig. 3.15) has been calculated as weighted average of the combined CLEO result, the BaBar $\mathrm{B} \to \rho e\nu$ result and BELLE's $\mathrm{B} \to \pi\ell\nu$ result. The weights are determined by the statistical error added in quadrature with the uncorrelated part of the systematic uncertainty. We assume that the systematic uncertainty is composed quadratically out of an uncorrelated part and a correlated part of about equal size, where the correlated part arises mainly from the modelling of the $b \to u$ feed-down background. The experimental error of the combined value includes this correlated contribution. The relative theoretical error is similar for all measurements; we take the one from the BaBar measurement. The result is

$$\boxed{|V_{ub}|_{excl} = (3.38 \ \pm \ 0.24_{exp\ ^{+0.37}_{-0.54\ th}}) \ \times \ 10^{-3} \,.} \tag{151}$$

5. B hadron lifetimes and lifetime differences

Beside the direct determination of inclusive and exclusive s.l. decay widths, there are several other measurements of B meson properties which are instrumental in testing some of the theoretical tools (OPE,

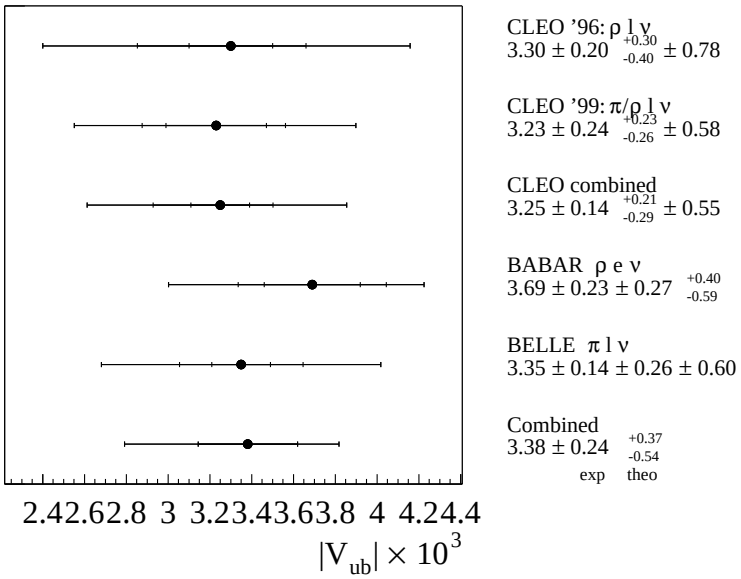

Fig. 3.15: *Current s.l. exclusive measurements of $|V_{ub}|$. The combined value is explained in the text.*

HQET, and lattice QCD) and are relevant in the precision determination of the CKM parameters. For instance, a precise evaluation of ΔM_d from the measurement of the time integrated $\mathrm{B}^0_d - \overline{\mathrm{B}}^0_d$ oscillation rate requires an accurate measurement of the $\overline{\mathrm{B}}^0_d$ meson lifetime. The accuracy of the $\overline{\mathrm{B}}^0_d$ lifetime and of the lifetime ratio of charged to neutral mesons are also a source of uncertainty in the extraction of $|V_{cb}|$ with the exclusive method. Measurements of B lifetimes test the decay dynamics, giving important information on non-perturbative QCD effects induced by the spectator quark(s). Decay rates are expressed using the OPE formalism, as an expansion in Λ_{QCD}/m_Q. Spectator effects contribute at $O(1/m^3_Q)$ and non-perturbative contributions can be reliably evaluated, at least in principle, using lattice QCD calculations.

Since the start of the data taking at LEP/SLC/Tevatron, an intense activity has been devoted to studies of inclusive and exclusive B hadron lifetimes. Most of the exclusive lifetime measurements are based on the reconstruction of the beauty hadron proper time by determining its decay length and momentum. The most accurate measurements are based on inclusive or partial reconstructions (such as topological reconstruction of B decay vertex and determination of its charge or reconstruction of $\mathrm{B} \to \mathrm{D}^{(*)}\ell^+\nu X$). These techniques exploit the kinematics offered by e^+e^- colliders at energies around the Z^0 peak, and also by hadron colliders, and the excellent tracking capabilities of the detectors. The accuracy of the results for B_d and B_u mesons, where the samples of candidates are larger, are dominated by systematics, including backgrounds, b-quark fragmentation, branching fractions and modelling of the detector response. In the case of B_s and Λ_b, the uncertainty is still statistical dominated. Final averages of the results obtained are given in Table 3.22 [262]. The averages for the B^0_d and B^+ lifetimes include also the recent very precise measurements by the B factories [263]. Fig. 3.16 gives the ratios of different B hadron lifetimes, compared with theory predictions (dark yellow bands). The achieved experimental precision of the hadron lifetimes – from a fraction of percent to a few percent – is quite remarkable. The phenomenological interpretation of these results in terms of exclusive lifetime ratios is discussed extensively in Sec 5.6.

The longer lifetime of charged B mesons as compared to the neutral ones has been established at 5σ level. The B^0_d and B^0_s lifetimes are found to be equal within a $\simeq$4% accuracy. The lifetimes of b-baryons appear to be shorter than those of B^0_d mesons. Although this is in qualitative agreement with

B Hadrons	Lifetime [ps]
$\tau(b)$	1.573 ± 0.007 (0.4 %)
$\tau(\mathrm{B}_d^0)$	1.540 ± 0.014 (0.9 %)
$\tau(\mathrm{B}^+)$	1.656 ± 0.014 (0.8 %)
$\tau(\mathrm{B}_s^0)$	1.461 ± 0.057 (3.9 %)
$\tau(\Lambda_b^0)$	1.208 ± 0.051 (4.2 %)

$\tau(\mathrm{B}_u^+)/\tau(\mathrm{B}_d^0) = 1.073 \pm 0.014$

$\tau(\mathrm{B}_s^0)/\tau(\mathrm{B}_d^0) = 0.949 \pm 0.038$

$\tau(\Lambda_b^0)/\tau(\mathrm{B}_d^0) = 0.798 \pm 0.052$

$\tau(b\,\mathrm{baryon})/\tau(\mathrm{B}_d^0) = 0.784 \pm 0.034$

Table 3.22: *Summary of B hadron lifetime results provided by the Lifetime Working Group [262].*

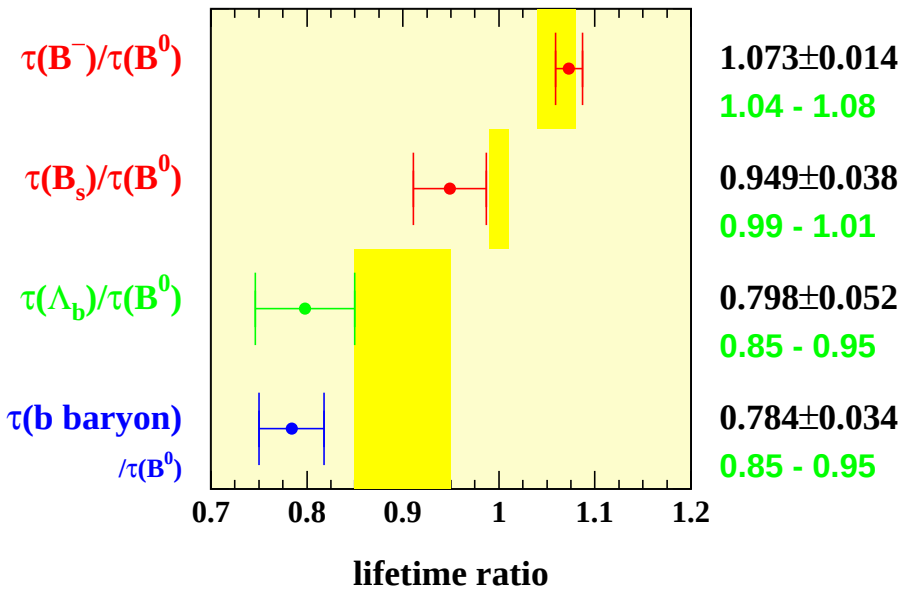

Fig. 3.16: *Ratios of exclusive B hadrons lifetimes [262], compared with the theoretical predictions given in Secs. 5.1. and 5.6. and shown by the dark yellow bands.*

expectations, the magnitude of the lifetime ratio of beauty baryons to mesons has been the subject of intense scrutiny, both by experiments and theorists, in view of a possible discrepancy. Indeed, recent calculations of higher order terms have improved the agreement of b baryon lifetime predictions with the present experimental results. The most precise determinations of the b baryon lifetimes come from two classes of partially reconstructed decays. The first has a Λ_c^+ baryon exclusively reconstructed in association with a lepton of opposite charge. The second uses more inclusive final states, where the enrichment in beauty baryons is obtained by requiring a proton or a Λ^0 to be tagged together with a lepton in the decay. These measurements are affected by uncertainties related to the Λ_b polarization and to poorly known beauty baryon fragmentation functions and decay properties.

Accessing the lifetime differences $\Delta\Gamma_s$ offers also an independent possibility of constraining the CKM unitarity triangle. This quantity is sensitive to a combination of CKM parameters very similar to the one entering ΔM_s (see Eq. (162) below), and an upper bound on $\Delta\Gamma_s$ translates in a upper bound on ΔM_s. With future accurate determinations, this method can therefore provide, in conjunction with the determination of ΔM_d, an extra constraint on the $\bar{\rho}$ and $\bar{\eta}$ parameters.

In the Standard Model the width difference $(\Delta\Gamma/\Gamma)$ of B_s mesons is expected to be rather large and within the reach of experiment in the near future. Recent experimental studies already provide an interesting bound on this quantity as will be detailed in Sec. 5.5. On the other hand, the two mass eigenstates of the neutral B_d system have in the SM only slightly different lifetimes. This is because the difference in the lifetimes is CKM-suppressed with respect to that in the B_s system. A rough estimate leads to $\frac{\Delta\Gamma_d}{\Gamma_d} \sim \frac{\Delta\Gamma_s}{\Gamma_s} \cdot \lambda^2 \approx 0.5\%$, where $\Delta\Gamma_s/\Gamma_s \approx 15\%$ [264,265].

5.1. Theoretical description of the width difference of B_s mesons

The starting point in the study of beauty hadron lifetimes is the construction of the effective weak Hamiltonian for the $\Delta B = 1$ transitions, which is obtained after integrating out the heavy degrees of freedom of the W and Z^0-bosons and of the top quark.

Neglecting the Cabibbo suppressed contribution of $b \to u$ transitions and terms proportional to $|V_{td}|/|V_{ts}|$ ($\sim \lambda$) in the penguin sector, the $\Delta B = 1$ effective Hamiltonian can be written as (cf. Eq. (26) of Chapter 1)

$$\mathcal{H}_{\rm eff}^{\Delta B=1} = \frac{G_F}{\sqrt{2}} V_{cb}^* \sum_i C_i(\mu) Q_i + h.c. \tag{152}$$

The explicit expressions for the various operators can be found e.g. in [266]. The Wilson coefficients $C_i(\mu)$ in the effective Hamiltonian contain the information about the physics at short distances (large energies) and are obtained by matching the full (Standard Model) and the effective theory ($\mathcal{H}_{\rm eff}^{\Delta B=1}$) at the scale $\mu \simeq M_W$. This matching, as well as the evolution from M_W to the typical scale $\mu \simeq m_b$, are known at the next-to-leading order (NLO) in perturbation theory [266].

Through the optical theorem, the width difference of B_s mesons can be related to the absorptive part of the forward scattering amplitude

$$\Delta\Gamma_{\mathrm{B}_s} = -\frac{1}{M_{\mathrm{B}_s}} \mathrm{Im}\langle \bar{\mathrm{B}}_s | \mathcal{T} | \mathrm{B}_s \rangle \,, \tag{153}$$

where the transition operator $\mathcal{T}$ is written as

$$\mathcal{T} = i \int d^4x \; T\left(\mathcal{H}_{eff}^{\Delta B=1}(x) \mathcal{H}_{eff}^{\Delta B=1}(0) \right) \,, \tag{154}$$

in terms of the $\Delta B = 1$ effective Hamiltonian.

Because of the large mass of the b-quark, it is possible to construct an OPE for the transition operator $\mathcal{T}$, which results in a sum of local operators of increasing dimension. The contributions of higher dimensional operators are suppressed by higher powers of the b-quark mass. In the case of the width

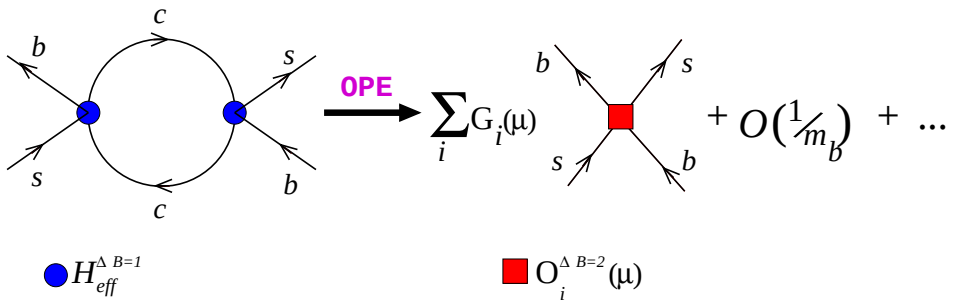

Fig. 3.17: *Heavy quark expansion: the non-local T-product of the l.h.s. (with the doubly inserted $\mathcal{H}_{eff}^{\Delta B=1}$) is expanded in the series in $1/m_b$, each coefficient being the sum of local $\Delta B = 2$ operators.*

difference $(\Delta\Gamma/\Gamma)_{B_s}$, the leading term in the expansion is parametrically of order $16\pi^2(\Lambda_{\rm QCD}/m_b)^3$. The result of this second OPE, which is illustrated in Fig. 3.17, reads

$$\Delta\Gamma_{\rm B_s} = \frac{G_F^2 m_b^2}{12\pi M_{\rm B_s}} |V_{cb}^* V_{cs}|^2 \left\{ G_1(\mu) \langle \bar{\rm B}_s | O_1(\mu) | {\rm B}_s \rangle + G_2(\mu) \langle \bar{\rm B}_s | O_2(\mu) | {\rm B}_s \rangle + \delta_{1/m_b} \right\}, \qquad (155)$$

where the $\Delta B = 2$ operators on the r.h.s. are

$$\begin{aligned} O_1 &= \bar{b}\gamma_\mu(1-\gamma_5)s\;\bar{b}\gamma_\mu(1-\gamma_5)s\,, \\ O_2 &= \bar{b}(1-\gamma_5)s\;\bar{b}(1-\gamma_5)s\,, \end{aligned} \qquad (156)$$

where a sum over repeated colour indices (i, j) is understood; δ_{1/m_b} contains the $1/m_b$ correction [267]. Contributions proportional to $1/m_b^n$ ($n \geq 2$) are neglected. The short distance physics effects (above the scale μ) are now encoded in the coefficient functions $G_{1,2}(\mu)$ which are combinations of the $\Delta B = 1$ Wilson coefficients.

The NLO corrections to the coefficients $G_{1,2}$ have been computed in Ref. [264]. They are large ($\sim 35\%$) and their inclusion is important. The long distance QCD dynamics is described in Eq. (155) by the matrix elements of the local operators O_1 and O_2, which are parametrized as

$$\langle \bar{\rm B}_s | O_1(\mu) | {\rm B}_s \rangle = \frac{8}{3} F_{\rm B_s}^2 M_{\rm B_s}^2 B_1(\mu)\,, \qquad \langle \bar{\rm B}_s | O_2(\mu) | {\rm B}_s \rangle = -\frac{5}{3} \left(\frac{F_{\rm B_s} M_{\rm B_s}^2}{m_b(\mu) + m_s(\mu)} \right)^2 B_2(\mu)\,, \quad (157)$$

where the B-parameters are equal to unity in the vacuum saturation approximation (VSA). To measure the deviations from the VSA one should also include the non-factorizable (non-perturbative) QCD effects. For such a computation a suitable framework is provided by the lattice QCD simulations. In principle, the lattice QCD approach allows the fully non-perturbative estimate of the hadronic quantities to an arbitrary accuracy. In practice, however, several approximations need to be made which, besides the statistical, introduce also a systematic uncertainty in the final results. The steady progress in increasing the computational power, combined with various theoretical improvements, helps reducing ever more systematic uncertainties. Various approximate treatments of the heavy quark on the lattice, and thus various ways to compute the B-parameters of Eq. (157), have been used:

- HQET: After discretizing the HQET lagrangian (to make it tractable for a lattice study), the matrix elements of Eq. (157) were computed in Ref. [268], but only in the static limit ($m_b \to \infty$).
- NRQCD: A step beyond the static limit has been made in Ref. [269], where the $1/m_b$-corrections to the NRQCD lagrangian have been included, as well as a large part of $1/m_b$-corrections to the

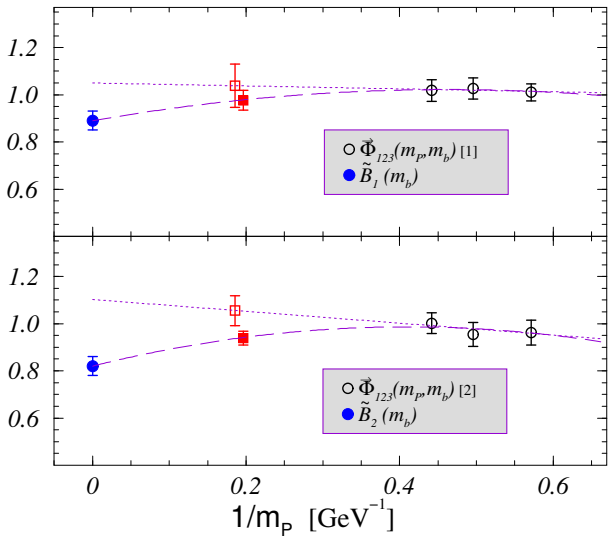

Fig. 3.18: *The lattice determination of $B_1(m_b)$ and $B_2(m_b)$ obtained in QCD with three heavy–light mesons m_P are combined with the static HQET result, $m_P \to \infty$. The result of the linear extrapolation to $1/M_{\mathrm{B}_s}$ is marked by the empty squares, whereas the interpolation is denoted by the filled squares.*

matrix elements of the four-fermion operators. It is important to note, however, that discretization errors associated with the light degrees of freedom cannot be reduced by taking a continuum limit, $a \to 0$, since the NRQCD expansion requires $a \sim 1/m_Q$. Instead, these errors are reduced by including higher and higher dimension operators whose coefficients are adjusted to improve the discretization. Such a procedure is difficult to carry out beyond terms of $O(a)$ and one must therefore show that the residual discretization and $1/m_b$ power-correction effects are small at finite a [270].

- Relativistic approach: In Ref. [271], the matrix elements were computed by using an $O(a)$-improved action in the region of masses close to the charm quark and then extrapolated to the b-quark sector by using the heavy quark scaling laws. However, this extrapolation can be significant and discretization errors will be amplified to varying degrees depending on the quantity studied, if it is performed before a continuum limit is taken. A discussion of this amplification in the context of neutral B meson mixing can be found in [272].

As of now, none of the above approaches is accurate enough on its own and all of them should be used to check the consistency of the obtained results.

A more accurate determination of the B-parameters relevant for $(\Delta\Gamma/\Gamma)_{B_s}$ has been recently obtained in Ref. [273]. To reduce the systematics of the heavy quark extrapolation, the results obtained in the static limit of the HQET [268] were combined with those of Ref. [271], where lattice QCD is employed for three mesons of masses in the region of D_s-mesons. As a result, one actually *interpolates* to the mass of the B_s-meson. This interpolation is shown in Fig. 3.18. The resulting values from Ref. [273], in the $\overline{\mathrm{MS}}$(NDR) scheme of Ref. [264], are

$$B_1(m_b) = 0.87(2)(5)\ , \qquad B_2(m_b) = 0.84(2)(4)\ , \tag{158}$$

where the first errors are statistical and the second include various sources of systematics. An important remark is that the above results are obtained in the quenched approximation ($n_f = 0$), and the systematic error due to quenching could not be estimated. The effect of the inclusion of the dynamical quarks has been studied within the NRQCD approach. The authors of Ref. [274] conclude that the B-parameters are

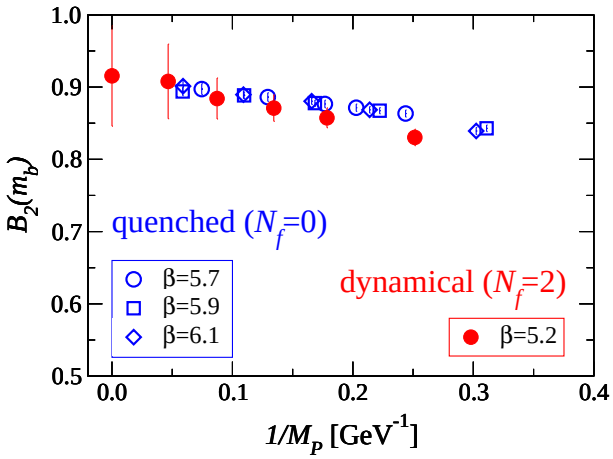

Fig. 3.19: *Results of the JLQCD collaboration [274], showing that the effects of quenching are negligible.*

essentially insensitive to the change from $n_f = 0$ to $n_f = 2$ (see Fig. 3.19). From their (high statistics) unquenched simulation, they quote

$$\begin{aligned} B_1(m_b)_{(n_f=2)} &= 0.83(3)(8)\ , \qquad & B_2(m_b)_{(n_f=2)} &= 0.84(6)(8)\ , \\ B_1(m_b)_{(n_f=0)} &= 0.86(2)(5)\ , \qquad & B_2(m_b)_{(n_f=0)} &= 0.85(1)(5)\ , \end{aligned} \tag{159}$$

where, for comparison, we also display their most recent results obtained in the quenched approximation [275]. The results of the two lattice approaches (Eqs. (158) and (159)) are in good agreement.

The theoretical estimate of $(\Delta\Gamma/\Gamma)_{\mathrm{B}_s}$ is obtained by combining the lattice calculations of the matrix elements with the Wilson coefficients. To that purpose two different formulas have been proposed which are both derived from Eq. (155):

- In Ref. [264] the width difference has been normalized by using the s.l. branching ratio $BR(\mathrm{B}_d \to X\ell\nu_\ell)$ which is experimentally determined. In this way one obtains the expression

$$\left(\frac{\Delta\Gamma}{\Gamma}\right)_{\mathrm{B}_s} = \frac{128\pi^2 BR(\mathrm{B_d} \to \mathrm{X}\ell\nu_\ell)}{3\, m_b^3\, g_{SL}\, \eta_{QCD}} |V_{cs}|^2 F_{\mathrm{B}_s}^2 M_{\mathrm{B}_s}\, \mathcal{M}\,, \tag{160}$$

  where

$$\mathcal{M} = G_1(z) B_1(m_b) + \frac{5}{8} \frac{M_{\mathrm{B}_s}^2}{\left(m_b(m_b) + m_s(m_b)\right)^2} G_2(z) B_2(m_b) + \tilde{\delta}_{1/m}\,, \tag{161}$$

  with $z = m_c^2/m_b^2$, and the phase space factor $g_{SL} = F(z)$ and $\eta_{QCD} = 1 - \frac{2}{3}\frac{\alpha_s}{\pi} f(z)$ are given in Sec. 2.4.

- Alternatively, one can use the measured mass difference in the B_d neutral meson system to write [271]:

$$\left(\frac{\Delta\Gamma}{\Gamma}\right)_{\mathrm{B}_s} = \frac{4\pi}{3}\frac{m_b^2}{M_W^2}\left|\frac{V_{cb}V_{cs}}{V_{td}V_{tb}}\right|^2 \left(\tau_{\mathrm{B}_s} \Delta M_{B_d} \frac{M_{\mathrm{B}_s}}{M_{B_d}}\right)^{(\mathrm{exp})} \frac{B_1(m_b)\xi^2}{\eta_B(m_b) S_0(x_t)}\, \mathcal{M}\,, \tag{162}$$

  where ξ is defined as $\xi = (F_{\mathrm{B}_s}\sqrt{\hat{B}_{\mathrm{B}_s}})/(f_{B_d}\sqrt{\hat{B}_{B_d}})$, and $S_0(x_t)$ is defined in Sec. 1.1. of Chapter 4.

From the point of view of the hadronic parameters, the advantage of the second formula is that it is expressed in terms of the ratio ξ, in the evaluation of which many systematic uncertainties of the lattice

calculations cancel. The estimate of ξ, however, is affected by an uncertainty due to the chiral extrapolation, which comes from the fact that in present lattice calculation it is not possible to simulate directly quark masses smaller than $\sim m_s/2$. Therefore an extrapolation to the physical d-quark mass is necessary. The first formula, instead, is expressed in terms of the decay constant F_{B_s} whose determination does not require a chiral extrapolation. However, other systematic uncertainties may be important in this case such as those coming from the value of the absolute lattice scale (inverse lattice spacing), the renormalization of the axial current and $1/m_b$-corrections.

In the numerical analysis, to derive a prediction for $(\Delta\Gamma/\Gamma)_{B_s}$, we use the values of parameters listed in Table 3.23. Notice that in the error for ξ the uncertainty due to the chiral extrapolation is quoted separately (second error).

Parameter	*Value and error*	*Parameter*	*Value and error*
$\alpha_s(m_b)$	0.22	m_t	165 ± 5 GeV
M_W	80.41 GeV	m_b	4.26 ± 0.09 GeV
M_{B_d}	5.28 GeV	m_c/m_b	0.28 ± 0.02
M_{B_s}	5.37 GeV	m_s	105 ± 25 MeV
τ_{B_s}	$1.461 \pm 0.057\, ps$	$\eta_B(m_b)$	0.85 ± 0.02
$\lvert V_{cb}\rvert$	0.0395 ± 0.0017	F_{B_s}	238 ± 31 MeV
$\lvert V_{ts}\rvert$	0.0386 ± 0.0013	ξ	$1.24 \pm 0.03 \pm 0.06$
$\lvert V_{cs}\rvert$	0.9756 ± 0.0005	$B_1(m_b)$	0.86 ± 0.06
$\lvert V_{td}\rvert$	0.0080 ± 0.0005	$B_2(m_b)$	0.84 ± 0.05
ΔM_{B_d}	$0.503 \pm 0.006\, ps^{-1}$	$G(z)$	0.030 ± 0.007
$BR(\mathrm{B}_d \to X l \nu_l)$	$10.6 \pm 0.3\%$	$G_S(z)$	0.88 ± 0.14

Table 3.23: *Average and errors of the main parameters used in the numerical analysis. When the error is negligible it has been omitted. The heavy-quark masses (m_t, m_b and m_c) are the $\overline{\mathrm{MS}}$ masses renormalized at their own values, e.g. $m_t = m_t^{\overline{\mathrm{MS}}}(m_t^{\overline{\mathrm{MS}}})$. The strange quark mass, $m_s = m_s^{\overline{\mathrm{MS}}}(\mu = 2\,GeV)$, is renormalized in $\overline{\mathrm{MS}}$ at the scale $\mu = 2$ GeV. The value for F_{B_s} and ξ are taken from Ref. [217].*

The value of the b-quark mass deserves a more detailed discussion. The b-*pole* mass, which corresponds at the NNLO to the $\overline{MS}$ mass $m_b = 4.26$ GeV quoted in Table 3.23, is $m_b^{pole} = 4.86$ GeV. Since the formulae for $(\Delta\Gamma/\Gamma)_{B_s}$ have been derived only at the NLO, however, it may be questionable whether to use $m_b^{pole} = 4.86$ GeV or $m_b^{pole} = 4.64$ GeV, corresponding to $m_b \simeq 4.26$ GeV at the NLO. That difference is very important for the value of $\tilde{\delta}_{1/m}$ which, computed in the VSA, varies between -0.4 and -0.6. In addition, a first principle non-perturbative estimates of the matrix elements entering the quantity $\tilde{\delta}_{1/m}$ is still lacking. For this reason we include $\pm 30\%$ of uncertainty in the estimate of $\tilde{\delta}_{1/m}$ stemming from the use of the VSA. We finally obtain the predictions:

$$\left(\frac{\Delta\Gamma}{\Gamma}\right)_{\mathrm{B}_s}^{Eq.\ (160)} = (8.5 \pm 2.8) \times 10^{-2}\,, \qquad \left(\frac{\Delta\Gamma}{\Gamma}\right)_{\mathrm{B}_s}^{Eq.\ (162)} = (9.0 \pm 2.8) \times 10^{-2}\,. \tag{163}$$

In Fig. 3.20 we show the corresponding probability distribution functions (pdf).

We see that the results obtained with the two formulas are in good agreement. From the pdfs we observe that $(\Delta\Gamma/\Gamma)_{B_s}$ can span a very large range of values, say between 0.03 and 0.15: the theoretical

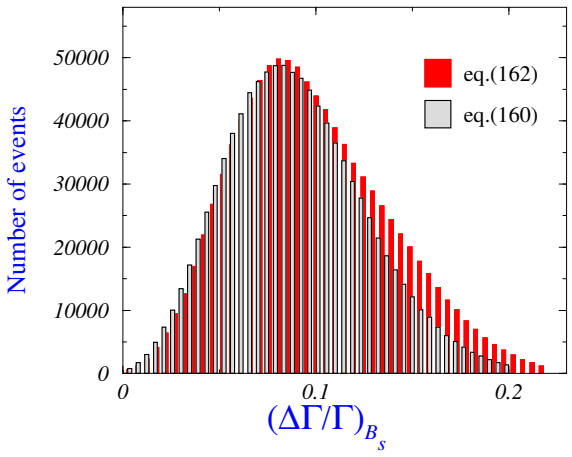

Fig. 3.20: *Probability density function (pdf) for* $(\Delta\Gamma/\Gamma)_{B_s}$ *using the formulas 160 and 162. The pdf corresponding to the smaller value is the one obtained with Eq. (160).*

uncertainty on this quantity is large. The main source of uncertainty, besides the assumption of local quark-hadron duality, comes from the $1/m_b$ corrections parameterized by $\tilde{\delta}_{1/m}$. That uncertainty is enhanced by a rather large cancellation between the leading contributions (first two terms of Eq. (161)) and it is very difficult to reduce, since it would require the non-perturbative estimate of many dimension-7, $\Delta B = 2$, operators. Such a calculation is very challenging and most probably beyond the present capability of the lattice QCD approach. Given the present theoretical uncertainty on $(\Delta\Gamma/\Gamma)_{\mathrm{B}_s}$ it is unlikely that signals of physics beyond the Standard Model may be detected from the measurement of this quantity.

5.2. Width difference of B_d mesons

The phenomenology of $\Delta\Gamma_d$ has been mostly neglected so far, in contrast to the lifetime difference in the B_s system, because the present data fall so short of the needed accuracy. However, in the prospect of experiments with high time resolution and large statistics, its study will become relevant. In fact, it may affect a precise determination of the CKM phase β, and it also provides several opportunities for detecting New Physics.

The width difference $\Delta\Gamma_d/\Gamma_d$ has been estimated in [276] including the $1/m_b$ contribution and part of the NLO QCD corrections. Adding the latter corrections decreases the value of $\Delta\Gamma_d/\Gamma_d$ computed at the leading order by a factor of almost 2. This yields

$$\Delta\Gamma_d/\Gamma_d = (2.6^{+1.2}_{-1.6}) \times 10^{-3}\,. \tag{164}$$

Using another expansion of the partial NLO QCD corrections proposed in [277], one gets

$$\Delta\Gamma_d/\Gamma_d = (3.0^{+0.9}_{-1.4}) \times 10^{-3}\,, \tag{165}$$

where preliminary values for the bag factors from the JLQCD collaboration [278] are used. The contributions to the error (in units of 10^{-3}) are ± 0.1 each from the uncertainties in the values of the CKM parameters and the parameter $x_d = (\Delta M_d/\Gamma)_d$, ± 0.5 each from the bag parameters and the mass of the b quark, ± 0.3 from the assumption of naive factorization made for the $1/m_b$ matrix elements, and $^{+0.5}_{-1.2}$ from the scale dependence. The error due to the missing terms in the NLO contribution is estimated to be ± 0.8 in the calculation of Eq. (164). Although it is reduced in the calculation of Eq. (165), a complete NLO calculation is definitely desirable for a more reliable result.

5.3. Relation between $\sin(2\beta)$ and $\Delta\Gamma_d$

The time-dependent CP asymmetry measured through the 'gold-plated' mode $\mathrm{B}_d \to J/\psi \mathrm{K}_\mathrm{S}$ is

$$\mathcal{A}_{CP} = \frac{\Gamma[\overline{\mathrm{B}}_d(t) \to J/\psi \mathrm{K}_S] - \Gamma[\mathrm{B}_d(t) \to J/\psi \mathrm{K}_S]}{\Gamma[\overline{\mathrm{B}}_d(t) \to J/\psi \mathrm{K}_S] + \Gamma[\mathrm{B}_d(t) \to J/\psi \mathrm{K}_S]} \approx \sin(\Delta M_d t)\sin(2\beta) \ , \tag{166}$$

which is valid when the lifetime difference, the direct CP violation, and the mixing in the neutral K mesons are neglected. As the accuracy of this measurement increases, the corrections due to these factors will need to be taken into account. Using the effective parameter $\bar{\epsilon}$ that absorbs several small effects and uncertainties, including penguin contributions (see [276] for a precise definition), and keeping only linear terms in that effective parameter, the asymmetry becomes

$$\begin{aligned} \mathcal{A}_{CP} \ = \ & \sin(\Delta M_d t)\sin(2\beta)\left[1 - \sinh\left(\frac{\Delta\Gamma_d t}{2}\right)\cos(2\beta)\right] \\ & +2\mathrm{Re}(\bar{\epsilon})\left[-1 + \sin^2(2\beta)\sin^2(\Delta M_d t) - \cos(\Delta M_d t)\right] \\ & +2\mathrm{Im}(\bar{\epsilon})\cos(2\beta)\sin(\Delta M_d t) \ . \end{aligned} \tag{167}$$

The first term represents the standard approximation of Eq. (166) together with the correction due to the lifetime difference $\Delta\Gamma_d$. The other terms include corrections due to CP violation in the B–$\bar{\mathrm{B}}$ and K–$\bar{\mathrm{K}}$ mixings.

Future experiments aim to measure β with an accuracy of 0.005 [279]. The corrections due to $\bar{\epsilon}$ and $\Delta\Gamma_d$ will become a large fraction of the systematic error. This error can be reduced by a simultaneous fit of $\sin(2\beta), \Delta\Gamma_d$ and $\bar{\epsilon}$. The BaBar Collaboration gives a bound on the coefficient of $\cos(\Delta M_d t)$ in Eq. (168), where other correction terms are neglected [280]. When measurements will become accurate enough to really constrain the $\cos(\Delta M_d t)$ term, all the other terms in Eq. (168) would also be measurable. In this case, the complete expression for $\mathcal{A}_{CP}$ needs to be used.

5.4. New Physics signals

The lifetime difference in neutral B mesons can be written in the form

$$\Delta\Gamma_q = -2|\Gamma_{21}|_q \cos(\Theta_q - \Phi_q) \ , \tag{168}$$

where $\Theta_q \equiv \mathrm{Arg}(\Gamma_{21})_q, \Phi_q \equiv \mathrm{Arg}(M_{21})_q$, and $q \in \{d, s\}$ (see Sec. 1.2.). In the B_s system, the new physics effects can only decrease the value of $\Delta\Gamma_s$ with respect to the SM [281]. In the B_d system, an upper bound for $\Delta\Gamma_d$ can be given, depending on the additional assumption of three-generation CKM unitarity:

$$\Delta\Gamma_d \leq \frac{\Delta\Gamma_d(\mathrm{SM})}{\cos[\mathrm{Arg}(1+\delta f)]} \ , \tag{169}$$

where δf depends on hadronic matrix elements. The bound in Eq. (169) can be calculated up to higher order corrections. In [276], $|\mathrm{Arg}(1+\delta f)| < 0.6$, so that $\Delta\Gamma_d < 1.2\ \Delta\Gamma_d(\mathrm{SM})$. A violation of this bound would indicate a violation of the unitarity of 3×3 CKM matrix. A complete NLO calculation would provide a stronger bound.

The ratio of two effective lifetimes can be used to measure the quantity $\Delta\Gamma_{obs(d)} \equiv \cos(2\beta)\Delta\Gamma_d/\Gamma_d$ (see Sec. 5.5.3.). In the presence of new physics, this quantity is in fact (see Eq. (168))

$$\Delta\Gamma_{obs(d)} = -2(|\Gamma_{21}|_d/\Gamma_d)\cos(\Phi_d)\cos(\Theta_d - \Phi_d), \tag{170}$$

where in the Standard Model

$$\Delta\Gamma_{obs(d)}(\mathrm{SM}) = 2(|\Gamma_{21}|_d/\Gamma_d)\cos(2\beta)\cos[\mathrm{Arg}(1+\delta f)] \tag{171}$$

is predicted to be positive. New physics is not expected to affect Θ_d, but it may affect Φ_d in such a way that $\cos(\Phi_d)\cos(\Theta_d - \Phi_d)$ changes sign. A negative sign of $\Delta\Gamma_{obs(d)}$ would therefore be a clear signal for New Physics. The time-dependent asymmetry in $J/\psi \mathrm{K}_S$ (or $J/\psi K_L$) measures $\mathcal{A}_{CP} = -\sin(\Delta M_d t)\sin(\Phi_d)$, where $\Phi_d = -2\beta$ in the SM. The measurement of $\sin(\Phi_d)$ still allows for a discrete ambiguity $\Phi_d \leftrightarrow \pi - \Phi_d$. If Θ_d can be determined independently of the mixing in the B_d system, then the measurement of $\Delta\Gamma_{obs(d)}$ will in principle resolve the discrete ambiguity.

In conclusion, the measurement of $\Delta\Gamma_d$ and related quantities should become possible in a near future, providing further important informations on the flavour sector of the SM.

5.5. Experimental review and future prospects for $\Delta\Gamma$ measurements

The width difference $\Delta\Gamma_s = \Gamma_{long} - \Gamma_{short}$ can be extracted from lifetime measurements of B_s decays. A first method is based on a double exponential lifetime fit to samples of events containing mixtures of CP eigenstates, like s.l. or $\mathrm{D_s}$-hadron B_s decays. A second approach consists in isolating samples of a single CP eigenstate, such as $\mathrm{B}_s \to J/\psi\phi$. The former method has a quadratic sensitivity to $\Delta\Gamma_s$, whereas the latter has a linear dependence and suffers from a much reduced statistics. A third method has been also proposed [299] and consists in measuring the branching fraction $\mathrm{B}_s \to \mathrm{D}_s^{(*)+}\mathrm{D}_s^{(*)-}$. More details on the different analyses performed are given in the following.

L3 [300] and DELPHI [301] use inclusively reconstructed B_s and $\mathrm{B}_s \to \mathrm{D}_s l\nu X$ events, respectively. If those sample are fitted assuming a single exponential lifetime, then, assuming $\frac{\Delta\Gamma_s}{\Gamma_s}$ is small, the measured lifetime is given by:

$$\tau_{\mathrm{B}_s^{incl.}} = \frac{1}{\Gamma_s}\frac{1}{1-\left(\frac{\Delta\Gamma_s}{2\Gamma_s}\right)^2} \ (\mathrm{incl.\,B}_s) \qquad ; \qquad \tau_{\mathrm{B}_s^{semi.}} = \frac{1}{\Gamma_s}\frac{1+\left(\frac{\Delta\Gamma_s}{2\Gamma_s}\right)^2}{1-\left(\frac{\Delta\Gamma_s}{2\Gamma_s}\right)^2} \ (\mathrm{B}_s \to \mathrm{D}_s l\nu X) \tag{172}$$

The single lifetime fit is thus more sensitive to the effect of $\Delta\Gamma$ in the s.l. case than in the fully inclusive one. The same method is used for the $\mathrm{B_s}$ world average lifetime (recomputed without the DELPHI measurement [302]) obtained by using only the s.l. decays. The technique of reconstructing only decays at defined CP has been exploited by ALEPH, DELPHI and CDF. ALEPH [299], reconstructs the decay $\mathrm{B_s} \to \mathrm{D_s^{(*)+}D_s^{(*)-}} \to \phi\phi\mathrm{X}$ which is predominantly CP even. The proper time dependence of the B_s^0 component is a simple exponential and the lifetime is related to $\Delta\Gamma_s$ via

$$\frac{\Delta\Gamma_\mathrm{s}}{\Gamma_\mathrm{s}} = 2\left(\frac{1}{\Gamma_\mathrm{s}}\frac{1}{\tau_{\mathrm{B_s^{short}}}} - 1\right). \tag{173}$$

Another method consists in using the branching fraction, $\mathrm{BR(B_s \to D_s^{(*)+}D_s^{(*)-})}$. Under several theoretical assumptions [303]

$$BR(\mathrm{B}_s \to \mathrm{D}_s^{(*)+}\mathrm{D}_s^{(*)-}) = \frac{\Delta\Gamma_s}{\Gamma_s\left(1+\frac{\Delta\Gamma_s}{2\Gamma_s}\right)}. \tag{174}$$

This is the only constraint on $\frac{\Delta\Gamma_s}{\Gamma_s}$ which does not rely on the measurement of the $\mathrm{B}_s^0(\mathrm{B}_d^0)$ lifetime. DELPHI [304] uses a sample of $\mathrm{B_s} \to \mathrm{D_s} - \mathrm{hadron}$, which is expected to have an increased CP-even component as the contribution due to $\mathrm{D}_s^{(*)+}\mathrm{D}_s^{(*)-}$ events is enhanced by selection criteria. CDF [305] reconstructs $\mathrm{B}_s \to J/\psi\phi$ with $J/\psi \to \mu^+\mu^-$ and $\phi \to \mathrm{K^+K^-}$ where the CP even component is equal to 0.84 ± 0.16 obtained by combining CLEO [306] measurement of CP even fraction in $\mathrm{B_d} \to \mathrm{J/\psi K^{*0}}$ and possible $SU(3)$ symmetry correction. The results, summarized in Table 3.24, are combined following the procedure described in [307]. The log-likelihood of each measurement are summed and normalized with respect to its minimum. Two measurements are excluded from the average for different reasons:

Experiment	B_s decays	$\Delta\Gamma_s/\Gamma_s$
DELPHI	$B_s \to D_s l\nu X$	< 0.47
Other s.l.	$B_s \to D_s l\nu X$	< 0.31
ALEPH	$B_s \to \phi\phi X$	$0.43^{+0.81}_{-0.48}$
ALEPH (BR method)	$B_s \to \phi\phi X$	$0.26^{+0.30}_{-0.15}$
DELPHI	$B_s \to D_s - \text{hadron}$	< 0.70
CDF	$B_s \to J/\psi\phi$	$0.36^{+0.50}_{-0.42}$

Table 3.24: *Summary of the available measurements on $\Delta\Gamma_s/\Gamma_s$ used to calculate the limit.*

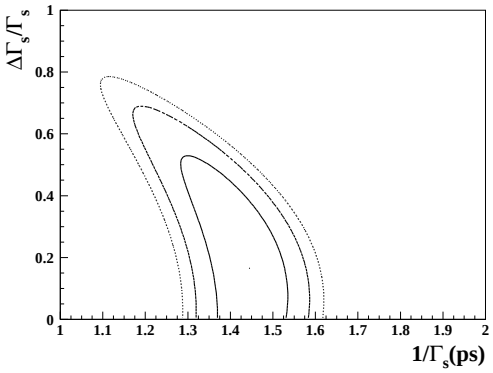

Fig. 3.21: 65%, 95% *and* 99% *C. L. contours of negative log-likelihood in the τ_{B_s}, $\Delta\Gamma_s/\Gamma_s$ plane.*

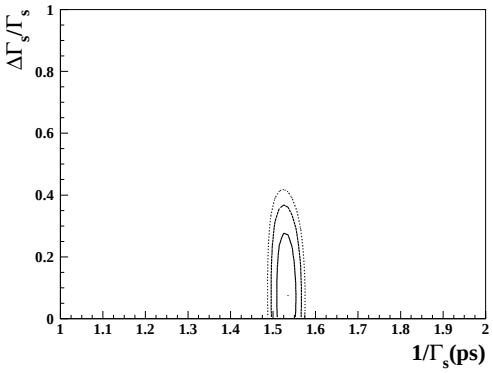

Fig. 3.22: *Same as Fig. 3.21 with the constraint $1/\Gamma_s = \tau_{B_d}$.*

- L3 inclusive analysis: the likelihood is not available and it cannot be reconstructed from the numerical result;
- ALEPH branching ratio analysis: the theoretical assumptions in Eq. (174) are controversial and the systematic error due to these assumptions has not been estimated.

The 65%, 95% and 99% confidence level contours are shown in Fig. 3.21. The result is

$$\Delta\Gamma_s/\Gamma_s = 0.16^{+0.15}_{-0.16}$$
$$\Delta\Gamma_s/\Gamma_s < 0.54 \text{ at } 95\% \text{ C.L.}$$

In order to improve the limit the constraint $1/\Gamma_s = \tau_{B_d}$ can be imposed. This is well motivated theoretically, as the total widths of the B_s^0 and the B_d^0 mesons are expected to be equal within less than 1% (see Fig. 3.16) and that $\Delta\Gamma_{B_d}$ is expected to be small. It results in:

$$\Delta\Gamma_s/\Gamma_s = 0.07^{+0.09}_{-0.07}$$
$$\Delta\Gamma_s/\Gamma_s < 0.29 \text{ at } 95\% \text{ C.L.}$$

The relative confidence level contours plot is shown in Fig. 3.22.

5.5.1. Prospects for Tevatron experiments

CDF measured the $B_s \to J/\psi\,\phi$ lifetime [308] and polarization [309] separately. In the future the idea is to combine these two measurements by fitting both the lifetime and the transversity angle*. The use of the transversity allows to separate the CP even from the CP odd component. A study has been performed, by assuming similar performances as those achieved during Run I (mass resolution, background fractions, etc.) and improved proper time resolution ($18\ \mu$m). With an integrated luminosity of 2 fb^{-1}, corresponding to about 4000 events, an accuracy on $\Delta\Gamma_s/\Gamma_s$ of 5% could be reached †. Using the same integrated luminosity and the impact parameter trigger [310], CDF could expect to reconstruct 2500 $B_s \to D_s^+ D_s^-$ events, with a signal-to-noise ratio of 1:1.5. Using this sample the lifetime of the short component can be measured with an error of 0.044 ps, which corresponds to $\sigma\left(\Delta\Gamma_s/\Gamma_s\right) = 0.06$. The $D_s\pi$ and $D_s 3\pi$ decays could be also used. Those events are flavour-specific, thus they correspond to well defined mixtures of B_s^{short} and B_s^{long}. By using $\sim 75,000$ events $1/\Gamma_s$ can be measured with an error of 0.007 ps. Combining together the flavour specific measurement and the $D_s^+ D_s^-$ analysis, CDF can reach an error $\sigma\left(\Delta\Gamma_s/\Gamma_s\right) = 0.04$.

DØ has based its studies of B_s lifetime difference measurements on its strong dimuon trigger and the extensive coverage of the calorimeter and the muon detector. It is expected that approximately 7000 $B_s \to J/\psi\,\phi$ events will be reconstructed with an integrated luminosity of 2 fb^{-1}. The sensitivity of the measurements depends on two parameters: (a) the fraction of the CP-even component of the $J/\psi\,\phi$ final state‡, and (b) the CP-violating phase ϕ in the mixing of the B_s system§. The methods discussed here invoke utilization of CP eigenstates, therefore an angular analysis is needed to disentangle the admixture of CP-even and CP-odd contributions.

The $J/\psi\,\phi$ channel can be exploited in two ways:

- by comparison of the CP-eigenstate lifetimes: the sensitivity in this measurement is proportional to $\Delta\Gamma_s\,\cos\phi = \Delta\Gamma_{CP}\,\cos^2\phi$.
- by comparison of a CP-eigenstate lifetime to that of a "50-50" admixture, *e.g.*: $\Delta\Gamma_s = 2\,\cos\phi \times [\Gamma(B_s^{\mathrm{CP\ even}}) - \Gamma(B_s^{\mathrm{CP\ 50-50}})]$. About 1000 events of the $B_s \to D_s\,\pi$ decay will be used for the extraction of $\Gamma(B_s^{\mathrm{CP\ 50-50}})$.

Additional decay channels may include $B_s \to J/\psi\,\eta$ and $J/\psi\,\eta'$ (both being CP-even states). Combining all modes, DØ can achieve a measurement on $\Delta\Gamma_s\,/\Gamma_s$ with precision between $\sigma = 0.04$ ($\mathrm{CP_{even}} = 100\%$) and $\sigma = 0.07$ ($\mathrm{CP_{even}} = 50\%$)

BTEV studied their $\Delta\Gamma_s/\Gamma_s$ reach in three different scenarios. Assuming a $b\bar{b}$ cross section of $100\ \mu$b, the number of expected events, using 2 fb^{-1} of integrated luminosity, are:

1. 91700 $B_s \to D_s\,\pi$
2. 1700 $B_s \to J/\psi\,\eta$ and 6400 $B_s \to J/\psi\,\eta\prime$, where $\tau_{B_s^{short}} = 1/\Gamma_s^{short}$ is measurable;
3. 41400 $B_s \to J/\psi\,\phi$ where the lifetime, $\tau_x = 1/\Gamma_s^x$, is a mixture of a Γ_s^{short} and a Γ_s^{long} components.

The analysis details are discussed in [277]. The results are summarised in Table 3.25, obtained under the assumption that $\Delta\Gamma_s/\Gamma_s = 0.15$.

*The transversity angle is defined as the angle between the μ^+ and the z axis in the rest frame of the J/ψ, where the z axis is orthogonal to the plane defined by the ϕ and K^+ direction.

†In this results it is assumed that the CP_{even} fraction is 0.77 ± 0.19. If $\mathrm{CP}_{even} = 0.5(1)$, the error becomes $\sigma\left(\Delta\Gamma_s/\Gamma_s\right) = 0.08\,(0.035)$.

‡The $\mathrm{CP_{even}}$ fraction has been measured by CDF in Run-I: (77±19)%.

§The CP-violating phase, defined by $\alpha_{CP}(B_s \to J/\psi\,\phi) \sim \sin\phi$, is expected to be small in the Standard Model.

Decay Modes Used	Error on $\Delta\Gamma_s/\Gamma_s$		
Integrated Luminosity in fb^{-1}	2	10	20
$D_s\pi$, $J/\psi\eta^{(\prime)}$	0.0273	0.0135	0.0081
$D_s\pi$, $J/\psi\phi$	0.0349	0.0158	0.0082
$D_s\pi$, $J/\psi\eta^{(\prime)}$,$J/\psi\phi$	0.0216	0.0095	0.0067

Table 3.25: *Projection for statistical error on $\Delta\Gamma_s/\Gamma_s$ which can be obtained by the BTeV experiment.*

	LHCb	ATLAS	CMS
$\sigma(\frac{\Delta\Gamma_s}{\Gamma_s})/\frac{\Delta\Gamma_s}{\Gamma_s}$	8.4%	11.3%	7.5%
$\sigma(\frac{\Delta\Gamma_s}{\Gamma_s})$	0.013	0.017	0.011
$\sigma(\Gamma_s)/\Gamma_s$	0.6%	0.7%	0.5%
$\sigma(A_{\|\|})/A_{\|\|}$	0.7%	0.8%	0.6%
$\sigma(A_\perp)/A_\perp$	2%	3%	2%
ϕ_s ($x_s = 20$)	0.02	0.03	0.014
ϕ_s ($x_s = 40$)	0.03	0.05	0.03

Table 3.26: *Expected statistical uncertainties on $B_s^0 \to J/\psi\phi$ parameters for each experiment under the assumptions presented in the text. The value $\frac{\Delta\Gamma_s}{\Gamma_s} = 0.15$ is used as input to the fit.*

5.5.2. Prospects for LHC experiments

The LHC experiments have investigated the measurement of $\Delta\Gamma_s$ in the exclusive $B_s^0 \to J/\psi\phi$ decay following the studies done in [312]. In these analyses, $\Delta\Gamma_s$ and Γ_s are fitted simultaneously with the weak phase $\phi_s = arg(V_{cs}^* V_{cb}/V_{cs}V_{cb}^*)$ and the two helicity amplitude values, $A_{||}$ and $A_\perp$, while the mixing parameter $x_s = \Delta m_s/\Gamma$ is assumed to be known and kept fixed. The results summarised in Table 3.26 correspond to 3 (5) years running at a luminosity of $10^{33}cm^{-2}s^{-1}(2 \cdot 10^{32}cm^{-2}s^{-1})$ for ATLAS and CMS (LCHb).

5.5.3. Measurement of $\Delta\Gamma_d/\Gamma_d$

In the case of $\Delta\Gamma_d/\Gamma_d$, the time resolution is no longer a limiting factor in the accuracy of lifetime measurements. At present, the only experimental limit comes from DELPHI [311], which has been obtained by fitting a sample of inclusive B decays to determine the mass difference ΔM_d without neglecting the $\Delta\Gamma_d$ term. At 90% C.L. $\Delta\Gamma_d/\Gamma_d < 0.20$. Given the large number of B_d produced at LHC and the proposed super B factories, it should be possible to measure $\Delta\Gamma_d/\Gamma_d \sim 0.5\%$. Using the time evolution of a single final state, however, is not sufficient as the time measurements of the decay of an untagged B_d to a single final state can only be sensitive to quadratic terms in $\Delta\Gamma_d/\Gamma_d$, [276]. This problem can be circumvented by combining the information from two different decay modes or by using angular distributions. It is then possible to have observables linear in $\Delta\Gamma_d/\Gamma_d$, which can provide $\Delta\Gamma_d/\Gamma_d \sim 0.5\%$. A viable option, perhaps the most efficient among those in [276], is to compare the measurements of the *average untagged lifetimes* of the s.l. decay mode τ_{SL} and of the CP-specific decay modes $\tau_{CP_\pm}$. The ratio between the two lifetimes is

$$\frac{\tau_{SL}}{\tau_{CP\pm}} = 1 \pm \frac{\cos(2\beta)}{2}\frac{\Delta\Gamma_d}{\Gamma_d} + \mathcal{O}\left[(\Delta\Gamma_d/\Gamma_d)^2\right] \quad . \tag{175}$$

The measurement of these two lifetimes will give a value of $|\Delta\Gamma_d|$, since $|\cos(2\beta)|$ will already be known with good accuracy by that time.

The LHC expects about 7×10^5 events of $J/\psi \mathrm{K}_S$ per year, whereas the number of s.l. decays at LHCb alone that will be directly useful in the lifetime measurements is expected to exceed 10^6 per year. The s.l. data sample may be further increased by including self-tagging decay modes, such as $\mathrm{D}_s^{(*)+}\mathrm{D}^{(*)-}$.

At hadronic machines, the $\mathrm{B}_d/\overline{\mathrm{B}}_d$ production asymmetry may be a stumbling block for the determination of the average untagged lifetimes. This drawback is obviously absent at the B factories. There, the most promising approach is to constrain $\Delta\Gamma_d/\Gamma_d$ by using $\Upsilon(4\mathrm{S})$ events where one B meson is fully reconstructed in a CP-specific decay mode, and the decay point of the second B meson is reconstructed using an inclusive technique that relies predominantly on s.l. and other self-tagging modes. For these events, only the *signed* difference of proper decay-times, $\Delta t = t_{\mathrm{CP}} - t_{\mathrm{tag}}$, i.e. not the decay times themselves, can be inferred since the production point cannot be reconstructed. The average value of Δt is given by

$$\langle \Delta t \rangle = \eta_{\mathrm{CP}} \cos(2\beta)\, \tau_{\mathrm{B}_d} \frac{\Delta\Gamma_d}{\Gamma_d} + \mathcal{O}\left[(\Delta\Gamma_d/\Gamma_d)^3\right] \tag{176}$$

where η_{CP} denotes the CP eigenvalue of the CP-specific final state considered. The BaBar potential has been studied using $J/\psi\, \mathrm{K}_S$ and similar charmonium final states. The expected statistical precision on $\Delta\Gamma_d/\Gamma_d$ is determined using the B reconstruction efficiencies and the experimental Δt resolution determined from BaBar's first data. From extrapolations based on published BaBar measurements of τ_{B_d} and $\sin(2\beta)$, the precision on τ_{B_d} and $\cos(2\beta)$ is expected to improve at the same time as the precision on $\langle \Delta t \rangle$, and to remain good enough to turn the $\langle \Delta t \rangle$ measurement into an evaluation of $\Delta\Gamma_d/\Gamma_d$. Using $\tau_{\mathrm{B}_d} = 1.55$ ps, $\sin(2\beta) = 0.6$ and 30 fb^{-1} of data one gets: $\sigma\left(\Delta\Gamma_d/\Gamma_d\right) = 0.073$. Using 300 fb^{-1} of data $\sigma\left(\Delta\Gamma_d/\Gamma_d\right) = 0.023$ is expected, and for 500 fb^{-1} $\sigma\left(\Delta\Gamma_d/\Gamma_d\right) = 0.018$.
At super B factories, 50 ab^{-1} of data may be obtained. A statistical precision at the 0.2 % level could be achieved. Strategies to reduce the systematic uncertainties to this level have not yet been studied in detail.

5.6. Theoretical description of b-hadron lifetimes and comparison with experiment

The same theoretical tools used to study $(\Delta\Gamma/\Gamma)_{B_s}$ in Sec. 5.1. can also be applied to describe the lifetime ratios of hadrons containing a b-quark, such as $\tau(\mathrm{B}_u)/\tau(\mathrm{B}_d)$, $\tau(\mathrm{B}_s)/\tau(\mathrm{B}_d)$, $\tau(\Lambda_b)/\tau(\mathrm{B}_d)$. The leading contributions in the heavy quark expansion (HQE) are represented, in the present case, by the dimension-3 operator $\bar{b}b$ ($\mathcal{O}(1)$) and the dimension-5 operator $\bar{b}\sigma_{\mu\nu}G^{\mu\nu}b$ ($\mathcal{O}(1/m_b^2)$). The first term in the expansion reproduces the predictions of the naïve quark spectator model. At this order, the hadronic decay is described in terms of the free b-quark decay, and the lifetime ratios of beauty hadrons are all predicted to be unity. The leading corrections, of $\mathcal{O}(1/m_b^2)$, describe the soft interactions of the spectator quark(s) inside the hadron, but give a small contribution ($\lesssim 2\%$) to the lifetime ratios.

The large lifetime difference of beauty hadrons which has been observed experimentally can be explained by considering hard spectator effects, that appear at $\mathcal{O}(1/m_b^3)$. Although suppressed by an additional power of $1/m_b$, these effects are enhanced with respect to the leading contributions by a phase-space factor of $16\pi^2$, being $2 \to 2$ processes instead of $1 \to 3$ decays (see Fig. 3.23). As in the case of the OPE for $(\Delta\Gamma/\Gamma)_{B_s}$, the starting point to describe the beauty hadron lifetimes is the effective $\Delta B = 1$ weak Hamiltonian, which enter the transition operator

$$\mathcal{T} = i \int d^4x\, T\left(\mathcal{H}_{\mathrm{eff}}^{\Delta B=1}(x)\mathcal{H}_{\mathrm{eff}}^{\Delta B=1}(0)\right) . \tag{177}$$

From the forward matrix elements of this operator, and using the optical theorem, one computes the

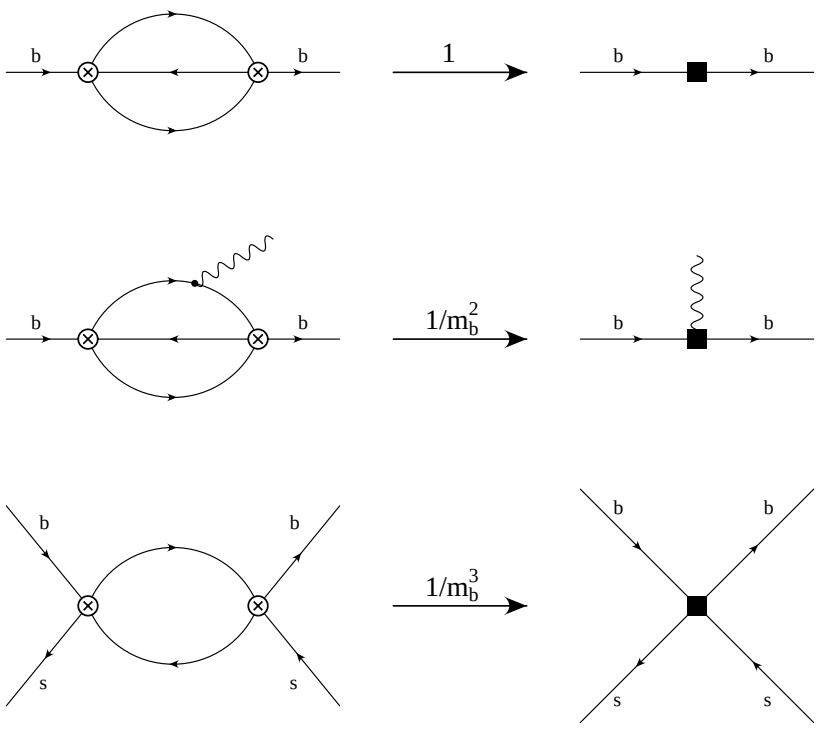

Fig. 3.23: *Examples of LO contributions to the transition operator $\mathcal{T}$ (left) and to the corresponding local operator (right). The crossed circles represent the insertions of the $\Delta B = 1$ effective Hamiltonian. The black squares represent the insertion of a $\Delta B = 0$ operator.*

inclusive decay width of a hadron H_b containing a b quark

$$\Gamma(H_b) = \frac{1}{M_{H_b}} \mathrm{Im} \langle H_b | \mathcal{T} | H_b \rangle \,. \tag{178}$$

The result of the HQE, in this case, is expressed in terms of matrix elements of $\Delta B = 0$ operators and it is given by

$$\Gamma(H_b) = \frac{G_F^2 |V_{cb}|^2 m_b^5}{192\pi^3} \left[c^{(3)} \frac{\langle H_b | \bar{b} b | H_b \rangle}{2M_{H_b}} + c^{(5)} \frac{g_s}{m_b^2} \frac{\langle H_b | \bar{b} \sigma_{\mu\nu} G^{\mu\nu} b | H_b \rangle}{2M_{H_b}} + \frac{96\pi^2}{m_b^3} \sum_k c_k^{(6)} \frac{\langle H_b | O_k^{(6)} | H_b \rangle}{2M_{H_b}} \right] , \tag{179}$$

where we have included all contributions up to $\mathcal{O}(1/m_b^2)$ and those $1/m_b^3$ corrections which are enhanced by the phase-space factor $16\pi^2$. The complete list of the dimension-6 operators $O_k^{(6)}$, which represent the contribution of hard spectator effects, includes

$$\begin{array}{ll} \mathcal{O}_1^q = (\bar{b}\, q)_{V-A}\, (\bar{q}\, b)_{V-A} \,, & \mathcal{O}_2^q = (\bar{b}\, q)_{S-P}\, (\bar{q}\, b)_{S+P} \,, \\ \mathcal{O}_3^q = (\bar{b}\, t^a q)_{V-A}\, (\bar{q}\, t^a b)_{V-A} \,, & \mathcal{O}_4^q = (\bar{b}\, t^a q)_{S-P}\, (\bar{q}\, t^a b)_{S+P} \,, \end{array} \tag{180}$$

with $q = u, d, s, c$, and the penguin operator

$$\mathcal{O}_P = (\bar{b} t^a b)_V \sum_{q=u,d,s,c} (\bar{q} t^a q)_V \,. \tag{181}$$

It is important to emphasize that the symbols b and $\bar{b}$ in the operators (180,181) denote the heavy quark field HQET. The reason is that renormalized operators, in QCD, mix with operators of lower dimension,

with coefficients proportional to powers of the b-quark mass. Therefore, the dimensional ordering of the HQE, based on the assumption that contributions of higher dimensional operators are suppressed by increasing powers of the b-quark mass, would be lost in this case. In order to implement the expansion, the matrix elements of the local operators should be cut-off at a scale smaller than the b-quark mass, which is naturally realized in the HQET. The HQE can be expressed in terms of QCD operators in those cases in which, because of their specific quantum numbers, these operators cannot mix with lower lower dimensional operators. This is the case, for instance, for the leading contributions in the HQE of $(\Delta\Gamma/\Gamma)_{B_s}$ and of the lifetime ratio $\tau(\mathrm{B}_u)/\tau(\mathrm{B}_d)$.

The Wilson coefficients $c^{(3)}$ and $c^{(5)}$ in Eq. (179) have been computed at the LO in Ref. [282], while the NLO corrections to $c^{(3)}$ have been evaluated in [92,283–285]. The NLO corrections to $c^{(5)}$ are still unknown, but their impact on the lifetime ratio is expected to be negligible. The coefficient functions $c_k^{(6)}$ of the current-current operators of dimension-6 have been computed at the LO in Refs. [286–288]. At this order the coefficient of the penguin operator $c_P^{(6)}$ vanishes. The NLO correction to $c_k^{(6)}$ for the operators $\mathcal{O}_k^q$ with $q = u, d$ has been recently completed in Refs. [289,290], and extended to $q = s$ in Ref. [289]. A complete list of these coefficients, calculated at NLO in the NDR-$\overline{\mathrm{MS}}$ scheme of Ref. [291], is given in Table 3.27. The operators containing the valence charm quark ($q = c$ in Eq. (180)) are expected to give a negligible contribution to the non-charmed hadron decay rates. The calculation of the NLO corrections to these coefficient functions, as well as the NLO calculation of the coefficient function of the penguin operator, have not been performed yet.

q	u	d	s
c_1^q	$-0.29^{+0.02}_{-0.04}$	$-0.03^{-0.01}_{+0.01}$	$-0.03^{-0.01}_{+0.01}$
c_2^q	$-0.02^{-0.01}_{+0.01}$	$0.03^{+0.01}_{-0.02}$	$0.04^{+0.00}_{-0.02}$
c_3^q	$2.37^{+0.12}_{-0.10}$	$-0.68^{-0.01}_{+0.01}$	$-0.58^{-0.00}_{+0.01}$
c_4^q	$-0.05^{-0.01}_{+0.00}$	$0.68^{-0.00}_{+0.00}$	$0.65^{-0.00}_{+0.00}$

Table 3.27: *Wilson coefficients $c_k^q(\mu_0)$ computed in the HQET, at NLO, at the scale $\mu_0 = m_b$. The coefficients also have a residual dependence on the renormalization scale μ_1 of the $\Delta B = 1$ operators, which is a NNLO effect. The uncertainty due to the variation of the scale μ_1 is reflected in the error bars (central values are obtained by using $\mu_1 = m_b$, upper error for $\mu_1 = m_b/2$ and the lower one for $\mu_1 = 2\,m_b$). In the evaluation we take $m_c/m_b = 0.28$. All the coefficients remain unchanged under the variation of $m_c/m_b = 0.28 \pm 0.02$ except for c_3^q, which changes by about 2%.*

The matrix elements of dimension-3 and dimension-5 operators, appearing in Eq. (179), can be expressed in terms of the HQET parameters $\mu_\pi^2(H_b)$ and $\mu_G^2(H_b)$ as

$$\begin{aligned}
\langle H_b|\bar{b}b|H_b\rangle &= 2M_{H_b}\left(1 - \frac{\mu_\pi^2(H_b) - \mu_G^2(H_b)}{2m_b^2} + \mathcal{O}(1/m_b^3)\right), \\
\langle H_b|\bar{b}g_s\sigma_{\mu\nu}G^{\mu\nu}b|H_b\rangle &= 2M_{H_b}\left(2\mu_G^2(H_b) + \mathcal{O}(1/m_b)\right).
\end{aligned} \tag{182}$$

Using these expansions in the lifetime ratio of two beauty hadrons one finds

$$\begin{aligned}
\frac{\tau(H_b)}{\tau(H_b')} &= 1 + \frac{\mu_\pi^2(H_b) - \mu_\pi^2(H_b')}{2m_b^2} - \left(\frac{1}{2} + \frac{2c^{(5)}}{c^{(3)}}\right)\frac{\mu_G^2(H_b) - \mu_G^2(H_b')}{m_b^2} \\
&\quad - \frac{96\pi^2}{m_b^3\, c^{(3)}}\sum_k c_k^{(6)}\left(\frac{\langle H_b'|O_k^{(6)}|H_b\rangle}{2M_{H_b}} - \frac{\langle H_b'|O_k^{(6)}|H_b'\rangle}{2M_{H_b'}}\right).
\end{aligned} \tag{183}$$

From the heavy hadron spectroscopy one obtains $\mu_\pi^2(\Lambda_b) - \mu_\pi^2(\mathrm{B}) \approx 0.01(3)$ GeV^2 and $\mu_\pi^2(\Lambda_b) - \mu_\pi^2(\mathrm{B}) \approx 0$. Therefore the impact of the second term in the above formula is completely negligible. On the other hand, $\mu_G^2(\mathrm{B}_q) = 3(M_{\mathrm{B}_q^*}^2 - M_{\mathrm{B}_q}^2)/4$, which gives $\mu_G^2(\mathrm{B}_{u,d}) \approx 0.36$ GeV^2, $\mu_G^2(\mathrm{B}_s) \approx 0.38$ GeV^2, while $\mu_G^2(\Lambda_b) = 0$. Therefore, only in the case $\tau(\Lambda_b)/\tau(\mathrm{B}_d)$, the third term gives a contribution that is visibly different from zero. By using $(1/2 + 2c^{(5)}/c^{(3)}) = -1.10(4)$, we thus obtain

$$\frac{\tau(\mathrm{B}^+)}{\tau(\mathrm{B}_d)} = 1.00 - \Delta_{\mathrm{spec}}^{\mathrm{B}^+}\,, \quad \frac{\tau(\mathrm{B}_s)}{\tau(\mathrm{B}_d)} = 1.00 - \Delta_{\mathrm{spec}}^{\mathrm{B}_s}\,, \quad \frac{\tau(\Lambda_b)}{\tau(\mathrm{B}_d)} = 0.98(1) - \Delta_{\mathrm{spec}}^{\Lambda}\,, \tag{184}$$

where the $\Delta_{\mathrm{spec}}^{H_b}$ represent the $1/m_b^3$ contributions of hard spectator effects (second line in Eq. (183)).

The comparison of Eq. (184) with the experimental results given in Table 3.28 shows that without inclusion of the spectator effects the experimental values could not be explained.

	Theory Prediction	World Average
$\frac{\tau(\mathrm{B}^+)}{\tau(\mathrm{B}_d)}$	1.06±0.02	1.073±0.014
$\frac{\tau(\mathrm{B}_s)}{\tau(\mathrm{B}_d)}$	1.00±0.01	0.949±0.038
$\frac{\tau(\Lambda_b)}{\tau(\mathrm{B}_d)}$	0.90±0.05	0.798±0.052

Table 3.28: *Comparison of theoretical expectations and experimental results for the ratios of exclusive lifetimes.*

Beside the coefficient functions presented in Table 3.27, the essential ingredients entering the corrections $\Delta_{\mathrm{spec}}^{H_b}$ are the hadronic matrix elements. We follow [292] and parameterize the B meson matrix elements as follows

$$\begin{aligned}
&\frac{\langle \mathrm{B}_q|\mathcal{O}_1^q|\mathrm{B}_q\rangle}{2M_{\mathrm{B}_q}} = \frac{F_{\mathrm{B}_q}^2 M_{\mathrm{B}_q}}{2}\,(B_1^q + \delta_1^{qq})\,, \quad
\frac{\langle \mathrm{B}_q|\mathcal{O}_3^q|\mathrm{B}_q\rangle}{2M_{\mathrm{B}_q}} = \frac{F_{\mathrm{B}_q}^2 M_{\mathrm{B}_q}}{2}\,(\varepsilon_1^q + \delta_3^{qq})\,,\\
&\frac{\langle \mathrm{B}_q|\mathcal{O}_2^q|\mathrm{B}_q\rangle}{2M_{\mathrm{B}_q}} = \frac{F_{\mathrm{B}_q}^2 M_{\mathrm{B}_q}}{2}\,(B_2^q + \delta_2^{qq})\,, \quad
\frac{\langle \mathrm{B}_q|\mathcal{O}_4^q|\mathrm{B}_q\rangle}{2M_{\mathrm{B}_q}} = \frac{F_{\mathrm{B}_q}^2 M_{\mathrm{B}_q}}{2}\,(\varepsilon_2^q + \delta_4^{qq})\,,\\
&\frac{\langle \mathrm{B}_q|\mathcal{O}_k^{q'}|\mathrm{B}_q\rangle}{2M_{\mathrm{B}_q}} = \frac{F_{\mathrm{B}_q}^2 M_{\mathrm{B}_q}}{2}\,\delta_k^{q'q} \quad , \qquad
\frac{\langle \mathrm{B}_q|\mathcal{O}_P|\mathrm{B}_q\rangle}{2M_{\mathrm{B}_q}} = \frac{F_B^2 M_B}{2}\,P^q\,.
\end{aligned} \tag{185}$$

where the parameters δ_k^{qq} are defined as the $\delta_k^{qq'}$ in the limit of degenerate quark masses ($m_q = m_{q'}$). For the Λ_b baryon we define

$$\begin{aligned}
&\frac{\langle \Lambda_b|\mathcal{O}_1^q|\Lambda_b\rangle}{2M_{\Lambda_b}} = \frac{F_B^2 M_B}{2}\,\left(L_1 + \delta_1^{\Lambda q}\right) \quad \text{for } q = u,d\,,\\
&\frac{\langle \Lambda_b|\mathcal{O}_3^q|\Lambda_b\rangle}{2M_{\Lambda_b}} = \frac{F_B^2 M_B}{2}\,\left(L_2 + \delta_2^{\Lambda q}\right) \quad \text{for } q = u,d\,,\\
&\frac{\langle \Lambda_b|\mathcal{O}_1^q|\Lambda_b\rangle}{2M_{\Lambda_b}} = \frac{F_B^2 M_B}{2}\,\delta_1^{\Lambda q} \quad \text{for } q = s,c\,,\\
&\frac{\langle \Lambda_b|\mathcal{O}_3^q|\Lambda_b\rangle}{2M_{\Lambda_b}} = \frac{F_B^2 M_B}{2}\,\delta_2^{\Lambda q} \quad \text{for } q = s,c\,,\\
&\frac{\langle \Lambda_b|\mathcal{O}_P|\Lambda_b\rangle}{2M_{\Lambda_b}} = \frac{F_B^2 M_B}{2}\,P^{\Lambda}\,.
\end{aligned} \tag{186}$$

In addition, in the case of Λ_b, the following relation holds up to $1/m_b$ corrections:

$$\langle \Lambda_b | \mathcal{O}_1^q | \Lambda_b \rangle = -2 \langle \Lambda_b | \mathcal{O}_2^q | \Lambda_b \rangle \,, \quad \langle \Lambda_b | \mathcal{O}_3^q | \Lambda_b \rangle = -2 \langle \Lambda_b | \mathcal{O}_4^q | \Lambda_b \rangle \,. \tag{187}$$

In Eqs.(185) and (186), $B_{1,2}$, $L_{1,2}$ and $\varepsilon_{1,2}$ are the "standard" bag parameters, introduced in Ref. [286]. Those parameters have already been computed in both the lattice QCD and QCD sum rule approaches. The parameters δ_k have been introduced in Ref. [292] to account for the corresponding penguin contractions. A non-perturbative lattice calculation of the δ_k parameters is possible, in principle. However, the difficult problem of subtractions of power-divergences has prevented their calculation.

In terms of parameters introduced above, the spectator contributions to the lifetime ratios, $\Delta_{\rm spec}^{H_b}$, are expressed in the form

$$\begin{aligned}
\Delta_{\rm spec}^{B^+} &= 48\pi^2 \frac{F_B^2 M_B}{m_b^3 c^{(3)}} \sum_{k=1}^{4} \left(c_k^u - c_k^d \right) \mathcal{B}_k^d \,, \\
\Delta_{\rm spec}^{\rm B_s} &= 48\pi^2 \frac{F_B^2 M_B}{m_b^3 c^{(3)}} \left\{ \sum_{k=1}^{4} \left[r\, c_k^s\, \mathcal{B}_k^s - c_k^d\, \mathcal{B}_k^d + \left(c_k^u + c_k^d \right) \left(r\, \delta_k^{ds} - \delta_k^{dd} \right) + \right. \right. \\
&\qquad \left. \left. c_k^s \left(r\, \delta_k^{ss} - \delta_k^{sd} \right) + c_k^c \left(r\, \delta_k^{cs} - \delta_k^{cd} \right) \right] + c_P \left(r P^s - P^d \right) \right\} \,, \\
\Delta_{\rm spec}^{\Lambda} &= 48\pi^2 \frac{F_B^2 M_B}{m_b^3 c^{(3)}} \left\{ \sum_{k=1}^{4} \left[\left(c_k^u + c_k^d \right) \mathcal{L}_k^\Lambda - c_k^d\, \mathcal{B}_k^d + \left(c_k^u + c_k^d \right) \left(\delta_k^{\Lambda d} - \delta_k^{dd} \right) + \right. \right. \\
&\qquad \left. \left. c_k^s \left(\delta_k^{\Lambda s} - \delta_k^{sd} \right) + c_k^c \left(\delta_k^{\Lambda c} - \delta_k^{cd} \right) \right] + c_P \left(P^\Lambda - P^d \right) \right\} \,.
\end{aligned} \tag{188}$$

where r denotes the ratio $(F_{\rm B_s}^2 M_{\rm B_s})/(F_B^2 M_B)$ and, in order to simplify the notation, we have defined the vectors of parameters

$$\begin{aligned}
\vec{\mathcal{B}}^q &= \{ B_1^q, B_2^q, \varepsilon_1^q, \varepsilon_1^q \} \,, \\
\vec{\mathcal{L}} &= \{ L_1, -L_1/2, L_2, -L_2/2 \} \,, \\
\vec{\delta}^{\Lambda q} &= \{ \delta_1^{\Lambda q}, -\delta_1^{\Lambda q}/2, \delta_2^{\Lambda q}, -\delta_2^{\Lambda q}/2 \} \,.
\end{aligned} \tag{189}$$

An important result of Eq. (188) is that, because of the $SU(2)$ symmetry, the non-valence (δs) and penguin (Ps) contributions cancel out in the expressions of the lifetime ratio $\tau(\rm B_u)/\tau(\rm B_d)$. Thus, the theoretical prediction of this ratio is at present the most accurate, since it depends only on the non-perturbative parameters actually computed by current lattice calculations. The prediction of the ratio $\tau(\Lambda_b)/\tau(\rm B_d)$, instead, is affected by both the uncertainties on the values of the δ and P parameters, and by the unknown expressions of the Wilson coefficients c_k^c and c_P at the NLO. For the ratio $\tau(\rm B_s)/\tau(\rm B_d)$ the same uncertainties exist, although their effect is expected to be smaller, since the contributions of non-valence and penguin operators cancel, in this case, in the limit of exact $SU(3)$ symmetry.

In the numerical analysis of the ratios $\tau(\rm B_s)/\tau(\rm B_d)$ and $\tau(\Lambda_b)/\tau(\rm B_d)$, we will neglect the non-valence and penguin contributions (*i.e.* we set all $\delta = P = 0$). The non-valence contributions vanish in the VSA, and present phenomenological estimates indicate that the corresponding matrix elements are suppressed, with respect to the valence contributions, by at least one order of magnitude [293,294]. On the other hand, the matrix elements of the penguin operators are not expected to be smaller than those of the valence operators. Since the coefficient function c_P vanishes at the LO, this contribution is expected to have the size of a typical NLO corrections. Thus, from a theoretical point of view, a quantitative evaluation of the non-valence and penguin operator matrix elements would be of the greatest interest to improve the determination of the Λ_B lifetime.

By neglecting the non valence and penguin contributions, and using for the Wilson coefficients the NLO results collected in Table 3.27, one obtains from Eq. (188) the following expressions

$$\begin{aligned}
\Delta^{B^+}_{\rm spec} &= -0.06(2)\, B_1^d - 0.010(3)\, B_2^d + 0.7(2)\, \varepsilon_1^d - 0.18(5)\, \varepsilon_2^d \,, \\
\Delta^{\rm B_s}_{\rm spec} &= -0.010(2)\, B_1^s + 0.011(3)\, B_2^s - 0.16(4)\, \varepsilon_1^s + 0.18(5)\, \varepsilon_2^s \\
&\quad + 0.008(2)\, B_1^d - 0.008(2)\, B_2^d + 0.16(4)\, \varepsilon_1^d - 0.16(4)\, \varepsilon_2^d \,, \\
\Delta^{\Lambda}_{\rm spec} &= -0.08(2)\, L_1 + 0.33(8)\, L_2 \\
&\quad + 0.008(2)\, B_1^d - 0.008(2)\, B_2^d + 0.16(4)\, \varepsilon_1^d - 0.16(4)\, \varepsilon_2^d \,,
\end{aligned} \tag{190}$$

For the charm and bottom quark masses, and the B meson decay constants we have used the central values and errors given in Table 3.29. The strong coupling constant has been fixed at the value $\alpha_s(m_Z) = 0.118$. The parameter $c^{(3)}$ in Eq. (188) is a function of the ratio m_c^2/m_b^2, and such a dependence has been consistently taken into account in the numerical analysis and in the estimates of the errors. For the range of masses given in Table 3.29, $c^{(3)}$ varies in the interval $c^{(3)} = 3.4 \div 4.2$ [285].

$B_1^d = 1.2 \pm 0.2$	$B_1^s = 1.0 \pm 0.2$
$B_2^d = 0.9 \pm 0.1$	$B_2^s = 0.8 \pm 0.1$
$\varepsilon_1^d = 0.04 \pm 0.01$	$\varepsilon_1^s = 0.03 \pm 0.01$
$\varepsilon_2^d = 0.04 \pm 0.01$	$\varepsilon_2^s = 0.03 \pm 0.01$
$L_1 = -0.2 \pm 0.1$	$L_2 = 0.2 \pm 0.1$
$m_b = 4.8 \pm 0.1$ GeV	$m_b - m_c = 3.40 \pm 0.06$ GeV
$F_B = 200 \pm 25$ MeV	$F_{\rm B_s}/F_B = 1.16 \pm 0.04$

Table 3.29: *Central values and standard deviations of the input parameters used in the numerical analysis. The values of m_b and m_c refer to the pole mass definitions of these quantities.*

As discussed before, for the ratio $\tau(\rm B_u)/\tau(\rm B_d)$ the HQE can be also expressed in terms of operators defined in QCD. The corresponding coefficient functions can be evaluated by using the matching between QCD and HQET computed, at the NLO, in Ref. [292]. In this way, one obtains the expression

$$\Delta^{B^+}_{\rm spec} = -0.05(1)\, \bar{B}_1^d - 0.007(2)\, \bar{B}_2^d + 0.7(2)\, \bar{\varepsilon}_1^d - 0.15(4)\, \bar{\varepsilon}_2^d \tag{191}$$

where the $\bar{B}$ and $\bar{\varepsilon}$ parameters are now defined in terms of matrix elements of QCD operators.

The errors quoted on the coefficients in Eq. (190) are strongly correlated, since they originate from the theoretical uncertainties on the same set of input parameters. For this reason, in order to evaluate the lifetime ratios, we have performed a Bayesian statistical analysis by implementing a short Monte Carlo calculation. The input parameters have been extracted with flat distributions, assuming as central values and standard deviations the values given in Table 3.29. The results for the B-parameters are based on the lattice determinations of Refs. [295,297] ¶. We have included in the errors an estimate of the uncertainties not taken into account in the original papers. The QCD results for the B meson B-parameters of Ref. [297] have been converted to HQET at the NLO [292]‖. The contributions of all the δ and P parameters have been neglected. In this way we obtain the final NLO predictions for the

¶ For recent estimates of these matrix elements based on QCD sum rules, see Refs. [298].

‖ With respect to [292], we use for the B meson B-parameters the results updated in [297].

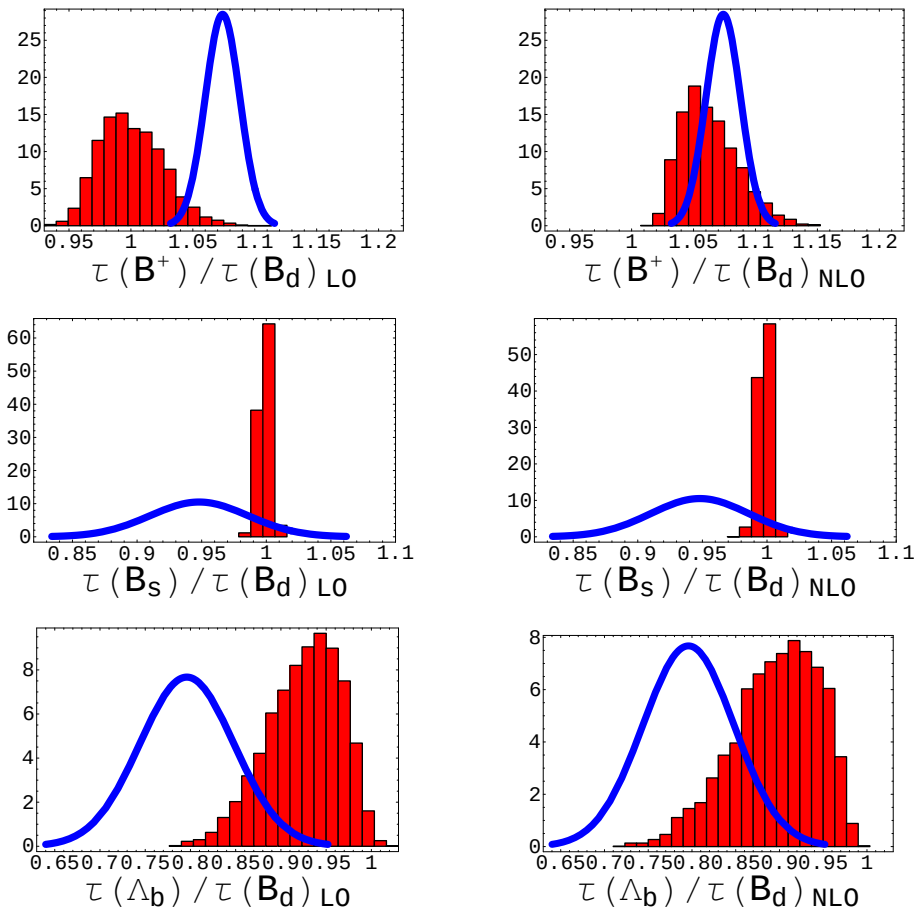

Fig. 3.24: *Theoretical (histogram) vs experimental (solid line) distributions of lifetime ratios. The theoretical predictions are shown at the LO (left) and NLO (right).*

lifetimes ratios summarised in Table 3.28. The central values and uncertainties correspond to the average and the standard deviation of the theoretical distributions, shown in Fig. 3.24, together with those from the experimental determinations. The uncertainty coming from the residual scale dependence represents less than 20% of the quoted errors.

With the inclusion of the NLO corrections, the theoretical prediction for the ratio $\tau(\mathrm{B}_u)/\tau(\mathrm{B}_d)$ is in good agreement with the experimental measurement, also summarised in Table 3.28. The agreement is also good for the ratio $\tau(\mathrm{B}_s)/\tau(\mathrm{B}_d)$, with the difference between theoretical predictions and experimental determinations below 1σ. A possible mismatch between the predicted and measured values for the ratio $\tau(\Lambda_b)/\tau(\mathrm{B}_d)$ has been much debated in past years. Interpretation in terms of a breakdown of the HQE framework and the appearance of a signal of quark-hadron duality violation have been claimed. The inclusion of higher order terms seems to reestablish a compatibility between predictions of the beauty baryon lifetime with the present experimental determinations. However, this issue will require further scrutiny in view of new, more precise results expected from the Tevatron Run II and from the fact that the theoretical predictions are less accurate in this case, since a reliable estimate of the contribution of the non-valence and penguin operators are not yet available.

5.7. Future prospects for *b*-hadron lifetime measurements

The B factories are now providing new, accurate determinations of the lifetimes of the B_d^0 and B^+ meson, which could decrease the relative error on to (0.4-0.5)%. Results from the Tevatron Run II are eagerly expected, since will provide precise measurements of the B_s^0 and Λ_b lifetimes and also results for the Ξ_b, Ω_b and the B_c beauty hadrons. Further improvements are then expected from the LHC experiments, with special regard to B_s^0 and baryon lifetimes.

CDF evaluated the lifetimes measurement capabilities exploiting separately the leptonic and the hadronic decay channels. The leptonic decays considered are only to $J/\psi \rightarrow \mu\mu$, this means exclusive decays. The uncertainties shown in Table 3.30 are only statistical and are obtained by scaling by a factor 50 the Run I measurements. The systematic uncertainty is expected to be the same order as that for the Run I analyses, at the level of 1%. Since in Run I there were no measurements based on hadronic decays, the Run II estimations had to be based on Monte Carlo simulations. The major interest is in measuring the B_s and Λ_b lifetime and the expected statistical errors are quoted in Table 3.30. With these measurements the $\mathrm{B}_s/\mathrm{B}^0$ lifetime ratio to will have an uncertainty of $\sim 0.5\%$, which is of the same order of the predicted deviation from unity. Λ_b baryons, reconstructed in the $\Lambda_c\pi$, $pD^0\pi$, $p\pi$ and pK decay channels, will allow a stringent test for the theoretical predictions of the lifetime ratio of Λ_b to B^0 if the signal to noise ratio of 1 can be obtained.

$\sigma\left(c\tau\right)/c\tau$	$\mathrm{B}^{\pm}$	B_d^0	B_s^0	Λ_b
Run II leptonic triggers	0.6%	0.6%	2%	3%
Run II hadronic trigger			0.5%	0.8%

Table 3.30: *CDF lifetime statistical error projections with leptonic and hadronic triggers for 2 fb*$^{-}1$ *of data. The systematic uncertainty is expected to be at the level of* 1%.

The DØ experiment has concentrated its studies on the projection for the Λ_b lifetime measurement. The preferred decay is $J/\psi\Lambda^0$ with $J/\psi \rightarrow \mu\mu$ and $\Lambda^0 \rightarrow p\pi^-$. In 2 fb^{-1} the expected number of reconstructed events is of order of 15,000, corresponding to a relative lifetime accuracy of 9%.

At LHC, lifetime measurements of different B hadron species will be based on even larger statistics, collected in individual exclusive channels. ATLAS [313,314] has performed a simulation for studying the statistical precision on the Λ_{b}^0 lifetime using the $\Lambda_{\mathrm{b}}^0 \rightarrow \Lambda^0\ \mathrm{J}/\psi$ decay channel. In three years of running at $10^{33} cm^{-2} s^{-1}$ luminosity, 75000 $\Lambda_{\mathrm{b}}^0 \rightarrow \Lambda^0\ \mathrm{J}/\psi$ signal decays can be reconstructed (with 1500 background events, mostly J/ψ paired to a primary Λ^0). Considering a proper time resolution of 0.073 ps, the estimated relative uncertainty on the Λ_{b}^0 lifetime is 0.3%.

References

[1] J. Chay, H. Georgi, and B. Grinstein, Phys. Lett. B **247** (1990) 399; M. Voloshin and M. Shifman, Sov. J. Nucl. Phys. **41** (1985) 120; A.V. Manohar and M.B. Wise, Phys. Rev. D **49** (1994) 1310; B. Blok *et al.*, Phys. Rev. D **49** (1994) 3356.

[2] I.I. Bigi *et al.*, Phys. Lett. B **293** (1992) 430; Phys. Lett. B **297** (1993) 477 (E); Phys. Rev. Lett. **71** (1993) 496.

[3] A.V. Manohar and M.B. Wise, Cambridge Monogr. Part. Phys. Nucl. Phys. Cosmol. **10** (2000) 1; I.I. Bigi, M.A. Shifman and N.G. Uraltsev, Ann. Rev. Nucl. Part. Sci. **47** (1997) 591 [hep-ph/9703290]; Z. Ligeti, eConf **C020805** (2002) L02 [hep-ph/0302031].

[4] N.G. Uraltsev, in *At the Frontier of Particle Physics: Handbook of QCD*, edited by M. Shifman (World Scientific, Singapore, 2001) [hep-ph/0010328].

[5] E.V. Shuryak, Phys. Lett. B **93** (1980) 134; E.V. Shuryak, Nucl. Phys. B **198** (1982) 83; J.E. Paschalis and G.J. Gounaris, Nucl. Phys. B **222** (1983) 473; F.E. Close, G.J. Gounaris and J.E. Paschalis, Phys. Lett. B **149** (1984) 209; S. Nussinov and W. Wetzel, Phys. Rev. D **36** (1987) 130.

[6] M.A. Shifman and M.B. Voloshin, Sov. J. Nucl. Phys. **45** (1987) 292 [Yad. Fiz. **45** (1987) 463].

[7] M.A. Shifman and M.B. Voloshin, Sov. J. Nucl. Phys. **47** (1988) 511 [Yad. Fiz. **47** (1988) 801].

[8] N. Isgur and M.B. Wise, Phys. Lett. B **232** (1989) 113.

[9] N. Isgur and M.B. Wise, Phys. Lett. B **237** (1990) 527.

[10] E. Eichten and F. Feinberg, Phys. Rev. D **23** (1981) 2724; W.E. Caswell and G.P. Lepage, Phys. Lett. B **167** (1986) 437; E. Eichten, Nucl. Phys. B Proc. Suppl. **4** (1988) 170; G.P. Lepage and B.A. Thacker, Nucl. Phys. B Proc. Suppl. **4** (1988) 199; H.D. Politzer and M.B. Wise, Phys. Lett. B **206** (1988) 681 and Phys. Lett. B **208** (1988) 504; E. Eichten and B. Hill, Phys. Lett. B **240** (1990) 193 and Phys. Lett. B **243** (1990) 427; B. Grinstein, Nucl. Phys. B **339** (1990) 253; H. Georgi, Phys. Lett. B **240** (1990) 447; A.F. Falk, H. Georgi, B. Grinstein and M.B. Wise, Nucl. Phys. B **343** (1990) 1; A.F. Falk, B. Grinstein and M.E. Luke, Nucl. Phys. B **357** (1991) 185; T. Mannel, W. Roberts and Z. Ryzak, Nucl. Phys. B **368** (1992) 204; J.G. Körner and G. Thompson, Phys. Lett. B **264** (1991) 185; S. Balk, J.G. Körner and D. Pirjol, Nucl. Phys. B **428** (1994) 499 [hep-ph/9307230].

[11] J.M. Flynn and N. Isgur, J. Phys. G **18** (1992) 1627 [hep-ph/9207223].

[12] M. Neubert, Phys. Rept. **245** (1994) 259 [hep-ph/9306320].

[13] M. Neubert, hep-ph/0001334.

[14] A.H. Hoang, hep-ph/0204299;
A. X. El-Khadra and M. Luke, Ann. Rev. Nucl. Part. Sci. **52** (2002) 201 [hep-ph/0208114].

[15] R. Tarrach, Nucl. Phys. B **183** (1981) 384;
A.S. Kronfeld, Phys. Rev. D **58** (1998) 051501 [hep-ph/9805215];
P. Gambino and P.A. Grassi, Phys. Rev. D **62** (2000) 076002 [hep-ph/9907254].

[16] I.I. Bigi, M.A. Shifman, N.G. Uraltsev and A.I. Vainshtein, Phys. Rev. D **50** (1994) 2234 [hep-ph/9402360]; M. Beneke and V.M. Braun, Nucl. Phys. B **426** (1994) 301 [hep-ph/9402364].

[17] N. Gray, D.J. Broadhurst, W. Grafe and K. Schilcher, Z. Phys. C **48** (1990) 673.

[18] K. Melnikov and T. v. Ritbergen, Phys. Lett. B **482** (2000) 99 [hep-ph/9912391]; K.G. Chetyrkin and M. Steinhauser, Nucl. Phys. B **573** (2000) 617 [hep-ph/9911434].

[19] A.H. Hoang *et al.*, Eur. Phys. J. direct C **3** (2000) 1 [hep-ph/0001286].

[20] I.I. Bigi, M.A. Shifman, N.G. Uraltsev and A.I. Vainshtein, Phys. Rev. D **56** (1997) 4017 [hep-ph/9704245].

[21] I.I. Bigi, M.A. Shifman, N.G. Uraltsev and A.I. Vainshtein, Phys. Rev. D **52** (1995) 196 [hep-ph/9405410].

[22] A. Czarnecki, K. Melnikov and N.G. Uraltsev, Phys. Rev. Lett. **80** (1998) 3189 [hep-ph/9708372].

[23] M. Beneke, Phys. Lett. B **434** (1998) 115 [hep-ph/9804241].

[24] Y. Schroder, Phys. Lett. B **447** (1999) 321 [hep-ph/9812205]. M. Peter, Phys. Rev. Lett. **78** (1997) 602 [hep-ph/9610209].

[25] A.H. Hoang, Z. Ligeti and A.V. Manohar, Phys. Rev. Lett. **82** (1999) 277 [hep-ph/9809423]; Phys. Rev. D **59** (1999) 074017 [hep-ph/9811239].

[26] A.H. Hoang and T. Teubner, Phys. Rev. D **60** (1999) 114027 [hep-ph/9904468].

[27] A. Pineda, JHEP **0106** (2001) 022 [hep-ph/0105008].

[28] V.A. Novikov, *et al.*, Phys. Rev. Lett. **38** (1977) 626 [Erratum-ibid. **38** (1977) 791]; L.J. Reinders, H. Rubinstein and S. Yazaki, Phys. Rept. **127** (1985) 1.

[29] M.B. Voloshin, Int. J. Mod. Phys. A **10** (1995) 2865 [hep-ph/9502224].

[30] J.H. Kühn, A.A. Penin and A.A. Pivovarov, Nucl. Phys. B **534** (1998) 356 [hep-ph/9801356].

[31] A.A. Penin and A.A. Pivovarov, Phys. Lett. B **435** (1998) 413 [hep-ph/9803363]; Nucl. Phys. B **549** (1999) 217 [hep-ph/9807421].

[32] A.H. Hoang, Phys. Rev. D **59** (1999) 014039 [hep-ph/9803454].

[33] K. Melnikov and A. Yelkhovsky, Phys. Rev. D **59** (1999) 114009 [hep-ph/9805270].

[34] M. Jamin and A. Pich, Nucl. Phys. Proc. Suppl. **74** (1999) 300 [hep-ph/9810259].

[35] A.H. Hoang, Phys. Rev. D **61** (2000) 034005 [hep-ph/9905550].

[36] M. Beneke and A. Signer, Phys. Lett. B **471** (1999) 233 [hep-ph/9906475].

[37] A.H. Hoang, hep-ph/0008102.

[38] J.H. Kuhn and M. Steinhauser, Nucl. Phys. B **619** (2001) 588 [Erratum-ibid. B **640** (2002) 415] [hep-ph/0109084].

[39] J. Erler and M. x. Luo, Phys. Lett. B **558** (2003) 125 [hep-ph/0207114].

[40] M. Eidemuller, hep-ph/0207237.

[41] J. Bordes, J. Penarrocha and K. Schilcher, hep-ph/0212083.

[42] A.H. Hoang and G. Corcella, Phys. Lett. B **554** (2003) 133 [hep-ph/0212297].

[43] A. Pineda and F.J. Yndurain, Phys. Rev. D **58** (1998) 094022 [hep-ph/9711287].

[44] A.H. Hoang, Nucl. Phys. Proc. Suppl. **86** (2000) 512 [hep-ph/9909356].

[45] N. Brambilla, Y. Sumino and A. Vairo, Phys. Rev. D **65** (2002) 034001 [hep-ph/0108084].

[46] M. A. Shifman, A. I. Vainshtein and V. I. Zakharov, Nucl. Phys. B **147** (1979) 385 and 448.

[47] M. Eidemuller and M. Jamin, Phys. Lett. B **498** (2001) 203 [hep-ph/0010334];
J. Penarrocha and K. Schilcher, Phys. Lett. B **515** (2001) 291 [hep-ph/0105222].

[48] G. Martinelli, *et al.*, Nucl. Phys. B **445** (1995) 81 [hep-lat/9411010].

[49] K. Jansen *et al.*, Phys. Lett. B **372** (1996) 275 [hep-lat/9512009].

[50] D. Becirevic, V. Lubicz and G. Martinelli, Phys. Lett. B **524** (2002) 115 [hep-ph/0107124].

[51] J. Rolf and S. Sint [ALPHA Collaboration], JHEP **0212** (2002) 007 [hep-ph/0209255].

[52] C.T. Davies *et al.*, Phys. Rev. Lett. **73** (1994) 2654 [hep-lat/9404012].

[53] V. Gimenez, L. Giusti, G. Martinelli and F. Rapuano, JHEP **0003** (2000) 018 [hep-lat/0002007].

[54] G. Martinelli and C.T. Sachrajda, Nucl. Phys. B **559** (1999) 429 [hep-lat/9812001].

[55] S. Collins, hep-lat/0009040.

[56] F. Di Renzo and L. Scorzato, JHEP **0102** (2001) 020 [hep-lat/0012011].

[57] J. Heitger and R. Sommer [ALPHA Collaboration], Nucl. Phys. Proc. Suppl. **106** (2002) 358 [hep-lat/0110016]; R. Sommer, hep-lat/0209162.

[58] D. Cronin-Hennessy *et al.* [CLEO Collaboration], Phys. Rev. Lett. **87** (2001) 251808 [hep-ex/0108033].

[59] D. Bloch *et al.* [DELPHI Collaboration], DELPHI 2002-070-CONF 604;
M. Battaglia *et al.* [DELPHI Collaboration], DELPHI 2002-071-CONF-605;
M. Calvi, hep-ex/0210046.

[60] B. Aubert *et al.* [BaBar Collaboration], hep-ex/0207184.

[61] M. Gremm, A. Kapustin, Z. Ligeti and M.B. Wise, Phys. Rev. Lett. **77** (1996) 20 [hep-ph/9603314].

[62] M.B. Voloshin, Phys. Rev. D **51** (1995) 4934 [hep-ph/9411296].

[63] M. Gremm and A. Kapustin, Phys. Rev. D **55** (1997) 6924 [hep-ph/9603448].

[64] C.W. Bauer and M. Trott, Phys. Rev. D **67** (2003) 014021 [hep-ph/0205039].

[65] C.W. Bauer, Z. Ligeti, M. Luke and A.V. Manohar, Phys. Rev. D **67** (2003) 054012 [hep-ph/0210027].

[66] N.G. Uraltsev, Nucl. Phys. B **491** (1997) 303.

[67] M. Jezabek and J.H. Kuhn, Nucl. Phys. B **320** (1989) 20;
A. Czarnecki, M. Jezabek and J.H. Kuhn, Acta Phys. Polon. B **20** (1989) 961;
A. Czarnecki and M. Jezabek, Nucl. Phys. B **427** (1994) 3 [hep-ph/9402326].

[68] M. Gremm and I. Stewart, Phys. Rev. D **55** (1997) 1226 [hep-ph/9609341].

[69] A.F. Falk, M.E. Luke and M.J. Savage, Phys. Rev. D **53** (1996) 2491 [hep-ph/9507284].

[70] A.F. Falk and M.E. Luke, Phys. Rev. D **57** (1998) 424 [hep-ph/9708327].

[71] M. Battaglia *et al.*, Phys. Lett. B **556** (2003) 41 [hep-ph/0210319].

[72] N.G. Uraltsev, Phys. Lett. B **545** (2002) 337 [hep-ph/0111166].

[73] A.S. Kronfeld and J.N. Simone, Phys. Lett. B **490** (2000) 228 [Erratum-ibid. B **495** (2000) 441] [hep-ph/0006345].

[74] S. Chen *et al.* [CLEO Collaboration], Phys. Rev. Lett. **87**, 251807 (2001).

[75] R. Briere *et al.* [CLEO Collaboration], CLEO-CONF-02-10, hep-ex/0209024.

[76] A.H. Hoang, Nucl. Phys. B, Proc. Suppl. **86** (2000) 512 [hep-ph/9909356]; A.H. Hoang and A.V. Manohar, Phys. Lett. B **483** (2000) 94 [hep-ph/9911461]; hep-ph/0008102; hep-ph/0102292.

[77] A.H. Mahmood *et al.* [CLEO Collaboration], CLNS 02/1810, CLEO 02-16, hep-ex/0212051.

[78] B. Aubert *et al.* [BaBar Collaboration], hep-ex/0207084.

[79] E.C. Poggio, H.R. Quinn and S. Weinberg, Phys. Rev. D **13** (1976) 1958.

[80] M. Greco, G. Penso and Y. Srivastava, Phys. Rev. D **21** (1980) 2520.

[81] M.A. Shifman, "Quark-hadron duality," in B. Ioffe Festschrift 'At the Frontier of Particle Physics / Handbook of QCD', ed. M. Shifman (World Scientific, Singapore, 2001), [hep-ph/0009131].

[82] I.I. Bigi and N.G. Uraltsev, Int. J. Mod. Phys. A **16** (2001) 5201 [hep-ph/0106346].

[83] C.G. Boyd, B. Grinstein and A.V. Manohar, Phys. Rev. D **54** (1996) 2081 [hep-ph/9511233].

[84] R.F. Lebed, N.G. Uraltsev, Phys. Rev. D **62** (2000) 094011 [hep-ph/0006346], and refs. therein.

[85] J. Chay, H. Georgi, B. Grinstein, Phys. Lett. B **247** (1990) 339.

[86] N. Isgur, Phys. Lett. B **448** (1999) 111 [hep-ph/9811377].

[87] A. Le Yaouanc, *et al.*, Phys. Lett. B **480** (2000) 119 [hep-ph/0003087].

[88] A. Le Yaouanc *et al.*, Phys. Rev. D **62** (2000) 074007 [hep-ph/0004246].

[89] A. Le Yaouanc *et al.*, Phys. Lett. B **517** (2001) 135 [hep-ph/010333].

[90] A. Le Yaouanc *et al.*, Phys. Lett. B **488** (2000) 153 [hep-ph/0005039].

[91] M. Luke, M.J. Savage and M.B. Wise, Phys. Lett. B **345** (1995) 301.

[92] Y. Nir, Phys. Lett. B **221** (1989) 184.

[93] N. Cabibbo and L. Maiani, Phys. Lett. B **79** (1978) 109; the original QED calculation is published in R.E. Behrends *et al.*, Phys. Rev. **101** (1956) 866.

[94] A. Czarnecki and K. Melnikov, Phys. Rev. D **59** (1998) 014036.

[95] N.G. Uraltsev, Int. J. Mod. Phys. A **11** (1996) 513.

[96] M. Voloshin and M. Shifman, Sov. J. Nucl. Phys. **41** (1985) 120;
J. Chay, H. Georgi and B. Grinstein, Phys. Lett. B **247** (1990) 399.

[97] D. Benson, I.I. Bigi, Th. Mannel, and N.G. Uraltsev, hep-ph/0302262.

[98] N.G. Uraltsev, Mod. Phys. Lett. A **17** (2002) 2317 [hep-ph/0210413].

[99] D.E. Groom *et al.*, Eur. Phys. J. C **15** (2000) 1.

[100] J. Bartelt *et al.* [CLEO Collaboration], CLEO CONF 98-21.

[101] Thorsten Brandt computed the average of b-hadron semileptonic partial width inclusive measurements available for the Workshop.

[102] The LEP Electroweak Working Group, `http://lepewwg.web.cern.ch/LEPEWWG/`, CERN-EP-2001-098 and hep-ex/0112021.

[103] B. Aubert *et al.* [BaBar Collaboration], hep-ex/0208018.

[104] K. Abe *et al.* [BELLE Collaboration], hep-ex/0208033.

[105] The LEP Vcb Working group, see `http://lepvcb.web.cern.ch/LEPVCB/`.

[106] K. Hagiwara *et al.*, Phys. Rev. D **66** (2002) 010001.

[107] M. Artuso and E. Barberio, hep-ph/0205163 (a shorter version has been included in [106] as a minireview on $|V_{cb}|$).

[108] T. van Ritbergen, Phys. Lett. B **454** (1999) 353 [hep-ph/9903226].

[109] N.G. Uraltsev, Int. J. Mod. Phys. A **14** (1999) 4641 [hep-ph/9905520].

[110] R. Fulton *et al.* [CLEO Collaboration], Phys. Rev. Lett. **64** (1990) 16;
J. Bartelt *et al.* [CLEO Collaboration], Phys. Rev. Lett. **71** (1993) 411;
H. Albrecht *et al.* [ARGUS Collaboration], Phys. Lett. B **255** (1991) 297.

[111] V.D. Barger, C.S. Kim and R.J. Phillips, Phys. Lett. B **251** (1990) 629;
A.F. Falk, Z. Ligeti and M.B. Wise, Phys. Lett. B **406** (1997) 225;
R.D. Dikeman and N.G. Uraltsev, Nucl. Phys. B **509** (1998) 378;
I.I. Bigi, R.D. Dikeman and N.G. Uraltsev, Eur. Phys. J. C **4** (1998) 453.

[112] C.W. Bauer, Z. Ligeti and M.E. Luke, Phys. Lett. B **479** (2000) 395 [hep-ph/0002161].

[113] G. Altarelli, *et al.*, Nucl. Phys. B **208** (1982) 365;
M. Wirbel, B. Stech, M. Bauer, Zeit. Phys. C **29** (1985) 637.

[114] N. Isgur *et al.*, Phys. Rev. D **39** (1989) 799.

[115] M. Neubert, Phys. Rev. D **49** (1994) 3392;
T. Mannel and M. Neubert, Phys. Rev. D **50** (1994) 2037.

[116] I.I. Bigi, M.A. Shifman, N.G. Uraltsev and A.I. Vainshtein, Int. J. Mod. Phys. A **9** (1994) 2467 [hep-ph/9312359].

[117] M. Neubert, Phys. Rev. D **49** (1994) 4623; A.L. Kagan and M. Neubert, Eur. Phys. J. C **7** (1999) 5 [hep-ph/9805303].

[118] I.I. Bigi and N.G. Uraltsev, Int. J. Mod. Phys. A **17** (2002) 4709 [hep-ph/0202175].

[119] U. Aglietti, Phys. Lett. B **515** (2001) 308 [hep-ph/0103002] and Nucl. Phys. B **610** (2001) 293 [hep-ph/0104020].

[120] A.K. Leibovich, I. Low and I.Z. Rothstein, Phys. Rev. D **61** (2000) 053006 [hep-ph/9909404].

[121] C.W. Bauer, M.E. Luke and T. Mannel, hep-ph/0102089 and Phys. Lett. B **543** (2002) 261 [hep-ph/0205150].

[122] I.I. Bigi and N.G. Uraltsev, Nucl. Phys. B **423** (1994) 33 [hep-ph/9310285];
M.B. Voloshin, Phys. Lett. B **515** (2001) 74 [hep-ph/0106040].

[123] A.K. Leibovich, Z. Ligeti and M.B. Wise, Phys. Lett. B **539** (2002) 242 [hep-ph/0205148].

[124] M. Neubert, Phys. Lett. B **543** (2002) 269 [hep-ph/0207002].

[125] A. Bornheim *et al.* [CLEO Collaboration], Phys. Rev. Lett. **88** (2002) 231803 [hep-ex/0202019].

[126] P. Abreu *et al.* [DELPHI Collaboration], Phys. Lett. B **478** (2000) 14.

[127] M. Neubert, JHEP **0007** (2000) 022 [hep-ph/0006068].

[128] C.W. Bauer, Z. Ligeti and M.E. Luke, Phys. Rev. D **64** (2001) 113004 [hep-ph/0107074].

[129] A. Bornheim *et al.* [CLEO Collaboration], hep-ex/0207064.

[130] R. Barate *et al.* [ALEPH Collaboration], Eur. Phys. J. C **6** (1999) 555;
G. Abbiendi *et al.* [OPAL Collaboration], Eur. Phys. J. C **21** (2001) 399.

[131] M. Acciarri *et al.* [L3 Collaboration], Phys. Lett. B436, 174 (1998).

[132] U. Aglietti, M. Ciuchini and P. Gambino, Nucl. Phys. B **637** (2002) 427 [hep-ph/0204140].

[133] R.V. Kowalewski and S. Menke, Phys. Lett. B **541** (2002) 29 [hep-ex/0205038].

[134] M. Neubert, Phys. Lett. B **264** (1991) 455.

[135] M. Neubert, Phys. Lett. B **338** (1994) 84 [hep-ph/9408290].

[136] C.G. Boyd, B. Grinstein and R.F. Lebed, Nucl. Phys. B **461** (1996) 493 [hep-ph/9508211].

[137] C.G. Boyd and R.F. Lebed, Nucl. Phys. B **485** (1997) 275 [hep-ph/9512363].

[138] C.G. Boyd, B. Grinstein and R.F. Lebed, Phys. Rev. D **56** (1997) 6895 [hep-ph/9705252].

[139] I. Caprini, L. Lellouch and M. Neubert, factors," Nucl. Phys. B **530** (1998) 153 [hep-ph/9712417].

[140] M. Neubert, Z. Ligeti and Y. Nir, Phys. Lett. B **301** (1993) 101 [hep-ph/9209271].

[141] M. Neubert, Z. Ligeti and Y. Nir, Phys. Rev. D **47** (1993) 5060 [hep-ph/9212266].

[142] Z. Ligeti, Y. Nir and M. Neubert, Phys. Rev. D **49** (1994) 1302 [hep-ph/9305304].

[143] J. D. Bjorken, *in* Proceedings of the 4th Recontres de Physique de la Vallèe d'Aoste, La Thuille, Italy, 1990, ed. M. Greco (Editions Frontières, Gif-Sur-Yvette, 1990);
N. Isgur and M. B. Wise, Phys. Rev. D **43** (1991) 819.

[144] M.B. Voloshin, Phys. Rev. D **46** (1992) 3062.

[145] A.G. Grozin and G.P. Korchemsky, Phys. Rev. D **53** (1996) 1378;
C.G. Boyd, B. Grinstein, and A.V. Manohar, Phys. Rev. D **54** (1996) 2081;
C.G. Boyd, Z. Ligeti, I.Z. Rothstein, and M.B. Wise, Phys. Rev. D **55** (1997) 3027.

[146] N.G. Uraltsev, Phys. Lett. B **501** (2001) 86 [hep-ph/0011124].

[147] M.E. Luke, Phys. Lett. B **252** (1990) 447.

[148] M.A. Shifman, N.G. Uraltsev, and A.I. Vainshtein, Phys. Rev. D **51** (1995) 2217 [hep-ph/9405207]; [Erratum-ibid. **52** (1995) 3149].

[149] A.F. Falk and M. Neubert, Phys. Rev. D **47** (1993) 2965 [hep-ph/9209268].

[150] A.S. Kronfeld, Phys. Rev. D **62**, 014505 (2000) [hep-lat/0002008].

[151] J. Harada, *et al.*, Phys. Rev. D **65**, 094514 (2002) [hep-lat/0112045].

[152] S. Hashimoto, *et al.*, Phys. Rev. D **66** (2002) 014503 [hep-ph/0110253].

[153] I.I. Bigi, M.A. Shifman and N.G. Uraltsev, Annu. Rev. Nucl. Part. Sci. **47** (1997) 591 [hep-ph/9703290].

[154] A. Czarnecki, K. Melnikov and N.G. Uraltsev, Phys. Rev. D **57** (1998) 1769 [hep-ph/9706311].

[155] A. Czarnecki, Phys. Rev. Lett. **76** (1996) 4124 [hep-ph/9603261].

[156] A. Czarnecki and K. Melnikov, Nucl. Phys. B **505** (1997) 65 [hep-ph/9703277].

[157] N.G. Uraltsev, hep-ph/9804275.

[158] T. Mannel, Phys. Rev. D **50** (1994) 428 [hep-ph/9403249].

[159] S. Ryan, Nucl. Phys. B Proc. Suppl. **106** (2002) 86 [hep-lat/0111010].

[160] A.X. El-Khadra, A.S. Kronfeld, and P.B. Mackenzie, Phys. Rev. D **55** (1997) 3933 [hep-lat/9604004].

[161] J. Harada, *et al.*, Phys. Rev. D **65** (2002) 094513 [hep-lat/0112044].

[162] S. Hashimoto *et al.*, Phys. Rev. D **61** (2000) 014502 [hep-ph/9906376].

[163] A.S. Kronfeld, P.B. Mackenzie, J.N. Simone, S. Hashimoto and S.M. Ryan, in *Flavor Physics and CP Violation*, edited by R.G.C. Oldemann, hep-ph/0207122.

[164] L. Randall and M.B. Wise, Phys. Lett. B **303** (1993) 135;
M.J. Savage, Phys. Rev. D **65** (2002) 034014 [hep-ph/0109190].

[165] D. Arndt, hep-lat/0210019.

[166] D. Scora and N. Isgur, Phys. Rev. D **52** (1995) 2783.

[167] Z. Ligeti, hep-ph/9908432.

[168] G.P. Lepage, *et al.*, Nucl. Phys. B Proc. Suppl. **106** (2002) 12 [hep-lat/0110175];
C. Morningstar, *ibid.* **109** (2002) 185 [hep-lat/0112023].

[169] D. Atwood and W.J. Marciano, Phys. Rev. D **41** (1990) 1736.

[170] E.S. Ginsberg, Phys. Rev. **171** (1968) 1675; **174** (1968) 2169(E); **187** (1969) 2280(E).

[171] A. Sirlin, Nucl. Phys. B **196** (1982) 83.

[172] R.A. Briere *et al.* [CLEO Collaboration], Phys. Rev. Lett. **89** (2002) 81803; [hep-ex/0203032].

[173] K. Abe *et al.* [BELLE Collaboration], Phys. Lett. B **526** (2002) 247; [hep-ex/0111060].

[174] P. Abreu *et al.* [DELPHI Collaboration], Phys. Lett. B **510** (2001) 55 [hep-ex/0104026].

[175] D. Buskulic *et al.* [ALEPH Collaboration], Phys. Lett. B **935** (1997) 373.

[176] G. Abbiendi *et al.* [OPAL Collaboration], Phys. Lett. B **482** (2000) 15.

[177] S. Anderson *et al.* [CLEO Collaboration], Nucl.Phys. A **663** (2000) [hep-ex/9908009].

[178] D. Buskulic *et al.* [ALEPH Collaboration], Z. Phys. C **73** (1997) 601.

[179] A. Anastassov *et al.* [CLEO Collaboration], Phys. Rev. Lett. **80** (1998) 4127.

[180] LEP/SLD Electroweak Heavy Flavor Group, results presented at the Winter 2001 Conferences, see `http://lepewwg.web.cern.ch/LEPEWWG/heavy/`

[181] D. Block *et al.* [DELPHI Collaboration], contributed paper to ICHEP 2000, DELPHI 2000-106 Conf. 45.

[182] ALEPH, CDF, DELPHI, L3, OPAL, SLD, CERN-EP/2001-050.

[183] V. Morenas *et al.*, Phys. Rev. D **59** (1997) 5668 [hep-ph/9706265];
M.Q. Huang, C. Li and Y.B. Dai, Phys. Rev. D **61** (2000) 54010 [hep-ph/9909307].

[184] A.K. Leibovich, Z. Ligeti, I.W. Stewart, M.B. Wise Phys. Rev. D **57** (1998) 308 [hep-ph/9705467] and Phys. Rev. Lett. **78** (1997) 3995 [hep-ph/9703213].

[185] LEP V_{cb} Working Group, Internal Note, see `http://lepvcb.web.cern.ch/LEPVCB/`

[186] CDF, LEP, SLD B Oscillations Working Group, Internal Note, see `http://lepbosc.web.cern.ch/LEPBOSC/`.

[187] CDF, LEP, SLD B-hadron Lifetime Working Group, Internal Note, see `http://claires.home.cern.ch/claires/lepblife.html`.

[188] J.E. Duboscq *et al.* [CLEO Collaboration], Phys. Rev. Lett. **76** (1996) 3898.

[189] B. Grinstein and Z. Ligeti, Phys. Lett. B **526** (2002) 345 [hep-ph/0111392].

[190] K. Abe *et al.* [BELLE Collaboration], Phys. Lett. B **526** (2002) 258 [hep-ex/0111082].

[191] J. Bartelt *et al.* [CLEO Collaboration], Phys. Rev. Lett. **82** (1999) 3746.

[192] L. Lellouch, hep-ph/9912353.

[193] K.'C. Bowler *et al.* [UKQCD Collaboration], Phys. Lett. B **486** (2000) 111 [hep-lat/9911011].

[194] A. Abada *et al.*, V. Lubicz and F. Mescia, Nucl. Phys. B **619** (2001) 565 [hep-lat/0011065].

[195] A.X. El-Khadra *et al.*, Phys. Rev. D **64** (2001) 014502 [hep-ph/0101023].

[196] S. Aoki *et al.* [JLQCD Collaboration], Phys. Rev. D **64** (2001) 114505 [hep-lat/0106024].

[197] B. Sheikholeslami and R. Wohlert, Nucl. Phys. B **259** (1985) 572.

[198] M. Luscher, S. Sint, R. Sommer and P. Weisz, Nucl. Phys. B **478** (1996) 365 [hep-lat/9605038].

[199] M. Luscher, S. Sint, R. Sommer and H. Wittig, Nucl. Phys. B **491** (1997) 344 [hep-lat/9611015].

[200] B.A. Thacker and G.P. Lepage, Phys. Rev. D **43** (1991) 196.

[201] G.P. Lepage, *et al.*, Phys. Rev. D **46** (1992) 4052 [hep-lat/9205007].

[202] G. Burdman, Z. Ligeti, M. Neubert and Y. Nir, Phys. Rev. D **49** (1994) 2331 [hep-ph/9309272].

[203] G. Burdman and J.F. Donoghue, Phys. Lett. B **280** (1992) 287.

[204] M.B. Wise, Phys. Rev. D **45** (1992) 2188.

[205] T.M. Yan, *et al.*, Phys. Rev. D **46** (1992) 1148 [Erratum-ibid. D **55** (1997) 5851].

[206] D. Becirevic, S. Prelovsek and J. Zupan, Phys. Rev. D **67** (2003) 054010 [hep-lat/0210048].

[207] R. Fleischer, Phys. Lett. B **303** (1993) 147.

[208] C.G. Boyd, B. Grinstein and R.F. Lebed, Phys. Rev. Lett. **74** (1995) 4603 [hep-ph/9412324].

[209] L. Lellouch, Nucl. Phys. B **479** (1996) 353 [hep-ph/9509358].

[210] D.R. Burford, *et al.* [UKQCD Collaboration], Nucl. Phys. B **447** (1995) 425 [hep-lat/9503002].

[211] L. Del Debbio, *et al.* [UKQCD Collaboration], Phys. Lett. B **416** (1998) 392 [hep-lat/9708008].

[212] J. Charles, *et al.*, Phys. Rev. D **60** (1999) 014001 [hep-ph/9812358].

[213] A. Khodjamirian, *et al.*, Phys. Rev. D **62** (2000) 114002 [hep-ph/0001297].

[214] S. Dürr, DESY-02-121, hep-lat/0208051.

[215] C. Bernard, *et al.*, hep-lat/0209086.

[216] S. Hashimoto *et al.* [JLQCD Collaboration], hep-lat/0209091.

[217] L. Lellouch, plenary talk presented at ICHEP-2002, Amsterdam, July 2002, hep-ph/0211359.

[218] J. M. Flynn *et al.* [UKQCD Collaboration], Nucl. Phys. B **461** (1996) 327 [hep-ph/9506398].

[219] B.H. Behrens *et al.* [CLEO Collaboration], Phys. Rev. D **61** (2000) 052001 [hep-ex/9905056].

[220] A. Abada *et al.*, Nucl. Phys. B **416** (1994) 675 [hep-lat/9308007].

[221] C.R. Allton *et al.* [APE Collaboration], Phys. Lett. B **345** (1995) 513 [hep-lat/9411011].

[222] J. Gill [UKQCD Collaboration], Nucl. Phys. Proc. Suppl. **106** (2002) 391 [hep-lat/0109035].

[223] A. Abada, *et al.* [SPQcdR Collaboration], hep-lat/0209116.

[224] M. Beneke and T. Feldmann, Nucl. Phys. B **592** (2001) 3 [hep-ph/0008255].

[225] J. Chay and C. Kim, Phys. Rev. D **65** (2002) 114016 [hep-ph/0201197].

[226] C.W. Bauer, D. Pirjol and I.W. Stewart, Phys. Rev. D **66** (2002) 054005 [hep-ph/0205289].

[227] M. Beneke, *et al.*, Nucl. Phys. B **643** (2002) 431 [hep-ph/0206152].

[228] P. Ball and V.M. Braun, Phys. Rev. D **58** (1998) 094016 [hep-ph/9805422].

[229] N. Yamada *et al.* [JLQCD Collaboration], Nucl. Phys. Proc. Suppl. **106** (2002) 397 [hep-lat/0110087].

[230] I.I. Balitsky, V.M. Braun and A.V. Kolesnichenko, Nucl. Phys. B **312** (1989) 509;
V.M. Braun and I.E. Filyanov, Z. Phys. C **44** (1989) 157.

[231] V.L. Chernyak and I.R. Zhitnitsky, Nucl. Phys. B **345** (1990) 137.

[232] V.M. Belyaev, A. Khodjamirian and R. Rückl, Z. Phys. C **60** (1993) 349.

[233] A. Khodjamirian, R. Rückl, S. Weinzierl and O. Yakovlev, Phys. Lett. B **410** (1997) 275;
E. Bagan, P. Ball and V.M. Braun, Phys. Lett. B **417** (1998) 154.

[234] P. Ball, JHEP **9809** (1998) 005.

[235] P. Ball and R. Zwicky, JHEP **0110** (2001) 019 [hep-ph/0110115].

[236] A. Ali, P. Ball, L.T. Handoko and G. Hiller, Phys. Rev. D **61** (2000) 074024.

[237] A. Khodjamirian and R. Ruckl, in *Heavy Flavors*, 2nd edition, eds., A.J. Buras and M. Lindner, World Scientific (1998), p. 345, hep-ph/9801443.

[238] V.M. Braun, hep-ph/9911206.

[239] P. Colangelo and A. Khodjamirian, *Boris Ioffe Festschrift 'At the Frontier of Particle Physics; Handbook of QCD'*, ed. M. Shifman (World Scientific, Singapore, 2001), p.1495 [hep-ph/0010175].

[240] M. Jamin and B.O. Lange, Phys. Rev. D **65** (2002) 056005.

[241] D. Becirevic and A.B. Kaidalov, Phys. Lett. B **478** (2000) 417 [hep-ph/9904490].

[242] V.M. Belyaev, V.M. Braun, A. Khodjamirian and R. Ruckl, Phys. Rev. D **51** (1995) 6177 [hep-ph/9410280]; A. Khodjamirian, R. Ruckl, S. Weinzierl and O. Yakovlev, Phys. Lett. B **457** (1999) 245 [hep-ph/9903421].

[243] K.C. Bowler *et al.* [UKQCD Collaboration], Phys. Lett. B **486** (2000) 111.

[244] H. Ishino [Belle Collaboration], talk at XXXVII Rencontres de Moriond, March 2002.

[245] J.P. Alexander *et al.* [CLEO Collaboration], Phys. Rev. Lett. **77** (1996) 5000.

[246] D. Scora and N. Isgur, Phys. Rev. D **52** (1995) 2783.

[247] D. Melikhov, Phys. Rev. D **53** (1996) 2160.

[248] M. Wirbel, B. Stech and M. Bauer, Z. Phys. C **29** (1985) 637.

[249] G. Burdman and J. Kambor, Phys. Rev. D **55** (1997) 2817 [hep-ph/9602353].

[250] J.M. Flynn *et al.*, Nucl. Phys. B **461** (1996) 327.

[251] B. Stech, Phys. Lett. B **354** (1995) 447.

[252] BELLE Collaboration, BELLE-CONF 0124 (2001).

[253] BELLE Collaboration, see `http://www.ichep02.nl/Transparencies/CP/CP-1/CP-1-4.kwon.pd` ICHEP (2002).

[254] BaBar Collaboration, hep-ex/0207080.

[255] Y. Kwon [BELLE Collaboration], ICHEP CP-1-4 (2002).

[256] M. Beyer and D. Melikhov, Phys. Lett. B **436** (1998) 344.

[257] N. Adam *et al.* [CLEO Collaboration], CLEO-CONF/02-09, ICHEP02-ABS931.

[258] F. De Fazio and M. Neubert, JHEP **9906** (1999) 017.

[259] Z. Ligeti and M.B. Wise, Phys. Rev. D **53** (1996) 4937. .

[260] BELLE Collaboration, BELLE-CONF 02/42, ICHEP ABS 732.

[261] CLEO Collaboration, talk at DPF-2002, see `http://dpf2002.velopers.net/talks_pdf/452talk.pdf`.

[262] LEP B Lifetime Working Group, see `http://lepbosc.web.cern.ch/LEPBOSC/lifetimes/ lepblife.html`

[263] B. Aubert *et al.* [BaBar Collaboration], Phys. Rev. Lett. **87** (2001) 201803;
K. Abe *et al.* [BELLE Collaboration], Phys. Rev. Lett. **88** (2002) 171801.

[264] M. Beneke *et al.*, Phys. Lett. B **459** (1999) 631 [hep-ph/9808385].

[265] M. Beneke and A. Lenz, J. Phys. G **G27** (2001) 1219 [hep-ph/0012222];
D. Becirevic, hep-ph/0110124 and refs. therein.

[266] A.J. Buras, M. Jamin, M.E. Lautenbacher and P.H. Weisz, Nucl. Phys. B **400** (1993) 37 [hep-ph/9211304]; A.J. Buras, M. Jamin and M.E. Lautenbacher, Nucl. Phys. B **400** (1993) 75 [hep-ph/9211321]; M. Ciuchini, E. Franco, G. Martinelli and L. Reina, Nucl. Phys. B **415** (1994) 403 [hep-ph/9304257].

[267] M. Beneke, G. Buchalla and I. Dunietz, Phys. Rev. D **54** (1996) 4419 [hep-ph/9605259].

[268] V. Gimenez and J. Reyes, Nucl. Phys. Proc. Suppl. **93** (2001) 95 [hep-lat/0009007].

[269] S. Hashimoto *et al.*, Phys. Rev. D **62** (2000) 114502 [hep-lat/0004022].

[270] S. Aoki *et al.* [JLQCD Collaboration], hep-lat/0208038.

[271] D. Becirevic *et al.*, Eur. Phys. J. C **18** (2000) 157 [hep-ph/0006135].

[272] L. Lellouch and C.J. Lin [UKQCD Collaboration], Phys. Rev. D **64** (2001) 094501 [hep-ph/0011086].

[273] D. Becirevic *et al.*, JHEP **0204** (2002) 025 [hep-lat/0110091].

[274] S. Hashimoto and N. Yamada [JLQCD Collaboration], hep-ph/0104080.

[275] S. Aoki *et al.* [JLQCD Collaboration], hep-lat/0208038.

[276] A.S. Dighe, *et al.*, Nucl. Phys. B **624** (2002) 377 [hep-ph/0109088] and hep-ph/0202070;
see also T. Hurth *et al.*, J. Phys. G **27** (2001) 1277 [hep-ph/0102159].

[277] K. Anikeev *et al.*, hep-ph/0201071.

[278] S. Hashimoto and N. Yamada [JLQCD Collaboration], hep-ph/0104080.

[279] P. Ball *et al.*, CERN-TH-2000-101, hep-ph/0003238.

[280] B. Aubert *et al.* [BaBar Collaboration], Phys. Rev. Lett. **87** (2001) 091801 [hep-ex/0107013].

[281] Y. Grossman, Phys. Lett. B **380** (1996) 99 [hep-ph/9603244].

[282] I.I. Bigi, N.G. Uraltsev and A.I. Vainshtein, Phys. Lett. B **293** (1992) 430; Erratum **297** (1993) 477 [hep-ph/9207214].

[283] Q. Ho-kim and X.-y. Pham, Phys. Lett. B **122** (1983) 297.

[284] E. Bagan, P. Ball, V.M. Braun and P. Gosdzinsky, Nucl. Phys. B **432** (1994) 3 [hep-ph/9408306].

[285] E. Bagan et al., Phys. Lett. B **342** (1995) 362; Erratum **374** (1996) 363 [hep-ph/9409440];
E. Bagan et al., Phys. Lett. B **351** (1995) 546 [hep-ph/9502338];
A.F. Falk et al., Phys. Lett. B **326** (1994) 145 [hep-ph/9401226].

[286] M. Neubert and C.T. Sachrajda, Nucl. Phys. B **483**, 339 (1997) [hep-ph/9603202].

[287] N.G. Uraltsev, Phys. Lett. B **376** (1996) 303 [hep-ph/9602324].

[288] M. Beneke and G. Buchalla, Phys. Rev. D **53** (1996) 4991 [hep-ph/9601249].

[289] E. Franco *et al.*, Nucl. Phys. B **633** (2002) 212 [hep-ph/0203089].

[290] M. Beneke *et al.*, hep-ph/0202106.

[291] V. Gimenez and J. Reyes, Nucl. Phys. B **545** (1999) 576 [hep-lat/9806023].

[292] M. Ciuchini, *et al.*, Nucl. Phys. B **625** (2002) 211 [hep-ph/0110375].

[293] V. Chernyak, Nucl. Phys. B **457** (1995) 96 [hep-ph/9503208].

[294] D. Pirjol and N.G. Uraltsev, Phys. Rev. D **59** (1999) 034012 [hep-ph/9805488].

[295] M. Di Pierro and C.T. Sachrajda [UKQCD Collaboration], Nucl. Phys. B **534** (1998) 373 [hep-lat/9805028].

[296] M. Di Pierro, C.T. Sachrajda and C. Michael [UKQCD Collaboration], Phys. Lett. B **468** (1999) 143 [hep-lat/9906031]; M. Di Pierro and C.T. Sachrajda [UKQCD Collaboration], Nucl. Phys. Proc. Suppl. **73** (1999) 384 [hep-lat/9809083].

[297] D. Becirevic, update of hep-ph/0110124 for the present work.

[298] P. Colangelo and F. De Fazio, Phys. Lett. B **387** (1996) 371 [hep-ph/9604425];
M.S. Baek, J. Lee, C. Liu and H.S. Song, Phys. Rev. D **57** (1998) 4091 [hep-ph/9709386];
H.Y. Cheng and K.C. Yang, Phys. Rev. D **59** (1999) 014011 [hep-ph/9805222];
C.S. Huang, C. Liu and S.L. Zhu, Phys. Rev. D **61** (2000) 054004 [hep-ph/9906300].

[299] ALEPH Collaboration, Phys. Lett. B **486** (2000) 286.

[300] L3 Collaboration, Phys. Lett. B **438** (1998) 417.

[301] DELPHI Collaboration, Eur. Phys. J. C **18** (2000) 229.

[302] ALEPH Collaboration, Phys. Lett. B **377** (1996) 205;
CDF Collaboration, Phys. Rev. D **59** (1999) 032004;
OPAL Collaboration, Phys. Lett. B **426** (1998) 161.

[303] R. Aleksan *et al.*, Phys. Lett. B **316** (1993) 567.

[304] DELPHI Collaboration, Eur. Phys. J. C **16** (2000) 555.

[305] CDF Collaboration, Phys. Rev. D **57** (1998) 5382.

[306] CLEO Collaboration, Phys. Rev. Lett. **79** (1997) 4533.

[307] ALEPH, CDF, DELPHI, L3, OPAL and SLD Collaborations, CERN-EP/2001-050.
See also `http://www.cern.ch/LEPBOSC`.

[308] CDF Collaboration, Phys. Rev. Lett. **77** (1996) 1945.

[309] CDF Collaboration, Phys. Rev. Lett. **75** (1995) 3068 and Phys. Rev. Lett. **85** (2000) 4668.

[310] W. Ashmanskas *et al.*, *Performance of the CDF Online Silicon Vertex Tracker* published in Proceedings of the 2001 IEEE Nuclear Science Symposium (NSS) and Medical Imaging Conference (MIC), San Diego, CA, November 2001.

[311] T. Allmendinger *et al.* [DELPHI Collaboration] DELPHI 2001-054 CONF 482.

[312] A. Dighe, I. Dunietz, H. Lipkin, J.L. Rosner, Phys. Lett. B **369** (1996) 144.

[313] M. Sevelda, PhD Thesis, Charles University of Prague, 1999.

[314] ATLAS TDR, CERN-LHCC-99-015.

Chapter 4

CKM ELEMENTS FROM K AND B MESON MIXING

Conveners : J.M. Flynn, M. Paulini, S. Willocq.
Contributors: D. Abbaneo, C. Bozzi, A.J. Buras, R. Forty, R. Gupta, R. Hawkings, A. Hoecker, M. Jamin, P. Kluit, A. Kronfeld, V. Lacker, F. Le Diberder, L. Lellouch, C. Leonidopoulos, D. Lin, V. Lubicz, H.G. Moser, U. Nierste, J. Ocariz, F. Parodi, C. Paus, P. Roudeau, Y. Sakai, O. Schneider, A. Stocchi, C. Weiser, N. Yamada.

1. Basic formulae for particle–antiparticle mixing

1.1. K sector: basic formula for ε_K

In the $\mathrm{K}^0 - \overline{\mathrm{K}}^0$ system, to lowest order in electroweak interactions $\Delta S = 2$ transitions are induced through the box diagrams of Fig. 4.1. Including leading and next-to-leading QCD corrections in renormalization group improved perturbation theory the effective Hamiltonian for the $\Delta S = 2$ transitions for scales $\mu < \mu_c = \mathcal{O}(m_c)$ is given by

$$\begin{aligned}\mathcal{H}_{\mathrm{eff}}^{\Delta S=2} &= \frac{G_{\mathrm{F}}^2}{16\pi^2} M_{\mathrm{W}}^2 \left[\lambda_c^2 \eta_1 S_0(x_c) + \lambda_t^2 \eta_2 S_0(x_t) + 2\lambda_c\lambda_t \eta_3 S_0(x_c, x_t)\right] \times \\ &\quad \times \left[\alpha_s^{(3)}(\mu)\right]^{-2/9} \left[1 + \frac{\alpha_s^{(3)}(\mu)}{4\pi} J_3\right] Q(\Delta S = 2) + \mathrm{h.c.} \qquad (1)\end{aligned}$$

where $\lambda_i = V_{is}^* V_{id}$, $\alpha_s^{(3)}$ is the strong coupling constant in an effective three flavour theory and $J_3 = 307/162 = 1.895$ in the NDR scheme [1]. In (1), the relevant operator

$$Q(\Delta S = 2) = (\bar{s}\gamma_\mu(1-\gamma_5)d)(\bar{s}\gamma^\mu(1-\gamma_5)d), \qquad (2)$$

is multiplied by the corresponding Wilson coefficient function. This function is decomposed into a charm-, a top- and a mixed charm-top contribution. The functions $S_0(x_i)$ and $S_0(x_c, x_t)$ are given by ($x_i = m_i^2/M_{\mathrm{W}}^2$):

$$S_0(x_t) = \frac{4x_t - 11x_t^2 + x_t^3}{4(1-x_t)^2} - \frac{3x_t^3 \ln x_t}{2(1-x_t)^3}, \qquad S_0(x_c) = x_c, \qquad (3)$$

$$S_0(x_c, x_t) = x_c \left[\ln \frac{x_t}{x_c} - \frac{3x_t}{4(1-x_t)} - \frac{3x_t^2 \ln x_t}{4(1-x_t)^2}\right], \qquad (4)$$

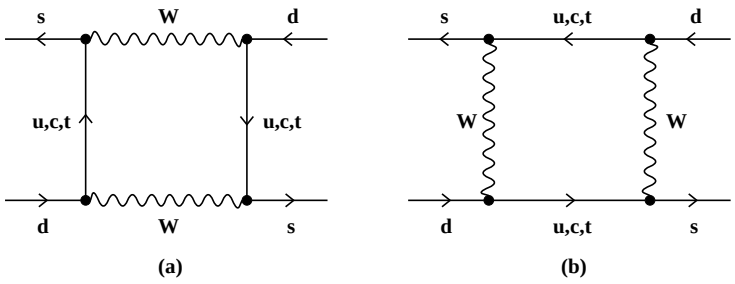

Fig. 4.1: *Box diagrams contributing to* $\mathrm{K}^0 - \overline{\mathrm{K}}^0$ *mixing in the SM.*

where we keep only linear terms in $x_c \ll 1$, but of course all orders in x_t. The exact expression can be found in [2].

Short-distance QCD effects are described through the correction factors η_1, η_2, η_3 and the explicitly $\alpha_{\rm s}$-dependent terms in (1). The NLO values of η_i are given as follows [1,3–6]:

$$\eta_1 = (1.32 \pm 0.32) \left(\frac{1.30\mathrm{GeV}}{m_c(m_c)}\right)^{1.1}, \qquad \eta_2 = 0.57 \pm 0.01, \qquad \eta_3 = 0.47 \pm 0.05\ . \tag{5}$$

It should be emphasized that the values of η_i depend on the definition of the quark masses m_i. The ones in (5) correspond to $m_t \equiv m_t(m_t)$ and $m_c \equiv m_c(m_c)$. With this definition the dependences of η_2 on m_t and of η_3 on m_t and m_c are fully negligible but the dependence of η_1 on m_c turns out to be significant. It can be well approximated by the formula in (5). The scale dependence in $m_t(\mu_t)$, where $\mu_t = \mathcal{O}(m_t)$, present generally in the functions $S_0(x_t)$ and $S_0(x_t, x_c)$ is canceled to an excellent accuracy in the products $\eta_2 S_0(x_t)$ and $\eta_3 S_0(x_t, x_c)$. The corresponding scale dependence in $m_c(\mu_c)$, where $\mu_c = \mathcal{O}(m_c)$, is cancelled to a large extent in the product $\eta_3 S_0(x_t, x_c)$ but remains still sizable in $\eta_1 S_0(x_c)$. As we use $m_c(m_c)$ and $m_t(m_t)$ we have included the left-over scale uncertainties due to μ_c and μ_t present in (1) in the errors of η_i that also include the uncertainties due to $\Lambda_{\overline{\rm MS}}$, the scale in the QCD running coupling. The small changes in η_1 and η_3 relative to the original papers are due to changes in $\alpha_s(M_Z)$.

Now, ε_K is defined by

$$\varepsilon_K = \frac{A(\mathrm{K_L} \to (\pi\pi)_{I=0})}{A(\mathrm{K_S} \to (\pi\pi)_{I=0})} \tag{6}$$

with I denoting isospin. From (6) one finds

$$\varepsilon_K = \frac{\exp(i\pi/4)}{\sqrt{2}\Delta M_K} \left(\mathrm{Im}M_{12} + 2\bar{\xi}\mathrm{Re}M_{12}\right), \qquad \bar{\xi} = \frac{\mathrm{Im}A_0}{\mathrm{Re}A_0} \tag{7}$$

with the off-diagonal element M_{12} in the neutral K-meson mass matrix representing K^0-$\overline{\mathrm{K}}^0$ mixing given by

$$2M_K M_{12}^* = \langle \overline{\mathrm{K}}^0 | \mathcal{H}_{\rm eff}(\Delta S = 2) | \mathrm{K}^0 \rangle\ . \tag{8}$$

The factor $2M_K$ reflects our normalization of external states and A_0 is the isospin amplitude. ΔM_K is the $\mathrm{K}_L - \mathrm{K}_S$ mass difference that is taken from experiment as it cannot be reliably calculated due to long distance contributions. The expression in (7) neglects higher order CP-violating terms: see the discussion in the review article in reference [7].

Defining the renormalization group invariant parameter $\hat{B}_K$ by [1]

$$\hat{B}_K = B_K(\mu) \left[\alpha_{\rm s}^{(3)}(\mu)\right]^{-2/9} \left[1 + \frac{\alpha_{\rm s}^{(3)}(\mu)}{4\pi} J_3\right], \tag{9}$$

$$\langle \overline{\mathrm{K}}^0 | Q(\Delta S = 2) | \mathrm{K}^0 \rangle \equiv \frac{8}{3} B_K(\mu) F_K^2 M_K^2 \tag{10}$$

and using (8) and (1) one finds

$$M_{12} = \frac{G_{\mathrm{F}}^2}{12\pi^2} F_K^2 \hat{B}_K M_K M_{\mathrm{W}}^2 \left[\lambda_c^{*2} \eta_1 S_0(x_c) + \lambda_t^{*2} \eta_2 S_0(x_t) + 2\lambda_c^* \lambda_t^* \eta_3 S_0(x_c, x_t) \right], \tag{11}$$

where $F_K = 160$ MeV is the K-meson decay constant and M_K the K-meson mass.

To proceed further we neglect the last term in (7) as in the standard CKM phase convention it constitutes at most a $2\,\%$ correction to ε_K. This is justified in view of other uncertainties, in particular those connected with $\hat{B}_K$. Inserting (11) into (7) we find

$$\varepsilon_K = C_\varepsilon \hat{B}_K \mathrm{Im}\lambda_t \left\{ \mathrm{Re}\lambda_c \left[\eta_1 S_0(x_c) - \eta_3 S_0(x_c, x_t) \right] - \mathrm{Re}\lambda_t \eta_2 S_0(x_t) \right\} \exp(i\pi/4), \tag{12}$$

where we have used the unitarity relation $\mathrm{Im}\lambda_c^* = \mathrm{Im}\lambda_t$ and have neglected $\mathrm{Re}\lambda_t/\mathrm{Re}\lambda_c = \mathcal{O}(\lambda^4)$ in evaluating $\mathrm{Im}(\lambda_c^* \lambda_t^*)$. The numerical constant C_ε is given by

$$C_\varepsilon = \frac{G_{\mathrm{F}}^2 F_K^2 M_K M_{\mathrm{W}}^2}{6\sqrt{2}\pi^2 \Delta M_K} = 3.837 \cdot 10^4 \,. \tag{13}$$

To this end we have used the experimental value of $\Delta M_K = 3.837 \cdot 10^{-15}$ GeV and $M_{\mathrm{W}} = 80.4$ GeV.

The main uncertainty in (12) resides in the parameter $\hat{B}_K$. The present status of $\hat{B}_K$ is discussed in Sec. 2.2. Here we note only that when $\hat{B}_K > 0$, as found by all non-perturbative methods, the formula (12) combined with the experimental value for ε_K implies $0 < \delta < \pi$ in the standard parametrization or equivalently $\bar{\eta} > 0$ in the Wolfenstein parametrization.

1.2. B sector: basic formulae for $\Delta M_{d,s}$ oscillation frequencies

The strengths of the $\mathrm{B}_{d,s}^0 - \overline{\mathrm{B}}_{d,s}^0$ mixings are described by the mass differences

$$\Delta M_{d,s} = M_H^{d,s} - M_L^{d,s} \tag{14}$$

where the subscripts H and L denote the heavy and light mass eigenstates respectively. The long distance contributions are estimated to be very small, in contrast to the situation for ΔM_K, and $\Delta M_{d,s}$ are very well approximated by the relevant box diagrams. Moreover, since $m_{u,c} \ll m_t$ only the top sector can contribute significantly to $\Delta M_{d,s}$. The charm and mixed top-charm contributions are entirely negligible.

$\Delta M_{d,s}$ can be expressed in terms of the off-diagonal element in the neutral B-meson mass matrix as follows

$$\Delta M_q = 2|M_{12}^{(q)}|, \qquad q = d, s \tag{15}$$

with M_{12} given by a formula analogous to (8)

$$2M_{B_q}|M_{12}^{(q)}| = |\langle \overline{\mathrm{B}}_q^0 | \mathcal{H}_{\mathrm{eff}}(\Delta B = 2) | \mathrm{B}_q^0 \rangle|. \tag{16}$$

In the case of $\mathrm{B}_d^0 - \overline{\mathrm{B}}_d^0$ mixing

$$\begin{aligned} \mathcal{H}_{\mathrm{eff}}^{\Delta B=2} &= \frac{G_{\mathrm{F}}^2}{16\pi^2} M_W^2 \left(V_{tb}^* V_{td}\right)^2 \eta_B S_0(x_t) \times \\ &\quad \times \left[\alpha_s^{(5)}(\mu_b)\right]^{-6/23} \left[1 + \frac{\alpha_s^{(5)}(\mu_b)}{4\pi} J_5\right] Q(\Delta B = 2) + h.c. \end{aligned} \tag{17}$$

Here $\mu_b = \mathcal{O}(m_b)$, $J_5 = 5165/3174 = 1.627$ in the NDR scheme [1],

$$Q(\Delta B = 2) = (\bar{b}\gamma_\mu(1-\gamma_5)d)(\bar{b}\gamma^\mu(1-\gamma_5)d) \tag{18}$$

and

$$\eta_B = 0.55 \pm 0.01 \tag{19}$$

summarizes the NLO QCD corrections [1,8]. In the case of $\mathrm{B}_s^0 - \overline{\mathrm{B}}_s^0$ mixing one should simply replace $d \to s$ in (17) and (18) with all other quantities and numerical values unchanged. Again $m_t \equiv m_t(m_t)$.

Defining the renormalization group invariant parameters $\hat{B}_{B_q}$ in analogy to (9) and (10)

$$\hat{B}_{B_q} = B_{B_q}(\mu)\left[\alpha_{\mathrm{s}}^{(5)}(\mu)\right]^{-6/23}\left[1 + \frac{\alpha_{\mathrm{s}}^{(5)}(\mu)}{4\pi}J_5\right], \tag{20}$$

$$\langle \overline{\mathrm{B}}_q^0 | Q(\Delta B = 2) | \mathrm{B}_q^0 \rangle \equiv \frac{8}{3} B_{B_q}(\mu) F_{B_q}^2 M_{B_q}^2 \tag{21}$$

one finds using (17)

$$\Delta M_q = \frac{G_{\mathrm{F}}^2}{6\pi^2}\eta_B M_{B_q}(\hat{B}_{B_q} F_{B_q}^2) M_{\mathrm{W}}^2 S_0(x_t)|V_{tq}|^2, \tag{22}$$

where F_{B_q} is the B_q-meson decay constant. This implies two approximate but rather accurate formulae

$$\Delta M_d = 0.50/\mathrm{ps} \cdot \left[\frac{\sqrt{\hat{B}_{B_d}}F_{B_d}}{230\mathrm{MeV}}\right]^2 \left[\frac{\overline{m}_{\mathrm{t}}(m_{\mathrm{t}})}{167\mathrm{GeV}}\right]^{1.52} \left[\frac{|V_{td}|}{7.8\cdot 10^{-3}}\right]^2 \left[\frac{\eta_B}{0.55}\right] \tag{23}$$

and

$$\Delta M_s = 17.2/\mathrm{ps} \cdot \left[\frac{\sqrt{\hat{B}_{B_s}}F_{B_s}}{260\mathrm{MeV}}\right]^2 \left[\frac{\overline{m}_{\mathrm{t}}(m_{\mathrm{t}})}{167\mathrm{GeV}}\right]^{1.52} \left[\frac{|V_{ts}|}{0.040}\right]^2 \left[\frac{\eta_B}{0.55}\right]. \tag{24}$$

The main uncertainty here stems from the parameters $F_{B_{d,s}}$ and $\hat{B}_{B_{d,s}}$. The most recent lattice and QCD sum rule results are summarized in Sec. 2.1.

1.3. Basic formulae for B oscillation probabilities

The probability $\mathcal{P}$ for a B_q^0 meson ($q = d, s$) produced at time $t = 0$ to decay as B_q^0 at proper time t is given as

$$\mathcal{P}(\mathrm{B}_q^0 \to \mathrm{B}_q^0) = \frac{1}{2}\Gamma_q\, e^{-\Gamma_q t}\,[\cosh(\frac{\Delta\Gamma_q}{2}t) \;+\; \cos(\Delta M_q t)]. \tag{25}$$

Here we neglect effects from CP violation, while $\Gamma_q = \frac{\Gamma_q^H + \Gamma_q^L}{2}$, $\Delta\Gamma_q = \Gamma_q^H - \Gamma_q^L$ and ΔM_q is defined in Eq. (14). The Standard Model predicts $\Delta\Gamma_q \ll \Delta M_q$. Neglecting a possible lifetime difference between the heavy and light mass eigenstates of the B_q^0, the above expression simplifies to:

$$\mathcal{P}_{B_q^0}^{\mathrm{unmix}} = \mathcal{P}(\mathrm{B}_q^0 \to \mathrm{B}_q^0) \;=\; \frac{1}{2}\Gamma_q\, e^{-\Gamma_q t}\,[1 + \cos(\Delta M_q t)] \tag{26}$$

Similarly, the probability for the B_q^0 to decay as $\overline{\mathrm{B}}_q^0$ is given by

$$\mathcal{P}_{B_q^0}^{\mathrm{mix}} = \mathcal{P}(\mathrm{B}_q^0 \to \overline{\mathrm{B}}_q^0) \;=\; \frac{1}{2}\Gamma_q\, e^{-\Gamma_q t}[1 - \cos(\Delta M_q t)]. \tag{27}$$

Thus, a measurement of the oscillation frequency gives a direct measurement of the mass difference between the two physical B meson states*.

Figure 4.2 shows the time evolution of $B^0 - \overline{\mathrm{B}}^0$ oscillations displaying the unmixed (solid) and mixed (dashed) contributions for two different oscillation frequencies ΔM. The sum of $\mathcal{P}^{\mathrm{mix}}$ and $\mathcal{P}^{\mathrm{unmix}}$ is just the exponential particle decay $\Gamma_q\,\mathrm{e}^{-\Gamma_q t}$ and is shown by the dotted line in Fig. 4.2.

*ΔM_q is usually given in ps^{-1}, where 1 ps^{-1} corresponds to 6.58 10^{-4}eV.

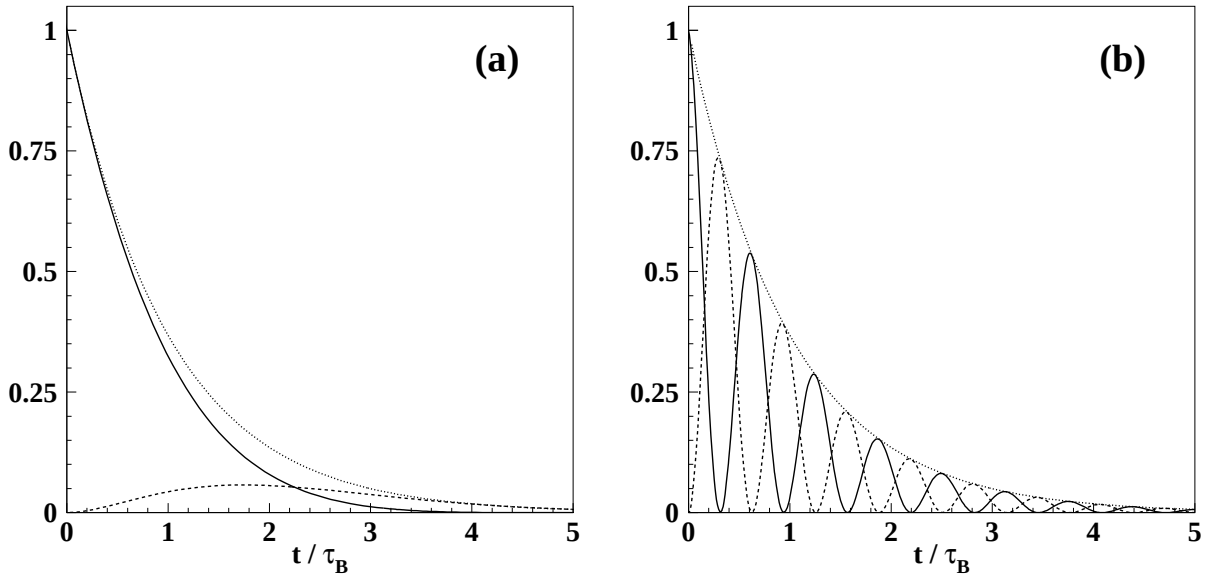

Fig. 4.2: *Time evolution of* B^0–$\overline{\mathrm{B}}^0$ *oscillations displaying the unmixed (solid) and the mixed (dashed) contribution as well as the sum of the two (dotted) for (a) slow and (b) fast oscillation frequencies* ΔM_q.

The integral of the probability $\mathcal{P}^{\rm mix}_{B^0_q}$ defined in Eq. (27) gives the mixing parameter:

$$\chi_q = \frac{x_q^2}{2\,(1+x_q^2)} \qquad \text{with} \quad x_q = \Delta M_q\,\tau_{B_q}, \tag{28}$$

where the lifetime $\tau_{B_q} = 1/\Gamma_q$.

2. Theoretical issues

2.1. Non-perturbative parameters for B meson mixing

From the discussion in Sec. 1.2. above, the main uncertainty in determining $|V_{td}|$ from ΔM_d comes from the factor $F_{B_d}\sqrt{\hat{B}_{B_d}}$ in Eq. 23. In the standard analysis of the Unitarity Triangle (see Chapter 5), ΔM_s is used in a ratio with ΔM_d, so that the important quantity is ξ, that is crucial for the determination of $|V_{td}|/|V_{ts}|$:

$$\frac{|V_{td}|}{|V_{ts}|} = \xi\sqrt{\frac{M_{\mathrm{B}_s}}{M_{\mathrm{B}_d}}}\sqrt{\frac{\Delta M_d}{\Delta M_s}}, \qquad \xi = \frac{F_{B_s}\sqrt{\hat{B}_{B_s}}}{F_{B_d}\sqrt{\hat{B}_{B_d}}}. \tag{29}$$

Although the quantities $F_{B_q}\sqrt{\hat{B}_{B_q}}$ for $q = d, s$ are needed for UT fits, it is common to find F_{B_q} and $\hat{B}_{B_q}$ separately.

2.1.1. F_{B_q} and ξ from lattice QCD

Lattice calculations are based on a first-principles evaluation of the path integral for QCD on a discrete space-time lattice. They have statistical errors arising from the stochastic (Monte Carlo) techniques used to evaluate the integral. They also have systematic errors from discretization effects, finite volume effects, the treatment of heavy quarks, chiral extrapolations and quenching (or partial quenching). We now briefly discuss these different sources of error.

Statistical, discretization and finite volume errors can all be addressed by brute-force improvement of numerical simulations. We can also use improved discretization procedures (to reduce discretization effects at a given lattice spacing) and understand (and even make use of) the finite volume effects.

Lattice results need to be matched either directly to physical quantities, or perhaps to quantities defined in some continuum renormalization scheme. On the lattice side this can be done using lattice perturbation theory, but with the development of non-perturbative renormalization methods, the uncertainty from the lattice can be systematically reduced. For a physical quantity (such as the decay constant F_{B_q}) this is the end of the story. If matching is made to a quantity in a continuum scheme (such as B_{B_q} in $\overline{\rm MS}$), the remaining uncertainty comes from the *continuum* perturbation theory: see for example the discussion in [9].

There are a number of ways to treat the heavy b-quark on the lattice. Results for $\rm B^0$–$\overline{\rm B}^0$ mixing obtained using different approaches broadly agree, suggesting that the heavy quark mass dependence is under control.

This leaves chiral extrapolations and quenching to consider. We will start with quenching. Recall that the QCD path integral is over both gauge and fermion fields. However, since the fermions appear quadratically in the action, the fermion integral can be done exactly to leave a determinant (actually a determinant for each flavour of quark). The calculation of the determinant is extremely intensive numerically, so the so-called *quenched approximation* replaces it with a constant, together with a shift in the bare couplings. This is not a controlled approximation, but today more and more lattice simulations are being done including the determinant for at least some of the quarks. The first dynamical quark algorithms produced sea quarks in degenerate pairs (in order to get a positive weight function for the Monte Carlo generation of the gauge field ensemble) and two-flavour ($N_f = 2$) dynamical simulations are still the most commonly encountered. However, methods are being developed to cope with single flavours of dynamical quark and $N_f = 2 + 1$ simulation results, with two degenerate light flavours and one heavy flavour, are beginning to appear, although there are still questions about the validity of some steps in the algorithm.

Each quark whose determinant is evaluated is labeled as a 'dynamical' or 'sea' quark in lattice parlance. A typical lattice calculation of a hadronic correlation function (from which masses and/or matrix elements may be extracted) involves an average over an ensemble of gauge fields of a combination of quark propagators. These propagators are evaluated on the background of each gauge field in the ensemble by means of a matrix inversion. The set of masses used for the propagators define the 'valence' masses of the simulation, which may or may not be the same as the dynamical masses which were incorporated (via determinant factors) when generating the gauge field ensemble. Usually the valence and sea masses are different and we talk of a 'partially quenched' calculation.

Results for F_B from quenched calculations have remained stable for a number of years. Numerical simulations using two flavours of dynamical quarks show an increase in F_B compared to quenched results. The latest developments have seen the first 3-flavour dynamical results [10,11], where two flavours are 'light' and one is heavier, around the strange quark mass. For the future, the development of more realistic dynamical simulations will continue.

Another important (and related) issue is that of chiral extrapolations, the subject of a panel discussion [12] at the Lattice 2002 conference. It is difficult to simulate realistically light (valence or sea) quarks, so that calculations of F_{B_q}, say, are made for a a set of (valence) quark masses m_q, typically in a range from about $m_s/2$ to $2m_s$ and the results are interpolated or extrapolated as required. Likewise, in partially quenched calculations, results from simulations with a range of sea quark masses need to be extrapolated. The control of these extrapolations is a serious issue for UT fits because of their effect on the final values of F_{B_d} and F_{B_s} and hence on the impact of the $\Delta M_s/\Delta M_d$ constraint. As far back as late 1994 Booth noted the striking difference between the quenched and QCD chiral logarithms [13] and posted a warning that F_{B_s}/F_{B_d} in QCD would be larger than in the quenched approximation. Recently, this issue has attracted much more attention [14–18].

Consider an idealized lattice calculation of the decay constant of a heavy-light pseudoscalar meson with valence content $Q\bar{q}$, where Q is the heavy quark and $\bar{q}$ a light quark. Imagine that the simulation is performed either with or without the presence of N_f flavours of (degenerate) sea quarks f and let ΔF_{B_q} be the correction to F_{B_q} depending on the mass(es) of the valence (q) and sea (f) quarks. With no sea quark effects included, the calculation is quenched. When $m_q \neq m_f$ the calculation is partially quenched and when $m_q = m_f$ it is QCD(-like). The dependence of ΔF_{B_q} on the valence and sea quark masses can be calculated in quenched (Q), partially quenched (PQ) or ordinary chiral perturbation theory, and shows up as dependence on the masses m_{qq}, m_{qf} and m_{ff} of pseudoscalar mesons made from the corresponding quarks [19]. The expressions are as follows

$$(\Delta F_{B_q})^{\rm QQCD} = \frac{1}{(4\pi f)^2}(X m_{qq}^2 + Y m_0^2)\ln\Big(\frac{m_{qq}^2}{\Lambda^2}\Big) \tag{30}$$

$$(\Delta F_{B_q})^{\rm PQQCD} = -\frac{(1+3g^2)}{(4\pi f)^2}\left[\frac{N_f}{2}m_{qf}^2\ln\Big(\frac{m_{qf}^2}{\Lambda^2}\Big) + \frac{(m_{ff}^2 - 2m_{qq}^2)}{2N_f}\ln\Big(\frac{m_{qq}^2}{\Lambda^2}\Big)\right] \tag{31}$$

$$(\Delta F_{B_q})^{\rm QCD} = -\frac{(1+3g^2)}{(4\pi f)^2}\Big(\frac{N_f}{2} - \frac{1}{2N_f}\Big)m_{qq}^2\ln\Big(\frac{m_{qq}^2}{\Lambda^2}\Big) \tag{32}$$

with $m_{qf}^2 = (m_{qq}^2 + m_{ff}^2)/2$ (at this order of calculation). In the factor $1/(4\pi f)^2$, f is equal to the common light pseudoscalar meson decay constant at leading order, while X, Y and m_0 are also built from coefficients of the effective Lagrangian. The dependence on the ultraviolet cutoff Λ is canceled by that of 'analytic terms' not shown here. The coupling g comes from the leading interaction term in the heavy meson chiral Lagrangian (see the textbook by Manohar and Wise [20] for details and original references) and fixes the $\mathrm{B}^*\mathrm{B}\pi$ coupling in the limit $M_B \to \infty$ by

$$g_{B^*B\pi} = \frac{2\,g\,M_B}{f} \tag{33}$$

where

$$\langle \mathrm{B}^+(p)\pi^-(q)|\mathrm{B}^*(\epsilon,p')\rangle = g_{B^*B\pi}\epsilon\cdot q. \tag{34}$$

The decay $\mathrm{B}^* \to \mathrm{B}\pi$ is not kinematically allowed, but g can be estimated using CLEO results [21] for $\mathrm{D}^* \to \mathrm{D}\pi$, or from a lattice QCD calculation of the matrix element of the light-quark axial current between B and B^* mesons [22] (or D and D^* [23]). The CLEO results lead to $g = 0.6$, consistent with the recent lattice calculation [23].

The expressions in Eqs. (30), (31) and (32) show that both the quenched and partially quenched 'chiral logarithms' diverge as the valence quark mass and hence m_{qq} vanishes while the sea quark mass is held fixed. In contrast, there are no divergences when the sea quark masses vanish with the valence masses held fixed. For the QCD-like case, things also remain finite as the joint valence and sea quark mass vanishes. The problem for lattice practitioners is how best to perform the chiral extrapolations from results calculated with sets of m_q and m_f values, particularly since it is very difficult to make the masses small enough to see the logarithmic dependence.

For F_{B_d} the situation is like the 'QCD' case above where the valence d quark in the B_d meson and (some of) the sea quarks are very light. For F_{B_s}, the valence mass is fixed at m_s and the sea quark masses are extrapolated to small values (more like the partially quenched case above). The JLQCD collaboration find [24] that these different extrapolations tend to decrease the value of F_{B_d} relative to F_{B_s}, and therefore increase ξ. However, a number of caveats must be kept in mind [25]. Although the data is consistent with the chiral logarithmic forms, all the data points are at masses beyond the region of strong variation in the logarithms. Moreover, at these larger masses, higher order terms in the chiral expansion may be required. Furthermore, in dynamical simulations the lattice spacing changes as the sea quark mass changes at fixed lattice coupling (β), so that care is needed not to interpret lattice-spacing

(and volume) dependence as sea-quark mass dependence. An added twist is that JLQCD find that their results for F_π are *not* consistent with the expected logarithmic behaviour.

The MILC collaboration have also estimated chiral logarithm effects as part of their extensive analysis of $N_f = 2$ simulations for heavy-light decay constants [17]. Their method is based on extrapolation of the ratio of the light-light to the heavy-light decay constant, where the chiral logarithmic terms cancel to a large extent. MILC's conclusion is that these effects do tend to increase the value of the ratio F_{B_s}/F_{B_d} and MILC ascribe a systematic error of $+0.04$ from chiral logarithms to a central value of 1.16 for F_{B_s}/F_{B_d}.

Kronfeld and Ryan (KR) [14] consider the ratios $\xi_f = F_{B_s}/F_{B_q}$ and $\xi_B = B_{B_s}/B_{B_q}$ as the mass of the quark q varies from the strange mass down to that of the light quarks u and d and match ChPT to lattice data for m_q not too far from m_s. Their analysis gives $\xi = 1.32(10)$. Another more recent phenomenological analysis (BFPZ) [18] supports the increase in ξ coming from chiral logarithms and leads to a consistent result $\xi = 1.22(7)$. This value is extracted using the double ratio

$$R = \frac{(F_{B_s}\sqrt{M_{B_s}})/(F_{B_d}\sqrt{M_{B_d}})}{F_K/F_\pi}. \tag{35}$$

An expression for R in leading order heavy meson and pion chiral perturbation theory (in full, 3-flavour QCD) is combined with the experimental ratio $(F_K/F_\pi)_{\rm expt} = 1.22(1)$ to extract F_{B_s}/F_{B_d}. Systematic error in both analyses arises from the uncertain values of parameters in the heavy meson and pion chiral Lagrangian, namely the coupling g in the leading interaction term, already encountered above, together with sums of coefficients of higher-order terms in the heavy meson chiral Lagrangian. In addition the analysis using R depends on L_5, the coefficient of a higher-order term in the pion chiral Lagrangian through its use of the ratio F_K/F_π.

In conclusion, lattice results for F_B can show significant light-quark mass dependence and more work is needed to understand to what extent this dependence is physical. At present a reasonable conservative view [25] is to allow a *decrease* of up to -10% in F_{B_d} with a negligible change in F_{B_s} as added systematic errors. These are included in the final estimates presented in Eq. (37).

A summary of lattice calculations for the decay constants, published after 1996, is given in Fig. 4.3 (taken from the review by Lellouch [25]), which shows results for F_{B_d} and the ratio F_{B_s}/F_{B_d}. The 'summary' numbers at the bottom of the plots give quenched averages for F_{B_d} and F_{B_s}/F_{B_d}, together with ratios of these quantities for $N_f = 2$ and $N_f = 0$:

$$\begin{aligned} F_{B_d}^{N_f=0} &= 178(20)\text{MeV} & \frac{F_{B_d}^{N_f=2}}{F_{B_d}^{N_f=0}} &= 1.09(6) \\ (F_{B_s}/F_{B_d})^{N_f=0} &= 1.14(3) & \frac{(F_{B_s}/F_{B_d})^{N_f=2}}{(F_{B_s}/F_{B_d})^{N_f=0}} &= 1.02(2) \end{aligned} \tag{36}$$

For the mixing parameter B_{B_q}, the situation with quenching and chiral extrapolation looks more favourable. Very little variation is observed between quenched ($N_f = 0$) and $N_f = 2$ results. The partially quenched chiral logarithm for B_{B_q} has a coefficient containing $1 - 3g^2 \simeq -0.1$ compared to $1 + 3g^2 \simeq 2.1$ in the F_{B_q} case (using $g = 0.6$ as discussed above) so the chiral extrapolation is better-controlled and leads to a small error in $\hat{B}_{B_s}/\hat{B}_{B_d}$ [14,25,16]. The heavy quark mass dependence is mild and different formulations agree at the physical point for B-mesons.

There is, however, an issue concerning lattice results for ξ which are normally quoted by combining results for F_B and $\hat{B}_B$. Of course, it is also possible to evaluate ξ directly from the ratio of $\Delta B = 2$ matrix elements. In this case ξ turns out to be larger, although with large errors [35,27]. Clearly the two procedures should give consistent answers, so this issue will need to be resolved.

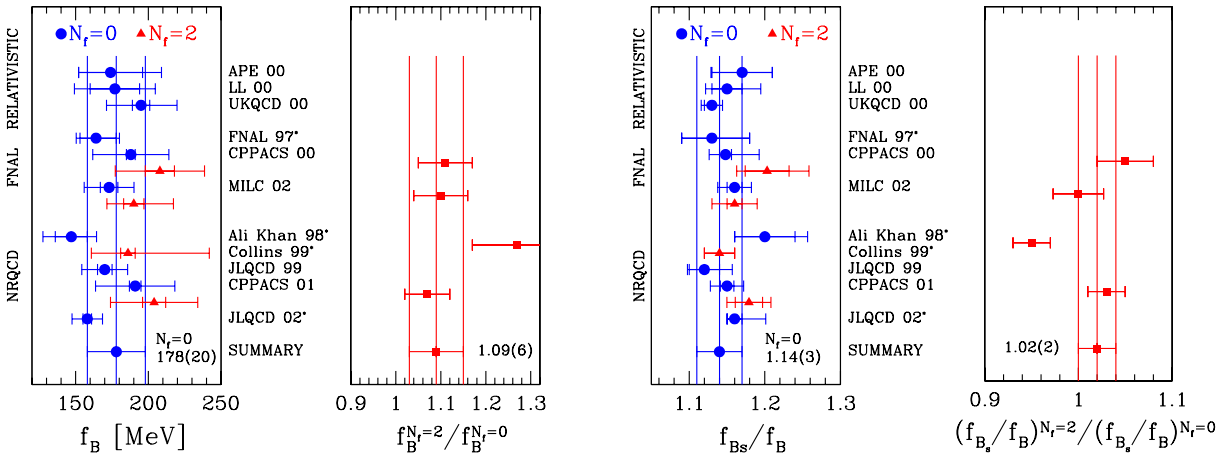

Fig. 4.3: *From left to right: lattice results published after 1996 for (a) F_{B_d} in quenched ($N_f = 0$) and two-flavour ($N_f = 2$) QCD, (b) the ratio $F_{B_d}^{N_F=2}/F_{B_d}^{N_f=0}$, (c) F_{B_s}/F_{B_d} in quenched ($N_f = 0$) and two-flavour ($N_f = 2$) QCD, (d) the ratio $(F_{B_s}/F_{B_d})^{N_f=2}/(F_{B_s}/F_{B_d})^{N_f=0}$. The results are grouped according to the formulation used to treat the heavy quark and the references are: APE 00 [26], LL 00 [27], UKQCD 00 [28], FNAL 97 [29], CPPACS 00 [30], MILC 02 [17], Ali Khan 98 [31], Collins 99 [32], JLQCD 99 [33], CPPACS 01 [34] and JLQCD 02 [16]. Figs. taken from [25].*

2.1.2. Summary on F_{B_q} and ξ from the lattice QCD

Using the quenched averages as a starting point together with the ratios of $N_f = 2$ to $N_f = 0$ results allows an extrapolation to $N_f = 3$ [25]. An additional systematic error equal to the shift from 2 to 3 flavours is added to account for the uncertainty in this procedure[†]. This leads to:

$$\boxed{\begin{array}{lll} F_{B_d} = 203(27)(^{0}_{20})\text{MeV} & F_{B_s} = 238(31)\text{MeV} & \dfrac{F_{B_s}}{F_{B_d}} = 1.18(4)(^{12}_{0}) \\ \hat{B}_{B_d} = 1.34(12) & \hat{B}_{B_s} = 1.34(12) & \dfrac{\hat{B}_{B_s}}{\hat{B}_{B_d}} = 1.00(3) \\ F_{B_d}\sqrt{\hat{B}_{B_d}} = 235(33)(^{0}_{24})\text{MeV} & F_{B_s}\sqrt{\hat{B}_{B_s}} = 276(38)\text{MeV} & \xi = 1.18(4)(^{12}_{0}) \end{array}} \quad . \tag{37}$$

Here, the last, asymmetric, error, where present, is due the uncertainty in the chiral extrapolation discussed above. The first error combines statistical and all other systematic errors. In UT analyses, the value of ξ given above should be understood as

$$\xi = 1.24(4)(6) \tag{38}$$

and likewise for other quantities affected by this asymmetric error. Note that this does not apply for F_{B_s} and $\hat{B}_{B_s}$, for which the chiral logarithmic uncertainties appear small compared to other systematic errors. The result for ξ in Eq. (38) is consistent with the KR [14] and BFPZ [18] analyses mentioned above.

2.1.3. F_{B_d} and F_{B_s} from QCD sum rules

Within the framework of QCD sum rules [36,37], the decay constants F_{B_d} and F_{B_s} can be calculated by equating phenomenological and theoretical spectral functions for the pseudoscalar B_d and B_s mesons,

[†]An alternative way to quote the final answer would be to use the $N_f = 2$ results extracted from Eq. (36) and add a systematic error for the extrapolation to $N_f = 3$. In this case, the final central value for F_{B_s}/F_{B_d} would be 1.16. The value of 1.18, however, is consistent with the latest preliminary MILC results for $N_f = 3$, which give $(F_{B_s}/F_{B_d})^{N_f=3} = 1.18(1)(^{4}_{1})$

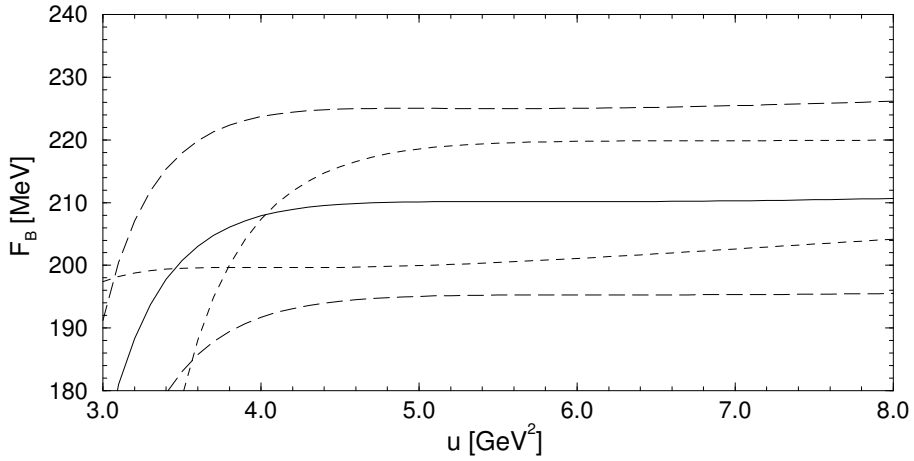

Fig. 4.4: F_{B_d} *as a function of the sum rule scale* u *for different sets of input parameters. Solid line: central values of Table 4.1; long-dashed line:* $m_b(m_b) = 4.16$ GeV *(upper line),* $m_b(m_b) = 4.26$ GeV *(lower line); dashed line:* $\mu_m = 3$ GeV *(lower line),* $\mu_m = 6$ GeV *(upper line).*

which leads to the relation [38–40]‡

$$M_B^4 F_{B_d}^2 = \int_0^{s_0} e^{(M_B^2 - s)/u} \rho(s)\, ds \tag{39}$$

for the B_d meson and analogously for B_s. Eq. (39) is the central relation for the sum rule analysis. The theoretical spectral function $\rho(s) \equiv \Im\Psi(s)/\pi$ can be obtained by calculating the two-point correlator of hadronic currents

$$\Psi(p^2) \equiv i \int dx\, e^{ipx}\, \langle 0|\, T\{\, j_5(x)\, j_5(0)^\dagger \}|0\rangle \tag{40}$$

in perturbative QCD, including corrections from the operator product expansion. For the B meson, the pseudoscalar current $j_5(x)$ takes the form

$$j_5(x) = (m_b + m_u)\, :\bar{u}(x)\, i\gamma_5 b(x):\ . \tag{41}$$

The parameter s_0 in Eq. (39) indicates the energy range up to which experimental knowledge of the phenomenological spectral function is available. This parameter will be further discussed below.

Substantial progress in determining the theoretical spectral function has been achieved very recently through a calculation of the perturbative three-loop order α_s^2 corrections [42,43]. These are important because the size of higher-order corrections depends on the renormalization scheme employed for the quark masses. As can be inferred from refs. [42,43], the α_s^2 term turns out to be of similar order to the leading contribution if pole quark masses are used, whereas good convergence of the perturbative series emerges for quark masses defined in the $\overline{\mathrm{MS}}$ scheme. Nevertheless, these scheme dependences influence only the theoretical uncertainties, since F_{B_d} and F_{B_s} are physical quantities which certainly should not depend on the quark mass definitions. Higher-dimensional operator corrections to the sum rule are known up to dimension six [39] and are also under good theoretical control.

Figure 4.4 shows numerical results for F_{B_d} of Ref. [39], plotted as a function of the sum rule scale u, after evaluating the sum rule of Eq. (39). Reliable values of F_{B_q} can be extracted from the sum rule if an energy region exists in which the physical quantity is only weakly dependent on u. For F_{B_d} this

‡A review of the procedure and further original references can be found in [41].

Parameter	Value	s_0	u_0	ΔF_{B_d}
$m_b(m_b)$	4.21 ± 0.08 GeV	$\begin{matrix}32.8\\34.6\end{matrix}$	$\begin{matrix}6.5\\5.0\end{matrix}$	∓ 24
μ_m	$3.0 - 6.0$ GeV	$\begin{matrix}33.5\\34.4\end{matrix}$	$\begin{matrix}6.8\\4.0\end{matrix}$	± 10
$\langle\bar{u}u\rangle(2\text{ GeV})$	$-(267 \pm 17\text{ MeV})^3$	$\begin{matrix}33.9\\33.3\end{matrix}$	$\begin{matrix}5.7\\5.5\end{matrix}$	± 6
$\mathcal{O}(\alpha_s^2)$	$\begin{matrix}2\times\mathcal{O}(\alpha_s^2)\\ \text{no } \mathcal{O}(\alpha_s^2)\end{matrix}$	33.6	5.6	± 2
$\alpha_s(M_Z)$	0.1185 ± 0.020	33.6	5.6	± 1

Table 4.1: *Values for the dominant input parameters, continuum thresholds* s_0 [GeV^2], *points of maximal stability* u_0 [GeV^2], *and corresponding uncertainties for* F_{B_d} [MeV].

Parameter	Value	s_0	u_0	ΔF_{B_s}
$m_b(m_b)$	4.21 ± 0.08 GeV	$\begin{matrix}34.3\\36.9\end{matrix}$	$\begin{matrix}5.8\\4.6\end{matrix}$	∓ 26
μ_m	$3.0 - 6.0$ GeV	$\begin{matrix}35.2\\37.2\end{matrix}$	$\begin{matrix}6.2\\3.6\end{matrix}$	$\begin{matrix}+8\\-9\end{matrix}$
$\langle\bar{s}s\rangle/\langle\bar{u}u\rangle$	0.8 ± 0.3	$\begin{matrix}35.9\\35.2\end{matrix}$	$\begin{matrix}5.3\\4.7\end{matrix}$	± 8
$\langle\bar{u}u\rangle(2\text{ GeV})$	$-(267 \pm 17\text{ MeV})^3$	$\begin{matrix}35.7\\35.3\end{matrix}$	$\begin{matrix}5.2\\4.9\end{matrix}$	$\begin{matrix}+5\\-4\end{matrix}$
$m_s(2\text{ GeV})$	100 ± 15 MeV	35.5	5.1	± 2
$\mathcal{O}(\alpha_s^2)$	$\begin{matrix}2\times\mathcal{O}(\alpha_s^2)\\ \text{no } \mathcal{O}(\alpha_s^2)\end{matrix}$	35.5	5.1	± 3
$\alpha_s(M_Z)$	0.1185 ± 0.020	35.5	5.1	± 1

Table 4.2: *Values for the dominant input parameters, continuum thresholds* s_0 [GeV^2], *points of maximal stability* u_0 [GeV^2], *and corresponding uncertainties for* F_{B_s} [MeV].

turns out to be the case in the range $4\text{ GeV}^2 \lesssim u \lesssim 6\text{ GeV}^2$. Averaging the results of refs. [38,39] in this energy range, one extracts the central results $F_{B_d} = 208$ MeV and $F_{B_s} = 242$ MeV.[§]

The dominant uncertainties in the sum rule determination of F_{B_d} and F_{B_s} arise from the strong dependence on the value of the bottom quark mass m_b and correspondingly on the scale μ_m at which the quark masses are renormalized. The ranges for the variation of these parameters and the corresponding variations of F_{B_d} and F_{B_s} have been collected in Tables 4.1 and 4.2 respectively. The reader should note that compared to Ref. [39], the error on $m_b(m_b)$ has been enlarged, in order to coincide with the value employed throughout this report, although the larger uncertainty should be considered very conservative. The Tables also list the values u_0 at which the sum rule displays optimal stability, as well as the parameters s_0 which can be determined consistently from an independent sum rule for the B_d and B_s meson masses. Additional smaller uncertainties are due to: variation of the strong coupling constant α_s; higher order QCD corrections; the value of the quark condensate $\langle\bar{u}u\rangle$ [44] which is the leading contribution from higher-dimensional operators; the strange condensate $\langle\bar{s}s\rangle$ and the strange quark mass m_s in the case of F_{B_s}. Ranges for these inputs together with the variations of F_{B_d} and F_{B_s} are also collected in Tables 4.1 and 4.2. For further details of the numerical analysis, the reader is referred to Ref. [39].

[§]Owing to the criticism put forward in Ref. [39], the result of Ref. [40] has not been included in the average, despite the apparent agreement for the numerical values.

Adding all errors for the various input parameters in quadrature, the final results for the B_d and B_s meson leptonic decay constants from QCD sum rules are:

$$F_{B_d} = 208 \pm 27 \text{ MeV} \qquad \text{and} \qquad F_{B_s} = 242 \pm 29 \text{ MeV}. \tag{42}$$

Owing to the strong sensitivity of these results on the bottom quark mass, one should note that for example using the very recent average $m_b(m_b) = 4.24$ GeV [45], the resulting values for F_{B_d} and F_{B_s} are lowered by almost 10 MeV.

2.1.4. B_{B_d} and B_{B_s} from QCD sum rules

The status of the determination of the hadronic B-parameters B_{B_d} and B_{B_s} from QCD sum rules is less satisfactory than for the decay constants. In principle, the B-parameters can be calculated from two different types of sum rules: namely three-point function sum rules with the insertion of two pseudoscalar currents and one four-quark operator [46,47], or two-point function sum rules with the insertion of two local four-quark operators [48,49]. However, both approaches are plagued with difficulties ¶.

The first determinations of the hadronic B-parameters [46,47] employed three-point function sum rules and found a value of $B_{B_d}(m_b) = 0.95 \pm 0.10$, slightly lower than the factorization approximation which results in $B_{B_d} = 1$. The dominant non-factorizable contribution due to the gluon condensate turned out to be negative, thus lowering the B-parameter. However, the perturbative part was only considered at the leading order, and thus the scale and scheme dependences of B_{B_d} were not under control. Besides, the analytic structure of three-point function sum rules is more delicate than for two-point correlators, and therefore great care has to be taken to properly extract the quantity in question [41].

For the case of the two-point function sum rules, next-to-leading order QCD corrections have been calculated in Ref. [48], which provides better control over the renormalization dependence of B_B. This analysis resulted in $B_{B_d}(m_b) = 1.0 \pm 0.15$. However, here the phenomenological parametrization of the spectral function is more complicated, since contributions from intermediate states containing B^* mesons have to be taken into account in addition to the B meson. Steps in this direction have recently been taken in Ref. [49] were the value $B_{B_d}(m_b) = 1.15 \pm 0.11$ was obtained, now indicating a positive correction.

Although averaging the results of the two approaches might appear problematic, we nevertheless decided to quote a common value for the B meson B-parameter from QCD sum rules:

$$B_{B_d}(m_b) = 1.10 \pm 0.15 \qquad \text{and} \qquad \hat{B}_{B_d} = 1.67 \pm 0.23, \tag{43}$$

which covers the outcome of both methods within the uncertainties. On the other hand, general agreement exists for the flavour dependence of the B-parameter. In all present sum rule approaches it was found to be negligible, thus yielding $B_{B_s}/B_{B_d} = 1$ to a good approximation.

2.2. K^0–$\overline{\mathrm{K}}^0$ mixing: determination of B_K

2.2.1. B_K from lattice QCD

The most commonly used method to calculate the matrix element $\langle \overline{\mathrm{K}}^0 \mid Z\ (\bar{s}d)_{V-A}(\bar{s}d)_{V-A}(\mu) \mid \mathrm{K}^0 \rangle$ is to evaluate the three point correlation function shown in Fig. 4.5. This corresponds to creating a K^0 at some time t_1 using a zero-momentum source; allowing it to propagate for time $t_{\mathcal{O}} - t_1$ to isolate the lowest state; inserting the four-fermion operator at time $t_{\mathcal{O}}$ to convert the K^0 to a $\overline{\mathrm{K}}^0$; and finally allowing the $\overline{\mathrm{K}}^0$ to propagate for long time $t_2 - t_{\mathcal{O}}$. To cancel the K^0 ($\overline{\mathrm{K}}^0$) source normalization at times t_1 and t_2 and the time evolution factors $e^{-E_K t}$ for times $t_2 - t_{\mathcal{O}}$ and $t_{\mathcal{O}} - t_1$ it is customary to divide this three-point function by the product of two 2-point functions as shown in Fig 1. If, in the 2-point functions, the

¶For a different approach see also Ref. [50].

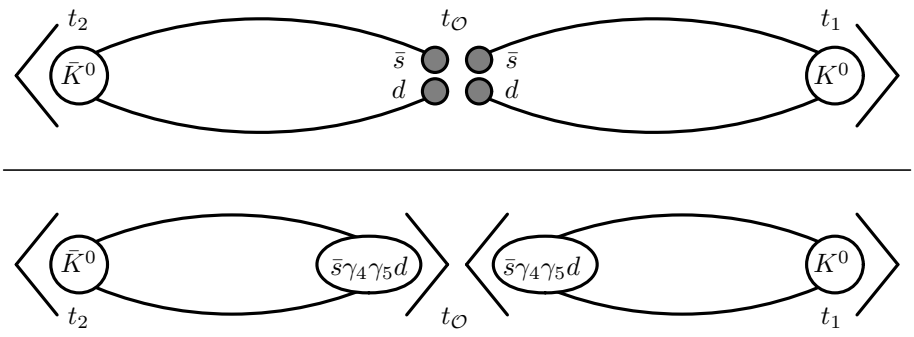

Fig. 4.5: *Ratio of lattice correlation functions used to calculate B_K.*

bilinear operator used to annihilate (create) the K^0 ($\overline{\mathrm{K}}^0$) at time $t_{\mathcal{O}}$ is the axial density $\bar{s}\gamma_4\gamma_5 d$, then the ratio of the 3-point correlation function to the two 2-point functions is $(8/3)B_K$.

B_K is defined to be the value of the matrix element at the physical kaon and normalized by the Vacuum Saturation Approximation value $8/3M_K^2F_K^2$

$$\langle \mathrm{K}^0 \mid Z\,(\bar{s}d)_{V-A}(\bar{s}d)_{V-A}(\mu) \mid \overline{\mathrm{K}}^0 \rangle \quad = \quad (8/3)B_K M_K^2 F_K^2\,.$$

The earliest calculations of B_K were done using Wilson fermions and showed significant deviations from this behaviour. It was soon recognized that these lattice artifacts are due to the explicit breaking of chiral symmetry in the Wilson formulation [51–55]. Until 1998, the only formulation that preserved sufficient chiral symmetry to give the right chiral behaviour was Staggered fermions. First calculations using this approach in 1989 gave the quenched estimate $B_K(\mathrm{NDR}, 2\mathrm{GeV}) = 0.70 \pm 0.01 \pm 0.03$. In hindsight, the error estimates were highly optimistic, however, the central value was only 10% off the current best estimate, and most of this difference was due to the unresolved $O(a^2)$ discretization errors.

In 1997, the staggered collaboration refined its calculation and obtained $0.62(2)(2)$ [56], again the error estimate was optimistic as a number of systematic effects were not fully included. The state-of-the-art quenched calculation using Staggered fermions was done by the JLQCD collaboration in 1997 and gave $B_K(2\mathrm{GeV}) = 0.63 \pm 0.04$ [57]. This estimate was obtained using six values of the lattice spacing between 0.15 and 0.04 fermi, thus allowing much better control over the continuum extrapolation as shown in Fig. 4.6 along with other published results. This is still the benchmark against which all results are evaluated and is the value exported to phenomenologists. This result has three limitations: (i) It is in the quenched approximation. (ii) All quenched calculations use kaons composed of two quarks of roughly half the "strange" quark mass and the final value is obtained by interpolation to a kaon made up of $(m_s/2, m_s/2)$ instead of the physical point (m_s, m_d). Thus, SU(3) breaking effects ($m_s \neq m_d$) have not been incorporated. (iii) There are large $O(a^2)$ discretization artifacts, both for a given transcription of the $\Delta S = 2$ operator on the lattice and for different transcriptions at a given value of the lattice spacing, so extrapolation to the continuum limit is not as robust as one would like. These limitations are discussed after a brief summary of the recent work.

In the last four years a number of new methods have been developed and the corresponding results are summarized in Table 4.3.

- The Rome collaboration has shown that the correct chiral behaviour can be obtained using $O(a)$ improved Wilson fermions provided non-perturbative renormalization constants are used. Their latest results, with two different "operators", are $B_K(2\mathrm{GeV}) = 0.63(10)$ and $0.70(12)$ [58]. These, while demonstrating the efficacy of this method, do not supplant the staggered result, as the continuum extrapolation is based on only three points and the data have larger errors. The discretization errors can be characterized as $B_K(a) = B_K(1 + a\Lambda)$ with $\Lambda \approx 400$MeV and are similar in magnitude to those with staggered fermions at $1/a = 2$ GeV, as are the differences in

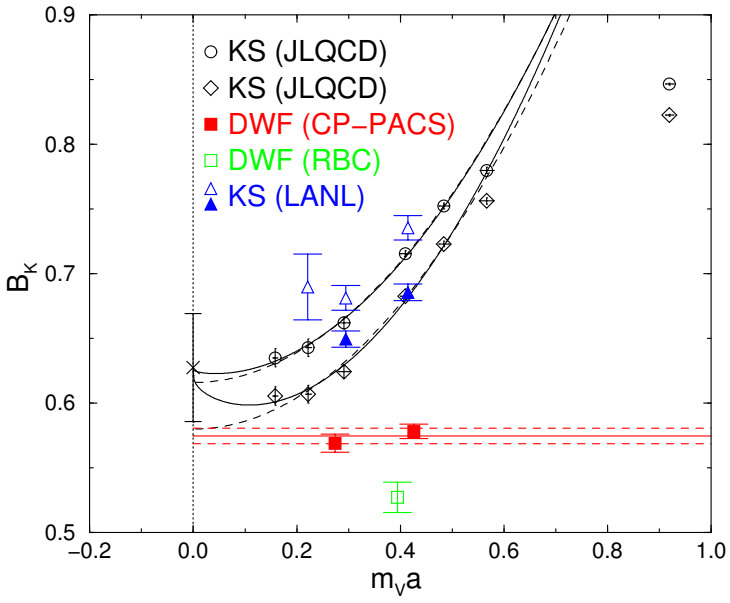

Fig. 4.6: *Published estimates of B_K with fermion formulations that respect chiral symmetry. All results are in the quenched approximation.*

Collaboration	year	B_K(2GeV)	Formulation	Renormalization	a^{-1} (GeV)
Staggered [56]	1997	0.62(2)(2)	staggered	1-loop	∞
JLQCD [57]	1997	0.63(4)	staggered	1-loop	∞
Rome [58]	2002	0.63(10)	Improved Wilson	NP	∞
Rome [58]	2002	0.70(12)	Improved Wilson	NP	∞
CP-PACS [59]	2001	0.58(1)	Domain Wall	1-loop	1.8 GeV
CP-PACS [59]	2001	0.57(1)	Domain Wall	1-loop	2.8 GeV
RBC [60]	2002	0.53(1)	Domain Wall	NP	1.9 GeV
DeGrand [61]	2002	0.66(3)	Overlap	1-loop	1.6 GeV
DeGrand [61]	2002	0.66(4)	Overlap	1-loop	2.2 GeV
GGHLR [62]	2002	0.61(7)	Overlap	NP	2.1 GeV

Table 4.3: *Quenched estimates for B_K evaluated in the NDR scheme at* 2GeV. *The fermion formulation used in the calculation, the method used for renormalizing the operators, and the lattice scale at which the calculation was done are also given. NP indicates non-perturbative renormalization using the RI/MOM scheme and $a^{-1} = \infty$ implies that the quoted result is after a continuum extrapolation.*

estimates with using different operators. In the staggered formulation, the artifacts are, however, $O(a^2\Lambda^2)$ and $O(\alpha_{\rm s}^2)$ and the data suggest an unexpectedly large $\Lambda \sim 900$MeV.

- Four collaborations have new results using domain wall and overlap fermions as shown in Table 4.3 [63,60,59,61,62]. Both formulations have built in chiral symmetry at finite a and $O(a)$ improvement. Each of these collaborations have used slightly different methodology, so they cannot be compared head on, or combined to do a continuum extrapolation. Thus, the results are quoted with reference to the lattice spacing at which the calculation was done. The differences reflect $O(a^2)$ (and $O(\alpha_s^2)$ in cases where perturbative renormalization constants have been used) artifacts.
- Calculations are in progress [64] using another method with good chiral behaviour, twisted mass QCD.

Deriving an estimate for the physical $\hat{B}_K$, starting from the current best quenched lattice estimate, the JLQCD staggered result $B_K(2{\rm GeV}) = 0.63(4)$, requires consideration of the following issues.

- The $O(a^2)$ errors in the staggered formulation are large. Nevertheless, the error 0.04 obtained by the JLQCD collaboration on including both $O(a^2)$ and $O(\alpha_{\rm s}^2)$ terms in the extrapolation is a reasonable 1σ estimate of both the statistical and the extrapolation to continuum limit errors.
- A choice for $\alpha_{\rm s}$ and the number of flavours in the perturbative expression has to be made to convert $B_K \to \hat{B}_K$. It turns out that the result is insensitive to whether one uses quenched or full QCD values. Using the 2-loop expression, the result for the central value is $\hat{B}_K = 0.86(6)$.
- An estimate of the systematic uncertainty associated with the quenched approximation and SU(3) breaking. Preliminary numerical estimates suggest that dynamical quarks would increase the value by about 5% [65,66]. Sharpe estimates, using ChPT, that unquenching would increase B_K by 1.05 ± 0.15, and SU(3) breaking effects would also increase it by 1.05 ± 0.05 [67]. This analysis of systematic errors is not robust and, furthermore, the two uncertainties are not totally independent. So one can take an aggressive and a conservative approach when quoting the final result for $\hat{B}_K$. In the aggressive approach, the error estimate is given by combining in quadrature the offset of the central values with respect to unity. This gives a 7% uncertainty and

$$\hat{B}_K = 0.86 \pm 0.06 \pm 0.06\,. \tag{44}$$

  In the conservative approach, advocated by Sharpe [67], one combines the uncertainty in quadrature to get a 16% uncertainty. The final result in this case is

$$\boxed{\hat{B}_K = 0.86 \pm 0.06 \pm 0.14} \tag{45}$$

Given the lack of a robust determination of the systematic error, it is important to decide how to fold these errors in a phenomenological analysis. One recommendation is to assume a flat distribution for the systematic error and add to it a Gaussian distribution with $\sigma = 0.06$ on either end, and do a separate analysis for the aggressive and conservative estimates. In other words, a flat distribution between 0.72 and 1.0 for a conservative estimate of $\hat{B}_K$ (or from 0.80 to 0.92 for the aggressive estimate) to account for systematic errors due to quenching and SU(3) breaking. Since this is the largest uncertainty, current calculations are focused on reducing it.

Finally, the reasons why the quenched lattice estimate of B_K has been stable over time and considered reliable within the error estimates quoted above are worth reemphasizing:

- The numerical signal is clean and accurate results are obtained with a statistical sample of even 50 decorrelated lattices.
- Finite size effects for quark masses $\geq m_s/2$ are insignificant compared to statistical errors once the quenched lattices are larger the 2 fermi.
- In lattice formulations with chiral symmetry, the renormalization constant connecting the lattice and continuum schemes is small ($< 15\%$), and reasonably well estimated by one-loop perturbation theory.

- For degenerate quarks, the chiral expansion for the matrix element has no singular quenched logarithms (they cancel between the AA and VV terms) that produce large artifacts at small quark masses in observables like M_π^2, f_π, etc. Also, the chiral expansions have the same form in the quenched and full theories [68–71].
- ChPT estimates of quenching and SU(3) breaking systematic errors are at the 7–16% level [70,65,66].

2.2.2. B_K from non-lattice approaches

The parameter B_K can also be calculated using other non-perturbative approaches to QCD, like QCD sum rules, the large-N_c expansion or the chiral quark model. As for the parameter B_B in the B-meson system, B_K can be obtained from sum rules by considering two-point [72–74] or three-point [75,76] correlation functions. However, both methods suffer from the same inadequacies as in the case of B_B. For the two-point function sum rule, the phenomenological spectral function is difficult to parametrise reliably, whereas for the three-point function sum rule no next-to-leading order QCD corrections are available and thus a proper matching with the Wilson coefficient function is at present not possible. For these reasons, we shall concentrate below on existing results in the large-N_c expansion [77–80], which in our opinion are developed furthest. After commenting on the large-N_c approach in more detail, the calculation of B_K within the chiral quark model [81] will also be briefly discussed.

Calculations of weak hadronic matrix elements in the framework of the large-N_c expansion were developed by Bardeen, Buras and Gérard in the nineteen-eighties. For B_K, at the next-to-leading order in $1/N_c$, this method resulted in $B_K = 0.7 \pm 0.1$ [77], to be compared with $B_K = 0.75$ in the strict large-N_c limit. However, at that time the next-to-leading order correction to the Wilson coefficient function [82] was not available, and anyhow it is debatable whether the result of [77] can be properly matched to the short distance coefficient. The proper matching of the scale and scheme dependencies in matrix elements as well as Wilson coefficients is, however, a crucial aspect for all approaches to weak hadronic matrix elements.

In the approach of [78] a significant dependence on the matching scale is still present, resulting in sizable uncertainties for B_K. Explicit cancellation of scale and scheme dependences was demonstrated in Ref. [79] within the chiral limit, and, to a lesser extent in Ref. [80], also for a physical strange quark. The main ingredients in the approaches of [79,80] are: the large-N_c expansion; chiral perturbation theory to control the low-energy end of the Green function required for the calculation of the matrix elements; the operator product expansion to control the higher-energy region of the Green function above roughly 1 GeV; a model which connects the low- and high energy regimes. To this end, in [79] the relevant Green function was saturated by the lowest lying vector meson, the ρ, whereas in [80] the extended Nambu-Jona-Lasinio model was applied which, however, does not display the correct QCD high-energy behaviour. The dependence on these models constitutes the dominant uncertainty for the latter approaches.

In the chiral limit, the findings $\hat{B}_K = 0.38 \pm 0.11$ [79] as well as $\hat{B}_K = 0.32 \pm 0.13$ [80] are in very good agreement with the current algebra result $\hat{B}_K = 0.33$ [83], obtained by relating $\hat{B}_K$ to the $K^+ \to \pi^+\pi^0$ decay rate. In fact, this agreement could be interpreted as a successful description of the $K^+ \to \pi^+\pi^0$ decay from large-N_c. The authors of Ref. [80] have also extended their calculation beyond the chiral limit with the result $\hat{B}_K = 0.77 \pm 0.07$. The smaller error compared to the chiral limit case is due to a reduced model dependence for a physical strange quark. However, as is obvious from these results, the chiral corrections amount to more than 100%, and it remains to be seen whether $\hat{B}_K$ of [80] incorporates all such corrections. Nevertheless, it is interesting to observe that the final result of Ref. [80] is again very close to the strict large-N_c prediction, and is also in good agreement with the average from lattice QCD quoted above.

An independent approach to hadronic matrix elements and to B_K in particular is the chiral quark model [81]. The chiral quark model provides a link between QCD and chiral perturbation theory and

bears some similarity to the extended Nambu-Jona-Lasinio model already mentioned above. In this framework, the hadronic matrix elements depend on the values of quark and gluon condensates, also present in the QCD sum rule approach, as well as constituent masses for the quarks. For values of these parameters which fit the $\Delta I = 1/2$ rule for $\mathrm{K} \to \pi\pi$ decays, the authors of [81] then obtain $\hat{B}_K = 1.1 \pm 0.2$, where the error is dominated by the variation of constituent quark mass and gluon condensate. However, owing to a poor matching between long- and short-distance contributions in the case of B_K, an additional systematic uncertainty of the order of 15% could be present in the result of Ref. [81].

3. Experimental methods for the study of B^0 and $\overline{\mathrm{B}}^0$ mixing

The system of neutral B mesons, B^0 and $\overline{\mathrm{B}}^0$, can be described in terms of states with well defined mass and lifetime exhibiting the phenomenon of particle-antiparticle oscillations. The frequency of B^0_d and B^0_s mixing can be described by the mass difference $\Delta M_{d,s}$ as defined in Eq. (14). This mass difference between the two mass eigenstates leads to a time-dependent phase difference between the particle wave functions. In the Standard Model, B^0–$\overline{\mathrm{B}}^0$ mixing is described via second order weak processes, as displayed for the case of K^0–$\overline{\mathrm{K}}^0$ mixing in Fig. 4.1. The mass difference $\Delta M_{d,s}$ can be determined by computing the electroweak box diagram, where the dominant contribution is through top quark exchange as can be seen in Eq. (22). A measurement of ΔM_d or ΔM_s in principle allows the determination of the Cabibbo-Kobayashi-Maskawa matrix elements $|V_{td}|$ or $|V_{ts}|$ as indicated by the relations in Eq. (23) and (24). The main uncertainty in relating measurements of the mixing frequency to the CKM matrix elements originates from the parameters $F_{B_{d,s}}$ and $\hat{B}_{B_{d,s}}$ as discussed in Sec. 2.1.. However, in the ratio $\Delta M_d/\Delta M_s$ several of the theoretical uncertainties cancel as is obvious from Eq. (29). Thus, the ratio $\Delta M_d/\Delta M_s$ is related to the ratio of CKM matrix elements $|V_{td}|/|V_{ts}|$ and will ultimately determine one of the sides of the CKM unitarity triangle.

3.1. Time integrated oscillation analyses and determination of B hadron production rates

At the $\Upsilon(4S)$, only B^0_d and B^+ mesons are produced, whereas at high energy colliders B^0_s mesons and b-baryons are also present. In the latter case, B^0_d and B^0_s mesons contribute to time integrated mixing measurements with a weight proportional to their relative production fractions:

$$\bar{\chi} = f_{\mathrm{B}^0_d}\,\chi_d \;+\; f_{\mathrm{B}^0_s}\,\chi_s. \tag{46}$$

Here, $f_{\mathrm{B}^0_d}$ and $f_{\mathrm{B}^0_s}$ are the production rates of B^0_d and B^0_s mesons in b quark jets, while $\chi_{d,s}$ are the respective mixing parameters defined in Eq. (28) [‖]. The non-linear relation between x and χ (see Eq. (28)) implies that χ becomes insensitive to x for values greater than $x \sim 5$. Thus, a time dependent oscillation analysis is necessary to observe fast oscillations as expected for B^0_s mesons. At the $\Upsilon(4S)$ resonance, a measurement of χ_d allows to directly extract x_d because only slowly oscillating B^0_d mesons are produced. A time integrated mixing analysis is, however, important to determine the hadron production fractions $f_{\mathrm{B}^0_d}$ and $f_{\mathrm{B}^0_s}$. For example, $f_{\mathrm{B}^0_d}$ is an essential input for a measurement of V_{cb} using $\overline{\mathrm{B}}^0_d \to D^{*+}\ell^-\bar{\nu}_\ell$ decays and the source of an important systematic error in ΔM_d measurements at high energy colliders. Furthermore, the sensitivity to B^0_s–$\overline{\mathrm{B}}^0_s$ oscillations in inclusive analyses depends on the B^0_s production rate $f_{\mathrm{B}^0_s}$.

The production rates of B hadrons in b quark jets can be obtained from the measured integrated oscillation rates of B mesons (see Eq. (46)). When measuring the time integrated oscillation parameter in a semileptonic sample, the mixing probability can be written as

$$\bar{\chi} = g_{\mathrm{B}^0_s}\chi_s + g_{\mathrm{B}^0_d}\chi_d, \tag{47}$$

[‖] The world average for the time integrated mixing parameter is $\bar{\chi}$=0.1194 ± 0.0043 [84].

b-hadron fractions	direct measurement	direct plus mixing
$f_{\mathrm{B}_s^0}$	$(9.2 \pm 2.4)\%$	$(9.3 \pm 1.1)\%$
$f_{b-\mathrm{baryon}}$	$(10.5 \pm 2.0)\%$	$(10.5 \pm 1.8)\%$
$f_{\mathrm{B}_d^0} = f_{\mathrm{B}^+}$	$(40.1 \pm 1.3)\%$	$(40.1 \pm 1.1)\%$

Table 4.4: *Average values of b-hadron production rates obtained from direct measurements and using time integrated mixing as of the ICHEP 2002 conference [87].*

where $g_{\mathrm{B}_s^0}$ and $g_{\mathrm{B}_d^0}$ are the fractions of B_d^0 and B_s^0 mesons in a semileptonic sample. Assuming that the semileptonic width is the same for all B hadrons, we obtain

$$g_{B_i} = f_{B_i} R_i \quad \text{where} \quad R_i = \frac{\tau_i}{\tau_B}. \tag{48}$$

This results in

$$\begin{aligned} f_{\mathrm{B}_s^0} &= \frac{1}{R_s} \frac{(1+r)\,\bar{\chi} - (1 - f_{b-\mathrm{baryon}}\, R_{b-\mathrm{baryon}})\,\chi_d}{(1+r)\,\chi_s - \chi_d} \\ f_{\mathrm{B}_d^0} &= \frac{1}{R_d} \frac{\bar{\chi} - (1 - f_{b-\mathrm{baryon}}\, R_{b-\mathrm{baryon}})\,\chi_s}{\chi_d - (1+r)\,\chi_s} \end{aligned} \tag{49}$$

where $r = R_u/R_d = \tau(B^+)/\tau(\mathrm{B}_d^0)$. We assume $f_{\mathrm{B}_d^0} = f_{\mathrm{B}^+}$, $f_{\mathrm{B}^+} + f_{\mathrm{B}_d^0} + f_{\mathrm{B}_s^0} + f_{b-\mathrm{baryon}} = 1$ and $\chi_s = 0.5$.

From the previous expressions, the values of $f_{\mathrm{B}_s^0}$ and $f_{\mathrm{B}_d^0}$ are determined and combined with those obtained from direct measurements (for more details see Ref. [85]). The results are shown in Table 4.4. It is clear that $f_{\mathrm{B}_s^0}$ is essentially determined from the time integrated mixing measurement. The error on $f_{\mathrm{B}_s^0}$ is dominated by the uncertainty on the integrated oscillation parameter $\bar{\chi}$, which is not expected to improve substantially in the near future. Different uncertainties contribute to the error on $f_{\mathrm{B}_d^0}$. The most important one is the poor knowledge of the b-baryon production rates. It has to be noted that $f_{\mathrm{B}_d^0}$ is essentially determined by the DELPHI direct measurement [86].

3.2. Flavour tagging techniques

In general, a measurement of the time dependence of B^0–$\overline{\mathrm{B}}^0$ oscillations requires the knowledge of:

- the proper decay time t of the B^0 meson (see Sec. 3.3.),
- the flavour of the B or $\overline{\mathrm{B}}$ meson at both production and decay in order to determine whether the B^0 meson has oscillated.

Events are classified on the basis of the sign of the production and decay tagging variables as mixed or unmixed. To accomplish this, it is necessary to determine the b quark content (b or $\bar{b}$) of the B meson at production and at decay time. The figure of merit to compare different flavour tags is the so-called effective tagging efficiency $\varepsilon(1 - 2\,p_W)^2$, where the efficiency ε represents the fraction of events for which a flavour tag exists and p_W is the mistag probability indicating the fraction of events with a wrong flavour tag. The mistag probability is related to the dilution $\mathcal{D}$, another quantity used to express the power of a flavour tag:

$$\mathcal{D} = 1 - 2\,p_W. \tag{50}$$

The dilution $\mathcal{D}$ is defined as the number of correctly tagged events N_R minus the number of incorrectly identified events N_W divided by the sum:

$$\mathcal{D} = \frac{N_R - N_W}{N_R + N_W}. \tag{51}$$

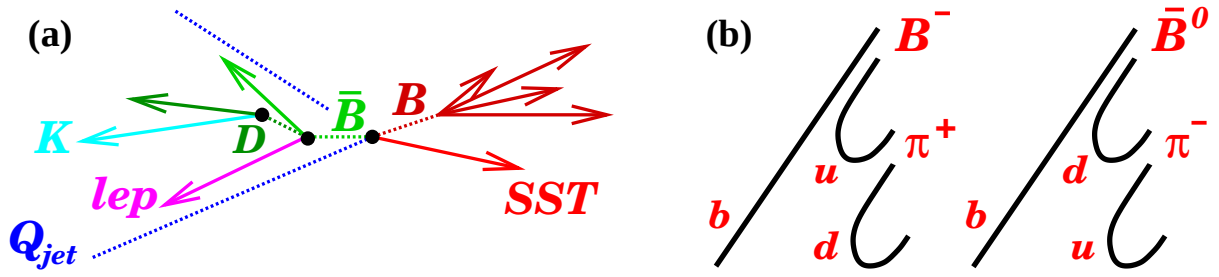

Fig. 4.7: *(a) Schematic sketch of a typical* $\mathrm{B\overline{B}}$ *event. (b) A simplified picture of* b *quark fragmentation into* B *mesons.*

Fig. 4.7(a) is a sketch of a $\mathrm{B\overline{B}}$ event showing the B and $\overline{\mathrm{B}}$ mesons originating from the primary production vertex and decaying at a secondary vertex indicating possible flavour tags on the decay vertex side (SST) and opposite side (lep, K, Q_{jet}).

3.2.1. Decay flavour tagging

Several techniques are used to determine the b quark flavour at decay time. The B flavour can be identified by the charge of a lepton from a semileptonic B decay. In a prompt $b \to \ell^-$ decay, the charge of the lepton reflects the b flavour. However, other processes can also give a lepton in the final state such as cascade decays $b \to c \to \ell^+$ resulting in a wrong sign tag, right sign cascade decays $b \to W^- \to \bar{c} \to \ell^-$, semileptonic τ decays $b \to W^- \to \tau^- \to \ell^-$ or $b \to J/\psi X \to \ell^\pm$ decays giving both sign leptons. These processes resulting in wrong sign leptons can be suppressed by using the lepton momentum or transverse momentum with respect to the b jet axis.

The b quark flavour can also be inferred from the charge of a reconstructed charm meson (D^{*-} from B^0_d or D^-_s from B^0_s) or that of a kaon assumed to come from a $b \to c \to s$ transition. In fully inclusive analyses, the b flavour can be obtained from the jet charge (see Eq. (52)), the charge of a reconstructed dipole or from multitags as further detailed in Sec. 3.4.

3.2.2. Production flavour tagging

Methods to tag the production b quark flavour differ somewhat between high energy colliders (LEP, SLC, Tevatron) and the B factories. At high-energy colliders, the production flavour tags can be divided into two groups, those that tag the initial charge of the b quark contained in the B candidate itself (same side tag) and those that tag the initial charge of the other quark ($\bar{b}$) produced in the same event (opposite side tag).

Same side tagging methods exploit correlations of the B flavour with the charge of particles produced in association with the B meson. Such correlations are expected to arise from b quark hadronization and from B^{**} decays. It has been suggested [88] that the electric charge of particles produced near a B meson can be used to determine its initial flavour. This can be understood in a simplified picture of b quark fragmentation as shown in Fig. 4.7(b). For example, if a b quark combines with a $\bar{u}$ quark to form a B^- meson, the remaining u quark may combine with a $\bar{d}$ quark to form a π^+. Similarly, if a b quark hadronizes to form a $\overline{\mathrm{B}}^0$ meson, the associated pion would be a π^-. A similar charge correlation is expected for a charged kaon produced in association with a B^0_s meson. Decays of the orbitally excited ($L = 1$) B^{**} mesons, $\mathrm{B}^{**0} \to \mathrm{B}^{(*)+}\pi^-$ or $\mathrm{B}^{**+} \to \mathrm{B}^{(*)0}\pi^+$, also produce pions with the same charge correlation. This tagging method has been successfully used for example at CDF [89,90].

There are several methods of opposite side flavour tagging as illustrated in Fig. 4.7(a). The methods using a lepton from the semileptonic decay of a B hadron, a kaon or the presence of a charmed particle from the other $\bar{B}$ hadron in the event, were already discussed above.

The technique based on the jet charge exploits the fact that the momentum weighted sum of the particle charges of a b jet is related to the b-quark charge. In the most basic form, the jet charge can be defined as:

$$Q_{\rm jet} = \frac{\sum_i q_i \cdot (\vec{p}_i \cdot \hat{a})}{\sum_i \vec{p}_i \cdot \hat{a}}, \tag{52}$$

where q_i and $\vec{p}_i$ are the charge and momentum of track i in the jet and $\hat{a}$ is a unit vector defining the jet direction. On average, the sign of the jet charge is the same as the sign of the b quark charge that produced the jet. More sophisticated weights (e.g. $(\vec{p}_i \cdot \hat{a})^\kappa$) or track impact parameter information are often introduced to improve the b flavour separation. The jet charge can also be used as a same side tag, if tracks from primary vertex can be efficiently distinguished with respect to those from secondary decay vertices.

Other tagging methods include the charge dipole method that aims of reconstructing the b hadron decay chain topologically. This method has been utilized at SLD taking advantage of the superb decay length resolution of the SLD CCD pixel vertex detector to separate tracks from the B decay point from tertiary tracks emitted at the charm decay vertex [91]. A charge dipole is defined as the distance between secondary and tertiary vertices signed by the charge difference between them (see also Sec. 3.4.).

Another interesting production flavour tagging method is available at SLD. It exploits the large polarized forward-backward asymmetry in $Z \to b\bar{b}$ decays [92–95]. This b flavour production tag makes use of the large electron beam polarization $P_e \sim 73\%$ at the SLC collider. A left- or right-handed incident electron tags the quark produced in the forward hemisphere as a b or $\bar{b}$ quark with a mistag rate p_W of 28% at nearly 100% efficiency [91].

At asymmetric e^+e^- B factories, $\mathrm{B}^0_d - \overline{\mathrm{B}}^0_d$ pairs are produced through the $\Upsilon(4S)$ resonance with a boost $\beta\gamma = 0.425$ and 0.55 at KEKB and PEP II, respectively. The two neutral B_d mesons produced from the $\Upsilon(4S)$ decay evolve in time in a coherent P-wave state where they keep opposite flavours until one of the B_d mesons decays. From this point in time onwards, the other B meson follows a time evolution according to the expression $\Gamma \mathrm{e}^{-\Gamma|\Delta t|}\,(1 \pm \cos\Delta M\,\Delta t)$ where Δt is the proper time difference between the two B decays. Hence, the production flavour tag of one of the B mesons can be taken as the decay flavour tag of the other. The main flavour tagging methods currently used at BaBar and Belle include $b \to \ell^-$ lepton tagging and $b \to c \to s$ kaon tagging.

It is common to combine different production tags in an oscillation analysis to achieve mistag probabilities of $p_W \sim 26\%$ at LEP [96–101] or even 22% for SLD [102]. An equivalent figure for CDF in Run I of the Tevatron is $p_W \sim 40\%$ [103]. Effective mistag probabilities of $p_W \sim 24\%$ are achieved by the BaBar and Belle experiments [104,105]. It is interesting to mention that the effect of B^0_d and B^0_s mixing substantially decreases the tagging power of opposite side tagging methods at high-energy colliders while mixing of the other B meson (i.e. the coherent mixing occurring before the first B decay) does not contribute to a mistag probability at the $\Upsilon(4S)$.

3.3. Analytical description of oscillation analyses

A physics function of the form $\Gamma \mathrm{e}^{-\Gamma t}\,(1 \pm \cos\Delta M\,t)$ is used to describe the signal in B oscillation analyses. At high energy colliders such as LEP, SLC or the Tevatron, the B meson decay proper time t can be obtained from a measurement of the distance L_B between the B production vertex and the B decay vertex. The proper time t is related to the decay distance L_B and to the boost $\beta\gamma$ by

$$c\,t = \frac{L_B}{\beta\gamma} = L_B\,\frac{M_B}{p_B}. \tag{53}$$

At asymmetric e^+e^- B factories, the proper time difference Δt between the two B candidate decays is the relevant measure. It is computed as:

$$\Delta t = \Delta z / \beta\gamma c, \tag{54}$$

where Δz is the spatial separation between the two B decay vertices along the boost direction.

The uncertainty on the decay time σ_t can be expressed in units of the B lifetime τ_B as

$$\frac{\sigma_t}{\tau_B} = \sqrt{\left(\frac{\sigma(L_B)}{L_B^0}\right)^2 + \left(\frac{t}{\tau_B}\frac{\sigma(p_B)}{p}\right)^2} \qquad \text{where} \quad L_B^0 = c\tau_B \cdot p_B/M_B. \tag{55}$$

The proper time resolution σ_t depends on the uncertainty $\sigma(L_B)$ to infer the decay length from the primary to the B decay vertex and on the B momentum resolution $\sigma(p_B)$. Note that the latter uncertainty scales with t/τ_B, while the vertexing resolution is independent of the proper time and only adds a constant error.

The dependence of B oscillations on the proper time resolution and other detector effects is illustrated in Fig. 4.8. Rather than plotting the mixed and unmixed probabilities $\mathcal{P}_{\text{unmix/mix}}(t) = 1/2\ \Gamma \mathrm{e}^{-\Gamma t}\,(1 \pm \cos\Delta M\, t)$ as introduced in Eq. (27) and Eq. (26), it is customary in B oscillation analyses to either determine a mixing asymmetry $\mathcal{A}_{\text{mix}}$ or to calculate the fraction of mixed events $\mathcal{F}_{\text{mix}}$

$$\mathcal{A}_{\text{mix}} = \frac{\mathcal{P}_{\text{unmix}} - \mathcal{P}_{\text{mix}}}{\mathcal{P}_{\text{unmix}} + \mathcal{P}_{\text{mix}}} = \cos\Delta M\, t, \qquad \mathcal{F}_{\text{mix}} = \frac{\mathcal{P}_{\text{mix}}}{\mathcal{P}_{\text{unmix}} + \mathcal{P}_{\text{mix}}} = (1 - \cos\Delta M\, t)/2. \tag{56}$$

As an example, Fig. 4.8(a) shows the oscillation pattern of $\mathcal{A}_{\text{mix}}$ for $\Delta M = 5$ ps^{-1} assuming an ideal case with perfect tagging, ideal proper time resolution and no background. The reduction of the amplitude due to a finite decay length resolution is shown in Fig. 4.8(b). Figure 4.8(c) indicates what happens when the resolution of the (silicon) vertex detector is not sufficient to resolve the oscillations: $\mathcal{A}_{\text{mix}}$ is completely smeared out and oscillations are no longer visible. The effect of a finite momentum resolution is displayed in Fig. 4.8(d). Since the uncertainty on the proper time coming from the momentum resolution is linear in proper time t, as seen in Eq. (55), the rapid oscillation damps in time while the first few "wiggles" can still be seen completely. The oscillation amplitude is reduced if a mistag probability is introduced, as can be seen in Fig. 4.8(e). Finally, in a real measurement, background will also be present which additionally reduces the relative importance of the oscillation amplitude. The effect of background on the mixing amplitude, in addition to a finite decay length and momentum resolution, as well as a non-zero mistag probability, is shown in Fig. 4.8(f). Note, however, that this "realistic" distribution is based on half a million signal events. Imagine the corresponding error bars for a measurement with a few hundred signal events and an oscillation frequency of $\Delta M = 20$ ps^{-1}.

In a B^0 mixing measurement, a value for ΔM is usually extracted from the data using a maximum likelihood method. In the following, we illustrate some of the essential steps for a B_d^0 analysis determining ΔM_d in more detail. We use the example of an analysis where like-sign (unlike-sign) events describe mixed (unmixed) events as would be the case, for example, in a dilepton analysis. The total probability to observe a like-sign tagged event at the reconstructed proper time t_{rec} is:

$$\mathcal{P}^{like}(t_{rec}) = f_{b\bar{b}} \sum_{q=d,s} f_{\mathrm{B_q}} p_W^{\mathrm{B_q}} \mathcal{P}^{\text{mix}}_{rec.\mathrm{B_q}}(t_{rec}) + f_b \sum_{q=u,d,s,baryons} f_{\mathrm{B_q}}(1 - p_W^{\mathrm{B_q}}) \mathcal{P}^{\text{unmix}}_{rec.\mathrm{B_q}}(t_{rec}) \quad + \\ f_{bkg.}(1 - p_W^{bkg.}) \mathcal{P}_{bkg.}(t_{rec}) \tag{57}$$

and correspondingly for an unlike-sign tagged event:

$$\mathcal{P}^{unlike}(t_{rec}) = f_{b\bar{b}} \sum_{q=d,s} f_{\mathrm{B_q}}(1 - p_W^{\mathrm{B_q}}) \mathcal{P}^{\text{mix}}_{rec.\mathrm{B_q}}(t_{rec}) + f_b \sum_{q=u,d,s,baryons} f_{\mathrm{B_q}} p_W^{\mathrm{B_q}} \mathcal{P}^{\text{unmix}}_{\mathrm{B_q}}(t_{rec}) \quad + \\ f_{bkg.} p_W^{bkg.} \mathcal{P}_{bkg.}(t_{rec}). \tag{58}$$

where $f_{b\bar{b}}$ is the fraction of $b\bar{b}$ events and p_W^i are the mistag probabilities. The probability $\mathcal{P}^{\text{mix}}_{rec.\mathrm{B_q}}(t_{rec})$ to observe the mixed B_d^0 or B_s^0 mesons at proper time t_{rec} is the result of a convolution of the oscillation probability function as given in Eq. (26) and Eq. (27) with the detector resolution function $\mathcal{R}$ and

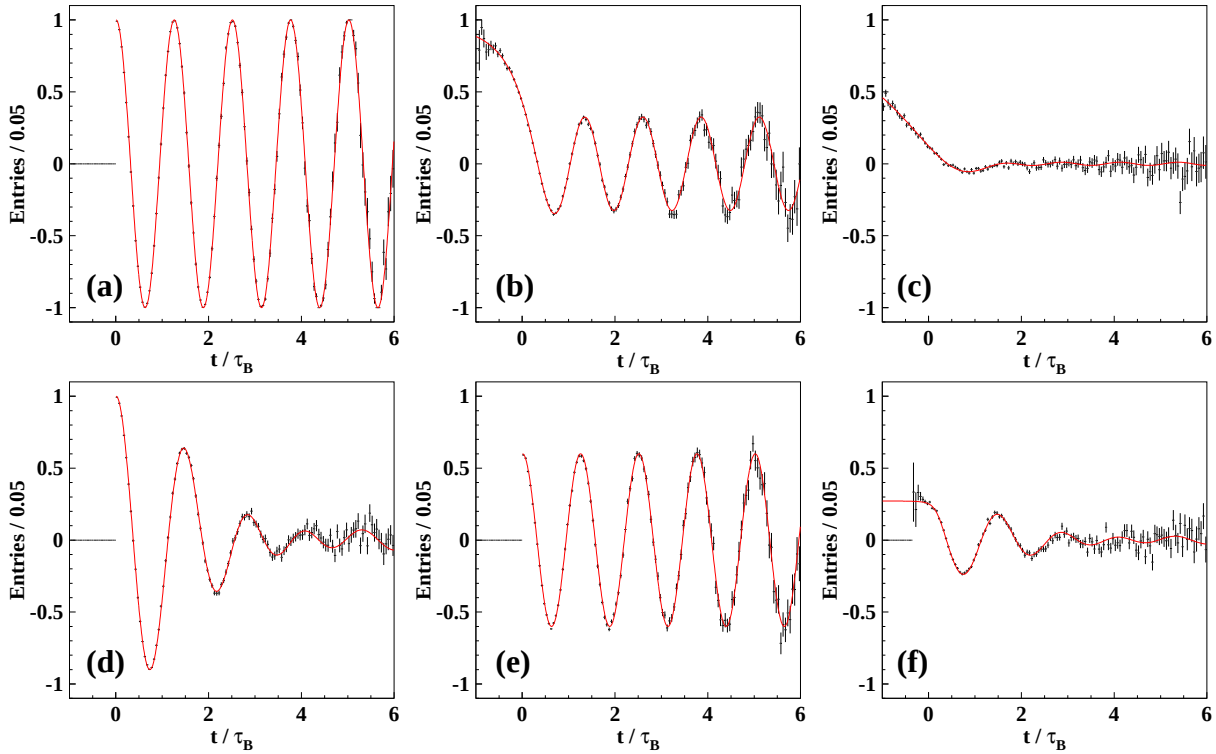

Fig. 4.8: *Illustration of various detector and analysis effects on the mixing amplitude $\mathcal{A}_{\rm mix}$: (a) perfect resolution, (b) good decay length resolution, (c) poor decay length resolution, (d) finite momentum resolution, (e) mistag probability and (f) decay length and momentum resolution plus mistag including background.*

weighted with an acceptance function $Acc(t)$

$$\mathcal{P}^{\rm (un)mix}_{rec.{\rm B_q}}(t_{rec}) = \int_0^\infty Acc(t)\mathcal{R}(t_{rec}-t,t)\mathcal{P}^{\rm (un)mix}_{\rm B_q}(t)dt. \tag{59}$$

To extract the value ΔM of the oscillation frequency, the following likelihood function is minimized :

$$\mathcal{L} = -\sum_{like-sign} \ln(\mathcal{P}^{like}(t_{rec})) - \sum_{unlike-sign} \ln(\mathcal{P}^{unlike}(t_{rec})). \tag{60}$$

In order to fully exploit the available statistics, more sophisticated mixing analyses make use of those variables on an event-by-event basis, or often divide the event sample into classes with e.g. different tagging capabilities.

3.3.1. The amplitude method

For ΔM_s measurements, the amplitude method [106] is used to set limits on ΔM_s and to combine results from different analyses. For the mixed and unmixed $\rm B^0_s$ events an amplitude A is introduced in the expressions describing the mixed and unmixed probabilities:

$$\mathcal{P}^{\rm unmix}_{\rm B^0_s} = \frac{1}{2}\Gamma_{\rm B_s} {\rm e}^{-\Gamma_{\rm B_s} t}[1 + A\cos\Delta M_s t] \tag{61}$$

and similarly:

$$\mathcal{P}^{\rm mix}_{\rm B^0_s} = \frac{1}{2}\Gamma_{\rm B_s} {\rm e}^{-\Gamma_{\rm B_s} t}[1 - A\cos\Delta M_s t] \tag{62}$$

The amplitude method works as follows. A B_s^0 oscillation amplitude A and its error σ_A are extracted as a function of a fixed test value of ΔM_s using a likelihood method in analogy to Eq. (60) based on the physics functions defined in Eq. (61) and Eq. (62). To a very good approximation, the statistical uncertainty on A is Gaussian and the experimental sensitivity is :

$$\mathcal{S} = \frac{1}{\sigma_A} \sim \sqrt{N/2}\, f_{\mathrm{sig}}\, (1 - 2p_w)\, \mathrm{e}^{-(\Delta M\, \sigma_t)^2/2} \tag{63}$$

where N and f_{sig} are the number of candidate events and the fraction of signal in the selected sample, p_W is the mistag probability to incorrectly tag a decay as mixed or unmixed characterizing the effective flavour tagging efficiency as discussed in Sec. 3.2., and σ_t is the resolution on proper time or proper time difference in the case of the B factories. The sensitivity $\mathcal{S}$ decreases rapidly as ΔM increases. This dependence is controlled by σ_t.

If ΔM_s equals its true value $\Delta M_s^{\mathrm{true}}$, the amplitude method expects $A = 1$ within the total uncertainty σ_A. If ΔM_s is tested far below its true value, a measurement consistent with $A = 0$ is expected. A value of ΔM_s can be excluded at 95% C.L. if $A + 1.645\, \sigma_A \leq 1$. If the true B_s^0 oscillation frequency $\Delta M_s^{\mathrm{true}}$ is very large, far above the experimental sensitivity, $A = 0$ is expected to be measured and all values of ΔM_s such that $1.645\, \sigma_A(\Delta M_s) < 1$ are expected to be excluded at 95% C.L. Because of proper time resolution, the quantity $\sigma_A(\Delta M_s)$ is an increasing function of ΔM_s. It is therefore expected that individual values of ΔM_s can be excluded up to $\Delta M_s^{\mathrm{sens}}$, where $\Delta M_s^{\mathrm{sens}}$ is called the sensitivity of the analysis defined by $1.645\, \sigma_A(\Delta M_s^{\mathrm{sens}}) = 1$. The results from different analyses and experiments can be combined by simple averaging different amplitude spectra.

3.4. Description of oscillation analyses

Many different analysis methods have been devised to study B_d^0 and B_s^0 mixing. These range from fully inclusive to fully exclusive analyses and, thus, they differ significantly in terms of selection efficiency, sample purity and mistag rates. Moreover, they make use of various production and decay tags. The methods also differ in the techniques used to reconstruct the B decay length and to estimate the B momentum, and therefore have different proper time resolutions. In the following, analysis methods developed to measure ΔM_d are discussed first and those used in the search for B_s^0 oscillations are presented afterwards.

3.4.1. B_d^0–$\overline{\mathrm{B}}_d^0$ *oscillation analyses*

Exclusive methods

The most straightforward and cleanest method relies on the exclusive reconstruction of the B_d^0 decay chain. However, because of its low efficiency, it has only recently become accessible with the advent of e^+e^- asymmetric B factories. Using samples of $\sim$30M $\mathrm{B\overline{B}}$ events, BaBar [107] and Belle [108] reconstruct the decays $\mathrm{B}_d^0 \to \mathrm{D}^{(*)-}\pi^+$, $\mathrm{D}^{(*)-}\rho^+$, $\mathrm{D}^{(*)-}a_1^+$, $J/\psi\mathrm{K}^{*0}$ (BaBar), and $\mathrm{B}_d^0 \to \mathrm{D}^{(*)-}\pi^+$, $\mathrm{D}^{*-}\rho^+$ (Belle), where charmed mesons are fully reconstructed in several D^{*-} and $\overline{\mathrm{D}}^0$ decay modes. Very clean signals are obtained, see Fig. 4.9, and the decay flavour is unambiguously determined by the charge of the $\mathrm{D}^{(*)}$ meson (or the charged kaon in case of the $J/\psi\mathrm{K}^{*0}$ decay).

The average separation of the two B decay points is $\Delta z = 255\ (200)\ \mu\mathrm{m}$ with $\sigma_z \simeq 180\ (140) \mu\mathrm{m}$ for Babar (Belle), which corresponds to a resolution on Δt (Eq. 54) of about $1.1\,\mathrm{ps}$. For a measurement of the B_d^0 oscillation frequency it is therefore critical to have good control over the resolution. Table 4.5 summarizes the number of events, signal mode purity and production flavour tag information for these as well as all other analyses presented below.

Decay modes	Analysis	Events/Signal	$f_{\rm mode}$	Production flavour tag
$\mathrm{B}^0_d \to \mathrm{D}^{(*)-} h^{+a}$	BaBar exclusive [107]	7380/6347	86%	Multiple tags
$J/\psi \mathrm{K}^{*0}$	Belle exclusive [108]	8325/6660	80%	Multiple tags
$\mathrm{B}^0_d \to \mathrm{D}^{*-}\pi^+$	Belle semi-incl. [116]	4899/3433	70%	Lepton
$\mathrm{B}^0_d \to \mathrm{D}^{(*)-} X$	ALEPH semi-excl. [113]	4059/2395	38?%	Lepton+jet charge
	CDF semi-excl. [103]	874/358	27%	Lepton
	DELPHI semi-excl. [114]	10030/4212	27?%	Jet charge
	OPAL semi-excl. [112]	347/253	48%	Lepton
$\mathrm{B}^0_d \to \mathrm{D}^{(*)-}\ell^+\nu$	BaBar semi-excl. [109]	17506/14182	74%	Multiple tags
	Belle semi-excl. [110]	16397/15118	80%	Multiple tags
	CDF semi-excl. [111]	888/530		Lepton
	CDF semi-excl. [89]	/6266		Same-side tag
	OPAL semi-excl. [112]	1200/926	65%	Jet charge
	DELPHI semi-incl. [114]	5958/4135	59%	Jet charge
	OPAL semi-incl. [115]	/7000	36%	Multiple tags
$\mathrm{B}^0_d \to X\ell^+\nu$	BaBar semi-incl. [120]	99k/	37%	Lepton
	Belle semi-incl. [121]	281k/		Lepton
	ALEPH semi-incl. [113]	5957/		Lepton
	CDF semi-incl. [117]	5968/	39%	Lepton ($\mu\mu$)
	CDF semi-incl. [103]	10180/		Lepton ($e\mu$)
	DELPHI semi-incl. [114]	4778/	33%	Lepton
	L3 semi-incl. [119]	1490/		Lepton
	L3 semi-incl. [119]	2596/	34%	Lepton (impact parameter)
	OPAL semi-incl. [100]	5357/		Lepton
	ALEPH semi-incl. [113]	62k/		Jet charge
	CDF semi-incl. [118]	13k/		Lepton+jet charge
	DELPHI semi-incl. [114]	60k/	29%	Jet charge
	OPAL semi-incl. [101]	95k/	30%	Jet charge
	L3 semi-incl. [119]	8707/		Jet charge
	SLD semi-incl. [93]	581/	51%	Polarization+jet charge
	SLD semi-incl. [92]	2609/	31%	Polarization+jet charge
$\mathrm{B}^0_d \to$ all	ALEPH inclusive [123]	423k/	35%	Jet charge
	DELPHI inclusive [122]	770k/	40%	Multiple tags
	SLD inclusive [94]	3291/	60%	Polarization+jet charge; Charge dipole decay tag
	SLD inclusive [94]	5694/	60%	Polarization+jet charge; Kaon decay tag 1993–95
	SLD inclusive [95]	7844/	60%	Multiple tags; Kaon decay tag 1996–98

[a] h^+ stands for π^+, ρ^+, a_1^+.

Table 4.5: *Summary of* B^0_d *mixing analyses showing the signal decay modes, analysis method, total number of selected events and estimated signal, fraction of signal decay mode in the selected sample (*$f_{\rm mode}$*), and production flavour tag.*

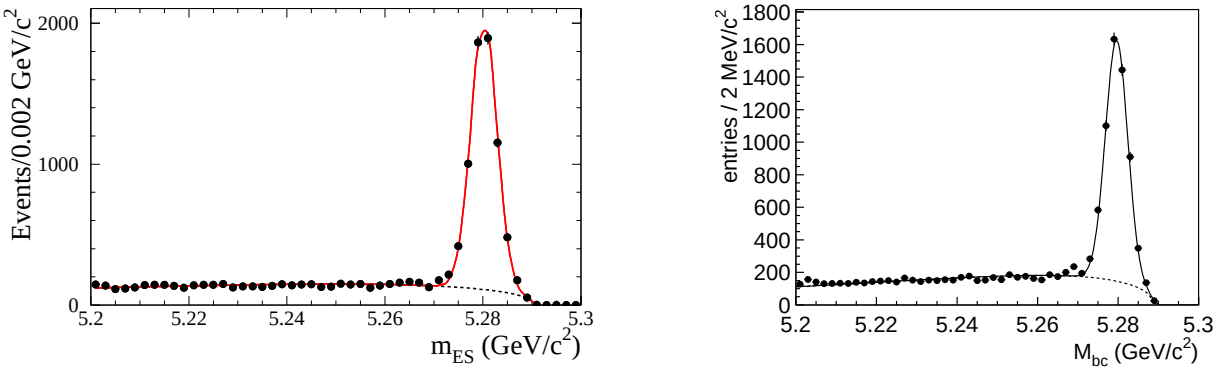

Fig. 4.9: *Distributions of beam-energy substituted mass for exclusively reconstructed* B^0_d *decays in the BaBar (left) and Belle (right) analyses.*

Semi-exclusive methods

Several analyses have combined an identified lepton with a fully reconstructed charmed hadron. Generally, the presence of a $\mathrm{D}^{(*)-}$, with charge opposite that of the lepton, tags the decay of a B^0_d meson. This simple picture is complicated by decays of the type $\mathrm{B}^+ \to \overline{\mathrm{D}}^{**0}\ell^+\nu$, where the $\overline{\mathrm{D}}^{**0}$ decays into a $\mathrm{D}^{(*)-}$ meson.

Measurements have been performed at B factories by BaBar [109] and Belle [110] and at high energy colliders by CDF [111,89] and OPAL [112]. B^0_d mesons are partially reconstructed in the mode $\mathrm{B}^0_d \to \mathrm{D}^{(*)-}\ell^+\nu$, where the D^{*-} or D^- meson is fully reconstructed. The selection relies on the kinematical properties of B^0_d and $\mathrm{D}^{(*)-}$ decays. In particular, the low Q value of the decay $\mathrm{D}^{*-} \to \overline{\mathrm{D}}^0\pi^-$ is exploited to identify D^{*-} mesons efficiently and cleanly. Fig. 4.10 shows the mass difference $\Delta M = M(\mathrm{D}^{*-}) - \mathrm{M}(\overline{\mathrm{D}}^0)$ in the BaBar and OPAL analyses. Signal purities range from ∼45% to ∼90% for the different experiments, depending mostly on the $\overline{\mathrm{D}}^0$ decay mode.

In order to increase the selection efficiency, analyses by ALEPH [113], CDF [103], DELPHI [114], and OPAL [112] select $\mathrm{B}^0_d \to \mathrm{D}^{(*)-}X$ decays, where the $\mathrm{D}^{(*)-}$ meson is also fully reconstructed. Despite the more inclusive nature of this method, the identification of a $\mathrm{D}^{(*)-}$ decay guarantees that the B^0_d purity remains high. However, $b\overline{b}$ tagging is generally needed to suppress the significant number of D^{*-} produced in $c\overline{c}$ events.

Semi-inclusive methods

One of the semi-inclusive methods selects $\mathrm{B}^0_d \to \mathrm{D}^{*-}\ell^+\nu$ decays without attempting to fully reconstruct the $\overline{\mathrm{D}}^0$ meson but only the lepton and the slow π^- from the $\mathrm{D}^{*-} \to \overline{\mathrm{D}}^0\pi^-$ decay. This partial reconstruction method yields much larger data samples than obtained with the exclusive reconstruction but suffers from higher background. It has been applied by DELPHI [114] and OPAL [115]. The combinatorial background can be studied with same-sign lepton-pion pairs and ΔM side bands. The $\mathrm{B}^+ \to \overline{\mathrm{D}}^{**0}\ell^+\nu$ component needs to be estimated from the simulation.

A similar technique is used by Belle [116] to reconstruct $\mathrm{B}^0_d \to \mathrm{D}^{*-}\pi^+$ decays. In this analysis, only the fast π^+ and the slow π^- are reconstructed. This information is sufficient to compute the $\overline{\mathrm{D}}^0$ missing mass, assuming that the B^0_d meson is at rest in the $\Upsilon(4\mathrm{S})$ rest frame and using energy and momentum conservation. The event is required to contain a high-momentum lepton to tag the other B meson flavour and to suppress the large non-$\mathrm{B}\overline{\mathrm{B}}$ background. This method is only possible at the $\Upsilon(4\mathrm{S})$ where sufficient kinematical constraints are available.

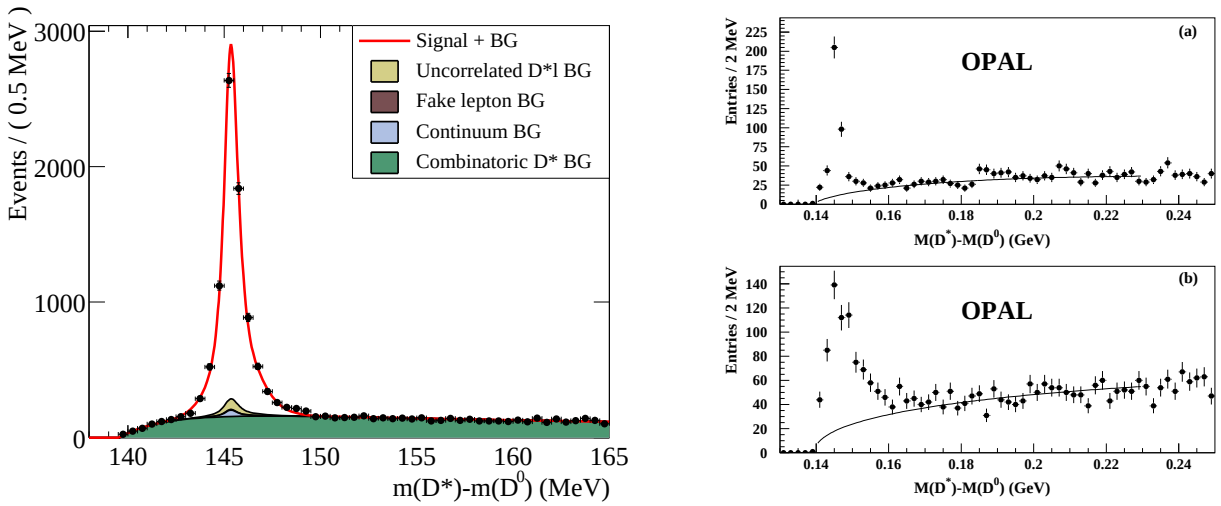

Fig. 4.10: *Distributions of the mass difference between* D^{*-} *and* $\overline{\mathrm{D}}^{0}$ *candidates for BaBar (left) and OPAL (right). The BaBar distribution is shown for* $\mathrm{D}^{*-}e^{+}\nu$ *candidates. The distributions on the right correspond to the modes* $\overline{\mathrm{D}}^{0} \to \mathrm{K}^{+}\pi^{-}$ *(top) and* $\overline{\mathrm{D}}^{0} \to \mathrm{K}^{+}\pi^{-}\pi^{0}$ *(bottom), where the* π^{0} *is not reconstructed.*

The most widely used method relies on the inclusive reconstruction of semileptonic decays. At high energy colliders, it has been employed by ALEPH [113], CDF [117,118,103], DELPHI [114], L3 [119], OPAL [100,101], and SLD [93,92]. This method is efficient since the decay rate for $\mathrm{B}^{0}_{d} \to X\ell^{+}\nu$ is approximately 20% (using electrons and muons) and the decay flavour tag is excellent. A high-p and high-p_T lepton is selected to suppress the contribution from cascade leptons (from $b \to c \to \ell^{+}$ transitions) and the accompanying charmed hadron (denoted "D" in the following) is reconstructed inclusively using charged tracks in the jet containing the lepton. The position of the B decay vertex and the B momentum are obtained using algorithms that aim to classify tracks as coming from either primary or secondary vertices. The B decay vertex is then obtained by intersecting the trajectories of the lepton and that of a D candidate.

The analyses are combined with a variety of different production flavour tags and are thus referred to as "dilepton", "lepton-jet charge" and "Multiple tags" analyses (see Table 4.5).

Dilepton analyses have also been performed by both BaBar [120] and Belle [121]. Here, there is no attempt to reconstruct the D decay and the time difference is extracted directly from the separation Δz between the intersections of the two leptons with the beam axis. Momentum and angular cuts are applied to reduce the wrong-sign background from cascade leptons. In the BaBar analysis, the main background consists of $\mathrm{B}^{+}\mathrm{B}^{-}$ events and is determined to be ∼55% and the main source of mistag originates from events containing one direct lepton and one cascade lepton, amounting to 13% of the total sample.

Inclusive methods

A few analyses rely on fully inclusive techniques to select large samples of B^{0}_{d} decays. These techniques aim to capture most decays by using topological vertexing. As for the semi-inclusive methods, the selection algorithms generally do not provide any enhancement in the B^{0}_{d} purity. The primary issue here is the decay flavour tag.

SLD uses two different decay tags: the charge of a kaon coming from the B decay chain [94,95] or the charge dipole of the secondary vertex [94]. These analyses require the net charge of all tracks associated with the decay to be zero to enhance the B^{0}_{d} fraction from ∼40% to ∼60%. The kaon decay tag is more efficient than the lepton decay tag but has a worse mistag rate of ∼20%. The charge dipole technique takes advantage of the $\mathrm{B}^{0}_{d} \to \mathrm{D}^{-}X^{+}$ dipole structure and the fact that the B^{0}_{d} and D^{-} vertices

are separated along the B_d^0 line of flight due to the finite charm lifetime. For the B_d^0 analyses the charge dipole is defined as the difference between the weighted mean location of the positive tracks and of the negative tracks along the axis joining the primary and secondary vertices. The track weights account for the uncertainty in determining the location of each track. A positive (negative) charge dipole tags the decay flavour of the $\overline{\mathrm{B}}_d^0$ (B_d^0) meson.

At LEP, DELPHI [122] also developed a fully inclusive method based on the charge dipole tag. The vertex algorithm uses topological and kinematical information to separate primary and secondary tracks. A secondary lepton is found in a subset of the vertices and provides the decay flavour tag (these leptons are referred to as "soft" leptons since decays with high p and p_T are used in other DELPHI analyses). For the remainder of the sample, the B decay products are boosted back into the B meson rest frame and a charge dipole is formed between the forward and backward hemispheres (as defined by the thrust axis). Given that the forward (backward) hemisphere contains mostly tracks from the D (B) decay vertex, one expects a ± 2 charge difference between the two hemispheres. The ALEPH inclusive analysis [123] reconstructs topological vertices in both event hemispheres as in the inclusive semileptonic analysis. The flavour tagging is performed by computing the product of the jet charges in the two hemispheres of each event. This product thus combines production and decay flavour tags and is sensitive to whether mixing occurred or not.

Table 4.5 summarizes the different B_d^0 mixing analyses. It should be noted that this Table provides only an approximate representation of the performance of each analysis. The reader is referred to the specific papers for more detailed comparisons.

3.4.2. B_s^0 *and* $\overline{\mathrm{B}}_s^0$ *oscillation analyses*

The study of time dependent B_s^0 oscillations has been performed with a wide range of analysis techniques at high energy colliders. The study of B_s^0 oscillations is more challenging than that of B_d^0 oscillations due to two main differences. Only about 10% of b quarks hadronize into B_s^0 mesons, as compared to about 40% into B_d^0 mesons. The B_s^0 oscillation frequency is expected to be at least a factor of 20 larger than that for B_d^0 oscillations. To address this, sophisticated analyses have been developed with an emphasis on lowering the mistag rate, increasing the B_s^0 purity and, especially, improving the proper time resolution, all of which affect the sensitivity to B_s^0 oscillations.

Exclusive methods

Fully exclusive analyses have been performed by ALEPH [124] and DELPHI [98] via the (all charged particles) modes $\mathrm{B}_s^0 \to \mathrm{D}_s^- \pi^+$, $\mathrm{D}_s^- a_1^+$, $\overline{\mathrm{D}}^0 \mathrm{K}^- \pi^+$, $\overline{\mathrm{D}}^0 \mathrm{K}^- a_1^+$ (last two for DELPHI only), where the D_s^- and $\overline{\mathrm{D}}^0$ are fully reconstructed in several decay modes. The decays $\mathrm{B}_s^0 \to \mathrm{D}_s^{*-} \pi^+$, $\mathrm{D}_s^{*-} a_1^+$ and $\mathrm{D}_s^{(*)-} \rho^+$ are also reconstructed by adding one or more photons to the above final states (ALEPH only) or by considering the events falling into the "satellite" mass region below the B_s^0 mass peak.

The number of selected signal decays is small (see Table 4.6) but the method provides excellent proper time resolution for two reasons. As there is no missing particle in the decay (at least for events in the main peak), the B_s^0 momentum is known with good precision and therefore the contribution of the momentum uncertainty to the proper time resolution is small. As a result, unlike all other methods, σ_t does not grow significantly when increasing the proper time t. In addition, the reconstructed channels are two-body or quasi two-body decays, with an opening angle of their decay products which is on average larger than that in multi-body final states; this results in a better accuracy on the B decay length. Despite the limited statistics, this method contributes to the study of B_s^0 oscillations at the highest values of ΔM_s. As detailed in Sec. 3.7., this is the preferred method for future studies of B_s^0 oscillations at hadron colliders.

Semi-exclusive methods

Many analyses have been developed with semi-exclusive methods. B_s^0 decays are partially reconstructed in the modes $\mathrm{B}_s^0 \to \mathrm{D}_s^- \ell^+ \nu_\ell X$ and $\mathrm{B}_s^0 \to \mathrm{D}_s^- h^+ X$, where h represents any charged hadron (or system of several hadrons) and the D_s^- meson decay is either fully or partially reconstructed in the modes $\mathrm{D}_s^- \to \phi\pi^-$, $\mathrm{K}^{*0}\mathrm{K}^-$, $K_s^0\mathrm{K}^-$, $\phi\rho^-$, $\mathrm{K}^{*0}\mathrm{K}^{*-}$, $\phi\pi^-\pi^+\pi^-$, $\phi\ell^-\overline{\nu}$, $\phi h^- X$. Partial reconstruction in $\mathrm{D}_s^- h^+$ modes has the benefit of larger statistics but the $\mathrm{D}_s^- \ell^+ \nu_\ell X$ channel has the advantage of a considerably higher B_s^0 purity, lower mistag rate and higher proper time resolution.

Analyses in the mode $\mathrm{B}_s^0 \to \mathrm{D}_s^- \ell^+ \nu$ have been performed by ALEPH [124], CDF [125], DELPHI [126] and OPAL [127]. Selection of D_s^- decays proceeds as described above. CDF only uses a partial reconstruction of the mode $\mathrm{D}_s^- \to \phi\pi^- X$. Some background suppression (especially from $\mathrm{B} \to \mathrm{D}_s \mathrm{D} X$) is achieved by requiring that the lepton and the D_s^- comes from the same vertex.

The hadronic channel $\mathrm{B}_s^0 \to \mathrm{D}_s^- h^+ X$ has been used by DELPHI [98] and SLD [128]. Fully reconstructed D_s^- decays are selected only in the modes $\mathrm{D}_s^- \to \phi\pi^-$ and $\mathrm{K}^{*0}\mathrm{K}^-$ because of their lower background level. D_s^- candidates are then combined with one or more secondary tracks to form B_s^0 decay candidates. Among B_s^0 decays contributing to the D_s^- signal, approximately 10% have the wrong decay flavour tag due to the process $W^+ \to \mathrm{D}_s^+$ ($b \to c\bar{c}s$ transition). This source of mistag is essentially absent in the semileptonic analyses. Despite lower statistics, the SLD analysis contributes to the B_s^0 oscillation sensitivity at large ΔM_s thanks to its excellent decay length resolution (see Table 4.6).

Semi-inclusive methods

The semi-inclusive lepton method, based on the process $\mathrm{B}_s^0 \to X \ell^+ \nu_\ell$, is the most sensitive method at LEP and has been used by ALEPH [124], DELPHI [126], OPAL [129] and SLD [130]. The principle of the method (see the discussion above in the case of B_d^0 mixing) is to reconstruct the D_s^- inclusively by relying on topological vertexing and kinematical information. Fairly loose criteria are applied to select large event samples, see Table 4.6.

For this method, it is important to reduce the contribution from cascade decays and to increase the B_s^0 purity of the sample (B_s^0 mesons represent about 10% of all b-hadrons produced, see Table 4.4). To enrich the sample in direct B_s^0 semileptonic decays, the following quantities are used: momentum and transverse momentum of the lepton, impact parameters of all tracks in the opposite hemisphere relative to the main event vertex, kaons at primary or secondary vertices in the same hemisphere, and charge of the secondary vertex. Those variables are usually combined in a global discriminant variable. The result of this procedure is to increase the B_s^0 purity by about 30%; the corresponding mistag rate at decay is $\sim$10% or less. The above information, as well as the proper time resolution, is then used on an event-by-event basis. As an example, Fig. 4.11 shows the neural network output distributions sensitive to the $b \to \ell^-$ fraction and the B_s^0 purities in the ALEPH data. The decay length resolution is somewhat worse than in the case of semi-exclusive analyses due to missing or mis-assigned tracks.

Inclusive methods

Fully inclusive methods are sensitive to most B decay modes and, thus, have high efficiency. Such techniques have been developed by DELPHI [122] and SLD [131]. The analyses rely on inclusive topological vertexing to select B decay products and to reconstruct the B decay vertex. The DELPHI analysis is the same as the one described earlier for B_d^0 mixing. A very large data sample is obtained but the mistag rates are high (see Table 4.6). SLD is able to exploit the excellent 3D spatial resolution of its CCD-pixel vertex detector to cleanly separate the charged decay products from secondary (originating directly from the B decay) and tertiary (originating from cascade D decays) vertices. The decay flavour is determined from the charge dipole δQ defined as the distance between secondary and tertiary vertices

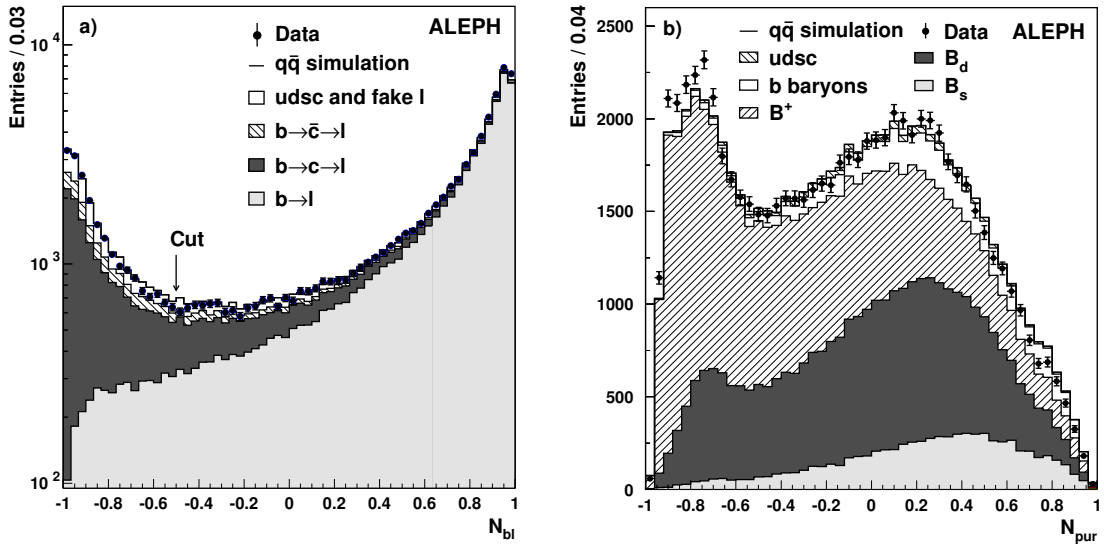

Fig. 4.11: *Distribution of (a) the $b \to \ell^-$ tagging variable and (b) the B_s^0 purity variable for data (points) and Monte Carlo simulation (histograms) in the ALEPH inclusive lepton analysis.*

signed by the charge difference between them. Positive (negative) values of δQ tag $\overline{\mathrm{B}^0}$ (B^0) decays as shown in Fig. 4.12.

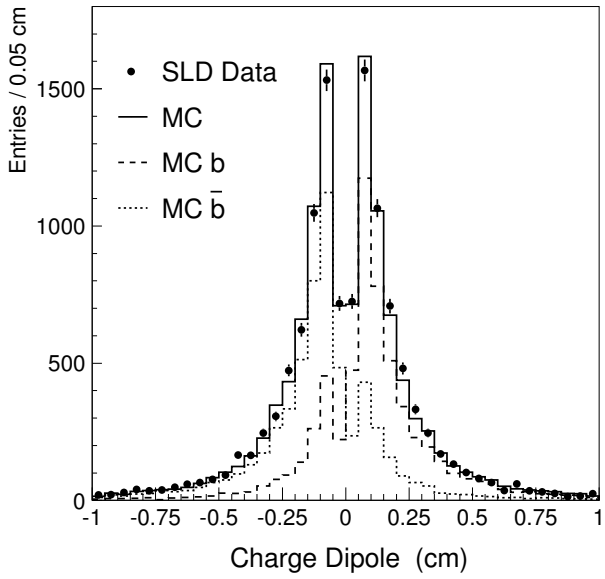

Fig. 4.12: *Distribution of the charge dipole for SLD data (points) and Monte Carlo (solid histogram). Also shown are the contributions from hadrons containing a b quark (dashed histogram) or a $\bar{b}$ quark (dotted histogram).*

Table 4.6 summarizes the different B_s^0 mixing analyses. It should be noted that the Table presents only the average performance of the analyses and that most analyses substantially increase their sensitivity by relying on event-by-event information.

Decay modes	Analysis	Events/Signal	$f_{\rm mode}$	p_W	σ_L	σ_p/p
$\mathrm{B}_s^0 \to \mathrm{D}_s^{(*)-} h^{+a}$	ALEPH [124]	80/29	36%	0	180 μm	0.005 (peak)
	exclusive					0.03 (satellite)
$\mathrm{B}_s^0 \to \mathrm{D}_s^{(*)-} h^{+a}$	DELPHI [98]	44/23	52%	0	117 μm (58%)	[b]
$\overline{\mathrm{D}}^0\mathrm{K}^- h'^+$	exclusive				216 μm (42%)	
$\mathrm{B}_s^0 \to \mathrm{D}_s^- X$	DELPHI [98]	3079/1266	50%	10%	260 μm (77%)	0.10 (77%)[c]
	semi-excl.				304 μm (13%)	0.26 (23%)
					650 μm (10%)	
	SLD [128]	361/174	55%	10%	50 μm (60%)	0.08 (60%)
	semi-excl.				151 μm (40%)	0.18 (40%)
$\mathrm{B}_s^0 \to \mathrm{D}_s^- \ell^+ \nu$	ALEPH [124]	333/156	47%		240 μm	0.11
	semi-excl.					
	CDF [125]	/1068	61%			
	semi-excl.					
	DELPHI [126]	/436	53%		200 μm (82%)	0.07 (82%)
	semi-excl.				740 μm (16%)	0.16 (16%)
	OPAL [127]	244/116	48%		500 μm	0.10
	semi-excl.					
$\mathrm{B}_s^0 \to X \ell^+ \nu$	ALEPH [124]	74k/	10%	13%[d]	251 μm (75%)	0.064 (60%)
	semi-incl.				718 μm (25%)	0.020 (40%)
	DELPHI [126]	68k/	10%	8-18%		
	semi-incl.					
	OPAL [129]	53k/	8%	12%[d]		
	semi-incl.					
	SLD [130]	2k/	16%	4%	55 μm (60%)	0.06 (60%)
	semi-incl.				217 μm (40%)	0.18 (40%)
$\mathrm{B}_s^0 \to$ all	DELPHI [122]	770k/	10%	43%[e]	400 μm	0.15
	inclusive			33%[f]		
	SLD [131]	11k/	16%	22%	78 μm (60%)	0.07 (60%)
	inclusive				304 μm (40%)	0.21 (40%)

[a] h^+ stands for π^+, ρ^+, a_1^+ and h'^+ stands for π^+, a_1^+.

[b] For the best data subset (B_s^0 peak and 1994-95 data).

[c] Evaluated at $t = 1$ ps for the best subset of data.

[d] Fraction of non-$(b \to \ell^-)$ decays.

[e] For 615k vertices with charge dipole tag.

[f] For 155k vertices with soft lepton tag.

Table 4.6: *Summary of* B_s^0 *mixing analyses showing the signal decay modes, analysis method, total number of selected events and estimated signal, fraction of signal mode in the selected sample* $f_{\rm mode}$*, decay flavour mistag rate* p_W *for* B_s^0 *decays, decay length and momentum resolutions. For semi-exclusive analyses, the number of signal events corresponds to the number of* D_s^- *signal decays (not the number of signal events in the selected decay mode) and* $f_{\rm mode}$ *represents the fraction of* B_s^0 *in the* D_s^- *signal.*

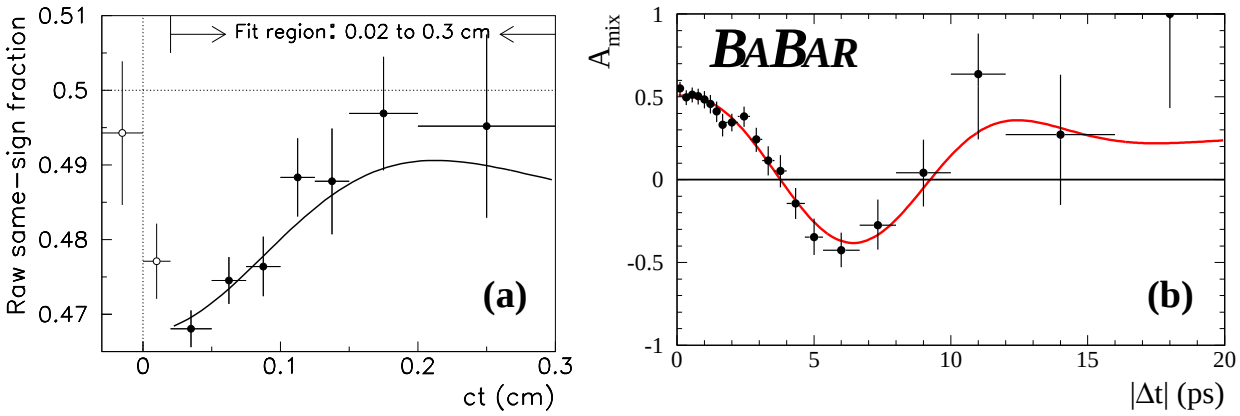

Fig. 4.13: *Examples of ΔM_d results from (a) CDF (Ref. [118]) and (b) BaBar (Ref. [120]). See text for details.*

3.5. B^0_d oscillation results. Measurement of the ΔM_d frequency

As detailed in Sec. 3.4., many methods and channels have been used to study B^0_d–$\overline{B}{}^0_d$ oscillations. These analyses have been performed by the ALEPH [113,123], BaBar [107,109,120], Belle [108,110,116,121], CDF [89,90,103,111,117,118], DELPHI [98,114,122], L3 [119], OPAL [112,115,100,101] and SLD [92–95] collaborations.

In the following, we will discuss the results of a few representative measurements of ΔM_d. Fig. 4.13(a) showss the fraction of mixed events as a function of proper decay length for a semi-inclusive analysis at CDF using a lepton sample with an inclusively reconstructed vertex combined, on the opposite side, with a lepton and jet charge tag to infer the production flavour [118]. Although this analysis is based on about 240,000 events, the total height of the oscillation amplitude is small (~ 0.05) due to an effective tagging efficiency of $\varepsilon(1-2p_W)^2 \sim 1\%$ for each tag yielding a value of $\Delta M_d = (0.500 \pm 0.052 \pm 0.043)$ ps^{-1}. In this analysis, a large mistag rate p_W resulting in $(1-2p_W)$ being small is compensated by the number of events N being large (see Eq. (63)). This result can be compared to a measurement from BaBar [120] based on about ~ 6300 neutral B mesons fully reconstructed in multihadronic modes (mainly $B^0_d \to \bar{D}^{(*)}X$). An opposite lepton and kaon tag with low mistag fractions of $p_W \sim 8\%$ and $\sim 16\%$, respectively, are the reason for an oscillation amplitude of ~ 0.5 in the mixed asymmetry as shown in Fig. 4.13(b). Note the statistical error on the ΔM_d value obtained by BaBar for this analysis: $\Delta M_d = (0.516 \pm 0.016 \pm 0.010)$ ps^{-1}. From this example we can see the trade-off between a poor tagging power in high statistics B samples produced for example in a hadronic $p\bar{p}$ environment at the Tevatron and lower statistics analyses with superior tagging and low mistag probabilities in an e^+e^- environment for example at the B factories. In addition, compared to inclusive methods, analyses with fully reconstructed B mesons have a higher sample purity.

Fig. 4.14 shows the result of two other ΔM_d analyses. One of the most precise single measurements performed at the Z^0 resonance is an inclusive D^* analysis by OPAL [115] using $B^0 \to D^{*-}\ell^+\nu$ decays. High statistics $D^{*-} \to \bar{D}^0\pi^-$ decays were reconstructed using the slow π^- from the D^{*-} decay while inferring the $\overline{D}{}^0$ with an inclusive technique. Same-sign lepton-pion pairs serve to constrain the combinatorial background in the opposite sign lepton-pion pair signature. A clear oscillation signal is observed in the fraction of mixed events as can be seen in Fig. 4.14(a). A value of $\Delta M_d = (0.497 \pm 0.024 \pm 0.025)$ ps^{-1} is extracted. Another example of a precise ΔM_d analysis at the Z^0 pole by DELPHI is shown in Fig. 4.14(b). A sample of 770,000 events with an inclusively reconstructed vertex has been selected. Tags based on several separating variables such as the jet charge, dipole charge and the transverse momentum of the (soft) lepton have been combined into a probability to determine the fraction of like-sign events as displayed in Fig. 4.14(b). DELPHI obtains a value of $\Delta M_d = (0.531 \pm 0.025 \pm 0.007)$ ps^{-1}.

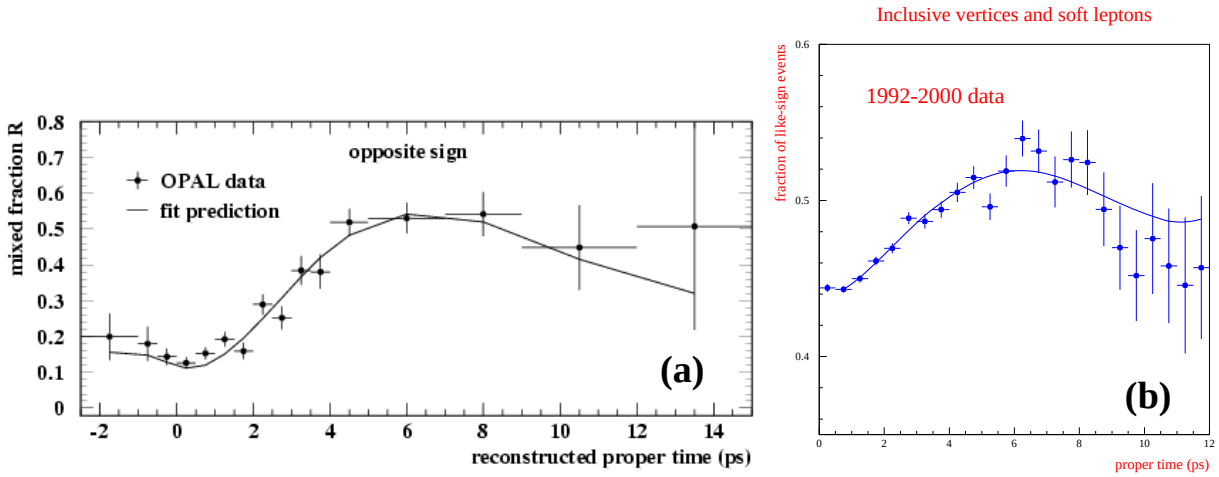

Fig. 4.14: *Examples of ΔM_d results from (a) OPAL (Ref. [115]) and (b) DELPHI (Ref. [122]). See text for details.*

In order to combine all individual ΔM_d results to obtain a world average value, possible statistical correlations between individual analyses have to be taken into account and also the systematic errors which are often not negligible have to be combined properly. The main sources of systematic uncertainties are determinations of sample compositions, mistag probabilities, b hadron production fractions and contributions from b hadron lifetimes. Before being combined, the measurements are adjusted on the basis of a common set of input values. Details of the averaging procedure are described in Ref. [85].

A compilation of all ΔM_d measurements available as of the 2002 ICHEP conference, can be found in Fig. 4.15. The individual results from each experiment are combined and averaged using the procedure described above. There exist also time-integrated measurements of B^0_d mixing from the ARGUS [132,133] and CLEO [134,135] collaborations which can be converted into a value for ΔM_d assuming the width difference $\Delta\Gamma_d$ in the B^0_d system to be zero and no CP violation in B^0_d mixing. The quoted world average, at the bottom of Fig. 4.15, also includes χ_d measurements by ARGUS and CLEO. The ΔM_d averages per experiment are displayed in Fig. 4.16.

The different results from the combination procedure are [87]:

$$\Delta M_d = \begin{cases} (0.491 \pm 0.041)\ \mathrm{ps}^{-1} & \text{Argus-CLEO (from } \chi_d\text{)} \\ (0.498 \pm 0.013)\ \mathrm{ps}^{-1} & \text{LEP-SLD-CDF} \\ (0.503 \pm 0.007)\ \mathrm{ps}^{-1} & \text{Belle-BaBar} \\ (0.503 \pm 0.006)\ \mathrm{ps}^{-1} & \text{world average} \end{cases} . \tag{64}$$

At the end of the LEP-CDF-SLD era, ΔM_d has been determined with a relative precision of about 2.6%. The LEP-CDF-SLD results are in excellent agreement with the Belle-BaBar measurements. After the inclusion of the results from B factories, the precision on ΔM_d is improved by a factor of two. The world average B^0_d mixing frequency is now dominated by the results of B factories.

3.6. Results on B^0_s oscillations. Limits on the ΔM_s frequency

B^0_s–$\overline{\mathrm{B}}^0_s$ oscillations have also been the subject of many studies by ALEPH [96,97,124], CDF [125], DELPHI [98,99,126,136], OPAL [127,129] and SLD [102,128,130,131]. No oscillation signal has been observed to date. To set lower limits on the oscillation frequency ΔM_s, all B^0_s mixing analyses use the amplitude method [106] described in Sec. 3.3.1.

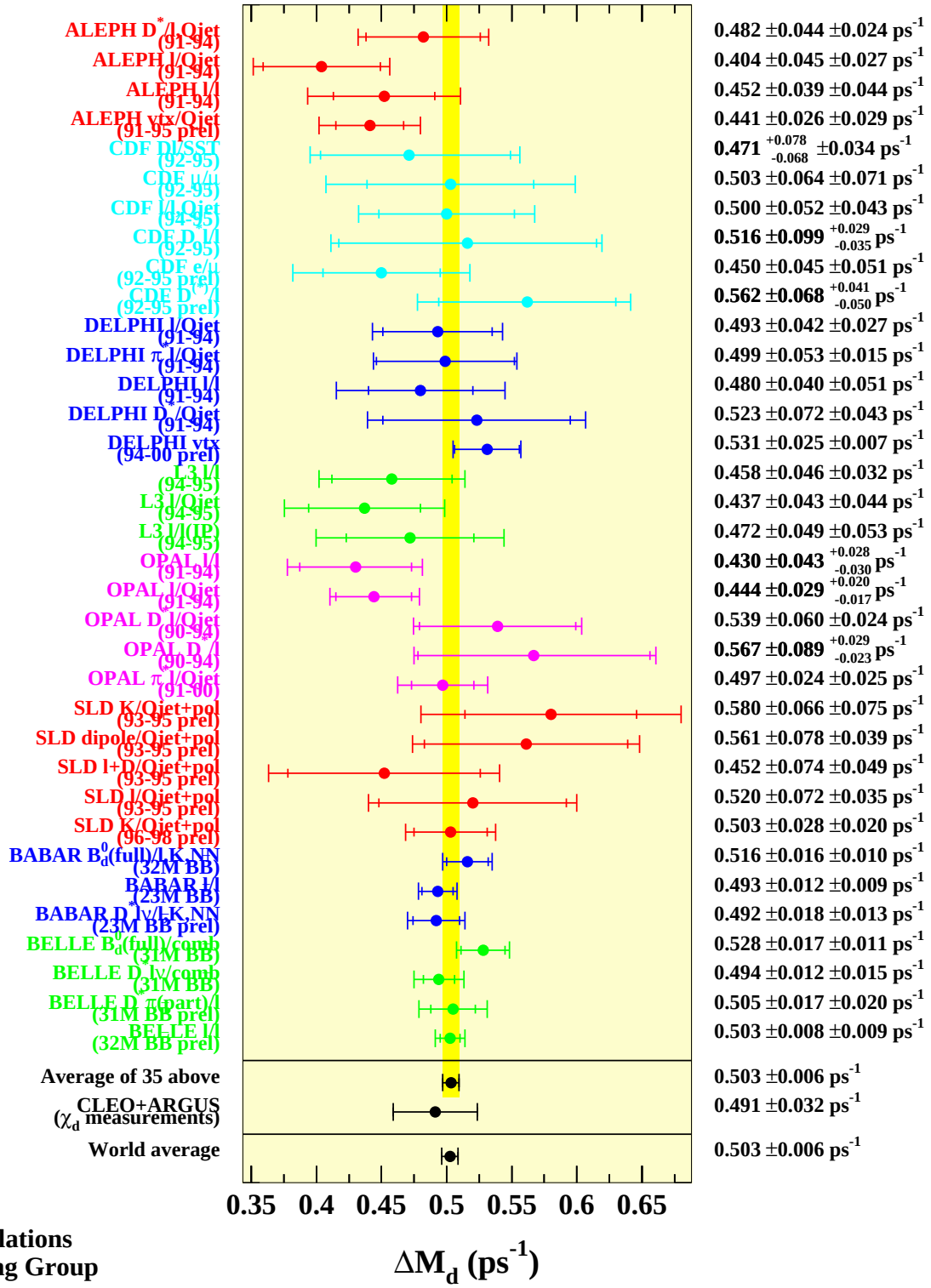

Fig. 4.15: *Individual and combined measurements of* ΔM_d *at* B *factories, LEP, SLD and CDF as of the ICHEP 2002 conference [87]. The quoted world average, at the bottom, also includes* χ_d *measurements performed by ARGUS and CLEO.*

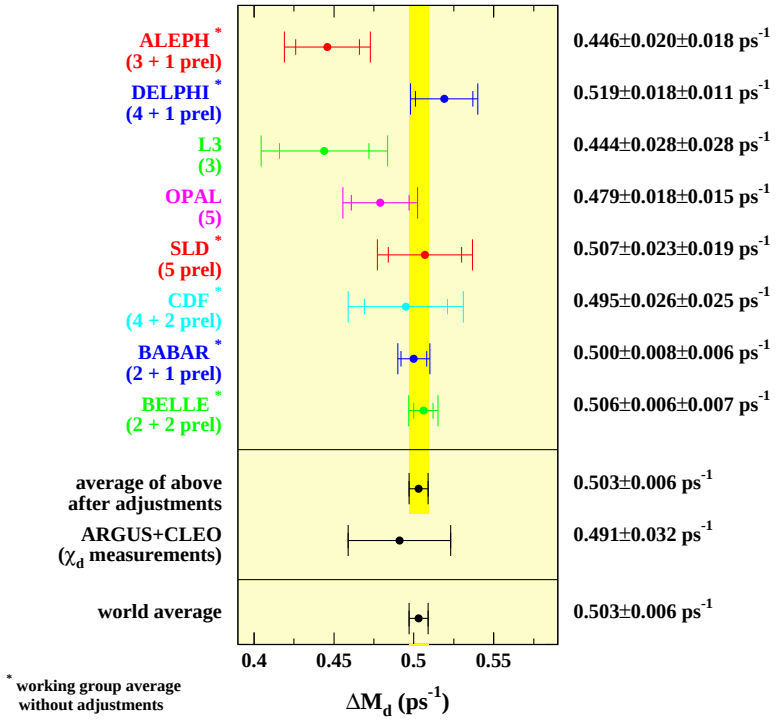

Fig. 4.16: *Combined measurements of ΔM_d averaged by experiment as of the ICHEP 2002 conference [87]. The quoted world average, at the bottom, also includes χ_d measurements by ARGUS and CLEO.*

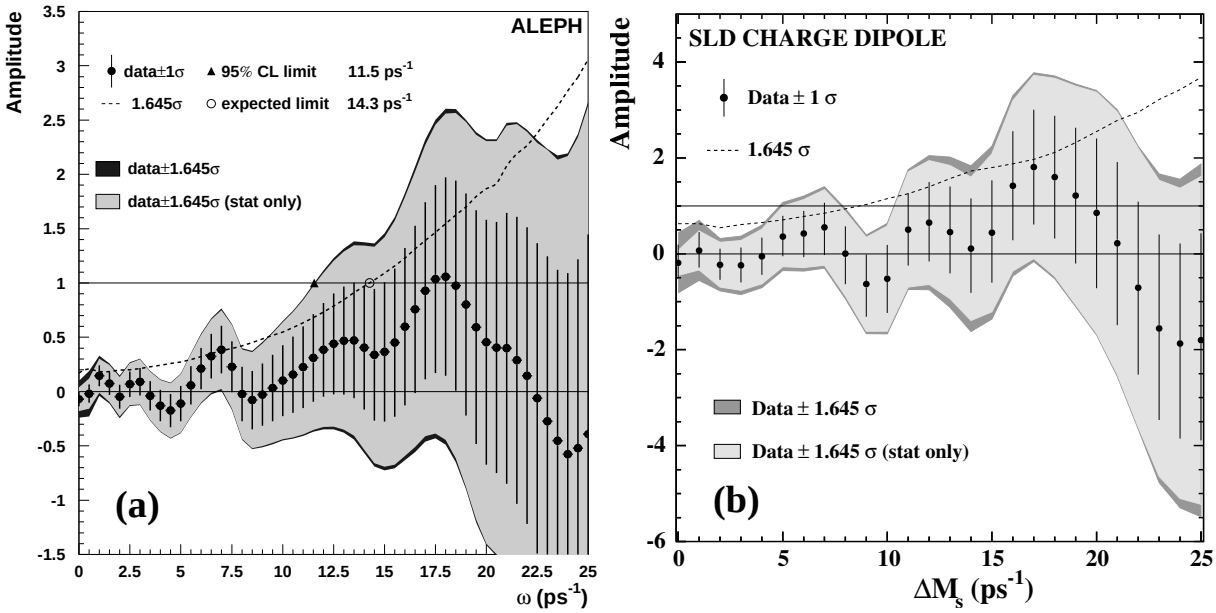

Fig. 4.17: *Examples of measured B_s^0 oscillation amplitudes as a function of the mixing frequency ΔM_s from (a) ALEPH (Ref. [124]) and (b) SLD (Ref. [131]). See text for details.*

Two examples of measured B_s^0 oscillation amplitudes as a function of the mixing frequency ΔM_s are shown in Fig. 4.17. The ALEPH collaboration recently presented an improved search for B_s^0 oscillations combining three analyses based on different final states [124]. First, fully reconstructed decays of B_s^0 mesons yield a small sample of B_s^0 candidates with excellent decay length and momentum resolution. Semileptonic decays with a reconstructed D_s^+ meson provide a second sample with larger statistics, high B_s^0 purity but with a poorer momentum and decay length resolution due to the partial decay reconstruction. Finally, semileptonic B hadron decays are inclusively selected and yield the data sample with the highest sensitivity to B_s^0 oscillations since the higher statistics compensates for the low average B_s^0 purity and the poorer proper time resolution. Fig. 4.17(a) shows the fitted amplitude spectrum as a function of ΔM_s for the third sample. From this inclusive semileptonic sample alone, ALEPH excludes all frequencies below 11.5 ps^{-1}, while the combined 95% C.L. limit from all three analyses yields $\Delta M_s > 10.9$ ps^{-1}.

Fig. 4.17(b) shows the amplitude spectrum from an analysis by SLD [131]. This analysis determined the B flavour at production time by exploiting the large forward-backward asymmetry of polarized $Z^0 \rightarrow b\bar{b}$ decays and uses additional information from the hemisphere opposite to that of the reconstructed B decay such as the jet charge, the lepton and kaon tags. The B flavour at decay is tagged by a charge dipole method as explained in Sec. 3.4.2. Although this analysis is based on only 11,000 decays, it reaches a sensitivity of 8.8 ps^{-1} because of the slower rise of the uncertainty on the amplitude due to the excellent proper time resolution.

No B_s^0 oscillation signal has been seen so far. The most sensitive analyses are the ones based on the inclusive lepton samples at LEP. Because of better proper time resolution, smaller data samples of inclusive decays analyzed at SLD as well as measurements using only a few fully reconstructed B_s^0 decays at LEP, turn out to be very useful to explore the high ΔM_s region. This point is illustrated in Fig. 4.18(a) showing the ΔM_s sensitivities for the different B_s^0 oscillation analysis methods. The uncertainty on the amplitude A (actually $1.645\,\sigma_A$) is plotted as a function of ΔM_s combining the existing results of the various B_s^0 analyses methods from different experiments. The combination of all fully inclusive methods crosses the dashed line corresponding to the condition $1.645\,\sigma_A = 1$ used to define the 95% C.L. sensitivity at about 9.5 ps^{-1}. This represents the combined sensitivity of all inclusive methods from the various experiments. Due to the combination of high statistics and adequate vertexing resolution, the inclusive lepton methods give currently the most sensitive results. The D_s^+-lepton samples also reach a high sensitivity while the exclusive methods that attempt to fully reconstruct hadronic B_s^0 decays have a lower sensitivity because of the small number of B_s^0 candidates that have been exclusively reconstructed to date. However, the slow growth of the amplitude error for the exclusive method can be inferred from Fig. 4.18(a). Note, the visible scattering of points for the exclusive method which results from the small number of events contributing in these analyses.

All available results on ΔM_s oscillations can be combined into a world average exclusion limit using the amplitude method. All data on the measurements of B_s^0 oscillation amplitudes versus ΔM_s, as provided by the experiments, are averaged to yield a combined amplitude A as a function of ΔM_s as shown in Fig. 4.18(b). The individual results have been adjusted to common physics inputs and all known correlations have been accounted for. The sensitivities of the inclusive analyses which depend on the assumed fraction, $f_{\mathrm{B}_s^0}$, of B_s^0 mesons have been re-scaled to a common average of $f_{\mathrm{B}_s^0} = 0.093 \pm 0.011$ (see Table 4.4). Figure 4.18(b) includes all results as of the ICHEP 2002 conference. The measurements are dominated by statistical uncertainties. Neighbouring points are statistically correlated. The combined result is [87]:

$$\boxed{\begin{array}{c}\Delta M_s > 14.4\ \mathrm{ps}^{-1}\ \text{at}\ 95\%\mathrm{C.L.} \\ \text{with a sensitivity of}\ \Delta\mathrm{M_s} = 19.2\ \mathrm{ps}^{-1}\end{array}} \tag{65}$$

Values between $14.4\,\mathrm{ps}^{-1}$ and $\sim 22\,\mathrm{ps}^{-1}$ cannot be excluded because the data appear to be compatible with a signal in this region. The amplitude plot presents a deviation from $A = 0$ at about $\Delta M_s \sim 17.5$ ps^{-1} for which a significance of $\sim 2.2\ \sigma$ can be derived. This means that there is not enough

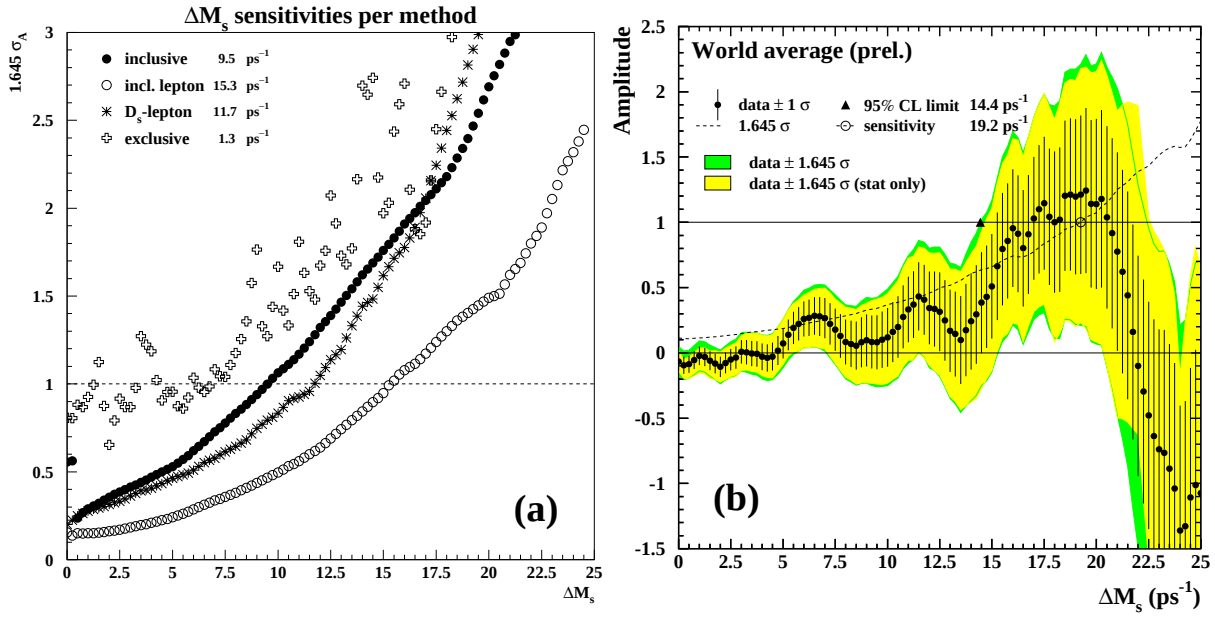

Fig. 4.18: *(a) Uncertainty ($1.645\,\sigma_A$) on the amplitude A as a function of ΔM_s for the various B_s^0 oscillation analyses. The dashed line corresponds to the condition $1.645\,\sigma_A = 1$ used to define the 95% C.L. sensitivity. (b) Combined measurements of the B_s^0 oscillation amplitude as a function of ΔM_s, including all results as of the ICHEP 2002 conference. Neighbouring points are statistically correlated.*

sensitivity for the observation of a B_s^0–$\overline{\mathrm{B}}_s^0$ signal at this frequency.

The different measurements of the B_s^0 oscillation amplitude as of the ICHEP 2002 conference are shown in Fig. 4.19, where the amplitudes for the various analyses are given at $\Delta M_s = 15$ ps^{-1} along with the relevant statistic and systematic errors. The exclusion sensitivities are also indicated Fig. 4.19 shows which analyses contribute most in the high ΔM_s region. Note that the individual measurements are quoted as in the original publications, but the averages include the effects of adjustments to a common set of input parameters.

Although all B_s^0 mixing results are presently limited by statistics, a discussion of systematic uncertainties in these analyses is relevant for a future measurement of B_s^0 oscillations. Critical analysis parameters (σ_L, σ_p and p_W) are extracted from detailed Monte Carlo simulation and are subject to modelling uncertainties. A first level of control is typically achieved with detailed comparisons between data and MC. In addition, measurements from calibration samples are performed to cross-check the parameters directly from the data but not all critical parameters can be tested in this manner. Of particular importance to the sensitivity at large ΔM_s values is the proper time resolution and, in particular, the decay length resolution. The latter has been tested with a variety of techniques: fit to the decay length distribution of τ decays, fit for the primary vertex in Z^0 decays to light-flavour quarks, study of tracks with negative impact parameter. These studies find that the decay length resolution is typically understood at the 10% level or better.

3.7. Future prospects for ΔM_d and ΔM_s determination

The current world average B_d^0 oscillation frequency constitutes a measurement at about 1% precision. It is dominated by the results of the B factories which will further improve the precision on Δm_d. The uncertainty on the B_d^0 lifetime starts to become a main contributor to the systematic error on future measurements of ΔM_d. A simultaneous fit of the B lifetime and ΔM_d will improve this situation as

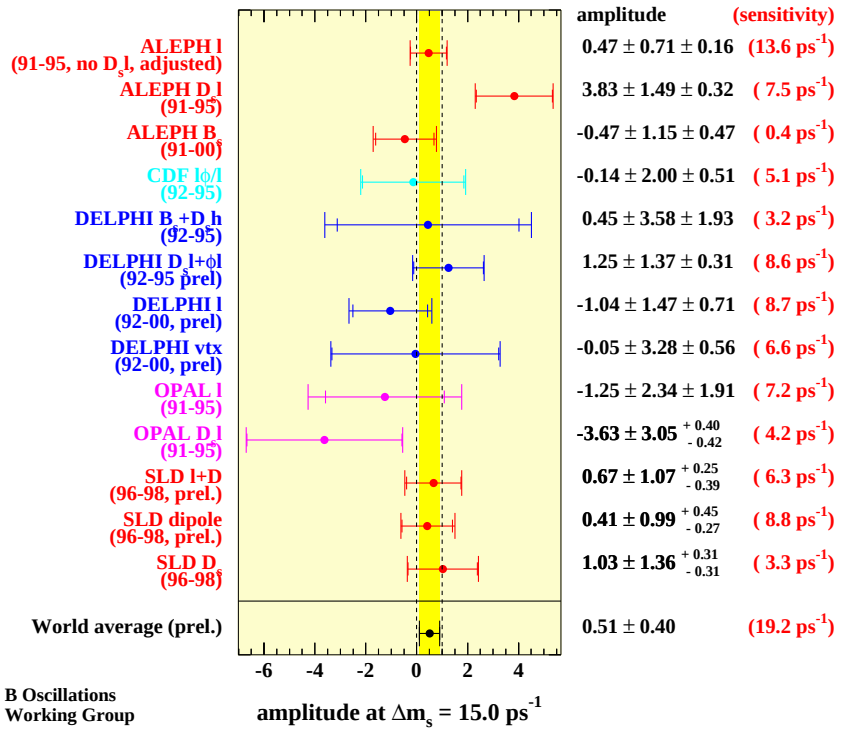

Fig. 4.19: *Measurements of the B_s^0 oscillation amplitude as of the ICHEP 2002 conference. The amplitudes are given at $\Delta M_s = 15\ ps^{-1}$ along with the relevant statistical and systematic errors. The exclusion sensitivities are indicated on the right, within in parentheses, The shaded area indicates the $\pm 1\ \sigma$ region on the average, and the dashed lines correspond to the values 0 and 1.*

demonstrated in Ref. [107]. For a data sample of 300 fb^{-1}, the BaBar and Belle experiments expect to improve the B_d^0 oscillation frequency by a factor two, down to a precision of about 0.4%

The future interest in B mixing clearly lies in a measurement of B_s^0 oscillations. Some of the still preliminary analyses from LEP and SLD are in the process of being finalized for publication while no new measurements or improved limits are to be expected. Since no B_s^0 mesons are produced at the B factories and running at the $\Upsilon(5S)$ resonance as a source of B_s^0 mesons is not foreseen in the near future, the hopes of the heavy flavour community focus on the Tevatron Collider experiments CDF and DØ to measure B_s^0 oscillations. For such a measurement it is important that the resolution of the vertexing device is good enough to resolve the expected (rapid) oscillations while a small boost correction will prevent the measured oscillations to damp out with proper time. The path to measure B_s^0 oscillations is therefore to use fully reconstructed B_s^0 mesons rather than higher statistics samples of partially reconstructed B_s^0 candidates from e.g. semileptonic decays.

A measurement of ΔM_s will be the next crucial test of the Standard Model probing whether the obtained result will fit to the current constraints on the CKM triangle which are all in beautiful agreement (see results in Chapter 5). It is noteworthy to mention that physics with B_s^0 mesons is unique to the Tevatron until the start of the LHC in 2007.

3.7.1. CDF and DØ detector upgrades in Run II at Tevatron

The Fermilab accelerator complex has undergone a major upgrade since the end of Run I in 1996. The centre-of-mass energy has been increased to 1.96 TeV and the Main Injector, a new 150 GeV proton storage ring, has replaced the Main Ring as injector of protons and anti-protons into the Tevatron. The Main Injector also provides higher proton intensity onto the anti-proton production target, with the goal

to allow for more than an order of magnitude higher luminosities. Run II officially started in March 2001. The design luminosity during the first phase of Run II (Run IIa) is 5-8·10^{31} cm^{-2}s^{-1} for a final integrated luminosity of ~ 2 fb^{-1} by the end of Run IIa.

Since 1996, the CDF and DØ detectors have also undergone major upgrades [138,139] to allow operation at high luminosities and bunch spacing of up to 132 ns. Details of the DØ detector upgrade can be found elsewhere [139]. The main upgrade for DØ is the installation of a tracking system contained in a 2T superconducting solenoid surrounded by a scintillator preshower detector. The tracking upgrade includes a silicon microstrip tracker which consists of six barrel segments with disks in between plus three more disks located at each end of the tracker. In addition, there are two large disks placed at the end of the silicon tracker to increase the pseudorapidity coverage. The silicon system is enclosed within a central fiber tracker providing momentum resolution at the level of $\sigma(p_T)/p_T = 0.02$-0.05 for low-p_T tracks with high tracking efficiency for charged particles with pseudo-rapidity $\eta < 2.5$. Vertex reconstruction is expected with a resolution of 15-30 μm in the $r\phi$-plane and about 80 μm in the rz-plane. A major upgrade of the muon system together with central and forward scintillators will allow DØ to trigger and reconstruct muon tracks. The B physics triggers at DØ allow to trigger on muons and electrons while a new Level 1 tracking trigger and a Level 2 silicon trigger are under construction.

The CDF detector improvements for Run II [138] were motivated by the shorter accelerator bunch spacing of up to 132 ns and the increase in luminosity by an order of magnitude. All front-end and trigger electronics has been significantly redesigned and replaced. A DAQ upgrade allows the operation of a pipelined trigger system. CDF's tracking devices were completely replaced. They consist of a new Central Outer Tracker (COT) with 30,200 sense wires arranged in 96 layers combined into four axial and four stereo superlayers. It also provides dE/dx information for particle identification. The Run II silicon vertex detector, covering a total radial area from 1.5-28 cm, consists of seven double sided layers and one single sided layer mounted on the beampipe. The silicon vertex detector covers the full Tevatron luminous region which has a RMS spread of about 30 cm along the beamline and allows for standalone silicon tracking up to a pseudo-rapidity $|\eta|$ of 2. The forward calorimeters have been replaced by a new scintillator tile based plug calorimeter which gives good electron identification up to $|\eta| = 2$. The upgrades to the muon system almost double the central muon coverage and extent it up to $|\eta| \sim 1.5$.

3.7.2. Prospects for B_s^0 mixing at CDF

The most important improvements for B physics at CDF are a Silicon Vertex Trigger (SVT) and a Time-of-Flight (ToF) system with a resolution of about 100 ps. The later employs 216 three-meter-long scintillator bars located between the outer radius of the COT and the superconducting solenoid. More details about the CDF II Time-of-Flight detector and its performance can be found in Ref. [140,141]. The ToF system will be most beneficiary for the identification of kaons with a 2 σ-separation between π and K for $p < 1.6$ GeV/c. This will enable CDF to make use of opposite side kaon tagging and allows to identify same side fragmentation kaons accompanying B_s^0 mesons [140,141].

In Run I, all B physics triggers at CDF were based on leptons including single and dilepton triggers. A newly implemented Silicon Vertex Trigger gives CDF access to purely hadronic B decays and makes CDF's B physics program fully competitive with the one at the e^+e^- B factories. The hadronic track trigger is the first of its kind operating successfully at a hadron collider. It works as follows: with a fast track trigger at Level 1, CDF finds track pairs in the COT with $p_T > 1.5$ GeV/c. At Level 2, these tracks are linked into the silicon vertex detector and cuts on the track impact parameter (e.g. $d > 100$ μm) are applied. The original motivation for CDF's hadronic track trigger was to select the two tracks from the rare decay $\mathrm{B}^0 \to \pi\pi$ but it will play a major role in collecting hadronic B_s^0 decays for the measurement of B_s^0 oscillations. Since the beginning of Run II, much work has gone into commissioning the CDF detector. The Silicon Vertex Trigger was fully operational at the beginning of 2002. A detailed discussion of the SVT and its initial performance can be found elsewhere [142,143].

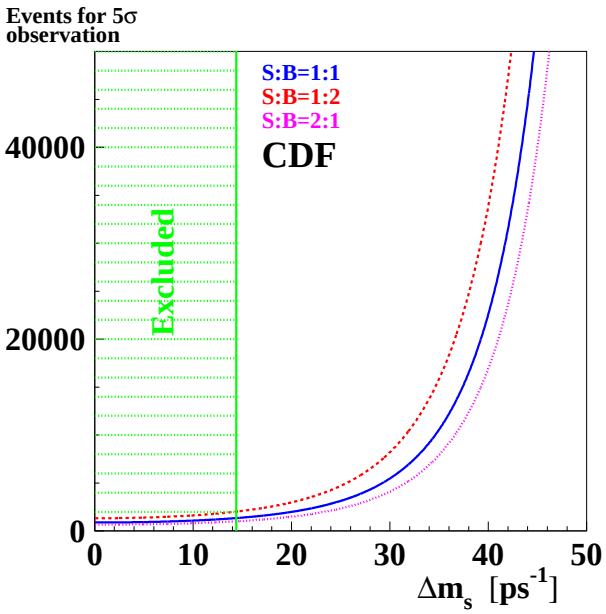

Fig. 4.20: *Expected event yield of fully reconstructed* B_s^0 *decays at CDF necessary for a* $5\,\sigma$*-observation of* B_s^0 *oscillations as a function of* ΔM_s *for different signal-to-background ratios.*

The CDF detector upgrades described above play an important role in CDF's prospects for measuring B_s^0 mixing. The inner layer of silicon mounted on the beampipe improves the time resolution for measuring the B_s^0 decay length from originally $\sigma_t = 0.060$ ps to 0.045 ps. This will be important if ΔM_s is unexpectedly large. The Time-of-Flight system will enhance the effectiveness of B flavour tagging, especially through same side tagging with kaons and opposite side kaon tagging, to a total expected $\varepsilon\mathcal{D}^2 \sim 11.3\%$ [144,141].

Fig. 4.20 shows the expected event yield of fully reconstructed B_s^0 decays necessary for a $5\,\sigma$ observation of B_s^0 oscillations as a function of the mixing frequency ΔM_s for different signal-to-background ratios. If the B_s^0 mixing frequency is around the current Standard Model expectation of $\Delta M_s \sim 18\mathrm{ps}^{-1}$ (see discussion in Sec. 6. of Chapter 5), Fig. 4.20 indicates that CDF would only need a few thousand fully reconstructed B_s^0 mesons to discover B_s^0 flavour oscillations. Originally, CDF estimated to fully reconstruct a signal of about 75,000 $\overline{\mathrm{B}}_s^0 \to \mathrm{D}_s^+\pi^-$ and $\overline{\mathrm{B}}_s^0 \to \mathrm{D}_s^+\pi^-\pi^+\pi^-$ events from the two-track hadronic trigger in 2 fb^{-1} [144]. This assumes all detector components and triggers work as expected. Although with the beginning of 2002, the CDF detector is in stable running conditions operating with reliable physics triggers, including the hadronic two-track trigger, there appear to be indications that the projected event yield might be overestimated. Given this and the small amount of data delivered by the Tevatron and recorded by CDF to date (about 100 pb^{-1} by the end of 2002) it will take some time until CDF can present first results on B_s^0 mixing [145].

3.7.3. Prospects for B_s^0 *mixing at DØ*

The major difference for a search of B_s^0 oscillations at DØ is the collection of B_s^0 candidate events. DØ currently does not operate a hadronic track trigger. However, it will be able to collect B_s^0 candidate events using lepton triggers. Various B_s^0 decay modes such as $\overline{\mathrm{B}}_s^0 \to \mathrm{D}_s^+\pi^-$, $\overline{\mathrm{B}}_s^0 \to \mathrm{D}_s^+\pi^-\pi^+\pi^-$ and $\overline{\mathrm{B}}_s^0 \to \mathrm{D}_s^+\ell^-\nu$ are under investigation by the DØ collaboration. The fully hadronic decay modes can be collected by single lepton triggers where the trigger lepton serves as an opposite side lepton tag and the B_s^0 meson is reconstructed on the other side. In this case the event yield is suppressed leaving DØ with a few thousand events of this type in a data sample of 2 fb^{-1}. If the B_s^0 oscillation frequency is

small enough, semileptonic B_s^0 decays can be used utilizing DØ's lepton trigger data. But due to the escaping neutrino, the boost resolution is reduced limiting the ΔM_s reach. DØ expects to collect about 40,000 events in the semileptonic channel in 2 fb^{-1}. Monte Carlo studies indicate that DØ will be able to measure B_s^0 oscillations in this mode up to a mixing frequency of $\Delta M_s \sim 20$ ps^{-1}.

4. Use of the amplitude spectrum for CKM fits

In this Section we discuss how to include ΔM_s information in CKM fits starting from the amplitude spectrum given by the LEP Oscillation Working Group [87].

The 95% C.L. limit and the sensitivity (see definition in Eq. (63)), are useful to summarize the results of the analysis. However to include ΔM_s in a CKM fit and to determine probability regions for the Unitarity Triangle parameters, continuous information about the degree of exclusion of a given value of ΔM_s is needed. We describe how to include this information in both Bayesian and frequentist approaches. The requirements for an optimal method are:

- the method should be independent of the significance of the signal: this criterion is important to avoid switching from one method to another because of the presence (absence) of a significant signal (whose definition is arbitrary);
- the probability regions derived should have correct coverage.

For the discussion in this Section we use the World Average computed by the LEP Oscillation Working Group [87] and presented a the CKM-Workshop, corresponding to a 95% C.L. lower limit at 15.0 ps^{-1} and to a sensitivity at 18.0 ps^{-1}.

In Sec. 4.1. we review and analyse how to include ΔM_s information for the CKM fits. Sec. 4.2. describes the newly-proposed frequentist method for including ΔM_s information in CKM fits.

4.1. Review of the available methods. The likelihood ratio method

Modified χ^2 method

The first CKM fits [146–148] used the χ^2 of the complete amplitude spectrum w.r.t. 1:

$$\chi^2 = \left(\frac{1-A}{\sigma_A}\right)^2 \tag{66}$$

The main drawback of this method is that the sign of the deviation of the amplitude with respect to the value $A = 1$ is not used. A signal might manifest itself by giving an amplitude value simultaneously compatible with $A = 1$ and incompatible with $A = 0$; in fact, with this method, values of $A > 1$ (but still compatible with $A = 1$) are disfavoured w.r.t. $A = 1$, while it is expected that, because of statistical fluctuations, the amplitude value corresponding to the "true" ΔM_s value could be higher than 1. This problem was solved, in the early days of using ΔM_s in CKM fits, by taking $A = 1$ whenever it was in fact higher.

A modified χ^2 has been introduced in [149] to solve the second problem:

$$\chi^2 = 2 \cdot \left[\mathrm{Erfc}^{-1}\left(\frac{1}{2}\mathrm{Erfc}\left(\frac{1-A}{\sqrt{2}\sigma_A}\right)\right)\right]^2 \tag{67}$$

Relation between the log-likelihood and the Amplitude

The log-likelihood values can be easily deduced from A and σ_A using the expressions given in [106]:

$$\Delta \log \mathcal{L}^{\infty}(\Delta M_s) \;=\; \frac{1}{2}\left[\left(\frac{A-1}{\sigma_A}\right)^2 - \left(\frac{A}{\sigma_A}\right)^2\right] = \left(\frac{1}{2} - A\right)\frac{1}{\sigma_A^2}\,, \tag{68}$$

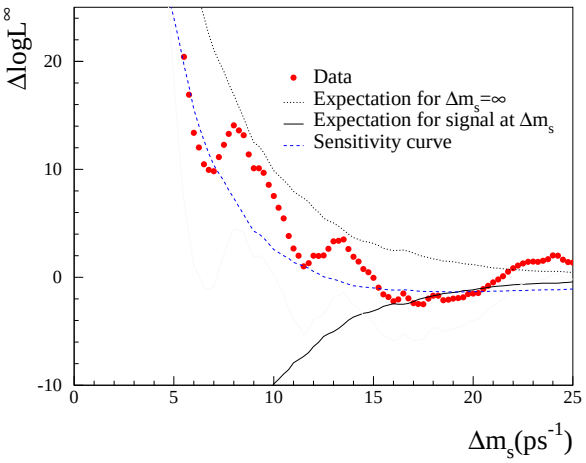

Fig. 4.21: *World average amplitude analysis:* $\Delta \log \mathcal{L}^{\infty}(\Delta M_s)$.

$$\Delta \log \mathcal{L}^{\infty}(\Delta M_s)_{\rm mix} = -\frac{1}{2}\frac{1}{\sigma_A^2}\,, \tag{69}$$

$$\Delta \log \mathcal{L}^{\infty}(\Delta M_s)_{\rm nomix} = \frac{1}{2}\frac{1}{\sigma_A^2}\,. \tag{70}$$

The last two equations give the average log-likelihood value for ΔM_s corresponding to the true oscillation frequency (mixing case) and for ΔM_s being far from the oscillation frequency ($|\Delta M_s - \Delta M_s^{\rm true}| \gg \Gamma/2$, no-mixing case). Γ is here the full width at half maximum of the amplitude distribution in case of a signal; typically $\Gamma \simeq 1/\tau_{\rm B_s^0}$. Fig. 4.21 shows the variation of $\Delta\mathcal{L}^{\infty}(\Delta M_s)$ corresponding to the amplitude spectrum of Fig. 4.18(b).

Likelihood ratio method R

Instead of the χ^2 or the modified χ^2 methods, the log-likelihood function $\Delta \log \mathcal{L}^{\infty}(\Delta M_s)$ can be used: this is the log-likelihood referenced to its value obtained for $\Delta M_s = \infty$ [150,151]. The log-likelihood values can easily be deduced from A and σ_A, in the Gaussian approximation, by using the expressions given in Eqs.(68), (69), (70). The Likelihood Ratio R, defined as,

$$\mathrm{R}(\Delta M_s) = e^{-\Delta \log \mathcal{L}^{\infty}(\Delta M_s)} = \frac{\mathcal{L}(\Delta M_s)}{\mathcal{L}(\Delta M_s = \infty)}\,, \tag{71}$$

has been adopted in [151] to incorporate the ΔM_s constraint.

Comparison between the two methods using the world average amplitude spectrum

The variation of the amplitude as a function of ΔM_s and the corresponding $\Delta \log \mathcal{L}^{\infty}(\Delta M_s)$ value are shown in Fig. 4.22-(a) and (b). The constraints obtained using the Likelihood Ratio method (R) and the Modified χ^2 method (χ^2) are shown in Fig. 4.22-(c). In this comparison the Modified χ^2 has been converted to a likelihood using $\mathcal{L} \propto \exp(-\chi^2/2)$. It is clear that the two methods (R and χ^2) give very different constraints. In particular the Modified χ^2 method, with the present World Average, corresponds to a looser constraint for CKM fits (and in particular for the determination of the $\bar{\rho}$ and γ parameters).

The toy Monte Carlo

In order to test and compare the statistical properties of the two methods it is necessary to generate several experiments having similar characteristics as the data used for the World Average. We will call

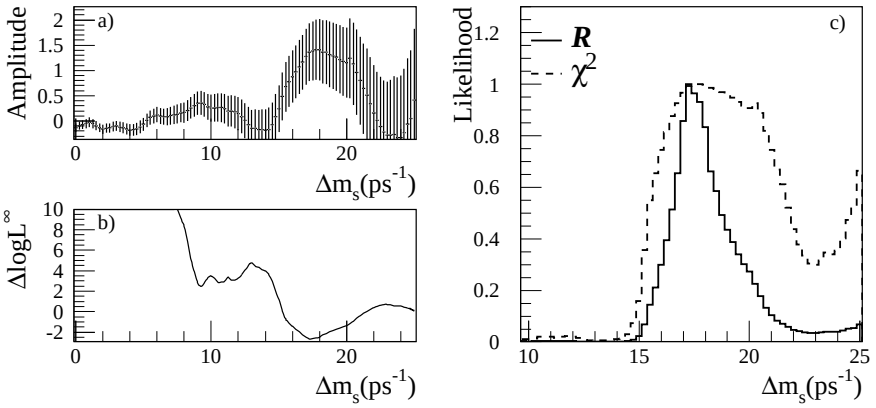

Fig. 4.22: *World Average amplitude analysis: (a) amplitude spectrum, (b) $\Delta \log \mathcal{L}^{\infty}(\Delta M_s)$, (c) comparison between the Likelihood Ratio method (R) and the Modified χ^2 method (χ^2). The information in (b) and in the solid histogram in (c) is identical.*

equivalent those experiments having the same dependence of σ_A as a function of ΔM_s.

The dependence of σ_A on ΔM_s can be reproduced by tuning the parameters of a fast simulation (toy-MC). The method used here is similar to the one presented in [152]. The error on the amplitude can be written as:

$$\sigma_A^{-1} = \sqrt{N}\,\eta_{\mathrm{B}_s^0}\,(2\epsilon_d - 1)\,(2\epsilon_p - 1)\,W(\sigma_L, \sigma_P, \Delta M_s) \tag{72}$$

where N is the total number of events, $\eta_{\mathrm{B}_s^0}$ the B_s^0 purity of the sample, $\epsilon_{d(p)}$ the tagging purity at the decay (production) time, σ_L the uncertainty on the B_s^0 flight length and σ_p the relative uncertainty in the B_s^0 momentum. W is the function that accounts for the damping of the oscillation due to the finite proper time resolution. The parameters σ_L, σ_p and the global factor that multiplies the W function are obtained by adjusting the simulated error distribution to the one measured with real events. Figure 4.23 shows the agreement between the toy-MC calculation and the real data up to $\Delta M_s = 25\,\mathrm{ps}^{-1}$ (the upper value of ΔM_s at which amplitudes are given). An additional problem is that, in principle, one would like to define the likelihood within the interval $[0, \infty]$ whereas the amplitude spectrum is measured only up to a certain value. For the present World Average the value is $25\,\mathrm{ps}^{-1}$. A procedure has to be introduced to continue σ_A and A.

The continuation for σ_A is shown in Fig.4.23. The continuation of A is more delicate. In particular it is more sensitive to the real amplitude spectrum. Nevertheless if $\Delta M_s^{\mathrm{sens}} << \Delta M_s^{\mathrm{last}}$, the significance S ($S = A/\sigma_A$) is approximately constant. It is then a good approximation to continue using:

$$A(\Delta M_s) = \frac{A(\Delta M_s^{\mathrm{last}})}{\sigma_A(\Delta M_s^{\mathrm{last}})}\sigma_A(\Delta M_s). \tag{73}$$

Although this procedure is reasonable, it should be stressed that it is very desirable to have all the amplitudes (with errors) up to the ΔM_s value where the significance remains stable.

Comparison of the methods in case of an oscillation signal

In this Section we compare the two methods in the presence of a clear ΔM_s oscillation signal. We perform several ΔM_s toy-MC analyses with the same σ_A versus ΔM_s behaviour as the World Average analysis. For this study we have generated a ΔM_s signal at $17\,\mathrm{ps}^{-1}$. This value corresponds to the value

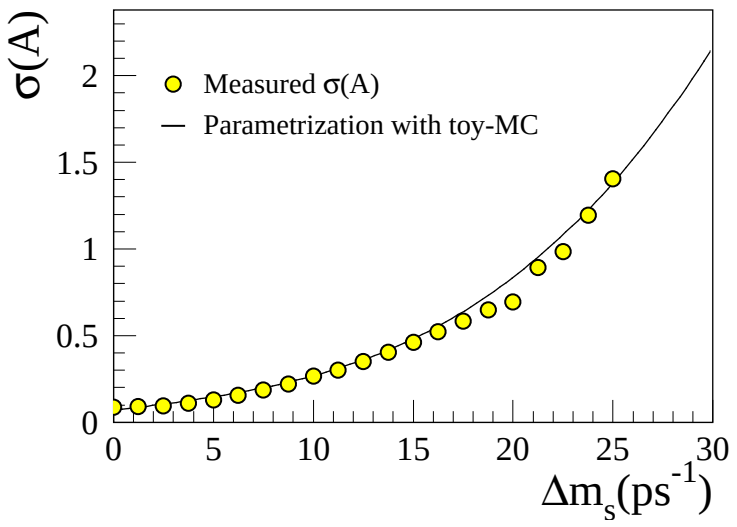

Fig. 4.23: *Comparison between the error distribution computed with the toy-MC (solid line) and the measured amplitude errors (circles).*

where there is the bump in the World Average amplitude spectrum. The statistics of the virtual experiments is much larger than the registered data, at present, so that clear oscillation signals are expected.

The results in Fig. 4.24 show that only the Likelihood Ratio method is able to see the signal at the correct ΔM_s value. The same exercise has been repeated for different generated values of ΔM_s, always giving the same result.

Test of the coverage of the two methods applied to CKM fits

In the absence of a clear B_s^0 oscillation signal, the Likelihood Ratio method results in a ΔM_s range which extends to infinity at any C.L. A criticism was made in [149] that it is then dangerous to use this information in a CKM fit. The best way to answer this objection is to test the coverage of the probability regions (68%, 95% and 99%) computed by the fit by performing a Monte Carlo simulation.

To do this we have prepared a simplified CKM fit where we measure the quantity R_t (see Chapter 1), using only the ΔM_d and the $\Delta M_d/\Delta M_s$ constraints. The set of constraints on the quantity R_t is:

$$\Delta M_d = a^2 R_t^2 \tag{74}$$

$$\Delta M_d/\Delta M_s = b^2 R_t^2 \qquad (\text{or } \Delta M_s = a^2/b^2) \tag{75}$$

where a and b are Gaussian distributed parameters with errors $\sigma_a = 20\%$ and $\sigma_b = 10\%$, thus taking into account the theoretical uncertainties.

Several experiments have been generated, each of them characterized by the following set of parameters:

R_t	
a_{theo}	extracted from the a distribution
b_{theo}	extracted from the b distribution
$\Delta M_d(\mathrm{theo})$	computed from R_t and a
$\Delta M_s(\mathrm{theo})$	computed from R_t and b
$\Delta M_d(\mathrm{exp})$	from $\Delta M_d(\mathrm{theo})$ smeared by the experimental resolution
Amplitude spectrum	from a toy-experiment generated with $\Delta M_s(\mathrm{theo})$

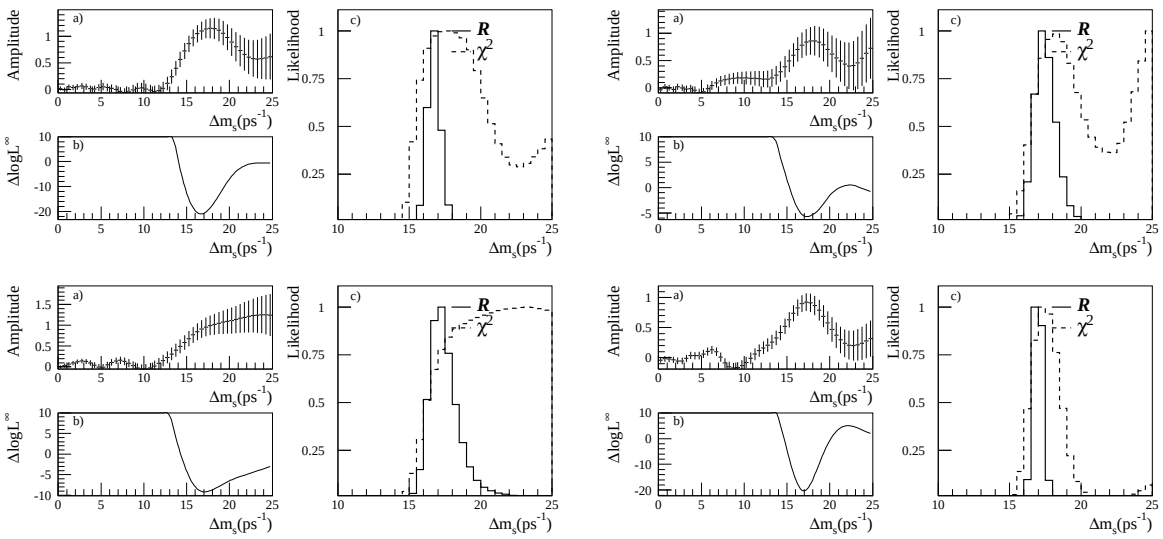

Fig. 4.24: *Toy-MC analyses with ΔM_s generated at $17\,\mathrm{ps}^{-1}$ corresponding to four virtual experiments. Each experiment is summarized in three plots: (a) amplitude spectrum, (b) $\Delta \log \mathcal{L}^{\infty}(\Delta M_s)$, (c) comparison between the Likelihood Ratio method (R) and the Modified χ^2 method (χ^2).*

	68%	95%	99%
$\Delta M_s = 10$	67.5 ± 1.5	93.1 ± 0.8	98.1 ± 0.4
$\Delta M_s = 18.2$	71.4 ± 1.4	96.1 ± 0.6	99.6 ± 0.2
$\Delta M_s = 25$	69.5 ± 1.5	96.4 ± 0.6	99.3 ± 0.3

Table 4.7: *Results obtained with the Likelihood Ratio method. For three different values of generated ΔM_s (left column) we indicate the percentage of "experiments" for which the generated true value of R_t falls inside the 68%, 95% and 99% probability interval.*

For each experiment the best-fit value for R_t was determined and it was counted how many times it fell inside the 68%, 95% and 99% probability regions defined by the Likelihood Ratio and by the Modified χ^2 methods. This exercise was repeated 1000 times. The measured frequencies for the three probability regions using the Likelihood Ratio or the Modified χ^2 method are given in Table 4.7 and 4.8 respectively.

For the Likelihood Ratio method the measured frequencies correspond to the confidence level intervals and the coverage is close to correct. This is not the case for the Modified χ^2 method where the confidence levels are significantly underestimated for the true value of ΔM_s. The effect stems from the fact that the χ^2 defined in Eq. 67 reaches its minimum systematically above the true value of ΔM_s.

Some conclusions

In this first part we have studied the problem of including in CKM fits the ΔM_s World Average amplitude spectrum. We have tested two different methods and compared the results in case of an oscillation signal. MC simulations also were performed for a CKM fit to test the coverage of the two methods. The conclusion is that the Likelihood Ratio method, proposed in [150,151], is optimal because it gives probability intervals with correct coverage and, in case of a signal, it also gives the correct value of ΔM_s.

	68%	95%	99 %
$\Delta M_s = 10$	48.6 ± 1.6	83.8 ± 1.2	94.3 ± 0.7
$\Delta M_s = 18.2$	64.6 ± 1.5	93.0 ± 0.8	99.2 ± 0.3
$\Delta M_s = 25$	77.5 ± 1.5	98.2 ± 0.4	99.7 ± 0.2

Table 4.8: *As for Table 4.7, but for the Modified χ^2 method.*

4.2. Use of the amplitude spectrum in a frequentist approach

The aim of this Section is to describe the frequentist method for incorporating experimental constraints derived from the amplitude spectrum as a function of the B_s^0 oscillation frequency (ΔM_s) into a global CKM fit. In other words, we address the questions: what is the pdf of a likelihood measurement of ΔM_s, and what is the confidence level (CL) as a function of ΔM_s to be associated with an observation obtained with a given level of sensitivity?

Infinite statistics

We assume that the x_s measurement is performed using the log-likelihood. The measured value of x_s ($x_\mathrm{s}^\mathrm{mes}$) is defined to be the one maximizing $\mathcal{L}(x_\mathrm{s})$: the outcome of one experiment $x_\mathrm{s}^\mathrm{mes}$ is a random number. For infinite statistics, the $x_\mathrm{s}^\mathrm{mes} = \Delta M_s \tau_b$ random number follows a (leading-order: lo) Gaussian probability density function:

$$\Phi_\mathrm{lo}^{x_\mathrm{s}}(x_\mathrm{s}^\mathrm{mes}) = \frac{1}{\sqrt{2\pi}\Sigma(x_\mathrm{s})} \exp\left(-\frac{1}{2}\left(\frac{x_\mathrm{s}^\mathrm{mes} - x_\mathrm{s}}{\Sigma(x_\mathrm{s})}\right)^2\right) \tag{76}$$

where the standard deviation $\Sigma(x_\mathrm{s})$ is given by the second derivative of the expected $\mathcal{L}$, through the integral A

$$(\sqrt{N}\Sigma(x_\mathrm{s}))^{-2} = \int_{-\infty}^{+\infty}\left(\frac{(\dot{\mathrm{P}}_-)^2}{\mathrm{P}_-} + \frac{(\dot{\mathrm{P}}_+)^2}{\mathrm{P}_+}\right)\mathrm{d}t_\mathrm{mes} \equiv \mathrm{A}(x_\mathrm{s}) \tag{77}$$

$$\dot{\mathrm{P}}_\pm = \frac{\partial \mathrm{P}_\pm}{\partial x_\mathrm{s}} = \mp f_\mathrm{s}\frac{1}{2} d\, t \sin(x_\mathrm{s} t) e^{-t} \otimes \mathrm{G_t} \tag{78}$$

N is the total number of mixed and unmixed events and the integrals are performed using the true value of x_s, not the measured one. It follows from Eq. (76) that one may set a confidence level $\mathrm{CL_{lo}}(x_\mathrm{s}^\mathrm{hyp})$ on a given hypothetical value $x_\mathrm{s}^\mathrm{hyp}$ using the χ^2 law:

$$\mathrm{CL_{lo}}(x_\mathrm{s}^\mathrm{hyp}) = \int_< \Phi_\mathrm{lo}^{x_\mathrm{s}^\mathrm{hyp}}(x_\mathrm{s}^{\mathrm{mes}\prime})\mathrm{d}x_\mathrm{s}^{\mathrm{mes}\prime} = \mathrm{Prob}(\chi^2, 1) \tag{79}$$

$$\chi \equiv \chi^{x_\mathrm{s}^\mathrm{hyp}}(x_\mathrm{s}^\mathrm{mes}) = \frac{x_\mathrm{s}^\mathrm{mes} - x_\mathrm{s}^\mathrm{hyp}}{\Sigma(x_\mathrm{s}^\mathrm{hyp})} \tag{80}$$

where the integral is performed over the $x_\mathrm{s}^{\mathrm{mes}\prime}$ domain where $\Phi_\mathrm{lo}^{x_\mathrm{s}^\mathrm{hyp}}(x_\mathrm{s}^{\mathrm{mes}\prime}) < \Phi_\mathrm{lo}^{x_\mathrm{s}^\mathrm{hyp}}(x_\mathrm{s}^\mathrm{mes})$, that is to say where $|\chi^{x_\mathrm{s}^\mathrm{hyp}}(x_\mathrm{s}^{\mathrm{mes}\prime})| > |\chi^{x_\mathrm{s}^\mathrm{hyp}}(x_\mathrm{s}^\mathrm{mes})|$.

If the log-likelihood is parabolic near its maximum, as is the case for infinite statistics, then, in the vicinity of $x_\mathrm{s}^\mathrm{mes}$, $\Sigma(x_\mathrm{s}^\mathrm{hyp}) \simeq \mathrm{cst} = \Sigma(x_\mathrm{s}^\mathrm{mes})$, and one can evaluate Σ as the second derivative of the experimental log-likelihood, taken at the measured value $x_\mathrm{s}^\mathrm{mes}$. In effect:

$$\frac{\partial^2 \mathcal{L}}{\partial {x_\mathrm{s}}^2}_{|x_\mathrm{s}=x_\mathrm{s}^\mathrm{mes}} = \sum_-\left(\frac{\ddot{\mathrm{P}}_-\mathrm{P}_- - (\dot{\mathrm{P}}_-)^2}{\mathrm{P}_-^2}\right)^2 + \sum_+\left(\frac{\ddot{\mathrm{P}}_+\mathrm{P}_+ - (\dot{\mathrm{P}}_+)^2}{\mathrm{P}_+^2}\right)^2 \tag{81}$$

$$\stackrel{N\to\infty}{=} \quad -N\mathrm{A}(x_\mathrm{s}) = -\Sigma^{-2} \tag{82}$$

where $\ddot{\mathrm{P}}_\pm$ denotes the second derivative with respect to x_s:

$$\ddot{\mathrm{P}}_\pm = \frac{\partial^2 \mathrm{P}_\pm}{\partial {x_\mathrm{s}}^2} = \mp f_\mathrm{s} \frac{1}{2} d\, t^2 \cos(x_\mathrm{s} t) e^{-t} \otimes \mathrm{G_t} \tag{83}$$

which does not appear in the final expression thanks to the normalization of the probability density function, and assuming that $x_\mathrm{s}^\mathrm{mes} = x_\mathrm{s}$ (which is true for infinite statistics).

Equivalently, one can evaluate Σ by locating the value of $x_\mathrm{s}^\mathrm{hyp}$ which yields a drop of $-1/2$ in the log-likelihood, for the experiment at hand, or one can compute the χ^2 directly using the approximation

$$\chi^2(x_\mathrm{s}^\mathrm{hyp}) = \left(\frac{x_\mathrm{s}^\mathrm{mes} - x_\mathrm{s}^\mathrm{hyp}}{\Sigma(x_\mathrm{s}^\mathrm{hyp})} \right)^2 \simeq 2(\mathcal{L}(x_\mathrm{s}^\mathrm{mes}) - \mathcal{L}(x_\mathrm{s}^\mathrm{hyp})) \equiv \tilde{\chi}^2(x_\mathrm{s}^\mathrm{hyp}) \tag{84}$$

Finite statistics

For large enough $x_\mathrm{s}^\mathrm{hyp}$, the approximation $\Sigma(x_\mathrm{s}^\mathrm{hyp}) \simeq \Sigma(x_\mathrm{s}^\mathrm{mes})$ breaks down since the sensitivity of the experiment vanishes: $\Sigma(x_\mathrm{s}^\mathrm{hyp}) \to \infty$ for $x_\mathrm{s}^\mathrm{hyp} \to \infty$. It follows that the likelihood is not parabolic for large enough $x_\mathrm{s}^\mathrm{hyp}$, however large the statistics.

The vanishing sensitivity makes χ^2, as defined by Eq. (80), a poor test statistic to probe for large x_s values. Furthermore, it is not a straightforward task to infer the correct $\mathrm{CL}(x_\mathrm{s}^\mathrm{hyp})$ from the χ^2 value: Eq. (79) does not apply (i.e., it is not a true χ^2) because Eq. (76) is a poor approximation**.

In the realistic case of finite statistics, the next-to-leading order statistical analysis of a likelihood measurement [153] is used here to obtain the key-formula expressing the probability density function of the random number $x_\mathrm{s}^\mathrm{mes}$ beyond the Gaussian approximation:

$$\Phi_\mathrm{nlo}^{x_\mathrm{s}}(x_\mathrm{s}^\mathrm{mes}) = \Phi_\mathrm{lo}^{x_\mathrm{s}}(x_\mathrm{s}^\mathrm{mes})\, e^{-{\mathrm{a_3}}^{x_\mathrm{s}} \chi^3} (1 + {\mathrm{a_0}}^{x_\mathrm{s}} \chi) \tag{85}$$

$${\mathrm{a_0}}^{x_\mathrm{s}} = \frac{2\mathrm{B} - \mathbb{C}}{2\mathrm{A}} \frac{1}{\sqrt{N\mathrm{A}}} = -\dot{\Sigma} \tag{86}$$

$${\mathrm{a_3}}^{x_\mathrm{s}} = \frac{3\mathrm{B} - \mathbb{C}}{6\mathrm{A}} \frac{1}{\sqrt{N\mathrm{A}}} \tag{87}$$

where $\mathrm{A}(x_\mathrm{s})$ is the integral defined in Eq. (77), $\mathrm{B}(\mathrm{x_s})$ and $\mathbb{C}(x_\mathrm{s})$ being two new integrals:

$$B(x_\mathrm{s}) = \int_{-\infty}^{+\infty} \left(\frac{\dot{\mathrm{P}}_- \ddot{\mathrm{P}}_-}{\mathrm{P}_-} + \frac{\dot{\mathrm{P}}_+ \ddot{\mathrm{P}}_+}{\mathrm{P}_+} \right) \mathrm{d}t_\mathrm{mes} \tag{88}$$

**The redefinition of the χ^2 using the right-hand side of Eq. (84) provides a test statistic more appropriate for large values of $x_\mathrm{s}^\mathrm{hyp}$. Although Eq. (79) does not apply, $\tilde{\chi}^2$ is capable of ruling out $x_\mathrm{s}^\mathrm{hyp}$ values lying beyond the sensitivity reach (if $\mathcal{L}(x_\mathrm{s}^\mathrm{mes})$ is large enough) provided one computes the CL using:

$$\mathrm{CL}(x_\mathrm{s}^\mathrm{hyp}) = \int_{\tilde{\chi}^2(x_\mathrm{s}^\mathrm{hyp})}^{\infty} \Psi^{x_\mathrm{s}^\mathrm{hyp}}(\tilde{\chi}^{2\prime})\, \mathrm{d}\tilde{\chi}^{2\prime}$$

where $\Psi^{x_\mathrm{s}^\mathrm{hyp}}$ is the probability density function of the $\tilde{\chi}^2$ test statistic, for $x_\mathrm{s} = x_\mathrm{s}^\mathrm{hyp}$, obtained using a toy Monte Carlo. The rejection of $x_\mathrm{s}^\mathrm{hyp}$ values beyond the sensitivity reach is not a paradox: it uses the fact that large values are unlikely to yield an indication of a clear signal, especially at low values of x_s. Such a treatment, as well as others (e.g., the minimum value of the likelihood could be used to define another test statistics) are satisfactory. We prefer here to use x_s^mes, and only this quantity, because an analytical expression for its probability density function is available (Eq. 85) and thus the computation of the CL can be carried out in practice. This is nothing but the standard choice made when dealing with better defined measurements.

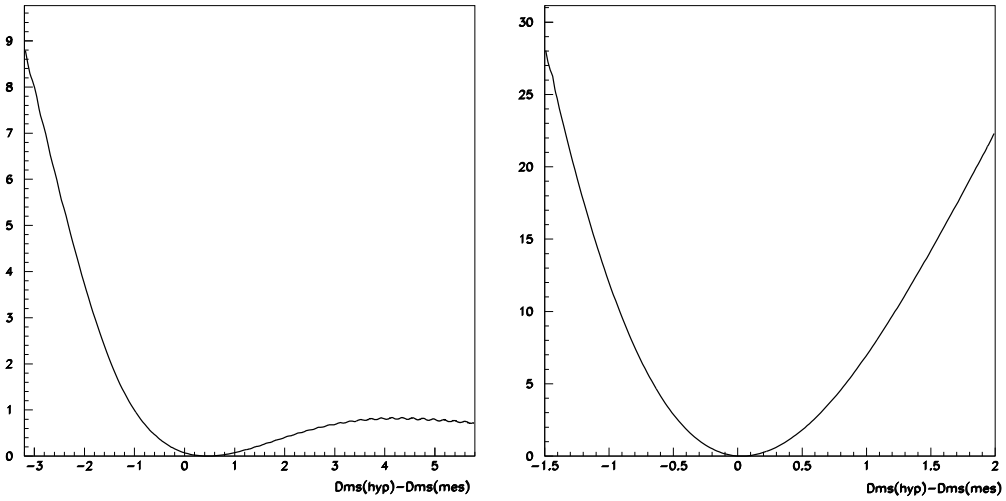

Fig. 4.25: *Left Plot: The equivalent χ^2 (cf. Eq. (79)) expressing the confidence levels computed using the next-to-leading order expression Eq. (85) in the actual situation where the maximum value of the likelihood is reached for $\Delta M_s(\mathrm{mes}) = 17.2\,\mathrm{ps}^{-1}$. The horizontal axis is the difference $\Delta M_s(\mathrm{hypothetical}) - \Delta M_s(\mathrm{mes})$. The minimum value of the equivalent χ^2 is not reached for $\Delta M_s(\mathrm{hypothetical}) = \Delta M_s(\mathrm{mes})$ because the maximum of the next-to-leading order probability density function is slightly shifted below the true ΔM_s value. The left hand side of the plot is nearly parabolic and resembles closely the one that a simplistic interpretation of the likelihood curve provides. The right hand side of the plot states that there is almost no constraint on high values of ΔM_s. One is far from dealing with a measurement in the usual (Gaussian) sense. Right Plot: The equivalent χ^2 in the would-be situation where the maximum value of the likelihood is reached for $\Delta M_s(\mathrm{mes}) = 10\,\mathrm{ps}^{-1}$. Although the equivalent χ^2 is not truly parabolic, the Gaussian limit is almost reached: one is close to dealing with a measurement in the usual (Gaussian) sense.*

$$C(x_\mathrm{s}) \;=\; \int_{-\infty}^{+\infty} \left(\frac{(\dot{\mathrm{P}}_-)^3}{\mathrm{P}_-^2} + \frac{(\dot{\mathrm{P}}_+)^3}{\mathrm{P}_+^2} \right) \mathrm{d}t_\mathrm{mes} \tag{89}$$

The integral ℂ tends to be small because, on the one hand the two contributions have opposite signs, and on the other hand the denominator is of order two: it follows that $\mathrm{a}_3 \simeq \mathrm{a}_0/2$. The right hand side of Eq. (86) links the next-to-leading order correction terms a_0 and a_3 to the dependence on x_s of Σ. When Σ depends significantly on x_s, not only is the standard treatment of Sec. 4.2. invalid, but the well-known formula Eq. (79) itself becomes incorrect, even if one uses the correct $\Sigma(x_\mathrm{s})$.

The expression Eq. (85) is identical to Eq. (76) for small χ values. Although it extends the range of validity to larger χ values, it cannot be trusted too far away from the origin, where higher order corrections start to play a role. In particular, Φ_nlo becomes negative (hence meaningless) for $\chi > -{\mathrm{a}_0}^{-1}$ (a_0 is negative since it is equal to minus the derivative of Σ with respect to x_s). Since Φ is sizable only when $\chi \sim \mathcal{O}(1)$ the next-to-leading order terms, when relevant, are of the form $N^{-\frac{1}{2}} \times (\mathrm{ratio\ of\ integrals})$: they are negligible for large enough N and for small enough ratio of integrals. The double-sided CL is computed as in Eq. (79), replacing Φ_lo by the next-to-leading order approximation. Using the right hand side of Eq. (79) to translate the confidence level thus obtained into a more familiar equivalent[††] χ^2, one obtains the results shown in Fig. (4.25) in two cases: first for the actual situation using the parametrization of the world average likelihood as described in Sec. 4.1. where the maximum of the likelihood is

[††] In the CKMfitter package, it is this equivalent χ^2 which is added to the overall χ^2.

reached at the boundary of the experimental sensitivity; second for a hypothetical situation where the maximum of the likelihood would be reached well within the sensitivity region.

In conclusion, we have presented a frequentist analysis of the B_s oscillation. Its domain of validity extends to the level of sensitivity reached by LEP and SLD. The treatment presented here provides, in a frequentist approach, a practical means to incorporate into a CKM fit the information on ΔM_s contained in the data, both present and future.

References

[1] A.J. Buras, M. Jamin and P.H. Weisz, Nucl. Phys. B **347** (1990) 491.

[2] A.J. Buras, W. Slominski and H. Steger, Nucl. Phys. B **245** (1984) 369.

[3] S. Herrlich and U. Nierste, Nucl. Phys. B **419** (1994) 292, [hep-ph/9310311].

[4] S. Herrlich and U. Nierste, Phys. Rev. D **52** (1995) 6505, [hep-ph/9507262].

[5] S. Herrlich and U. Nierste, Nucl. Phys. B **476** (1996) 27, [hep-ph/9604330].

[6] M. Jamin and U. Nierste (2003). Recent update for this document.

[7] E. de Rafael, in Proceedings of TASI 1994 (1995), hep-ph/9502254.

[8] J. Urban, F. Krauss, U. Jentschura and G. Soff, Nucl. Phys. B **523** (1998) 40, [hep-ph/9710245].

[9] M. Ciuchini *et al.*, JHEP **07** (2001) 013, [hep-ph/0012308].

[10] C. Bernard *et al.*, Nucl. Phys. Proc. Suppl. **106** (2002) 412, [hep-lat/0110072].

[11] MILC Collaboration, C. Bernard *et al.*, hep-lat/0209163.

[12] C. Bernard *et al.*, in Proceedings of Lattice 2002 (2002) hep-lat/0209086.

[13] M.J. Booth, Phys. Rev. D **51** (1995) 2338, [hep-ph/9411433].

[14] A.S. Kronfeld and S.M. Ryan, Phys. Lett. B **543** (2002) 59, [hep-ph/0206058].

[15] JLQCD Collaboration, N. Yamada *et al.*, Nucl. Phys. Proc. Suppl. **106** (2002) 397, [hep-lat/0110087].

[16] N. Yamada, in Proceedings of 20th Int. Symp. on Lattice Field Theory, Lattice 2002, Boston, June 2002 (2002) hep-lat/0210035.

[17] MILC Collaboration, C. Bernard *et al.*, Phys. Rev. D **66** (2002) 094501, [hep-lat/0206016].

[18] D. Becirevic, S. Fajfer, S. Prelovsek and J. Zupan, hep-ph/0211271.

[19] S.R. Sharpe and Y. Zhang, Phys. Rev. D **53** (1996) 5125, [hep-lat/9510037].

[20] A.V. Manohar and M.B. Wise, Heavy Quark Physics, vol. 10 of Cambridge Monographs on Particle Physics, Nuclear Physics and Cosmology (Cambridge University Press, 2000).

[21] CLEO Collaboration, S. Ahmed *et al.*, Phys. Rev. Lett. **87** (2001) 251801, [hep-ex/0108013].

[22] UKQCD Collaboration, G.M. de Divitiis *et al.*, JHEP **10** (1998) 010, [hep-lat/9807032].

[23] A. Abada *et al.*, hep-lat/0209092.

[24] JLQCD Collaboration, S. Hashimoto *et al.*, hep-lat/0209091.

[25] L. Lellouch, in Proceedings of ICHEP 2002, 31st Int. Conf. on High Energy Physics, Amsterdam, July 2002, hep-ph/0211359.

[26] D. Becirevic *et al.*, Nucl. Phys. B **618** (2001) 241, [hep-lat/0002025].

[27] UKQCD Collaboration, L. Lellouch and C.J.D. Lin, Phys. Rev. D **64** (2001) 094501, [hep-ph/0011086].

[28] UKQCD Collaboration, K.C. Bowler *et al.*, Nucl. Phys. B **619** (2001) 507, [hep-lat/0007020].

[29] A.X. El-Khadra *et al.*, Phys. Rev. D **58** (1998) 014506, [hep-ph/9711426].

[30] CP-PACS Collaboration, A. Ali Khan *et al.*, Phys. Rev. D **64** (2001) 034505, [hep-lat/0010009].

[31] A. Ali Khan *et al.*, Phys. Lett. B **427** (1998) 132, [hep-lat/9801038].

[32] S. Collins *et al.*, Phys. Rev. D **60** (1999) 074504, [hep-lat/9901001].

[33] JLQCD Collaboration, K.I. Ishikawa *et al.*, Phys. Rev. D **61** (2000) 074501, [hep-lat/9905036].

[34] CP-PACS Collaboration, A. Ali Khan *et al.*, Phys. Rev. D **64** (2001) 054504, [hep-lat/0103020].

[35] C.W. Bernard, T. Blum and A. Soni, Phys. Rev. D **58** (1998) 014501, [hep-lat/9801039].

[36] M.A. Shifman, A.I. Vainshtein and V.I. Zakharov, Nucl. Phys. B **147** (1979) 385.

[37] M.A. Shifman, A.I. Vainshtein and V.I. Zakharov, Nucl. Phys. B **147** (1979) 448.

[38] A.A. Penin and M. Steinhauser, Phys. Rev. D **65** (2002) 054006, [hep-ph/0108110].

[39] M. Jamin and B.O. Lange, Phys. Rev. D **65** (2002) 056005, [hep-ph/0108135].

[40] S. Narison, Phys. Lett. B **520** (2001) 115, [hep-ph/0108242].

[41] P. Colangelo and A. Khodjamirian, hep-ph/0010175.

[42] K.G. Chetyrkin and M. Steinhauser, Phys. Lett. B **502** (2001) 104, [hep-ph/0012002].

[43] K.G. Chetyrkin and M. Steinhauser, Eur. Phys. J. C **21** (2001) 319, [hep-ph/0108017].

[44] M. Jamin, Phys. Lett. B **538** (2002) 71, [hep-ph/0201174].

[45] A.X. El-Khadra and M. Luke, hep-ph/0208114.

[46] A.A. Ovchinnikov and A.A. Pivovarov, Phys. Lett. B **207** (1988) 333.

[47] L.J. Reinders and S. Yazaki, Phys. Lett. B **212** (1988) 245.

[48] S. Narison and A.A. Pivovarov, Phys. Lett. B **327** (1994) 341, [hep-ph/9403225].

[49] K. Hagiwara, S. Narison and D. Nomura, Phys. Lett. B **540** (2002) 233, [hep-ph/0205092].

[50] V. Chernyak, Nucl. Phys. B **457** (1995) 96 [hep-ph/9503208].

[51] N. Cabibbo, G. Martinelli and R. Petronzio, Nucl. Phys. B **244** (1984) 381.

[52] R.C. Brower, G. Maturana, M. Belen Gavela and R. Gupta, Phys. Rev. Lett. **53** (1984) 1318.

[53] C.W. Bernard, in Proceedings of Gauge Theory On A Lattice, Argonne (1984), p. 85.

[54] C.W. Bernard *et al.*, Phys. Rev. Lett. **55** (1985) 2770.

[55] M.B. Gavela *et al.*, Nucl. Phys. B **306** (1988) 677.

[56] Staggered Collaboration, G. Kilcup, R. Gupta and S.R. Sharpe, Phys. Rev. D **57** (1998) 1654, [hep-lat/9707006].

[57] JLQCD Collaboration, S. Aoki *et al.*, Phys. Rev. Lett. **80** (1998) 5271, [hep-lat/9710073].

[58] SPQCDR Collaboration, D. Becirevic *et al.*, [hep-lat/0209136].

[59] CP-PACS Collaboration, A. Ali Khan *et al.*, Phys. Rev. D **64** (2001) 114506, [hep-lat/0105020].

[60] RBC Collaboration, T. Blum *et al.*, hep-lat/0110075.

[61] MILC Collaboration, T. DeGrand, hep-lat/0208054.

[62] GGHLR Collaboration, N. Garron *et al.*, hep-lat/0212015.

[63] T. Blum and A. Soni, Phys. Rev. Lett. **79** (1997) 3595, [hep-lat/9706023].

[64] M. Guagnelli *et al.*, hep-lat/0110097.

[65] N. Ishizuka *et al.*, Phys. Rev. Lett. **71** (1993) 24.

[66] G. Kilcup, Phys. Rev. Lett. **71** (1993) 1677.

[67] S. Sharpe, Nucl. Phys. Proc. Suppl. **53** (1997) 181, [hep-lat/9609029].

[68] J. Bijnens, H. Sonoda and M.B. Wise, Phys. Rev. Lett. **53** (1984) 2367.

[69] S.R. Sharpe, Phys. Rev. D **46** (1992) 3146, [hep-lat/9205020].

[70] S.R. Sharpe, hep-ph/9412243.

[71] M.F.L. Golterman and K.C. Leung, Phys. Rev. D **57** (1998) 5703, [hep-lat/9711033].

[72] J. Prades *et al.*, Z. Phys. C **51** (1991) 287.

[73] M. Jamin and A. Pich, Nucl. Phys. B **425** (1994) 15, [hep-ph/9402363].

[74] S. Narison, Phys. Lett. B **351** (1995) 369, [hep-ph/9409428].

[75] L.J. Reinders and S. Yazaki, Nucl. Phys. B **288** (1987) 789.

[76] N. Bilic, C.A. Dominguez and B. Guberina, Z. Phys. C **39** (1988) 351.

[77] W. Bardeen, A. Buras and J.M. Gérard, Phys. Lett. **211** (1988) 343.

[78] T. Hambye, G.O. Köhler and P.H. Soldan, Eur. Phys. J. C **10** (1999) 271, [hep-ph/9902334].

[79] S. Peris and E. de Rafael, Phys. Lett. B **490** (2000) 213, [hep-ph/0006146].

[80] J. Bijnens and J. Prades, J. High Energy Phys. **01** (2000) 002, [hep-ph/9909244].

[81] S. Bertolini, J.O. Eeg, M. Fabbrichesi and E.I. Lashin, Nucl. Phys. B **514** (1998) 63, [hep-ph/9705244].

[82] A.J. Buras, M. Jamin and P.H. Weisz, Nucl. Phys. B **347** (1990) 491.

[83] J.F. Donoghue, E. Golowich and B.R. Holstein, Phys. Lett. B **119** (1982) 412.

[84] LEP/SLD Electroweak Working Group, CERN-EP/2001-021.

[85] LEP/SLD/CDF Collaborations, CERN-EP/2001-050.

[86] DELPHI Collaborations, EPS-HEP99, contributed paper 5.515.

[87] The LEP B Oscillation Working Group, http://www.cern.ch/LEPBOSC/.

[88] M. Gronau, A. Nippe and J.L. Rosner, Phys. Rev. D **47** (1993) 1988, [hep-ph/9211311].

[89] CDF Collaboration, F. Abe *et al.*, Phys. Rev. Lett. **80** (1998) 2057, [hep-ex/9712004].

[90] CDF Collaboration, F. Abe *et al.*, Phys. Rev. D **59** (1999) 032001, [hep-ex/9806026].

[91] P.C. Rowson, D. Su and S. Willocq, Ann. Rev. Nucl. Part. Sci. **51** (2001) 345, [hep-ph/0110168].

[92] SLD Collaboration (1996). SLAC-PUB-7228, contribution to ICHEP96 Warsaw.

[93] SLD Collaboration, K. Abe *et al.*, SLAC-PUB-7229, contribution to ICHEP96 Warsaw.

[94] SLD Collaboration, SLAC-PUB-7230, contribution to ICHEP96 Warsaw.

[95] J.L. Wittlin (2001). Ph.D. thesis, SLAC-R-582.

[96] ALEPH Collaboration, R. Barate *et al.*, Eur. Phys. J. C **4** (1998) 367.

[97] ALEPH Collaboration, R. Barate *et al.*, Eur. Phys. J. C **7** (1999) 553, [hep-ex/9811018].

[98] DELPHI Collaboration, P. Abreu *et al.*, Eur. Phys. J. C **18** (2000) 229, [hep-ex/0105077].

[99] DELPHI Collaboration, P. Abreu *et al.*, Eur. Phys. J. C **16** (2000) 555, [hep-ex/0107077].

[100] OPAL Collaboration, K. Ackerstaff *et al.*, Z. Phys. C **76** (1997) 417, [hep-ex/9707010].

[101] OPAL Collaboration, K. Ackerstaff *et al.*, Z. Phys. C **76** (1997) 401, [hep-ex/9707009].

[102] J. Thom, SLAC-R-585 (2002).

[103] CDF Collaboration, M. Paulini, Int. J. Mod. Phys. A **14** (1999) 2791, [hep-ex/9903002].

[104] BABAR Collaboration, B. Aubert *et al.*, Phys. Rev. Lett. **87** (2001) 091801, [hep-ex/0107013].

[105] Belle Collaboration, K. Abe *et al.*, Phys. Rev. Lett. **87** (2001) 091802, [hep-ex/0107061].

[106] H.G. Moser and A. Roussarie, Nucl. Instrum. Meth. A **384** (1997) 491.

[107] BABAR Collaboration, B. Aubert *et al.*, Phys. Rev. Lett. **88** (2002) 221802, [hep-ex/0112044].

[108] Belle Collaboration, T. Tomura *et al.*, Phys. Lett. B **542** (2002) 207, [hep-ex/0207022].

[109] BABAR Collaboration, B. Aubert *et al.*, [hep-ex/0212017].

[110] Belle Collaboration, K. Hara *et al.* Phys. Rev. Lett. **89** (2002) 251803, [hep-ex/0207045].

[111] CDF Collaboration, T. Affolder *et al.*, Phys. Rev. D **60** (1999) 112004, [hep-ex/9907053].

[112] OPAL Collaboration, G. Alexander *et al.*, Z. Phys. C **72** (1996) 377.

[113] ALEPH Collaboration, D. Buskulic *et al.*, Z. Phys. C **75** (1997) 397.

[114] DELPHI Collaboration, P. Abreu *et al.*, Z. Phys. C **76** (1997) 579.

[115] OPAL Collaboration, G. Abbiendi *et al.*, Phys. Lett. B **493** (2000) 266, [hep-ex/0010013].

[116] Belle Collaboration, Y. Zheng *et al.*, to appear in Phys. ReV. D, [hep-ex/0211065].

[117] CDF Collaboration, F. Abe *et al.*, Phys. Rev. D **60** (1999) 051101.

[118] CDF Collaboration, F. Abe *et al.*, Phys. Rev. D **60** (1999) 072003, [hep-ex/9903011].

[119] L3 Collaboration, M. Acciarri *et al.*, Eur. Phys. J. C **5** (1998) 195.

[120] BABAR Collaboration, B. Aubert *et al.*, Phys. Rev. Lett. **88** (2002) 221803, [hep-ex/0112045].

[121] Belle Collaboration, N. Hastings *et al.*,to appear in Phys. Rev. D, [hep-ex/0212033].

[122] DELPHI Collaboration, J. Abdallah *et al.*, CERN-EP-2002-078.

[123] ALEPH Collaboration, D. Buskulic *et al.*, ALEPH-97/027, contribution to EPS-HEP97 Jerusalem.

[124] ALEPH Collaboration, A. Heister *et al.*, CERN-EP-2002-016.

[125] CDF Collaboration, F. Abe *et al.*, Phys. Rev. Lett. **82** (1999) 3576.

[126] DELPHI Collaboration, J. Abdallah *et al.* DELPHI 2002-073, contribution to ICHEP 2002 Amsterdam.

[127] OPAL Collaboration, G. Abbiendi *et al.*, Eur. Phys. J. C **19** (2001) 241, [hep-ex/0011052].

[128] SLD Collaboration, K. Abe *et al.*, Phys. Rev. D **66** (2002) 032009, [hep-ex/0207048].

[129] OPAL Collaboration, G. Abbiendi *et al.*, Eur. Phys. J. C **11** (1999) 587, [hep-ex/9907061].

[130] SLD Collaboration, K. Abe *et al.*, SLAC-PUB-8568, [hep-ex/0012043].

[131] SLD Collaboration, K. Abe *et al.*, Phys. Rev. D **67** (2003) 012006, [hep-ex/0209002].

[132] ARGUS Collaboration, H. Albrecht *et al.*, Z. Phys. C **55** (1992) 357.

[133] ARGUS Collaboration, H. Albrecht *et al.*, Phys. Lett. B **324** (1994) 249.

[134] CLEO Collaboration, J. Bartelt *et al.*, Phys. Rev. Lett. **71** (1993) 1680.

[135] CLEO Collaboration, B.H. Behrens *et al.*, Phys. Lett. B **490** (2000) 36, [hep-ex/0005013].

[136] DELPHI Collaboration, W. Adam *et al.*, Phys. Lett. B **414** (1997) 382.

[137] Particle Data Group Collaboration, K. Hagiwara *et al.*, Phys. Rev. D **66** (2002) 010001.

[138] CDF-II Collaboration, R. Blair *et al.*, FERMILAB-PUB-96-390-E.

[139] D0 Collaboration, J. Ellison, prepared for 15th International Workshop on High-Energy Physics and Quantum Field Theory (QFTHEP 2000), Tver, Russia, 14-20 Sep 2000.

[140] S. Cabrera *et al.*, Nucl. Instrum. Meth. A **494** (2002) 416.

[141] C. Grozis *et al.*, hep-ex/0209027.

[142] CDF Collaboration, A. Cerri, presented at 31st International Conference on High Energy Physics (ICHEP 2002), Amsterdam, The Netherlands, 24-31 Jul 2002.

[143] CDF Collaboration, D. Lucchesi, presented at Beauty 2002: 8th International Conference on B Physics at Hadron machines, Santiago de Compostela, Spain, 17-21 Jun 2002.

[144] K. Anikeev *et al.*, hep-ph/0201071.

[145] CDF Collaboration, M. Paulini, hep-ex/0302016.

[146] P. Paganini, F. Parodi, P. Roudeau and A. Stocchi, Phys. Scripta **58** (1998) 556, [hep-ph/9711261].

[147] Y. Grossman, Y. Nir, S. Plaszczynski and M.H. Schune, Nucl. Phys. B **511** (1998) 69, [hep-ph/9709288].

[148] F. Parodi, P. Roudeau and A. Stocchi, Nuovo Cim. A **112** (1999) 833, [hep-ex/9903063].

[149] A. Hoecker, H. Lacker, S. Laplace and F. Le Diberder, Eur. Phys. J. C **21** (2001) 225, [hep-ph/0104062].

[150] P. Checchia, E. Piotto and F. Simonetto (1999), hep-ph/9907300.

[151] M. Ciuchini *et al.*, JHEP **07** (2001) 013, [hep-ph/0012308].

[152] G. Boix and D. Abbaneo, JHEP **08** (1999) 004, [hep-ex/9909033].

[153] R.N. Cahn, Private communication.

Chapter 5

FIT OF THE UNITARITY TRIANGLE PARAMETERS

Conveners : A.J. Buras, F. Parodi.
Contributors : M. Ciuchini, G. Dubois-Felsmann, G. Eigen, P. Faccioli, E. Franco, A. Hocker, D. Hitlin, H. Lacker, S. Laplace, F. LeDiberder, V. Lubicz, G. Martinelli, F. Porter, P. Roudeau, L. Silvestrini, A. Stocchi, M. Villa

1. Introduction

In this Chapter we will discuss the determination of the Unitarity Triangle (UT) using as input the values of $|V_{us}|$, $|V_{cb}|$, and $|V_{ub}|$ from Chapters 2 and 3 and the constraints from ε_K and $\Delta M_{d,s}$ with the values of the non-perturbative parameters $\hat{B}_K$, $F_{B_d}\sqrt{\hat{B}_{B_d}}$, $F_{B_s}\sqrt{\hat{B}_{B_s}}$ and ξ determined in Chapter 4. We will also include in this analysis the most recent results for the CP asymmetry in $\mathrm{B}_d \to J/\psi \mathrm{K}_S$ that allows to determine the angle β of the UT essentially without any theoretical uncertainty. The list of the common quantities which have been used for the analyses performed in this Chapter are summarised in Table 5.1.

A very important issue in constraining the apex $(\bar{\varrho}, \bar{\eta})$ of the UT is the treatment of the experimental and especially the theoretical uncertainties. In the literature five different approaches can be found: Gaussian approach [1], Bayesian approach [2], frequentist approach [3], 95% C.L. scan method [4] and the simple (naive) scanning within one standard deviation. Moreover the fact that different authors often use different input parameters makes the comparison of various analyses very difficult.

This situation is clearly unsatisfactory as different analyses give generally different allowed ranges for $(\bar{\varrho}, \bar{\eta})$. While all these analyses find presently the SM consistent with all the available data, the situation may change in the future when the experimental and theoretical uncertainties will be reduced and additional decays relevant for the determination of the UT will be available.

It is then conceivable that some approaches will find the SM consistent with the data whereas other will claim an indication for new physics contributions. This clearly would be rather unfortunate. However, even in the absence of new physics contributions, the increasing accuracy of the data and the expected reduction of theoretical uncertainties calls for an extensive comparison of the different methods to gain the best understanding on the UT.

Another important issue is the sensitivity of the UT analysis to theoretical uncertainties. Some theoretical parameters have more impact on this analysis than others and it is important to identify those for which the reduction of errors through improved non-perturbative calculations can contribute to the quality of the determination of the UT most efficiently.

Parameter	Value	Gaussian σ	Theory uncertainty
λ	0.2240(0.2210)	0.0036 (*0.0020*)	-
$\|V_{cb}\|$ $(\times 10^{-3})$ (excl.)	42.1	2.1	-
$\|V_{cb}\|$ $(\times 10^{-3})$ (incl.)	41.4 (*40.4*)	0.7	0.6(*0.8*)
$\|V_{ub}\|$ $(\times 10^{-4})$ (excl.)	33.0(*32.5*)	2.4(*2.9*)	4.6(*5.5*)
$\|V_{ub}\|$ $(\times 10^{-4})$ (incl.)	40.9	4.6	3.6
ΔM_d (ps^{-1})	0.503 (*0.494*)	0.006 (*0.007*)	-
ΔM_s (ps^{-1})	$>$ 14.4 (*14.9*) at 95% C.L.	sensitivity 19.2 (*19.3*)	
m_t (GeV)	167	5	-
m_c (GeV)	1.3	-	0.1
$F_{B_d}\sqrt{\hat{B}_{B_d}}$(MeV)	223 (*230*)	33 (*30*)	12 (*15*)
$\xi = \frac{F_{B_s}\sqrt{\hat{B}_{B_s}}}{F_{B_d}\sqrt{\hat{B}_{B_d}}}$	1.24(1.18)	0.04 (*0.03*)	0.06 (*0.04*)
$\hat{B}_K$	0.86	0.06	0.14
sin 2β	0.734 (*0.762*)	0.054 (*0.064*)	-

Table 5.1: *Latest values of the relevant quantities entering into the expressions of ϵ_K, ΔM_d and ΔM_s. In the third and fourth columns the Gaussian and the flat part of the uncertainty are given, respectively. The values within parentheses are the ones available at the time of the Workshop and used when comparing different fitting procedures. In case of asymmetric theoretical errors, like for $|V_{ub}|$ exclusive, the central values have been shifted to make them symmetric.*

The goals of this Chapter are:

- to describe in some detail two of the most developed methods: the Bayesian approach and the frequentist approach,
- to compare the resulting allowed regions for $(\bar{\varrho}, \bar{\eta})$ obtained from the Bayesian and frequentist approaches for the same input parameters,
- to identify those non-perturbative parameters for which the reduction of the uncertainty is most urgent.

This Chapter is organized as follows. In Section 2. we express the constraints from $|V_{ub}/V_{cb}|$, ε_K and $\Delta M_{d,s}$ in terms of Wolfenstein parameters [5] including the generalization of [6]. The Bayesian method and the frequentist methods are discussed in Sections 3.1. and 3.2., respectively. The discussion in the frequentist case includes the *R*fit and the scanning methods. In Section 4. the impact of the uncertainties of theoretical parameters on the determination of the UT is discussed in detail using both the Bayesian approach and the scanning method. Finally in Section 5. we compare the Bayesian and *R*fit methods and draw conclusions. In Section 6. we show some important results obtained in testing the consistency of the CKM picture of the Standard Model.

2. Constraints on the Unitarity Triangle parameters

Five measurements restrict at present the range of $(\bar{\varrho}, \bar{\eta})$ within the SM:

- The $|V_{ub}|$ constraint:

The length of the side AC of the UT (see Fig. 5.1) is determined from

$$R_b = \sqrt{\bar{\varrho}^2 + \bar{\eta}^2} = (1 - \frac{\lambda^2}{2})\frac{1}{\lambda}\left|\frac{V_{ub}}{V_{cb}}\right|. \tag{1}$$

The constraint in the $(\bar{\varrho}, \bar{\eta})$ plane resulting from (1) is represented by a circle of radius R_b that is centered at $(\bar{\varrho}, \bar{\eta}) = (0, 0)$ (for the visualisation of this and following constraints see Fig. 5.1).

- The ε_K–constraint:

$$\bar{\eta}\left[(1-\bar{\varrho})A^2\eta_2 S(x_t) + P_c(\varepsilon)\right] A^2 \hat{B}_K = 0.187 \left(\frac{0.224}{\lambda}\right)^{10}, \tag{2}$$

that follows from the experimental value for ε_K and the formula (Eq. (12) of Chapter 4). Here

$$P_c(\varepsilon) = [\eta_3 S_0(x_c, x_t) - \eta_1 x_c]\frac{1}{\lambda^4}, \qquad x_t = \frac{m_{\rm t}^2}{M_{\rm W}^2}. \tag{3}$$

$P_c(\varepsilon) = 0.29 \pm 0.07$ [7] summarizes the contributions of box diagrams with two charm quark exchanges and the mixed charm-top exchanges. We observe a very strong dependence of the r.h.s. in (2) on the parameter $\lambda = |V_{us}|$. However, this dependence is cancelled to a large extent by the λ dependence of $P_c(\varepsilon)$ and of $A = |V_{cb}|/\lambda^2$ that enter the l.h.s of (2). The main uncertainties in the constraint (2) reside then in $\hat{B}_K$ and to some extent in the factor A^4 or equivalently $|V_{cb}|^4$ which multiplies the dominant term. The status of $\hat{B}_K$ has been reviewed in Chapter 4. Eq. (2) specifies an hyperbola in the $(\bar{\varrho}, \bar{\eta})$ plane. This hyperbola intersects the circle found from the $|V_{ub}|$ constraint in two points which correspond to two solutions for the angle γ.

- The ΔM_d–constraint:
The length R_t of the side AB of the UT (see Fig. 5.1) can be determined from the observed $\mathrm{B}_d^0 - \overline{\mathrm{B}}_d^0$ mixing, parametrized by ΔM_d and given in Eq. 22 (in Chapter 4), with the result

$$R_t = \sqrt{(1-\bar{\varrho})^2 + \bar{\eta}^2} = \frac{1}{\lambda}\frac{|V_{td}|}{|V_{cb}|} = 0.85 \cdot \left[\frac{|V_{td}|}{7.8 \cdot 10^{-3}}\right]\left[\frac{0.041}{|V_{cb}|}\right] \tag{4}$$

where

$$|V_{td}| = 7.8 \cdot 10^{-3}\left[\frac{230\mathrm{MeV}}{\sqrt{F_{B_d}\hat{B}_{B_d}}}\right]\sqrt{\frac{\Delta M_d}{0.50/\mathrm{ps}}}\sqrt{\frac{0.55}{\eta_B}}\sqrt{\frac{2.34}{S_0(x_t)}}\,. \tag{5}$$

Since $m_{\rm t}$, ΔM_d and η_B are already rather precisely known, the main uncertainty in the determination of R_t and $|V_{td}|$ from $\mathrm{B}_d^0 - \overline{\mathrm{B}}_d^0$ mixing comes from $F_{B_d}\sqrt{\hat{B}_{B_d}}$. Its theoretical status has been reviewed in Chapter 4. R_t suffers from additional uncertainty in $|V_{cb}|$. The constraint in the $(\bar{\varrho}, \bar{\eta})$ plane resulting from (4) is represented by a circle of radius R_t that is centered at $(\bar{\varrho}, \bar{\eta}) = (1, 0)$.

- The $\Delta M_d/\Delta M_s$–constraint:
The measurement of $\mathrm{B}_s^0 - \overline{\mathrm{B}}_s^0$ mixing parametrized by ΔM_s together with ΔM_d allows to determine R_t in a different manner:

$$R_t = \frac{1}{\lambda}\xi\sqrt{\frac{M_{\mathrm{B}_s}}{M_{\mathrm{B}_d}}}\sqrt{\frac{\Delta M_s}{\Delta M_d}}(1 - \frac{\lambda^2}{2} + \bar{\varrho}\lambda^2), \qquad \xi = \frac{F_{B_s}\sqrt{\hat{B}_s}}{F_{B_d}\sqrt{\hat{B}_d}}\,. \tag{6}$$

This constraint follows from Eq. (22) (in Chapter 4) with the factor $(1 - \lambda^2/2 + \bar{\varrho}\lambda^2)$ representing the departure of $|V_{ts}/V_{cb}|$ from unity. For $0 \le \bar{\varrho} \le 0.5$ this factor deviates from unity by less than 2%. Neglecting this correction gives ($\lambda = 0.224$)

$$R_t = 0.86\sqrt{\frac{\Delta M_d}{0.50/\mathrm{ps}}}\sqrt{\frac{18.4/\mathrm{ps}}{\Delta M_s}}\left[\frac{\xi}{1.18}\right]. \tag{7}$$

The advantage of determining R_t by means of the ratio $\Delta M_d/\Delta M_s$ with respect to the ΔM_d constraint are smaller hadronic uncertainties in ξ than in $F_{B_d}\sqrt{\hat{B}_d}$ and the absence of m_t and $|V_{cb}|$ dependence. The present status of ξ has been reviewed in Chapter 4.

- The $a(\psi K_S)$–constraint:
  The mixing induced CP asymmetry $a_{\psi K_S}$ in $\mathrm{B} \to \psi \mathrm{K_S}$ allows to determine the angle β of the UT essentially without any hadronic uncertainties through

$$(\sin 2\beta)_{\psi K_S} = 0.734 \pm 0.054 \ . \tag{8}$$

  The value given in (8) is the world average from [8] and is dominated by the results of the BaBar [9] and Belle [10] Collaborations.

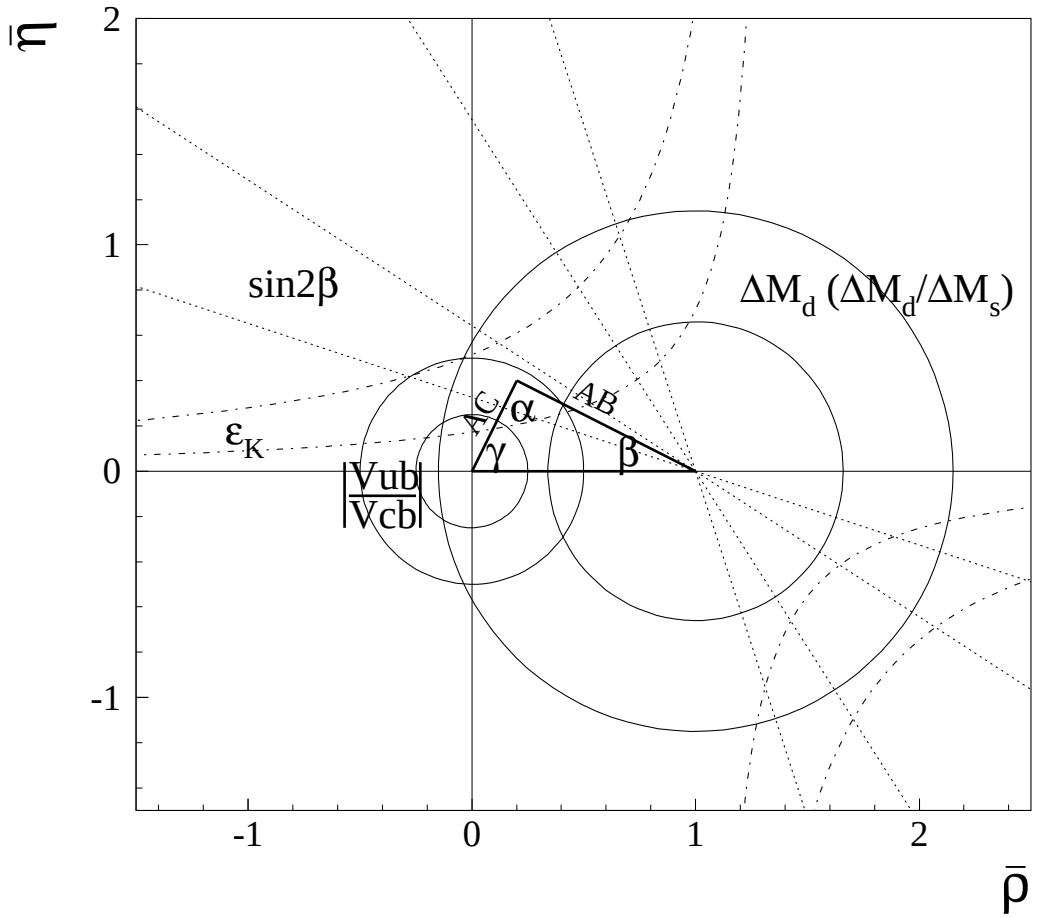

Fig. 5.1: *Constraints which are contributing to the Unitarity Triangle parameter determination.*

3. Statistical methods for CKM fits

In this Section we describe the basic ingredients for the different statistical approaches. The plots and the results presented here have to be taken as illustrations of the methods. Quantitative results and comparisons are given in the next Sections.

3.1. Bayesian methods

In this Section we describe the basic ingredients of the Bayesian approach and discuss the role of the systematic and theoretical uncertainties in deriving probability intervals for the relevant parameters.

Each of Eqs. (1, 2, 4, 6, 8) relates a constraint c_j to the parameters $\bar{\rho}$ and $\bar{\eta}$, via the set of additional parameters $\mathbf{x}$, where $\mathbf{x} = \{x_1, x_2, \ldots, x_N\}$ stand for all experimentally determined or theoretically calculated quantities on which the various c_j depend ($m_t,\ \xi$ ...)

$$c_j = c_j(\bar{\rho}, \bar{\eta}; \mathbf{x}). \tag{9}$$

In an ideal case of exact knowledge of c_j and $\mathbf{x}$, each of the constraints provides a curve in the $(\bar{\rho}, \bar{\eta})$ plane. In a realistic case, the analysis suffers from several uncertainties on the quantities c_j and $\mathbf{x}$. This means that, instead of a single curve (9) in the $(\bar{\rho}, \bar{\eta})$ plane, we have a family of curves which depends on the distribution of the set $\{c_j, \mathbf{x}\}$. As a result, the points in the $(\bar{\rho}, \bar{\eta})$ plane get different weights (even if they were taken to be equally probable *a priori*) and the *confidence* on the values of $\bar{\rho}$ and $\bar{\eta}$ clusters in a region of the plane.

The above arguments can be formalized by using the so called Bayesian approach (see [11] for an introduction). In this approach, the uncertainty is described in terms of a probability density function (pdf) which quantifies the confidence on the values of a given quantity. Applying Bayes Theorem in the case of a single constraint we obtain

$$\begin{aligned} f(\bar{\rho}, \bar{\eta}, c_j, \mathbf{x} \,|\, \hat{c}_j) &\propto f(\hat{c}_j \,|\, c_j, \bar{\rho}, \bar{\eta}, \mathbf{x}) \cdot f(c_j, \bar{\rho}, \bar{\eta}, \mathbf{x}) &(10)\\ &\propto f(\hat{c}_j \,|\, c_j) \cdot f(c_j \,|\, \bar{\rho}, \bar{\eta}, \mathbf{x}) \cdot f(\mathbf{x}, \bar{\rho}, \bar{\eta}) &(11)\\ &\propto f(\hat{c}_j \,|\, c_j) \cdot \delta(c_j - c_j(\bar{\rho}, \bar{\eta}, \mathbf{x})) \cdot f(\mathbf{x}) \cdot f_\circ(\bar{\rho}, \bar{\eta})\,, &(12) \end{aligned}$$

where $\hat{c}_j$ is the experimental best estimate of c_j and $f_\circ(\bar{\rho}, \bar{\eta})$ denotes the *prior* distribution.

The various steps follow from probability rules, by assuming the independence of the different quantities and by noting that $\hat{c}_j$ depends on ($\bar{\rho}, \bar{\eta}, \mathbf{x}$) only via c_j. This is true since c_j is unambiguously determined, within the Standard Model, from the values of $\bar{\rho}$, $\bar{\eta}$ and $\mathbf{x}$.

The extension of the formalism to several constraints is straightforward. We can rewrite Eq. (10) as

$$f(\bar{\rho}, \bar{\eta}, \mathbf{x} \,|\, \hat{c}_1, ..., \hat{c}_{\rm M}) \;\propto\; \prod_{j=1,{\rm M}} f_j(\hat{c}_j \,|\, \bar{\rho}, \bar{\eta}, \mathbf{x}) \times \prod_{i=1,{\rm N}} f_i(x_i) \times f_\circ(\bar{\rho}, \bar{\eta})\,. \tag{13}$$

M and N run over the constraints and the parameters respectively. In the derivation of (13), we have used the independence of the different quantities. By integrating Eq. (13) over $\mathbf{x}$ we obtain

$$f(\bar{\rho}, \bar{\eta} \,|\, \hat{\mathbf{c}}, \mathbf{f}) \propto \mathcal{L}(\hat{\mathbf{c}} \,|\, \bar{\rho}, \bar{\eta}, \mathbf{f}) \times f_\circ(\bar{\rho}, \bar{\eta})\,, \tag{14}$$

where $\hat{\mathbf{c}}$ stands for the set of measured constraints, and

$$\mathcal{L}(\hat{\mathbf{c}} \,|\, \bar{\rho}, \bar{\eta}, \mathbf{f}) = \int \prod_{j=1,{\rm M}} f_j(\hat{c}_j \,|\, \bar{\rho}, \bar{\eta}, \mathbf{x}) \prod_{i=1,{\rm N}} f_i(x_i)\, {\rm d}x_i \tag{15}$$

is the effective overall likelihood which takes into account all possible values of x_j, properly weighted. We have written explicitly that the overall likelihood depends on the best knowledge of all x_i, described by $f(\mathbf{x})$. Whereas *a priori* all values for $\bar{\rho}$ and $\bar{\eta}$ are considered equally likely ($f_\circ(\bar{\rho}, \bar{\eta})$=cst), *a posteriori* the probability clusters around the point which maximizes the likelihood.

In conclusion, the final (unnormalized) pdf obtained starting from a uniform pdf for $\bar{\rho}$ and $\bar{\eta}$ is

$$f(\bar{\rho}, \bar{\eta}) \propto \int \prod_{j=1,{\rm M}} f_j(\hat{c}_j \,|\, \bar{\rho}, \bar{\eta}, \mathbf{x}) \prod_{i=1,{\rm N}} f_i(x_i)\, {\rm d}x_i\,. \tag{16}$$

The integration can be performed by Monte Carlo methods and the normalization is trivial. Starting from the pdf for $\bar{\rho}$ and $\bar{\eta}$, probability regions $P(w)$ are defined by the conditions:

$$\begin{array}{l} (\bar{\rho}, \bar{\eta}) \in P(w) \text{ if } f(\bar{\rho}, \bar{\eta}) \;>\; z_w \\ \int_{P(w)} f(\bar{\rho}, \bar{\eta}) d\bar{\rho} d\bar{\eta} = w \end{array}$$

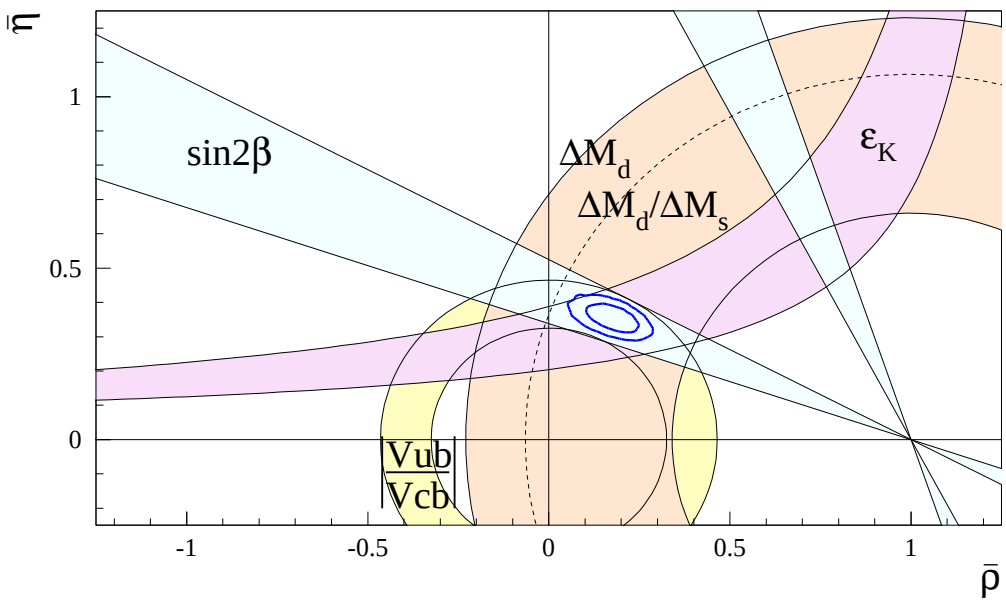

Fig. 5.2: *The contours at 68%, 95% probability regions in $\bar{\rho}$ and $\bar{\eta}$ as obtained using the Bayesian method, superimposed to the experimental constraints.*

An example of the typical output of this fit approach is shown in Fig. 5.2 where the probability regions at 68% and 95% are shown together with the experimental constraints.

It is important to note that this method does not make any distinction on whether the individual likelihood associated with some constraint is different from zero only in a narrow region (and we usually refer to this case as "measurement"), or if it goes to zero only on one side (e.g. when $c_j \to \infty$ or 0). In the latter case, the data only provide an upper/lower bound to the value of the constraint. This is precisely what happens, at present, with ΔM_s. Therefore, the experimental information about this constraint enters naturally in the analysis.

One of the feature of the Bayesian approach is that there is no conceptual distinction between the uncertainty due to random fluctuations, which might have occurred in the measuring process, the uncertainty about the parameters of the theory, and the uncertainty about systematics of not-exactly-known value, which can be both of experimental or theoretical origin (in the Bayesian jargon there are often indicated as influence parameters).

We can simply extend the notation to include in $\mathbf{x}$ these influence parameters responsible for the systematic uncertainty, and use Eq. (15) in an extended way. Irrespectively of the assumptions made on the pdf of $\mathbf{x}$, the overall likelihoods $f(\hat{c}_j)$ are approximately Gaussian because of a mechanism similar to the central limit theorem (i.e. just a matter of combinatorics). This makes the results largely stable against variations within choices of the distributions used to describe the uncertainties due to theory or systematics. For this reason we simplify the problem, by reducing the choice to only two possibilities. We choose a Gaussian model when the uncertainty is dominated by statistical effects, or there are many comparable contributions to the systematic errors, so that the central limit theorem applies ($\mathcal{G}(x - x_0)$). We choose a uniform pdf if the parameter is believed to be (almost) certainly in a given interval, and the points inside this interval are considered as equally probable. The second model is applied to some theoretical uncertainties. $\mathcal{U}(x) = 1/2\sigma_{\rm theo}$ for $x \in [x_0 - \sigma_{\rm theo}, x_0 + \sigma_{\rm theo}]$ and $\mathcal{U}(x) = 0$ elsewhere. The combined pdf $\mathcal{P}$ is then obtained by convoluting the Gaussian pdf $\mathcal{G}$ with the uniform pdf $\mathcal{U}$: $\mathcal{P} = \mathcal{G} \otimes \mathcal{U}$. When several determinations of the same quantity are available, the final p.d.f, in the Bayesian approach, is obtained by the product of the single pdfs.

An important point is how to evaluate the compatibility among individual constraints. In the CKM fits based on χ^2 minimization, a conventional evaluation of compatibility stems automatically from the value of the χ^2 at its minimum.

The compatibility between constraints in the Bayesian method is evaluated by comparing partial pdfs obtained when removing each constraint at a time. The integral over the overlap between the pdf with and without a given constraint quantifies the compatibility. In case of poor overlap the difference Δ_j between the two pdfs can be determined, for each constraint c_j, by substituting

$$c_j \to c_j(1 + \Delta_j). \tag{17}$$

Further investigation (based on physics and not on statistics) will be necessary to tell if the difference Δ_j comes from an incorrect evaluation of the input parameters or from new physics.

3.2. Frequentist methods

As said in the introduction theoretical quantities play an important role in the formulae relating the measured quantities to the UT parameters. These quantities are often inferred from theoretical calculations with uncertainties which can be associated to approximations. Uncertainties due to approximations are often estimated from more or less educated guesswork. For example, we recall that i) The quenched approximation in Lattice QCD calculations; ii) Model calculations of form factors where model parameters are varied within some range; iii) Higher order terms neglected in a power series for which the error is estimated from the "natural size" of the expansion parameter or a scale dependence in a perturbative series where the error is estimated by varying the scale within some *reasonable* range. This has driven the developments of statistical approaches based on a frequentist understanding of systematic theoretical uncertainties, which cannot be treated as statistically distributed quantities.

In this framework two approaches are presented: the *R*fit method and the Scanning method. In both methods, the "theoretically allowed" values for some theoretical parameters are "scanned", *i.e.* no statistical weight is assigned to these parameters as long as their values are inside a "theoretically allowed" range.

The *R*fit method starts by choosing a point in a parameter subspace of interest, *e.g.* a point in the $\bar{\rho}$-$\bar{\eta}$ plane, and ask for the best set of theoretical parameters for this given point. This set is determined by minimizing a χ^2 function with respect to all model parameters, except $\bar{\rho}$ and $\bar{\eta}$. The theoretical parameters are free to vary inside their theoretically allowed range without obtaining any statistical weight. In this way, upper limits of confidence levels in the parameter subspace of interest can be determined.

The basic idea of the Scanning method is to choose a possible set of values for the theoretical parameters and to ask whether this particular model leads to an acceptable fit for the given data set. If so, a confidence contour is drawn in a parameter subspace of interest, *e.g.* the $\bar{\rho}$-$\bar{\eta}$ plane, representing the constraints obtained for this particular set of model parameters. This procedure is repeated for a large number of possible theoretical models by scanning allowed ranges of the non-perturbative parameters. The single confidence level contours cannot be compared from a statistical point of view. This method has been extended to facilitate an analysis of the relative influence of experimental and theoretical uncertainties in determining the consistency of the measurements with theory.

*3.2.1. The R*fit *approach*

The CKM analysis using the *R*fit method * is performed in three steps: 1. Testing the overall consistency between data and the theoretical framework, here the SM. 2. If data and the SM are found to be in reasonable agreement, confidence levels (CL) in parameter subspaces are determined. 3. Testing extensions of the SM.

*The *R*fit method is implemented in the software package *CKMfitter* [12]. More details can be found in [3].

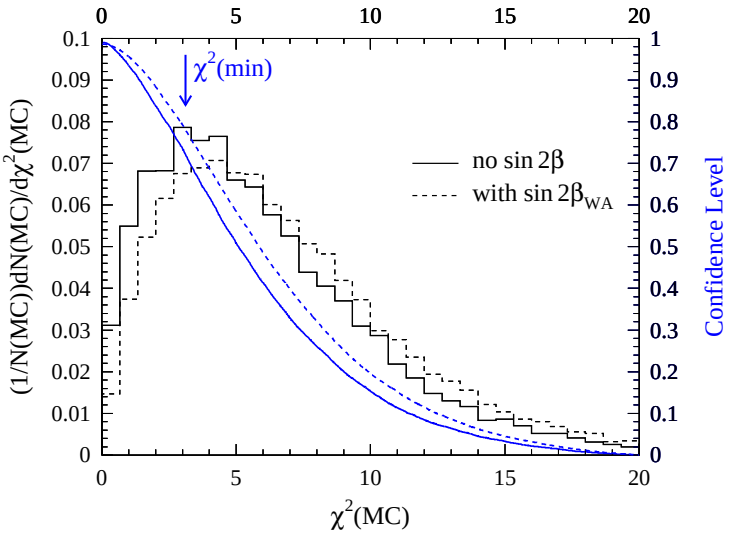

Fig. 5.3: *Determination of CL(SM). The histograms show the test statistics $F(\chi^2)$ built from the Monte Carlo technique as described in the text for two different fits, including or excluding the* $\sin 2\beta$ *measurement. Integration of the distributions above* χ^2_{min} *provides CL(SM).*

The quantity $\chi^2 = -2\ln\mathcal{L}(y_{\rm mod})$ is minimized in the fit, where the likelihood function is defined by $\mathcal{L}(y_{\rm mod}) = \mathcal{L}_{\rm exp}(x_{\rm exp} - x_{\rm theo}(y_{\rm mod})) \cdot \mathcal{L}_{\rm theo}(y_{\rm QCD})$. The experimental part, $\mathcal{L}_{\rm exp}$, depends on measurements, $x_{\rm exp}$, and theoretical predictions, $x_{\rm theo}$, which are functions of model parameters, $y_{\rm mod}$. The theoretical part, $\mathcal{L}_{\rm theo}$, describes our "knowledge" of the theoretical parameters, $y_{\rm QCD} \in \{y_{\rm mod}\}$. We set $\mathcal{L}_{\rm theo} = 1$ within an "allowed range" $\mathcal{R}$ provided by a theoretical estimate, and $\mathcal{L}_{\rm theo} = 0$ outside $\mathcal{R}$. That is, the $y_{\rm QCD}$ are free to vary within $\mathcal{R}$ without changing the $\mathcal{L}_{\rm theo}$ part of the χ^2 function. It should be kept in mind that the choice of $\mathcal{R}$ is statistically not well-defined and reflects an intrinsic problem of all statistical analyses when dealing with theoretical uncertainties.

It is worthwhile to emphasize that a uniform likelihood function is not identical to a uniform pdf. Whereas a uniform likelihood means that the theoretical parameter is free to vary within $\mathcal{R}$, a uniform pdf states that each value within $\mathcal{R}$ has equal probability and hence introduces a statistical weight. This has important consequences if more than one theoretical parameter enter a constraint or if the constraint depends on a nonlinear function of a theoretical parameter. For example, the ε_K constraint depends on the product $P = \hat{B}_K \cdot |V_{cb}|^4$. The theoretical likelihood for $|V_{cb}|^4$ reads $\mathcal{L}_{\rm theo}(|V_{cb}|^4) = 1$ for all theoretically allowed $|V_{cb}|$ values given by $\mathcal{L}_{\rm theo}(|V_{cb}|) = 1$. The theoretical likelihood for the product P reads $\mathcal{L}_{\rm theo}(P) = 1$ for any value of $\hat{B}_K$ and $|V_{cb}|$ given by $\mathcal{L}_{\rm theo}(\hat{B}_K) = 1$ and $\mathcal{L}_{\rm theo}(|V_{cb}|) = 1$, respectively. That is, in *R*fit, no statistical weight is introduced for any value of P, independent of the fact whether the single theoretical parameters are bound or unbound and independent of the particular parametrization chosen. On the contrary, the pdf for the theoretical part of $|V_{cb}|^4$ is proportional to $(|V_{cb}|)^{-3/4}$ if the theoretical pdf for $|V_{cb}|$ is chosen to be uniform. The pdf for the product P would be proportional to $-\log|P|$ in leading order if the pdfs for $\hat{B}_K$ and $|V_{cb}|^4$ were chosen to be uniform [3].

The agreement between data and the SM is gauged by the global minimum $\chi^2_{{\rm min};y_{\rm mod}}$, determined by varying freely all model parameters $y_{\rm mod}$. For $\chi^2_{{\rm min};y_{\rm mod}}$, a confidence level CL(SM) is computed by means of a Monte Carlo simulation. For the optimal set of model parameters $y_{\rm mod}$, a large number of pseudo-measurements is generated using the experimental likelihood function $\mathcal{L}_{\rm exp}$. For each set of pseudo-measurements, the minimum $\chi^2_{\rm min}$ is determined and used to build a test statistics $F(\chi^2)$. The CL is then calculated as $\mathrm{CL(SM)} = \int_{\chi^2_{{\rm min};y_{\rm mod}}}^{\infty} F(\chi^2)d\chi^2$ as illustrated in Fig. 5.3. If there is a hint of an incompatibility between data and the SM one has to investigate in detail which constraint leads to a small value for $\mathrm{CL(SM)}$.

If the hypothesis "the CKM picture of the SM is correct" is accepted, CLs in parameter subspaces a, *e.g.* $a = (\bar{\rho}, \bar{\eta}), \sin 2\beta, ...$, are evaluated. For a given point in a, one determines the best agreement between data and theory. One calculates $\Delta\chi^2(a) = \chi^2_{\mathrm{min};\mu}(a) - \chi^2_{\mathrm{min};y_{\mathrm{mod}}}$, by varying freely all model parameters μ (including y_{QCD}) with the exception of a. The corresponding CL is obtained from $\mathrm{CL}(a) = \mathrm{Prob}(\Delta\chi^2(a), N_{\mathrm{dof}})$ (see e.g. Fig. 5.3) where N_{dof} is the number of degrees of freedom, in general the dimension of the subspace a. It has to be stressed that $\mathrm{CL}(a)$ depends on the choice of $\mathcal{R}$. The usage of $\mathrm{Prob}(\Delta\chi^2(a), N_{\mathrm{dof}})$ assumes Gaussian shapes for $\mathcal{L}_{\mathrm{exp}}$. The CL obtained has been verified for several examples using a Monte Carlo simulation similar to the one described in the last section.

If the SM cannot accommodate the data, the analysis has to be repeated within extensions of the SM. Even in the case of a good agreement between data and the SM, it is worthwhile to perform the analysis for possible extensions of the SM in order to constrain New Physics parameters, see *e.g.* Ref. [13], or to determine the precision needed to study or exclude certain models.

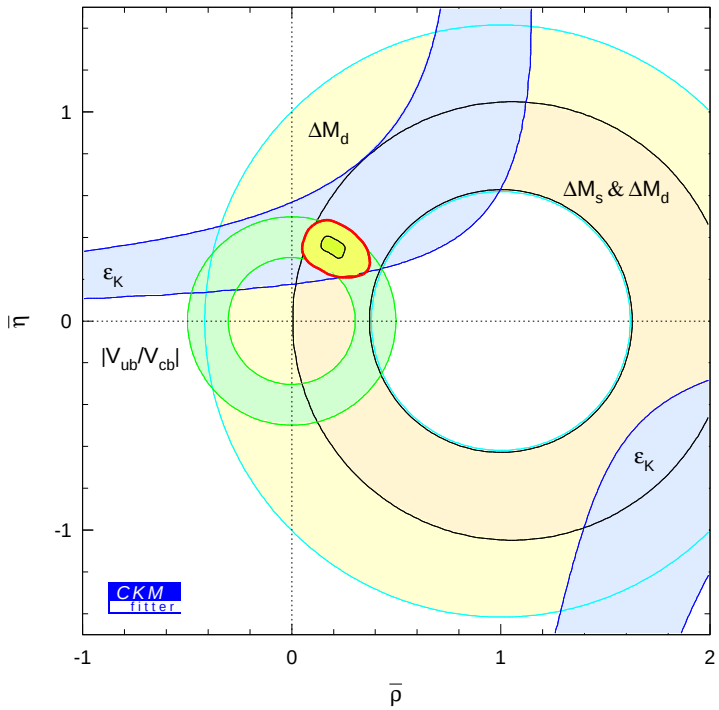

Fig. 5.4: *Different single constraints in the $\bar{\rho} - \bar{\eta}$ plane shown at 95 % CL contours. The 95 % and 10 % CL contours for the combined fit are also shown.*

3.2.2. The Scanning Method

In the scanning method the following procedure is set to deal with "not-statistically" distributed quantities: we select a specific set of theoretical parameters called a "model",

$$\mathcal{M} \equiv \{\mathcal{F}_{D*}(1),\ \tilde{\Gamma}^c_{incl},\ \tilde{\Gamma}^u_{excl}, \tilde{\Gamma}^u_{incl},\ F_{B_d}\sqrt{\hat{B}_{B_d}}, \hat{B}_K,\ \xi,\ \eta_1, \eta_2,\ \eta_3,\ \eta_B\}, \tag{18}$$

where $\mathcal{F}_{D*}(1)$ is the Isgur-Wise function of $\mathrm{B} \to \mathrm{D}^*\ell\nu$ at zero recoil corrected for finite b-quark mass, $\tilde{\Gamma}^c_{incl}$ denotes the reduced decay rate for $b \to c\ell\nu$, $\tilde{\Gamma}^u_{excl}$ ($\tilde{\Gamma}^u_{incl}$) represents the reduced decay rate for $\mathrm{B} \to \rho\ell\nu$ ($b \to u\ell\nu$), F_{B_d} (F_{B_s}) is the B^0_d (B^0_s) decay constant, B_{B_d}, B_{B_s} and $\hat{B}_K$ parameterize the values of the hadronic matrix elements appearing in $\mathrm{B}^0_d - \overline{\mathrm{B}}^0_d$ mixing, $\mathrm{B}^0_s - \overline{\mathrm{B}}^0_s$ mixing and $\mathrm{K}^0 - \overline{\mathrm{K}}^0$ mixing, respectively, $\xi = F_{B_s}/F_{B_d}\sqrt{(\hat{B}_{B_s}/\hat{B}_{B_d})}$, and η_1, η_2, η_3, and η_B denote QCD parameters. Such a set of theoretical parameters carries by definition non-probabilistic uncertainties but still may

involve probabilistic errors. By choosing many different "models" we map out the allowed ranges of these theoretical parameters.

For each "model" $\mathcal{M}$ we construct and minimize the function

$$\chi^2_{\mathcal{M}}(A,\bar{\rho},\bar{\eta}) = \sum_i \left[\frac{E_i - \mathcal{E}_i(A,\bar{\rho},\bar{\eta};C_k;\mathcal{M})}{\sigma_{E_i}}\right]^2, \tag{19}$$

where the E_i are observables based on measured quantities, $\mathcal{E}_i(A,\bar{\rho},\bar{\eta};C_k;\mathcal{M})$ is their parameterization in terms of A, $\bar{\rho}$, and $\bar{\eta}$, C_k denotes measured quantities that possess experimentally derived or other probabilistic uncertainties, such as masses and lifetimes, and the σ_{E_i} denote all measurement uncertainties contributing to both E_i and $\mathcal{E}_i(A,\bar{\rho},\bar{\eta};C_k;\mathcal{M})$. This includes all uncertainties on the theoretical parameters that are statistical in nature.

The inputs used are those given in Table 5.1. To incorporate results on ΔM_s searches we include a χ^2-term defined as the maximum between the log-likelihood ratio used in [2] and 0:

$$-2ln\mathcal{L}_\infty(\Delta M_s) = \max\left(\frac{(1-2\mathcal{A})}{\sigma^2_{\mathcal{A}}}, 0\right) \tag{20}$$

$\mathcal{A}$ is the amplitude spectrum as function of ΔM_s.

The minimization solution $(A,\bar{\rho},\bar{\eta})_{\mathcal{M}}$ for a particular "model" $\mathcal{M}$ incorporates no prior distribution for non-probabilistic uncertainties of the theoretical parameters and meets the frequency interpretation. All uncertainties depend only on measurement errors and other probabilistic uncertainties including any probabilistic component of the uncertainties on the theoretical parameters relevant to each particular measurement. At the moment, for practical reasons, we have treated the comparatively small uncertainties arising from η_1, η_2, η_3, and η_B as probabilistic. The effects of this simplification will be explored in future fits.

A "model" $\mathcal{M}$ and its best-fit solution are kept only if the probability of the fit satisfies $\mathcal{P}(\chi^2_{\mathcal{M}}) > \mathcal{P}_{min}$, which is typically chosen to be 5%. For each "model" $\mathcal{M}$ accepted, we draw a 95% C.L. contour in the $(\bar{\rho},\bar{\eta})$ plane. The fit is repeated for other "models" $\mathcal{M}$ by scanning through the complete parameter space specified by the theoretical uncertainties. This procedure derives from the technique originally described in [14].

The χ^2 minimization thus serves three purposes:

1. If a "model" $\mathcal{M}$ is consistent with the data, we obtain the best estimates for the three CKM parameters, and 95% C.L. contours are determined.
2. If a "model" $\mathcal{M}$ is inconsistent with the data the probability $\mathcal{P}(\chi^2_{\mathcal{M}})$ will be low. Thus, the requirement of $\mathcal{P}(\chi^2_{\mathcal{M}})_{min} > 5\%$ provides a test of compatibility between data and its theoretical description.
3. By varying the theoretical parameters beyond their specified range we can determine correlations on them imposed by the measurements. The first results of this study are shown in Section 4.2.

If no "model" were to survive we would have evidence of an inconsistency between data and theory, independent of the calculations of the theoretical parameters or the choices of their uncertainties. Since the goal of the CKM parameter fits is to look for inconsistencies of the different measurements within the Standard Model, it is important to be insensitive to artificially produced effects and to separate the non-probabilistic uncertainties from Gaussian-distributed errors.

In order to demonstrate the impact of the different theoretical quantities on the fit results in the $(\bar{\rho},\bar{\eta})$ plane, Figs. 5.5a–f show contours for fits in which only one parameter was scanned while the others were kept at their central values. These plots demonstrate the impact of the model dependence in $|V_{ub}|$ and $|V_{cb}|$ as well as that of $F_{B_d}\sqrt{\hat{B}_{B_d}}$ and $\hat{B}_K$, ξ, and η_1, respectively. For each parameter we consider

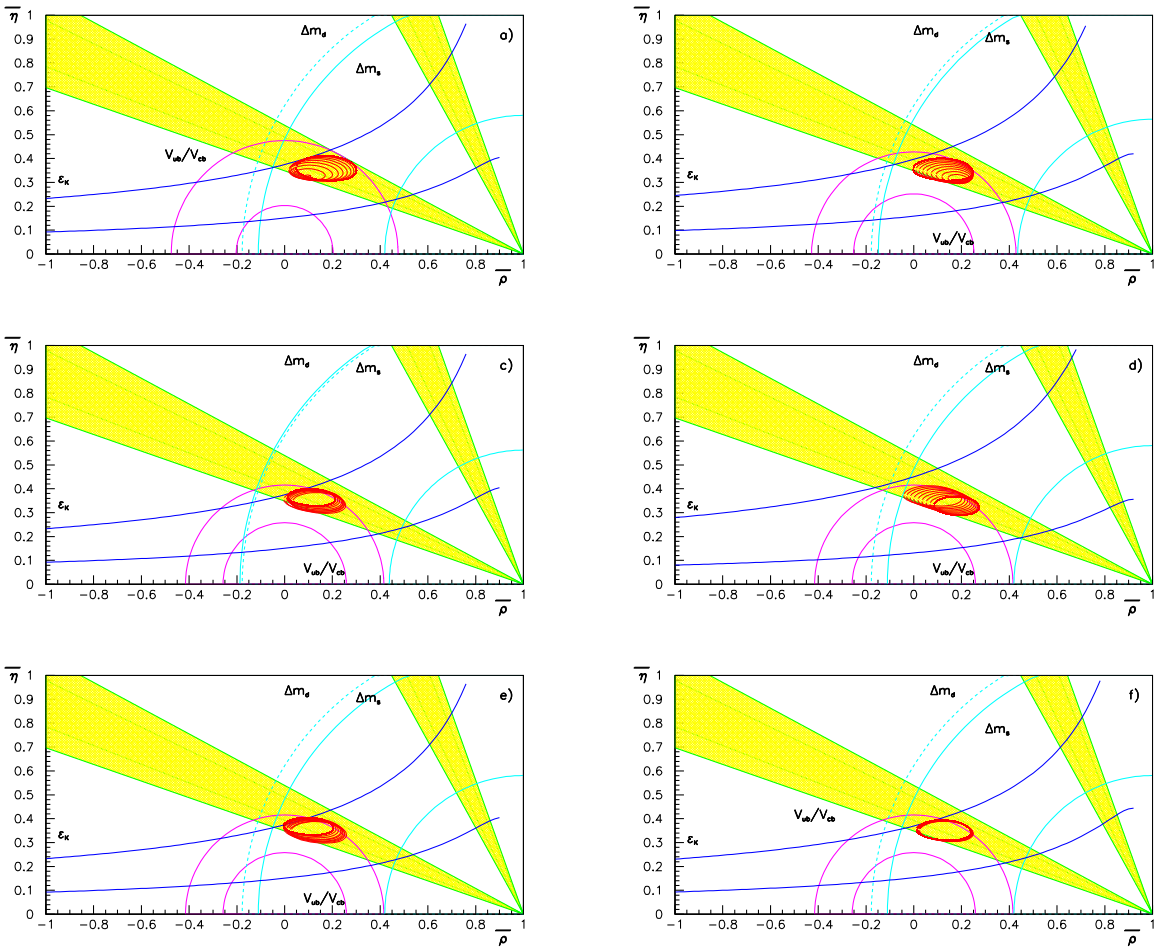

Fig. 5.5: *Contours of different models in the $(\bar{\rho}, \bar{\eta})$ plane, by varying only one theoretical parameter at a time, a) $\tilde{\Gamma}_{excl}$, b) $\mathcal{F}_{D^*}(1)$, c) $F_{B_d}\sqrt{\hat{B}_{B_d}}$, d) $\hat{B}_K$, e) ξ (where ΔM_s is included in the fit), and f) η_1. In each plot nine different models are considered by varying the theoretically-allowed range from the minimum value to the maximum value. The figures are arranged with a) in the upper left, b) in the upper right, etc..*

nine different models which span its range equidistantly, starting with the smallest allowed value. Since these plots just serve illustrative purposes we use only the measurements of $|V_{ub}|$, $|V_{cb}|$, ΔM_d, and ϵ_K in the fits, except for Fig. 5.5e where the information of ΔM_s has been included in addition. To guide the eye we show the boundaries of the three bands for $|V_{ub}/V_{cb}|$, $|V_{td}/V_{cb}|$, and ϵ_K. Since the theoretical parameters are kept at their central values except for the one being varied, the bands corresponding to the other parameters reflect only experimental uncertainties.

We now turn to scanning all parameters simultaneously within their theoretically "allowed" ranges. Figure 5.6 shows the resulting contours for a set of representative "models", when all available constraints are included. Note that there is no frequency interpretation for comparing which models are to be "preferred", other than the statement that at most one model is correct. In this analysis we cannot, and do not, give any relative probabilistic weighting among the contours, or their overlap regions. Indeed, the entire purpose of the scanning method is to make clear the relative importance of measurable experimental errors and a-priori unknown theoretical uncertainties.

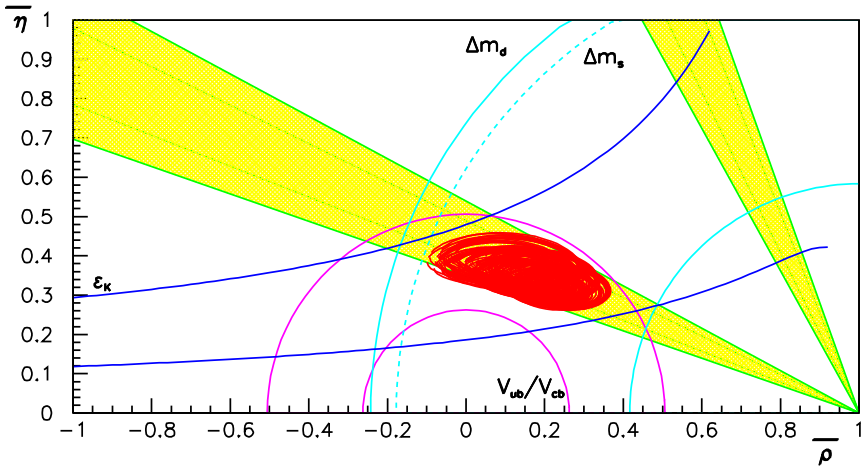

Fig. 5.6: *Contours in the* $(\bar{\rho}, \bar{\eta})$ *plane for different models, scanning theoretical parameters* $\tilde{\Gamma}_{excl}$, $\mathcal{F}_{D^*}(1)$, $F_{B_d}\sqrt{\hat{B}_{B_d}}$, $\hat{B}_K$, *and* ξ, *based on measurements of* $|V_{ub}|$, $|V_{cb}|$, ΔM_d, ϵ_K, *the amplitude for* ΔM_s, *and* $\sin 2\beta$.

4. Impact of the uncertainties on theoretical quantities in CKM Fits

As described in the previous sections, the "correct" way to treat the theoretical parameters is not unambiguously defined but depends on the adopted statistical approach. In this section we will not discuss the problems and the virtues of the different statistical approaches on this point, and concentrate on the impact of the uncertainties on theoretical parameters in constraining $\bar{\rho}$ and $\bar{\eta}$.

Two numerical analyses will be presented: one in the Bayesian framework and one in the frequentist framework. In the first analysis we study the effect on the UT fit from a modification (or a removal) of some theoretical parameter used as input parameter. The second analysis introduces a graphical method to represent, in the space of the theoretical parameters, the goodness of the UT fit and to evaluate the relevance of the knowledge on these parameters.

4.1. Bayesian analysis

In the framework of the Bayesian method the input knowledge is expressed in terms of pdfs for all quantities (theoretical and experimental parameters). Following the procedure described in Section 3.1., the output pdf can be computed for $\bar{\rho}$, $\bar{\eta}$ and for any other quantity of interest.

The impact of the uncertainty on a given quantity, which enters as a parameter in a given constraint, is naturally evaluated by comparing the results obtained excluding the corresponding constraint or by varying the error of the input parameter. When the information on a certain quantity is excluded the corresponding input pdf is taken as uniform. The common set of inputs used for this analysis are the ones available at the time of the Workshop (Table 5.1).

4.1.1. Determination of $F_{B_d}\sqrt{\hat{B}_{B_d}}$

First we consider the $F_{B_d}\sqrt{\hat{B}_{B_d}}$ parameter. Quite remarkably the remaining constraints determine precisely this quantity and, from the output distribution shown in the left part of Fig. 5.7, we get

$$F_{B_d}\sqrt{\hat{B}_{B_d}} = (223 \pm 12)\ \text{MeV} \tag{21}$$

This is in perfect agreement with the results from lattice calculation (see Table 5.1) and has a significantly smaller error. This suggests that, unless the lattice error on $F_B\sqrt{\hat{B}_B}$ does not become smaller than 12 MeV, the theoretical knowledge of this quantity is not quite relevant in UT fits. The Table in Fig. 5.7 quantifies the effect of changing the uncertainty on $F_{B_d}\sqrt{\hat{B}_{B_d}}$ (keeping the same central value).

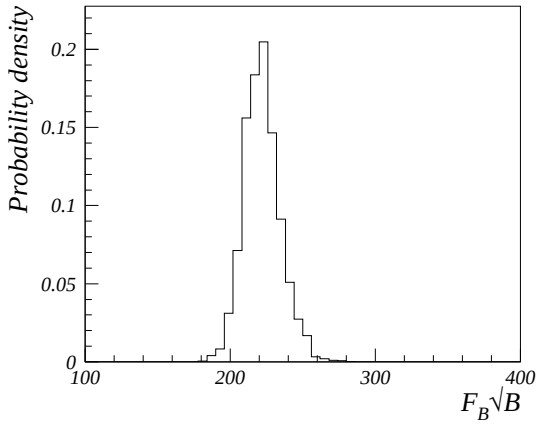

$\sigma \pm \Delta/2$	$\bar{\rho}$	$\bar{\eta}$
$\pm 16 \pm 6$	0.183 ± 0.040	0.355 ± 0.027
$\pm 33 \pm 12$	0.173 ± 0.046	0.357 ± 0.027
$\pm 66 \pm 24$	0.173 ± 0.046	0.355 ± 0.027
∞	0.175 ± 0.049	0.355 ± 0.027

Fig. 5.7: *Left: output distribution for $F_{B_d}\sqrt{\hat{B}_{B_d}}$ assuming a flat input distribution. Right: table reporting the results of the UT fit for $\bar{\rho}$ and $\bar{\eta}$ assuming different input values for the errors on $F_{B_d}\sqrt{\hat{B}_{B_d}}$ (in MeV) (σ is the Gaussian error and $\Delta/2$ is the half-width of the systematic range). The last column ("infinite error") is obtained with a uniform input distribution.*

4.1.2. Determination of $\hat{B}_K$

Here the same exercise has been repeated with the parameter $\hat{B}_K$. Assuming for $\hat{B}_K$ a uniform input distribution between 0 and 2, from the output distribution shown in Fig. 5.8 we obtain

$$\hat{B}_K = 0.73^{+0.13}_{-0.07} \tag{22}$$

The fitted value is again in perfect agreement with the lattice value (see Table 5.1), but in this case the fitted (output) uncertainty is similar to the theoretical (input) one. We then expect that "lattice information" plays a non negligible role, in particular in the determination of $\bar{\eta}$ (because of simple geometrical arguments). Table in Fig. 5.8 shows that, in fact, removing the information coming from Lattice QCD (last row) the error on $\bar{\eta}$ increases by 50%.

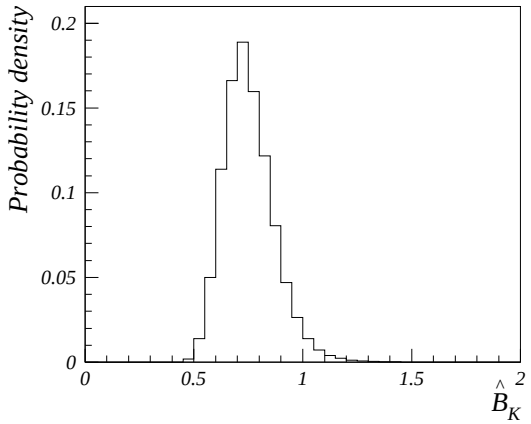

$\sigma \pm \Delta/2$	$\bar{\rho}$	$\bar{\eta}$
$\pm 0.03 \pm 0.065$	0.181 ± 0.040	0.349 ± 0.025
$\pm 0.06 \pm 0.13$	0.173 ± 0.046	0.357 ± 0.027
$\pm 0.12 \pm 0.26$	0.163 ± 0.052	0.365 ± 0.030
∞	0.161 ± 0.055	0.361 ± 0.042

Fig. 5.8: *Left: output distribution for $\hat{B}_K$ assuming a flat input distribution. Right: table reporting the results of the CKM Fits for $\bar{\rho}$ and $\bar{\eta}$ assuming different input values for the errors on $\hat{B}_K$ (σ is the Gaussian error and $\Delta/2$ is the half-width of the systematic range). The last column ("infinite error") is obtained with a flat input distribution.*

4.1.3. Determination of ξ

Since ΔM_s has not yet been measured, ξ cannot be determined by the data. Assuming a uniform distribution between 0.6 and 2 (the upper bound is obviously arbitrary), the output distribution shown in Fig. 5.9 is obtained. The tail on the right part of the plot shows that, at present, ξ is only weakly constrained by experimental data; for this reason the information on the ξ parameter is very important, in particular in the determination of $\bar{\rho}$, as shown in the table in Fig. 5.9.

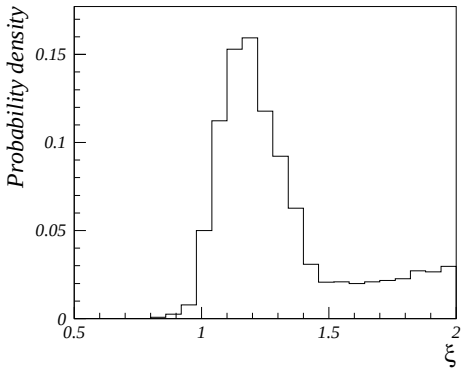

$\sigma \pm \Delta/2$	$\bar{\rho}$	$\bar{\eta}$
$\pm 0.02 \pm 0.025$	0.183 ± 0.037	0.353 ± 0.025
$\pm 0.04 \pm 0.05$	0.173 ± 0.046	0.357 ± 0.027
$\pm 0.08 \pm 0.10$	0.167 ± 0.062	0.357 ± 0.030
$[0.4, 2]$	0.203 ± 0.080	0.347 ± 0.035

Fig. 5.9: *Left: output distribution for ξ assuming a flat input distribution between 0.6 and 2. Right: table reporting the results of the CKM Fits for $\bar{\rho}$ and $\bar{\eta}$ assuming different input values for the errors on ξ (σ is the Gaussian error and $\Delta/2$ is the half-width of the systematic range). The last column is obtained with a flat input distribution between 0.6 and 2.*

4.2. Scan analysis

In the study of the sensitivity of the UT fit to a given theoretical parameter one should define how to treat the remaining parameters. In the Bayesian approach (described in the previous section) the remaining parameters are integrated using their input pdf while in the standard frequentist approach the confidence level for a parameter is computed irrespectively of the values of all the remaining parameters (logical "OR" over the values of the parameters).

The technique presented here aims at studying and visualizing the sensitivity of UT fits to theoretical uncertainties, in the theoretical parameters space (T), minimizing a priori inputs and intermediate combinations of parameters. The method tries to represent pairs or triplets of theoretical parameters while keeping some information on the remaining (undisplayed) parameters. The input knowledge on a theoretical parameter is described by a "nominal central value" and a "theoretical preferred range". In two dimensions the procedure is as follows:

- Pick two of the parameters T for display. Call these the *primary parameters*, T_1 and T_2.
- Pick a third T parameter, the *secondary parameter* T_s. This parameter is singled out for special attention to the effects of projecting over it.
- Call all the other T parameters the *undisplayed parameters*, T_X.
- For each point P in the grid of scanned values of $T_1 \otimes T_2$, a number of fits will have been attempted, covering all the scanned values of T_s and T_X. For each P, evaluate the following hierarchy of criteria against the ensemble of results of these fits, deriving for the point a value, we call it the "Level", which is an integer between 0 and 5 inclusive:

  1. Define a minimum acceptable value for $P(\chi^2)$. Did any of the fits for P pass this cut? If not, assign Level = 0 and stop; otherwise assign Level = 1 and continue.
  2. Did any of the remaining fits lie within the "theoretically preferred region" for *all* the undisplayed parameters T_X? If not, stop; if yes, assign Level = 2 and continue.

3. Did any of the remaining fits have the secondary parameter T_s within its "theoretically preferred region"? If not, stop; if yes, assign Level = 3 and continue.
4. Did any of the remaining fits have T_s equal to its "nominal central value"? (That value must have been included in the scan grid for this to make sense.) If not, stop; if yes, assign Level = 4 and continue.
5. Did any of the remaining fits have *all* the undisplayed parameters T_X also at their "nominal central values"? If not, stop; if yes, assign Level = 5 and stop.

- Now display contours of the quantity Level over the grid in the $T_1 \otimes T_2$ plane. Assign a unique color to each parameter T, so the contours for T_s at Level = 3,4 are drawn in the color corresponding to that parameter. The contours for Level = 4,5, which correspond to restrictions of parameters exactly to their central values, are also drawn distinctively, with dashing.
  The Level 3 contour (solid, colored), in particular, displays the allowed region, at the selected confidence level, for T_1 and T_2, based on the experimental data and on limiting all other theoretical parameters to their preferred ranges. Study of the relative spacing of the Level 2, 3, and 4 contours readily reveals the effects of the application of the T_s bounds on the fit results.
- Overlay the contours with straight lines showing the theoretically preferred ranges and nominal central values for T_1 and T_2, in their respective unique colors, again with dashing for the central value. This allows the theoretical bounds on T_1 and T_2 to be evaluated directly for consistency against all other available data, yet avoiding any convoluted use of priors for these two parameters. Comparison of these theoretical bounds for T_1 and T_2 with the Level 3 contour that shows the experimental information, constrained by the application of the theoretical bounds on T_s and the T_x, allows a direct visual evaluation of the consistency of all available information, with the effects of the application of all theoretical bounds manifest, not obscured by convolutions performed in the fit itself.

Figure 5.10 shows the results of the previous procedure, using $F_B\sqrt{\hat{B}_B}$ and V_{ub} as primary parameters, $\hat{B}_K$ as secondary parameter, while the undisplayed parameter (there is just one in this case) is ξ. What can be seen immediately is that the entire theoretically allowed region for the primary parameters, shown by the crossing of the solid lines, is consistent with all the other data, including the theoretical bound on $\hat{B}_K$, and that even when all parameters are constrained to their central values the resulting fit (there can be only one at that point) is fully consistent. Changing the role of primary, secondary, and undisplayed parameters in many different ways, helps to understand the role of these parameters in the fit.

These plots can be extended in three dimensions by drawing the three bi-dimensional projections of the allowed region. Several three dimensional plots and further details can be found in [15].

5. Fit comparison

In this section we compare the results on the CKM quantities obtained following two approaches: Bayesian and *R*fit. The common set of inputs are the ones available at the time of the Workshop (Table 5.1). The Scan method has not been included in the comparison because it does not evaluate overall allowed regions for the CKM parameters. As explained in the previous sections, the main difference between the Bayesian and the *R*fit analyses originates from the computation of the Likelihood functions (identified with pdfs in the Bayesian case) for each parameter and in the treatment of the Likelihood fit.

5.1. Input likelihoods and combination of likelihoods

In general a determination of a given quantity is characterized by a central value, a statistical error and a systematical error. Starting from such a splitting of the errors Bayesian and frequentist approaches may describe this quantity according to different likelihood functions.

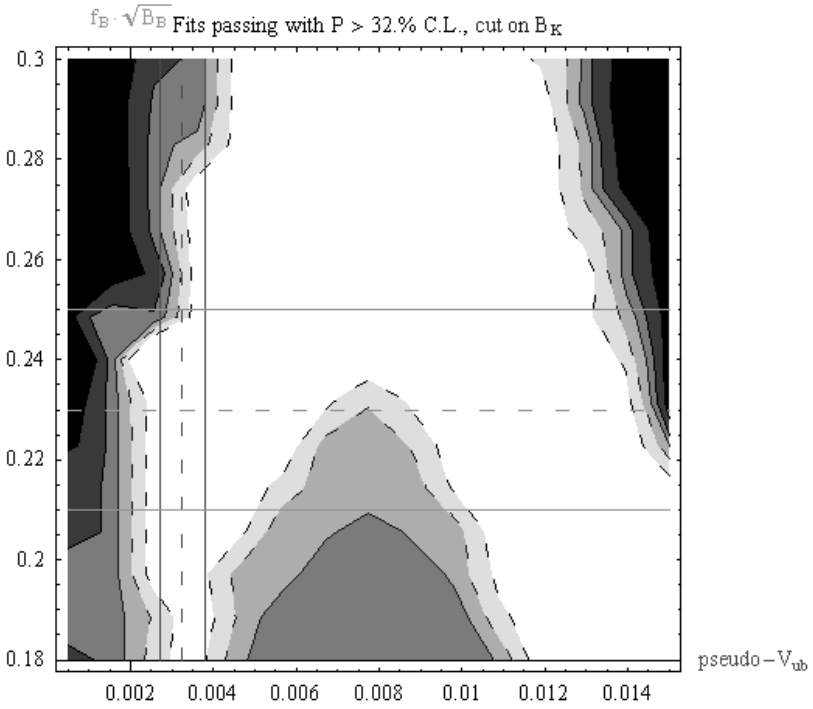

Fig. 5.10: *Results of the procedure described in the text, using $F_{B_d}\sqrt{\hat{B}_{B_d}}$ and V_{ub} as primary parameters, $\hat{B}_K$ as secondary parameter, and ξ as undisplayed parameter.*

In the Bayesian approach, the basic assumption is that the value of any quantity is distributed according to a pdf. The final pdf of a certain quantity is obtained by convoluting the pdfs corresponding to the different uncertainties affecting the quantity. In particular, the uncertainty on a quantity is usually splitted in two parts: a statistical part which can be described by a Gaussian pdf, $\mathcal{G}(x - x_0)$ (this part may contain many sources of uncertainties which have been already combined into a single pdf) and another part which is usually of theoretical origin and is often related to uncertainties due to theoretical parameters. In the following we will denote it as theoretical systematics. It is often described using an uniform pdf: $\mathcal{U}(x) = 1/2\sigma_{\rm theo}$ for $x \in [x_0 - \sigma_{\rm theo}, x_0 + \sigma_{\rm theo}]$ and $\mathcal{U}(x) = 0$ elsewhere. The combined pdf $\mathcal{P}$ is then obtained by convoluting the Gaussian pdf $\mathcal{G}$ with the uniform pdf $\mathcal{U}$: $\mathcal{P} = \mathcal{G} \otimes \mathcal{U}$.

In the frequentist analysis, no statistical meaning is attributed to the uncertainties related to theoretical systematics. The likelihood function $\mathcal{L}$ for the quantity x contains a statistical part, $\mathcal{L}_{\rm exp}(x - x'_0)$, described by a Gaussian with mean value x'_0, and a "not-statistical" part, $\mathcal{L}_{\rm theo}(x'_0)$. The function $\mathcal{L}_{\rm theo}(x'_0)$, as denoted *R*fit likelihood, is a uniform function $\mathcal{L}_{\rm theo}(x'_0) = 1$ for $x'_0 \in [x_0 - \sigma_{\rm theo}, x_0 + \sigma_{\rm theo}]$ and $\mathcal{L}_{\rm theo}(x'_0) = 0$ elsewhere. The final likelihood is given by the product $\mathcal{L} = \mathcal{L}_{\rm exp}(x - x'_0) \cdot \mathcal{L}_{\rm theo}(x'_0)$. In conclusion, when a quantity contains an uncertainty to which the frequentists do not attribute any statistical meaning, the likelihood which describes this quantity is obtained as a product between this uncertainty and the statistical one.

When several determinations of the same quantity are available one may combine them to obtain a single input for a quantity entering the fit (these considerations apply for example to the determinations of $|V_{ub}|$ and $|V_{cb}|$). We suppose, in the following, that these determinations are not correlated. In addition, it is assumed that the various determinations of these quantities are compatible. Then, for the combination, the Bayesian approach calculates the product of the single pdfs, whereas the frequentist approach calculates the product of the individual likelihoods. Hence, the mathematical concepts for the

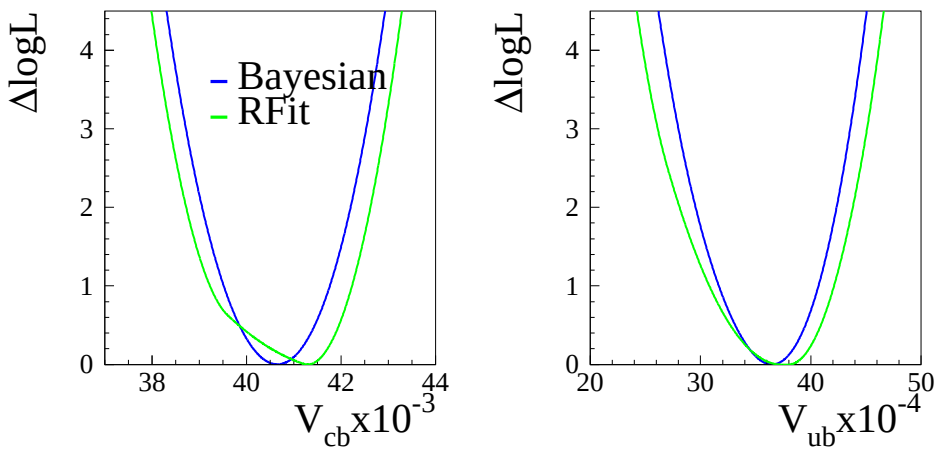

Fig. 5.11: *The ΔLikelihood for $|V_{cb}|$ and $|V_{ub}|$ using the Bayesian and frequentist approaches when combining the inclusive and the exclusive determinations.*

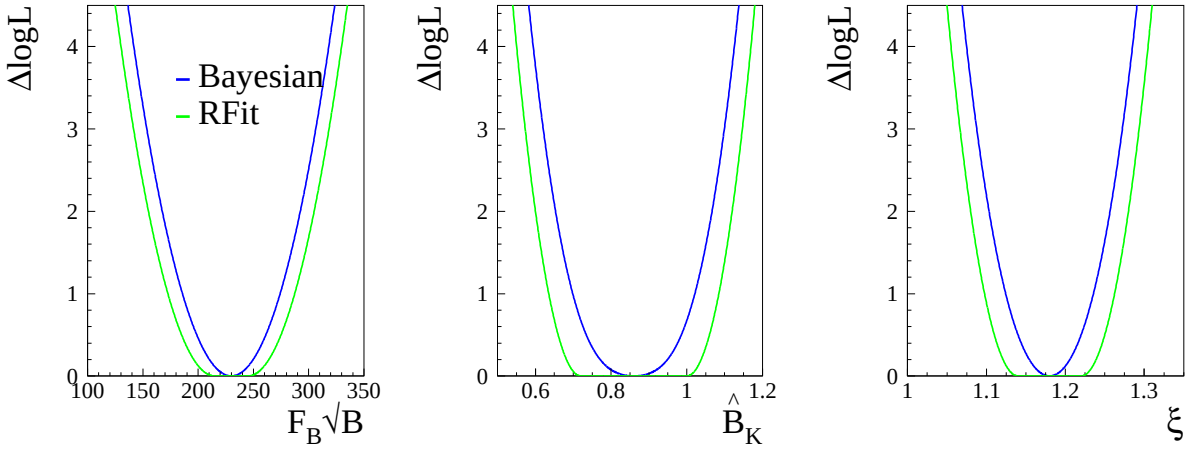

Fig. 5.12: *The ΔLikelihood for $F_{B_d}\sqrt{\hat{B}_{B_d}}$, $\hat{B}_K$ and ξ using the Bayesian and frequentist approaches.*

combination procedure of the two statistical approaches are identical.

5.2. Distributions for the relevant quantities in the CKM fits

The relevant quantities entering the fit are summarized in Table 5.1 given at the beginning of this Chapter. Figures. 5.11 and 5.12 show the Δ Log(Likelihood) for $|V_{cb}|$,$|V_{ub}|$ and for the non-perturbative QCD parameters, $F_{B_d}\sqrt{\hat{B}_{B_d}}$, ξ and $\hat{B}_K$ as obtained following the Bayesian and the frequentist methods. To be more explicit, in Table 5.2. we show the 68% and 95% ranges as obtained following the Bayesian and the *R*fit methods. It can be noticed that differences on the input quantities between the two approaches can be important and depend upon the chosen splitting of the errors. In the Bayesian approach the splitting of the total error in two errors is not really important, since, the two errors are often, already, the results of the convolution of many different source of errors. It has been also shown that the choice of the shape of the pdf to be attributed to the error has a moderate impact on the final results [16], once the central value and the r.m.s. of the pdf has been fixed. In the *R*fit this splitting is crucial and a careful breakdown of the sources of the errors which contribute to it should be done. For this comparison we

have decided to keep this splitting and to classify certain errors as a flat pdf and "non statistical" for the Bayesian and *R*fit approaches, respectively.

Parameters	68% range	95% range
$\hat{B}_K$ *R*fit (Bayes) [ratio R/B]	0.68-1.06 (0.76-0.98) [1.70]	0.62-1.12 (0.67-1.06) [1.25]

Table 5.2: *68% and 95% ranges for some relevant quantities used in the CKM fits in the* R*fit and Bayes approaches.*

5.3. Results and Comparison

*R*fit Method			
Parameter	$\leq 5\%$ CL	$\leq 1\%$ CL	$\leq 0.1\%$ CL
$\bar{\rho}$	0.091 - 0.317	0.071 - 0.351	0.042 - 0.379
$\bar{\eta}$	0.273 - 0.408	0.257 - 0.423	0.242 - 0.442
$\sin 2\beta$	0.632 - 0.813	0.594 - 0.834	0.554 - 0.855
γ°	42.1 - 75.7	38.6 - 78.7	36.0 - 83.5

Bayesian Method			
Parameter	5% CL	1% CL	0.1% CL
$\bar{\rho}$	0.137 - 0.295	0.108 - 0.317	0.045 - 0.347
$\bar{\eta}$	0.295 - 0.409	0.278 - 0.427	0.259 - 0.449
$\sin 2\beta$	0.665 - 0.820	0.637 - 0.841	0.604 - 0.863
γ°	47.0 - 70.0	44.0 - 74.4	40.0 - 83.6

Ratio *R*fit/Bayesian Method			
Parameter	5% CL	1% CL	0.1% CL
$\bar{\rho}$	1.43	1.34	1.12
$\bar{\eta}$	1.18	1.12	1.05
$\sin 2\beta$	1.17	1.18	1.16
γ°	1.46	1.31	1.09

Table 5.3: *Ranges at difference C.L for $\bar{\rho}$, $\bar{\eta}$, sin 2β and γ. The measurements of $|V_{ub}|$ / $|V_{cb}|$ and ΔM_d, the amplitude spectrum for including the information from the $\mathrm{B}_s^0 - \overline{\mathrm{B}}_s^0$ oscillations, $|\varepsilon_K|$ and the measurement of sin 2β have been used.*

For the comparison of the results of the fit we use $\bar{\rho}$, $\bar{\eta}$, sin 2β and γ. Those quantities are compared at the 95%, 99% and 99.9% C.L. It has to be stressed that in the frequentist approach those confidence levels correspond to $\geq$95%, $\geq$99% and $\geq$99.9%. All the available constraints have been used: the measurements of $|V_{ub}|$ / $|V_{cb}|$, ΔM_d, the amplitude spectrum for including the information from the $\mathrm{B}_s^0 - \overline{\mathrm{B}}_s^0$ oscillations, $|\varepsilon_K|$ and the measurement of sin 2β. It has to be stressed once more that the inputs used are the same in the two approaches (in term of Gaussian and uniform uncertainties), but

they correspond to different input likelihoods, for $|V_{cb}|$, $|V_{ub}|$, $F_{B_d}\sqrt{\hat{B}_{B_d}}$, $\hat{B}_K$ and ξ as shown in the previous figures. Figure 5.13 shows the comparison on the ($\bar{\rho}$, $\bar{\eta}$) plane. The numerical results are given in Table 5.3. Figure 5.14 shows the comparison between the allowed regions obtained using Bayesian or *R*fit methods if the constraint from the direct measurement of sin2β is removed from the fit.

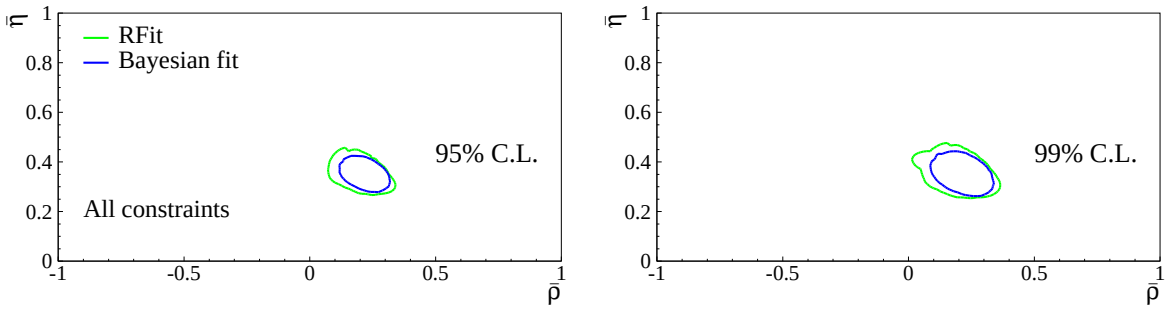

Fig. 5.13: *Comparison Bayesian/*R*fit Methods. Allowed regions for $\bar{\rho}$ and $\bar{\eta}$ at 95% (left plot) and 99% (right plot) using the measurements of $|V_{ub}|$ / $|V_{cb}|$, ΔM_d, the amplitude spectrum for including the information from the $B_s^0 - \overline{B}_s^0$ oscillations, $|\varepsilon_K|$ and the measurement of sin 2β.*

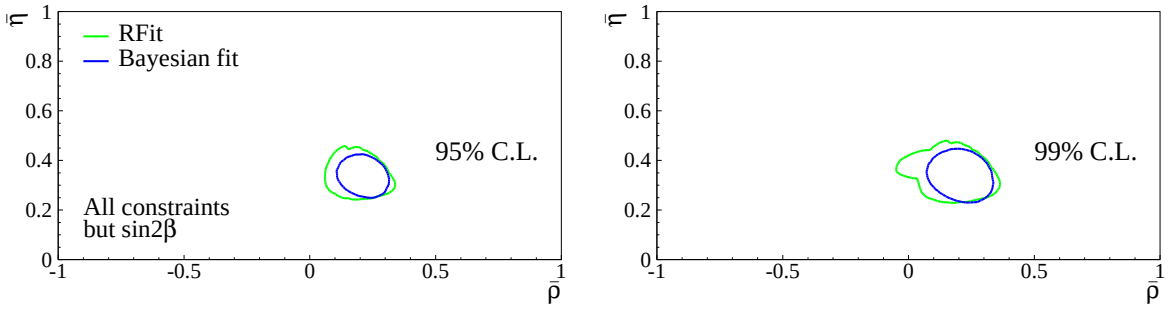

Fig. 5.14: *Comparison Bayesian/*R*fit Methods. Allowed regions for $\bar{\rho}$ and $\bar{\eta}$ at 95% (left plot) and 99% (right plot) using the measurements of $|V_{ub}|$ / $|V_{cb}|$, ΔM_d, the amplitude spectrum for including the information from the $B_s^0 - \overline{B}_s^0$ oscillations and $|\varepsilon_K|$*

5.3.1. Further comparisons

To further the orogin of the residual difference between the two methods, we have performed the following test: both methods use the distributions as obtained from *R*fit or from the Bayesian method to account for the information on input quantities. The results of the comparison using the input distributions as obtained from *R*fit are shown in Figs. 5.15 (Table 5.4). In some cases (0.1% C.L.) the ranges selected by the Bayesian approach are wider. The comparison using the input distributions, as obtained from the Bayesian method, give a maximal difference of 5%. These two tests show that, if same input likelihood are used, the results on the output quantities are very similar. The main origin of the residual difference on the output quantities, between the Bayesian and the *R*fit method comes from the likelihood associated to the input quantities.

5.3.2. Some conclusions on the fit comparison

The Bayesian and the *R*fit methods are compared in an agreed framework in terms of input and output quantities. For the input quantities the total error has been splitted in two errors. The splitting and the p.d.f distribution associated to any of the errors is not really important in the Bayesian approach. It becomes central in the *R*fit approach where the systematic errors are treated as “non statistical” errors.

Parameter	5% CL	1% CL	0.1% CL
$\bar{\rho}$	1.20	1.13	0.96
$\bar{\eta}$	1.03	0.99	0.94
$\sin 2\beta$	1.07	1.08	1.07
γ°	1.24	1.12	0.95

Table 5.4: *Comparison. Ratio for confidence levels* R*fit/Bayesian using the distributions as obtained from* R*fit to account for the information on input quantities*

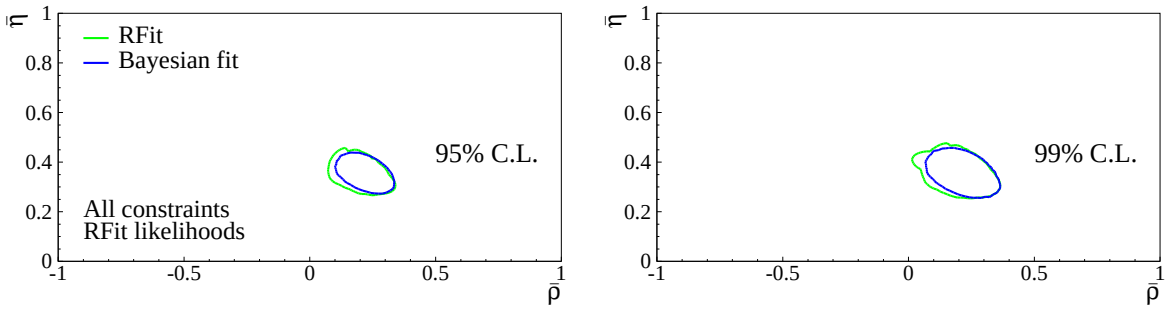

Fig. 5.15: *Comparison Bayesian/*R*fit Methods using the distributions as obtained from* R*fit to account for the information on input quantities. Allowed regions for $\bar{\rho}$ and $\bar{\eta}$ at 95% (left plot) and 99%(right plot) using the measurements of $|V_{ub}|$ / $|V_{cb}|$ and ΔM_d the amplitude spectrum for including the information from the $\mathrm{B}_s^0 - \overline{\mathrm{B}}_s^0$ oscillations, $|\varepsilon_K|$ and the measurement of sin 2β.*

The result is that, even if the same central values and errors are used in the two methods, the likelihood associated to the input parameters, which are entering in the fitting procedure, can be different. The output results ($\bar{\rho}$,$\bar{\eta}$, sin2 β, γ) differ by 15%-45%, 10%-35% and 5-15% if the 95%, 99% and 99.9% confidence regions are compared, respectively, with ranges from the frequentist method being wider. If the same likelihoods are used the output results are very similar.

6. Test of the CKM picture in the Standard Model

After comparing different statistical methods, in this final Section we show how the present data can be used to test the CKM picture of the Standard Model. The results presented here have been obtained with a Bayesian fit to the latest inputs of Table 5.1. The central values, errors and 68% (95%) [and 99%] C.L. ranges obtained for various quantities of interest are collected in Table 5.5.

The most crucial test is the comparison between the UT parameters determined with quantities sensitive to the sides of the UT (semileptonic B decays and oscillations) with the measurement of CP violation in the kaon sector ($|\varepsilon_K|$) and, also with the one in the B (sin2β) sector. This test is shown in Fig. 5.16. It can be translated quantitatively into a comparison between the values of sin2β obtained from the measurement of the CP asymmetry in the $J/\psi \mathrm{K}_\mathrm{S}^0$ decays and the one determined from "sides" measurements:

$$\begin{array}{ll} \sin 2\beta = & 0.685 \pm 0.052\ (0.581, 0.789) \quad \text{indirect} - \text{sides only} \\ \sin 2\beta = & 0.734 \pm 0.054\ (0.628, 0.840) \qquad \mathrm{B}^0 \to \mathrm{J}/\psi \mathrm{K}_\mathrm{S}^0\ , \end{array}$$

where, within parentheses, we give also the 95% probability region. The spectacular agreement between these values shows the consistency of the Standard Model in describing the CP violation phenomena

$\|V_{cb}\| \times 10^3$	41.5 ± 0.8	(39.9,43.1) [39.1,43.9]
$\bar{\eta}$	0.341 ± 0.028	(0.288,0.397) [0.271,0.415]
$\bar{\rho}$	0.178 ± 0.046	(0.085,0.265) [0.052,0.297]
$\sin 2\beta$	0.705 ± 0.037	(0.636,0.779) [0.612,0.799]
$\sin 2\alpha$	-0.19 ± 0.25	(–0.62,0.33) [–0.75,0.47]
γ(degrees)	61.5 ± 7.0	(49.0,77.0) [44.3,82.1]
$\Delta M_s(ps^{-1})$	18.3 ± 1.7	(15.6,22.2) [15.1,27.0]

Table 5.5: *Values and errors for different quantities using the present knowledge summarized in Table 5.1. Within parentheses and brackets the 95% and 99% probability regions are, respectively, given.*

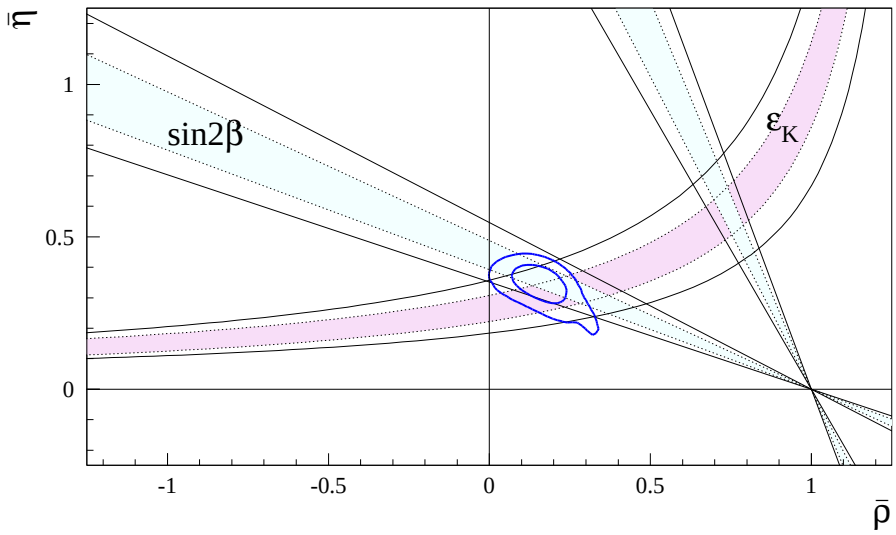

Fig. 5.16: *The allowed regions for $\overline{\rho}$ and $\overline{\eta}$ (contours at 68%, 95%) as selected by the measurements of $|V_{ub}|$ / $|V_{cb}|$, ΔM_d, and by the limit on $\Delta M_s/\Delta M_d$ are compared with the bands (at 68% and 95% C.L.) from CP violation in the kaon (ϵ_K) and in the B (sin2β) sectors.*

in terms of one single complex parameter η. Conversely, assuming the validity of the SM, this is also an important test of the OPE, HQET and LQCD theories which have been used to extract the CKM parameters. It has to be noted that the test is significant provided that the errors on sin 2β from the two determinations are comparable. Presently, the accuracy of both is at the 10% level. It is also of interest to explicitly make predictions for quantities which will be measured in the next future. We concentrate on ΔM_s which will be soon measured at Tevatron. The results obtained by excluding (or including) the information from the $\mathrm{B}_s^0 - \bar{\mathrm{B}}_s^0$ analyses are:

$$\begin{array}{rc} \Delta M_s(\text{with } \Delta M_s \text{ included}) = & 18.3 \pm 1.7\ (15.6, 22.2)\ [15.1, 27.0]\ \text{ps}^{-1} \\ \Delta M_s(\text{without } \Delta M_s\ ) = & 20.6 \pm 3.5\ (14.2, 28.1)\ [12.8, 30.7]\ \text{ps}^{-1}\ . \end{array}$$

where, within parentheses, we give the 95% and the 99% regions.

It will be interesting to compare these results with future measurements with the goal of identifying new physics contributions. Moreover a precise measurement of ΔM_s will reduce significantly the uncertainties in the output quantities in Table 5.5.

References

[1] A. Ali and D. London, Eur. Phys. J. C **18** (2001) 665;
S. Mele, Phys. Rev. D **59** (1999) 113011;
D. Atwood and A. Soni, Phys. Lett. B **508** (2001) 17.

[2] M. Ciuchini, G. D'Agostini, E. Franco, V. Lubicz, G. Martinelli, F. Parodi, P. Roudeau, A. Stocchi, JHEP 0107 (2001) 013, [hep-ph/0012308].

[3] A. Höcker, H. Lacker, S. Laplace, F. Le Diberder, Eur. Phys. J. C **21** (2001) 225, [hep-ph/0104062].

[4] Y. Grossman, Y. Nir, S. Plaszczynski and M.-H. Schune, Nucl. Phys. B **511** (1998) 69;
S. Plaszczynski and M.-H. Schune, hep-ph/9911280.

[5] L. Wolfenstein, Phys. Rev. Lett. **51** (1983) 1945.

[6] A.J. Buras, M.E. Lautenbacher and G. Ostermaier, Phys. Rev. D **50** (1994) 3433.

[7] S. Herrlich and U. Nierste, Nucl. Phys. B **419** (1994) 192, Phys. Rev. D **52** (1995) 6505 and recent update by M. Jamin and U. Nierste.

[8] Y. Nir, hep-ph/0208080.

[9] B. Aubert *et al.*, BaBar Collaboration, hep-ex/0207042.

[10] K. Abe *et al.*, Belle Collaboration, hep-ex/0208025.

[11] G. D'Agostini, CERN Report 99–03.

[12] "*CKMfitter*: code, numerical results and plots", http://ckmfitter.in2p3.fr

[13] S. Laplace, Z. Ligeti, Y. Nir, G. Perez, Phys. Rev. D **65**:094040 (2002)

[14] The BaBar Physics Book, BaBar Collaboration, (P.F. Harrison and H.R. Quinn, eds.). SLAC-R-0504 (1998).

[15] G.P. Dubois-Felsmann D.G. Hitlin, F.C. Porter and G. Eigen, CALT 68-2396 (2002).

[16] F. Parodi, P. Roudeau and A. Stocchi, Nuovo Cim. **112A** (1999) 833.

Chapter 6

FUTURE DIRECTIONS

This chapter contains a few contributions related to future possibilities for the extraction of the CKM elements and of the CP violating phases. They include general strategies for the determination of the CKM matrix elements, radiative rare B decays, weak phase determination from hadronic B decays and rare $K \to \pi\nu\bar{\nu}$ decays. Since these topics have not been the subject of a dedicated working group at this meeting of the Workshop, we present them in the form of collected papers under individual authorship.

1. General strategies for the CKM matrix

A.J. Buras, F. Parodi and A. Stocchi

During the last two decades several strategies have been proposed that should allow one to determine the CKM matrix and the related unitarity triangle (UT). We have already discussed a number of processes that can be used for the determination of the CKM parameters in Chapters 2–4. Additional processes and the related strategies will be discussed in this part. They are also reviewed in [1–5]. In this first opening section we want to address the determination of the CKM matrix and of the UT in general terms leaving the discussion of specific strategies to the following sections.

To be specific let us first choose as the independent parameters

$$|V_{us}|, \qquad |V_{cb}|, \qquad \bar{\varrho}, \qquad \bar{\eta}\ . \tag{1}$$

The best place to determine $|V_{us}|$ and $|V_{cb}|$, as discussed already in detail in Chapters 2 and 3, are the semi-leptonic K and B decays, respectively. The question that we want address here is the determination of the remaining two parameters $(\bar{\varrho}, \bar{\eta})$.

There are many ways to determine $(\bar{\varrho}, \bar{\eta})$. As the length of one side of the rescaled unitarity triangle is fixed to unity, we have to our disposal two sides, R_b and R_t and three angles, α, β and γ. These five quantities can be measured by means of rare K and B decays and in particular by studying CP-violating observables. While until recently only a handful of strategies could be realized, the present decade should allow several independent determinations of $(\bar{\varrho}, \bar{\eta})$ that will test the KM picture of CP violation and possibly indicate the physics beyond the Standard Model (SM).

The determination of $(\bar{\varrho}, \bar{\eta})$ in a given strategy is subject to experimental and theoretical errors and it is important to identify those strategies that are experimentally feasible and in which hadronic uncertainties are as much as possible under control. Such strategies are reviewed in [1–5] and in the following sections below.

Here we want to address a different question. The determination of $(\bar{\varrho}, \bar{\eta})$ requires at least two independent measurements. In most cases these are the measurements of two sides of the UT, of one side

and one angle or the measurements of two angles. Sometimes $\bar{\eta}$ can be directly measured and combining it with the knowledge of one angle or one side of the UT, $\bar{\varrho}$ can be found. Analogous comments apply to measurements in which $\bar{\varrho}$ is directly measured. Finally in more complicated strategies one measures various linear combinations of angles, sides or $\bar{\varrho}$ and $\bar{\eta}$.

Restricting first our attention to measurements in which sides and angles of the UT can be measured independently of each other, we end up with ten different pairs of measurements that allow the determination of $(\bar{\varrho}, \bar{\eta})$. The question then arises which of the pairs in question is most efficient in the determination of the UT? That is, given the same relative errors on R_b, R_t, α, β and γ, we want to find which of the pairs gives the most accurate determination of $(\bar{\varrho}, \bar{\eta})$.

The answer to this question depends necessarily on the values of R_b, R_t, α, β and γ but as we will see below just the requirement of the consistency of R_b with the measured value of $|V_{ub}/V_{cb}|$ implies a hierarchy within the ten strategies mentioned above.

During the 1970's and 1980's α_{QED}, the Fermi constant G_F and the sine of the Weinberg angle ($\sin\theta_W$) measured in the ν-N scattering were the fundamental parameters in terms of which the electroweak tests of the SM were performed. After the Z^0 boson was discovered and its mass precisely measured at LEP-I, $\sin\theta_W$ has been replaced by M_Z and the fundamental set used in the electroweak precision studies in the 1990's has been (α_{QED}, G_F, M_Z). It is to be expected that when M_W will be measured precisely this set will be changed to (α_{QED}, M_W, M_Z) or (G_F, M_W, M_Z).

We anticipate that an analogous development will happen in this decade in connection with the CKM matrix. While the set (1) has clearly many virtues and has been used extensively in the literature, one should emphasize that presently no direct independent measurements of $\bar{\eta}$ and $\bar{\varrho}$ are available. $|\bar{\eta}|$ can be measured cleanly in the decay $\mathrm{K}_L \to \pi^0\nu\bar{\nu}$. On the other hand to our knowledge there does not exist any strategy for a clean independent measurement of $\bar{\varrho}$.

Taking into account the experimental feasibility of various measurements and their theoretical cleanness, the most obvious candidate for the fundamental set in the quark flavour physics for the coming years appears to be [6]

$$|V_{us}|, \qquad |V_{cb}|, \qquad R_t, \qquad \beta \tag{2}$$

with the last two variables describing the V_{td} coupling that can be measured by means of the $\mathrm{B}^0 - \bar{B}^0$ mixing ratio $\Delta M_d/\Delta M_s$ and the CP-asymmetry $a_{\psi \mathrm{K}_S}$, respectively. In this context, we investigate [6], in analogy to the $(\bar{\varrho}, \bar{\eta})$ plane and the planes $(\sin 2\beta, \sin 2\alpha)$ [7] and $(\gamma, \sin 2\beta)$ [8] considered in the past, the (R_t, β) plane for the exhibition of various constraints on the CKM matrix. We also provide the parametrization of the CKM matrix given directly in terms of the variables (2).

While the set (2) appears to be the best choice for the coming years, our analysis shows that in the long run other choices could turn out to be preferable. In this context it should be emphasized that several of the results and formulae presented here are not entirely new and have been already discussed by us and other authors in the past. In particular in [9] it has been pointed out that only a moderately precise measurement of $\sin 2\alpha$ can be as useful for the UT as a precise measurement of the angle β. This has been recently reemphasized in [10–12], see contribution in this Chapter, Sec. 3.3.. Similarly the measurement of the pair (α, β) has been found to be a very efficient tool for the determination of the UT [13,14] and the construction of the full CKM matrix from the angles of various unitarity triangles has been presented in [15]. Next, the importance of the pair $(R_t, \sin 2\beta)$ has been emphasized recently in a number of papers [16–20]. Many useful relations relevant for the unitarity triangle can also be found in [21,22]. Finally, in a recent paper [6] we have presented a systematic classification of the strategies in question and their comparison. In fact the results of this paper constitute the main part of this section.

1.1. Basic formulae

Let us begin our presentation by listing the formulae for $\bar{\varrho}$ and $\bar{\eta}$ in the strategies in question that are labeled by the two measured quantities as discussed above.

$\boldsymbol{R_t}$ and $\boldsymbol{\beta}$

$$\bar{\varrho} = 1 - R_t \cos\beta, \qquad \bar{\eta} = R_t \sin\beta \; . \tag{3}$$

$\boldsymbol{R_b}$ and $\boldsymbol{\gamma}$

$$\bar{\varrho} = R_b \cos\gamma, \qquad \bar{\eta} = R_b \sin\gamma \; . \tag{4}$$

$\boldsymbol{R_b}$ and $\boldsymbol{R_t}$

$$\bar{\varrho} = \frac{1}{2}(1 + R_b^2 - R_t^2), \qquad \bar{\eta} = \sqrt{R_b^2 - \bar{\varrho}^2} \tag{5}$$

where $\bar{\eta} > 0$ has been assumed.

$\boldsymbol{R_t}$ and $\boldsymbol{\gamma}$

This strategy uses (4) with

$$R_b = \cos\gamma \pm \sqrt{R_t^2 - \sin^2\gamma} \; . \tag{6}$$

The two possibilities can be distinguished by the measured value of R_b.

$\boldsymbol{R_b}$ and $\boldsymbol{\beta}$

This strategy uses (3) and

$$R_t = \cos\beta \pm \sqrt{R_b^2 - \sin^2\beta} \; . \tag{7}$$

The two possibilities can be distinguished by the measured value of R_t.

$\boldsymbol{R_t}$ and $\boldsymbol{\alpha}$

$$\bar{\varrho} = 1 - R_t^2 \sin^2\alpha + R_t \cos\alpha \sqrt{1 - R_t^2 \sin^2\alpha}, \tag{8}$$

$$\bar{\eta} = R_t \sin\alpha \left[R_t \cos\alpha + \sqrt{1 - R_t^2 \sin^2\alpha} \right] \tag{9}$$

where $\cos\gamma > 0$ has been assumed. For $\cos\gamma < 0$ the signs in front of the square roots should be reversed.

$\boldsymbol{R_b}$ and $\boldsymbol{\alpha}$

$$\bar{\varrho} = R_b^2 \sin^2\alpha - R_b \cos\alpha \sqrt{1 - R_b^2 \sin^2\alpha}, \tag{10}$$

$$\bar{\eta} = R_b \sin\alpha \left[R_b \cos\alpha + \sqrt{1 - R_b^2 \sin^2\alpha} \right] \tag{11}$$

where $\cos\beta > 0$ has been assumed.

$\boldsymbol{\beta}$ and $\boldsymbol{\gamma}$

$$R_t = \frac{\sin\gamma}{\sin(\beta+\gamma)}, \qquad R_b = \frac{\sin\beta}{\sin(\beta+\gamma)} \tag{12}$$

and (5).

$\boldsymbol{\alpha}$ and $\boldsymbol{\gamma}$

$$R_t = \frac{\sin\gamma}{\sin\alpha}, \qquad R_b = \frac{\sin(\alpha+\gamma)}{\sin\alpha} \tag{13}$$

and (5).

$\boldsymbol{\alpha}$ and $\boldsymbol{\beta}$

$$R_t = \frac{\sin(\alpha+\beta)}{\sin\alpha}, \qquad R_b = \frac{\sin\beta}{\sin\alpha} \tag{14}$$

and (5).

Finally we give the formulae for the strategies in which $\bar{\eta}$ is directly measured and the strategy allows to determine $\bar{\varrho}$.

$\bar{\boldsymbol{\eta}}$ and $\boldsymbol{R_t}$ or $\boldsymbol{R_b}$

$$\bar{\varrho} = 1 - \sqrt{R_t^2 - \bar{\eta}^2}, \qquad \bar{\varrho} = \pm\sqrt{R_b^2 - \bar{\eta}^2}\,, \tag{15}$$

where in the first case we have excluded the + solution in view of $R_b \leq 0.5$ as extracted from the experimental data on $|V_{ub}|$.

$\bar{\boldsymbol{\eta}}$ and $\boldsymbol{\beta}$ or $\boldsymbol{\gamma}$

$$\bar{\varrho} = 1 - \frac{\bar{\eta}}{\tan\beta}, \qquad \bar{\varrho} = \frac{\bar{\eta}}{\tan\gamma}\,. \tag{16}$$

1.2. CKM matrix and the fundamental variables

It is useful for phenomenological purposes to express the CKM matrix directly in terms of the parameters selected in a given strategy. This can be easily done by inserting the formulae for $\bar{\varrho}$ and $\bar{\eta}$ presented here into the known expressions for the CKM elements in terms of these variables [23,13] as given in Chapter 1.

Here we give explicit result only for the set (2). In order to simplify the notation we use λ instead of $|V_{us}|$ as $V_{us} = \lambda + \mathcal{O}(\lambda^7)$. We find

$$V_{ud} = 1 - \frac{1}{2}\lambda^2 - \frac{1}{8}\lambda^4 + \mathcal{O}(\lambda^6), \qquad V_{ub} = \frac{\lambda}{1-\lambda^2/2}|V_{cb}|\left[1 - R_t e^{i\beta}\right], \tag{17}$$

$$V_{cd} = -\lambda + \frac{1}{2}\lambda|V_{cb}|^2 - \lambda|V_{cb}|^2\left[1 - R_t e^{-i\beta}\right] + \mathcal{O}(\lambda^7), \tag{18}$$

$$V_{cs} = 1 - \frac{1}{2}\lambda^2 - \frac{1}{8}\lambda^4 - \frac{1}{2}|V_{cb}|^2 + \mathcal{O}(\lambda^6), \tag{19}$$

$$V_{tb} = 1 - \frac{1}{2}|V_{cb}|^2 + \mathcal{O}(\lambda^6), \qquad V_{td} = \lambda|V_{cb}|R_t e^{-i\beta} + \mathcal{O}(\lambda^7), \tag{20}$$

$$V_{ts} = -|V_{cb}| + \frac{1}{2}\lambda^2|V_{cb}| - \lambda^2|V_{cb}|\left[1 - R_t e^{-i\beta}\right] + \mathcal{O}(\lambda^6)\,. \tag{21}$$

1.3. Hierarchies of the various strategies

The numerical analysis of various strategies listed above was performed using the Bayesian approach as described in the previous Chapter. The main results of this analysis are depicted in Figs. 6.1, 6.2, 6.3 and 6.4. In Figs. 6.1 and 6.2 we plot the correlation between the precisions on the variables relevant for a given strategy required to reach the assumed precision on $\bar{\eta}$ and $\bar{\varrho}$, respectively. For this exercise we have used, for $\bar{\eta}$ and $\bar{\rho}$, the central values obtained in the previous Chapter. Obviously strategies described by curves in Figs. 6.1 and 6.2 that lie far from the origin are more effective in the determination of the unitarity triangle than those corresponding to curves placed close to the origin.

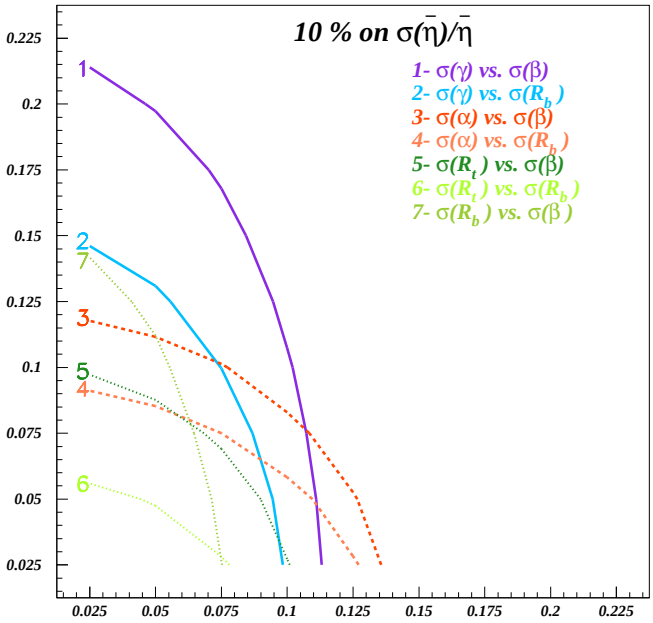

Fig. 6.1: *The plot shows the curves of the 10% relative precision on $\bar{\eta}$ as a function of the precision on the variables of the given strategy.*

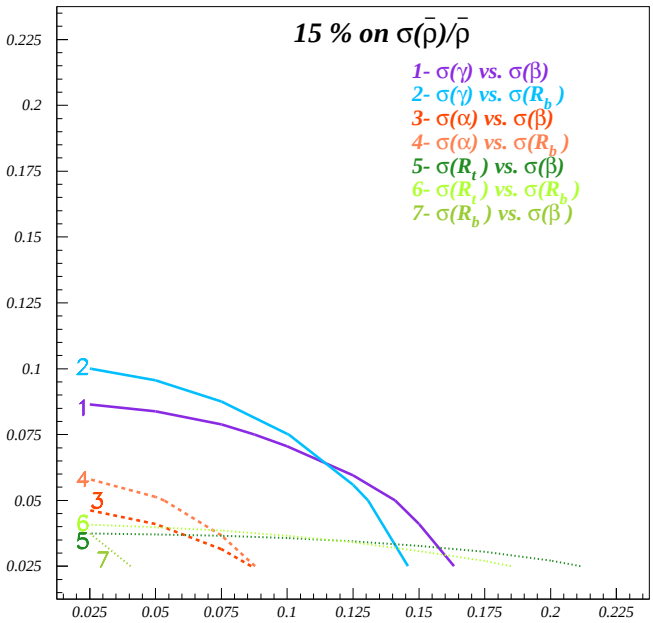

Fig. 6.2: *The plot shows the curves of the 15% relative precision on $\bar{\varrho}$ as a function of the precision on the variables of the given strategy.*

Figures 6.1 and 6.2 reveal certain hierarchies within the strategies in question. In order to find these hierarchies and to eliminate the weakest ones not shown in these figures we divided first the five variables under consideration into two groups:

$$(R_t, \alpha, \gamma), \qquad (R_b, \beta)\ . \tag{22}$$

It turned out then that the four strategies (R_t, α), (R_t, γ), (α, γ) and (R_b, β) which involve pairs of variables belonging to the same group are not particularly useful in the determination of $(\bar{\varrho}, \bar{\eta})$. In the case of (R_b, β) this is related to the existence of two possible solutions as stated above. If one of these solutions can easily be excluded on the basis of R_t, then the effectiveness of this strategy can be increased. We have therefore included this strategy in our numerical analysis. The strategy (R_t, γ) turns out to be less useful in this respect. Similarly the strategy (γ, α) is not particularly useful due to strong correlation between the variables in question as discussed previously by many authors in the literature.

The remaining six strategies that involve pairs of variables belonging to different groups in (22) are all interesting. While some strategies are better suited for the determination of $\bar{\eta}$ and the other for $\bar{\varrho}$, as clearly seen in Figs. 6.1 and 6.2, on the whole a clear ranking of strategies seems to emerge from our analysis.

If we assume the same relative error on α, β, γ, R_b and R_t we find the following hierarchy:

$$1)\ (\gamma, \beta), \quad (\gamma, R_b) \qquad 2)\ (\alpha, \beta), \quad (\alpha, R_b) \qquad 3)\ (R_t, \beta), \quad (R_t, R_b), \quad (R_b, \beta). \tag{23}$$

We observe that in particular the strategies involving R_b and γ are very high on this ranking list. This is related to the fact that $R_b < 0.5 < R_t$ and consequently the action in the $(\bar{\varrho}, \bar{\eta})$ plane takes place closer to the origin of this plane than to the corner of the UT involving the angle β. Consequently the accuracy on R_b and γ does not have to be as high as for R_t and β in order to obtain the same accuracy for $(\bar{\varrho}, \bar{\eta})$. This is clearly seen in Figs. 6.1 and 6.2.

This analysis shows how important is the determination of R_b and γ in addition to β that is already well known. On the other hand the strategy involving R_t and β will be most probably the cleanest one before the LHC experiments unless the error on angle γ from B factories and Tevatron can be significantly decreased below 10% and the accuracy on R_b considerably improved. The explicit strategies for the determination of γ are discussed in the following sections.

The strategies involving α are in our second best class. However, it has to be noticed that in order to get $10\%(15\%)$ relative precision on $\bar{\eta}(\bar{\rho})$ it is necessary (see Figs. 6.1 and 6.2) to determine α with better than 10% relative precision. If $\sin 2\alpha$ could be directly measured this could be soon achieved due to the high sensitivity of $\sin 2\alpha$ to α for α in the ball park of 90° as obtained from the standard analysis of the unitarity triangle. However, from the present perspective this appears to be very difficult in view of the penguin pollution that could be substantial as indicated by the most recent data from Belle [24]. On the other hand, as the BaBar data [25] do not indicate this pollution, the situation is unclear at present. These issues are discussed in detail in the following sections.

We have also performed a numerical analysis for the strategies in which $|\bar{\eta}|$ can be directly measured. The relevant formulae are given in (15) and (16). It turns out that the strategy $(\gamma, \bar{\eta})$ can be put in the first best class in (23) together with the strategies (γ, β) and (γ, R_b).

In Fig. 6.3 we show the resulting regions in the $(\bar{\varrho}, \bar{\eta})$ plane obtained from leading strategies assuming that each variable is measured with 10% accuracy. This figure is complementary to Figs. 6.1 and 6.2 and demonstrates clearly the ranking given in (23).

While at present the set (2) appears to be the leading candidate for the fundamental parameter set in the quark flavour physics for the coming years, it is not clear which set will be most convenient in the

second half of this decade when the B-factories and Tevatron will improve considerably their measurements and LHC will start its operation. Therefore it is of interest to investigate how the measurements of three variables out of $\alpha,\ \beta,\ \gamma$, R_b and R_t will determine the allowed values for the remaining two variables. We illustrate this in Fig. 6.4 assuming a relative error of 10% for the constraints used in each plot. While this figure is self explanatory a striking feature consistent with the hierarchical structure in (23) can be observed. While the measurements of (α, R_t, R_b) and (α, β, R_t) as seen in the first two plots do not appreciably constrain the parameters of the two leading strategies (β, γ) and (R_b, γ), respectively, the opposite is true in the last two plots. There the measurements of (R_b, γ, α) and (β, γ, α) give strong constraints in the (β, R_t) and (R_b, R_t) plane, respectively. The last two plots illustrate also clearly that measuring only α and γ does not provide a strong constraint on the unitarity triangle.

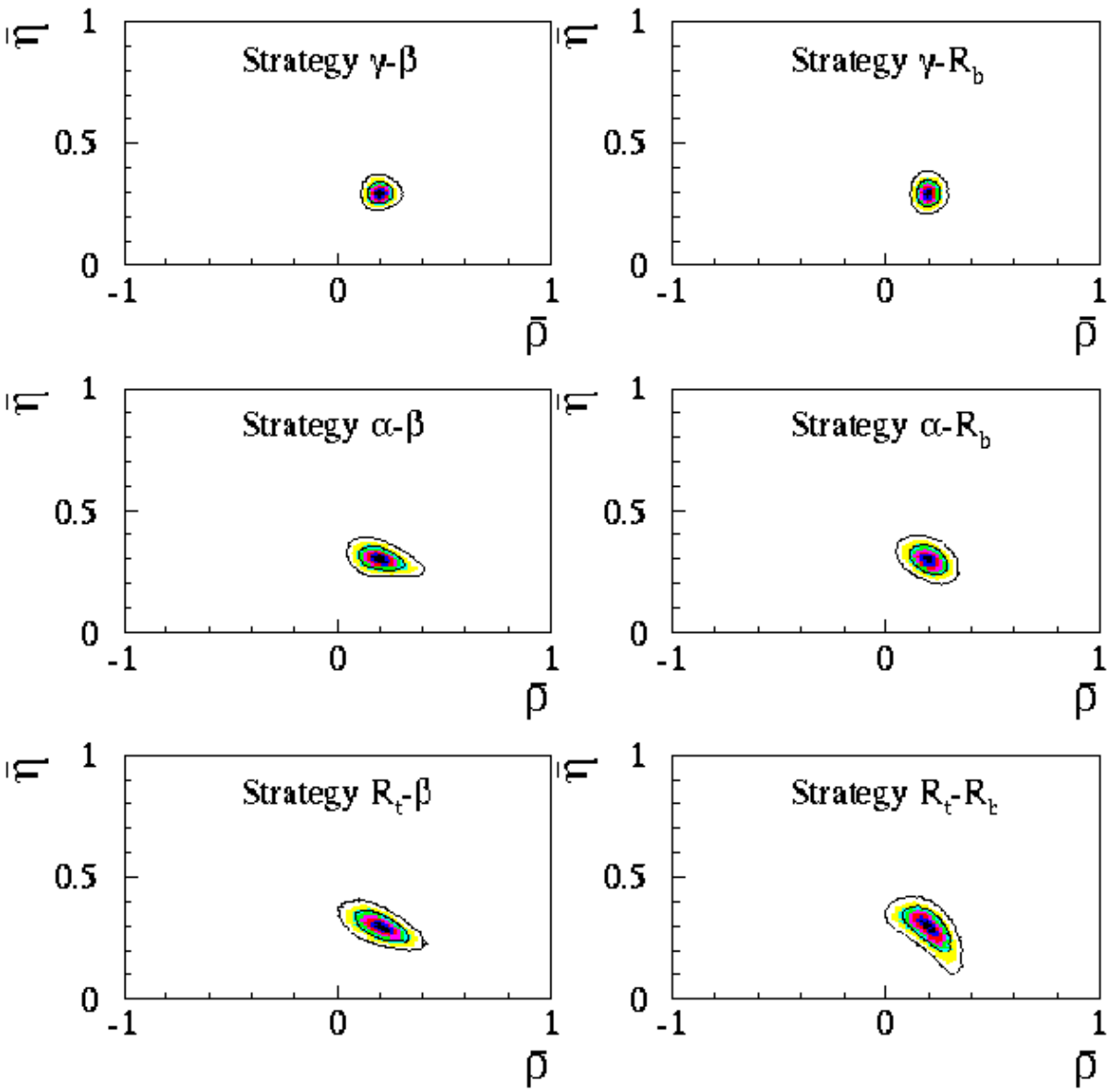

Fig. 6.3: *The plots show the allowed regions (68% and 95%) in the $(\bar{\varrho}, \bar{\eta})$ plane obtained from the leading strategies assuming that each variable is measured with* 10% *accuracy.*

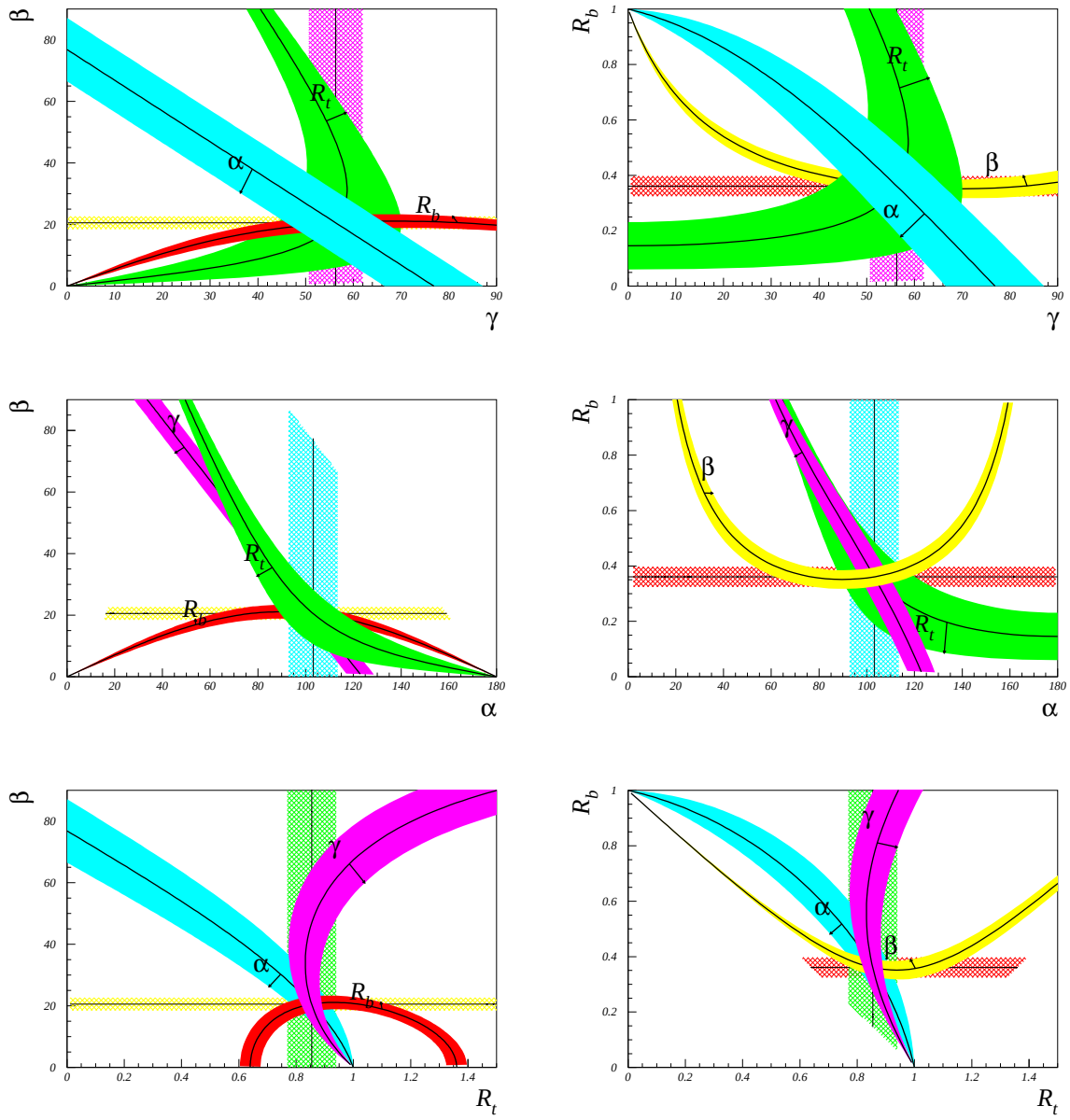

Fig. 6.4: *The plots show the different constraints (assuming a relative error of 10%) in the different planes corresponding to the leading stategies of equation 23. The small arrow indicates the range corresponding to an increase of 10% of the corresponding quantity.*

1.4. Results for the presently available strategies

At present the concrete results can be obtained only for the strategies (R_t, β), (R_b, R_t) and (R_b, β) as no direct measurements of γ and α are available.

The results for $\bar{\rho}$ and $\bar{\eta}$ for the three strategies in question are presented in Table 6.1 and in Figs. 6.5, 6.6 and 6.7. To obtain these results we have used the direct measurement of sin 2β [26], R_t as extracted from ΔM_d and $\Delta M_d/\Delta M_s$ by means of the formulae in [5,27] and R_b as extracted from $|V_{ub}|$.

Strategy	$\bar{\rho}$	$\bar{\eta}$
(R_t, β)	$0.157\ ^{+0.056}_{-0.054}$	$0.367\ ^{+0.036}_{-0.034}$
	[0.047-0.276]	[0.298-0.439]
(R_t, R_b)	$0.161^{+0.055}_{-0.057}$	$0.361\ ^{+0.041}_{-0.045}$
	[0.043-0.288]	[0.250-0.438]
(R_b, β)	$0.137\ ^{+0.135}_{-0.135}$	$0.373\ ^{+0.049}_{-0.063}$
	[-0.095-0.357]	[0.259-0.456]

Table 6.1: *Results for $\bar{\rho}$ and $\bar{\eta}$ for the three indicated strategies using the present knowledge summarized in Table 5.1 in Chapter 5. For the strategy (R_t, β), the solution compatible with the region selected by the R_b constraint has been considered. In squared brackets the 95% probability regions are also given.*

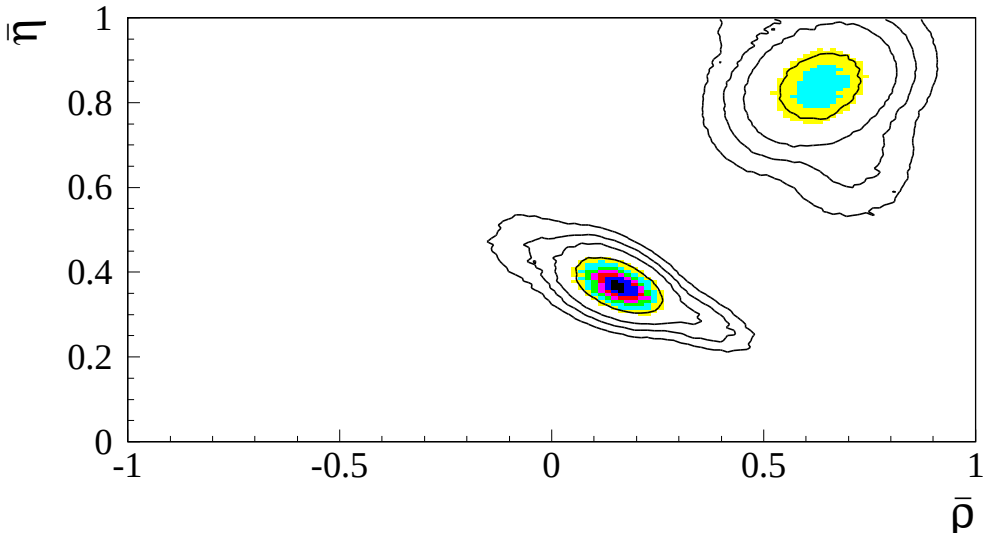

Fig. 6.5: *The plot shows the presently allowed regions (68%,95%,99% and 99.9%) in the $(\bar{\rho}, \bar{\eta})$ plane using the (R_t, β) strategy: the direct measurement of sin 2β and R_t from ΔM_d and $\Delta M_d/\Delta M_s$.*

The experimental and theoretical inputs are summarized in Chapter 4 It should be emphasized that these three presently available strategies are the weakest among the leading strategies listed in (23). Among them (R_t, β) and (R_t, R_b) appear to be superior to (R_b, β) at present. We expect that once ΔM_s has been measured and the error on $\sin 2\beta$ reduced, the strategy (R_t, β) will be leading among these three. Therefore in Fig. 6.8 we show how the presently available constraints look like in the (R_t, β) plane.

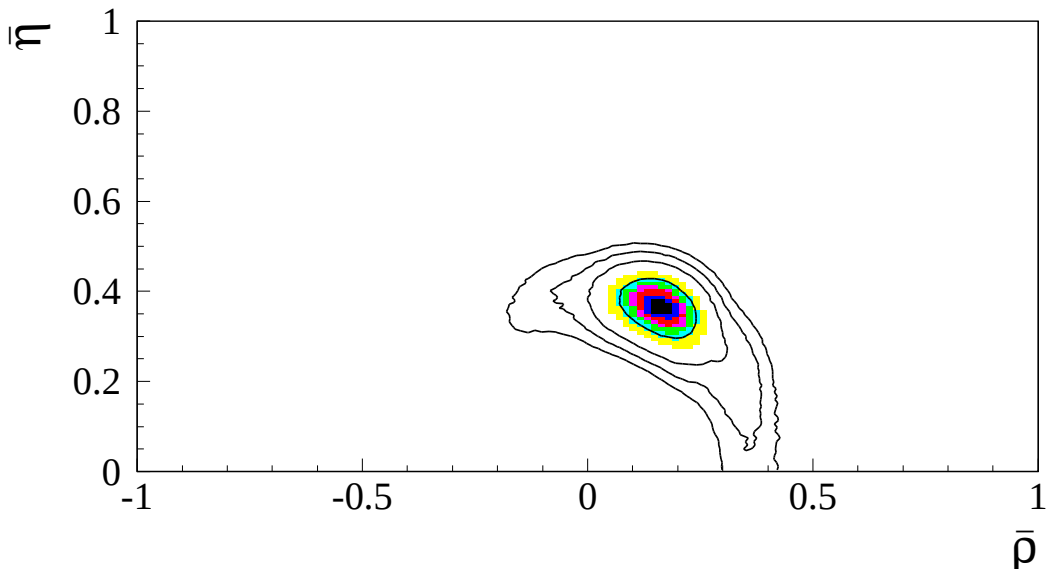

Fig. 6.6: *The plot shows the allowed regions (68%,95%,99% and 99.9%) in the $(\bar{\rho}, \bar{\eta})$ plane using the (R_t, R_b) strategy: R_t from ΔM_d and $\Delta M_d/\Delta M_s$ and R_b from $|V_{ub}|$.*

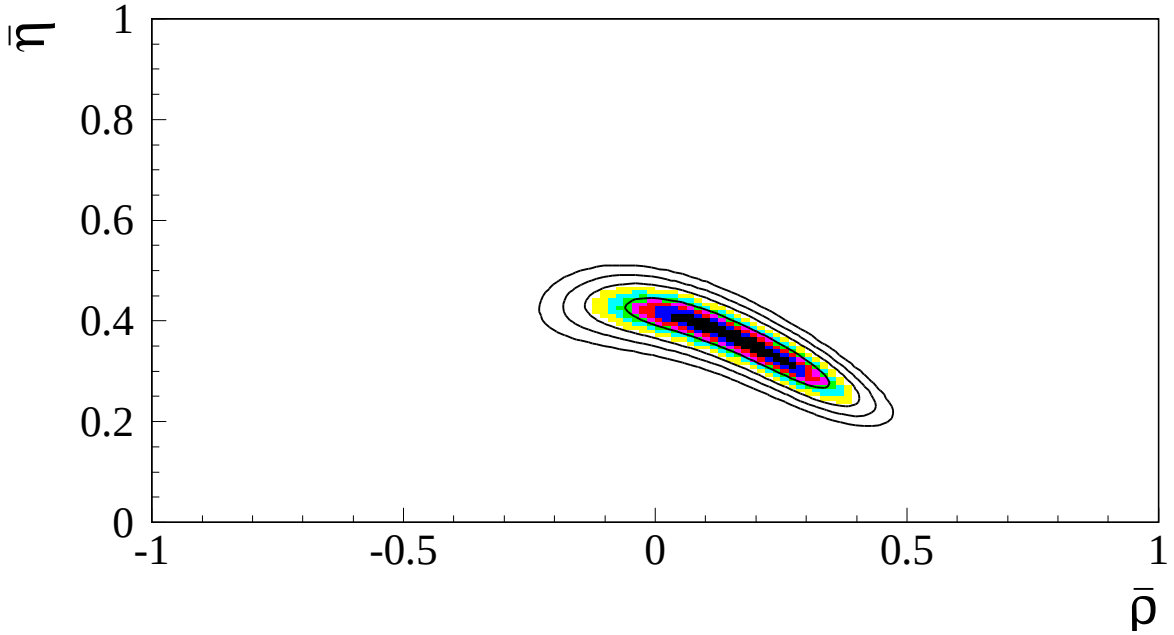

Fig. 6.7: *The plot shows the allowed regions (68%,95%,99% and 99.9%) in the $(\bar{\rho}, \bar{\eta})$ plane using the (R_b, β) strategy: direct measurement of sin 2β and R_b from $|V_{ub}/V_{cb}|$.*

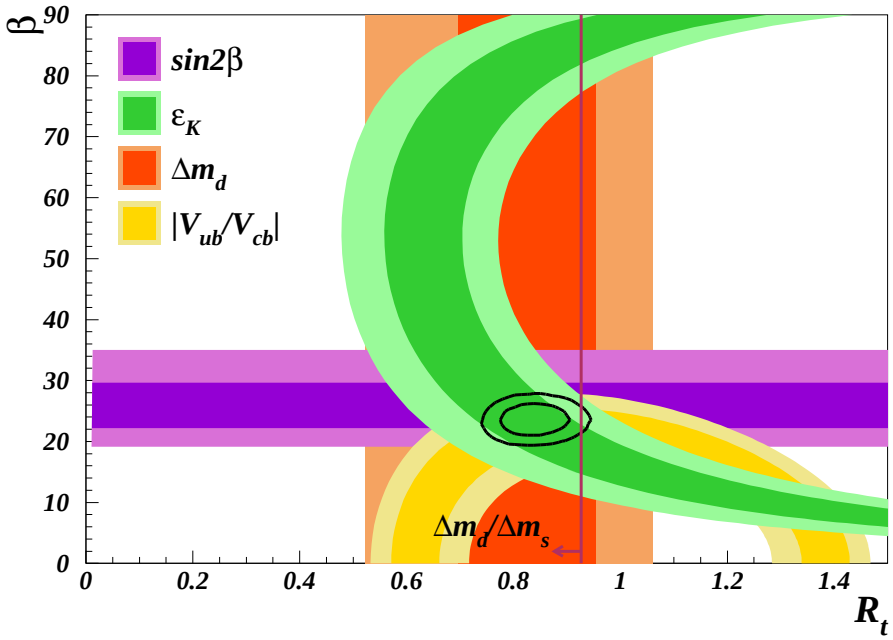

Fig. 6.8: *The plot shows the allowed regions (68% and 95%) in the (R_t, β) plane. Different constraints are also shown.*

1.5. Summary

We have presented a numerical analysis of the unitarity triangle from a different point of view, that emphasizes the role of different strategies in the precise determination of the unitarity triangle parameters. While we have found that the pairs (γ, β), (γ, R_b) and $(\gamma, \bar{\eta})$ are most efficient in determining $(\bar{\varrho}, \bar{\eta})$, we expect that the pair (R_t, β) will play the leading role in the UT fits in the coming years, in particular, when ΔM_s will be measured and the theoretical error on ξ decreased. For this reason we have proposed to plot available constraints on the CKM matrix in the (R_t, β) plane.

It will be interesting to compare in the future the allowed ranges for $(\bar{\varrho}, \bar{\eta})$ resulting from different strategies in order to see whether they are compatible with each other. Any discrepancies will signal the physics beyond the SM. We expect that the strategies involving γ will play a very important role in this comparison.

For the fundamental set of parameters in the quark flavour physics given in (2) we find within the SM

$$|V_{us}| = 0.2240 \pm 0.0036,\ |V_{cb}| = (41.3 \pm 0.7)10^{-3},\ R_t = 0.91 \pm 0.05,\ \beta = (22.4 \pm 1.4)^\circ,$$

where the errors represent one standard deviations and the result for β corresponds to $\sin 2\beta = 0.705 \pm 0.035$.

A complete analysis of the usefulness of a given strategy should also include the discussion of its experimental feasibility and theoretical cleanness. Extensive studies of these two issues can be found in [1–5] and in these proceedings. Again among various strategies, the (R_t, β) strategy is exceptional as the theoretical uncertainties in the determination of these two variables are small and the corresponding experiments are presently feasible. In the long run, when γ will be cleanly measured in $\mathrm{B}_d \to \mathrm{D}\pi$ and $\mathrm{B}_s \to \mathrm{D}_s\mathrm{K}$ decays and constrained through other decays as reviewed in the following sections, we expect that the strategy (γ, β) will take over the leading role. Eventually the independent direct determinations of the five variables in question will be crucial for the tests of the SM and its extensions.

2. Radiative rare B decays

A. Ali and M. Misiak

The transitions $b \to s(d)\gamma$ and $b \to s(d)\ell^+\ell^-$ receive sizable contributions from loops involving the top quark (Fig. 6.9). Their dependence on V_{ts} and V_{td} may be used to test unitarity of the CKM matrix and to overconstrain the Wolfenstein parameters $\bar{\rho}$ and $\bar{\eta}$. The considered transitions manifest themselves in exclusive $\overline{\rm B}$-meson decays like $\overline{\rm B} \to {\rm K}^\star\gamma$, $\overline{\rm B} \to {\rm K}^*\ell^+\ell^-$, $\overline{\rm B} \to \rho\gamma$ and $\overline{\rm B} \to \rho\ell^+\ell^-$. The corresponding inclusive decays $\overline{\rm B} \to X_{s(d)}\gamma$ and $\overline{\rm B} \to X_{s(d)}\ell^+\ell^-$ are experimentally more challenging, but the theoretical predictions are significantly more accurate, thanks to the use of OPE and HQET. The exclusive processes remain interesting due to possible new physics effects in observables other than just the total branching ratios (photon polarization, isospin- and CP-asymmetries), as well as due to information they provide on non-perturbative form-factors. This information is particularly required in analyzing exclusive modes generated by the $b \to d\gamma$ transition, in which case there is little hope for an inclusive measurement.

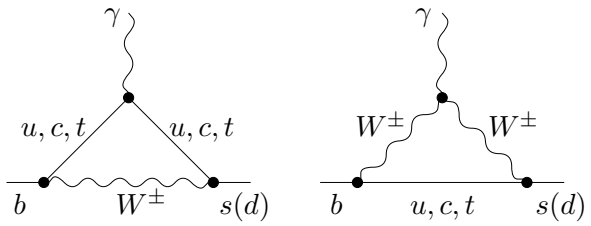

Fig. 6.9: *Leading-order Feynman diagrams for $b \to s(d)\gamma$ in the SM.*

In this section we discuss briefly the generic features of the CKM phenomenology in the considered rare B-decays. The transitions $b \to s\gamma$ and $b \to s\ell^+\ell^-$ involve the CKM matrix elements from the second and third column of this matrix, with the unitarity constraint taking the form $\sum_{u,c,t} \lambda_i = 0$, with $\lambda_i = V_{ib}V_{is}^*$. This equation yields a unitarity triangle which is highly squashed, as one of the sides of this triangle $\lambda_u = V_{ub}V_{us}^* \simeq A\lambda^4(\bar{\rho} - i\bar{\eta})$ is doubly Cabibbo suppressed, compared to the other two sides $\lambda_c \simeq -\lambda_t = A\lambda^2 + ...$ Hence, the transitions $b \to s\gamma$ and $b \to s\ell^+\ell^-$ are not expected to yield useful information on the parameters $\bar{\rho}$ and $\bar{\eta}$, which define the apex of the unitarity triangle of current interest (see Chapt. 1). The test of unitarity for the $b \to s$ transitions in rare B-decays lies in checking the relation $\lambda_t \simeq -\lambda_c$, which holds up to corrections of order λ^2.

The impact of the decays $b \to d\gamma$ and $b \to d\ell^+\ell^-$ on the CKM phenomenology is, however, quite different. These transitions involve the CKM matrix elements in the first and third column, with the unitarity constraints taking the form $\sum_{u,c,t} \xi_i = 0$, with $\xi_i = V_{ib}V_{id}^*$. Now, all three matrix elements are of order λ^3, with $\xi_u \simeq A\lambda^3(\bar{\rho} - i\bar{\eta})$, $\xi_c \simeq -A\lambda^3$, and $\xi_t \simeq A\lambda^3(1 - \bar{\rho} - i\bar{\eta})$. This equation leads to the same unitarity triangle as studied through the constraints V_{ub}/V_{cb}, ΔM_{B_d} (or $\Delta M_{B_d}/\Delta M_{B_s}$). Hence, the transitions $b \to d\gamma$ and $b \to d\ell^+\ell^-$ lead to complementary constraints on the CKM parameters $\bar{\rho}$ and $\bar{\eta}$, as illustrated in the following. Thus, the role of rare B-decays is that they provide complementary constraints on the CKM matrix elements, hence test the CKM unitarity, but they also constrain extensions of the Standard Model, and by that token can act as harbinger of new physics.

A theoretical framework for analyzing the $b \to s\gamma$ transition is set by the effective interaction Hamiltonian

$$\mathcal{H}_{\rm eff} = -\frac{4G_F}{\sqrt{2}} V_{ts}^* V_{tb} \sum_{i=1}^{8} C_i(\mu) Q_i. \tag{24}$$

The generic structure of the operators Q_i is as follows:

$$Q_i = \begin{cases} (\bar{s}\Gamma_i c)(\bar{c}\Gamma'_{\underline{i}} b), & i = 1,2, \\ (\bar{s}\Gamma_i b)\sum_q (\bar{q}\Gamma'_{\underline{i}} q), & i = 3,4,5,6, \qquad (q = u,d,s,c,b) \\ \frac{e m_b}{16\pi^2}\bar{s}_L \sigma^{\mu\nu} b_R F_{\mu\nu}, & i = 7, \\ \frac{g_s m_b}{16\pi^2}\bar{s}_L \sigma^{\mu\nu} T^a b_R G^a_{\mu\nu}, & i = 8. \end{cases} \tag{25}$$

Here, Γ_i and Γ'_i denote various combinations of the colour and Dirac matrices. Everything that is not important for $b \to s\gamma$ at the leading order in $\alpha_{\rm em}$, m_b/m_W, m_s/m_b and V_{ub}/V_{cb} has been neglected in Eq. (24).

Perturbative calculations (see Ref. [28] and refs. therein) are used to find the Wilson coefficients in the $\overline{\rm MS}$ scheme, at the renormalization scale $\mu_b \sim m_b$

$$C_i(\mu_b) = C_i^{(0)}(\mu_b) + \frac{\alpha_s(\mu_b)}{4\pi} C_i^{(1)}(\mu_b) + \left(\frac{\alpha_s(\mu_b)}{4\pi}\right)^2 C_i^{(2)}(\mu_b) + \ldots . \tag{26}$$

Here, $C_i^{(n)}(\mu_b)$ depend on α_s only via the ratio $\eta \equiv \alpha_s(\mu_0)/\alpha_s(\mu_b)$, where $\mu_0 \sim m_W$. In the Leading Order (LO) calculations, everything but $C_i^{(0)}(\mu_b)$ is neglected in Eq. (26). At the Next-to-Leading Order (NLO), one takes $C_i^{(1)}(\mu_b)$ into account. The Wilson coefficients contain information on the short-distance QCD effects due to hard gluon exchanges between the quark lines of the leading one-loop electroweak diagrams (Fig. 6.9). Such effects enhance the perturbative branching ratio $\mathcal{B}(b \to s\gamma)$ by roughly a factor of three [29].

The same formalism applies to $b \to d\gamma$, too. The corresponding operators Q_i are obtained by replacing $\bar{s} \to \bar{d}$ in Eq. (25), and by including the u-quark analogues of $Q_{1,2}$. The latter operators are no longer CKM-suppressed. The matching conditions $C_i(\mu_0)$ and the solutions of the RG equations, yielding $C_i(\mu_b)$, coincide with those needed for the process $b \to s\gamma$.

2.1. Inclusive $\overline{\rm B} \to X_{s(d)}\gamma$ decay

The inclusive branching ratio $\mathcal{B}(\overline{\rm B} \to X_s\gamma)$ was measured for the first time by CLEO in 1995 [30]. The present world averages

$$\mathcal{B}(\overline{\rm B} \to X_s\gamma \ (E_\gamma > 1.6 \text{ GeV})) = \left(3.28\ ^{+0.41}_{-0.36}\right) \times 10^{-4}, \tag{27}$$

$$\mathcal{B}(\overline{\rm B} \to X_s\gamma \ (E_\gamma > \tfrac{1}{20} m_b\ )) = \left(3.40\ ^{+0.42}_{-0.37}\right) \times 10^{-4} \tag{28}$$

are found from the following four measurements

$$\mathcal{B}(\overline{\rm B} \to X_s\gamma\,(E_\gamma > \tfrac{1}{20}m_b)) = \left[3.88 \pm 0.36_{\rm stat} \pm 0.37_{\rm sys}\ \left(^{+0.43}_{-0.23}\right)_{\rm theory}\right] \times 10^{-4}, \quad \text{(BABAR [31])},$$

$$\mathcal{B}(\overline{\rm B} \to X_s\gamma\,(E_\gamma > \tfrac{1}{20}m_b)) = \left[3.21 \pm 0.43_{\rm stat} \pm 0.27_{\rm sys}\ \left(^{+0.18}_{-0.10}\right)_{\rm theory}\right] \times 10^{-4}, \quad \text{(CLEO [32])},$$

$$\mathcal{B}(\overline{\rm B} \to X_s\gamma\,(E_\gamma > \tfrac{1}{20}m_b)) = \left[3.36 \pm 0.53_{\rm stat} \pm 0.42_{\rm sys}\ \left(^{+0.50}_{-0.54}\right)_{\rm theory}\right] \times 10^{-4}, \quad \text{(BELLE [33])},$$

$$\mathcal{B}(b \to s\gamma) = (3.11 \pm 0.80_{\rm stat} \pm 0.72_{\rm sys}) \times 10^{-4}, \quad \text{(ALEPH [34])},$$

in which full correlation of the "theory" errors has been assumed. The averages (27) and (28) are perfectly consistent with the SM predictions [35,36]

$$\mathcal{B}(\overline{\rm B} \to X_s\gamma \ (E_\gamma > 1.6 \text{ GeV}))_{\rm SM} = (3.57 \pm 0.30) \times 10^{-4}, \tag{29}$$

$$\mathcal{B}(\overline{\rm B} \to X_s\gamma \ (E_\gamma > \tfrac{1}{20} m_b\ ))_{\rm SM} = 3.70 \times 10^{-4}. \tag{30}$$

By convention, contributions to $\overline{\rm B} \to X_s\gamma$ from the intermediate real ψ and ψ' are treated as background, while all the continuum $c\bar{c}$ states are included assuming quark-hadron duality. Non-continuum states other than ψ and ψ' have negligible effect.

When the theoretical result (29) is reevaluated without use of the CKM unitarity in the dominant contributions (i.e. everywhere except for three small ($< 2.5\%$) corrections), comparison with the experiment (27) leads to the following constraint on the CKM matrix elements

$$| \, 1.69 \, \lambda_u \, + \, 1.60 \, \lambda_c \, + \, 0.60 \, \lambda_t \, | \;\; = \;\; (\, 0.94 \; \pm \; 0.07 \,) \, |V_{cb}|. \tag{31}$$

After using the numerical values of $\lambda_c \simeq |V_{cb}| = (41.0 \pm 2.1) \times 10^{-3}$ and λ_u from the PDG [37], this equation yields $\lambda_t \simeq -47 \times 10^{-3}$ with an error of around 17%. This is consistent with the unitarity relation $\lambda_c \simeq -\lambda_t$. This relation, however, holds in the SM with much better accuracy than what has just been derived from Eq. (31). On the other hand, if the SM with 3 generations is not valid, Eq. (31) is not valid either.

Contrary to $\mathcal{B}(\overline{\rm B} \to X_s\gamma)$, the branching ratio $\mathcal{B}(\overline{\rm B} \to X_d\gamma)$, if measured, would provide us with useful constraints on the Wolfenstein parameters $\bar\rho$ and $\bar\eta$. After using the CKM unitarity, it can be written as

$$\mathcal{B}(\overline{\rm B} \to X_d\gamma) = \frac{|\xi_t|^2}{|V_{cb}|^2} D_t + \frac{|\xi_u|^2}{|V_{cb}|^2} D_u + \frac{Re(\xi_t^* \xi_u)}{|V_{cb}|^2} D_r + \frac{Im(\xi_t^* \xi_u)}{|V_{cb}|^2} D_i \, . \tag{32}$$

The factors ξ_i have been defined earlier. The quantities D_a ($a = t, u, r, i$), which depend on various input parameters such as m_t, m_b, m_c, μ_b and α_s, are given in Ref. [38]. Typical values of these quantities (in units of λ^4) are: $D_t = 0.154, D_u = 0.012, D_r = -0.028$, and $D_i = 0.042$, corresponding to the scale $\mu = 5$ GeV, and the pole quark mass ratio $m_c/m_b = 0.29$. The charge-conjugate averaged branching ratio $\langle \mathcal{B}(B \to X_d\gamma) \rangle$ is obtained by discarding the last term on the right hand side of Eq. (32).

It is convenient to consider the ratio

$$\begin{aligned} \frac{\langle \mathcal{B}(B \to X_d\gamma) \rangle}{\langle \mathcal{B}(B \to X_s\gamma) \rangle} \;\; &= \;\; \frac{|\xi_t|^2}{|\lambda_t|^2} + \frac{D_u}{D_t} \frac{|\xi_u|^2}{|\lambda_t|^2} + \frac{D_r}{D_t} \frac{Re(\xi_t^* \xi_u)}{|\lambda_t|^2} \\ &= \;\; \lambda^2 \left[(1-\bar\rho)^2 + \bar\eta^2 + \frac{D_u}{D_t} (\bar\rho^2 + \bar\eta^2) + \frac{D_r}{D_t} (\bar\rho(1-\bar\rho) - \bar\eta^2) \right] + O(\lambda^4) \\ &\simeq \;\; 0.036 \quad [\text{for } (\bar\rho, \bar\eta) = (0.22, 0.35)] \; . \end{aligned} \tag{33}$$

The above result together with Eq. (30) implies $\langle \mathcal{B}(\overline{\rm B} \to X_d\gamma) \rangle \simeq 1.3 \times 10^{-5}$ in the SM. Thus, with $O(10^8)$ $\rm B\overline{B}$ events already collected at the B factories, $O(10^3)$ $b \to d\gamma$ decays are already produced. However, extracting them from the background remains a non-trivial issue.

Apart from the total branching ratios, the inclusive decays $\overline{\rm B} \to X_{s(d)}\gamma$ provide us with other observables that might be useful for the CKM phenomenology. First, as discussed in Chapt. 3, the $\overline{\rm B} \to X_s\gamma$ photon spectrum is used to extract the HQET parameters that are crucial for the determination of V_{ub} and $|V_{cb}|$. Second, CP-asymmetries contain information on the CKM phase. These asymmetries can be either direct (i.e. occur in the decay amplitudes) or induced by the $\rm B\overline{B}$ mixing.

The mixing-induced CP-asymmetries in $\overline{\rm B} \to X_{s(d)}\gamma$ are very small ($\mathcal{O}(m_{s(d)}/m_b)$) in the SM, so long as the photon polarizations are summed over. It follows from the particular structure of the dominant operator Q_7 in Eq. (25), which implies that photons produced in the decays of B and $\overline{\rm B}$ have opposite *circular* polarizations. Thus, in the absence of new physics, observation of the mixing-induced CP-violation would require selecting particular *linear* photon polarization with the help of matter-induced photon conversion into e^+e^- pairs [39].

The SM predictions for the direct CP-asymmetries read

$$\mathcal{A}_{\rm CP}({\rm B} \to X_s\gamma) \equiv \frac{\Gamma(\overline{\rm B} \to X_s\gamma) - \Gamma({\rm B} \to X_{\overline{s}}\gamma)}{\Gamma(\overline{\rm B} \to X_s\gamma) + \Gamma({\rm B} \to X_{\overline{s}}\gamma)} \simeq \frac{{\rm Im}(\lambda_t^* \lambda_u) D_i}{|\lambda_t|^2 \, D_t} \;\; \simeq \;\; 0.27 \, \lambda^2 \bar\eta \;\sim\; 0.5\%, \tag{34}$$

$$\mathcal{A}_{\rm CP}(\mathrm{B}\to \mathrm{X_d}\gamma) \equiv \frac{\Gamma(\overline{\mathrm{B}}\to \mathrm{X_d}\gamma)-\Gamma(\mathrm{B}\to \mathrm{X}_{\overline{\mathrm{d}}}\gamma)}{\Gamma(\overline{\mathrm{B}}\to \mathrm{X_d}\gamma)+\Gamma(\mathrm{B}\to \mathrm{X}_{\overline{\mathrm{d}}}\gamma)} \simeq \frac{\mathrm{Im}(\xi_{\rm t}^*\xi_{\rm u})\mathrm{D_i}}{|\xi_{\rm t}|^2\,\mathrm{D_t}} \;\simeq\; \frac{-0.27\,\bar\eta}{(1-\bar\rho)^2+\bar\eta^2} \sim -13\%, \quad (35)$$

where $\bar\rho = 0.22$ and $\bar\eta = 0.35$ have been used in the numerical estimates. As stressed in Ref. [38], there is considerable scale uncertainty in the above predictions, which would require a NLO calculation of D_i to be brought under theoretical control. The smallness of $\mathcal{A}_{\rm CP}(\mathrm{B}\to X_s\gamma)$ is caused by three suppression factors: λ_u/λ_t, α_s/π and m_c^2/m_b^2. This SM prediction is consistent with the CLEO bound $-0.27 < \mathcal{A}_{\rm CP}(\mathrm{B}\to X_s\gamma) < +0.10$ at 95% C.L. [40].

No experimental limit has been announced so far on either the branching ratio $\mathcal{B}(\overline{\mathrm{B}}\to X_d\gamma)$ or the CP asymmetry $\mathcal{A}_{\rm CP}(\mathrm{B}\to X_d\gamma)$. While experimentally challenging, the measurement of these quantities might ultimately be feasible at the B-factories which would provide valuable and complementary constraints on the CKM parameters.

2.2. Exclusive radiative B decays

The effective Hamiltonian sandwiched between the B-meson and a single meson state (say, K^* or ρ in the transitions $\mathrm{B}\to(\mathrm{K}^\star,\rho)\gamma$) can be expressed in terms of matrix elements of bilinear quark currents inducing heavy-light transitions. These matrix elements are dominated by strong interactions at small momentum transfer and cannot be calculated perturbatively. They have to be obtained from a non-perturbative method, such as the lattice-QCD and the QCD sum rule approach. As the inclusive branching ratio $\mathcal{B}(\mathrm{B}\to X_s\gamma)$ in the SM is in striking agreement with data, the role of the branching ratio $\mathcal{B}(\mathrm{B}\to \mathrm{K}^*\gamma)$ is that it will determine the form factor governing the electromagnetic penguin transition, $T_1^{\mathrm{K}^*}(0)$.

To get a firmer theoretical prediction on the decay rate, one has to include the perturbative QCD radiative corrections arising from the vertex renormalization and the hard spectator interactions. To incorporate both types of QCD corrections, it is helpful to use a factorization Ansatz for the heavy-light transitions at large recoil and at leading order in the inverse heavy meson mass, introduced in Ref. [41]. Exemplified here by the $\mathrm{B}\to V\gamma^*$ transition, a typical amplitude $f_k(q^2)$ can be written in the form

$$f_k(q^2) = C_{\perp k}\xi_\perp(q^2) + C_{\parallel k}\xi_\parallel(q^2) + \Phi_B\otimes T_k(q^2)\otimes\Phi_V, \quad (36)$$

where $\xi_\perp(q^2)$ and $\xi_\parallel(q^2)$ are the two independent form factors in these decays remaining in the heavy quark and large energy limit; $T_k(q^2)$ is a hard-scattering kernel calculated to $O(\alpha_s)$; Φ_B and Φ_V are the light-cone distribution amplitudes of the B- and vector-meson, respectively, the symbol $\otimes$ denotes convolution with T_k, and $C_k = 1 + O(\alpha_s)$ are the hard vertex renormalization coefficients. In a number of papers [42–44], the factorization Ansatz of Eq. (36) is shown to hold in $O(\alpha_s)$, leading to the explicit $O(\alpha_s)$ corrections to the amplitudes $\mathrm{B}\to V\gamma$ and $\mathrm{B}\to V\ell^+\ell^-$.

Experiment	$\mathcal{B}_{\rm exp}(\mathrm{B}^0(\overline{\mathrm{B}}^0)\to \mathrm{K}^{*0}(\overline{\mathrm{K}}^{*0})+\gamma)$	$\mathcal{B}_{\rm exp}(\mathrm{B}^\pm\to \mathrm{K}^{*\pm}+\gamma)$
CLEO [45]	$(4.55^{+0.72}_{-0.68}\pm 0.34)\times 10^{-5}$	$(3.76^{+0.89}_{-0.83}\pm 0.28)\times 10^{-5}$
BELLE [46]	$(3.91\pm 0.23\pm 0.25)\times 10^{-5}$	$(4.21\pm 0.35\pm 0.31)\times 10^{-5}$
BABAR [47]	$(4.23\pm 0.40\pm 0.22)\times 10^{-5}$	$(3.83\pm 0.62\pm 0.22)\times 10^{-5}$

Table 6.2: *Experimental branching ratios for the decays* $\mathrm{B}^0(\overline{\mathrm{B}}^0)\to \mathrm{K}^{*0}(\overline{\mathrm{K}}^{*0})\gamma$ *and* $\mathrm{B}^\pm\to \mathrm{K}^{*\pm}\gamma$.

We first discuss the exclusive decay $\mathrm{B}\to \mathrm{K}^*\gamma$, for which data from the CLEO, BABAR, and BELLE measurements are available and given in Table 6.2 for the charge conjugated averaged branching ratios. We note that the BELLE data alone has reached a statistical accuracy of better than 10%.

Adding the statistical and systematic errors in quadrature, we get the following world averages for the branching ratios:

$$\begin{aligned} \mathcal{B}(\mathrm{B}^0 \to \mathrm{K}^{*0}\gamma) &= (4.08 \pm 0.26) \times 10^{-5} , \\ \mathcal{B}(\mathrm{B}^\pm \to \mathrm{K}^\pm\gamma) &= (4.05 \pm 0.35) \times 10^{-5} . \end{aligned} \tag{37}$$

The two branching ratios are completely consistent with each other, ruling out any significant isospin breaking in the respective decay widths, which is not expected in the SM [48] but anticipated in some beyond-the-SM scenarios. Likewise, the CP asymmetry in $\mathrm{B} \to \mathrm{K}^*\gamma$ decays, which in the SM is expected to be of the same order of magnitude as for the inclusive decay, namely $\mathcal{A}_{\rm CP}(\mathrm{B} \to \mathrm{K}^*\gamma) \le 1\%$, is completely consistent with the present experimental bounds, the most stringent of which is posted by the BELLE collaboration [46]: $\mathcal{A}_{\rm CP}(\mathrm{B} \to \mathrm{K}^*\gamma) = -0.022 \pm 0.048 \pm 0.017$. In view of this, we shall concentrate in the following on the branching ratios in $\mathrm{B} \to \mathrm{K}^*\gamma$ decays to determine the form factors.

Ignoring the isospin differences in the decay widths of $\mathrm{B} \to \mathrm{K}^*\gamma$ decays, the branching ratios for $\mathrm{B}^\pm \to \mathrm{K}^{*\pm}\gamma$ and $\mathrm{B}^0(\overline{\mathrm{B}}^0) \to \mathrm{K}^{*0}(\overline{\mathrm{K}}^{*0})\gamma$ can be expressed as:

$$\begin{aligned} \mathcal{B}_{\rm th}(\mathrm{B} \to \mathrm{K}^*\gamma) &= \tau_B\, \Gamma_{\rm th}(\mathrm{B} \to \mathrm{K}^*\gamma) \\ &= \tau_B\, \frac{G_F^2 \alpha |V_{tb}V_{ts}^*|^2}{32\pi^4}\, m_{b,\rm pole}^2\, M^3\, \left[\xi_\perp^{(\mathrm{K}^*)}\right]^2 \left(1 - \frac{m_{\mathrm{K}^*}^2}{M^2}\right)^3 \left| C_7^{(0)\rm eff} + A^{(1)}(\mu)\right|^2 , \end{aligned} \tag{38}$$

where G_F is the Fermi coupling constant, $\alpha = \alpha(0) = 1/137$ is the fine-structure constant, $m_{b,\rm pole}$ is the pole b-quark mass, M and M_{K^*} are the B- and K*-meson masses, and τ_B is the lifetime of the B^0- or B^+-meson. The quantity $\xi_\perp^{K^*}$ is the soft part of the form factor $T_1^{K^*}(q^2 = 0)$ in the $\mathrm{B} \to \mathrm{K}^*\gamma$ transition, to which the symmetries in the large energy limit apply. The two form factors $\xi_\perp^{K^*}$ and $T_1^{K^*}(q^2 = 0)$ are related by perturbative $(O(\alpha_s))$ and power $(O(\Lambda_{\rm QCD}/m_b))$ corrections [50]. Thus, one could have equivalently expressed the $O(\alpha_s)$-corrected branching ratio for $\mathrm{B} \to \mathrm{K}^*\gamma$ in terms of the QCD form factor $T_1^{K^*}(q^2 = 0)$, and a commensurately modified expression for the explicit $O(\alpha_s)$ correction in the above equation [43]. In any case, the form factor $T_1^{K^*}(q^2 = 0)$ or $\xi_\perp^{K^*}$ has to be determined by a non-perturbative method.

The function $A^{(1)}$ in Eq. (38) can be decomposed into the following three components:

$$A^{(1)}(\mu) = A_{C_7}^{(1)}(\mu) + A_{\rm ver}^{(1)}(\mu) + A_{\rm sp}^{(1)K^*}(\mu_{\rm sp}) . \tag{39}$$

Here, $A_{C_7}^{(1)}$ and $A_{\rm ver}^{(1)}$ are the $O(\alpha_s)$ (i.e. NLO) corrections due to the Wilson coefficient $C_7^{\rm eff}$ and in the $b \to s\gamma$ vertex, respectively, and $A_{\rm sp}^{(1)K^*}$ is the $\mathcal{O}(\alpha_s)$ hard-spectator correction to the $\mathrm{B} \to \mathrm{K}^*\gamma$ amplitude computed in [42–44]. This formalism leads to the following branching ratio for $\mathrm{B} \to \mathrm{K}^*\gamma$ decays:

$$\mathcal{B}_{\rm th}(\mathrm{B} \to \mathrm{K}^*\gamma) \simeq (7.2 \pm 1.1) \times 10^{-5} \left(\frac{\tau_B}{1.6\ \mathrm{ps}}\right) \left(\frac{m_{b,\rm pole}}{4.65\ \mathrm{GeV}}\right)^2 \left(\frac{\xi_\perp^{(K^*)}}{0.35}\right)^2 , \tag{40}$$

where the default values of the three input parameters are made explicit, with the rest of the theoretical uncertainties indicated numerically; the default value for the form factor $\xi_\perp^{(K^*)}(0)$ is based on the light-cone QCD sum rule estimates [49].

The non-perturbative parameter $\xi_\perp^{(K^*)}(0)$ can now be extracted from the data on the branching ratios for $\mathrm{B} \to \mathrm{K}^*\gamma$ decays, given in Eq. (37), leading to the current world average $\langle \mathcal{B}(\mathrm{B} \to \mathrm{K}^*\gamma)\rangle = (4.06 \pm 0.21) \times 10^{-5}$, which then yields

$$\bar{\xi}_\perp^{(K^*)}(0) = 0.25 \pm 0.04, \qquad \left[\bar{T}_1^{(K^*)}(0, \bar{m}_b) = 0.27 \pm 0.04\right] , \tag{41}$$

where we have used the $O(\alpha_s)$ relation between the effective theory form factor $\xi_\perp^{(K^*)}(0)$ and the full QCD form factor $T_1^{(K^*)}(0,\bar{m}_b)$, worked out in [50]. This estimate is significantly smaller than the corresponding predictions from the QCD sum rules analysis $T_1^{(K^*)}(0) = 0.38 \pm 0.06$ [51,49] and from the lattice simulations $T_1^{(K^*)}(0) = 0.32^{+0.04}_{-0.02}$ [52]. Clearly, more work is needed to calculate the $\mathrm{B} \to \mathrm{K}^*\gamma$ decay form factors precisely.

As already discussed, inclusive $b \to d\gamma$ transitions are not yet available experimentally. This lends great importance to the exclusive decays, such as $\mathrm{B} \to \rho\gamma, \omega\gamma$, to whose discussion we now turn. These decays differ from their $\mathrm{B} \to \mathrm{K}^*\gamma$ counterparts, in that the annihilation contributions are not Cabibbo-suppressed. In particular, the isospin-violating ratios and CP-asymmetries in the decay rates involving the decays $\mathrm{B}^\pm \to \rho^\pm\gamma$ and $\mathrm{B}^0(\overline{\mathrm{B}^0}) \to \rho^0\gamma$ are sensitive to the penguin and annihilation interference in the amplitudes.

We recall that ignoring the perturbative QCD corrections to the penguin amplitudes the ratio of the branching ratios for the charged and neutral B-meson decays in $\mathrm{B} \to \rho\gamma$ can be written as [53,54]

$$\frac{\mathcal{B}(\mathrm{B}^- \to \rho^-\gamma)}{2\mathcal{B}(\mathrm{B}^0 \to \rho^0\gamma)} \simeq \left| 1 + \epsilon_A \mathrm{e}^{i\phi_A} \frac{V_{ub}V_{ud}^*}{V_{tb}V_{td}^*} \right|^2 , \tag{42}$$

where $\epsilon_A \mathrm{e}^{i\phi_A}$ includes the dominant W-annihilation and possible sub-dominant long-distance contributions. We shall use the value $\epsilon_A \simeq +0.30 \pm 0.07$ for the decays $\mathrm{B}^\pm \to \rho^\pm\gamma$ [55,56], obtained assuming factorization of the annihilation amplitude. The corresponding quantity for the decays $\mathrm{B}^0 \to \rho^0\gamma$ is suppressed due to the electric charge of the spectator quark in B^0 as well as by the unfavourable colour factors. Typical estimates for ϵ_A in $\mathrm{B}^0 \to \rho^0\gamma$ put it at around 5% [55,56]. The strong interaction phase ϕ_A vanishes in $\mathcal{O}(\alpha_s)$ in the chiral limit and to leading twist [54], giving theoretical credibility to the factorization-based estimates. Thus, in the QCD factorization approach the phase ϕ_A is expected to be small and one usually sets $\phi_A = 0$. Of course, $O(\alpha_s)$ vertex and hard spectator corrections generate non-zero strong phases, as discussed later. The isospin-violating correction depends on the unitarity triangle phase α due to the relation:

$$\frac{V_{ub}V_{ud}^*}{V_{tb}V_{td}^*} = -\left| \frac{V_{ub}V_{ud}^*}{V_{tb}V_{td}^*} \right| \mathrm{e}^{i\alpha} . \tag{43}$$

The NLO corrections to the branching ratios of the exclusive decays $\mathrm{B}^\pm \to \rho^\pm\gamma$ and $\mathrm{B}^0 \to \rho^0\gamma$ are derived very much along the same lines as outlined for the decays $\mathrm{B} \to \mathrm{K}^*\gamma$. Including the annihilation contribution, the $\mathrm{B} \to \rho\gamma$ branching ratios, isospin- and CP-violating asymmetries are given in [43,44].

Concentrating on the decays $\mathrm{B}^\pm \to \rho^\pm\gamma$, the expression for the ratio $R(\rho\gamma/\mathrm{K}^*\gamma) \equiv \mathcal{B}(B^\pm \to \rho^\pm\gamma)/\mathcal{B}(\mathrm{B}^\pm \to \mathrm{K}^{*\pm}\gamma)$ (where an average over the charge-conjugated modes is implied) can be written as [44]

$$R(\rho\gamma/\mathrm{K}^*\gamma) = S_\rho \left| \frac{V_{td}}{V_{ts}} \right|^2 \frac{(M_B^2 - M_\rho^2)^3}{(M_B^2 - M_{K^*}^2)^3} \zeta^2 (1 + \Delta R) , \tag{44}$$

where $S_\rho = 1$ for the $\rho^\pm$ meson, and $\zeta = \xi_\perp^\rho(0)/\xi_\perp^{K^*}(0)$, with $\xi_\perp^\rho(0)(\xi_\perp^{K^*}(0))$ being the form factors (at $q^2 = 0$) in the effective heavy quark theory for the decays $\mathrm{B} \to \rho\gamma(\mathrm{B} \to \mathrm{K}^*\gamma)$. The quantity $(1 + \Delta R)$ entails the explicit $O(\alpha_s)$ corrections, encoded through the functions $A_\mathrm{R}^{(1)K^*}$, $A_\mathrm{R}^{(1)t}$ and A_R^u, and the long-distance contribution L_R^u. For the decays $\mathrm{B}^\pm \to \rho^\pm\gamma$ and $\mathrm{B}^\pm \to \mathrm{K}^{*\pm}\gamma$, this can be written after charge conjugated averaging as

$$\begin{aligned} 1 + \Delta R^\pm &= \left| \frac{C_7^d + \lambda_u L_R^u}{C_7^s} \right|^2 \left(1 - 2A_R^{(1)K^*} \frac{\Re C_7^s}{|C_7^s|^2} \right) \\ &\quad + \frac{2}{|C_7^s|^2} \Re \left[(C_7^d + \lambda_u L_R^u)(A_R^{(1)t} + \lambda_u^* A_R^u) \right] . \end{aligned} \tag{45}$$

$\zeta = 0.76 \pm 0.10$	$L_R^u = -0.095 \pm 0.022$
$A^{(1)K^*} = -0.113 - i0.043$	$A^{(1)t} = -0.114 - i0.045$
$A^u = -0.0181 + i0.0211$	
$\eta_{tt} = 0.57$	$\eta_{cc} = 1.38 \pm 0.53$
$\eta_{tc} = 0.47 \pm 0.04$	$\hat{B}_K = 0.86 \pm 0.15$
$\eta_B = 0.55$	$F_{B_d}\sqrt{\hat{B}_{B_d}} = 235 \pm 33^{+0}_{-24}$ MeV
$\xi_s = 1.18 \pm 0.04^{+0.12}_{-0}$	
$\lambda = 0.221 \pm 0.002$	$\lvert V_{ub}/V_{cb}\rvert = 0.097 \pm 0.010$
$\epsilon_K = (2.271 \pm 0.017)\ 10^{-3}$	$\Delta M_{B_d} = 0.503 \pm 0.006\ \text{ps}^{-1}$
$a_{\psi K_s} = 0.734 \pm 0.054$	$\Delta M_{B_s} \geq 14.4\ \text{ps}^{-1}$ (95% C.L.)

Table 6.3: *Theoretical parameters and measurements used in* $\mathrm{B} \to \rho\gamma$ *observables and in the CKM unitarity fits. For details and references, see [57,17]*

In the SM, $C_7^d = C_7$, as in the $b \to s\gamma$ decays; however, in beyond-the-SM scenarios, this may not hold making the decays $\mathrm{B} \to \rho\gamma$ interesting for beyond-the-SM searches [57]. The definitions of the quantities $A^{(1)K^*}$, $A^{(1)t}$, A^u and $L_R^u = \epsilon_A\, C_7^{(0)\text{eff}}$ can be seen in [44]. Their default values together with that of ζ are summarized in Table 6.3, where we have also specified the theoretical errors in the more sensitive parameters ζ and L_R^u.

What concerns the quantity called ζ, we note that there are several model-dependent estimates of the same in the literature. Some representative values are: $\zeta = 0.76 \pm 0.06$ from the light-cone QCD sum rules [55]; a theoretically improved estimate in the same approach yields [49]: $\zeta = 0.75 \pm 0.07$; $\zeta = 0.88 \pm 0.02(!)$ using hybrid QCD sum rules [58], and $\zeta = 0.69 \pm 10\%$ in the quark model [59]. Except for the hybrid QCD sum rules, all other approaches yield a significant SU(3)-breaking in the magnetic moment form factors. In the light-cone QCD sum rule approach, this is anticipated due to the appreciable differences in the wave functions of the K^* and ρ-mesons. To reflect the current dispersion in the theoretical estimates of ζ, we take its value as $\zeta = 0.76 \pm 0.10$. A lattice-QCD based estimate of the same is highly desirable.

The isospin breaking ratio

$$\Delta(\rho\gamma) \equiv \frac{(\Delta^{+0} + \Delta^{-0})}{2}, \qquad \Delta^{\pm 0} = \frac{\Gamma(\mathrm{B}^\pm \to \rho^\pm\gamma)}{2\Gamma(\mathrm{B}^0(\overline{\mathrm{B}}^0) \to \rho^0\gamma)} - 1 \tag{46}$$

is given by

$$\begin{aligned}\Delta(\rho\gamma) \;&=\; \left|\frac{C_7^d + \lambda_u L_R^u}{C_7^d}\right|^2 \left(1 - \frac{2\Re C_7^d (A_R^{(1)t} + \lambda_u^* A_R^u)}{|C_7^d|^2}\right) \\ &\quad + \frac{2}{|C_7^d|^2}\Re\left[(C_7^d + \lambda_u L_R^u)(A_R^{(1)t} + \lambda_u^* A_R^u)\right] - 1\,,\end{aligned} \tag{47}$$

and the CP asymmetry $A_{CP}^\pm(\rho\gamma) = (\mathcal{B}(\mathrm{B}^- \to \rho^-\gamma) - \mathcal{B}(\mathrm{B}^+ \to \rho^+\gamma))/(\mathcal{B}(\mathrm{B}^- \to \rho^-\gamma) + \mathcal{B}(\mathrm{B}^+ \to \rho^+\gamma))$ is

$$A_{CP}^\pm(\rho\gamma) = -\frac{2\Im\left[(C_7^d + \lambda_u L_R^u)(A_I^{(1)t} + \lambda_u^* A_I^u)\right]}{|C_7^d + \lambda_u L_R^u|^2}\,. \tag{48}$$

The observables $R^0(\rho\gamma/\mathrm{K}^*\gamma) \equiv \bar{\mathcal{B}}(\mathrm{B}^0 \to \rho^0\gamma)/\mathcal{B}(\overline{\mathrm{B}}^0 \to \mathrm{K}^{*0}\gamma)$ (where $\bar{\mathcal{B}}$ is the average of the B^0 and $\overline{\mathrm{B}}^0$ modes) and $A_{CP}^0(\rho\gamma) = (\mathcal{B}(\mathrm{B}^0 \to \rho^0\gamma) - \mathcal{B}(\overline{\mathrm{B}}^0 \to \rho^0\gamma))/(\mathcal{B}(\mathrm{B}^0 \to \rho^-\gamma) + \mathcal{B}(\overline{\mathrm{B}}^0 \to \rho^0\gamma))$ are

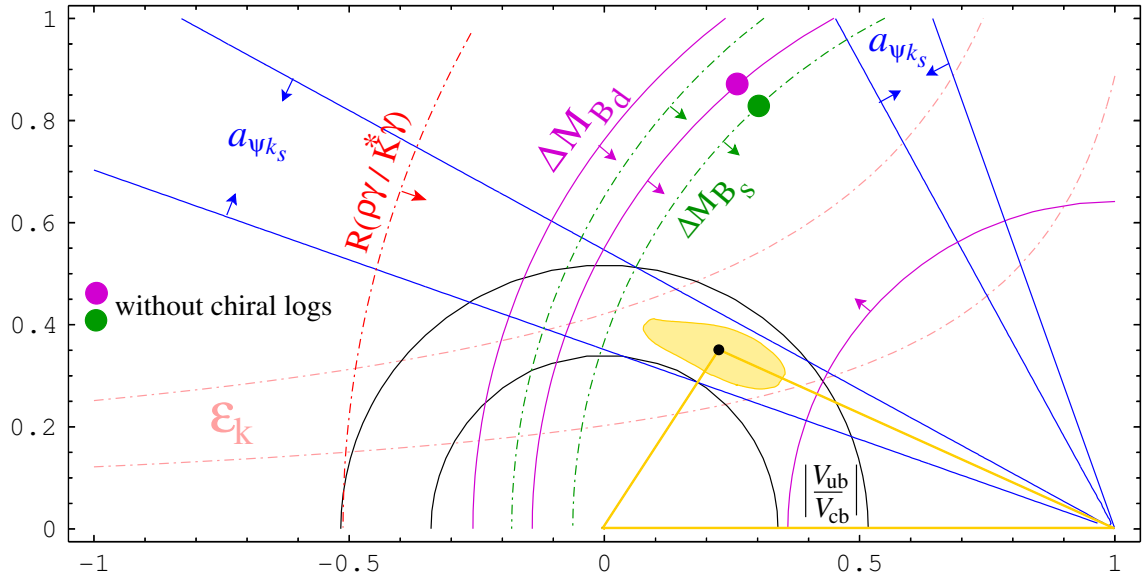

Fig. 6.10: Unitary triangle fit in the SM and the resulting 95% C.L. contour in the $\bar{\rho}$ - $\bar{\eta}$ plane. The impact of the $R(\rho\gamma/\mathrm{K}^*\gamma) < 0.047$ constraint is also shown (from Ref. [57]).

obtained from Eqs. (44, 45, 48) in the limit $L_R^u = 0$ and $S_\rho = 1/2$. The numerical estimates for the various observables depend, apart from the hadronic parameters specific to the $\mathrm{B} \to V\gamma$ ($V = \mathrm{K}^*, \rho$) decays, also on the CKM parameters, in particular $\bar{\rho}$ and $\bar{\eta}$. A typical analysis of the constraints in the $(\bar{\rho}, \bar{\eta})$ plane from the unitarity of the CKM matrix [57], including the measurements of the CP asymmetry $a_{\psi K_s}$ in the decays $\mathrm{B}^0/\overline{\mathrm{B}^0} \to J/\psi \mathrm{K}_s$ (and related modes) [60] is shown in Fig. 6.10. Note that for the hadronic parameters $F_{B_d}\sqrt{\hat{B}_{B_d}}$ and ξ_s, the recent lattice estimates [61] have been adopted that take into account uncertainties induced by the so-called chiral logarithms [62]. These errors are extremely asymmetric and, once taken into account, reduce sizeably the impact of the $\Delta M_{B_s}/\Delta M_{B_d}$ lower bound on the unitarity triangle analysis, as shown in Fig. 6.10. The 95% CL contour is drawn taking into account chiral logarithms uncertainties. The fitted values for the Wolfenstein parameters are $\bar{\rho} = 0.22 \pm 0.07$ and $\bar{\eta} = 0.35 \pm 0.04$. This yields $\Delta R^\pm = 0.055 \pm 0.130$ and $\Delta R^0 = 0.015 \pm 0.110$ [44,57]. The impact of the current upper limit $R(\rho\gamma/\mathrm{K}^*\gamma) \leq 0.047$ [63] is also shown. While not yet competitive to the existing constraints on the unitarity triangle, this surely is bound to change with the anticipated $O(1\ (\mathrm{ab})^{-1})$ $\Upsilon(4S) \to \mathrm{B}\overline{\mathrm{B}}$ data over the next three years at the B-factories.

Taking into account these errors and the uncertainties on the theoretical parameters presented in Table 6.3, leads to the following SM expectations for the $\mathrm{B} \to (\mathrm{K}^*, \rho)\gamma$ decays [57]:

$$R^\pm(\rho\gamma/\mathrm{K}^*\gamma) = 0.023 \pm 0.012\ , \tag{49}$$
$$R^0(\rho\gamma/\mathrm{K}^*\gamma) = 0.011 \pm 0.006\ , \tag{50}$$
$$\Delta(\rho\gamma) = 0.04^{+0.14}_{-0.07}\ , \tag{51}$$
$$A_{CP}^\pm(\rho\gamma) = 0.10^{+0.03}_{-0.02}\ , \tag{52}$$
$$A_{CP}^0(\rho\gamma) = 0.06 \pm 0.02\ . \tag{53}$$

The above estimates of $R^\pm(\rho\gamma/\mathrm{K}^*\gamma)$ and $R^0(\rho\gamma/\mathrm{K}^*\gamma)$ can be combined with the measured branching ratios for $\mathrm{B} \to \mathrm{K}^*\gamma$ decays given earlier to yield:

$$\mathcal{B}(\mathrm{B}^\pm \to \rho^\pm\gamma) = (0.93 \pm 0.49) \times 10^{-6}\ , \quad \mathcal{B}(\mathrm{B}^0 \to \rho^0\gamma) = (0.45 \pm 0.24) \times 10^{-6}\ . \tag{54}$$

The errors include the uncertainties on the hadronic parameters and the CKM parameters $\bar{\rho}$, $\bar{\eta}$, as well as the current experimental error on $\mathcal{B}(\mathrm{B} \to \mathrm{K}^*\gamma)$. While there is as yet no experimental bounds

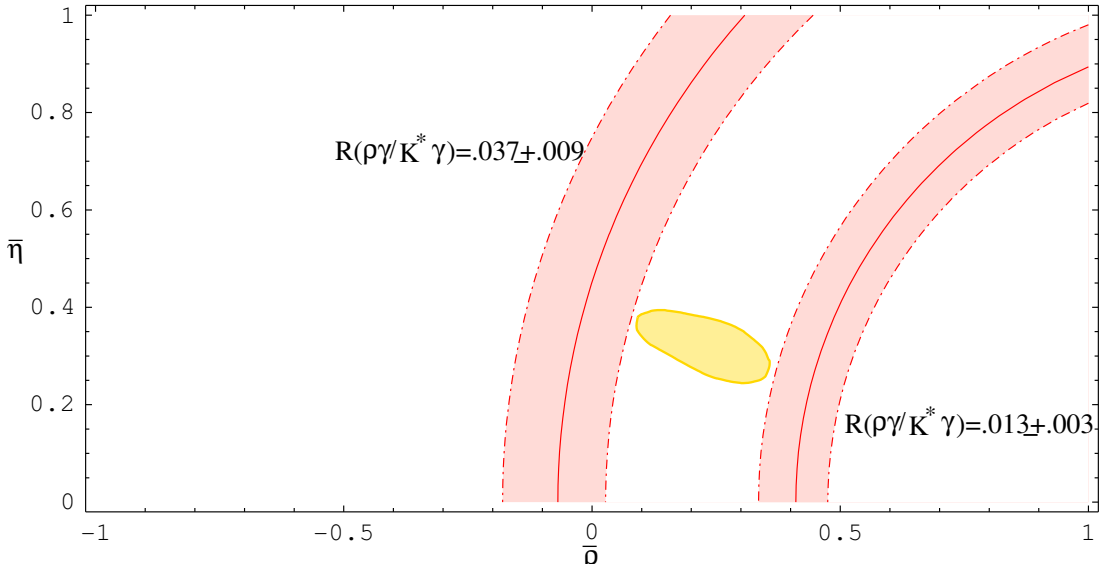

Fig. 6.11: Extremal values of $R(\rho\gamma/\mathrm{K}^*\gamma)$ t hat are compatible with the SM unitarity triangle analysis (from Ref. [57]).

on the isospin- and CP-violating quantities, $\Delta(\rho\gamma)$, $A_{CP}^{\pm}(\rho\gamma)$ and $A_{CP}^{0}(\rho\gamma)$, the upper limits on the branching ratios $R^{\pm}(\rho\gamma/\mathrm{K}^*\gamma)$ and $R^{0}(\rho\gamma/\mathrm{K}^*\gamma)$ have been significantly improved by the BABAR [63] and BELLE [46] collaborations recently. Averaged over the charge conjugated modes, the current best upper limits are [63]: $\mathcal{B}(\mathrm{B}^0 \to \rho^0\gamma) < 1.4 \times 10^{-6}$, $\mathcal{B}(\mathrm{B}^{\pm} \to \rho^{\pm}\gamma) < 2.3 \times 10^{-6}$ and $\mathcal{B}(\mathrm{B}^0 \to \omega\gamma) < 1.2 \times 10^{-6}$ (at 90% C.L.). They have been combined, using isospin weights for $\mathrm{B} \to \rho\gamma$ decays and assuming $\mathcal{B}(\mathrm{B}^0 \to \omega\gamma) = \mathcal{B}(\mathrm{B}^0 \to \rho^0\gamma)$, to yield the improved upper limit $\mathcal{B}(\mathrm{B} \to \rho\gamma) < 1.9 \times 10^{-6}$. The current measurements of the branching ratios for $\mathrm{B} \to \mathrm{K}^*\gamma$ decays by BABAR [47], $\mathcal{B}(\mathrm{B}^0 \to \mathrm{K}^{*0}\gamma) = (4.23 \pm 0.40 \pm 0.22) \times 10^{-5}$ and $\mathcal{B}(\mathrm{B}^+ \to \mathrm{K}^{*+}\gamma) = (3.83 \pm 0.62 \pm 0.22) \times 10^{-5}$, are then used to set an upper limit on the ratio of the branching ratios $R(\rho\gamma/\mathrm{K}^*\gamma) \equiv \mathcal{B}(\mathrm{B} \to \rho\gamma)/\mathcal{B}(\mathrm{B} \to \mathrm{K}^*\gamma) < 0.047$ (at 90% C.L.) [63]. This bound is typically a factor 2 away from the SM estimates given above [44,57]. However, in beyond-the-SM scenarios, this bound provides highly significant constraints on the relative strengths of the $b \to d\gamma$ and $b \to s\gamma$ transitions [57].

The extremal values of $R(\rho\gamma/\mathrm{K}^*\gamma)$ compatible with the SM UT-analysis are shown in Fig. 6.11 where the bands correspond to the values 0.037 ± 0.007 and 0.013 ± 0.003 (the errors are essentially driven by the uncertainty on ζ). The meaning of this figure is as follows: any measurement of $R(\rho\gamma/\mathrm{K}^*\gamma)$, whose central value lies in the range $(0.013, 0.037)$ would be compatible with the SM, irrespective of the size of the experimental error. The error induced by the imprecise determination of the isospin breaking parameter ζ limits currently the possibility of having a very sharp impact from $R(\rho\gamma/\mathrm{K}^*\gamma)$ on the UT analysis. This aspect needs further theoretical work.

3. Weak phases from hadronic B decays

M. Beneke, G. Buchalla (coordinator), M. Ciuchini, R. Fleischer, E. Franco, Y.-Y. Keum, G. Martinelli, M. Pierini, J.L. Rosner and L. Silvestrini

The next five contributions discuss the problem of extracting weak phases from hadronic B decays. The emphasis is on determining the CKM parameters γ and α, or equivalent constraints on $\bar{\rho}$ and $\bar{\eta}$, from exclusive modes with two light mesons in the final state, such as $\mathrm{B} \to \pi\mathrm{K}$ and $\mathrm{B} \to \pi\pi$. This problem is difficult since the underlying weak interaction processes are dressed by QCD dynamics, which is prominent in purely hadronic decays. Despite the general difficulty, there are several circumstances that help us to control strong interaction effects and to isolate the weak couplings:

- **Flavour symmetries:** The impact of strong interactions may be reduced by eliminating hadronic matrix elements through a combination of different channels, exploiting approximate flavour symmetries of QCD. Important examples are isospin, U-spin (doublet (d, s)) or, more generally, $SU(3)_F$.
- **Heavy-quark limit:** The fact that $m_b \gg \Lambda_{QCD}$ can be used to simplify the theoretical description of QCD dynamics in B decays. Within this framework amplitudes are expanded in Λ_{QCD}/m_b, long-distance and short-distance contributions are factorized, and the latter can be treated in perturbative QCD. As a result the impact of nonperturbative hadronic physics is reduced.
- **Rich phenomenology:** A large number of decay channels exists, which allows us to explore different approaches, to apply various strategies based on QCD flavour symmetries and to obtain cross-checks for dynamical calculations based on factorization.

It has to be emphasized that this field is in a state of ongoing development, both theoretically and experimentally. On the theory side important questions still need further study (general proof of factorization, light-cone dynamics of the B meson, numerical accuracy of heavy-quark limit in various situations, size of $SU(3)_F$-breaking corrections), while many valuable new data continue to be collected by the experiments. It is worth noting that the approaches based on flavour symmetries and those using dynamical calculations in the heavy-quark limit are complementary to each other. For instance, corrections from flavour symmetry breaking can be estimated within factorization. One may expect that the most important results might eventually be obtained from the combined use of all the available options mentioned above.

The following contributions summarize the status of the subject as it was discussed at this workshop. The contributions of J.L. Rosner and R. Fleischer highlight strategies based on QCD flavour symmetries to extract α and γ from $\mathrm{B} \to \pi\mathrm{K}$, $\pi\pi$ decays. The status of factorization is outlined by M. Beneke. A critical point of view on extracting γ from global fits to hadronic modes is presented by M. Ciuchini et al.. Finally, a phenomenological analysis based on the hypothesis of hard-gluon dominance of $\mathrm{B} \to \pi$ form factors is described by Y.-Y. Keum.

3.1. Weak coupling phases

J.L. Rosner[*]

The phases of CKM matrix elements describing charge-changing weak couplings of quarks are fundamental quantities. They are sometimes described in terms of angles $\alpha = \phi_2$, $\beta = \phi_1$, and $\gamma = \phi_3$ in the unitarity triangle. Now that BaBar and Belle are converging on a value of $\sin(2\beta)$, attention has turned to ways of learning α and $\gamma = \pi - \beta - \alpha$. This summary describes some recent work on the subject.

In Sec. 3.1.1. we discuss $\mathrm{B}^0 \to \pi^+\pi^-$ in the light of recent measurements at BaBar [64] and Belle [24] of time-dependent asymmetries. This work was performed in part in collaboration with M. Gronau [11,65,66] and in part with Z. Luo [12]. We then mention how to learn γ from various $\mathrm{B} \to \mathrm{K}\pi$ decays (Sec. 3.1.2., collaboration with M. Gronau [11] and with M. Neubert [67,68]), $2\beta + \gamma$ from $\mathrm{B} \to \mathrm{D}^{(*)}\pi$ (Sec. 3.1.3., collaboration with D. Suprun and C.W. Chiang [69]), and α and γ from tree-penguin interference in $\mathrm{B} \to PP,\ PV$ decays, where P is a light pseudoscalar and V a light vector meson (Sec. 3.1.4., collaboration with C.W. Chiang [70]). Sec. 3.1.5. is a short guide to other recent work, while we summarize in Sec. 3.1.6.

[*]J.L. Rosner would like to thank C.-W. Chiang, M. Gronau, Z. Luo, M. Neubert, and D. Suprun for enjoyable collaborations on these subjects.

3.1.1. *Determination of α from $B^0 \to \pi^+\pi^-$ decays*

We regard α, γ as uncertain to about $\pi/4$: $126^\circ \geq \alpha \geq 83^\circ$, $32^\circ \leq \gamma \leq 75^\circ$ [11], in accord with $122^\circ \geq \alpha \geq 75^\circ$, $37^\circ \leq \gamma \leq 80^\circ$ [71]. If $B^0 \to \pi^+\pi^-$ were dominated by the "tree" amplitude T with phase $\gamma = \mathrm{Arg}(V_{ub}^* V_{ud})$, the parameter $\lambda_{\pi\pi} \equiv e^{-2i\beta} A(\overline{B}^0 \to \pi^+\pi^-)/A(B^0 \to \pi^+\pi^-)$ would be just $e^{2i\alpha}$ and the indirect CP-violating asymmetry $S_{\pi\pi} = 2\mathrm{Im}\lambda_{\pi\pi}/(1+|\lambda_{\pi\pi}|^2)$ would be $\sin 2\alpha$. Here

$$\frac{d\Gamma}{dt}\left\{ \begin{array}{l} B^0|_{t=0} \to f \\ \overline{B}^0|_{t=0} \to f \end{array} \right\} \propto e^{-\Gamma t}[1 \mp S_{\pi\pi}\sin\Delta M_d t \pm C_{\pi\pi}\cos\Delta M_d t] \quad , \tag{55}$$

$C_{\pi\pi} = (1-|\lambda_{\pi\pi}|^2)/(1+|\lambda_{\pi\pi}|^2)$, and $\Delta\Gamma \simeq \Delta M_d/200$ has been neglected. In the presence of non-zero $\Delta\Gamma$ one can also measure $A_{\pi\pi} = 2\mathrm{Re}\lambda_{\pi\pi}/(1+|\lambda_{\pi\pi}|^2)$. Since $|S_{\pi\pi}|^2 + |C_{\pi\pi}|^2 + |A_{\pi\pi}|^2 = 1$ one has $|S_{\pi\pi}|^2 + |C_{\pi\pi}|^2 \leq 1$. However, one also has a penguin amplitude P involving a $\bar{b} \to \bar{d}$ loop transition involving contributions $\sim V_{ud}^* V_{ub}$, $V_{cd}^* V_{cb}$, and $V_{td}^* V_{tb} = -V_{ud}^* V_{ub} - V_{cd}^* V_{cb}$. The decay amplitudes are then

$$A(B^0 \to \pi^+\pi^-) = -(|T|e^{i\delta_T}e^{i\gamma} + |P|e^{i\delta_P}),\ A(\overline{B}^0 \to \pi^+\pi^-) = -(|T|e^{i\delta_T}e^{-i\gamma} + |P|e^{i\delta_P}), \tag{56}$$

where the strong phase difference $\delta \equiv \delta_P - \delta_T$. It will be convenient to define $R_{\pi\pi} \equiv \overline{\mathcal{B}}(B^0 \to \pi^+\pi^-)/\overline{\mathcal{B}}(B^0 \to \pi^+\pi^-)_{\mathrm{tree}}$, where $\overline{\mathcal{B}}$ refers to a branching ratio averaged over B^0 and $\overline{B}^0$. One may use $S_{\pi\pi}$ and $C_{\pi\pi}$ to learn α, δ, resolving a discrete ambiguity with the help of $R_{\pi\pi}$ [65]. Alternatively, one may directly use $S_{\pi\pi}$, $C_{\pi\pi}$, and $R_{\pi\pi}$ to learn α, δ, and $|P/T|$ [66,72].

Explicit expressions for $R_{\pi\pi}$, $S_{\pi\pi}$ and $C_{\pi\pi}$ may be found in [65,66]. In [65] we estimated $|P/T| = 0.276 \pm 0.064$ (see also [10]), obtaining $|P|$ from $B^+ \to K^0\pi^+$ via (broken) flavor SU(3) and $|T|$ from $B \to \pi\ell\nu$. Plotting $C_{\pi\pi}$ against $S_{\pi\pi}$ for various values of α in the likely range, one obtains curves parametrized by δ which establish a one-to-one correspondence between a pair $(S_{\pi\pi}, C_{\pi\pi})$ and a pair (α, δ) as long as $|\delta| \leq 90^\circ$. However, if $|\delta|$ is allowed to exceed about 90° these curves can intersect with one another, giving rise to a discrete ambiguity corresponding to as much as 30° uncertainty in α when $C_{\pi\pi} = 0$. In this case, when $\delta = 0$ or π, one has $|\lambda_{\pi\pi}| = 1$ and $S_{\pi\pi} = \sin 2(\alpha + \Delta\alpha)$, where $\tan(\Delta\alpha) = \pm(|P/T|\sin\gamma)/(1 \pm (|P/T|\cos\gamma)$ is typically $\pm 15^\circ$. One can resolve the ambiguity either by comparing the predicted $R_{\pi\pi}$ with experiment (see [65] for details) , or by comparing the allowed (ρ, η) region with that determined by other observables [71]. An example is shown in [11].

Once errors on $R_{\pi\pi}$ are reduced to ± 0.1 (they are now about three times as large [65]), a distinction between $\delta = 0$ and $\delta = \pi$ will be possible when $S_{\pi\pi} \simeq 0$, as appears to be the case for BaBar [64]. For the Belle data [24], which suggest $S_{\pi\pi} < 0$, the distinction becomes easier; it becomes harder for $S_{\pi\pi} > 0$. With 100 fb^{-1} at each of BaBar and Belle, it will be possible to reduce $\Delta|T|^2/|T|^2$ from its present error of 44% and $\overline{\mathcal{B}}(B^0 \to \pi^+\pi^-)$ from its present error of 21% each to about 10% [12], which will go a long way toward this goal. In an analysis independent of $|P/T|$ performed since the workshop, the somewhat discrepant BaBar and Belle values of $S_{\pi\pi}$ and $C_{\pi\pi}$, when averaged, favor α between about 90° and 120° (see Fig. 1 of [66]).

3.1.2. *Determination of γ from $B \to K\pi$ decays*

γ from $B^0 \to K^+\pi^-$ and $B^+ \to K^0\pi^+$

We mention some results of [11] on information provided by $B^0 \to K^+\pi^-$ decays, which involve both a penguin P' and a tree T' amplitude. One can use the flavor-averaged branching ratio $\overline{\mathcal{B}}$ and the CP asymmetry in these decays, together with P' information from the $B^+ \to K^0\pi^+$ decay rate (assuming it is equal to the charge-conjugate rate, which must be checked) and T' information from $B \to \pi\ell\nu$ and flavor SU(3), to obtain constraints on γ. One considers the ratio $R \equiv [\overline{\mathcal{B}}(B^0 \to K^+\pi^-)/\overline{\mathcal{B}}(B^+ \to K^0\pi^+)][\tau_+/\tau_0]$, where the B^+/B^0 lifetime ratio τ_+/τ_0 is about 1.07. Once the error on this quantity is reduced to ± 0.05 from its value of ± 0.14 as of February 2002, which should be possible with 200

fb^{-1} at each of BaBar and Belle, one should begin to see useful constraints arising from the value of R, especially if errors on the ratio $r \equiv |T'/P'|$ can be reduced with the help of better information on $|T'|$.

γ from $\mathrm{B}^+ \to \mathrm{K}^+\pi^0$ and $\mathrm{B}^+ \to \mathrm{K}^0\pi^+$

One can use the ratio $R_c \equiv 2\overline{\mathcal{B}}(\mathrm{B}^+ \to \mathrm{K}^+\pi^0)/\overline{\mathcal{B}}(\mathrm{B}^+ \to \mathrm{K}^0\pi^+)$ to determine γ [11,67,68]. Given the values as of February 2002, $R_c = 1.25 \pm 0.22$, $A_c \equiv [\mathcal{B}(\mathrm{B}^- \to \mathrm{K}^-\pi^0) - \mathcal{B}(\mathrm{B}^+ \to \mathrm{K}^+\pi^0)]/\overline{\mathcal{B}}(\mathrm{B}^+ \to \mathrm{K}^0\pi^+) = -0.13 \pm 0.17$, and $r_c \equiv |T' + C'|/|p'| = 0.230 \pm 0.035$ (here C' is a color-suppressed amplitude, while p' is a penguin amplitude including an electroweak contribution), and an estimate [67,68] of the electroweak penguin contribution, one finds $\gamma \leq 90^\circ$ or $\gamma \geq 140^\circ$ at the 1σ level, updating an earlier bound [11] $\gamma \geq 50^\circ$. A useful determination would involve $\Delta R_c = \pm 0.1$, achievable with 150 fb^{-1} each at BaBar and Belle.

3.1.3. Determination of $2\beta + \gamma$ from $\mathrm{B} \to \mathrm{D}^{(*)}\pi$ decays

The "right-sign" (RS) decay $\mathrm{B}^0 \to \mathrm{D}^{(*)-}\pi^+$, governed by the CKM factor $V_{cb}^* V_{ud}$, and the "wrong-sign" (WS) decay $\overline{\mathrm{B}}^0 \to \mathrm{D}^{(*)-}\pi^+$, governed by $V_{cd}^* V_{ub}$, can interfere through B^0–$\overline{\mathrm{B}}^0$ mixing, leading to information on the weak phase $2\beta + \gamma$. One must separate out the dependence on a strong phase δ between the RS and WS amplitudes, measuring time-dependent observables

$$A_\pm(t) = (1 + R^2) \pm (1 - R^2)\cos\Delta m t, \;\; B_\pm(t) = -2R\sin(2\beta + \gamma \pm \delta)\sin\Delta m t, \qquad (57)$$

where $R \equiv |\mathrm{WS/RS}| = r|V_{cd}^* V_{ub}/V_{cb}^* V_{ud}| \simeq 0.02r$, with r a parameter of order 1 which needs to be known better. In Ref. [69] we use the fact that R can be measured in the decay $\mathrm{B}^+ \to \mathrm{D}^{*+}\pi^0$ to conclude that with 250 million $\mathrm{B}\bar{B}$ pairs one can obtain an error of less than ± 0.05 on $\sin(2\beta + \gamma)$, which is expected to be greater than about 0.89 in the standard model. Thus, such a measurement is not likely to constrain CKM parameters, but has potential for an interesting non-standard outcome.

3.1.4. Determination of α and γ from $\mathrm{B} \to PP,\ PV$ decays

Some other processes which have a near-term potential for providing information on tree-penguin interference (and hence on α and γ) are the following [70: (1) the CP asymmetries in $\mathrm{B}^+ \to \pi^+\eta$ and $\pi^+\eta'$; (2) rates in $\mathrm{B}^+ \to \eta'\mathrm{K}^+$ and $\mathrm{B}^0 \to \eta'\mathrm{K}^0$; (3) rates in $\mathrm{B}^+ \to \eta\mathrm{K}^{*+}$ and $\mathrm{B}^0 \to \eta\mathrm{K}^{*0}$; and (4) rates in $\mathrm{B}^+ \to \omega\mathrm{K}^+$ and $\mathrm{B}^0 \to \omega\mathrm{K}^0$. Other interesting branching ratios include those for $\mathrm{B}^0 \to \pi^-\mathrm{K}^{*+}$, $\mathrm{B}^0 \to \mathrm{K}^+\rho^-$, $\mathrm{B}^+ \to \pi^+\rho^0$, $\mathrm{B}^+ \to \pi^+\omega$, and $\mathrm{B}^{(+,0)} \to \eta'\mathrm{K}^{*(+,0)}$, with a story for each [70]. In order to see tree-penguin interference at the predicted level one needs to measure branching ratios at the level of $\Delta\overline{\mathcal{B}} = (1 - 2) \times 10^{-6}$.

3.1.5. References to other work

For other recent suggestions on measuring α and γ, see the review of [73] and the contributions of [74] on the isospin triangle in $\mathrm{B} \to \pi\pi$ (α), [75,76] on $\mathrm{B}^+ \to \mathrm{DK}^+$ (γ), [77] on $\mathrm{B}^0 \to \mathrm{DK}_S$ ($2\beta+\gamma$), [78] on $\mathrm{B}^0 \to \mathrm{K}\pi$ (γ), [79] on $\mathrm{B}^0 \to \pi^+\pi^-$ and $\mathrm{B_s} \to \mathrm{K}^+\mathrm{K}_-$ (γ), and [80] on $\mathrm{B}^0 \to \mathrm{K}^+\pi^-$ and $\mathrm{B_s} \to \mathrm{K}^-\pi^+$ (γ). These contain references to earlier work.

3.1.6. Summary

CKM phases will be learned in many ways. While β is well-known now and will be better-known soon, present errors on α and γ are about 45°. To reduce them to 10° or less, several methods will help. (1) Time-dependent asymmetries in $\mathrm{B}^0 \to \pi^+\pi^-$ already contain useful information. The next step will come when both BaBar and Belle accumulate samples of at least 100 fb^{-1}. (2) In $\mathrm{B}^0 \to \pi^+\pi^-$

an ambiguity between a strong phase δ near zero and one near π (if the direct asymmetry parameter $C_{\pi\pi}$ is small) can be resolved experimentally, for example by better measurement of the $\mathrm{B}^0 \to \pi^+\pi^-$ branching ratio and the $\mathrm{B} \to \pi\ell\nu$ spectrum. (3) Several $\mathrm{B} \to \mathrm{K}\pi$ modes, when compared, can constrain γ through penguin-tree interference. This has been recognized, for example, in [71]. (4) The rates in several $\mathrm{B} \to \mathrm{PP},\ \mathrm{PV}$ modes are sensitive to tree-penguin interference. One needs to measure branching ratios with errors less than 2×10^{-6} to see such effects reliably.

3.2. Extracting γ through flavour-symmetry strategies

R. Fleischer[†]

An important element in the testing of the Kobayashi–Maskawa picture of CP violation is the direct determination of the angle γ of the unitarity triangle of the CKM matrix. Here the goal is to overconstrain this angle as much as possible. In the presence of new physics, discrepancies may arise between different strategies, as well as with the "indirect" results for γ that are provided by the usual fits of the unitarity triangle, yielding at present $\gamma \sim 60^\circ$ [6,8,27].

There are many approaches on the market to determine γ (for a detailed review, see Ref. [81]). Here we shall focus on $\mathrm{B} \to \pi\mathrm{K}$ modes [11,78], [82–90], which can be analysed through flavour-symmetry arguments and plausible dynamical assumptions, and the U-spin-related decays $\mathrm{B}_d \to \pi^+\pi^-$, $\mathrm{B}_s \to \mathrm{K}^+\mathrm{K}^-$ [79]. The corresponding flavour-symmetry strategies allow the determination of γ and valuable hadronic parameters with a "minimal" theoretical input. Alternative approaches, relying on a more extensive use of theory, are provided by the recently developed "QCD factorization" [41,10] and "PQCD" [91] approaches, which allow furthermore a reduction of the theoretical uncertainties of the flavour-symmetry strategies discussed here. Let us note that these approaches are also particularly promising from a practical point of view: BaBar, Belle and CLEO-III may probe γ through $\mathrm{B} \to \pi\mathrm{K}$ modes, whereas the U-spin strategy, requiring also a measurement of the B_s-meson decay $\mathrm{B}_s \to \mathrm{K}^+\mathrm{K}^-$, is already interesting for run II of the Tevatron [3], and can be fully exploited in the LHC era [2]. A variant for the B-factories [92], where $\mathrm{B}_s \to \mathrm{K}^+\mathrm{K}^-$ is replaced by $\mathrm{B}_d \to \pi^\mp\mathrm{K}^\pm$, points already to an exciting picture [93].

3.2.1. Studies of $\mathrm{B} \to \pi\mathrm{K}$ *decays*

Using the isospin flavour symmetry of strong interactions, relations between $\mathrm{B} \to \pi\mathrm{K}$ amplitudes can be derived, which suggest the following combinations to probe γ: the "mixed" $\mathrm{B}^\pm \to \pi^\pm\mathrm{K}$, $\mathrm{B}_d \to \pi^\mp\mathrm{K}^\pm$ system [83–86], the "charged" $\mathrm{B}^\pm \to \pi^\pm\mathrm{K}$, $\mathrm{B}^\pm \to \pi^0\mathrm{K}^\pm$ system [67,68,88], and the "neutral" $\mathrm{B}_d \to \pi^0\mathrm{K}$, $\mathrm{B}_d \to \pi^\mp\mathrm{K}^\pm$ system [78,88]. Interestingly, already CP-averaged $\mathrm{B} \to \pi\mathrm{K}$ branching ratios may lead to non-trivial constraints on γ [84,67,68]. In order to *determine* this angle, also CP-violating rate differences have to be measured. To this end, we introduce the following observables [88]:

$$\left\{ \begin{array}{c} R \\ A_0 \end{array} \right\} \equiv \left[\frac{\mathrm{BR}(\mathrm{B}^0_{\mathrm{d}} \to \pi^-\mathrm{K}^+) \pm \mathrm{BR}(\overline{\mathrm{B}^0_{\mathrm{d}}} \to \pi^+\mathrm{K}^-)}{\mathrm{BR}(\mathrm{B}^+ \to \pi^+\mathrm{K}^0) + \mathrm{BR}(\mathrm{B}^- \to \pi^-\overline{\mathrm{K}^0})} \right] \frac{\tau_{B^+}}{\tau_{B^0_d}} \tag{58}$$

$$\left\{ \begin{array}{c} R_{\mathrm{c}} \\ A_0^{\mathrm{c}} \end{array} \right\} \equiv 2 \left[\frac{\mathrm{BR}(\mathrm{B}^+ \to \pi^0\mathrm{K}^+) \pm \mathrm{BR}(\mathrm{B}^- \to \pi^0\mathrm{K}^-)}{\mathrm{BR}(\mathrm{B}^+ \to \pi^+\mathrm{K}^0) + \mathrm{BR}(\mathrm{B}^- \to \pi^-\overline{\mathrm{K}^0})} \right] \tag{59}$$

$$\left\{ \begin{array}{c} R_{\mathrm{n}} \\ A_0^{\mathrm{n}} \end{array} \right\} \equiv \frac{1}{2} \left[\frac{\mathrm{BR}(\mathrm{B}^0_d \to \pi^-\mathrm{K}^+) \pm \mathrm{BR}(\overline{\mathrm{B}^0_d} \to \pi^+\mathrm{K}^-)}{\mathrm{BR}(\mathrm{B}^0_d \to \pi^0\mathrm{K}^0) + \mathrm{BR}(\overline{\mathrm{B}^0_d} \to \pi^0\overline{\mathrm{K}^0})} \right]. \tag{60}$$

[†]R. Fleischer would like to thank Andrzej Buras, Thomas Mannel and Joaquim Matias for pleasant collaborations on the topics discussed below.

If we employ the isospin flavour symmetry and make plausible dynamical assumptions, concerning mainly the smallness of certain rescattering processes, we obtain parametrizations of the following structure [86,88] (for alternative ones, see Ref. [87]):

$$R_{(\mathrm{c,n})},\, A_0^{(\mathrm{c,n})} = \text{functions}\left(q_{(\mathrm{c,n})}, r_{(\mathrm{c,n})}, \delta_{(\mathrm{c,n})}, \gamma\right). \tag{61}$$

Here $q_{(\mathrm{c,n})}$ denotes the ratio of electroweak (EW) penguins to "trees", $r_{(\mathrm{c,n})}$ is the ratio of "trees" to QCD penguins, and $\delta_{(\mathrm{c,n})}$ the strong phase between "trees" and QCD penguins. The EW penguin parameters $q_{(\mathrm{c,n})}$ can be fixed through theoretical arguments: in the mixed system [83–85], we have $q \approx 0$, as EW penguins contribute only in colour-suppressed form; in the charged and neutral $\mathrm{B} \to \pi\mathrm{K}$ systems, q_{c} and q_{n} can be fixed through the $SU(3)$ flavour symmetry without dynamical assumptions [67,68,78,88]. The $r_{(\mathrm{c,n})}$ can be determined with the help of additional experimental information: in the mixed system, r can be fixed through arguments based on factorization [83,85,41,10] or U-spin [80], whereas r_{c} and r_{n} can be determined from the CP-averaged $\mathrm{B}^{\pm} \to \pi^{\pm}\pi^0$ branching ratio by using only the $SU(3)$ flavour symmetry [82,67,68]. The uncertainties arising in this programme from $SU(3)$-breaking effects can be reduced through the QCD factorization approach [41,10], which is moreover in favour of small rescattering processes. For simplicity, we shall neglect such FSI effects in the discussion given below.

Since we are in a position to fix the parameters $q_{(\mathrm{c,n})}$ and $r_{(\mathrm{c,n})}$, we may determine $\delta_{(\mathrm{c,n})}$ and γ from the observables given in (61). This can be done separately for the mixed, charged and neutral $\mathrm{B} \to \pi\mathrm{K}$ systems. It should be emphasized that also CP-violating rate differences have to be measured to this end. Using just the CP-conserving observables $R_{(\mathrm{c,n})}$, we may obtain interesting constraints on γ. In contrast to $q_{(\mathrm{c,n})}$ and $r_{(\mathrm{c,n})}$, the strong phase $\delta_{(\mathrm{c,n})}$ suffers from large hadronic uncertainties. However, we can get rid of $\delta_{(\mathrm{c,n})}$ by keeping it as a "free" variable, yielding minimal and maximal values for $R_{(\mathrm{c,n})}$:

$$R^{\mathrm{ext}}_{(\mathrm{c,n})}\Big|_{\delta_{(\mathrm{c,n})}} = \text{function}\left(q_{(\mathrm{c,n})}, r_{(\mathrm{c,n})}, \gamma\right). \tag{62}$$

Keeping in addition $r_{(\mathrm{c,n})}$ as a free variable, we obtain another – less restrictive – minimal value

$$R^{\mathrm{min}}_{(\mathrm{c,n})}\Big|_{r_{(\mathrm{c,n})},\delta_{(\mathrm{c,n})}} = \text{function}\left(q_{(\mathrm{c,n})}, \gamma\right)\sin^2\gamma. \tag{63}$$

These extremal values of $R_{(\mathrm{c,n})}$ imply constraints on γ, since the cases corresponding to $R^{\mathrm{exp}}_{(\mathrm{c,n})} < R^{\mathrm{min}}_{(\mathrm{c,n})}$ and $R^{\mathrm{exp}}_{(\mathrm{c,n})} > R^{\mathrm{max}}_{(\mathrm{c,n})}$ are excluded. Present experimental data seem to point towards values for γ that are *larger* than 90°, which would be in conflict with the CKM fits, favouring $\gamma \sim 60^\circ$ [6,8,27]. Unfortunately, the present experimental uncertainties do not yet allow us to draw definite conclusions, but the picture should improve significantly in the future.

An efficient way to represent the situation in the $\mathrm{B} \to \pi\mathrm{K}$ system is provided by allowed regions in the $R_{(\mathrm{c,n})}$–$A_0^{(\mathrm{c,n})}$ planes [89,93], which can be derived within the Standard Model and allow a direct comparison with the experimental data. A complementary analysis in terms of γ and $\delta_{\mathrm{c,n}}$ was performed in Ref. [90]. Another recent $\mathrm{B} \to \pi\mathrm{K}$ study can be found in Ref. [11], where the $R_{(\mathrm{c})}$ were calculated for given values of $A_0^{(\mathrm{c})}$ as functions of γ, and were compared with the B-factory data. In order to analyse $\mathrm{B} \to \pi\mathrm{K}$ modes, also certain sum rules may be useful [94].

3.2.2. The $\mathrm{B}_d \to \pi^+\pi^-$ and the $\mathrm{B}_s \to \mathrm{K}^+\mathrm{K}^-$ decays

As can be seen from the corresponding Feynman diagrams, $\mathrm{B}_s \to \mathrm{K}^+\mathrm{K}^-$ is related to $\mathrm{B}_d \to \pi^+\pi^-$ through an interchange of all down and strange quarks. The decay amplitudes read as follows [79]:

$$A(\mathrm{B}^0_d \to \pi^+\pi^-) \propto \left[e^{i\gamma} - de^{i\theta}\right], \quad A(\mathrm{B}^0_s \to \mathrm{K}^+\mathrm{K}^-) \propto \left[e^{i\gamma} + \left(\frac{1-\lambda^2}{\lambda^2}\right)d'e^{i\theta'}\right], \tag{64}$$

where the CP-conserving strong amplitudes $de^{i\theta}$ and $d'e^{i\theta'}$ measure, sloppily speaking, ratios of penguin to tree amplitudes in $\mathrm{B}^0_d \to \pi^+\pi^-$ and $\mathrm{B}^0_s \to \mathrm{K}^+\mathrm{K}^-$, respectively. Using these general parametrizations, we obtain expressions for the direct and mixing-induced CP asymmetries of the following kind:

$$\mathcal{A}_{\mathrm{CP}}^{\mathrm{dir}}(\mathrm{B}_d \to \pi^+\pi^-) = \mathrm{function}(d,\theta,\gamma),\ \mathcal{A}_{\mathrm{CP}}^{\mathrm{mix}}(\mathrm{B}_d \to \pi^+\pi^-) = \mathrm{function}(d,\theta,\gamma,\phi_d = 2\beta) \tag{65}$$

$$\mathcal{A}_{\mathrm{CP}}^{\mathrm{dir}}(\mathrm{B}_s \to \mathrm{K}^+\mathrm{K}^-) = \mathrm{function}(d',\theta',\gamma),\ \mathcal{A}_{\mathrm{CP}}^{\mathrm{mix}}(\mathrm{B}_s \to \mathrm{K}^+\mathrm{K}^-) = \mathrm{function}(d',\theta',\gamma,\phi_s \approx 0). \tag{66}$$

Consequently, we have four observables at our disposal, depending on six "unknowns". However, since $\mathrm{B}_d \to \pi^+\pi^-$ and $\mathrm{B}_s \to \mathrm{K}^+\mathrm{K}^-$ are related to each other by interchanging all down and strange quarks, the U-spin flavour symmetry of strong interactions implies

$$d'e^{i\theta'} = d\,e^{i\theta}. \tag{67}$$

Using this relation, the four observables in (65,66) depend on the four quantities d, θ, $\phi_d = 2\beta$ and γ, which can hence be determined [79]. The theoretical accuracy is only limited by the U-spin symmetry, as no dynamical assumptions about rescattering processes have to be made. Theoretical considerations give us confidence into (67), as it does not receive U-spin-breaking corrections in factorization [79]. Moreover, we may also obtain experimental insights into U-spin breaking [79,95].

The U-spin arguments can be minimized, if the B^0_d–$\overline{\mathrm{B}}^0_d$ mixing phase $\phi_d = 2\beta$, which can be fixed through $\mathrm{B}_d \to J/\psi\mathrm{K}_{\mathrm{S}}$, is used as an input. The observables $\mathcal{A}_{\mathrm{CP}}^{\mathrm{dir}}(\mathrm{B}_d \to \pi^+\pi^-)$ and $\mathcal{A}_{\mathrm{CP}}^{\mathrm{mix}}(\mathrm{B}_d \to \pi^+\pi^-)$ allow us then to eliminate the strong phase θ and to determine d as a function of γ. Analogously, $\mathcal{A}_{\mathrm{CP}}^{\mathrm{dir}}(\mathrm{B}_s \to \mathrm{K}^+\mathrm{K}^-)$ and $\mathcal{A}_{\mathrm{CP}}^{\mathrm{mix}}(\mathrm{B}_s \to \mathrm{K}^+\mathrm{K}^-)$ allow us to eliminate the strong phase θ' and to determine d' as a function of γ. The corresponding contours in the γ–d and γ–d' planes can be fixed in a *theoretically clean* way. Using now the U-spin relation $d' = d$, these contours allow the determination both of the CKM angle γ and of the hadronic quantities d, θ, θ'; for a detailed illustration, see Ref. [79]. This approach is very promising for run II of the Tevatron and the experiments of the LHC era, where experimental accuracies for γ of $\mathcal{O}(10^\circ)$ [3] and $\mathcal{O}(1^\circ)$ [2] may be achieved, respectively. It should be emphasized that not only γ, but also the hadronic parameters d, θ, θ' are of particular interest, as they can be compared with theoretical predictions, thereby allowing valuable insights into hadron dynamics. For other recently developed U-spin strategies, the reader is referred to [80,96].

3.2.3. The $\mathrm{B}_d \to \pi^+\pi^-$ and the $\mathrm{B}_d \to \pi^\mp\mathrm{K}^\pm$ decays and implications for $\mathrm{B}_s \to \mathrm{K}^+\mathrm{K}^-$ decay

A variant of the $\mathrm{B}_d \to \pi^+\pi^-$, $\mathrm{B}_s \to \mathrm{K}^+\mathrm{K}^-$ approach was developed for the e^+e^- B-factories [92], where $\mathrm{B}_s \to \mathrm{K}^+\mathrm{K}^-$ is not accessible: as $\mathrm{B}_s \to \mathrm{K}^+\mathrm{K}^-$ and $\mathrm{B}_d \to \pi^\mp\mathrm{K}^\pm$ are related to each other through an interchange of the s and d spectator quarks, we may replace the B_s mode approximately through its B_d counterpart, which has already been observed by BaBar, Belle and CLEO. Following these lines and using experimental information on the CP-averaged $\mathrm{B}_d \to \pi^\mp\mathrm{K}^\pm$ and $\mathrm{B}_d \to \pi^+\pi^-$ branching ratios, the relevant hadronic penguin parameters can be constrained, implying certain allowed regions in observable space [93]. An interesting situation arises now in view of the recent B-factory measurements of CP violation in $\mathrm{B}_d \to \pi^+\pi^-$, allowing us to obtain new constraints on γ as a function of the B^0_d–$\overline{\mathrm{B}}^0_d$ mixing phase ϕ_d, which is fixed through $\mathcal{A}_{\mathrm{CP}}^{\mathrm{mix}}(\mathrm{B}_d \to J/\psi\mathrm{K}_{\mathrm{S}})$ up to a twofold ambiguity, $\phi_d \sim 51^\circ$ or 129°. If we assume that $\mathcal{A}_{\mathrm{CP}}^{\mathrm{mix}}(\mathrm{B}_d \to \pi^+\pi^-)$ is positive, as indicated by recent Belle data, and that ϕ_d is in agreement with the "indirect" fits of the unitarity triangle, i.e. $\phi_d \sim 51^\circ$, also the corresponding values for γ around 60° can be accommodated. On the other hand, for the second solution $\phi_d \sim 129^\circ$, we obtain a gap around $\gamma \sim 60^\circ$, and could easily accommodate values for γ larger than 90°. Because of the connection between the two solutions for ϕ_d and the resulting values for γ, it is very desirable to resolve the twofold ambiguity in the extraction of ϕ_d directly. As far as $\mathrm{B}_s \to \mathrm{K}^+\mathrm{K}^-$ is concerned, the data on the CP-averaged $\mathrm{B}_d \to \pi^+\pi^-$, $\mathrm{B}_d \to \pi^\mp\mathrm{K}^\pm$ branching ratios imply a very constrained allowed region in the space of $\mathcal{A}_{\mathrm{CP}}^{\mathrm{mix}}(\mathrm{B}_s \to \mathrm{K}^+\mathrm{K}^-)$ and $\mathcal{A}_{\mathrm{CP}}^{\mathrm{dir}}(\mathrm{B}_s \to \mathrm{K}^+\mathrm{K}^-)$ within the Standard Model, thereby providing a narrow target range for run II of the Tevatron and the experiments of the LHC era [93]. Other recent studies related to $\mathrm{B}_d \to \pi^+\pi^-$ can be found in Refs. [11,97].

3.3. Determining γ with QCD factorization

M. Beneke [‡]

3.3.1. Outline of the method

The QCD factorization approach [41,98] puts the well-known factorization ansatz [99] for hadronic two-body B decay matrix elements on a firm theoretical basis. It replaces the factorization ansatz by a factorization formula that includes radiative corrections and spectator scattering effects. Where it can be justified, the factorization ansatz emerges in the simultaneous limit, when m_b becomes large and when radiative corrections are neglected.

The QCD factorization approach uses heavy quark expansion methods ($m_b \gg \Lambda_{\rm QCD}$) and soft-collinear factorization (particle energies $\gg \Lambda_{\rm QCD}$) to compute the matrix elements $\langle f|O_i|\bar{\rm B}\rangle$ relevant to hadronic B decays in an expansion in $1/m_b$ and α_s. Only the leading term in $1/m_b$ assumes a simple form. The basic formula is

$$\begin{aligned}\langle M_1M_2|O_i|\overline{\rm B}\rangle \;=\; & F^{B\to M_1}(0)\int_0^1 du\, T^I(u)\Phi_{M_2}(u)\\ & +\int d\xi du dv\, T^{II}(\xi,u,v)\,\Phi_B(\xi)\Phi_{M_1}(v)\Phi_{M_2}(u),\end{aligned}\tag{68}$$

where $F^{B\to M_1}$ is a (non-perturbative) form factor, Φ_{M_i} and Φ_B are light-cone distribution amplitudes and $T^{I,II}$ are perturbatively calculable hard scattering kernels. Although not strictly proven to all orders in perturbation theory, the formula is presumed to be valid when both final state mesons are light. (M_1 is the meson that picks up the spectator quark from the B meson.) The formula shows that there is no long-distance interaction between the constituents of the meson M_2 and the (BM_1) system at leading order in $1/m_b$. This is the precise meaning of factorization. For a detailed discussion of (68) I refer to [10,98]. A summary of results that have been obtained in the QCD factorization approach is given in [100].

Factorization as embodied by (68) is not expected to hold at subleading order in $1/m_b$. Some power corrections related to scalar currents are enhanced by factors such as $m_\pi^2/((m_u+m_d)\Lambda_{\rm QCD})$. Some corrections of this type, in particular those related to scalar penguin amplitudes nevertheless appear to be calculable and turn out to be important numerically. On the other hand, attempts to compute subleading power corrections to hard spectator-scattering in perturbation theory usually result in infrared divergences, which signal the breakdown of factorization. At least these effects should be estimated and included into the error budget. All weak annihilation contributions belong to this class of effects and often constitute the dominant source of theoretical error.

3.3.2. Uses of QCD factorization

If the corrections to (68) were negligible and if all the quantities in (68) were known or computed with sufficient accuracy, the QCD factorization approach would allow one to determine directly weak CP-violating phases from branching fraction or CP asymmetry measurements, if the corresponding decay has two interfering amplitudes with different phases. In practice, depending on the particular decay mode, one is often far from this ideal situation. Depending on the theoretical uncertainty or one's confidence in theoretical error estimates, I can imagine the following uses of the QCD factorization approach, where in ascending order one makes stronger use of theoretical rather than experimental input.

1) Many strategies to determine γ are based on relating the strong interaction dynamics of different decay channels such that a sufficient set of measurements yields the weak phase together with the

[‡]M. Beneke would like to thank Gerhard Buchalla, Matthias Neubert and Chris Sachrajda for collaborations on the topics discussed in this article.

strong amplitudes (see the contributions by Fleischer and Rosner in this Chapter). QCD factorization can complement this approach where it has to rely on assumptions. For instance, it may be used to estimate SU(3) flavour symmetry breaking or to provide an estimate of small contributions to the decay amplitude that one would otherwise have to neglect to make use of the amplitude relations.

2) The QCD factorization approach generically predicts small strong rescattering phases, because rescattering is either perturbatively loop-suppressed, or power-suppressed in the heavy-quark limit. (Exceptions to the rule of small phases occur when the leading term in the α_s- or $1/m_b$-expansion is suppressed, for instance by small Wilson coefficients.) Even if the quantitative prediction of the strong phases turns out to be difficult, the qualitative result of small phases can be used to sharpen the bounds on γ that follow from some amplitude relations, or to turn the bounds into determinations of γ. An example of this in the context of a method suggested in [68] will be discussed below.
3) For predicting CP violation the ratio of two strong interaction amplitudes, P/T, (often a ratio of a pure penguin and a dominantly tree amplitude, which are multiplied by different weak phases) is a particularly important quantity. While P/T is computed in the QCD factorization approach, one may decide to use only the calculation of the absolute value $|P/T|$ and to dismiss the quantitative phase information. The rationale for this procedure could be that the calculation of the imaginary part is usually less accurate than the real part, because a one-loop calculation determines the phase only to leading order. For the same reason the value of the phase is more sensitive to uncalculable power corrections. In this procedure the phase information must be provided by an additional measurement, for instance a direct CP asymmetry.
4) The full information of the QCD factorization approach is employed to compute two-body branching fractions as functions of the parameters of the CKM matrix. Since the b quark mass is not very large it will be important to estimate the theoretical error from power corrections.

The development of QCD factorization has not yet reached the stage where one can decide which of these strategies will turn out to be most useful. (The strategy of choice obviously also depends on the amount of experimental information available that would allow one to drop one or the other piece of theoretical input.) Calculations of $\pi\pi$ and πK final states showed [10] that one obtains naturally the right magnitude of penguin and tree amplitudes. The accuracy of the calculation of strong phases is less clear at present, but forthcoming measurements of direct CP asymmetries should shed light on this question. The current limits favour small strong phases, but a quantitative comparison may require a complete next-to-leading order calculation of the absorptive parts of the amplitudes. It will also be important to clarify the relevance of weak annihilation effects in the decay amplitudes. While the current data do not favour the assumption of large annihilation contributions, they can also not yet be excluded. Bounds on rare annihilation-dominated decays will limit the corresponding amplitudes.

3.3.3. Results related to the determination of γ

The possibility to determine the CP-violating angle γ by comparing the calculation of branching fractions into $\pi\pi$ and $\pi\mathrm{K}$ final states with the corresponding data has been investigated in [10] (see also [101]). In the following I summarize the main results, referring to [10] for details and to [102,103] for partial updates of the analysis of [10].

γ from CP-averaged charged $\mathrm{B} \to \pi\mathrm{K}$ decay

The ratio

$$R_* = \frac{\mathrm{Br}(\mathrm{B}^+ \to \pi^+\mathrm{K}^0) + \mathrm{Br}(\mathrm{B}^- \to \pi^-\bar{\mathrm{K}}^0)}{2[\mathrm{Br}(\mathrm{B}^+ \to \pi^0\mathrm{K}^+) + \mathrm{Br}(\mathrm{B}^- \to \pi^0\mathrm{K}^-)]}\,, \tag{69}$$

currently measured as 0.71 ± 0.10, provides a useful bound on γ [68,87]. The theoretical expression is

$$\begin{aligned} R_*^{-1} &= 1 + 2\bar{\varepsilon}_{3/2}\cos\phi\,(q - \cos\gamma) + \bar{\varepsilon}_{3/2}^2(1 - 2q\cos\gamma + q^2) \\ &< \left(1 + \bar{\varepsilon}_{3/2}\,|q - \cos\gamma|\right)^2 + \bar{\varepsilon}_{3/2}^2\sin^2\gamma, \end{aligned} \tag{70}$$

where $\bar{\epsilon}_{3/2}e^{i\phi}$ is a tree-to-penguin ratio, whose magnitude can be fixed with SU(3) symmetry, and q an electroweak penguin contribution, which can be determined theoretically. (In this expression, a rescattering contribution ε_a, which QCD factorization predicts to be small, is neglected.) The inequality is obtained by allowing the relative strong phase ϕ to take any value. If R_* is smaller than one, the bound implies an exclusion region for $\cos\gamma$. The bound can be considerably sharpened, and the requirement $R_* < 1$ relaxed, if the phase is known to be small. QCD factorization as well as bounds on direct CP asymmetries suggest that $\cos\phi > 0.9$. In [10] it was shown that assuming the more conservative range $\cos\phi > 0.8$, the measurement of R_* combined with $|V_{ub}/V_{cb}|$ provides a determination of γ with a theoretical error of about 10°, if R_* is close to 1.

γ from $\mathrm{B}_d(t) \to \pi^+\pi^-$ decay

The QCD factorization approach allows us to interpret directly the mixing-induced and direct CP asymmetry in $\mathrm{B}_d \to \pi^+\pi^-$ decay without resort to other decay modes, since the tree and penguin amplitudes are both computed. The time-dependent asymmetry is defined by

$$\begin{aligned} A_{\mathrm{CP}}^{\pi\pi}(t) &= \frac{\mathrm{Br}(\mathrm{B}^0(t) \to \pi^+\pi^-) - \mathrm{Br}(\overline{\mathrm{B}}^0(t) \to \pi^+\pi^-)}{\mathrm{Br}(\mathrm{B}^0(t) \to \pi^+\pi^-) + \mathrm{Br}(\overline{\mathrm{B}}^0(t) \to \pi^+\pi^-)} \\ &= -S_{\pi\pi}\sin(\Delta M_B\,t) + C_{\pi\pi}\cos(\Delta M_B\,t). \end{aligned} \tag{71}$$

Assuming that the $\mathrm{B}\bar{\mathrm{B}}$ mixing phase is determined experimentally via the mixing-induced CP asymmetry in $\mathrm{B}_d(t) \to J/\psi\mathrm{K}$ decay, both $S_{\pi\pi}$ and $C_{\pi\pi}$ are measures of CP violation in the decay amplitude and determine γ. In [10] it was shown that even a moderately accurate measurement of $S_{\pi\pi}$ translates into a stringent constraint in the $(\bar{\rho}, \bar{\eta})$ plane. The predicted correlation between $S_{\pi\pi}$ and $C_{\pi\pi}$ is shown in [102].

3.3.4. γ from CP-averaged $\mathrm{B} \to \pi\mathrm{K}$, $\pi\pi$ decay

Since the branching fractions are computed as functions of the Wolfenstein parameters $(\bar{\rho}, \bar{\eta})$, one can perform a fit of $(\bar{\rho}, \bar{\eta})$ to the six measured CP-averaged $\mathrm{B} \to \pi\pi, \pi\mathrm{K}$ branching fractions. The result of this fit is shown in Fig. 6.12 based on the data as of May 2002. (The details of the fit procedure can be found in [10], the input data in [102]). The result of the fit is consistent with the standard fit based on meson mixing and $|V_{ub}|$. However, the $\pi\pi$, $\pi\mathrm{K}$ data persistently exhibit a preference for γ near 90°, or, for smaller γ, smaller $|V_{ub}|$. The significance and interpretation of this observation remains to be clarified.

3.3.5. Weak annihilation

Weak annihilation contributions are power-suppressed and not calculable in the QCD factorization approach. (This is one of the important differences between the QCD factorization approach and the pQCD approach described by Y. Keum in this Chapter.) The results discussed above include an estimate of annihilation effects together with an uncertainty derived from a $\pm 100\%$ variation of this estimate, encoded in the constraint $|\rho_A| < 1$ for a certain weak annihilation parameter [10]. Since this constraint is often a key factor in the overall theoretical uncertainty estimate, it will be important to obtain experimental information on weak annihilation. The current data on $\pi\pi$ and $\pi\mathrm{K}$ final states do not favour large annihilation contributions, but also do not exclude this possibility. The upper limits on annihilation-dominated

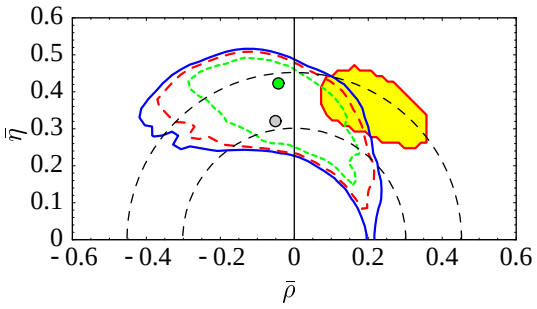

Fig. 6.12: *95% (solid), 90% (dashed) and 68% (short-dashed) confidence level contours in the* $(\bar{\rho}, \bar{\eta})$ *plane obtained from a global fit to the CP averaged* $\mathrm{B} \to \pi\mathrm{K}, \pi\pi$ *branching fractions, using the scanning method as described in [8]. The darker dot shows the overall best fit, whereas the lighter dot indicates the best fit for the default hadronic parameter set. The light-shaded region indicates the region preferred by the standard global fit [8], including the direct measurement of* $\sin(2\beta)$.

charmless decays are not yet tight enough to provide interesting constraints. However, we can adapt the estimate of annihilation contributions to $\bar{\mathrm{B}}_d \to \mathrm{D}^+\pi^-$ performed in [98] to the annihilation-dominated decay $\bar{\mathrm{B}}_d \to \mathrm{D}_s^+\mathrm{K}^-$, recently observed with a branching fraction $(3.8 \pm 1.1) \cdot 10^{-5}$ [104]. This results in a branching fraction estimate of $1.2 \cdot 10^{-5}$ for central parameters, or an upper limit $5 \cdot 10^{-5}$ upon assigning a 100% error to the annihilation amplitude. While the annihilation mechanism in $\bar{\mathrm{B}}_d \to \mathrm{D}_s^+\mathrm{K}^-$ is not identical to the dominant penguin annihilation term in $\mathrm{B} \to \pi\mathrm{K}$ decay, the comparison nevertheless supports the phenomenological treatment of annihilation suggested in [10,98].

3.4. $\mathrm{B} \to \mathrm{K}\pi$, charming penguins and the extraction of γ

M. Ciuchini, E. Franco, G. Martinelli, M. Pierini and L. Silvestrini

3.4.1. Main formulae

In this section we collect the main formulae for the amplitudes of $\mathrm{B} \to \mathrm{K}\pi, \pi\pi$, introducing the parametrization used in the analysis. We refer the reader to the literature for any detail on the origin and the properties of these parameters [105,106,107,108]. From Ref. [107], one reads

$$
\begin{aligned}
A(\mathrm{B}_d \to \mathrm{K}^+\pi^-) &= \frac{G_F}{\sqrt{2}}\Big(\lambda_t^s P_1 - \lambda_u^s (E_1 - P_1^{GIM})\Big) \\
A(\mathrm{B}^+ \to \mathrm{K}^+\pi^0) &= \frac{G_F}{2}\Big(\lambda_t^s P_1 - \lambda_u^s (E_1 + E_2 - P_1^{GIM} + A_1)\Big) + \Delta A \\
A(\mathrm{B}^+ \to \mathrm{K}^0\pi^+) &= \frac{G_F}{\sqrt{2}}\Big(- \lambda_t^s P_1 + \lambda_u^s (A_1 - P_1^{GIM})\Big) + \Delta A \\
A(\mathrm{B}_d \to \mathrm{K}^0\pi^0) &= \frac{G_F}{2}\Big(- \lambda_t^s P_1 - \lambda_u^s (E_2 + P_1^{GIM})\Big) + \Delta A \\
A(\mathrm{B}_d \to \pi^+\pi^-) &= \frac{G_F}{\sqrt{2}}\Big(\lambda_t^d (P_1 + P_3) - \lambda_u^d (E_1 + A_2 - P_1^{GIM}) - P_3^{GIM}\Big) \\
A(\mathrm{B}_d \to \pi^+\pi^0) &= \frac{G_F}{2}\Big(- \lambda_u^d (E_1 + E_2)\Big) + \Delta A \\
A(\mathrm{B}_d \to \pi^0\pi^0) &= \frac{G_F}{2}\Big(- \lambda_t^s (P_1 + P_3) - \lambda_u^s (E_2 + P_1^{GIM} + P_3^{GIM} - A_2)\Big) + \Delta A\,,
\end{aligned}
\tag{72}
$$

$\lvert V_{cb}\rvert\times 10^3$	$\lvert V_{ub}\rvert\times 10^3$	$\hat{B}_K$	$F_{B_d}\sqrt{B_d}$ (MeV)	ξ
40.9 ± 1.0	3.70 ± 0.42	$0.86\pm0.06\pm0.14$	$230\pm30\pm15$	$1.16\pm0.03\pm0.04$
$f_K(M_K^2)$	$\mathcal{B}(\mathrm{K}^+\pi^-)\times 10^6$	$\mathcal{B}(\mathrm{K}^+\pi^0)\times 10^6$	$\mathcal{B}(\mathrm{K}^0\pi^+)\times 10^6$	$\mathcal{B}(K^0\pi^0)\times 10^6$
0.32 ± 0.12	18.6 ± 1.1	11.5 ± 1.3	17.9 ± 1.7	8.9 ± 2.3
$f_\pi(M_\pi^2)$	$\mathcal{B}(\pi^+\pi^-)\times 10^6$	$\mathcal{B}(\pi^+\pi^0)\times 10^6$	$\mathcal{B}(\pi^0\pi^0)\times 10^6$	
0.27 ± 0.08	5.2 ± 0.6	4.9 ± 1.1	<3.4 *BaBar*	

Table 6.4: *Values of the input parameters used in our analysis. The CP-averaged branching ratios $\mathcal{B}$ are taken from Ref. [109].*

where $\lambda^q_{q'} = V_{q'q}V^*_{q'b}$. Neglecting the A_i, these parameters can be rewritten as

$$\begin{aligned} &E_1 = a_1^c A_{\pi\mathrm{K}}\,, \quad E_2 = a_2^c A_{K\pi}\,, \quad A_1 = A_2 = 0\,, \\ &P_1 = a_4^c A_{\pi K} + \tilde{P}_1\,, \quad P_1^{GIM} = (a_4^c - a_4^u)A_{\pi K} + \tilde{P}_1^{GIM}\,. \end{aligned} \tag{73}$$

The terms proportional to a_i^q give the parameters computed in the limit $m_b \to \infty$ using QCD factorization. Their definition, together with those of $A_{\pi K}$, $A_{K\pi}$, etc., can be found for instance in Refs. [41,98,10], although power-suppressed terms included there, proportional to the chiral factors $r^\chi_{K,\pi}$, should be discarded in eqs. (73). In our case, in fact, terms of $O(\Lambda_{QCD}/m_b)$ are accounted for by two phenomenological parameters: the charming-penguin parameter $\tilde{P}_1$ and the GIM-penguin parameter $\tilde{P}_1^{GIM}$. In $\mathrm{B}\to\mathrm{K}\pi$ there are no other contributions, once flavour $SU(2)$ symmetry is used and few other doubly Cabibbo-suppressed terms, including corrections to emission parametes E_1 and E_2, some annihilations (A_1) and the Zweig-suppressed contractions (ΔA), are neglected [107]. On the contrary, further power-suppressed terms (A_2, P_3, P_3^{GIM}) enter the $\mathrm{B}\to\pi\pi$ amplitudes, all with the same power of the Cabibbo angle. Therefore, these modes are subject to a larger uncertainty than the $\mathrm{B}\to\mathrm{K}\pi$ ones.

Using the inputs collected in Table 6.4, we fit the value of the complex parameter $\tilde{P}_1 = (0.13 \pm 0.02)\, e^{\pm i(114\pm35)^\circ}$. Notice that the sign of the phase is practically not constrained by the data. This result is almost independent of the inputs used for the CKM parameters ρ and η, namely whether these parameters are taken from the usual unitarity triangle analysis (UTA) [27,110] or only the constraint from $|V_{ub}/V_{cb}|$ is used.

Mode	UTA		$\lvert V_{ub}/V_{cb}\rvert$	
	$\mathcal{B}$ (10^{-6})	$\lvert\mathcal{A}_{CP}\rvert$	$\mathcal{B}$ (10^{-6})	$\lvert\mathcal{A}_{CP}\rvert$
$\pi^+\pi^-$	8.9 ± 3.3	0.37 ± 0.17	8.7 ± 3.6	0.39 ± 0.20
$\pi^+\pi^0$	5.4 ± 2.1	–	5.5 ± 2.2	–
$\pi^0\pi^0$	0.44 ± 0.13	0.61 ± 0.26	0.69 ± 0.27	0.45 ± 0.27
$\mathrm{K}^+\pi^-$	18.4 ± 1.0	0.21 ± 0.10	18.8 ± 1.0	0.21 ± 0.12
$\mathrm{K}^+\pi^0$	10.3 ± 0.9	0.22 ± 0.11	10.7 ± 1.0	0.22 ± 0.13
$\mathrm{K}^0\pi^+$	19.3 ± 1.2	0.00 ± 0.00	18.1 ± 1.5	0.00 ± 0.00
$\mathrm{K}^0\pi^0$	8.7 ± 0.8	0.04 ± 0.02	8.2 ± 1.2	0.04 ± 0.03

Table 6.5: *Predictions for CP-averaged branching ratios $\mathcal{B}$ and absolute value of the CP asymmetries $|\mathcal{A}_{CP}|$. The left (right) columns show results obtained using constraints on the CKM parameters ρ and η obtained from the UTA (the measurement of $|V_{ub}/V_{cb}|$). The last four channels are those used for fitting the charming penguin parameter $\tilde{P}_1$.*

For the sake of simplicity, we also neglect here the contribution of $\tilde{P}_1^{GIM}$. The $\mathrm{B} \to \mathrm{K}\pi$ data do not constrain this parameter very effectively, since its contribution is doubly Cabibbo suppressed with respect to $\tilde{P}_1$. The remaining $\pi^+\pi^-$ mode alone is not sufficient to fully determine the complex parameter $\tilde{P}_1^{GIM}$. It is interesting, however, to notice that the GIM-penguin contribution is potentially able to enhance the $\mathcal{B}(\mathrm{B} \to \pi^0\pi^0)$ up to few $\times 10^{-6}$ [108].

Table 6.5 shows the predicted values of the CP-averaged branching ratios $\mathcal{B}$ and the absolute value of the CP-asymmetries $|\mathcal{A}_{CP}|$ for the $\mathrm{B} \to \mathrm{K}\pi$ and $\mathrm{B} \to \pi\pi$ modes, since the data are not able to fix the sign of asymmetries. Charming penguins are able to reproduce the $\mathrm{K}\pi$ data and are also consistent with the only $\pi\pi$ mode measured so far. It is interesting to notice that the latest measurements improve the consistency, for a comparison see refs. [106,108].

3.4.2. Remarks on different approaches

Since the different approaches aiming at evaluating power-suppressed terms contain phenomenological parameters, it is natural to ask whether, after all, they are equivalent or not, even if the physical mechanism invoked to introduce the parameters is not the same. To answer this question, it is useful to compute the parameters $\tilde{P}_1$ and $\tilde{P}_1^{GIM}$ within *improved* QCD factorization. They read

$$\tilde{P}_1 = r_K^\chi a_6^c A_{\pi K} + b_3 B_{\pi K}\,,\ \tilde{P}_1^{GIM} = r_K^\chi (a_6^c - a_6^u) A_{\pi K}\,, \tag{74}$$

where the functions a_i^q (b_i) contain the complex parameter ρ_H (ρ_A), see Ref. [10] for the definitions. These two parameters account for chirally-enhanced terms, originating from hard-spectator interactions and annihilations respectively, which are not computable within the *improved* QCD factorization.

The functional dependence of the amplitudes on the phenomenological parameters in the two approaches is different. For instance, the GIM-penguin parameter is a pure short-distance correction in the *improved* QCD factorization, since the ρ_H dependence cancels out in the difference $a_6^c - a_6^u$. In practice, however, the main contribution of the phenomenological parameters to the $\mathrm{B} \to \mathrm{K}\pi$ amplitudes comes from the annihilation term b_3, i.e. from ρ_A . This term behaves effectively as the charming-penguin parameter, enhancing the Cabibbo-favored amplitude.

Notice that a vanishing ρ_A (and ρ_H), which turns out to be compatible with the data, does not mean that the phenomenological contribution is negligible. In fact, the parameters are defined so that the phenomenological terms are functions of $X_{A(H)} = (1 + \rho_{A(H)}) \log(m_B/\mu_h)$, where the scale μ_h is assumed to be 0.5 GeV [10].

3.4.3. On the possibility of extracting γ

The presence of complex phenomenological parameters in the amplitudes makes the extraction of γ very problematic. Using the $|V_{ub}/V_{cb}|$-constrained fit, almost any value of γ is allowed, given the uncertainty on $\tilde{P}_1$, see Fig. 6.13 (left). This seems a general problem which make us doubt recent claims proposing non-leptonic B decays as an effective tool for the CKM matrix determination. Even more, we think that the combination of the constraint from $\mathrm{B} \to \mathrm{K}\pi$ decays on γ with the others can even be misleading. The reason is very simple: γ is looked for through the effect of interefence terms in the branching ratios. The presence of a competing amplitude with a new phase, i.e. the one containing the phenomenological parameter, makes the extraction of γ much more complicated. Although weak and strong phases can be disentangled in principle, in practice we checked that not only the task is very difficult now, but the situation improves slowly as data become more accurate, even when the CP asymmetries will be measured.

Concerning various analyses based on the *improved* QCD factorization claiming to find a "large" value of $\gamma \sim 90^\circ$, we just notice that, as far as we know, they all assume the bound $|\rho_A| < 1$, suggested in Ref. [10] as a theoretical prejudice and supported by the observation that even $|\rho_A| = 0$ produces a

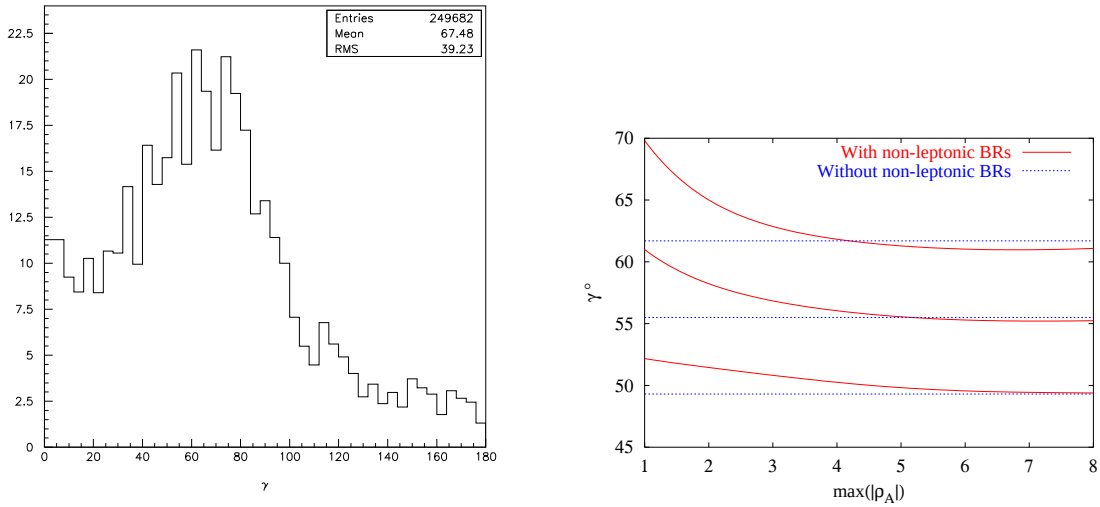

Fig. 6.13: *Fits of γ from* $\mathrm{B} \to \mathrm{K}\pi$ *using charming penguins (left) and UTA + improved QCD factorization as a function of* $\max|\rho_A|$ *(right).*

good fit to $\mathcal{B}(\mathrm{B} \to \mathrm{K}\pi)$. A better fit, however, can be obtained letting $|\rho_A|$ take values up to about 3. As shown in the right plot of Fig. 6.13, by doing so, the contribution of the constraint from non-leptonic B decays to a global fit of γ becomes totally negligible. In other words, for $|\rho_A| \sim 3$, the annihilation amplitude containing ρ_A becomes competitive with the others, improving the fit to the $\mathcal{B}$s on the one hand and weakening the predictivity on γ on the other.

3.5. Determination of the weak phases ϕ_2 and ϕ_3 from $\mathrm{B} \to \pi\pi, \mathrm{K}\pi$ in the pQCD method

Y.-Y. Keum[§].

In this section, we focus on the $\mathrm{B} \to \pi^+\pi^-$ and $\mathrm{K}\pi$ processes, providing promising strategies to determine the weak phases of ϕ_2 and ϕ_3, by using the perturbative QCD method. The perturbative QCD method (pQCD) has a predictive power demonstrated sucessfully in exclusive two body B-meson decays, specially in charmless B-meson decay processes[111]. By introducing parton transverse momenta $k_\perp$, we can generate naturally the Sudakov suppression effect due to resummation of large double logarithms $Exp[-\frac{\alpha_s C_F}{4\pi}\ln^2(\frac{Q^2}{k_\perp^2})]$, which suppress the long-distance contributions in the small $k_\perp$ region and give a sizable average $< k_\perp^2 > \sim \bar{\Lambda} M_B$. This can resolve the end point singularity problem and allow the applicability of pQCD to exclusive decays. We found that almost all of the contribution to the exclusive matrix elements come from the integration region where $\alpha_s/\pi < 0.3$ and the pertubative treatment can be justified.

In the pQCD approach, we can predict the contribution of non-factorizable term and annihilation diagram on the same basis as the factorizable one. A folklore for annihilation contributions is that they are negligible compared to W-emission diagrams due to helicity suppression. However the operators $O_{5,6}$ with helicity structure $(S-P)(S+P)$ are not suppressed and give dominant imaginary values, which is the main source of strong phase in the pQCD approach. So we have a large direct CP violation in $\mathrm{B} \to \pi^\pm\pi^\mp, \mathrm{K}^\pm\pi^\mp$, since large strong phase comes from the factorized annihilation diagram, which can distinguish pQCD from other models (see the previous two subsections).

[§]Y.-Y. Keum would like to thank G. Buchalla and members of PQCD working group for fruitful collaboration and joyful discussions.

3.5.1. *Extraction of $\phi_2(=\alpha)$ from $\mathrm{B} \to \pi^+\pi^-$ decay*

Even though isospin analysis of $\mathrm{B} \to \pi\pi$ can provide a clean way to determine ϕ_2, it might be difficult in practice because of the small branching ratio of $\mathrm{B}^0 \to \pi^0\pi^0$. In reality to determine ϕ_2, we can use the time-dependent rate of $\mathrm{B}^0(\mathrm{t}) \to \pi^+\pi^-$ including sizable penguin contributions. In our analysis we use the c-convention. The amplitude can be written as:

$$A(\mathrm{B}^0 \to \pi^+\pi^-) = -(|\mathrm{T_c}|\ \mathrm{e}^{\mathrm{i}\delta_\mathrm{T}}\ \mathrm{e}^{\mathrm{i}\phi_3} + |\mathrm{P_c}|\ \mathrm{e}^{\mathrm{i}\delta_\mathrm{P}}) \tag{75}$$

Penguin term carries a different weak phase than the dominant tree amplitude, which leads to generalized form of the time-dependent asymmetry.

When we define $R_{\pi\pi} = \overline{Br}(\mathrm{B}^0 \to \pi^+\pi^-)/\overline{Br}(\mathrm{B}^0 \to \pi^+\pi^-)|_{tree}$, where $\overline{Br}$ stands for a branching ratio averaged over B^0 and $\bar{\mathrm{B}}^0$, the explicit expression for $S_{\pi\pi}$ and $C_{\pi\pi}$ are given by:

$$\begin{aligned} R_{\pi\pi} &= 1 - 2\,R_c\,\cos\delta\,\cos(\phi_1+\phi_2) + R_c^2, & (76)\\ R_{\pi\pi}S_{\pi\pi} &= \sin 2\phi_2 + 2\,R_c\,\sin(\phi_1-\phi_2)\,\cos\delta - R_c^2 sin2\phi_1, & (77)\\ R_{\pi\pi}C_{\pi\pi} &= 2\,R_c\,\sin(\phi_1+\phi_2)\,\sin\delta. & (78) \end{aligned}$$

with $R_c = |P_c/T_c|$ and the strong phase difference between penguin and tree amplitudes $\delta = \delta_P - \delta_T$. The time-dependent asymmetry measurement provides two equations for $C_{\pi\pi}$ and $S_{\pi\pi}$ in terms of R_c, δ and ϕ_2.

If we know R_c and δ, then we can determine ϕ_2 from the experimental data on $C_{\pi\pi}$ versus $S_{\pi\pi}$.

Since the pQCD method provides $R_c = 0.23^{+0.07}_{-0.05}$ and $-41^\circ < \delta < -32^\circ$, the allowed range of ϕ_2 at present stage is determined as $55^\circ < \phi_2 < 100^\circ$ as shown in Fig. 6.14. Since we have a relatively large strong phase in pQCD, in contrast to the QCD-factorization ($\delta \sim 0^\circ$), we predict large direct CP violation effect of $A_{cp}(B^0 \to \pi^+\pi^-) = (23 \pm 7)\%$ which will be tested by more precise experimental measurement in future. Since the data by Belle Collaboration [24] is located outside allowed physical regions, we only considered in the numerical analysis the recent BaBar measurement[112] with 90% C.L. interval taking into account the systematic errors:

- $S_{\pi\pi} = \quad 0.02 \pm 0.34 \pm 0.05 \qquad$ [-0.54, +0.58]
- $C_{\pi\pi} = -0.30 \pm 0.25 \pm 0.04 \qquad$ [-0.72, +0.12].

The central point of BaBar data corresponds to $\phi_2 = 78^\circ$ in the pQCD method.

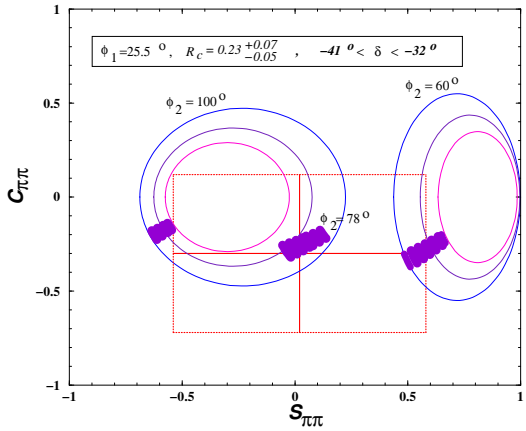

Fig. 6.14: *Plot of $C_{\pi\pi}$ versus $S_{\pi\pi}$ for various values of ϕ_2 with $\phi_1 = 25.5^\circ$, $0.18 < R_c < 0.30$ and $-41^\circ < \delta < -32^\circ$ in the pQCD method. Here we consider the allowed experimental ranges of BaBar measurment whinin 90% C.L. Dark areas is allowed regions in the pQCD method for different ϕ_2 values.*

3.5.2. *Extraction of $\phi_3(=\gamma)$ from $B^0 \to K^+\pi^-$ and $B^+ \to K^0\pi^+$ decays*

By using tree-penguin interference in $B^0 \to K^+\pi^-(\sim T' + P')$ versus $B^+ \to K^0\pi^+(\sim P')$, CP-averaged $B \to K\pi$ branching fraction may lead to non-trivial constraints on the ϕ_3 angle [84,67,68]. In order to determine ϕ_3, we need one more useful information on CP-violating rate differences[11]. Let's introduce the following observables :

$$\begin{aligned} R_K &= \frac{\overline{Br}(B^0 \to K^+\pi^-)\ \tau_+}{\overline{Br}(B^+ \to K^0\pi^+)\ \tau_0} = 1 - 2\ r_K\ \cos\delta\ \cos\phi_3 + r_K^2 \\ A_0 &= \frac{\Gamma(\bar{B}^0 \to K^-\pi^+) - \Gamma(B^0 \to K^+\pi^-)}{\Gamma(B^- \to \bar{K}^0\pi^-) + \Gamma(B^+ \to \bar{K}^0\pi^+)} \\ &= A_{cp}(B^0 \to K^+\pi^-)\ R_K = -2r_K\ \sin\phi_3\ \sin\delta. \end{aligned} \tag{79}$$

where $r_K = |T'/P'|$ is the ratio of tree to penguin amplitudes in $B \to K\pi$ and $\delta = \delta_{T'} - \delta_{P'}$ is the strong phase difference between tree and penguin amplitudes. After elimination of $\sin\delta$ in Eqs. (8)–(9), we have

$$R_K = 1 + r_K^2 \pm \sqrt{4r_K^2\cos^2\phi_3 - A_0^2\cot^2\phi_3}. \tag{80}$$

Here we obtain $r_K = 0.201 \pm 0.037$ from the pQCD analysis[111] and $A_0 = -0.11 \pm 0.065$ by combining recent BaBar measurement on CP asymmetry of $B^0 \to K^+\pi^-$: $A_{cp}(B^0 \to K^+\pi^-) = -10.2 \pm 5.0 \pm 1.6\%$ [112] with present world averaged value of $R_K = 1.10 \pm 0.15$ [113].

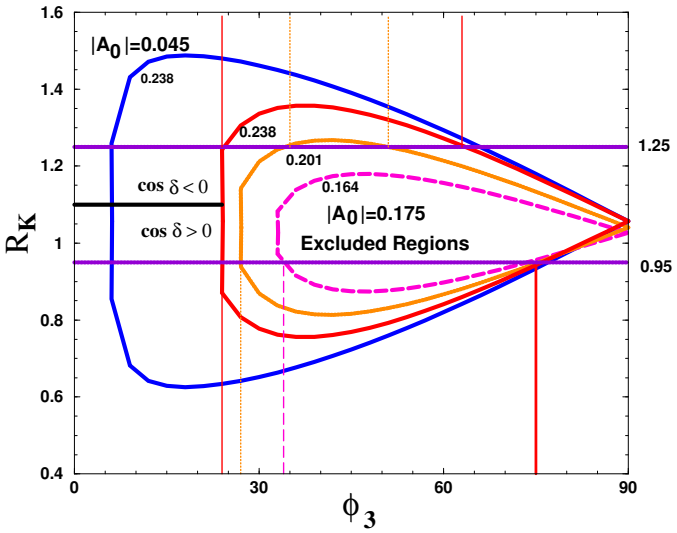

Fig. 6.15: *Plot of R_K versus ϕ_3 with $r_K = 0.164, 0.201$ and 0.238.*

From Table 2 of Ref. [114], we obtain $\delta_{P'} = 157^\circ$, $\delta_{T'} = 1.4^\circ$ and the negative $\cos\delta$: $\cos\delta = -0.91$. As shown in Fig. 6.15, we can constrain the allowed range of ϕ_3 within $1\,\sigma$ range of World Averaged R_K as follows:

- For $\cos\delta < 0$, $r_K = 0.164$: we can exclude $0^\circ \le \phi_3 \le 6^\circ$.
- For $\cos\delta < 0$, $r_K = 0.201$: we can exclude $0^\circ \le \phi_3 \le 6^\circ$ and $35^\circ \le \phi_3 \le 51^\circ$.
- For $\cos\delta < 0$, $r_K = 0.238$: we can exclude $0^\circ \le \phi_3 \le 6^\circ$ and $24^\circ \le \phi_3 \le 62^\circ$.

When we take the central value of $r_K = 0.201$, ϕ_3 is allowed within the ranges of $51^\circ \le \phi_3 \le 129^\circ$, which is consistent with the results of the model-independent CKM-fit in the $(\bar{\rho}, \bar{\eta})$ plane.

3.5.3. Conclusion

We discussed two methods to determine the weak phases ϕ_2 and ϕ_3 within the pQCD approach through 1) Time-dependent asymmetries in $B^0 \to \pi^+\pi^-$, 2) $B \to K\pi$ processes via penguin-tree interference. We can already obtain interesting bounds on ϕ_2 and ϕ_3 from present experimental measurements. Our predictions within pQCD method is in good agreement with present experimental measurements in charmless B-decays. Specially our pQCD method predicted a large direct CP asymmetry in $B^0 \to \pi^+\pi^-$ decay, which will be a crucial touch stone in order to distinguish our approach from others in future precise measurements. More detail works on other methods in $B \to K\pi$ and $D^{(*)}\pi$ processes will appear elsewhere [114].

4. $K \to \pi\nu\bar{\nu}$ decays

G. Isidori and D.E. Jaffe

4.1. Theoretical description

The $s \to d\nu\bar{\nu}$ transition is one of the rare examples of weak processes whose leading contribution starts at $\mathcal{O}(G_F^2)$. At the one-loop level it receives contributions only from Z-penguin and W-box diagrams, as shown in Fig. 6.16, or from pure quantum electroweak effects. Separating the contributions to the one-loop amplitude according to the intermediate up-type quark running inside the loop, we can write

$$\mathcal{A}(s \to d\nu\bar{\nu}) = \sum_{q=u,c,t} V_{qs}^* V_{qd} \mathcal{A}_q \quad \sim \quad \begin{cases} \mathcal{O}(\lambda^5 m_t^2) + i\mathcal{O}(\lambda^5 m_t^2) & (q=t) \\ \mathcal{O}(\lambda m_c^2) + i\mathcal{O}(\lambda^5 m_c^2) & (q=c) \\ \mathcal{O}(\lambda \Lambda_{\rm QCD}^2) & (q=u) \end{cases} \tag{81}$$

where V_{ij} denote the elements of the CKM matrix. The hierarchy of these elements would favour up- and charm-quark contributions; however, the *hard* GIM mechanism of the perturbative calculation implies $\mathcal{A}_q \sim m_q^2/M_W^2$, leading to a completely different scenario. As shown on the r.h.s. of (81), where we have employed the standard CKM phase convention ($\mathrm{Im}V_{us} = \mathrm{Im}V_{ud} = 0$) and expanded the V_{ij} in powers of the Cabibbo angle, the top-quark contribution dominates both real and imaginary parts. This structure implies several interesting consequences for $\mathcal{A}(s \to d\nu\bar{\nu})$: it is dominated by short-distance dynamics, therefore its QCD corrections are small and calculable in perturbation theory; it is very sensitive to V_{td}, which is one of the less constrained CKM matrix elements; it is likely to have a large CP-violating phase; it is very suppressed within the SM and thus very sensitive to possible new sources of quark-flavour mixing.

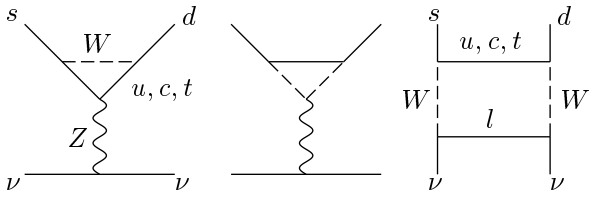

Fig. 6.16: *One-loop diagrams contributing to the $s \to d\nu\bar{\nu}$ transition.*

Short-distance contributions to $\mathcal{A}(s \to d\nu\bar{\nu})$, are efficiently described, within the SM, by the following effective Hamiltonian [115]

$$\mathcal{H}_{eff} = \frac{G_F}{\sqrt{2}} \frac{\alpha}{2\pi \sin^2\Theta_W} \sum_{l=e,\mu,\tau} \left[\lambda_c X_{NL}^l + \lambda_t X(x_t)\right] (\bar{s}d)_{V-A} (\bar{\nu}_l \nu_l)_{V-A} \,, \tag{82}$$

where $x_t = m_t^2/M_W^2$ and, as usual, $\lambda_q = V_{qs}^* V_{qd}$. The coefficients X_{NL}^l and $X(x_t)$, encoding charm- and top-quark loop contributions, are known at the NLO accuracy in QCD [116,117] and can be found

explicitly in [115]. The theoretical uncertainty in the dominant top contribution is very small and it is essentially determined by the experimental error on m_t. Fixing the $\overline{\rm MS}$ top-quark mass to $\overline{m}_t(m_t) = (166 \pm 5)$ GeV we can write

$$X(x_t) = 1.51 \left[\frac{\overline{m}_t(m_t)}{166\ {\rm GeV}}\right]^{1.15} = 1.51 \pm 0.05\ . \tag{83}$$

The simple structure of $\mathcal{H}_{eff}$ leads to two important properties of the physical $\mathrm{K} \to \pi\nu\bar{\nu}$ transitions:

- The relation between partonic and hadronic amplitudes is exceptionally accurate, since hadronic matrix elements of the $\bar{s}\gamma^\mu d$ current between a kaon and a pion can be derived by isospin symmetry from the measured K_{l3} rates.
- The lepton pair is produced in a state of definite CP and angular momentum, implying that the leading SM contribution to $\mathrm{K}_L \to \pi^0\nu\bar{\nu}$ is CP-violating.

The largest theoretical uncertainty in estimating $\mathcal{B}(\mathrm{K}^+ \to \pi^+\nu\bar{\nu})$ originates from the charm sector. Following the analysis of Ref. [115], the perturbative charm contribution is conveniently described in terms of the parameter

$$P_0(X) = \frac{1}{\lambda^4}\left[\frac{2}{3}X_{NL}^e + \frac{1}{3}X_{NL}^\tau\right] = 0.42 \pm 0.06\ . \tag{84}$$

The numerical error in the r.h.s. of Eq. (84) is obtained from a conservative estimate of NNLO corrections [115]. Recently also non-perturbative effects introduced by the integration over charmed degrees of freedom have been discussed [118]. Despite a precise estimate of these contributions is not possible at present (due to unknown hadronic matrix-elements), these can be considered as included in the uncertainty quoted in Eq. (84).[¶] Finally, we recall that genuine long-distance effects associated to light-quark loops are well below the uncertainties from the charm sector [119].

With these definitions the branching fraction of $\mathrm{K}^+ \to \pi^+\nu\bar{\nu}$ can be written as

$$\mathcal{B}(\mathrm{K}^+ \to \pi^+\nu\bar{\nu}) = \frac{\bar{\kappa}_+}{\lambda^2}\ \left[(\mathrm{Im}\lambda_t)^2 X^2(x_t) + \left(\lambda^4 \mathrm{Re}\lambda_c P_0(X) + \mathrm{Re}\lambda_t X(x_t)\right)^2\right]\ , \tag{85}$$

where [115]

$$\bar{\kappa}_+ = r_{K^+}\frac{3\alpha^2 \mathcal{B}(\mathrm{K}^+ \to \pi^0 e^+\nu)}{2\pi^2 \sin^4\Theta_W} = 7.50 \times 10^{-6} \tag{86}$$

and $r_{K^+} = 0.901$ takes into account the isospin breaking corrections necessary to extract the matrix element of the $(\bar{s}d)_V$ current from $\mathcal{B}(\mathrm{K}^+ \to \pi^0 e^+\nu)$ [120].

The case of $\mathrm{K}_L \to \pi^0\nu\bar{\nu}$ is even cleaner from the theoretical point of view [121]. Because of the CP structure, only the imaginary parts in (82) –where the charm contribution is absolutely negligible– contribute to $\mathcal{A}(\mathrm{K}_2 \to \pi^0\nu\bar{\nu})$. Thus the dominant direct-CP-violating component of $\mathcal{A}(\mathrm{K}_L \to \pi^0\nu\bar{\nu})$ is completely saturated by the top contribution, where QCD corrections are suppressed and rapidly convergent. Intermediate and long-distance effects in this process are confined only to the indirect-CP-violating contribution [9] and to the CP-conserving one [122], which are both extremely small. Taking into account the isospin-breaking corrections to the hadronic matrix element [120], we can write an expression for the $\mathrm{K}_L \to \pi^0\nu\bar{\nu}$ rate in terms of short-distance parameters, namely

$$\mathcal{B}(\mathrm{K}_L \to \pi^0\nu\bar{\nu})_{\rm SM} = \frac{\bar{\kappa}_L}{\lambda^2}(\mathrm{Im}\lambda_t)^2 X^2(x_t) = 4.16 \times 10^{-10} \times \left[\frac{\overline{m}_t(m_t)}{167\ {\rm GeV}}\right]^{2.30}\left[\frac{\mathrm{Im}\lambda_t}{\lambda^5}\right]^2\ , \tag{87}$$

which has a theoretical error below 3%.

[¶] The natural order of magnitude of these non-perturbative corrections, relative to the perturbative charm contribution is $m_K^2/(m_c^2 \ln(m_c^2/M_W^2)) \sim 2\%$.

At present the SM predictions of the two $\mathrm{K} \to \pi\nu\bar{\nu}$ rates are not extremely precise owing to the limited knowledge of both real and imaginary parts of λ_t. Taking into account all the indirect constraints in a global Gaussian fit, the allowed ranges read [123,124][‖]

$$\mathcal{B}(\mathrm{K}^+ \to \pi^+\nu\bar{\nu})_{\mathrm{SM}} = (0.72 \pm 0.21) \times 10^{-10} , \tag{88}$$

$$\mathcal{B}(\mathrm{K}_L \to \pi^0\nu\bar{\nu})_{\mathrm{SM}} = (0.28 \pm 0.10) \times 10^{-10} . \tag{89}$$

The high accuracy of the theoretical predictions of $\mathcal{B}(\mathrm{K}^+ \to \pi^+\nu\bar{\nu})$ and $\mathcal{B}(\mathrm{K}_L \to \pi^0\nu\bar{\nu})$ in terms of modulus and phase of $\lambda_t = V_{ts}^* V_{td}$ clearly offers the possibility of very interesting tests of flavour dynamics. Within the SM, a measurement of both channels would provide two independent pieces of information on the unitary triangle, or a complete determination of $\bar{\rho}$ and $\bar{\eta}$ from $\Delta S = 1$ transitions. In particular, $\mathcal{B}(\mathrm{K}^+ \to \pi^+\nu\bar{\nu})$ defines an ellipse in the $\bar{\rho}$–$\bar{\eta}$ plane and $\mathcal{B}(\mathrm{K}_\mathrm{L}^0 \to \pi^0\nu\bar{\nu})$ an horizontal line (the height of the unitarity triangle). Note, in addition, that the determination of $\sin 2\beta$ which can be obtained by combining $\mathcal{B}(\mathrm{K}_\mathrm{L}^0 \to \pi^0\nu\bar{\nu})$ and $\mathcal{B}(\mathrm{K}^+ \to \pi^+\nu\bar{\nu})$ is extremely clean, being independent from uncertainties due to m_t and V_{cb} (contrary to the separate determinations of $\bar{\rho}$ and $\bar{\eta}$) [9].

In principle a very precise and highly non-trivial test of the CKM mechanism could be obtained by the comparison of the following two sets of data [9]: the two $\mathrm{K} \to \pi\nu\bar{\nu}$ rates on one side, the ratio $\Delta M_{B_d}/\Delta M_{B_s}$ and $a_{\mathrm{CP}}(B \to J/\Psi K_S)$ on the other side. The two sets are determined by very different loop amplitudes ($\Delta S = 1$ FCNCs and $\Delta B = 2$ mixing) and both suffer from very small theoretical uncertainties. In particular, concerning the $\mathrm{K}^+ \to \pi^+\nu\bar{\nu}$ mode, we can write [123]

$$\mathcal{B}(\mathrm{K}^+ \to \pi^+\nu\bar{\nu}) = \bar{\kappa}_+ |V_{cb}|^4 X^2(x_t) \left[\sigma R_t^2 \sin^2\beta + \frac{1}{\sigma} \left(R_t \cos\beta + \frac{\lambda^4 P_0(X)}{|V_{cb}|^2 X(x_t)} \right)^2 \right] , \tag{90}$$

where R_t is determined by $\Delta M_{B_d}/\Delta M_{B_s}$ [115],[**]

$$R_t = \frac{\xi}{\lambda} \sqrt{\frac{\Delta M_{B_d}}{\Delta M_{B_s}}} \tag{91}$$

and $\sin\beta$ from $a_{\mathrm{CP}}(B \to J/\Psi \mathrm{K}_S)$. In the next few years, when the experimental determination of $a_{\mathrm{CP}}(B \to J/\Psi \mathrm{K}_S)$, $\Delta M_{B_d}/\Delta M_{B_s}$, and $\mathcal{B}(\mathrm{K}^+ \to \pi^+\nu\bar{\nu})$ will substantially improve, this relation could provide one of the most significant tests of the Standard Model in the sector of quark-flavour dynamics.

Present experimental data on $\mathrm{K} \to \pi\nu\bar{\nu}$ rates do not allow yet to fully explore the high-discovery potential of these CKM tests. Nonetheless, we stress that the evidence of the $\mathrm{K}^+ \to \pi^+\nu\bar{\nu}$ decay obtained by BNL-E787 already provides highly non-trivial constraints on realistic scenarios with large new sources of flavour mixing (see e.g. Ref. [123,125,126]).

4.2. Experimental status and future prospects

The Brookhaven experiment E787 [127] searched for the decay $\mathrm{K}^+ \to \pi^+\nu\bar{\nu}$ by stopping approximately 25% of a 670, 710, 730 or 790 MeV/c K^+ beam at $\sim$ 5 MHz with $\sim$ 25% π^+ contamination in a scintillating-fiber target along the axis of a 1-T solenoidal magnetic spectrometer. The range (R), momentum (P) and energy (E) of charged decay products are measured using the target, central drift chamber and a cylindrical range stack composed of 21 layers of plastic scintillator with two layers of

[‖] As pointed out in Ref. [124], the errors in Eqs. (88)–(89) can be reduced if $\mathrm{Re}\lambda_t$ and $\mathrm{Im}\lambda_t$ are directly extracted from $a_{\mathrm{CP}}(B \to J/\Psi \mathrm{K}_S)$ and ϵ_K; however, this procedure introduces a stronger sensitivity to the probability distribution of the (theoretical) estimate of B_K.

[**] As usual we define $\xi = (F_{B_s}/F_{B_d})\sqrt{B_{B_s}/B_{B_d}}$ and $\sigma = 1/(1 - \frac{\lambda^2}{2})^2$.

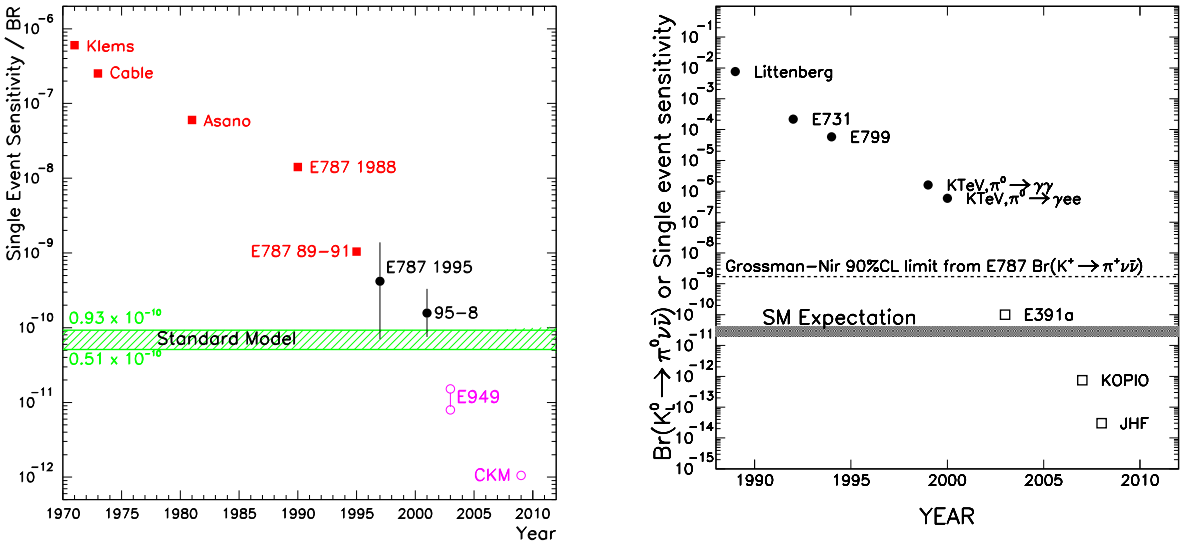

Fig. 6.17: *History and prospects for the study of* $\mathcal{B}(\mathrm{K}^+ \to \pi^+\nu\bar{\nu})$*(left) and* $\mathcal{B}(\mathrm{K}_\mathrm{L}^0 \to \pi^0\nu\bar{\nu})$*(right). The points with error bars are measured branching fractions, the solid points are upper limits at 90% CL and the open points or squares are single event sensitivities. The dashed line is a nearly model-independent limit based on the E787's results for* $\mathcal{B}(\mathrm{K}^+ \to \pi^+\nu\bar{\nu})$ *[126]. The horizontal bands are the 68% CL SM expectations.*

tracking chambers. Detection of the decay sequence $\pi^+ \to \mu^+ \to e^+$ in the range stack provided a powerful tool against $\mathrm{K}^+ \to \mu^+\nu(\gamma)$ decays. A 4π-sr calorimeter consisting of lead/scintillator layers in the barrel (14 radiation lengths) and undoped CsI crystals in the endcap (13.5 radiation lengths) were used to veto photons and suppress $\mathrm{K}^+ \to \pi^+\pi^0$ background. Incident kaons were detected and identified by Čerenkov, tracking and energy loss detectors along the beam that aided in the suppression of backgrounds due to scattered beam pions and the charge exchange process that resulted in $\mathrm{K}_L^0 \to \pi^+\ell^-\nu$ decays ($\ell^- = e^-$,μ^-) in the target.

E787 has a long history, summarized in Fig. 6.17, that has lead to the development of a relatively robust analysis strategy. The strategy begins with *a priori* identification of background sources and development of experimental tools to suppress each background source with at least two independent cuts. In the search for such rare processes, background rejection cannot be reliably simulated, instead it is measured by alternatively inverting independent cuts and measuring the rejection of each cut taking any correlations into account. To avoid bias, cuts are determined using 1/3 of the data and then the backgrounds rates are measured with the remaining 2/3 sample. Background estimates are verified by loosening cuts and comparing the observed and predicted rates, first in the 1/3 sample, then in the 2/3 sample. Simulated signal events are used to measure the geometrical acceptance for $\mathrm{K}^+ \to \pi^+\nu\bar{\nu}$ and the acceptance is verified with a measurement of $\mathcal{B}(\mathrm{K}^+ \to \pi^+\pi^0)$. The pre-defined signal region in R, P and E is not examined until all background estimates are verified. It is anticipated that similar strategies will be employed in further investigations of $\mathrm{K} \to \pi\nu\bar{\nu}$ decays.

Brookhaven E787 was completed in 1998 and has observed two candidates for the decay $\mathrm{K}^+ \to \pi^+\nu\bar{\nu}$ in the pion momentum region 211 to 229 MeV/c with an estimated background of 0.15 ± 0.05 in a sample of 5.9×10^{12} stopped K^+ that corresponds to [127]

$$\mathcal{B}(\mathrm{K}^+ \to \pi^+\nu\bar{\nu}) = (15.7^{+17.5}_{-8.2}) \times 10^{-11} \ . \tag{92}$$

The probability that the two candidates are entirely due to background is 0.02% . In addition a search

in the momentum interval 140 to 195 MeV/c in a sample of 1.1×10^{12} stopped K^+ yielded a single candidate upon an estimated background of 0.73 ± 0.18 corresponding to a limit $\mathcal{B}(K^+ \to \pi^+\nu\bar{\nu}) < 420 \times 10^{-11}$ at 90% C.L. [128]. Such a search below the peak of the two body $K^+ \to \pi^+\pi^0$ decays has the potential not only to augment the statistics of the higher momentum sample, but also to investigate the shape of the $P(\pi^+)$ distribution predicted by the SM. In addition, the search is somewhat complementary to that of the higher momentum interval because the background is dominated by $K^+ \to \pi^+\pi^0$ decays in which the charged pion undergoes a nuclear interaction in the target near the kaon decay vertex.

E949 is an upgraded version of E787 with an expected net increase in sensitivity of at least a factor of 5 based on 6000 hours of running time or 5-10 SM events [129]. The main detector upgrades are an increased photon veto capability, both in the endcap and barrel regions, as well as trigger and data acquisition improvements. E949 recently accumulated 1.9×10^{12} stopped kaons ($\sim 1/9$ of E949's goal) and additional running is expected in 2003 assuming sufficient funding is forthcoming.

The CKM experiment at Fermilab expects to attain a single event sensitivity of 1×10^{-12} that would correspond to ~ 100 $K^+ \to \pi^+\nu\bar{\nu}$ events assuming the SM value of the branching fraction [130]. Such a measurement would achieve a statistical precision comparable to the current theoretical uncertainty in the branching fraction. CKM departs from the E787/E949 technique by using kaon decays in flight in a 22 GeV/c, 50 MHz debunched beam with 60% kaon purity. The experiment will use photon veto technology similar to E787 and KTeV with the addition of ring-imaging Čerenkov detectors to aid in kinematic suppression of backgrounds. The use of in-flight kaon decays means that the dominant $K^+ \to \pi^+\pi^0$ background in E787's search in the lower momentum region should not be present at CKM [131]. CKM should be taking data in the second half of this decade.

The progress concerning the neutral mode is much slower. No dedicated experiment has started yet and the best direct limit is more than four orders of magnitude above the SM expectation [132]. An indirect model-independent upper bound on $\Gamma(K_L \to \pi^0\nu\bar{\nu})$ can be obtained by the isospin relation [126]

$$\Gamma(K^+ \to \pi^+\nu\bar{\nu}) = \Gamma(K_L \to \pi^0\nu\bar{\nu}) + \Gamma(K_S \to \pi^0\nu\bar{\nu}) \tag{93}$$

which is valid for any $s \to d\nu\bar{\nu}$ local operator of dimension ≤ 8 (up to small isospin-breaking corrections). Using the BNL-E787 result (92), this implies $\mathcal{B}(K_L \to \pi^0\nu\bar{\nu}) < 1.7 \times 10^{-9}$ (90% CL). Any experimental information below this figure can be translated into a non-trivial constraint on possible new-physics contributions to the $s \to d\nu\bar{\nu}$ amplitude.

The first $K_L \to \pi^0\nu\bar{\nu}$ dedicated experiments are E391a at KEK [133] and KOPIO at Brookhaven [134]. E391a is envisioned as a two-stage experiment and will attempt to use a highly collimated K_L^0 beam and a hermetic veto to observe high transverse momentum π^0 near the endpoint of the $K_L^0 \to \pi^0\nu\bar{\nu}$ spectrum with a technique similar to previous searches [132]. The first stage of E391a is regarded as a pilot experiment and will use the KEK 12 GeV/c proton beam and should begin data taking in 2003. If successful, it could push the limit on $\mathcal{B}(K_L^0 \to \pi^0\nu\bar{\nu})$ to within an order of magnitude of the SM expectation (Fig. 6.18). An aggressive second stage envisions use of the high intensity 50 GeV/c proton beam from the Japanese Hadron Facility(JHF) to reach a single event sensitivity of 3×10^{-14} or, equivalently, ~ 1000 SM events.

The KOPIO experiment will attempt a new approach, using a microbunched, low momentum beam, time-of-flight and a high precision electromagnetic preradiator and calorimeter to fully reconstruct the kinematics of the $K_L^0 \to \pi^0\nu\bar{\nu}$ decay. Coupled with highly efficient charged particle and photon vetoes, KOPIO will be able to exploit the E787 strategy of independent kinematic and veto cuts to measure all backgrounds with the data. The goal of KOPIO is a single event sensitivity of 7.5×10^{-13} or the capability to obtain 40 SM events with a signal to background of 2 corresponding to a precision on $\mathcal{J}$ or $\bar{\eta}$ of $\sim 10\%$.

As anticipated, one of the most interesting test of the CKM mechanism could be obtained by the comparison of the two $K \to \pi\nu\bar{\nu}$ rates on one side vs. the ratio $\Delta M_{B_d}/\Delta M_{B_s}$ and $a_{CP}(B \to$

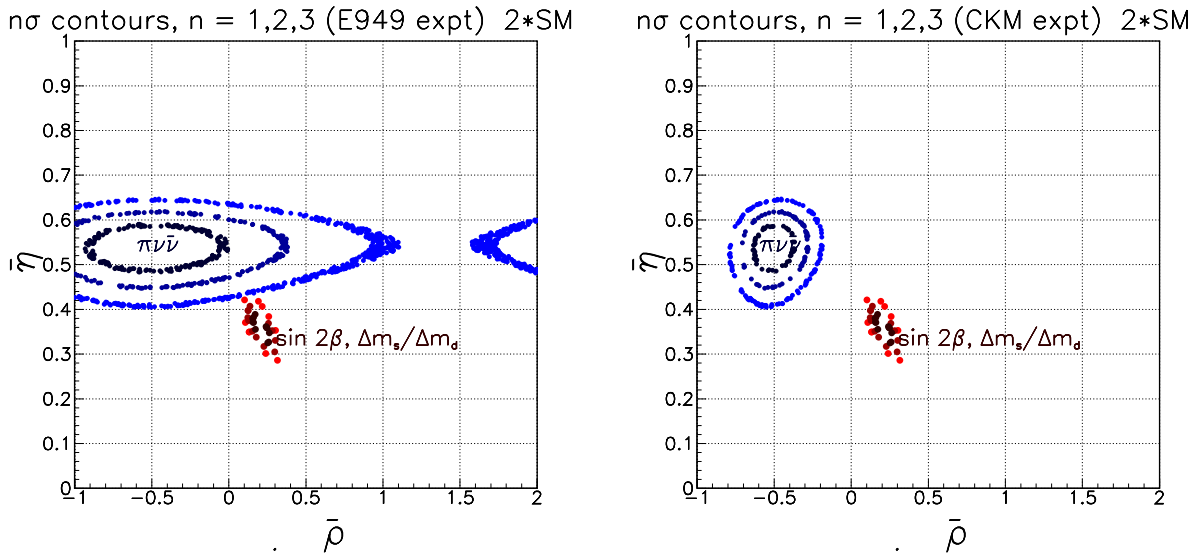

Fig. 6.18: *Comparison of the impact of hypothetical measurements of the* $\mathrm{K} \to \pi\nu\bar{\nu}$ *branching fractions by E949 and KOPIO(left) or CKM and KOPIO(right) in the* $\bar{\rho}, \bar{\eta}$ *plane with hypothetical measurements of* $\sin 2\beta$ *and* $\Delta M_s/\Delta M_d$*. Contours at 68.3, 95.45 and 99.7% CL are indicated for the K measurements. For the B measurements, the points indicating the three contours overlap. See text for details.*

$\mathrm{J}/\Psi\mathrm{K_S}$) on the other side. As an illustration, in Figure 6.18 we consider the comparison of the two B-physics measurements, assumed to be $a_{\mathrm{CP}}(B \to J/\Psi \mathrm{K}_S) = 0.75 \pm 0.02$ and $\Delta M_{B_d}/\Delta M_{B_s} = 17.0 \pm 1.7\ \mathrm{ps}^{-1}$, with the two $\mathrm{K} \to \pi\nu\bar{\nu}$ rates, both assumed to be twice the corresponding SM prediction. The uncertainties on $\mathcal{B}(\mathrm{K} \to \pi\nu\bar{\nu})$ measurements are those expected by E949, CKM and KOPIO experiments attaining their expected sensitivities. The corresponding constraints in the $\bar{\rho}$–$\bar{\eta}$ plane have been derived assuming Gaussian uncertainties for all quantities, using the Bayesian statistics option of the CKM fitter program [135]. Negligible uncertainty in $|V_{cb}|$ is assumed in placing the K measurements in this *B-centric* rendering of the UT. Note that the alternative, equally fundamental, parametrization of the UT using the λ_t plane would remove the need for this assumption [136].

References

[1] The BaBar Physics Book, eds. P. Harrison and H. Quinn, 1998, SLAC report 504.

[2] B Decays at the LHC, eds. P. Ball, R. Fleischer, G.F. Tartarelli, P. Vikas and G. Wilkinson, hep-ph/0003238.

[3] B Physics at the Tevatron, Run II and Beyond, K. Anikeev et al., hep-ph/0201071.

[4] A.J. Buras and R. Fleischer, Adv Ser. Direct. High. Energy Phys. **15** (1998) 65; [hep-ph/9704376].

[5] A.J. Buras, hep-ph/0101336, lectures at the International Erice School, August, 2000;
Y. Nir, hep-ph/0109090, lectures at 55th Scottish Univ. Summer School, 2001.

[6] A.J. Buras, F. Parodi and A. Stocchi, JHEP **0301** (2003) 029 [hep-ph/0207101].

[7] J.M. Soares and L. Wolfenstein, Phys. Rev. D **47** (1993) 1021; Y. Nir and U. Sarid, Phys. Rev. D **47** (1993) 2818; Y. Grossman and Y. Nir, Phys. Lett. B **313** (1993) 126; R. Barbieri, L.J. Hall and A. Romanino, Phys. Lett. B **401** (1997) 47; M. Ciuchini, E. Franco, L. Giusti, V. Lubicz and G. Martinelli, Nucl. Phys. B **573** (2000) 201-222; P. Paganini, F. Parodi, P. Roudeau and A. Stocchi, Physica Scripta **58** (1998) 556-569; F. Parodi, P. Roudeau and A. Stocchi Nuovo Cimento **112A (1999) 833.**

[8] A. Höcker, H. Lacker, S. Laplace and F. Le Diberder, Eur. Phys. J. C **21** (2001) 225.

[9] G. Buchalla and A.J. Buras, Phys. Rev. D **54** (1996) 6782.

[10] M. Beneke, G. Buchalla, M. Neubert, and C. Sachrajda, Nucl. Phys. B **606** (2001) 245.

[11] M. Gronau and J. L. Rosner, Phys. Rev. D **65** (2002) 013004 [E: D **65** (2002) 079901].

[12] Z. Luo and J. L. Rosner, Phys. Rev. D **65** (2002) 054027.

[13] A.J. Buras, M.E. Lautenbacher and G. Ostermaier, Phys. Rev. D **50** (1994) 3433.

[14] A.J. Buras, Phys. Lett. B **333** (1994) 476; Nucl. Instr. Meth. **A368** (1995) 1.

[15] R. Aleksan, B. Kayser and D. London, Phys. Rev. Lett. **73** (1994) 18;
J.P. Silva and L. Wolfenstein, Phys. Rev. D **55** (1997) 5331;
I.I. Bigi and A.I. Sanda, hep-ph/9909479.

[16] A.J. Buras, P. Gambino, M. Gorbahn, S. Jäger and L. Silvestrini, Phys. Lett. B **500** (2001) 161.

[17] A. Ali and D. London, Eur. Phys. J. C **9** (1999) 687 [hep-ph/9903535]; Phys. Rep. **320** (1999), 79 [hep-ph/9907243]; hep-ph/0002167; Eur. Phys. J. C **18** (2001) 665.

[18] A.J. Buras and R. Fleischer, Phys. Rev. D **64** (2001) 115010.

[19] A.J. Buras, P.H. Chankowski, J. Rosiek and L. Slawianowska, Nucl. Phys. B **619** (2001) 434.

[20] G. D'Ambrosio and G. Isidori, Phys. Lett. B **530** (2002) 108.

[21] G.C. Branco, L. Lavoura and J. Silva, (1999), CP Violation, Oxford Science Publications, Press Clarendon, Oxford.

[22] F.J. Botella, G.C. Branco, M. Nebot and M.N. Rebelo, Nucl. Phys. B **651** (2003) 174 [hep-ph/0206133].

[23] L. Wolfenstein, Phys. Rev. Lett. **51** (1983) 1945.

[24] Belle Collaboration, K. Abe et al., Phys. Rev. Lett. **89** (2002) 071801, hep-ex/0204002.

[25] Talk by A. Farbin (BaBar Collaboration), XXXVIIth Recontres de Moriond, Electroweak Interactions and Unified Theories, Les Arcs, France, 9-16 March 2002, http://moriond.in2p3.fr/EW/2002/.

[26] Average from Y. Nir hep-ph/0208080 based on: R. Barate et al. (ALEPH Collaboration) *Phys. Lett.* B **492** (2000), 259; K. Ackerstaff et al. (OPAL Collaboration) *Eur. Phys.* C **5** (1998) 379; T. Affolder at al. Phys. ReV. D61 (2000) 072005; B. Aubert et al. (Babar Collaboration) hep-ex/0207042; K. Abe at al. (Belle Collaboration) hep-ex/0207098.

[27] M. Ciuchini, G. D'Agostini, E. Franco, V. Lubicz, G. Martinelli, F. Parodi, P. Roudeau, A. Stocchi, JHEP **0107** (2001) 013 [hep-ph/0012308].

[28] T. Hurth, Rev. Mod. Phys. (to appear) [hep-ph/0212304]; A. J. Buras and M. Misiak, Acta Phys. Pol. B 33 (2002) 2597 [hep-ph/0207131].

[29] S. Bertolini, F. Borzumati and A. Masiero, Phys. Rev. Lett. **59** (1987) 180;
N.G. Deshpande *et al.*, Phys. Rev. Lett. **59** (1987) 183.

[30] M. S. Alam *et al.* (CLEO Collaboration), Phys. Rev. Lett. **74** (1995) 2885.

[31] B. Aubert *et al.* (BABAR Collaboration), hep-ex/0207076.

[32] S. Chen *et al.* (CLEO Collaboration), Phys. Rev. Lett. **87** (2001) 251807 [hep-ex/0108032].

[33] K. Abe *et al.* (BELLE Collaboration), Phys. Lett. B **511** (2001) 151 [hep-ex/0103042].

[34] R. Barate *et al.* (ALEPH Collaboration), Phys. Lett. B **429** (1998) 169.

[35] P. Gambino and M. Misiak, Nucl. Phys. B **611** (2001) 338 [hep-ph/0104034].

[36] A.J. Buras, A. Czarnecki, M. Misiak and J. Urban, Nucl. Phys. B **631** (2002) 219 [hep-ph/0203135].

[37] K. Hagiwara *et al.* (Particle Data Group Collaboration), Phys. Rev. D **66** (2002) 010001.

[38] A. Ali, H. Asatrian and C. Greub, Phys. Lett. B **429** (1998) 87 [hep-ph/9803314];
A. L. Kagan and M. Neubert, Phys. Rev. D **58** (1998) 094012 [hep-ph/9803368].

[39] Y. Grossman and D. Pirjol, JHEP **0006** (2000) 02 [hep-ph/0005069].

[40] T.E. Coan *et al.* (CLEO Collaboration), Phys. Rev. Lett. **86** (2001) 5661 [hep-ex/0010075].

[41] M. Beneke, G. Buchalla, M. Neubert and C. T. Sachrajda, Phys. Rev. Lett. **83** (1999) 1914 [hep-ph/9905312].

[42] M. Beneke, T. Feldmann and D. Seidel, Nucl. Phys. B **612** (2001) 25 [hep-ph/0106067].

[43] S. W. Bosch and G. Buchalla, Nucl. Phys. B **621** (2002) 459 [hep-ph/01060].

[44] A. Ali and A. Y. Parkhomenko, Eur. Phys. J. C **23** (2002) 89 [hep-ph/0105302].

[45] T. E. Coan *et al.* (CLEO Collaboration), Phys. Rev. Lett. **84** (2000) 5283 [hep-ex/9912057].

[46] S. Nishida (BELLE Collaboration), Talk presented at the 31st. International Conference on High Energy Physics, July 24 - 31, 2002, Amsterdam, The Netherlands.

[47] B. Aubert *et al.* (BABAR Collaboration) Phys. Rev. Lett. **88** (2002) 101805 [hep-ex/0110065].

[48] A. L. Kagan and M. Neubert, Phys. Lett. B **539**, 227 (2002) [hep-ph/0110078].

[49] P. Ball and V. M. Braun, Phys. Rev. D **58** (1998) 094016 [hep-ph/9805422].

[50] M. Beneke and T. Feldmann, Nucl. Phys. B **592** (2001) 3 [hep-ph/0008255].

[51] A. Ali, V. M. Braun and H. Simma, Z. Phys. C **63** (1994) 437 [hep-ph/9401277].

[52] L. Del Debbio, J. M. Flynn, L. Lellouch and J. Nieves (UKQCD Collaboration), Phys. Lett. B **416** (1998) 392 [hep-lat/9708008].

[53] A. Ali, L. T. Handoko and D. London, Phys. Rev. D **63** (2000) 014014 [hep-ph/0006175].

[54] B. Grinstein and D. Pirjol, Phys. Rev. D **62** (2000) 093002 [hep-ph/0002216].

[55] A. Ali and V. M. Braun, Phys. Lett. B **359** (1995) 223 [hep-ph/9506248].

[56] A. Khodjamirian, G. Stoll and D. Wyler, Phys. Lett. B **358** (1995) 129 [hep-ph/9506242].

[57] A. Ali and E. Lunghi, DESY-02-089, hep-ph/0206242.

[58] S. Narison, Phys. Lett. B **327** (1994) 354 [hep-ph/9403370].

[59] D. Melikhov and B. Stech, Phys. Rev. D **62** (2000) 014006 [hep-ph/0001113].

[60] Y. Nir, hep-ph/0208080.

[61] See, for example, L. Lellouch, plenary talk at the 31st. International Conference on High Energy Physics, July 24 - 31, 2002, Amsterdam, The Netherlands.

[62] A. S. Kronfeld and S. M. Ryan, Phys. Lett. B **543** [hep-ph/0206058].

[63] C. Jessop (BABAR Collaboration), Talk presented at the 31st. International Conference on High Energy Physics, July 24 - 31, 2002, Amsterdam, The Netherlands.

[64] BaBar Collaboration, B. Aubert et al., SLAC preprint SLAC-PUB-9229, hep-ex/0205082, presented at 37th Rencontres de Moriond on Electroweak Interactions and Unified Theories, Les Arcs, France, 9–16 Mar 2002.

[65] M. Gronau and J. L. Rosner, Phys. Rev. D **65** (2002) 093012.

[66] M. Gronau and J. L. Rosner, Phys. Rev. D **66** (2002) 119901.

[67] M. Neubert and J. L. Rosner, Phys. Lett. B **441** (1998) 403.

[68] M. Neubert and J. L. Rosner, Phys. Rev. Lett. **81** (1998) 5076.

[69] D. A. Suprun, C.-W. Chiang, and J. L. Rosner, Phys. Rev. D **65** (2002) 054025.

[70] C.-W. Chiang and J. L. Rosner, Phys. Rev. D **65** (2002) 074035.

[71] A. Höcker, H. Lacker, S. Laplace, and F. Le Diberder, in *Proceedings of the 9th International Symposium on Heavy Flavor Physics*, Pasadena, California, 10–13 Sep 2001, AIP Conf. Proc. **618** (2002) 27.

[72] J. Charles, Phys. Rev. D **59** (1999) 054007.

[73] R. Fleischer, in *Proceedings of the 9th International Symposium on Heavy Flavor Physics*, Pasadena, California, 10–13 Sep 2001, AIP Conf. Proc. **618** (2002) 266.

[74] M. Gronau, D. London, N. Sinha, and R. Sinha, Phys. Lett. B **514** (2001) 315.

[75] M. Gronau, Phys. Rev. D **58** (1998) 037301.

[76] D. Atwood, I. Dunietz, and A. Soni, Phys. Rev. D **63** (2001) 036005.

[77] B. Kayser and D. London, Phys. Rev. D **63** (2000) 116013.

[78] A. J. Buras and R. Fleischer, Eur. Phys. J. C **16** (2000) 97.

[79] R. Fleischer, Phys. Lett. B **459** (1999) 306.

[80] M. Gronau and J. L. Rosner, Phys. Lett. B **482** (2000) 71.

[81] R. Fleischer, Phys. Rep. **370** (2202) 537 [hep-ph/0207108].

[82] M. Gronau, J. L. Rosner and D. London, Phys. Rev. Lett. **73** (1994) 21.

[83] R. Fleischer, Phys. Lett. B **365** (1996) 399.

[84] R. Fleischer and T. Mannel, Phys. Rev. D **57** (1998) 2752.

[85] M. Gronau and J. L. Rosner, Phys. Rev. D **57** (1998) 6843.

[86] R. Fleischer, Eur. Phys. J. C **6** (1999) 451.

[87] M. Neubert, JHEP **9902** (1999) 014.

[88] A. J. Buras and R. Fleischer, Eur. Phys. J. C **11** (1999) 93.

[89] R. Fleischer and J. Matias, Phys. Rev. D **61** (2000) 074004.

[90] M. Bargiotti *et al.*, Eur. Phys. J. C **24** (2002) 361.

[91] H.-n. Li and H. L. Yu, Phys. Rev. D **53** (1996) 2480;
Y. Y. Keum, H.-n. Li and A. I. Sanda, Phys. Lett. B **504** (2001) 6;
Y. Y. Keum and H.-n. Li, Phys. Rev. D **63** (2001) 074006.

[92] R. Fleischer, Eur. Phys. J. C **16** (2000) 87.

[93] R. Fleischer and J. Matias, Phys. Rev. D. **66** (2002) 054009, [hep-ph/0204101].

[94] J. Matias, Phys. Lett. B **520** (2001) 131.

[95] M. Gronau, Phys. Lett. B **492** (2000) 297.

[96] R. Fleischer, Eur. Phys. J. C **10** (1999) 299, Phys. Rev. D **60** (1999) 073008;
P. Z. Skands, JHEP **0101** (2001) 008.

[97] M. Gronau and J. L. Rosner, Phys. Rev. D **65** (2002) 093012, 113008 and hep-ph/0205323;
C.-D. Lü and Z.-j. Xiao, Phys. Rev. D **66** (2002) 074011 [hep-ph/0205134].

[98] M. Beneke, G. Buchalla, M. Neubert and C. T. Sachrajda, Nucl. Phys. B **591** (2000) 313.

[99] M. Wirbel, B. Stech and M. Bauer, Z. Phys. C **29** (1985) 637;
M. Bauer, B. Stech and M. Wirbel, Z. Phys. C **34** (1987) 103.

[100] M. Beneke, in: Proceedings of the 5th KEK Topical Conference: Frontiers in Flavor Physics (KEKTC5), Tsukuba, Ibaraki, Japan, 20-22 Nov 2001 [hep-ph/0202056].

[101] D. Du, H. Gong, J. Sun, D. Yang and G. Zhu, Phys. Rev. D **65** (2002) 074001.

[102] M. Beneke, in: Proceedings of: Flavor Physics and CP Violation (FPCP), Philadelphia, Pennsylvania, 16-18 May 2002 [hep-ph/0207228].

[103] M. Neubert, in: Proceedings of the International Workshop on Heavy Quarks and Leptons, Salerno, Italy, 27 May - 1 Jun 2002 [hep-ph/0207327].

[104] BaBar Collaboration, hep-ex/0207053; P. Krokovny [Belle Collaboration], talk at ICHEP2002, Amsterdam, July 2002.

[105] M. Ciuchini, E. Franco, G. Martinelli and L. Silvestrini, Nucl. Phys. B **501** (1997) 271 [hep-ph/9703353].

[106] M. Ciuchini, R. Contino, E. Franco, G. Martinelli and L. Silvestrini, Nucl. Phys. B **512** (1998) 3 [Erratum-ibid. B **531** (1998) 656] [hep-ph/9708222].

[107] A. J. Buras and L. Silvestrini, Nucl. Phys. B **569** (2000) 3 [hep-ph/9812392].

[108] M. Ciuchini, E. Franco, G. Martinelli, M. Pierini and L. Silvestrini, Phys. Lett. B **515** (2001) 33 [hep-ph/0104126].

[109] R. Patterson, summary talk at FPCP02, http://www.hep.upenn.edu/FPCP/talks/1803/180303Patterson.pdf.

[110] M. Ciuchini, Nucl. Phys. Proc. Suppl. **109** (2002) 307 [hep-ph/0112133].

[111] Y.Y. Keum, H.n. Li and A.I. Sanda, Phys. Lett. B **504** (2001) 6; Phys. Rev. D **63** (2001) 054008; hep-ph/0201103; Y.Y. Keum and H.n. Li, Phys. Rev. D **63** (2001) 074006; C.D. Lu, K. Ukai and M.Z. Yang, Phys. Rev. D **63** (2001) 074009; C.-H. Chen, Y.Y. Keum and H.-n. Li, Phys.Rev.D **64** (2001) 112002; hep-ph/0204166; S. Mishima, Phys.Lett. B **521** (2001) 252.

[112] BaBar Collaboration (B. Aubert et al.), hep-ex/0207055.

[113] R. Bartoldus, talk on Review of rare two-body B decays at FPCP workshop, May 17, 2002.

[114] Y.Y. Keum, Proceeding at the 3rd workshop on Higher Luminosity B Factory, Aug. 6-7, 2002; hep-ph/0209002; hep-ph/0209014; Y.Y. Keum et al., in preparation.

[115] G. Buchalla and A. J. Buras, Nucl. Phys. B **548** (1999) 309 [hep-ph/9901288].

[116] G. Buchalla and A. J. Buras, Nucl. Phys. B **398** (1993) 285; **400** (1993) 225; **412** (1994) 106 [hep-ph/9308272];

[117] M. Misiak and J. Urban, Phys. Lett. B. **451** (1999) 161 [hep-ph/9901278].

[118] A. F. Falk, A. Lewandowski and A. A. Petrov, Phys. Lett. B. **505** (2001) 107 [hep-ph/0012099].

[119] M. Lu and M. Wise, Phys. Lett. B. **324** (1994) 461 [hep-ph/9401204].

[120] W.J. Marciano and Z. Parsa, Phys. Rev. D **53** (1996) R1.

[121] L. Littenberg, Phys. Rev. D39 (1989) 3322.

[122] G. Buchalla and G. Isidori, Phys. Lett. B. **440** (1998) 170 [hep-ph/9806501];
D. Rein and L.M. Sehgal, Phys. Rev. D39 (1989) 3325.

[123] G. D'Ambrosio and G. Isidori, Phys. Lett. B. **530** (2002) 108 [hep-ph/0112135].

[124] S. Kettell, L. Landsberg and H. Nguyen, hep-ph/0212321.

[125] A. J. Buras *et al.*, Nucl. Phys. B **566** (2000) 3 [hep-ph/9908371].

[126] Y. Grossman and Y. Nir, Phys. Lett. B **398** (1997) 163 [hep-ph/9701313].

[127] S. Adler *et al.* [E787 Collaboration], Phys. Rev. Lett. **88** (2002) 041803 and references therein.

[128] S. Adler *et al.* [E787 Collaboration], Phys. Lett. B **537** (2002) 211 [hep-ex/0201037].

[129] http://www.phy.bnl.gov/e949/

[130] P.S. Cooper, Nucl. Phys. Proc. Suppl. **99B** (2001) 121;
http://www.fnal.gov/projects/ckm/Welcome.html

[131] M.V.Diwan, hep-ex/0205089, La Thuile, Italy, 2002.

[132] A. Alavi-Harati *et al.* [KTeV Collaboration], Phys. Rev. D **61** (2000) 072006 [hep-ex/9907014].

[133] http://psux1.kek.jp/∼e391/

[134] A. Konaka, hep-ex/9903016; http://pubweb.bnl.gov/people/e926/

[135] H. Höcker, H. Lacker, S. Laplace and F. Le Diberder, Eur. Phys. J. C **21** (2001) 225, hep-ph/0104062, http://ckmfitter.in2p3.fr/

[136] L.S. Littenberg, hep-ex/0201026, to appear in the Proc. 9th Intl. Symp. on Heavy Flavor Physics.

Chapter 7

SUMMARY AND HIGHLIGHTS

With over two hundred participants, more than eighty presentations in plenary and parallel sessions, and twelve discussion sessions, the first Workshop on the CKM Unitarity Triangle provided an opportunity for an exploration of the status, open issues, and future directions in the understanding of the quark mixing matrix. Thirteen more months for the preparation of this report have allowed to update results, refine most of the studies presented in February 2002, and add coherence to their presentation. It has also been an opportunity for the participants to discuss further, and to reach a consensus on several issues which had been debated at the Workshop. As a result, these proceedings could be written in the form of a coherent document with a common signatory list for each chapter, corresponding to the original working groups. On some issues we agreed to disagree: the continuation of this Workshop series will have to address these subjects.

The main goal of this first Workshop was to review the status of the CKM Unitarity Triangle at the end of the B physics studies at LEP, SLD and CESR and during the hand-over of the responsibility for their continuation, with even higher accuracy and sensitivity, to the B factories and the Tevatron. Chapter 1 introduces the CKM matrix and the Unitarity Triangle (UT), briefly describes the theoretical framework, and recalls the development of the B physics studies throughout a decade characterized by the operation of the LEP and SLC colliders, the Tevatron Run I, and their role in complementing the data obtained at CESR.

The cleanest way to measure the individual elements of the CKM mixing matrix is the determination of the yield of tree-level semileptonic processes which can be reliably computed. These measurements have reached their full maturity thanks to both the increasingly large data sample available, and the advancements in the theoretical understanding. Chapter 2 is devoted to the determination of $|V_{us}|$ from $K_{\ell 3}$ decays and that of $|V_{ud}|$ from super-allowed Fermi transitions and neutron beta decay. The relative accuracy on $|V_{us}|$ has now reached the 1% level while that on $|V_{ud}|$ is approaching a factor of twenty better. This requires special attention in evaluating the theoretical uncertainties that affect these determinations. In fact, they represent a large fraction of the total uncertainty in both cases. A likely explanation of the present 2.2 σ discrepancy in the unitarity relation $|V_{ud}|^2 + |V_{us}|^2 + |V_{ub}|^2 = 1$ is an underestimate of these effects. In the absence of a clear indication of which uncertainty has been underestimated, it has been proposed to take the value $|V_{us}| = 0.2240 \pm 0.0036$ as a conservative estimate of $|V_{us}|$, which assumes CKM unitarity. Possible improvements, which can be expected for both $|V_{us}|$ and $|V_{ud}|$ in the near future, are discussed. Particularly promising is the extraction of $|V_{us}|$ from $K_{\ell 3}$ decays. Here we soon expect new, precise data with a consistent treatment of radiative corrections and, at the same time, new theoretical evaluations of the $SU(3)$ breaking effects. Concerning $|V_{ud}|$, a challenging opportunity for experiment is offered by the theoretically clean π_{e3} decay.

The other class of tree-level decays which is central to the CKM UT studies is represented by the

$b \to c\ell\bar{\nu}$ and $b \to u\ell\bar{\nu}$ processes, which give access to $|V_{cb}|$ and $|V_{ub}|$, respectively. The discussion of the status of the extraction of these two CKM elements has attracted a large part of the participants and of the presentations at the Workshop. The third chapter of this report tries to summarize the status, with important updates from the Summer 2002 conferences.

With the statistical accuracy approaching the few percent level for some of these measurements, an important issue here is to carefully test the underlying theoretical assumptions. Both inclusive and exclusive decays are routinely studied. The measurement of $|V_{cb}|$ from exclusive decays is limited by the theoretical uncertainty on the value of the form factor at maximum q^2 (see Table 7.1). A detailed analysis of lattice QCD results and their uncertainty is now available. Progress in these studies, as well as more precise data from the B factories, are expected. Important progress has been made during and after the Workshop on the $|V_{cb}|$ extraction from inclusive semileptonic decays. The current accuracy of experimental measurements is at the percent level. While perturbative QCD corrections have been studied in different frameworks and the related uncertainty seems under control, the non-perturbative parameters appearing in the Operator Product Expansion (OPE) have to be constrained using experimental data. Several new analyses of the moments of distributions in semileptonic and radiative decays have appeared in the last year. Their results demonstrate that a significant fraction of the uncertainty on $|V_{cb}|$, arising from these parameters, can be absorbed in the experimental uncertainty. As shown in Table 7.1, the remaining theoretical uncertainty is now at the level of a percent. The consistent picture emerging from these preliminary studies represents a remarkable success for the OPE and bolsters confidence in the inclusive $|V_{cb}|$ determination, as no violation of parton-hadron duality has been detected at the present level of accuracy.

The CKM-suppressed counterpart of the $b \to c\ell\bar{\nu}$ process is the $b \to u\ell\bar{\nu}$ decay which measures $|V_{ub}|$, the smallest element in the CKM mixing matrix. Since its rate is only about 1/60 of that for $b \to c$ transition, measuring this charmless decay accurately is a formidable experimental challenge. We have known for more than a decade that this process is present, thanks to pioneering measurements by ARGUS and CLEO. The non-vanishing of $|V_{ub}|$ is a pre-requisite for explaining CP violation within the Standard Model (SM). Knowing its magnitude accurately is a top priority for testing the CKM UT. In this respect, significant progress has been made. Theorists have devised a number of strategies to pin down the value of $|V_{ub}|$ with good accuracy. Large data sets, complementary kinematical characteristics of the signal events at $\Upsilon(4S)$ and Z^0 energies, and experimental ingenuity have provided a significant set of results. None of them is approaching the accuracy obtained on $|V_{cb}|$ and the debate in the community on these fairly recent developments is still lively. But the results, obtained with very different methods, are all consistent and the overall accuracy amounts to better than 15% (see Table 7.1).

Another important area of studies of tree-level B decays, discussed in Chapter 3, is represented by the determination of the exclusive and inclusive b-hadron lifetimes. Those for the lighter mesons are presently known to an accuracy of one percent, or better. For B_s^0 and b-baryons important data has already been gathered and the Tevatron is expected to reach soon a similar accuracy. Lifetime differences between b-hadrons have been compared with expectations from OPE to test our understanding of the non-spectator contributions to beauty hadron decays. While this comparison has shown a consistent agreement between predictions and measurements in the meson sector, the measured ratio of baryon to meson lifetimes deviates from its initial expectation. This has been interpreted as a possible signal of problems in the underlying theory assumptions. However, much better agreement with data is re-established once the NLO corrections are included.

There remain two CKM elements, $|V_{ts}|$ and $|V_{td}|$, which have been so far accessed only through box diagrams. They can be probed by $\mathrm{K}^0 - \overline{\mathrm{K}}^0$ and $\mathrm{B}^0_{d,s} - \overline{\mathrm{B}}^0_{d,s}$ mixing. The experimental status of these studies and that of the non-perturbative calculations of $\hat{B}_K$, $\sqrt{\hat{B}_{B_d}}F_{B_d}$, $\sqrt{\hat{B}_{B_s}}F_{B_s}$, and ξ is reviewed in Chapter 4.

The theoretical discussion has centred on the determination of the non-perturbative parameters for

Parameter	Value	Experimental uncertainty	Theory uncertainty
λ	0.2240	0.0036	-
$\|V_{cb}\|\,(\times 10^{-3})$ (excl.)	42.1	1.1	1.9
$\|V_{cb}\|\,(\times 10^{-3})$ (incl.)	41.4	0.7	0.6
$\|V_{ub}\|\,(\times 10^{-4})$ (excl.)	33.0	2.4	4.6
$\|V_{ub}\|\,(\times 10^{-4})$ (incl. LEP)	40.9	5.8	3.3
$\|V_{ub}\|\,(\times 10^{-4})$ (incl. CLEO)	40.8	5.2	3.9
ΔM_d (ps^{-1})	0.503	0.006	-
ΔM_s (ps^{-1})	> 14.4 at 95% C.L.	sensitivity 19.2	
$F_{B_d}\sqrt{\hat{B}_{B_d}}$(MeV)	223	33	12
$\xi = \frac{F_{B_s}\sqrt{\hat{B}_{B_s}}}{F_{B_d}\sqrt{\hat{B}_{B_d}}}$	1.24	0.04	0.06
$\hat{B}_K$	0.86	0.06	0.14
sin 2β	0.734	0.054	-

Table 7.1: *Main experimental and theoretical results entering the UT determination. Other parameters of interest can be found in Chapters 2-5.*

neutral meson mixing. For F_{B_q} and ξ, lattice calculations with two dynamical flavours of quarks are becoming common and the first $2{+}1$ dynamical calculations have appeared. Much attention has focused on the chiral extrapolations needed to obtain the physical results, particularly for ξ, with a final lattice value for UT fits given as $\xi = 1.24(4)(6)$. QCD sum rules give very consistent results for the B meson decay constants, slightly less so for the B-parameters. For neutral kaon mixing the benchmark lattice calculations are quenched and lead to the final result given in Table 7.1. The systematic uncertainty includes the estimate for quenching effects and is considered to be very conservative (a more aggressive error estimate is given in Sec. 2.2. of Chapter 4). The best-developed alternative technique to evaluate $\hat{B}_K$ is the large-N_c expansion and gives a consistent result, although the chiral corrections are more than 100% in this case.

The time structure of B^0-$\overline{\mathrm{B}}^0$ oscillations has been precisely measured in the B^0_d sector. The LEP, Tevatron and SLC results are in excellent agreement with those obtained at the B factories. After the inclusion of the latter, the oscillation frequency ΔM_d is known with a precision of about 1% (see Table 7.1). Further improvements are expected, which should bring the accuracy on ΔM_d to a few per mille.

On the other hand, B^0_s-$\overline{\mathrm{B}}^0_s$ oscillations have not been observed yet, even though the experimental effort has allowed to largely exceed the anticipated sensitivity. Today we know that B^0_s mesons oscillate at least thirty times faster than B^0_d mesons. The final result of the searches at LEP and SLC is $\Delta M_s > 14.4$ ps^{-1} at 95% C.L., with a sensitivity of $\Delta M_s = 19.2$ ps^{-1}. While this much sought-after phenomenon has so far eluded searches, the consequent lower limit on ΔM_s has already a significant impact on the determination of the UT parameters.

The extraction of the UT parameters from all these inputs, within the Standard Model, is discussed in Chapter 5, which represents a central part of this Workshop. Five quantities have been considered to constrain the upper apex of the UT in the $\bar{\rho}$-$\bar{\eta}$ plane. These are ϵ_K, $|V_{ub}|/|V_{cb}|$, ΔM_d, the limit on ΔM_s and sin 2β from the measurement of the CP asymmetry in the $J/\psi\mathrm{K}^0$ decays. Comparing

the measured values of these observables with their theoretical predictions (in the SM or in a different model) yields a set of constraints, which however depend on several parameters, like quark masses, decay constants of B mesons and non-perturbative parameters, such as $\hat{B}_K$. Their values are constrained by both measurements and theoretical calculations which are reviewed in Chapter 4.

Different methods have been proposed to combine this information and extract the UT parameters. They differ in the treatment of the theoretical uncertainties for which they adopt either a frequentist or a Bayesian approach. Despite much interest in these studies, no systematic comparison of these methods had been performed before this Workshop. Moreover, different assumptions on the input parameters made any comparison of published results difficult. At the Workshop, different groups agreed to share a common set of input values (see Table 5.1), provided by the relevant working groups. In spite of using the same central values and errors, the likelihood functions associated with the input parameters are different in the two approaches. As a consequence, the region defining the 95% (99%) confidence level for the UT parameters is wider by 30% (20%) in the frequentist as compared to the Bayesian approach. Further tests have shown that, if the same likelihoods are used for input quantities, the output results become almost identical. The main origin of the difference between the results in the Bayesian and the frequentist method is therefore the likelihood associated to the input quantities. But these differences will decrease progressively as the theoretical uncertainties will be reduced or related to experimental ones. An example of the latter is the extraction of $|V_{cb}|$ from inclusive decays, where — as already mentioned — experimental constraints from the moments have replaced theoretical estimates in the aftermath of the Workshop. It is also expected that additional inputs will be determined using unquenched Lattice simulations.

Independently of the statistical method adopted, a crucial outcome of these investigations is the remarkable agreement of the UT parameters, as determined by means of CP conserving quantities sensitive to the UT sides, with the CP violation measurements in the kaon sector (ϵ_K) and in the B sector (sin2β). This agreement tells us that, at the present level of accuracy, the SM mechanism of flavour and CP violation describes the data well. At the same time, it is also an important test of the OPE, HQET and Lattice QCD, on which the extraction of the CKM parameters rests. The present accuracy is at the 10% level; the B factories and a next generation of facilities will improve the sensitivity of these tests by an order of magnitude. The study of the impact of the uncertainties in the theoretical parameters on the UT fits has shown that the uncertainties in $\sqrt{\hat{B}_{B_d}}F_{B_d}$ have to be decreased by at least a factor of two in order to have a significant impact on the UT fits — unless future calculations result in $\sqrt{\hat{B}_{B_d}}F_{B_d}$ values which differ significantly from present results. In the case of $\hat{B}_K$ and in particular ξ, even a modest reduction of the theoretical uncertainty could already have an important impact on the UT fits.

The output for various quantities of interest can be found in Table 5.5; a pictorial representation of the fit is shown in Fig. 5.2. UT fits can also be used to obtain predictions for quantities that will only be measured in the future, such as the ΔM_s oscillation frequency, predicted to be < 22.2 ps^{-1}, and the angle γ, predicted to be between 49.0° and 77.0°. These 95% confidence levels ranges may be considered as a reference to which the direct measurements will need to be compared for identifying possible signals of New Physics.

While the determination of the triangle sides and the definition of the procedures for the UT fits had a central role at the Workshop, a number of topics, which will become of increasing importance at future meetings, started to be addressed. They are presented as individual contributions in Chapter 6. At this stage, general strategies for the determination of the UT need to be formulated. Preliminary studies show that the pairs of measurements (γ, β), (γ, R_b) and $(\gamma, \overline{\eta})$ offer the most efficient sets of observables to determine $(\bar{\rho}, \bar{\eta})$. On the other hand the pair (R_t, β) will play the leading role in the UT fits in the coming years and for this reason it has been suggested to plot the available constraints on the CKM matrix in the (R_t, β) plane. The present (R_t, β) plot corresponding to the usual $(\bar{\rho}, \bar{\eta})$ plot can be found in Fig. 6.5.

There are more measurements of B decays which are relevant to the CKM studies. Radiative rare B-decays, very sensitive to New Physics in loops, have been reviewed for their potential relevance in probing the CKM UT. The combined studies of radiative decays into non-strange hadrons are sensitive to $(\bar{\rho}, \bar{\eta})$ and could in principle provide interesting constraints on the UT, provided that the theoretical errors can be reduced and that the branching fractions are accurately measured.

The decays $\mathrm{B} \to \pi\mathrm{K}$, $\mathrm{B} \to \pi\pi$ and $\mathrm{B} \to \mathrm{K}\overline{\mathrm{K}}$ are emphasised as useful tools for the determination of the angles α and γ. Here flavour symmetries and recent dynamical approaches like QCD factorization and pQCD play the dominant role in the phenomenology. The status of QCD factorization has been outlined and also the critical points in view of a possible extraction of γ have been described.

Finally, the potential of the rare decays $\mathrm{K}^+ \to \pi^+\nu\overline{\nu}$ and $\mathrm{K_L} \to \pi^0\nu\overline{\nu}$ with respect to the determination of the UT has been discussed. These decays are essentially free of theoretical uncertainties but are subject to parametric uncertainties such as m_c for $\mathrm{K}^+ \to \pi^+\nu\overline{\nu}$ and V_{cb} for both decays. These uncertainties should be reduced in the coming years so that the future measurements of these decays will provide very important independent measurements of V_{td} and $\sin 2\beta$ and more generally of the UT parameters. The comparison of these measurements with those obtained by B decays offers a very powerful tool for testing the SM and its extensions.

The CKM Workshop contributed to demonstrate the richness and variety of the physics landscape related to the CKM matrix and the Unitarity Triangle. Results from the LEP, SLC, CESR and Tevatron experiments have already provided us with an impressionistic outline of this landscape, which the B factories and the Run II at the Tevatron are now revealing in greater detail. While the CKM matrix appears likely to be the dominant source of flavour and CP violation, New Physics contributions may still modify the shape of the UT and be revealed by forthcoming studies. In this context the measurements of the angle γ in non-leptonic B decays and those of ΔM_s will mark important new steps in the search for New Physics in the $\bar{\rho}$-$\bar{\eta}$ plane. The present deviation from the SM expectation of the CP asymmetry in $\mathrm{B}^0_d \to \phi\mathrm{K}_S$ also awaits a clarification, and the improved data on several rare decays will be very important in this programme. All this will be the subject of future CKM Workshops.